MERCAPTOBENZOTHIAZOLE-ON-GOLD BIOSENSOR SYSTEMS FOR ORGANOPHOSPHATE AND CARBAMATE PESTICIDE COMPOUNDS

Vernon Sydwill Somerset

Summary

Organophosphate and carbamate pesticides are powerful neurotoxins that impede the activity of cholinesterase enzyme leading to severe health effects. This study firstly reports the development, characterisation, and application of thick-film acetylcholinesterase (AChE) biosensors based on a gold electrode modified with a mercaptobenzothiazole (MBT) self-assembled monolayer and either poly(o-methoxyaniline) (POMA) or poly(2,5-dimethoxyaniline) (PDMA) in the presence of polystyrene(*4*-sulphonic acid) (PSSA). The Au/MBT/POMA-PSSA/AChE and Au/MBT/PDMA-PSSA/AChE biosensors were then applied to successfully detect standard organophosphorous and carbamate pesticides in a 0.1 M phosphate buffer, 0.1 M KCl (pH 7.2) solution. Secondly, it reports the construction of the Au/MBT/PANI/AChE/PVAc thick-film biosensor for the determination of certain organophosphate and carbamate pesticide solutions in selected aqueous organic solvent solutions. The Au/MBT/PANI/AChE/PVAc electrocatalytic biosensor device was constructed by encapsulating acetylcholinesterase (AChE) enzyme in the PANI polymer composite, followed by the coating of poly(vinyl acetate) (PVAc) on top to secure the biosensor film from falling off. The electroactive substrate called acetylthiocholine (ATCh) was also chosen to replace acetylcholine (ACh) as substrate, since ATCh has better redox activity and can both be oxidised and reduced to provide better movement of electrons in the amperometric biosensor. The voltammetric results have shown that the current shifts more anodically as the

Au/MBT/PANI/AChE/PVAc biosensor responded to successive acetylthiocholine (ATCh) substrate addition under anaerobic conditions in 0.1 M phosphate buffer, KCl (pH 7.2) solution. For the Au/MBT/PANI/AChE/PVAc biosensor, various performance and stability parameters were evaluated. These factors include the optimal enzyme loading, effect of pH, long-term stability of the biosensor, temperature stability of the biosensor, the effect of polar organic solvents, and the effect of non-polar organic solvents on the amperometric behaviour of the biosensor. The Au/MBT/PANI/AChE/PVAc biosensor was then applied to detect a series of 5 organophosphorous and carbamate standard pesticide solutions. The organophosphorous pesticides studied were diazinon, fenthion, parathion-methyl, malathion and chlorpyrifos; while the carbamate pesticides included dioxacarb, aldicarb, carbaryl, carbofuran and methomyl. Very good detection limits were obtained for the standard pesticide solutions and they were within the nanomolar range. The detection limit values for the individual pesticides were 0.137 nM (diazinon), 0.826 nM (fenthion), 1.332 nM (parathion-methyl), 0.189 nM (malathion), 0.018 nM (chlorpyrifos), 1.572 nM (dioxacarb), 1.209 nM (aldicarb), 0.880 nM (carbaryl), 0.249 nM (carbofuran) and 0.111 nM (methomyl). The detection limit results showed that the thick-film Au/MBT/PANI/AChE/PVAc biosensor was more sensitive to organophosphorous and carbamate pesticides compared to other biosensor results found in the literature.

Dedication

To my son, Enver Stuart and daughter, Emma Marion.

"So that others may learn, experiment and report."

Acknowledgements

Table of Contents

List of Figures

List of Tables

Acronyms and Abbreviations

A	Area of electrode
AChE	Acetylcholinesterase
ACh	Acetylcholine
AChI	Acetylcholine iodide
Ag/AgCl	Saturated Silver/ Silver chloride reference electrode
ATCh	Acetylthiocholine
ATChCl	Acetylthiocholine chloride
Au	Gold
Au/MBT	Gold/Mercaptobenzothiazole
a_s	Activity of the substance S
a.c.	Alternating current
BuChE	Butyrylcholinesterase
BTCh	Butyrylthiocholine
C	Concentration of redox active species in bulk solution
C_i	Analyte ion concentration
C_I	Inhibitor concentration
ChE	Cholinesterase
CPE	Carbon paste elecrode
CPs	Conducting polymers
CSA	Camphor sulphonic acid
CV	Cyclic Voltammetry
CNT	Carbon nanotube
d.c.	Direct current
D_e	Electron diffusion coefficient
D_o	Diffusion coefficient
DBSA	Dodecyl benzenesulphonic acid
DMA	*2,5*-dimethoxyaniline
DPV	Differential Pulse Voltammetry
E	(i) Applied potential, or (ii) Enzyme
$E_{\frac{1}{2}}$	Half-wave potential
EM	Emeraldine
ES	(i) Enzyme-substrate complex, or (ii) Emeraldine salt
E^0	Standard redox potential
$E_{p,a}$	Anodic peak potential
$E_{p,c}$	Cathodic peak potential
E^o	Formal electrode potential
ΔE_p	Separation peak potential
Ep	Peak potential
$E_{p/2}$	Half-peak potential
F	Faraday's constant
Fc	Ferrocene

FETs	Field effect transistors
GCE	Glassy carbon electrode
GOx	Glucose oxidase
H_2O_2	Hydrogen peroxide
H_2SO_4	Sulphuric acid
HCl	Hydrochloric acid
ISE	Ion selective electrode
I %	Inhibition degree or percentage inhibition
I	Current
$I_{p,a}$	Anodic peak current
$I_{p,c}$	Cathodic peak current
I_{max}	Maximum current
K_m^{app}	Apparent Michaelis-Menten constant
K_m^{Inhib}	Apparent Michaelis-Menten constant for the inhibitor
Log P	Logarithm of the partition coefficient
LB	Leucoemeraldine base
M	Molar concentration
MBT	Mercaptobenzothiazole
MBC	Methyl *2*-benzimidazole carbamate
nM	Nanomolar concentration
OMA	*O*-methoxyaniline (or o-anisidine or 2-methoxyaniline)
Ox	Oxidised form of an electrochemically active species
OSWV	Osteryoung Square Wave Voltammetry
PANI	Polyaniline
PANIs	Polyanilines
PBS	Phosphate buffered saline solution
PCB	Polycarbazole
PFU	Polyfuran
pH	Acidity or alkalinity of a solution
POMA	Poly(*o*-methoxyaniline)
PDMA	Poly(*2,5*-dimethoxyaniline)
PS	Pernigraniline salt
PSSA	Poly(*4*-styrene sulphonic acid)
PPy	Polypyrrole
PPN	Poly(*p*-phenylene)
Pt	Platinum
PT	Polythiophene
PVAc	Poly(vinyl acetate)
ppm	Parts per million
ppb	Parts per billion
PTC	Positive temperature coefficient
PVC	polyvinylchloride
Q	Charge
Red	Reduced from of an electrochemically active species
S	Substrate

SAM	Self-assembled monolayer
SAMs	Self-assembled monolayers
SPEs	Screen-printed electrodes
SWV	Square Wave Voltammetry
T	Temperature
t	time
TCNQ	*7,7,8,8*-Tetracyanoquinodimethane
TSA	*p*-Toluene sulphonic acid
V_{max}	Maximal rate
WE	Working electrode
WHO	World Health Organisation
Γ	Surface concentration
v	Scan rate
α	Transfer coefficient
ψ	Mathematical function for quasi-reversible electron transfer processes
γ	Activity coefficient

List of Publications and Presentations

Papers

1. **Vernon S. Somerset**, Michael J. Klink, Mantoa M. C. Sekota, Priscilla G.L. Baker and Emmanuel I. Iwuoha. (**2006**). Polyaniline-mercaptobenzothiazole biosensor for organophosphate and carbamate pesticides. *Analytical Letters,* 39 (8): 1683 – 1698.

2. Emmanuel I. Iwuoha, Sipho E Mavundla, **Vernon S Somerset**, Leslie F Petrik, Michael J Klink, Mantoa Sekota and Priscilla Baker. (**2006**). Electrochemical and Spectroscopic Properties of Fly Ash-Polyaniline Matrix Nanorod Composites. *Michrochimica Acta, 155 (3-4):* 453 – 458.

3. **Vernon S. Somerset**, Michael J. Klink, Priscilla G. L. Baker & Emmanuel I. Iwuoha. (**2007**). Acetylcholinesterase-polyaniline biosensor investigation of organophosphate pesticides in selected organic solvents. *Journal of Environmental Science and Health*, *B42 (*3): 297 – 304.

4. Immaculate N. Michira, M. Klink, R. O. Akinyeye, **V. Somerset**, M. Sekota, A. Al-Ahmed, P. G. L Baker, Emmanuel I. Iwuoha. (**2007**). Anthracene Sulfonic Acid-Doped Polyanilines: Electrodynamics and Application as Amperometric Peroxide Biosensor. *Book chapter: Recent Advances in Conducting Polymer (In Review)*

5. **V.S. Somerset**, M.J. Klink, M. Sekota, P.G.L. Baker and E.I. Iwuoha. (**2007**). Acetylcholinesterasepoly(*2,5dimethoxyaniline*) pesticide (nano)biosensor for organophosphate pesticide detection. In E. Mvula, H.R. Lofty, I. Mapaure, S. Singh & B. Mapani (eds.). Proceedings of the East and Southern Africa Environmental Chemistry Workshop (ESAECW) and the Sixt Theoretical Chemistry Workshop in Africa (TCWA). University of Namibia, Windhoek, Namibia. 5-9 December 2005*: 89 – 102.*

6. **V. Somerset**, M. Klink, R. Akinyeye, M. Sekota, A. Al-Ahmed, P. Baker and E.I. Iwuoha. (**2007**). Spectroelectrochemical Reactivities of Novel Polyaniline Nanotube Pesticide Biosensors. *Macromolecular Symposia, 2007 (In Press)*

7. Michira I. N, Klink M., Akinyeye R., **Somerset V**., Sekota M., Al-Ahmed A., Baker P. and Iwuoha E. (**2007**). Electrochemical Synthesis of Anthracene Sulfonic Doped Polyanilines: Spectroscopic Characterization and Application in Hydrogen Peroxide Sensing. *Macromolecular Symposia, 2007 (In Press)*

Oral and Poster Presentations at Conferences

➢ **Enviromin 2004 Environmental Conference**
Kasane, Botswana, 27 June – 1 July 2004
"Fly ash-conducting polymer matrix composites: structural and electrochemical impedance characterisation."
Mavundla S, **Somerset V**, Petrik L, Baker P & Iwuoha E.

➢ **37th South African Chemical Institute (SACI) Convention**
CSIR International Convention Centre, CSIR Campus,, Pretoria, RSA. 4 – 8 July 2004.
"Nanobiosensor systems for organophosphate pesticides 1: Template synthesized polyaniline nanocomposites on mercaptobenzothiazole-modified gold electrodes."
Somerset V, Mabula T, Baker P & Iwuoha E.

➢ **Faraday Discussions, 128: Self Organising Polymers Conference**
University of Leeds, UK, 19 – 21 July 2004
"Template Synthesized Polyaniline Nanocomposites on Mercaptobenzothiazole Modified Gold Electrodes."
Iwuoha E, **Somerset V**, Mabula T & Baker P.

➢ **10th Student Symposium on Atmospheric Chemistry, Electrochemistry and Separations**
Chemistry Department, Stellenbosch University, Stellenbosch, RSA. 29 November 2004.
"Voltammetric analysis of template synthesized polyaniline doped with acetylcholinesterase."
Somerset V, Klink M, Baker P & Iwuoha E.

➢ **XVIIIth International Symposium on BIOELECTROCHEMISTRY and BIOENERGETICS**
3rd Spring Meeting – Bioelectrochemistry. Coimbra, 19 – 24 June 2005, Spain
"Amperometric and Impedimetric Reactivities of Metabolic Enzyme Bioelectrodes in Nanotubular Polyaniline matrix."
E.I. Iwuoha, M.J. Klink, **V.S. Somerset**, S.E. Mavundla, P. Baker and M. Sekota

➢ **8th UNESCO School & UNESCO/IUPAC Conference on Macromolecules**
Department of Chemistry, Faculty of Science, University of Mauritius, Réduit, Mauritius, 6 – 9 June 2005
"Electrochemical preparation and characterisation of novel poly(pyrrole) and thiophene condutive polymers."
PGL Baker, **V Somerset**, R Akinyeye, M Klink and E Iwuoha.

➢ **5th International Kenya Chemical Society Conference**

Kenyatta University, Nairobi, Kenya, 22 – 26 August 2005.
(i) "Self-assembled acetylcholinesterase-polyaniline pesticide (nano)biosensor on mercaptobenzothiazole-modified gold electrodes."
V.S. Somerset, M.J. Klink, M. Sekota, P.G.L. Baker and E.I. Iwuoha.

(ii) "Preparation and spectroelectro-chemical reactivities of novel polyaniline nanotubes."
<u>E.I. Iwuoha,</u> M.J. Klink, **V.S. Somerset**, M. Sekota and P.G.L. Baker

- **2nd International Workshop on Biosensors for Food Safety and Environmental Monitoring.**
  Université Hassan II-Mohammedia, Faculté des Sciences et Techniques, 10 – 12 November 2005, Agadir, Morocco.
  "Spectroelectrochemical Reactivities Of Novel Polyaniline Nanotube Pesticide Biosensors."
  E.I. Iwuoha, M.J. Klink, **V. Somerset**, P. Baker and M. Sekota.

- **East and Southern Africa Environmental Chemistry Workshop (ESAECW) and the Sixt Theoretical Chemistry Workshop in Africa (TCWA).**
  University of Namibia, 5 – 9 December 2005, Windhoek, Namibia.
  (i) "Acetylcholinesterasepoly(2,5dimethoxyaniline) pesticide (nano)biosensor for organophosphate pesticide detection."
  V.S. Somerset, M.J. Klink, M. Sekota, P.G.L. Baker and E.I. Iwuoha.

  (ii) "Electrochemical Properties of Novel Polyaniline Nanotubes and Nanomicelles."
  M.J.Klink, **V.S.Somerset**, S.E.Mavundla, M.Sekota, P.Baker, E.Iwuoha. (2005).

  (iii) "Spectroscopic and Electrochemical Properties of Novel Polyaniline Nanaotubes."
  <u>E.I. Iwuoha,</u> I.N. Michira, M.J. Klink, **V. Somerset**, P. Baker and M. Sekota.

- **Ninth World Congress on Biosensors 2006**
  Sheraton Centre, 10 – 12 May 2006, Toronto, Canada.
  "Acetylcholinesterase-polyaniline biosensor investigation of organophosphosphate pesticides in selected organic solvents."
  V.S. Somerset, M.J. Klink, P.G.L. Baker and E.I. Iwuoha.

- **International Conference on Pesticide Use in Developing Countries: Environmental Fate, Effects and Public Health Implications**
  Organized by ANCAP in Collaboration with SETAC Africa branch, 16th - 20th October 2006, Arusha International Conference Centre, Arusha, Tanzania.
  "Electrochemical Polyaniline Biosensor For Diazinon Detection."
  I.N. Michira, **V. Somerset**, M. Klink, R. Akinyeye, P. Baker and E I Iwuoha.

- **9th Annual NESCO/IUPAC Conference on Macromolecules: Polymers for Advanced Applications**
  Stellenbosch University, 20 – 23 November 2006, Stellenbosch, South Africa.
  (i) "Spectroelectrochemical Reactivities of Novel Polyaniline Nanotube Pesticide Biosensors."
  V. Somerset, M. Klink, R. Akinyeye, M. Sekota, A. Al-Ahmed, P. Baker and E.I. Iwuoha

  (ii) "Electrochemical Synthesis of Anthracene Sulfonic Doped Polyanilines: Spectroscopic Characterization and Application in Hydrogen Peroxide Sensing."
  Michira I. N, Klink M., Akinyeye R., **Somerset V**., Sekota M., Al-Ahmed A., Baker P. and Iwuoha E.

- **9th International Symposium on Kinetics in Analytical Chemistry (KAC)**
  4 – 6 November 2006, Marrakech, Morocco.
  "Electrokinetics and sensor applications of polypyrrole modified with 1, 4-naphthaquinone sulfonic acid (NQSA)."
  <u>Richard Akinyeye</u>, Immaculate Michira, Michael Klink, **Vernon Somerset**, Mantoa Sekota, Amir-Al Ahmed, Priscilla Baker, Emmanuel Iwuoha.

- **South African Nanotechnology Initiative (SANI) NanoAfrica 2006 Conference**
  26 – 29 November 2006, University of Cape Town, Cape Town, South Africa.
  "Electrochemical and Spectroscopic Properties of Fly Ash-Polyaniline Matrix Nanorod Composites."
  Vernon S Somerset, Sipho E Mavundla, Leslie F Petrik, Michael J Klink, Mantoa Sekota, Amir Al-Ahmed, Priscilla Bakers, Emmanuel I. Iwuoha.

- **38th Convention of the South African Chemical Institute**
  3 – 8 December 2006, University of KwaZulu-Natal, Howard College Campus, Durban, South Africa.
  (i) "The assembling and application of an acetylcholinesterase-polyaniline biosensor for organophosphate and carbamate pesticides."
  V.S. Somerset, M.J. Klink, P.G.L. Baker and E.I. Iwuoha.

  (ii) "Novel Phenol and Phenol-derivative Sensor based on Poly(2,5 dimethoxyaniline) (PDMA) Sulphonic Acid (ASA) nanostructured conducting polymer as a redox mediator."
  Michael Klink, **Vernon Somerset**, Mantoa Sekota, Priscilla Baker and Emmanuel Iwuoha.

  (iii) "Polyanilino Matrices for Horse Radish Peroxidase (HRP) Encapsulation in a Peroxide Sensing Scheme."

I.N. Michira, M. J. Klink, R. Akinyeye, **V. Somerset**, M. Sekota, P. Baker and E. Iwuoha.

(iv) "4-(thiophen-3-yl) aniline based electrochemical biosensors for determination of glufosinate, glyphosate, and their major metabolites in genetically modified foodstuffs."
E. Songa, L. Ticha, **V. Somerset**, P.G.L. Baker and E. Iwuoha.

➢ **Southern and East African Network of Analytical Chemists (SEANAC) International Conference (Theme: Chemistry for Health)**
15 – 18 July 2007, Gaborone Sun Hotel, Gaborone, Botswana.
"Poly (2, 5-dimethoxyaniline)-poly (4-styrene sulfonic acid)-based biosensor for determination of glyphosate and glufosinate."
E.A. Songa, **V.S. Somerset**, A. Al-Ahmed, P.G.L. Baker, E.I. Iwuoha.

➢ **International Conference on Materials for Advanced Technologies 2007 (ICMAT)**
1 – 6 July 2007, Suntec Singapore International Convcention & Exhibition Centre, Singapore.
(i) "Reactivities of Novel Nanostructured Derivatised Polyaniline Amperometric Biosensor Devices for Detection of Various Analytes."
N. Michira, R. O. Akinyeye, **V. S. Somerset**, M. J. Klink, P. G. L. Baker and E. I. Iwuoha.

(ii) "Impedimetric Applications of Nanostructured Conducting Polypyrroles for the Determination of Some Anthropogenic Organic Pollutants in Waste Water."
R. O. Akinyeye, I. N. Michira, M. Klink, **V. Somerset**, O. A. Arotiba, J. O. Owino, A. Ignaszack, A. Al-Ahmed, T. T. Tsafaye, P. G. L. Baker and E. I. Iwuoha.

CHAPTER 1

Introduction

1.1   Introduction

This thesis describes the development and characterisation of a suitable organic phase amperometric biosensor for the detection of organophosphorus and carbamate pesticides in organic solvents.

Chapter 1 discusses what a biosensor is and defining sensors in general, followed by the use of self-assembled monolayers (SAMs), conducting polymers and the role of pesticides. This is followed by a discussion of the motivation, aims, and layout of the thesis.

1.2   Biosensors

Biosensors operate on the direct spatial coupling of an immobilised biologically active compound with a signal transducer and an electronic amplifier (Scheller and Schubert 1992:7; Karube and Nomura 2000:177-178).
A biosensor can be defined as:

> *"a compact analytical device incorporating a biological or biologically-derived sensing element either integrated within or intimately associated with a physicochemical transducer. The usual aim of a biosensor is to produce either discrete or continuous digital electronic signals that are proportional to a single analyte or a related group of analytes."*

(Newman *et al.* 2001:6; Morrin 2002:3; Keane *et al*. 2002:103; Evtugyn *et al*. 1998:467; Jin & Brennan 2002:16).
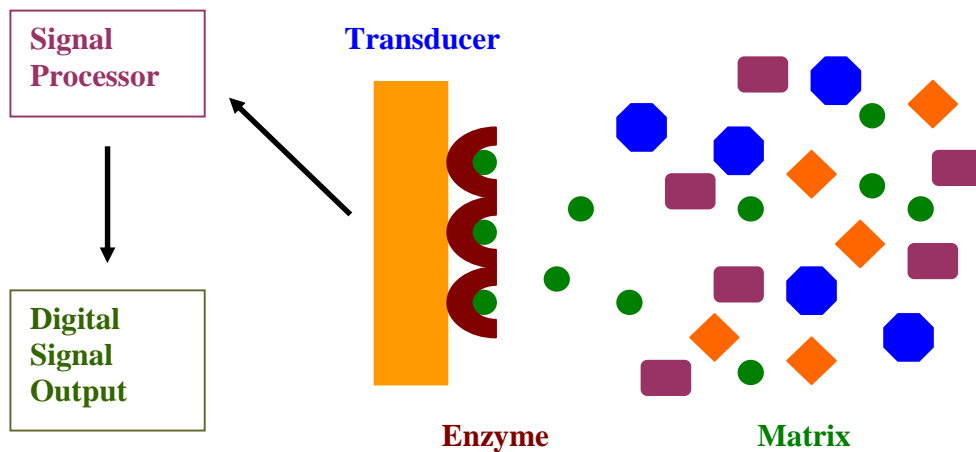
Figure 1.1 **Schematic diagram showing the functioning of a biosensor device.**

As shown in Figure 1.1, the first step in the above-mentioned interaction is the specific complex formation of the immobilised biologically active substance, called the enzyme, with the target analyte. The complex formation causes physiochemical changes such as change of layer thickness, refractive index, light absorption or electrical charge. These changes may be indicated by means of opto-electronic

sensors, potentiometric sensors, or field effect transistors. After the measurement, the initial state must be regenerated by splitting of the complex (Scheller and Schubert 1992:7-9; Evtugyn *et al*. 1998:467).

The following sequence of processes takes place in biosensors:

(I)   specific recognition of the analyte;

(II)   transduction of the physiochemical effect caused by the interaction with the receptor into an electrical signal;

(III)   signal processing and amplification.

In operation the biosensor measures the change in the concentration of a co-reactant that reacts with the analyte or a co-product, which is produced with the analyte of a biological reaction (e.g. enzyme reaction). When we have the use of an electrode as a transducer in a biosensor, the electrode converts the change in concentration of a product of a biological reaction into an electrical signal (Karube & Nomura 2000:178).

1.3   Self-Assembling Monolayers (SAMs)

Self-assembled monolayers are ordered molecular assemblies, which are formed by the adsorption of active surfactants on a solid surface, i.e. a solid electrode. This technique provides an elegant route to the preparation of well-defined organic

assemblies on solid surfaces. The monolayers are formed due to a specific interaction between a terminal functional group and a specific surface.

The use of *1*-alkanethiols as SAMs on a gold surface is formed by the adsorption of the monolayers from solution onto the gold surface. Alkanethiols are composed of molecules with ten or more carbon atoms per alkyl chain, and they are highly ordered and densely packed. Besides the methyl-terminated *1*-alkanethiols, ω-substituted *1*-alkanethiols of the formula $HS(CH_2)_nX$, where X is, for example, a halogen atom, or a hydroxyl, amino, carboxylic acid, ester, or nitrile group, have also been employed as well as mixed monolayers of *1*-alkanethiols with different terminal substituents. The uses of SAMs include several advantages such as their ease of preparation, stability, and the possibility of introducing different chemical functionalities. They further allow the preparation of surfaces with tailor-made properties, since monolayers with the appropriate chemical functionality with some molecular level control, can be used (Chellappan and Ohsaka 2001:44; Mazur & Krysinski 2001:3963; Yourdshahyan *et al*. 2001:1; Bruto *et al.* 2003:53).

The formation of SAMs on gold electrodes has yielded very promising results for the construction of electrochemical biosensors, the advantages of which are:

(i)   improved electrocatalysis,

(ii)   freedom from surface fouling, and

(iii)   prevention of undesirable reactions competing kinetically with the desired electrode process.

Particular emphasis has been placed on alkanethiol monolayers, which are known to form well-ordered assemblies that can be used to immobilise protein close to the

electrode surface, with a high degree of control over the molecular architecture of the recognition interface. Alkanethiols have also been modified to include electroactive moieties (for mediator or electron transfer function), so that the SAMs can be used for electrical wiring or communication between the redox-active enzymes and the electrode surface (Kerman *et al.* 2002:39-40; Zhang *et al.* 2002:150; Bruto *et al.* 2003:53).

1.4   Conducting Polymers

The type of organic materials, called conjugated polymers, has attracted a lot of attention lately, as materials for possible applications in micro-electronic devices. The reasons for this are their unique properties and versatility. Since the discovery of polythiazyl, $(SN)_x$, as the first conjugated polymer, the idea of using polymers for their electrical conducting properties has created much interest since then. Other conducting polymers having π-electron conjugated structures, such as polyaniline (PANI), polypyrrole (PPY), polythiophene (PT), polyfuran (PFU), poly(*p*-phenylene) (PPN) and polycarbazole (PCB) have been synthesized for possible use in micro-electronic devices (Palys *et al*. 2000:111; Saxena and Malhotra 2003:293-294).

Polyaniline (PANI) as conducting polymer has been studied the most because of its widespread application in micro-electronic devices. The PANI molecule consists of two segments, a flat structure of two imine groups and a quinoid ring (see

Figure 2.27). It also contains tetrahedral segments of two amine groups, which in turn

separates three benzenoid rings (Laska 2004:13).

It is furthermore possible to transfer PANI by redox reactions into states of

strongly differing electrical conductivity. Due to this characteristic property, PANI

and other conducting polymers have also been classified as organic metals. Recent

developments has seen the use of conducting polymers as active layers in chemical

sensors, since there is evidence that adsorbed gas molecules and organic vapours

cause a change of electrical conductivity in the polymer matrix of organic metals.

Conducting polymers further lends itself to direct electrochemical deposition onto

certain surfaces. This type of deposition also allows the preparation of films at a well-

defined redox potential in the presence of a given counter ion, which in turn defines

the level and characteristics of the doping reaction (Pruneanu *et al.* 1999:2733;

Mathebe *et al.* 2004:115; Reemts *et al.* 2004:320).

1.5   Thick film electrodes

Currently different technologies exist to develop thick-film biosensors for

pesticide detection (Joshi *et al.* 2005:54; Albereda-Sirvent *et al.* 2001:36). Albareda-

Sirvent *et al.* (2000:154) divide these different technologies into three categories of

(i) multiple-layer deposition with biological deposition by hand or electrochemically,

(ii) using screen-printing techniques of composite inks or pastes in two or more steps

with biological deposition done by screen-printing, (iii) using a one-step deposition layer also called the biocomposite strategy. One of the main aims of this work was to develop an electrode, which can be exposed to organic solutions containing potential inhibitors without having the polymer layer separating from the electrode surface, after use or drying thereby using polyvinyl acetate as the binder to circumvent this problem. Cellulose acetate is known to be used as a synthetic resin in screen-printing inks to improve printing qualities or as a selective membrane over platinum anodes to reduce interferences (McGovern *et al.* 2005:659; Hart *et al.* 1999:7).

1.6   Pesticides

The Environmental Protection Agency (EPA) of the USA defines a pesticide as follows:

> *"A pesticide is any substance or mixture of substances*
>
> *intended for preventing, destroying, repelling, or mitigating*
>
> *any pest. Pests can be insects, mice and other animals,*
>
> *unwanted plants (weeds), fungi, or microorganisms like*
>
> *bacteria and viruses. Though often misunderstood to*
>
> *refer only to insecticides, the term pesticide also applies*
>
> *to herbicides, fungicides, and various other substances used*
>
> *to control pests. Under United States law, a pesticide is also*

any substance or mixture of substances intended for use as a

plant regulator, defoliant, or desiccant."

(EPA 2006).

Greenhalgh *et al.* (1980:2563) defines a pesticide as a compound that can be used to effectively control the target organism for a critical period of time during its growth and is then degraded to products that are harmless to humans and other organisms. Ideally that is what is expected from pesticides that they will degrade in as short a time as possible but it is not the case for all pesticides.

Pesticides are used extensively in the agriculture sector for the eradication of unwanted insect and pests, thereby enhancing food production. With this widespread use of pesticides in the public and agricultural domains, severe environmental pollution and potential health hazards have increased including severe acute and chronic cases of human poisonings. The World Health Organisation (WHO) has estimated that the incidence of pesticide poisonings in developing countries has doubled during the past 10 years. Although in 1982 developing countries accounted for only 15% of the worldwide use of pesticides, in these countries over 50% of pesticide poisoning cases occurred due to misuse (Wang *et al.* 2003:255; Abdollahi *et al*. 2004:29; Deo *et al.* 2005:185).

Organophosphate pesticides have been used against a broad spectrum of insects and on food crops, in residential and commercial buildings, on plants and lawns and for mosquito control. Carbamate pesticides have been widely used against insects, fungi and weeds, as well as on agricultural crops and on residential lawns. Since their

has been an increase in the amount of pesticides applied to agricultural commodities, serious concerns have been raised about the increasing risk to human health.

Carbamates form part of the major classes of pesticides synthesized on a large scale worldwide because of its broad biological activity. Due its worldwide use, concerns have been raised about the exposure of people to the pesticide during manufacture and application (Li *et al.* 2004:547). Carbamates and organophosphates are pesticides known to inhibit insect acetylcholinesterase (AChE) activity, but they also strongly interfere with neural transmissions in other organisms, including humans. These pesticides therefore represent a potential hazard for the environment and human health, requiring continuous assessment, and monitoring (Albareda-Sirvent *et al.* 2001:35; Chough *et al.* 2001:4; Del Carlo *et al.* 2004: 651).

1.7   Objectives of the Study

The main objective for the research presented in this dissertation is to expand the current existing knowledge base of both the physical and chemical properties of organic phase amperometric biosensors for the detection of organophosphorous and carbamate pesticides in organic solvents. Secondly, to introduce the novel use of a self-assembled monolayer (SAM) immobilised on a gold electrode for thick-film biosensor configuration and construction.

Motivation

This will be done to obtain information and a complete understanding of the physical and chemical properties of organic phase amperometric biosensors for the detection of organophosphorous and carbamate pesticides in organic solvents. The detection of pesticides in non-aqueous environments has been reported but few publications refer to the use of immobilised AChE biosensors in non-aqueous media. Organophosphorous pesticides are characterised by a low solubility in water and a higher solubility in organic solvents. It is for this fact that the extraction and concentration of pesticides from fruits, vegetables, etc. are carried out in organic solvents. It is known that some enzymes, e.g. glucose oxidase, work well in both water and organic solvents, while other enzymes require a minimum amount of water to retain catalytic activity. To circumvent the problem of hydrophilic solvents stripping the enzymes of essential water of hydration necessary for enzymatic activity, it is recommended that 1-10% water be added to the organic solvent for sufficient hydration of the active site of the enzyme (Klibanov 2003:428; Andreescu *et al.* 2002:173; Wilkins *et al.* 2000:789; Palchetti *et al.* 1997:316; Iwuoha *et al.* 1995:756).

Areas that were considered are:

(a)   To assess critically the use and implementation of the prepared AChE thick-film biosensor to real organophosphate and carbamate pesticide samples in aqueous mixtures of organic solvents of acetone, acetonitrile, ethanol, n-hexane, and diethyl ether.

(b)   Identification of the factors, which could result in the successful and optimum use of the AChE thick-film biosensor to real organophosphate and carbamate pesticide samples.

(c)   To use the information gained during the course of this work, to provide information on whether the AChE thick-film biosensor can be applied to detect real organophosphate and carbamate pesticides in industrial samples.

Approach

Certain key research questions for this study were identified, which includes:

(i)   Preparation of an electrode platform for biosensor construction by employing a self-assembled monolayer (SAM) of the thiol called mercaptobenzothiazole (MBT), coated on a gold (Au) electrode surface.

(ii)   Construction of novel thick film electrodes by employing a self-assembled monolayer (SAM) of the thiol called mercaptobenzothiazole (MBT) as the first layer in the sequential layer-by-layer biosensor construction.

(iii)   The use of the conducting polymer called polyaniline (PANI) or its derivatives as a mediator for enzyme immobilisation in the biosensor construction.

(iv)   The use of acetylcholinesterase (AChE) as enzyme for immobilisation in a polymer matrix of polyaniline (PANI) and its derivatives, e.g. poly(*o*-methoxyaniline) (POMA), or poly(*2,5*-dimethoxyaniline) (PDMA), in the

construction of enzyme electrodes and corresponding biosensors for organophosphate and carbamate pesticide detection.

(v)   Employing the principle of enzyme inhibition for the design of the biosensor.

(vi)   Characterisation of the biosensors by dc and ac voltammetric techniques in phosphate buffer and aqueous mixtures of organic solvents.

(vii)   Determination of organophosphorous and carbamate pesticide residues in appropriate standard samples.

(vii)   Application and characterisation of the constructed AChE biosensor to real samples containing organophosphate and carbamate pesticides.

The specific aims/objectives of this thesis are:

(i)   Coating of a gold (Au) electrode with a mercaptobenzothiazole (MBT) self-assembled monolayer (SAM) followed by characterisation of the Au/MBT electrode. This will be followed by *in situ* electropolymerisation of *o*-methoxyaniline (*o*-anisidine) (OMA) and *2,5*-dimethoxyaniline (DMA) monomers on the Au/MBT SAM electrode, in the presence of a surfactant of poly(*4*-styrene sulphonic acid) (PSSA), in order to aggregate the polymer on the electrode surface. In a different reaction step, *in situ* electropolymerisation of aniline as monomer on the Au/MBT SAM electrode, in the absence of a surfactant will be performed, in order to polymerise the polymer on the electrode surface and to get a polymer that is not too soluble in aqueous solution. The synthesis will be followed by electrochemical characterisation of either polyaniline (PANI), poly(*o*-methoxyaniline) (POMA) or poly(*2,5*-

dimethoxyaniline) (PDMA) polymer films on the Au/MBT SAM electrode, employing cyclic voltammetric measurements, in a 0.1 M phosphate buffer, KCl (pH 7.2) solution and a 0.1 M HCl solution.

(ii)   Construction and characterisation of the Au/MBT/POMA-PSSA/AChE and Au/MBT/PDMA-PSSA/AChE thick-film biosensors with acetylcholine (ACh) as substrate, employing cyclic voltammetry, square wave voltammetry and differential pulse voltammetry as techniques.

(iii)   Application and characterisation of the Au/MBT/POMA-PSSA/AChE and Au/MBT/PDMA-PSSA/AChE biosensors to detect standard organophosphate (e.g. diazinon, chlorpyrifos) and carbamate (e.g. carbofuran and carbaryl) pesticides in 0.1 M phosphate buffer, KCl (pH 7.2) solutions.

(iv)   Construction, characterisation and optimisation of the Au/MBT/PANI/AChE thick film biosensor with poly(vinyl acetate) (PVAc) as the final binder coated on top of the biosensor using acetylthiocholine chloride (ATChCl) as substrate, employing cyclic voltammetry, square wave voltammetry and differential pulse voltammetry as techniques.

(v)   Application and characterisation of the Au/MBT/PANI/AChE/PVAc biosensor to standard organophosphate (e.g. diazinon, chlorpyrifos) and carbamate (e.g. carbofuran and carbaryl) pesticides in a 0.1 M phosphate buffer, KCl (pH 7.2) solution, and aqueous mixtures of organic solvents of acetone, acetonitrile, ethanol, *n*-hexane and diethyl ether.

(vi)   Application and characterisation of the Au/MBT/PANI/AChE/PVAc biosensor to real organophosphate (e.g. diazinon, chlorpyrifos) and carbamate

(e.g. carbofuran and carbaryl) pesticide samples in aqueous mixtures of organic solvents of acetone, acetonitrile, ethanol, *n*-hexane and diethyl ether.

1.8   Layout of the Thesis

The thesis is divided into the following chapters:

Chapter 1   An introduction to the dissertation on *"Mercaptobenzothiazole-on-Gold Biosensor Systems for the determination of organophosphate and carbamate pesticide compounds"* is given and the main aims and objectives, as well as the layout of the dissertation is provided.

Chapter 2   A review of literature surrounding the sciences of biosensors, self-assembling monolayers, conducting polymers, thick-film biosensor configuration, and pesticides is presented.

Chapter 3   The sample preparation and experimental procedures for the preparation of the gold electrode, self-assembling monolayer formation, *in situ* electropolymerisation of the polymers onto the electrodes, and the biosensor construction are presented.

The electrochemical characterisation of the biosensor construction and pesticide detection were done using techniques such as cyclic voltammetry, Osteryoung square wave voltammetry and differential pulse voltammetry techniques.

Chapter 4   The results for the Assembling and Optimisation of Polyaniline-Based

Enzyme Biosensors prepared on gold thiol-modified electrodes are

presented and discussed.

Chapter 5   The   results   for   the   Analysis   and   Application   of   an

Acetylcholinesterase-Poly(o-methoxyaniline)   Biosensor   for   the

Determination of Selected Organophosphate and Carbamate Pesticide

Compounds in 0.1 M Phosphate buffer (pH = 7.2) Saline Solution are

presented and discussed.

Chapter 6   The   results   for   the   Analysis   and   Application   of   an

Acetylcholinesterase-Polyaniline Biosensor for the Determination of a

Series of Organophosphate and Carbamate Pesticide Compounds in

Aqueous Organic Solvent Solutions are presented and discussed.

Chapter 7   Conclusions, Recommendations, and Future Work

Chapter 8   References

CHAPTER 2

Literature Review

2.1   Introduction

Due to ever-increasing environmental pollution a strong demand for environmental monitoring technologies has surfaced. Water can be polluted by toxins (e.g. cyanide, heavy metals or pesticides) and/or eutrophicants (e.g. phosphate or nitrogen compounds). The effect of eutrophicants in water leads to overgrowth of plants and toxic algae, thereby making the water unsuitable for drinking or industrial uses. The monitoring of these contaminants in water has become an extremely important task, considering the impact that polluted water would have on our everyday lives (Karube & Nomura 2000:177; Keane *et al*. 2002:103).

The increasing use of pesticides adds to environmental problems. Pesticides are very toxic compounds and is known to be responsible for many ecological problems and damages to human health. The intensive use of pesticides in agriculture, medicine and industry has significantly contributed to the environmental problems experienced with pesticide application (Pogačnik & Franko 1999:569; Montesinos *et al*. 2001:231; Andreescu *et al.* 2002:169).

Several established techniques exist for pesticide detection, which include high performance liquid chromatography (HPLC), gas chromatography (GC) coupled to mass spectrometry (GC-MS) and other analytical techniques. The rational behind the development of biosensors is not to compete with the aforementioned techniques, but rather to complement them by providing fast and effective detection of pollutants onsite in field analysis (Albareda-Sirvent *et al.* 2001:35; Wilkins *et al.* 2000:786). Sotiropoulou *et al.* (2005a:199) indicate that enzyme-based biosensors have emerged as the most promising technology for direct pesticide monitoring. Mulchandani *et al.* (2001:225) has also concluded that biosensors, which operate on the inhibition of cholinesterases, offer the highest sensitivity.

Environmental pollutants, whether they are readily degradable or recalcitrant, are expected to continue to be widespread in the ecosystem over the next three decades or even longer. In this regard, environmental biosensors represent a significant breakthrough to help with the monitoring of pollutants in contaminated matrices. This is because the sensors have the unique ability to measure the interaction of specific compounds with biological systems through highly sensitive bio-recognition processes (Keane *et al*. 2002:103).

2.2. Sensors

2.2.1 Introduction to Chemical Sensors

A chemical sensor is different from a physical transducer in that it provides the user with information about the chemical nature of its environment. This sensor may consist of:

- a physical transducer (e.g. a thermistor or piezo-electric crystal),

- or reference electrode (e.g. a Ag/AgCl wire) at its core,

- and a chemically selective membrane, film or layer at the sensing tip.

A chemical sensor is defined as:

"a device which furnishes the user with information about its environment; it consists of a physical transducer and a chemically selective layer" (Diamond 1998:2-3).

The composition and form of the chemically selective layer is of crucial importance to the construction and functioning of the sensor, as it also determines the effectiveness of the sensor. It further controls the selectivity, sensitivity, lifetime and response time of the sensor (Diamond 1998:2).

The differentiation between chemical and biosensors is a difficult task, but it is said that a biosensor is different, since it incorporates a biological entity (e.g. enzyme, antibody, etc.) as a fundamental part of the sensing process (Diamond 1998:3).

2.2.2 Introduction to Biosensors

Biosensors are currently used to replace conventional analytical methods of sample analysis, which tend to be complicated, time-consuming, expensive and not suitable for *in situ* monitoring (Kukla *et. al.* 1999:213; Reay *et al.* 1996:450; Evtugyn *et al.* 1998:465; Andreescu *et al.* 2002:169).

Problems have also surfaced with stability and reproducibility in using biosensors, due to the inherent instability of biomaterials used as sensing elements. In this regard several intelligent immobilisation methods that may help to overcome these difficulties have emerged. See section 2.2.5.9.3.

Various biosensors for the detection of insecticides are currently described in literature. Some of these sensors include the following (Andreescu *et al.* 2002:169-170):

I)   Biological sensors based on organophosphate hydrolase, which catalyse the hydrolysis of organophosphorus pesticides with *p*-nitrophenyl substituents into a direct detectable compound called *p*-nitrophenol.

II)   The determination of pesticides based on their inhibitory effect on enzyme activity has also been reported. This involves the decrease of enzyme activity caused by inhibition, which is correlated to the concentration of pesticides in the sample or their metabolites in the sample. Tyrosinase-based or Acetylcholinesterase-based sensors have been developed for the detection of

enzymes inhibitors with a detection limit in the range of micromolar concentrations.

III)   Many of the traditional methods refer to the use of cholinesterases (ChE), acetylcholinesterase (AChE) or butyryl-cholinesterase (BuChE). They are the real biological target of main organophosphorus and carbamate insecticides, representing 40% of the world market of these classes of compounds.

2.2.3 Components of Biosensors

2.2.3.1 Transducer

The physiochemical change of the biologically active material that results from the interaction with the analyte, need to be converted into an electrical output signal by an appropriate transducer. Broadly applicable transducers may be used for this purpose, which indicate general parameters such as reaction enthalpy (thermistor), mass change (piezo-electric crystal), or layer thickness (reflectometry). In the case of potentiometric and amperometric electrodes, a specific output signal is achieved relating the analyte being detected. The potentiometric and amperometric sensors can be used for species such as H^+, OH^-, CO_2, NH_3 or H_2O_2, or with optical methods such as photometry or fluorimetry (Scheller and Schubert 1992:10).

2.2.3.2 Biomaterials: Use of Enzymes

Enzymes play an important role as biomaterials for biosensors and it is this role that is discussed in the following paragraphs. Enzymes are often referred to as biocatalysts since they play an important role in all the biochemical reactions that make up the complexity of living systems. Enzyme-catalyzed reactions exhibit higher reaction rates than uncatalyzed reactions, typically 10^6 to 10^{12} times greater. Furthermore, these reactions can normally occur under relatively mild conditions of temperature and pH. On the other hand, there are also enzymes that can function under extreme conditions of temperature and pH, and it is those properties that are often exploited for commercial and other applications.

Enzymes display a range of specificities, as some enzymes react only with a single molecule (or substrate). This is referred to absolute specificity. This quality can be used as a key factor in the selection of an enzyme for use in a specific sensor. Other enzymes may react with a variety of substrates and in that way can be used in other specific reactions (Diamond 1998:133-134).

In enzymes, substrate recognition depends on shape matching between the enzyme and its specific subtrate as illustrated in Figure 2.1.
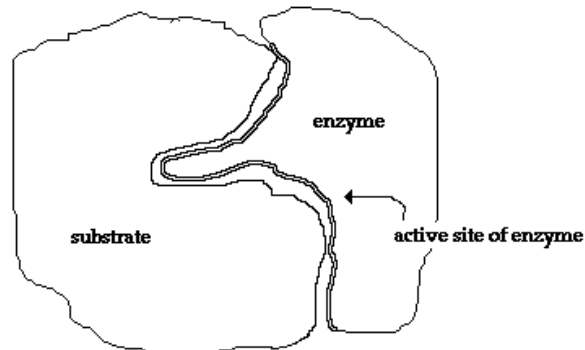
Figure 2.1   **Schematic representation of a substrate binding to an enzyme.**

If any changes in the conformation of the enzyme occur it will interfere with its ability to bind substrate and catalyse reactions. Enzymes are not changed by the catalytic reactions in which they participate and an enzyme molecule can be used repeatedly. The binding site for the substrate to the enzyme is called the active site. Some enzymes may have other binding sites, which are called control sites that can interact with other molecules. These other molecules may improve or interfere with the enzyme's ability to recognize and bind its substrate. Enzymes may also have co-enzymes that will assist in the functioning of a specific enzyme and they serve as hydrogen or electron acceptors (Mathews and Van Holde 1990:351).

2.2.3.2.1 The Kinetics of Enzymatic Catalysis

An enzyme is nothing but a catalyst and consequently it cannot alter the equilibrium of a chemical reaction. This means that an enzyme accelerates the forward and reverse reaction by precisely the same factor. The rate of catalysis, V, varies with the substrate concentration, $[S]$, which is the case for many enzymes. This is shown in Figure 2.2 (Stryer 1975:111; Mathews and Van Holde 1990:358).

Substrate concentration, [S]
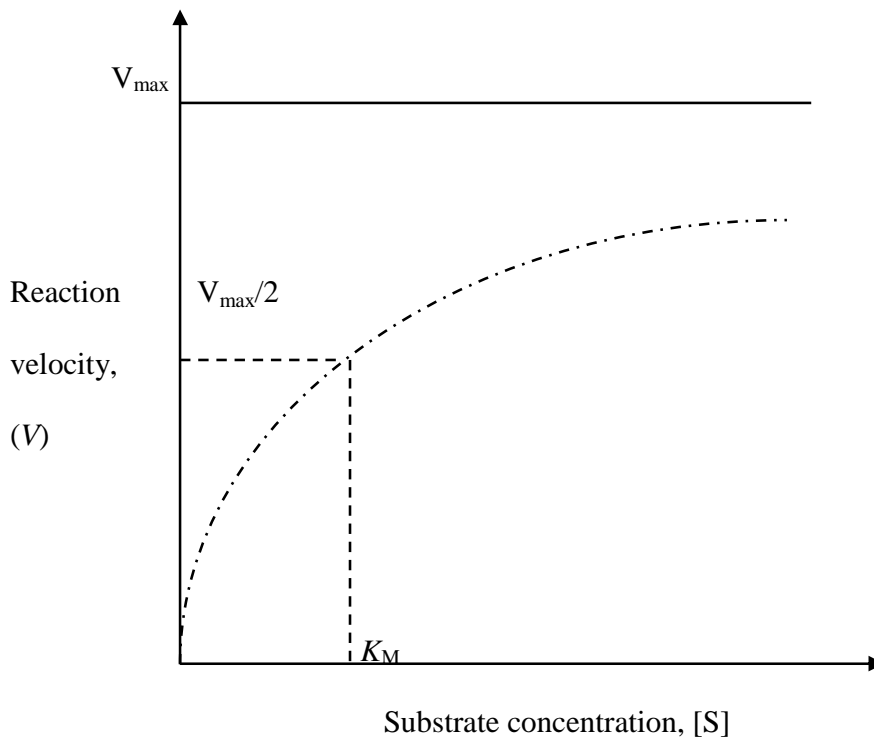
Figure 2.2   **A graph of the reaction velocity, *V*, as a function of the substrate concentration, [S], for an enzyme that obeys Michaelis-Menten kinetics (V_{max} is the maximal velocity and K_M is the Michaelis constant).**

Figure 2.2 indicates that at a fixed concentration of enzyme, *V* is almost linearly proportional to [S] when [S] is small. On the other hand, at high [S], V is nearly independent of [S]. Using the above data, Leonor Michaelis and Maud Menten (Stryer 1975:110; Mathews and Van Holde 1990:358), proposed a simple model to account for these kinetic characteristics. Assuming that a specific ES complex is a necessary intermediate in catalysis, the model proposed for the kinetic properties of many enzymes is:

$$E + S \underset{k_2}{\overset{k_1}{\Longleftrightarrow}} ES \overset{k_3}{\rightarrow} E + P$$

Eqn. 2.1
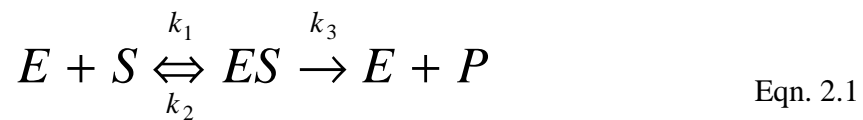
In equation 2.1 an enzyme, E, combines with a substrate S to form an ES complex, with a rate constant k_1. It is also assumed that none of the product reverts to the initial stage (Stryer 1975:111; Mathews and Van Holde 1990:357). What was needed is an expression that relates the rate of catalysis to the concentration of substrate and enzyme and the rates of the individual steps. We may thus express the reaction rate or velocity, defined as the rate of formation of products as:

$$V = k_3[ES]$$

Eqn. 2.2

In equation 2.2 the catalytic rate is equal to the product of the concentration of the ES complex and k_3. When ES is expressed in terms of known quantities, the rates of formation and breakdown of ES can be written as:

Rate of formation of ES $= k_1[ES]$ Eqn. 2.3

Rate of breakdown of ES $= (k_2 + k_3)[ES]$ Eqn. 2.4

The catalytic rate under steady-state conditions should be considered, since in a *steady state*, the concentrations of intermediates stay the same while the concentrations of starting materials and products are changing. This will occur when the rates of formation and breakdown of the ES complex are equal, so that equation 2.3 is equal to equation 2.4, as follows:

$$k_1[E][S] = (k_2 + k_3)[ES]$$

Eqn. 2.5

When equation 2.5 is rearranged, it can be written as (Stryer 1975:111-112; Mathews and Van Holde 1990:359-362):

$$[ES] = \frac{[E] \cdot [S]}{(k_2 + k_3)/k_1}$$

Eqn. 2.6

Equation 2.6 can be simplified by defining a new constant, K_M, called the *Michaelis constant*, so that equation 2.6 then becomes:

$$K_M = \frac{k_2 + k_3}{k_1}$$

Eqn. 2.7

When equation 2.7 is substituted into equation 2.6, it then becomes:

$$[ES] = \frac{[E] \cdot [S]}{K_M}$$

Eqn. 2.8

When the numerator is examined in equation 2.8, it can be deduced that the concentration of uncombined substrate, [S], is very nearly equal to the total substrate concentration. This will only be if the concentration of enzyme is much lower than that of the substrate. Furthermore, the concentration of uncombined enzyme, [E], is equal to the total enzyme concentration, E_T, minus the concentration of the ES complex, as shown in equation 2.9.

$$[E] = [E_T] - [ES]$$

Eqn. 2.9

On substituting equation 2.9 for [E] into equation 2.8, the expression becomes,

$$[ES] = ([E_T] - [ES]) \cdot [S]/K_M \qquad \text{Eqn. 2.10}$$

When equation 2.10 is solved for [ES], it changes to,

$$[ES] = [E_T] \cdot \frac{[S]/K_M}{1 + [S]/K_M} \qquad \text{Eqn. 2.11}$$

that can also be written as:

$$[ES] = [E_T] \cdot \frac{[S]}{[S] + K_M} \qquad \text{Eqn. 2.12}$$

When this expression for [ES] is substituted into equation 2.2, we get

$$V = k_3 \cdot [E_T] \cdot \frac{[S]}{[S] + K_M} \qquad \text{Eqn. 2.13}$$

The *maximal rate*, V_{max}, is obtained when the enzyme sites are saturated with substrate, in which case [S] is much greater than K_M, so that $[S]/([S] + K_M)$

approaches 1. When this happens, equation 2.13 changes to (Stryer 1975:112; Mathews and Van Holde 1990:359):

$$V_{max} = k_3 \cdot [E_T]$$

Eqn. 2.14

Therefore, when equation 2.14 is substituted into equation 2.13, the *Michaelis-Menten equation* is obtained:

$$V = V_{max} \cdot \frac{[S]}{[S] + K_M}$$

Eqn. 2.15

Equation 2.15 accounts for the kinetic data given in Figure 2.2, so that at low substrate concentration, when [S] is much less than K_M, $V = [S] \cdot V_{max} / K_M$. This means that the rate is directly proportional to the substrate concentration. On the other hand, at high substrate concentration when [S] is much greater than K_M, $V = V_{max}$. This indicates that the rate is maximal, and independent of substrate concentration. It can further be deduced from equation 2.15 that when $[S] = K_M$, then $V = V_{max}/2$. This indicates that, K_M is equal to the substrate concentration at which the reaction is half of its maximal value.

Determination of V_{max} and K_M by varying the substrate concentration

If an enzyme operates according to the scheme given in equation 2.1, then the *Michaelis constant*, K_M, and the *maximal rate*, V_{max}, can be readily derived for rates of catalysis at different substrate concentrations. In order to simplify analysis, the *Michaelis-Menten* equation can be transformed into one that gives a straight line plot. When the reciprocal of both sides of equation 2.15 is taken, it gives the following equation (Stryer 1975:113; Mathews and Van Holde 1990:361-362):

$$\frac{1}{V} = \frac{1}{V_{max}} + \frac{K_M}{V_{max}} \cdot \frac{1}{[S]}$$ Eqn. 2.16

From equation 2.16 it is deduced that a plot of 1/V versus 1/[S] will give a straight line with y-intercept equal to $1/V_{max}$ and slope equal to K_M/V_{max}, as shown in Figure 2.3.
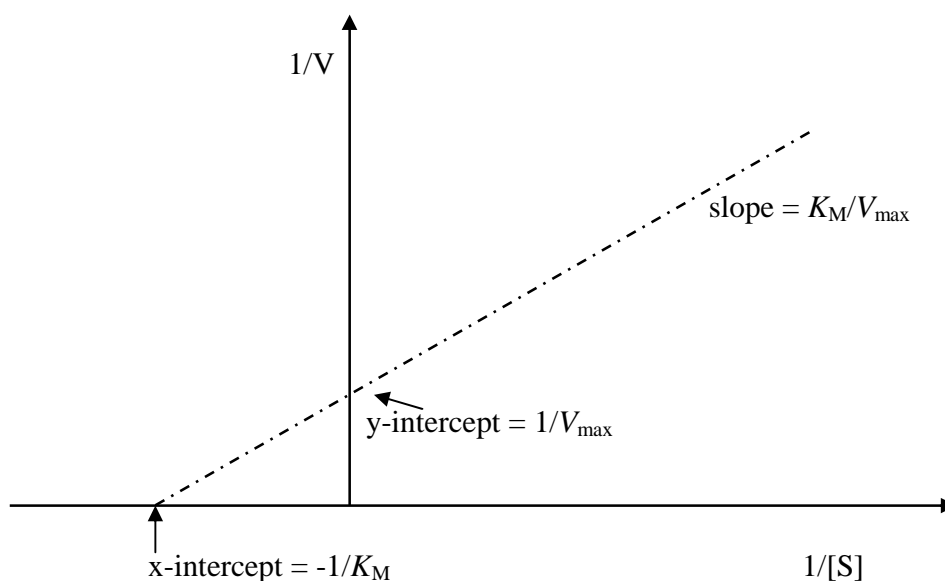
Figure 2.3   A graph of 1/V versus 1/[S]. The slope is K_M/V_{max}, the y-intercept is 1/V_{max}, and the x-intercept is -1/K_M.

The linear graph shown in Figure 2.3 is obtained by using a double reciprocal plot, which is called *the Lineweaver-Burk plot*. A Lineweaver-Burk graph is also an easy way to test whether you have adherence to Michaelis-Menten kinetics and allows easy evaluation of the critical constants shown in equation 2.16 (Mathews and Van Holde 1990:362).

The Lineweaver-Burk plot does have one major disadvantage, in that it requires a long extrapolation to determine K_M, with corresponding uncertainty in the results. To eliminate this disadvantage, alternative ways of plotting the data are sometimes used. If equation 2.15 is rearranged into the form:

$$V = V_{\max} - \frac{K_M \cdot V}{[S]}$$

Eqn. 2.17

and a graph of V versus $V/[S]$ is plotted, it yields what is called an *Eadie-Hofstee plot*, as shown in Figure 2.4 (Mathews and Van Holde 1990:362).
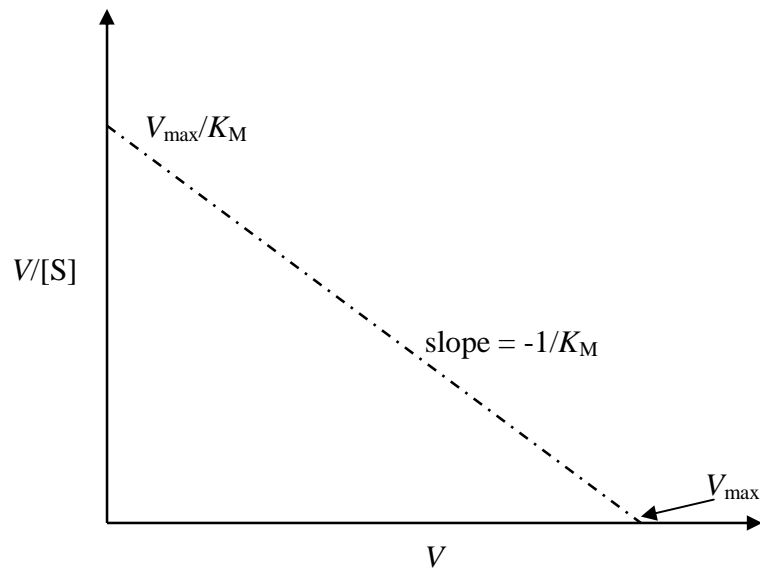
Figure 2.4 **An Eadie-Hofstee plot of V versus $V/[S]$, to obtain $V_{\max}$ at $(V/[S]) = 0$ and K_M from the slope of the line.**

2.2.3.2.2 Types of Enzyme Inhibition

Different types of inhibition can be observed between the enzyme's active site, an inhibitor and a selective substrate for a specific enzyme. As known, a number

of substances can cause a reduction in the rate of an enzyme catalysed reaction such as an inhibitor. This loss of activity caused by an inhibitor can occur either reversibly or irreversibly. If it is reversible, activity may be restored by the removal of the inhibitor, while if it's irreversible the loss of activity is time dependent and cannot be recovered during the timescale of interest during the reaction. When the inhibited enzyme becomes totally inactive, irreversible inhibition behaves as a time-dependant loss of enzyme concentration leading to a lower V_{max} for the reaction. If incomplete inactivation occurs time-dependent changes may be observed in both the *Michaelis constant*, K_M, and the *maximal rate*, V_{max}.

The effect of reversible inhibitors is important for most enzyme-catalysed processes and it can be explained in terms of a simple extension to the Michaelis-Menten reaction scheme.

$$E + S \xleftrightarrow{k_{+1}} ES \xrightarrow{\quad k_{+2} \quad} P$$
$$+I \Updownarrow K_i \qquad\qquad K_i' \Updownarrow +I$$
$$EI \qquad\qquad ESI$$
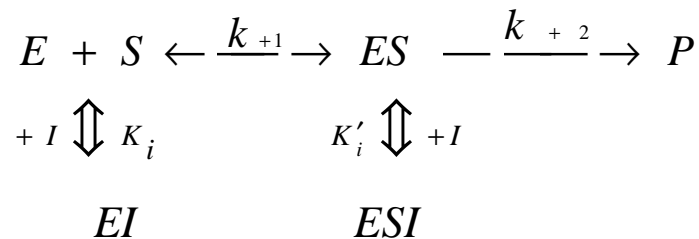
Eqn. 2.18

where the reversible inhibitor is represented by I and the inhibitory (dissociation) constants K_i and K_i' are expressed as

$$K_i = \frac{[E]\cdot[I]}{[EI]}$$

Eqn. 2.19

and,

$$K_i' = \frac{[ES]\cdot[I]}{[ESI]}$$

Eqn. 2.20

If it is assumed that none of EI or ESI is reacting to form product, equilibrium

between EI and ESI is allowed, although it makes no net contribution to the rate

equation as it must be equivalent to the equilibrium established through:

$$EI + S \Leftrightarrow E + S + I \Leftrightarrow ES + I \Leftrightarrow ESI$$

Eqn. 2.21

It should also be noted that inhibitors may change with the pH of the solution and

result in the independent variation of both K_i and K_i' with pH

(http://www.lsbu.ac.uk/biology/enztech/inhibition.html). Some of the types of

inhibition and its enzyme kinetics are explained in the following paragraphs.

(a)   Competitive Inhibitors

This type of inhibitor refers to a compound that bears a close structural and chemical similarity to the substrate of the enzyme, and this similarity causes the inhibitor to bind to the enzyme's active site instead of the substrate. However, it should be noted that the subtrate and inhibitor are not identical and therefore the enzyme will be unable to convert the inhibitor into product and it will just block the active site of the enzyme as illustrated in Figure 2.5. Also, if the substrate binds to the active site before the inhibitor, the inhibitor is incapable of binding to the enzyme (http://orion1.paisley.ac.uk/kinetics/Chapter_3/chapter3_1.html; http://campus.northpark.edu/biology/cell/enzymes.html).
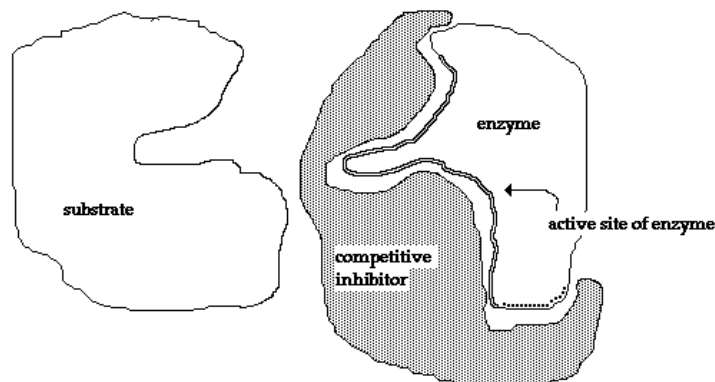
Figure 2.5   Schematic representation of a competitive inhibitor blocking the active site of an enzyme for its substrate.

In terms of enzyme kinetics it is found that for competitive inhibition, K_i' (Eqn. 2.20) is much greater than the total inhibitor concentration and the ESI complex (Eqn. 2.21) is not formed. Since both the substrate and inhibitor compete for binding to the active site of the enzyme, the inhibition is most noticeable at low substrate concentration but can be overcome at sufficiently high substrate concentration as the value of V_{max} remains unaffected. The rate equation can then be expressed as:

$$V = \frac{V_{max} \cdot [S]}{K_m{}^{app} + [S]}$$

Eqn. 2.22

where $K_m{}^{app}$ represents the apparent K_m for the reaction, which can be expressed as:

$$K_m{}^{app} = K_m \left[1 + \frac{[I]}{K_i} \right]$$

Eqn. 2.23

It should be noted that the competitive inhibitor bears some structural similarity to the substrate and is often a reaction product. In this case there is product inhibition that can cause a substantial loss of productivity when high degrees of conversion are required. Using equations 2.22 and 2.23 the rate equation for product inhibition can then be derived as:

$$V = \frac{V_{max} \cdot [S]}{K_m \left[1 + \dfrac{[P]}{K_p} \right] + [S]}$$

Eqn. 2.24

(http://www.lsbu.ac.uk/biology/enztech/inhibition.html).

(b) Non-competitive Inhibitors

A non-competitive inhibitor is able to bind to the control site of an enzyme and partially block the active site or alter the shape of the enzyme completely as shown in Figure 2.6. In some cases the inhibitor(s) may bind so firmly to the enzyme that it is not easily removed and in this case it permanently disrupt the functioning of the enzyme molecule and acts as a poison. In other cases the inhibitor attaches to the enzyme for a brief period only and temporarily blocks the enzyme's activity (http://campus.northpark.edu/biology/cell/enzymes.html).
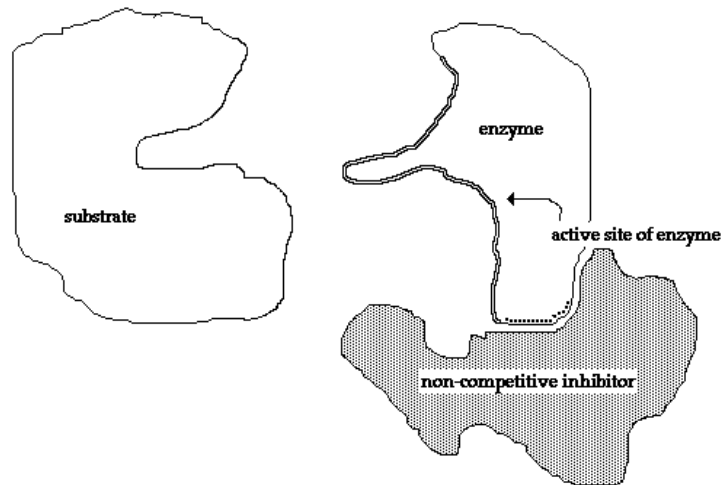
Figure 2.6 **Schematic representation of a non-competitive inhibitor altering the shape of an enzyme.**

In the enzyme kinetics observed for non-competitive inhibition it is observed that K_i (Eqn. 2.19) is now much greater than the total inhibitor concentration and the EI complex (Eqn. 2.21) is not formed. This is the case when the inhibitor binds to a site which only becomes available after the substrate (S_1) in Eqn. 2.25 has bound to the active site of the enzyme. It should be noted that this inhibition is most commonly encountered in multi-substrate reactions where the inhibitor is competitive with respect to one substrate (e.g. S_2) but uncompetitive with respect to another (e.g. S_1). In this case the reaction scheme can be represented by the following equation:

$$E + S_1 \Leftrightarrow ES_1 + S_2 \Leftrightarrow ES_1 S_2 \rightarrow product$$

$$E + S_1 \Leftrightarrow ES_1 + I \Leftrightarrow ES_1 I \neq S \qquad \text{Eqn. 2.25}$$
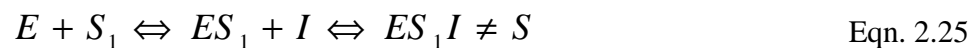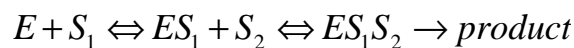
From Eqn. 2.25 it is deduced that the inhibition is most noticeable at high substrate concentrations (S_1) and cannot be overcome as both the values of V_{max} and K_M are equally reduced. The rate equation can then be expressed as:

$$V = \frac{V_m{}^{app} \cdot [S]}{K_m{}^{app} + [S]}$$

Eqn. 2.26

where $V_{max}{}^{app}$ and $K_m{}^{app}$ represents the apparent V_{max} and K_m for the reaction, which can be expressed as:

$$V_{max}^{app} = \frac{V_{max}}{1 + \dfrac{[I]}{K_i'}}$$

Eqn. 2.27

and

$$K_m^{app} = \frac{K_m}{1 + \dfrac{[I]}{K_i'}}$$

Eqn. 2.28

It should be further noted that the specificity constant remains unaffected by the inhibition and normally the uncompetitive inhibitor also bears some structural similarity to one of the substrates, which is often a reaction product (http://www.lsbu.ac.uk/biology/enztech/inhibition.html).

2.2.3.2.3 Various methods for immobilisation of biomolecules

The biomaterial component of a biosensor can be divided into two distinct groups called catalytic and non-catalytic. The catalytic biomaterials includes enzymes, micro-organisms and tissues, while non-catalytic biomaterials includes antibodies, receptors and nucleic acids, etc (Sharma *et al.* 2003:307). When used in sensors the biomaterials of enzymes, multi-enzyme complex, tissues, micro-organisms, organelles, cell receptors, antibodies, nucleic acids or whole cells are responsible for recognition of the analyte. Very minute quantities of the biomaterials are required in biosensor construction but the purity of the biomaterials play a vital role in the reliability of the biosensor (Sharma *et al.* 2003:308). In the construction of a biosensor, there is a need for electrons to pass from the enzyme-based biocomponents to the amplifier or microprocessor. It is for this reason that the reagent layer in a biosensor forms an essential component. The creation of these layers requires the immobilisation of the recognition elements to be used for detection and various methods are available for immobilisation of the biomolecules. However, not all of these methods are appropriate for biosensor manufacturing but the most commonly used immobilisation techniques for designing and development of specific sensors include physical adsorption, entrapment, intermolecular cross-linking and covalent binding as shown in Figure 2.7 (Sharma *et al.* 2003:308).

When the technique of *adsorption* is used, the enzyme is adsorbed onto substrates such as cellulose, silica gel, glass, hydroxyappatite and collagen as illustrated in Figure 2.7 (Sharma *et al.* 2003:308).
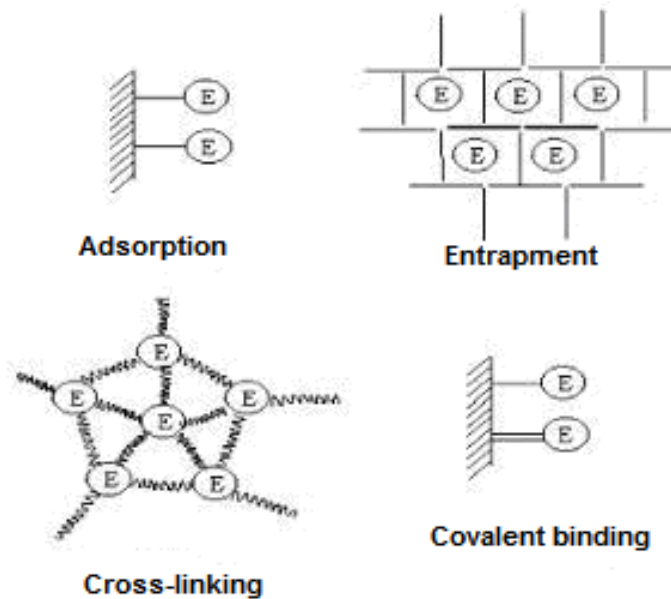
Figure 2.7   Various methods used for enzyme immobilisation (Sharma *et al.* 2003:308)

When *entrapment* is used, a polymeric gel is prepared in a solution that contains the biomolecules that becomes trapped within the gel matrix as shown in Figure 2.7. Matrices that can be used for this technique include polyacramide, starch, nylon and siliastic gel (Sharma *et al.* 2003:308).

In using *cross-linking* as technique, intermolecular cross-linking of biomolecules is done using bi-functional or multi-functional reagents such as

glutaraldehyde,   hexamethylene   di-isocyanate,   1,5-difluoro-2,4-dinitrobenzene, (Sharma *et al.* 2003:308).

With *covalent binding*, a functional group in the enzyme that is not essential for its catalytic activity is used. Normally the nucleophilic functional groups present in amino acid side chains of proteins such as amino, carboxylic, imidazole, thiol, hydroxyl, etc. are used for coupling (Sharma *et al.* 2003:308).

2.2.4 Electrochemical Biosensors

Since electrochemical transduction has become available, the mass production of low-cost, disposable devices using either thick or thin film technologies has been possible. This has made electrochemical sensing systems open to miniaturisation and widespread application (Morrin 2002:20).

One of the most widely-used features in electrochemical biosensor construction, is the method of electronic coupling between the redox enzymes and the transducer itself. Developing new techniques and methods has been the subject of intense research and new methods for shuttling electrons between enzymes and electrodes have been evolving since the 1960s. In the beginning the biosensors was based on the electroactivity of the enzyme substrate or product to deliver the *first generation* biosensors. This was followed by the integration of a redox mediator into the sensor to deliver the *second generation* biosensor, which was able to eliminate matrix interferences. When *third generation* biosensors was developed, the mediator

was removed to provide superior selectivity and to obtain direct electron transfer onto the transducer (Morrin 2002:21).

2.2.4.1 First generation electrochemical biosensors

Biosensors that were based on the Clark model are commonly referred to as the *first generation* biosensors. These biosensors are based on the direct electrochemical detection of substrates or products of an enzymatic reaction. In the original glucose enzyme biosensor, molecular oxygen was used as the oxidising agent. Since oxygen is of low molecular weight, it served as the electron acceptor by shuttling electrons between the enzyme redox site and the electrode surface, as shown below (Morrin 2002:20):

$$\beta\text{-D-glucose} \ + \ O_2 \ \xrightarrow{\textbf{GOx}} \ \text{D-gluconic acid} + H_2O_2 \qquad \text{Eqn. 2.29}$$

The biosensor was constructed by covering a platinum electrode with a polyethylene membrane that is permeable to oxygen. The glucose oxidase was then sandwiched between this membrane and a cellulose acetate membrane, which is permeable to both oxygen and glucose. The oxygen was then reduced using voltammetry and the cell current was directly proportional to the oxygen concentration (Morrin 2002:21):

$$O_2 + e^- \longrightarrow O_2^- \qquad -0.6 \text{ V vs Ag/AgCl} \qquad\qquad \text{Eqn. 2.30}$$
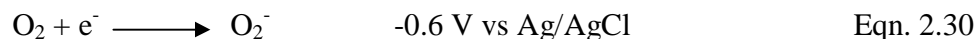
Alternatively, the measurement of hydrogen peroxide can be carried out by applying a positive potential (Morrin 2002:21):

$$H_2O_2 \longrightarrow 2H^+ + 2e^- + O_2 \qquad 0.6 \text{ V vs Ag/AgCl} \qquad\qquad \text{Eqn. 2.31}$$
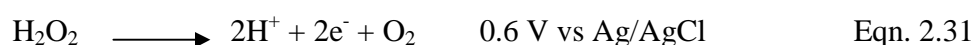
The last approach was then used to develop the first commercially available electrochemical biosensor.

Some limitations were experienced in using oxygen as electron acceptor due to its limited solubility and environmental fluctuation. Since high potentials are required for oxidation, it can cause the measurement of interfering species such as ascorbate. These and other problems experienced drove research into the development of other novel mediated sensors and *second generation* biosensors came into existence (Morrin 2002:21).

2.2.4.2 Second generation electrochemical biosensors

One of the drawbacks of first generation biosensors was the use of a too high potential during operation, which saw the focus shifting to the use of other mediators. New mediators were used consisting of small active molecules that could diffuse in

and react with the active site of the enzyme, followed by diffusing out and reacting with the electrode surface, thereby shuttling electrons between the enzyme and the electrode. The use of ferrocyanide as an alternative redox couple enabled the shuttling of electrons to the electrode surface and eliminated the problems encountered of oxygen and hydrogen peroxide monitoring (Morrin 2002:21-22).

Ferrocene derivatives rank as the most successful mediators been used in *second generation* biosensors (Morrin 2002:21-22). Their success can be attributed to the fact that they react rapidly, exhibit reversible kinetics, have a low oxidising potential and are stable in the reduced and oxidised forms. In Figure 2.8 a cyclic diagram of a ferrocene-mediated biosensor for glucose monitoring is shown.
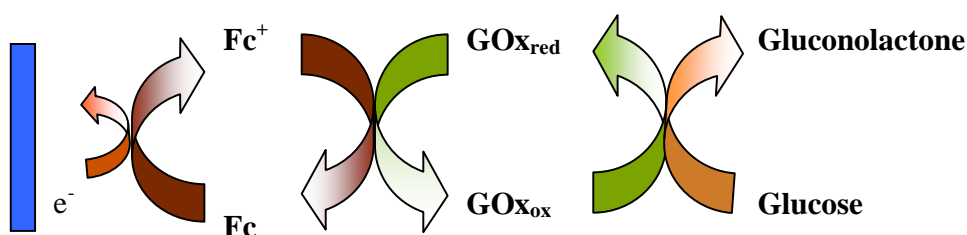
Figure 2.8 **A ferrocene-mediated biosensor for glucose: Glucose is oxidised by GOx. GOx becomes reduced during this process but is immediately reoxidised by the Fc^+ mediator. This mediator, which has become reduced to Fc is reoxidised directly at the electrode surface. The current flowing through the electrode is an amperometric measurement of the glucose concentration (Morrin 2002:22).**

A number of soluble mediators have also been integrated into immunosensors with peroxidase as common enzyme tracer label. Suitable mediators described for this

peroxidase coupled amperometric detection are ferrocene, iodine, hydroquinone and tetrathiafulvalene (Morrin 2002:22).

Second generation biosensors saw further progress been made with the use of flexible polymers onto which mediating functionalities were bound. This paved the way for the use of mediators that were bound and could not diffuse or leach into solution, thereby improving biosensor stability. A good example is ferrocene that has been used as an integral part of a cross-linking polyacrylamide as shown in Figure 2.9. The ferrocene-cross-linked-polyacrylamide is a gel-like material that provides an excellent medium for encapsulation of actives enzymes, while the ferrocene provides a non-diffusional electron-transfer mediator (Morrin 2002:22-23).
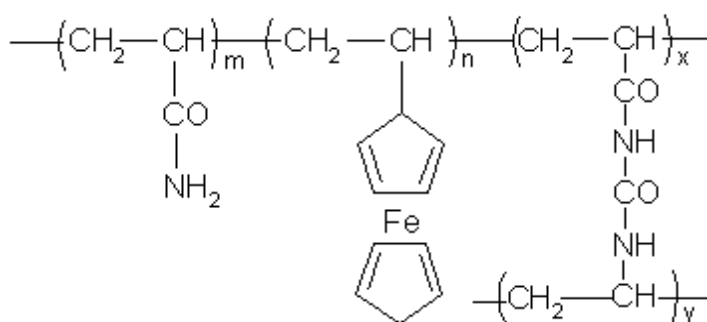
Figure 2.9   A cross-linked polyacrylamide gel containing ferrocene (Morrin 2002:22).

2.2.4.3 Third generation electrochemical biosensors

Trends in research then moved away from soluble mediators towards direct enzyme-electrode coupling in order to produce *reagentless biosensors* that are now known as *third generation* biosensors. In third generation biosensors, non-diffusional mediators (i.e. there is no shuttling of mediator) are used. These biosensors saw a three-way shuttling of the electrons from the enzyme redox centre to the electrode surface, known as non-diffusional type coupling. The latter was achieved by forming a biocomplex with a large redox polymer. These biosensors should operate in a potential window that is close to the redox potential of the enzyme itself, in order to be less prone to interfering reactions as was experienced in second generation biosensors (Morrin 2002:23).

Conducting polymer-based biosensors consisting of immobilised biomolecules in electropolymerised films is gaining high importance, since the discovery of electractive polymers two decades ago. At first these materials were heralded for their high conductivity-to-weight ratio, but later the fascination turned to their unique chemical properties. These polymers can be synthesised under mild conditions and enable a range of biological moieties (e.g. enzymes, antibodies, and whole living cells) that can be incorporated into the polymer structure. Furthermore, the unique electronic properties of conducting polymers, allow direct and interactive communication with the biochemistries incorporated, to produce a range of analytical signals (Morrin 2002:23-24).

The transition metals osmium and ruthenium have been coordinated within polymers to produce examples of new generation biosensors. The electroactivity of these polymers is associated with the reversible redox behaviour of the metal centres. These sensors see the biomolecule being "molecularly wired" onto the sensor surface, with non-diffusionally mediating species bound in long polymer chains. This results in direct electrical communication between the biomolecule and the electrode surface (Morrin 2002:24).

The electronically conducting polymers have perhaps been the most fascinating of the electrofunctional polymers as far as use in analytical devices is concerned. Conducting polymers are capable of functioning as electron transfer mediators and redox changes are not localised at a specific centre but are rather delocalised over a number of conducting polymer groups. Examples of these polymers are polyacetylene, polypyrrole, polyaniline and polythiophene as shown in Figure 2.10 (Morrin 2002:24-25).

Polyacetylene   Polypyrrole

Polyaniline   Polythiophene
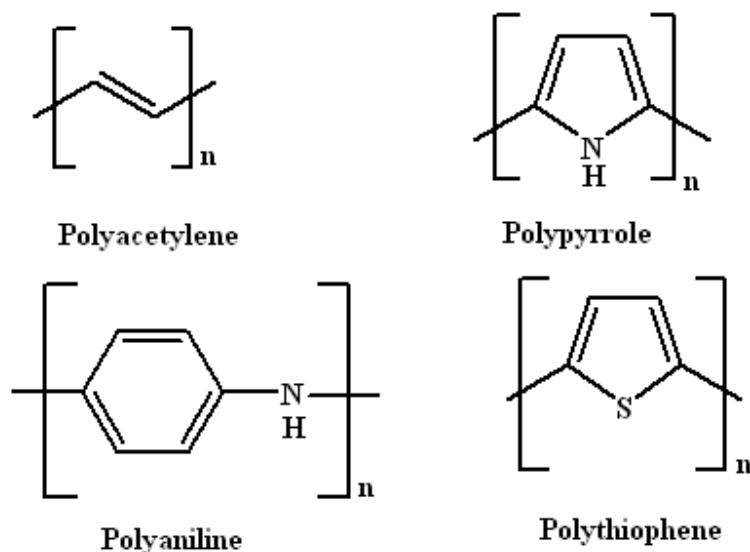
Figure 2.10   Structures of some electronically conducting polymers.

Both electrochemical and chemical oxidative polymerisation techniques can be employed in the synthesis of conducting polymers. Electrochemical synthesis is rapidly becoming the preferred method in application because of its simplicity and increased reproducibility, especially in the case of polyaniline. Electrochemical polymerisation is generally employed by galvanostatic, potentiostatic or potentiodynamic methods. Electrode surfaces commonly used for electrochemical synthesis of conducting polymers include carbon, platinum, gold, indium-tin oxide coated glass and palladium (Morrin 2002:25).

Polyaniline can be grown on the surface of an electrode by either using a potentiostatic or a potentiodynamic technique. In a potentiodynamic fashion, a more homogeneous film is achieved. In a potentiodynamic technique, cyclic voltammetry

has found application in biosensor development using PANI-modified electrodes. PANI has also been doped with polyvinylsulphonate to enhance the morphology and electrical conductivity of the polymer at non-acidic pH, thus rendering it ideal for the application in enzyme electrodes or immunosensors (Iwuoha *et al*. 1997:750-751; Killard *et al*. 1999:110-111; Morrin 2002:26).

2.2.5 Overview of Differentiation in Sensors

To date different types of sensors exist, depending on the method of operation and the field of application. Some of these different sensors will be explained in the following paragraphs.

2.2.5.1 Amperometric sensors

Amperometric biosensors are classified as analytical devices making use of a biological material as a biological catalyst, used in combination with an electrical transducer. The sensor responds to an analyte in a sample and interprets its concentration as an electrical signal via a biological system connected to an electrochemical transducer. The range of biological material used, also referred to as catalysts include enzymes, antibodies, chemoreceptors, cell organelle and cellular tissue (Diamond 1998:119).

With an Amperometric biosensor, the magnitude of response depends on a number of factors, including:

- kinetics of the enzymatic reaction,

- the construction of the enzyme electrode, and

- the mode of operation of the electrode.

The response obtained from the electrode can either be diffusionally or kinetically controlled. When it is kinetically controlled, the enzyme loading is sufficiently low that the response depends on the concentration of enzyme and the kinetics of the enzymatic reaction. There are limitations to this mode of operation as response saturation occurs at low substrate concentration. When the electrode is diffusionally controlled, it possesses very high enzyme loadings such that the current is independent of small changes in enzyme concentration. As a consequence, the current response is then a function of analyte concentration and diffusion (Diamond 1998:119-120).

Several new approaches and different techniques have been investigated in the design and construction of amperometric biosensors. Several of these biosensor designs are listed below.

Nunes *et al.* (1999:37-38) constructed an improved biosensor by lowering its enzymatic charge and thereby lowering the substrate with the purpose of increasing sensitivity and stability. This biosensor used cholinesterase on a chemically modified carbon paste electrode for trace determination of carbamates in fruit, vegetable and water samples.

Tsai and Doong (2005:1796-1800) have constructed an array-based biosensor for the simultaneous analysis of multiple samples in the presence of multiple unrelated analytes. They developed an array-based enzymatic optical biosensor for the simultaneous determination of pH, urea, acetylcholine and heavy metal concentrations.

Quintino *et al.* (2005:215-216) have constructed a new stable glucose sensor using glassy carbon and gold electrodes modified with tetraruthenated Ni-porphyrin by electropolymerisation in alkaline medium. They reported that the sensor presents favourable characteristics for the oxidative catalysis of sugars, very low detection limit, a wide linear response region, high frequency of analysis, simplicity and reproducibility of preparation.

In another study, Chao *et al.* (2005:784-785) have developed an amperometric gas sensor using a three-electrode configuration for the measurement of hydrogen in the atmosphere containing carbon monoxide. In this sensor the working electrode was based on a platinum black electrode that was deposited on a porous Teflon substrate.

Tao *et al.* (2005:332–333) developed an amperometric hydrogen peroxide biosensor using hemoglobin immobilised in a poly(*o*-aminophenol) film at a iron–cobalt hexacyanoferrate-modified gold electrode for H_2O_2 sensing.

Erdem *et al.* (2000:349-350) developed an amperometric horseradish peroxidase-modified carbon paste electrode (HRP-CPE) for the analysis of drugs with oxidisable groups (e.g. acetominophen, epinephrine, pyrogallol, pyrocatechol, resorcinol) in the presence of H_2O_2 in solution.

Wang *et al.* (2003:255-256) developed an amperometric organophosphorus-hydrolase biosensor for flow injection measurements of organophorous compounds. This study illustrated a microfabricated thin film biosensor coupled to a flow-injection operation for fast, sensitive and selective monitoring of organophosphorus compounds.

Deo *et al.* (2005:185-186) developed a carbon nanotube-organophosphorus hydrolase (CNT-OPH) electrochemical biosensor for the amperometric determination of organophosphate pesticides. This sensor employed the ability of the CNT modified electrodes to promote the oxidation of phenolic compounds (including *p*-nitrophenol that is the product of the OPH reaction) and to minimise surface fouling that is associated with the oxidation processes occuring at the electrode surface.

Chough *et al*. (2002:273-274) reports another amperometric organophosphorus hydrolase (OPH) biosensor for the determination of parathion, paraoxon and fenitrothion using OPH immobilised on a nylon net in direct contact with a carbon paste electrode. The study demonstrated that with nylon net a very minimal amount of OPH is required for immobilisation, which is 100 times less as in the case of optical or electrochemical sensor methods.

2.2.5.2 Thermometric indication with thermistors

The same enthalpy change that occurs in chemical reactions is exhibit by enzyme-catalysed reactions. Inasmuch as they increase the reaction rate, they also

enhance the rate of enthalpy change substantially. Therefore thermometric indication is universally applicable in enzyme sensors. Only one reaction step producing sufficient heat is required and no "measurable" reaction product must be formed (Scheller and Schubert 1992:10).

For thermistors, several new approaches and different techniques have also been reported and several of these new approaches are listed below.

Chatterjee and Maiti (2001:294) have developed a positive temperature coefficient (PTC) thermistor that functions with vapour phase diffusion, which could be very useful particularly for thin specimens.

Huang *et al.* (2003:523) have developed a thick-film integrated temperature-humidity sensor and investigated the design, preparation and characteristics of such a design in detail. They further presented the relationship between resistance-temperature characteristics and the composition of the negative temperature coefficient thermistor materials.

In a study by Kimura and Toshima (2003:239), they have developed a new p-n junction temperature-sensor operating on a constant applied voltage, in which the temperature-sensitivity of the sensors can be adjusted by the forward bias-voltage of the sensor.

2.2.5.3 Potentiometric sensors

In the functioning of potentiometric sensor, a general operating condition of near-zero current flow is maintained and it measures the difference in potential between the working electrode and the reference electrode. The transducer may be an ion selective electrode (ISE), which is an electrochemical sensor, based on thin films or selective membranes as recognition materials. The output of a potentiometric sensor is a potential difference as a function of time. It should be noted that potentiometry is less sensitive than amperometry with a detection limit usually in the order of millimoles (Hou 2005:17).

Enzyme-based biosensors, also known as enzyme electrodes, may also operate on the principle of potentiometry. In potentiometry, the change in the voltage that accompanies the reaction of the enzyme and a specific target compound, is measured at constant current.

Varamban *et al.* (2005:94) explains that a potentiometric sensor is a galvanic cell in which the sensor electromotive force (emf) is measured and then logaritmically correlated to the concentration of the electroactive species through the Nernst equation.

Several new approaches and different techniques have been reported in the development of potentiometric sensors and some of these approaches are listed below.

In another study by Mashhadizadeh *et al.* (2004:1048), they have developed a novel ion selective membrane potentiometric sensor for the direct determination of

Fe(III) in the presence of Fe(II) ions. They prepared the new PVC membrane using 2-[(2-hydroxy-1-propenyl-buta-1,3-dienylimino)-methyl]-4-p-tolylazo-phenol [HPDTP] as a suitable carrier.

Pijanowska *et al.* (2004:350-351), have developed a flow-through potentiometric sensor for an integrated microdialysis system, which was designed as part of a lab-on-a chip system and consists of a microdialysis probe, a sensor array and a calibration facility.

In another study by Moghimi *et al.* (2004:169), a polymeric membrane sensor for the potentiometric determination of vanadyl (VO^{2+}) ions was developed. In this work new electrodes were prepared by incorporating a new calix[4]arene derivative into a plasticised poly(vinyl chloride) matrix.

Gupta and Agarwal (2005:730-731) have developed polyvinyl chloride (PVC) based membranes containing a metalloporphyrin of 5,10,15,20-tetrakis (*4*-methoxyphenyl) porphyrinatocobalt(II) as electroactive material in a potentiometric sensor for arsenate. They further used dibutyl butyl phosphonate (DBBP), dioctyl phthalate (DOP), *1*-chloronaphthalene (CN), tri-*n*-butyl phosphate (TBP) and tris(*2*-ethylhexyl) phosphate (TEP) as plasticising solvent mediators in the sensor for arsenite determination.

In the work done by Tymecki *et al.* (2004:3-4), screen-printed reference electrodes for potentiometric measurements were developed. This new method entails the fabrication of Ag/AgCl/KCl reference half-cell in planar format, in one fully automated step, using screen-printing technology, without additional chemical or electrochemical steps.

2.2.5.4 Conductometric sensors

In the operation of conductometric biosensors, sensing is based on measuring the time dependence of the change in conductivity as a result of the receptor recognition of its complimentary analyte. The measuring signal reflects the migration of all ions in the biofilm (Hou 2005:17-18).

Several new approaches and different techniques have been reported in the development of conductometric sensors and some of these approaches are listed below.

Sergeyeva *et al.* (1999:105-106) have developed molecularly imprinted polymer membranes that contains artificial recognition sites for atrazine, prepared by photopolymerisation using atrazine as a template, methacrylic acid as a functional monomer and tri(ethylene glycol)-dimethacrylate as cross-linker. Furthermore, oligourethane acrylate was added to the monomer mixture to obtain thin, flexible and mechanically stable membranes.

Chouteau *et al.* (2004:1089-1090) have developed a novel biosensor that is based on the immobilisation of whole cell *Chlorella vulgaris* microalgae as the bioreceptors on interdigitated conductometric electrodes. The biosensor was used for the testing of alkaline phospatase activity (APA) and the detection of cadmium ions in aquatic habitats.

Dable *et al.* (2004:284) have demonstrated in their work the quantitative, multicomponent and multivariate calibration of microhotplate (MHP) conductometric

sensors for binary and tertiary mixtures of light gases in air. To differentiate between analytes in the mixtures analysed, titanium and tin oxides (TiO_2 and SnO_2) were used in four element microsensor arrays with surface-dispersed gold, while the SnO_2 consited of two grain structures.

Barkauskas (1997:1107) investigated and optimised conductometric humidity sensors wherein the sensing film of the devices was prepared from polyvinylalcohol and a graphitised carbon black dispersed phase. The sensing film was further investigated in terms of composition, thermal treatment and design.

In a study by Shvarev *et al.* (2001:500) a potassium-selective conductometric sensor has been constructed using potassium-selective membranes for potentiometric ion-selective electrodes, which were studied in ac-impedance mode. The results have shown that the bulk resistance of the thin membranes of 20-250 μm thickness depends on the composition of the aqueous bathing solution.

2.2.5.5 Opto-electronic sensors

The basic type of opto-electronic sensor combines light-conducting fibres (optic fibres) with techniques such as spectrophotometry, fluorimetry or reflectometry. This enables the sensors to indicate changes of optical parameters such as light absorption, wavelength, or refraction index, occurring in that part of the measuring medium immediately surrounding the fibre. These devices incorporate

either a single or a dual optical fibre bundle for the incident light and for the light beam to be measured (Scheller and Schubert 1992:13).

Several new approaches and different techniques have been reported in the development of opto-electronic sensors and some of these approaches are listed below.

In a study by Di Natale *et al.* (2000:220-221), a porphyrins-based opto-electronic nose for the detection of volatile organic compounds have been developed. The study involved the development of thin films of different metallophorphyrins that was used as sensing materials in the construction of optical sensors for the detection of different volatile organic compounds (VOCs).

In another study by Wolfbeis *et al*. (1998:17), they have developed a sensing scheme that is capable of measuring the ten parameters most important in the analysis of blood gases, electrolytes and enzyme substrates. For this sensor detection is based on the variation in the decay time of the luminescence of a single class of luminophores, namely the ruthenium diimine complexes. Furthermore, the set of luminescence decay time based chemical sensors developed for clinical applications have shown that when it is operated within a limited range of modulation frequencies, the sensors are consistent in terms of spectroscopy and analytical wavelengths.

2.2.5.6 Calorimetric sensors

The automotive industry has seen a growing interest in exhaust constituent sensors because of increasingly stringent emission standards and the regulatory requirement for catalytic converter self-diagniosis. It is for this reason that the calorimetric sensor has been considered for use as an exhaust hydrocarbon sensor. When a calorimetric sensor is used in combination with various diagnostic strategies, it has shown to be able to determine the deterioration of converter catalysts. The principle, on which a calometric sensor operates, is that of a direct proportionality between the heat generated by catalytic exothermic reactions and the concentrations of hydrocarbons in the exhaust. In a calorimetric sensor, a thermocouple measures the temperature rise caused by exothermic reactions as compared to other hydrocarbon sensing techniques, such as mixed potential electrochemical sensors and electromotive force (proton pumping) electrochemical sensors. The calorimetric sensor also offers several advantages for exhaust applications. It has a simple chemistry and a well-understood principle, followed by the device essentially measuring the heating values of hydrocarbon molecules, giving rise to a signal proportional to the total hydrocarbons, thereby providing reliable readings of overall hydrocarbon concentrations from engine to engine and converter to converter. The calorimetric sensor can also be fabricated with a micro-machining technique to improve the output signal and response time, and has proved to be ideally suitable for diesel exhaust applications where the engine is operated in the far lean oxygen region and the exhaust flow rate is fairly constant. Furthermore, the high oxygen

concentration in the diesel exhaust provides an oxidative environment for catalytic combustion, which is needed for the calorimetric sensor (Wu and Micheli 2004:291).

Several new approaches and different techniques have been reported in the development of calorimetric sensors and some of these approaches are listed below.

The specific details of the sensor developed by Wu and Micheli (2004:291), indicates that they have developed a calorimetric sensor that utilises a thermoelectric device, supported on a planar alumina substrate. This sensor operated on a highly selective carbon monoxide (CO) catalyst and a non-selective platinum (Pt) catalyst, and was able to detect either CO or hydrocarbons with high selectivity.

In a study by Casey *et al.* (2003:114), the fabrication, characterisation and gas response of a planar calorimetric combustible gas sensor is reported. This sensor utilises thin film thermoelectric elements and operates at ambient temperatures. The basic principle on which the sensor operates is the catalytic combustion of the analyte gas and the heat that evolves during combustion is subsequently utilised to generate a dc voltage at a semiconductor-inert metal Seebeck junction.

2.2.5.7 Piezoelectric sensors

This type of sensor operates on the principle that the frequency of vibration of an oscillating crystal is decreased by the adsorption of a foreign material on its surface. The crystal can be sensitised by covering it with material binding or reacting with the analyte. Piezoelectric sensors are used for the measurement of ammonia,

nitrous oxide (NO_x), carbon monoxide, hydrocarbons, hydrogen, methane, sulphur dioxide, and certain organophosphate compounds (Scheller and Schubert 1992:18).

Cui *et al*. (2000:94) have shown that by combining quartz crystal microbalance (QCM) devices with interdigitated electrode sensor pairs, with both devices containing conducting poly(pyrrole) coatings, *2*-D odour maps can be constructed. Furthermore, they have constructed a *2*-D map to demonstrate the feasibility of discriminating odourants and mixtures using a lower number of combined sensors with a lower number of different polymer coatings, compared with single property measurement systems.

In the work done by Kim and Nam (1997:495) it was shown that a micro-depth control system that does not require a position sensor but rather uses piezoelectric voltage feedback can be developed. The device operates on the principle of hysteresis, refers to a reference input voltage that is calculated by computer, and then uses the actuator/sensor characteristics of piezoelectric materials.

Sun and Huang (2001:434-435) derived a formula for the modelling of the behaviour of laminated composite beams with an integrated piezoelectric sensor and actuator. The major goal of their work was to develop a set of governing equations for laminated composite beams with piezoelectric laminae using Hamilton's principle by introducing the electric potential function.

The work done by Halámek *et al.* (2005:337-338) reports the development of piezoelectric affinity sensors for cocaine and cholinesterase inhibitors. The functioning of these sensors is based on the formation of affinity complexes between an immobilised cocaine derivative and an anti-cocaine antibody or cholinesterase. To

perform both binding reactions, a compound called benzoylecgonine-1,8-diamino-3,4-dioxaoctane (BZE-DADOO) was immobilised on the surface of the sensor. During the immobilisation step, pre-conjugated BZE-DADOO coupled with 11-mercaptomonoundecanoic acid (MUA) via 2-(5-norbornen-2,3-dicarboximide)-1,1,3,3-tetramethyluronium-tetrafluoroborate (TNTU) allowed the formation of a chemisorbed monolayer on the piezosensor surface.

2.2.5.8 Organic phase enzyme electrodes (OPEEs)

Organic phase enzyme electrodes (OPEEs), also known as organic phase biosensors, have been used for the analysis of compounds such as cholesterol, alcohols, organic peroxides and phenols. These electrodes constitute a new class of biosensor that can be used in cases where the substrate or matrices are insoluble or scarcely soluble in aqueous media, thereby enabling the analysis of these compounds in organic phase media (Campanella *et al*. 2001:235).

Since in OPEEs the enzymes are insoluble in organic solvents, enzyme immobilisation may often be achieved by simply absorbing it onto a solid or gel support. Once the enzyme is absorbed, it is not liable to desorbs from the surface and immobilisation is easily achieved by impregnation of the support medium by an aqueous solution of the enzyme. It has therefore not become necessary for covalent linking or entrapment procedures used in conventional aqueous-based systems.

Moreover, organic solvents may attack the covalent binding of enzymes to the support (Campanella *et al*. 2001:236; Wang and Dong 2000:45).

Particles that are finely divided or macroporous structures with large surface areas may be used to absorb enzymes onto solid surfaces. Applicable materials are therefore alumina, graphite foil, carbon fibre, porous glass beads and porous glass beads (Campanella *et al*. 2001:235).

Another important aspect of immobilised enzymes in organic solvents is the possibility of the support altering the microenvironment in the neighbourhood of the enzyme. Hydrophilic supports, e.g. calcium alginate, are compatible with enzymes and can be used to increase the level of enzyme hydration. The use of highly polar supports may limit the rate of mass transfer of hydrophobic substrates to the enzyme layer. This problem can be solved by using hydrophobic supports, e.g. polyurethanes, but this may limit or reduce the compatibility with hydrophilic enzymes. Another possible solution to the above problem is the use of gels based on photo-polymerizable resins and urethane macromonomers to vary the ratio between hydrophilic and hydrophobic moieties in the monomer molecules (Campanella *et al*. 2001:236).

Other important points concerning OPEES developments are that a number of studies (Campanella *et al*. 2001:238-339; Campanella *et al*. 1998:595-596) have been done on good activities of several enzymes in hydrophobic organic solvents and their possible analytical advantages. Although the above developments have been made, the development and application of enzymatic biosensors in organic solvents is still a comparatively recent innovation. For the task of indirect food moistening monitoring,

various enzymes displaying organic-phase activity have been considered and tyrosinase was selected. The reason for the selection is the fact that tyrosinase has a strong action in non-aqueous media and the low potential detection of its quinone product, which in itself minimizes potential interferences from electroactive constituents of food samples (Campanella *et al*. 2001:239).

Different OPEEs have recently been developed for hydrogen peroxide determination in several polar (e.g. chloroform) and low polar (e.g. toluene) organic solvents, using immobilised catalase as enzyme (Campanella *et al*. 2001:240).

Inhibition OPEEs have also become the focus of recent studies (Campanella *et al*. 2001:243) for example the amperometric determination of the extent to which the catalytic reaction between H_2O_2 and the immobilised peroxidase was inhibited by pesticide compounds, working both in aqueous and organic phases (i.e. toluene, acetonitrile and chloroform).

2.2.5.8.1 Rationale for organic phase biosensors

The main objective and interest for the development of organic phase biosensors, arises from the limitations encountered in the detection of hydrophobic analytes that are only sparingly soluble in water. These hydrophobic analytes and their matrices are readily soluble in organic solvents. Other advantages arising from the use of organic phase biosensors include:

(i)   the elimination of microbial contamination,

(ii)   reduced interference from water-soluble compounds,

(iii)   an extended biosensor linear range,

(iv)   a solvent-induced change in the substrate specificity of the enzyme,

(v)   immobilisation of the enzyme through adsorption onto non-porous surfaces is satisfactory as enzymes are unable to desorb from these surfaces in non-aqueous media,

(vi)   and enhanced thermostability and sensitivity (Konash and Magner 2006:117; Li *et al.* 1998:69-70; Wang *et al.* 1991:2993; Cosnier *et al.* 1998:165; Campanella *et al.* 1999:109).

The activity and specificity of enzymes can be extensively changed due to the effects of organic solvents. This is due to the fact that the specificity of the enzymes depends on non-covalent interactions such as hydrogen bonding, as well as ionic, hydrophobic and van der Waals forces. Therefore, the factors that include the enzyme immobilisation procedure, the means of communication between the transducer and the enzyme (i.e. direct or mediated electron transfer), and the physico-chemical properties of the solvent used, are important since they can have a significant influence on the micro-environment of the biocatalyst (Konash and Magner 2006:117; Klibanov 1989:141; Iwuoha *et al.* 1995:662).

It should also be noted that some drawbacks with the use of organic solvents do exist. These drawbacks include:

(i)   inactivation of the immobilised enzyme molecules due to denaturation by the non-aqueous surroundings,

(ii)   and reduction in the rate of the enzymatic reaction by the organic media (Cosnier *et al.* 1998:165).

In fact, it should be noted that the activity of enzymes in organic media is strongly dependent on their hydration layer, which is essential for their conformational flexibility, thus necessitating the use of water-organic solvent mixtures in some cases (Cosnier *et al.* 1998:165).

Campanella *et al.* (1998:595) did further investigative work into the functioning of enzymes in organic media and looked into a possible correlation between biosensor sensitivity (i.e. enzymatic activity) and indicators, such as the dielectric constant value (DEC), or the log P value of the organic solvent used.

The detection of pesticides is often done in aqueous solutions, but often these compounds are characterised by a low solubility in water and a higher solubility in organic solvents. When solid matrices (e.g. fruit, vegetables, etc.) are prepared for pesticide analysis, extraction and concentration of pesticides from these matrices are commonly carried out in organic solvents. Therefore, the ability of enzymes to work in non-aqueous media is very important. The nature and amount of the organic solvent affects the enzyme's activity, but for some enzymes such as glucose oxidase and tyrosinase, it was found that they function equally well in various organic solvents as in water. However, in all cases the enzyme requires a minimum amount of water to retain its catalytic activity. Cholinesterase (ChE) has shown to be more sensitive towards organic solvents, compared to the previously named enzymes. The influence of organic solvents on free AChE activity has been reported and few publications refer to the detection of pesticides with immobilized AChE in organic

media (Andreescu *et al.* 2002:169-170; Ronzani 1993:3867; Fennouh *et al.* 1997:97-99).

It was earlier stated that the immobilisation procedure is important since it can influence the micro-environment of the biocatalyst. In the case of hydrophilic matrices they are compatible with enzymes and can be used to increase the level of enzyme hydration, although polar supports may limit the rate of mass transfer of hydrophobic substrates to the enzyme layer. In the work done by Konash and Magner (2006:116-117) it was shown that using a polymer such as Eastman AQ, which combines hydrophilic and hydrophobic structural features, the above-stated problem can be solved.

Several new approaches and different techniques have since been reported in the development of organic phase sensors.

Iwuoha *et al.* (1995:661) investigated the effects of polar organic solvents on the activity of tyrosinase that was entrapped in a poly(estersulphonic acid) polymer matrix. They investigated the behaviour of an organic phase phenol sensor in the solvents acetonitrile, acetone and tetrahydrofuran containing 20% v/v water, and found that the enzyme electrode is effective in the three media in the presence of 100 μM phenol.

In another study by Montesino *et al.* (2001:231-232) it was shown that a disposable cholinesterase biosensor assembled on screen-printed electrodes can be manufactured. The biosensor was used to assess the effect of three miscible organic solvents (acetonitrile, ethanol, dimethyl sulfoxide) on the acetylcholinesterase

(AChE) activity and on the inhibitory effect of organophosphorous pesticides on AChE activity.

2.2.5.8.2 Enzyme behaviour in organic solvents

The use of enzymes in organic media (with low or no water content) has been one of the most exciting facets of enzymology in recent times and it has been investigated by several scientists (Gupta and Roy 2004:2575).

Water activity in nearly anhydrous media is very important. Less than a monolayer of water is needed for an enzyme to start showing biological activity, while the addition of more water molecules increases biological activity. It was further showed that the higher the water content on the enzyme, the higher the reaction rate for the enzyme (Gupta and Roy 2004:2575-2576).

Furthermore, the pH is also an important factor since the correct protonation state of the side chains of amino acids residues of the enzyme is important in non-aqueous media as well (Gupta and Roy 2004:2575-2576).

The work by Kröger *et al.* (1998:219-220) indicated that for enzymes operating in organic solvents, a major mechanism of solvent-induced disruption is the disturbance of the enzyme hydration shell and water molecules associated with the active centre of the enzyme. They further indicated that solvents can be classified into three groups, including:

(i)   water-immiscible solvents in which there is no interaction between the enzyme and hydration shell,

(ii)   partially water-miscible solvents, which have the hydration shell removed, but low levels of water in the bulk solution can prevent inhibition,

(iii)   and water-miscible solvents which are mainly the alcohols and when applied pure, they can strip the essential water from the enzyme.

They also indicated that significant free activity was observed for acetylcholinesterase (AChE) when it is dissolved in solvents from the first two categories, while the last category has proved to be destructive for AChE (Kröger *et al.* 1998:219-220).

Iwuoha *et al.* (1995:661) also reports that hydrophilic solvents are understood to strip enzymes of the essential water of hydration needed for enzyme activity. They further indicated that when enzymes are operated in organic media, the hydration level of the active site of the enzyme should be maintained.

In another study done by Chowdary and Prapulla (2003:127) it was reported that the polar nature of ethanol causes inhibition of enzymes, especially in esterification reactions since it strips the hydration layer around the enzyme surface, resulting in low enzyme activity.

In the work done by Klibanov (2003:427), it is clearly stated that in hydrophobic solvents, enzymes have a higher enzymatic activity than in hydrophilic solvents. In the case of hydrophobic solvents a few clusters of water molecules, presumably mainly bound to charged groups on the surface of the enzyme molecules, are available for enzymatic activity. Hydrophilic solvents on the other hand, strip

some of the essential water off the enzyme molecules, thereby lowering the enzyme's catalytic activity. The lowering of enzymatic activity in organic media can be prevented by adding small quantities of water to the solvent. Furthermore, higher catalytic activities for enzymes in organic solvents are also obtained if the enzyme is lyophilised from an aqueous solution of optimum pH for enzyme activity, or if that aqueous solution contains a ligand for the enzyme or a lyoprotectant (Klibanov 2003:427-428).

Since enzymes were able to function in non-aqueous solvents, the optimum biochemical parameters had to be defined for the functioning of the enzymes in non-aqueous solvents. In this regard, new correlations were found between classical indicators such as the log P values of several solvents, as well as new empirical indicators. These empirical indicators included the current variation and the current variation rate, which may be monitored with a biosensor by dipping it directly into an organic solvent. It was also found that neither solvent apolarity nor water immiscibility by itself is essential for optimal enzymatic activity, and that immobilised enzyme preparations can exhibit increased catalytic efficiency of at least one to two orders of magnitude over lyophilized powders in low-water organic reaction systems (Adányi and Váradi 2004:432-433; Sirotkin *et al.* 2000:114).

In the work done by Khmelnitsky *et al.* (1993:73) it was shown that micellar enzymology (i.e. enzymes entrapped in reversed micelles in organic solvents) plays an important part in the studying of the behaviour of enzymes in organic media, since several enzymes retain their catalytic properties upon entrapment in reversed micelles. A common approach to produce enzyme-containing reversed micelles is to

use the so-called injection method. This entails the injection of a small amount of

aqueous stock enzyme solution directly into the surfactant solution in organic solvent.

The next step involves the mechanical shaking or stirring until a clear monophasic

system is formed in which enzyme molecules are incorporated in inner aqueous

cavities of hydrated reversed micelles. It should be noted that the enzymes remain in

a bulk aqueous solution during the time period between the injection and actual

solubilisation of the enzyme.

2.2.5.9 Biosensors for inhibitor determination

Biosensors for the estimation of the content of inhibitors involve a two-step

process, which involves the measurement of:

(i)   the initial response of a biosensor,

(ii)   and its decay after being in contact with the inhibitor solution (Evtugyn *et al.*

        1998:465).

This may result in a biosensor for the measurement of inhibition being too

complicated. It is often the case that the mechanism of the enzyme-inhibitor

interaction is well-known, but the immobilisation of the enzyme and the

heterogeneous kinetics of the enzymatic reaction affect other parameters. These

parameters include the experimental kinetic parameters of inhibition and the optimal

conditions of the determination of inhibitors. It is also found that the analytical

characteristics of inhibitor determination are often far from those obtained with native

enzymes. However, with the high sensitivity of biosensors, new opportunities exist for purposeful modification of the sensitivity and selectivity of the determination of inhibitors (Evtugyn *et al.* 1998:466).

Futhermore, with careful investigation of the substrate-inhibitor system of both the native and immobilised enzyme, it is possible to optimise the measurement procedure and the detection system. This enables the elaboration of the analytical characteristics of the determination of inhibitors and allows control of the dynamic range and detection limits, depending on the particular analytical problem to be solved (Evtugyn *et al.* 1998:466).

The inhibition degree (I %) is used to express the inhibiting effect of the chemicals on the response of the biosensor, after the biosensor was in contact with the sample tested. If the degree of inhibition is not used, the absolute value of the response of a biosensor can be used for the plotting of calibration curves. For irreversible inhibitors, an empirical linear calibration curve can be constructed by plotting the inhibition degree (I %) or biosensor response versus log C_I (with C_I being the inhibitor concentration). In the case of reversible inhibitors, a calibration curve is plotted in linear coordinates of the inhibition degree (I %) versus the inhibitor concentration (C_I). For these constructed graphs, the sensitivity of a biosensor towards an inhibitor can be defined as the slope of the calibration curve (Evtugyn *et al.* 1998:468).

Three steps are involved in determining the inhibiting effect and the inhibitor concentration for inhibitor biosensors. These steps involve:

(i)   the determination of the initial response value of the constructed biosensor,

(ii)   incubating the biosensor in an inhibitor solution (incubation stage),

(iii)   and the repeated determination of the reduced response of the biosensor after

          exposure to the inhibitor (Evtugyn *et al.* 1998:468).

          For the second stage it should be noted that for irreversible inhibitors, only the

inhibitor is present and no substrate, while the the resulting decay of the enzyme

activity and of the response of the biosensor increase with the duration

of the contact (i.e. with the time of incubation). For reversible inhibitors, the working

solution will contain the inhibitor and the substrate, so that the incubation takes place

in the presence of the substrate. After the completion of stage three, the degree of

inhibition can be calculated as well as the relative decrease of the response value of

the biosensor (Evtugyn *et al.* 1998:468).

2.2.5.9.1 Choosing an enzyme for inhibitor determination

          To choose an enzyme for inhibitor determination and to establish how it

affects the enzyme's activity, the mechanism of their toxic effect on living beings

should be considered. Specific enzymes and its common inhibitors include the

following:

(i)   Since the cholinesterase of insects is the target for the commercial

          preparations of organophosphorus and carbamate insectoacaricides, the

          presence of these pesticides may be determined with cholinesterase.

(ii)   The presence of dithiocarbamate fungicides can be determined with biosensors containing aldehyde dehydrogenase, which is considered as a target.

(iii)   It is known that herbicides suppress photosynthetic reactions and the activity of tyrosinase and peroxidase as enzymes.

(iv)   Cyanide ions is known to inhibit the activity of the enzyme called cytochrome oxidase.

(v)   Heavy metals are known to inhibit the activity of catalase (Evtugyn *et al.* 1998:469).

In constructing any of the above biosensors for inhibitor determination, it is important to check on the commercial availability of the enzyme preparations, the stability of the enzyme during storage and application, as well as the convenience of the detection of the enzymatic reaction (Evtugyn *et al.* 1998:469).

Cholinesterase is one of the most popular enzymes used for inhibitor determination, since this enzyme catalyse the hydrolysis of the natural neurotransmitter, acetylcholine, which is commonly found in insects and humans (Evtugyn *et al.* 1998:469).

Native or immobilised cholinesterase can be applied in a biosensor to determine a wide range of pollutants, which include the organophosphorus and carbamate pesticides, heavy metal ions, fluorides, cationic surfactants, and etcetera. Furthermore, cholinesterases obtained from insects are more sensitive to insecticides than those obtained from mammals. On the other hand, the isolation of these enzymes

and their stablisation are considered to be the weak point in their practical application (Evtugyn *et al.* 1998:470-471).

2.2.5.9.2 Kinetics of enzyme-inhibitor interaction

The mechanism of the enzyme-inhibitor determination plays a vital role in establishing the optimal procedure for the measurement of the inhibiting effect of an inhibitor biosensor application. The enzyme-inhibitor interaction encountered for irreversible inhibitors, results in the formation of a covalent bond between the enzyme's active centre and the inhibitor. This interaction means that the decomposition of the enzyme-inhibitor complex results in the destruction of the inhibitor molecule via its hydrolysis, oxidation, etc. This destruction proceeds stepwise as shown in Scheme 2.1 for phosphorylated cholinesterase, which can be accelerated by special reagents (Evtugyn *et al.* 1998:471).

$$E + I \rightleftharpoons E\text{-}I \longrightarrow E\text{-}I' \longrightarrow E$$
$$P_i' \qquad P_i''$$
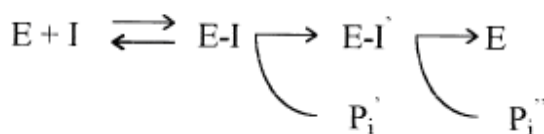
Scheme 2.1 **Reaction scheme of the enzyme-inhibitor complex for a irreversible inhibitor, as for phosphorylated cholinesterase (Evtugyn *et al.* 1998:471).**

In the case of irreversible inhibitors, the following equation can be used for the determination of the inhibitor concentration (C_I), or the bimolecular rate constant (k_{II}) of the enzyme-inhibitor interaction as shown in equation 2.32 (Evtugyn *et al.* 1998:472):

$$\ln(\upsilon_o / \upsilon_t) = k_{II} C_I \tau \qquad \text{Eqn. 2.32}$$

Where τ is the incubation time, υ_0 and υ_t are the initial rates of an enzyme prior to and after the contact of the enzyme with the inhibitor, respectively. Equation 2.32 is valid for a short incubation period ($\tau < 10$–15 min) and when the concentration of the inhibitor is much higher than that of the active centers of the enzyme.

In Scheme 2.2, the influence of a reversible inhibitor (or activator) on the two-step enzyme reaction is presented. In this scheme it is assumed that the inhibitor reacts with the enzyme of enzyme-substrate complex, ES, in a ratio 1:1 (Evtugyn *et al.* 1998:472).

$$E + S \xleftrightarrow{\quad K_s \quad} ES \xrightarrow{\quad k_2 \quad} E + P$$

$$+ I \Updownarrow K_I \qquad\qquad + I \Updownarrow \alpha \cdot K_I$$

$$EI + S \xleftrightarrow{\quad \alpha \cdot K_s \quad} EIS \xrightarrow{\quad \beta \cdot k_2 \quad} EI + P$$
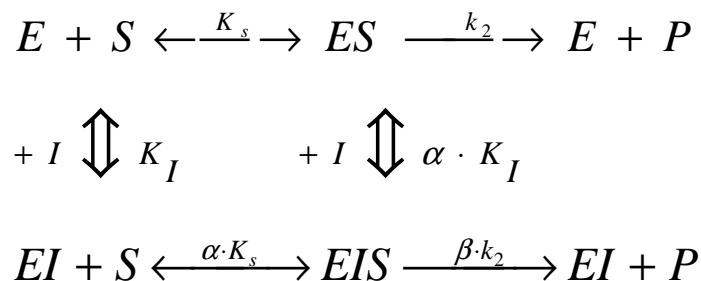
Scheme 2.2   **Reaction scheme of the enzyme-inhibitor complex for a reversible inhibitor (Evtugyn *et al.* 1998:472).**

2.2.5.9.3 Enzyme immobilsation and the role of surface factors

A very important part in the development of a biosensor is the immobilisation of the enzyme. If an immobilised enzyme can be used in multiple applications, it reduces the cost of measurement. Furthermore, an immobilised enzyme is more stable towards extreme working conditions, such as high temperature, and it can be easily combined with an appropriate sensor in the biosensor assembly (Evtugyn *et al.* 1998:473).

The economic advantages are not so compelling for inhibitor determination, since inhibition implies that the enzyme activity decays and a limited number of consecutive measurements with the same batch of immobilised enzyme can be performed. However, certain conditions in the operating of the inhibitor biosensor can be optimised to obtain maximum response (Evtugyn *et al.* 1998:473-474).

The content of the membrane influences the analytical characteristics of the determination of an inhibitor, which is more pronounced for thick membranes with a high activity of the enzymes, such as for a gelatine membrane. In the case of thin enzyme films, which are formed directly on the electrode surface, the diffusion limitation is not as high. Furthermore, the results obtained are much more affected by the nature of the enzyme and by the specific enzyme's activity. To this extent it was found that with a pH-sensitive field effect transistor (FET) covered with an ultra-thin layer of cholinesterase and a potentiometric biosensor with a replaceable membrane, the detection limits of organophosphorus pesticides are similar to each other for each sensor respectively (Evtugyn *et al.* 1998:475).

In the case of biosensors that are based on potentiometric pH sensitive ion-selective electrodes or field effect transistors (FETs), the consideration of kinetic limitations should be extended to the acid formed in the enzyme reaction. A pH shift of 1 – 1.5 units in a weak buffer medium can be observed in a membrane body. This will cause changes in both the activity of an enzyme and in the kinetic parameters of inhibition, which are also pH sensitive. Another important factor is the pH value of the working solution, which is commonly selected close to the pH maximum of the enzyme activity observed for a native enzyme. If there is a pH shift in the membrane body, it results in an additional decrease in the sensitivity of an immobilised enzyme to the inhibitor, when compared to that of a native enzyme in similar working conditions (Evtugyn *et al.* 1998:475).

For amperometric biosensors, the response of the sensor to various inhibitors is often considered to be a linear function of the enzyme's activity. Calculations of

the kinetic parameters based on this assumption are in good agreement with the results obtained with traditional measurements of the specific activity of the immobilised enzyme (Evtugyn *et al.* 1998:475-476).

2.2.5.9.4 pH of the working solution

The pH value of the working solution is usually regarded as the most important factor in determining the performance of a biosensor and its sensitivity towards inhibitors. It is thus a rule that the pH maximum of the enzyme activity is evaluated as most appropriate for the substrate and inhibitor determination. And there is agreement that the pH-dependence of the observed inhibiting effect often corresponds to that of the response of a biosensor. Thus when enzyme sensors utilising various esterases are constructed, they are most sensitive to organophosphates at the pH 8 – 9 when the response of the biosensor is maximal (Evtugyn *et al.* 1998:475-476).

In the presence of multicharged ions, the inhibiting effect on the enzyme cholinesterase is preceded by their partial hydrolysis and the formation of the hydroxyl ions, $MeOH^+$. It therefore indicated that the pH maximum of inhibition depends on the appropriate equilibrium constants of hydrolysis (Evtugyn *et al.* 1998:478).

The importance of the pH value of the working solution has been noted, but the actual pH shift in a membrane body during the formation of the response of a

biosensor, is determined by the nature of the buffer solution. The effect caused by the use of a specific buffer on the inhibition degree obtained, can result from the change of the capacity of the buffer or the ion strength. For example, the use of borate buffer for cholinesterase, demonstrate a weak inhibiting effect of the enzyme. Furthermore, the concentration of the supporting electrolyte is not as important for biosensor response, as the pH value of the working solution (Evtugyn *et al.* 1998:478).

It should be noted that there can be a shift of the pH value from the optimum for the enzyme-substrate or enzyme-inhibitor interaction, to meet the needs of accurately detecting the enzyme reaction or the stability of the sensor. Since electrodes based on the composition of epoxy resin and carbon is unstable in basic media, the pH can be adjusted when this composition containing cholinesterase is used for inhibitor determination, and all measurements can be performed at pH = 7.0 (Evtugyn *et al.* 1998:478).

In the case of irreversible inhibitors, the incubation procedure is performed before the substrate is added to test the inhibitor effect, following the initial testing of the biosensor with the same substrate. The conditions of the initial response of the biosensor, followed by the conditions of inhibition and of the following determination of the reduced response after inhibition, can differ and there are some limitations that should be avoided. If a cholinesterase biosensor is incubated in a non-buffered media at pH = 7 – 7.5, followed by determination of the response in standard conditions for this enzyme (e.g. phosphate buffer at pH 8.0), it will be possible to detect both heavy metal ions and organophosphorus pesticides. If incubation is done in a phosphate buffer at pH 8.0 under the same conditions of response measurement,

it will result in the selective determination of organophosphates in the presence of heavy metal ions. For the determination of organophosphates, incubation can be conducted immediately in organic solvents that were used for extraction of the pesticides. The biosensor is then washed to eliminate the interfering influence of the organic solvent on the response of the biosensor in standard buffer solution (Evtugyn *et al.* 1998:478).

2.2.5.9.5 Measurements in organic media

The measurement of a biosensor's response in non-aqueous media has become a very attractive prospect and the employing of enzymes in organic media allows an increase in the solubility of non-polar substrates and or inhibitors. It further allows shifting of the sensitivity of the enzymes towards various substrates and effectors (Evtugyn *et al.* 1998:479).

It is a known fact that only a few enzymes retain their activity when the content of water does not exceed a certain percentage. Two enzyme- based biosensors, e.g. tyrosinase and peroxidase, have been widely investigated for the determination of various substrates and inhibitors in organic solvents, containing various amounts of water, acetonitrile, alcohols, 1,4-dioxane, acetone, chloroform, etc. Biosensors for measurements in organic solvents are subjected to more stringent requirements for immobilisation of the enzyme. The appropriate carrier used for the immobilisation of the enzyme, should neither dissolve nor swell in organic media and

the immobilised enzyme must retain its activity in the biosensor working conditions. Several materials (e.g. polymers, membranes, etc.) have been used for enzyme immobilisation (Evtugyn *et al.* 1998:479).

In biosensors, enzymes use the presence of a water phase for the establishing of electric conductivity that is necessary for electrochemical measurements. When non-polar solvents are used, a two-phase solution result with the addition of water or buffer, which can also be used since the organic phase forms reversed micelles. These micelles will contain a low amount of aqueous buffer solution that will maintain the enzyme activity and the electric conductivity (Evtugyn *et al.* 1998:479).

It was found that most enzymes reduce their activity in the presence of water-miscible solvents. The use of these solvents follows the same goals as for the use of organic media in measurements. That is the increase of solubility of the inhibitors to be determined and the possibility of direct analysis of extracts taken directly from plants or soil, without having to evaporate the extracting agent, etc. It should be noted that the maximum amount of solvent to be used in the working solution depends on the nature of the enzyme and the membrane material (Evtugyn *et al.* 1998:479).

In order to overcome the limitations of organic solvents, i.e. resulting in insufficient electric conductivity and low enzyme stability, the biosensor incubation can be performed in organic media and the response measurement after incubation in aqueous standard or buffer solution. To do this, a 30 minute incubation time is suggested for pure alkanes (C_6 – C_{12}), benzene, butyl acetate, ethyl ether and acetonitrile since it does not significantly alter the activity of acetylcholinesterase. On the other hand, solvents such as alcohols, dimethyl sulphoxide and chloroform

diminish the activity of the enzyme by 50 – 100%. The parameter log P was used to characterise the influence of the solvent on the activity of the enzyme. Log P is defined as the logarithm of the partition coefficient in a standard octanol-water two-phase system, with $P = (C_{solvent})_{octanol}/(C_{solvent})_{water}$. The highest enzyme activities (as high as 120% for free enzyme and up to 115% for immobilised cholinesterase) were obtained after the incubation in hydrophobic solvents, with log $P > 4$ for free and 2 for immobilised enzyme (Evtugyn *et al.* 1998:479).

The role the organic solvent plays in the inhibition effect is unclear. In the case of reversible inhibitors it may depend on the hydrophilic/hydrophobic properties of the substrate and inhibitor. While for irreversible inhibitors, the influence of the organic solvent on the inhibiting effect is considered to be lower than in the case of reversible inhibitors (Evtugyn *et al.* 1998:480).

2.2.5.9.6 Using enzyme effectors

This involves the incorporation of stabilisers and effectors of the enzyme in the working solution during the biosensor assembly. This area is most promising but has been less investigated as one of the key directions for progress in the development of biosensors for the determination of inhibitors. As an example, the detection limits of mercury (II) that inhibits peroxidase from horse serum, can decrease by a factor of 100, if the enzyme is first incubated in a diluted solution of thiourea. Moreover, this treatment of the biosensor prevents the interfering effect of other heavy metals with the biosensor response, and with the choice of appropriate

substrates this approach resulted in the development of highly selective methods of mercury determination with low detection limits (Evtugyn *et al.* 1998:480).

Another example consists of the activating effect of calcium ions and some other doubly charged cations on the response of amperometric biosensors, with butyrylcholinesterase immobilised in cellulose dinitrate and its sensitivity towards irreversible inhibitors. The sensitizing effect can be observed within narrow limits of experimental conditions of a pH between 9 and 10 and with low concentrations of the supporting electrolyte (Evtugyn *et al.* 1998:480).

2.2.5.9.7 Future prospects of biosensors for inhibitor determination

It may seem that the practical application of inhibitor biosensors are currently much more complicated than that of substrate biosensors, but the potentialities of the former type of biosensors are far from being exhausted. This is especially the case in the application of biosensors for environmental monitoring. Unlike the use of conventional techniques and analytical equipment that is sometimes costly and cumbersome in transporting field samples to the lab, inhibitor biosensors make the direct detection (without pre-concentration or sample treatment) of dangerous pollutants on-site and in the field possible. The detection limits achieved in the application of most inhibitor biosensors, refer to the maximum permissible levels of pollution in environmental samples. The ease of operation, simple response measurement as well as user-friendly design, make these types of biosensors very

attractive for the preliminary estimation of pollutant levels in field conditions. The use of inhibitor biosensors does not come without some limitations or problems, which include:

(i)   the selectivity of response,

(ii)   the calibration of biosensors in multi-component media,

(iii)   the influence of natural enzyme effectors,

(iv)   and the directional regulation for biosensor performance depending on particular analytical problems (Evtugyn *et al.* 1998:481).

Recent research calls for modes that provide further improvement of biosensors based on well-known enzymes (i.e. cholinesterase, peroxidase, tyrosinase, etc.) applied to the development of novel sensors-transducers for the better provision of operating conditions (e.g. response time, lifetime of enzymatic membrane, etc.). The sensitivity of the sensors can be improved by the optimisation of the working conditions that may include the incorporation of enzyme activators into the membrane or electrode material, as well as in the working solution (Evtugyn *et al.* 1998:482).

2.2.5.10   Thick film biosensors

2.2.5.10.1   Introduction

Recent years have seen increasing interest in the application of simple, rapid, inexpensive and disposable biosensors for use in the fields of clinical, environmental

or industrial analysis. To produce disposable biosensors thick-film technology is generally considered. In thick-film technology biosensor configuration, one normally sees layers of special inks or pastes that are deposited sequentially onto an insulating support or substrate (Albareda-Sirvent *et al.* 2000:153).

Different thick-film biosensor configurations have been proposed and designed. All these planar configurations can be classified into three groups (Albareda-Sirvent *et al.* 2000:153):

(i)   multi-layer deposition with biological material deposition by hand or electrochemically,

(ii)   screen-printing of composite inks or pastes using two steps with biological material deposition by screen printing,

(iii)   one-step deposition layer using a biocomposite ink or paste.

The thick-film technique comprises of a specific method of film deposition namely screen printing, which is one of the oldest forms of graphic art reproduction. The construction and production of sensors and biosensors with the use of thick-film technology is an emerging field. The sensing or active membrane and its adhesion to the transducer layer is the most critical point in the manufacturing of thick-film biosensors (Albareda-Sirvent *et al.* 2000:153).

The different layers in a thick-film biosensor configuration can be classified as follows:

(i)   a conducting pad consisting of carbon ink or paste,

(ii)   the free enzyme or mixed with an entrapment agent or cross-linker and a stabiliser or additive is applied in one or more layers,

(iii)   outer selector layer (used in some applications) like cellulose or Nafion is applied with the aim of avoiding any interferences,

(iv)   the mediators, stabilisers and additives, depending on the application of the device, can be included in any of the ink or paste layers (Albareda-Sirvent *et al.* 2000:153-154).

2.2.5.10.2   **Examples of thick-film biosensors**

Several different approaches and techniques have been reported in the development of thick-film biosensors and some of these approaches are listed below.

In the work done by Palchetti *et al.* (l997:315) it is reported that a choline amperometric biosensor based on screen-printed electrodes was constructed to assess the inhibitory effect of organophosphorous and carbamate pesticides on acetylcholinesterase activity in both standard solutions and real samples. In the construction of the sensor a layer of silver ink was printed on polyester film, followed by a carbon pad positioned over the silver track, and a final insulating layer to avoid contact between the carbon pad and the analyte solution. Graphite-based ink manually mixed with ruthenium-activated carbon was prepared to use in the working electrode and after printing the sheets were heated at 110 ºC for 10 minutes. Choline oxidase was immobilised on the surface of the working electrode by adsorption to obtain the choline sensor.

Martorell *et al.* (1997:305) reported the construction of a multilayer amperometric biosensor for the determination of organophosphorous and carbamate pestcides. The biosensor consisted of a robust, machinable biocomposites containing graphite powder, a non-conducting epoxy resin, the electronic mediator 7,7,8,8-tetracyanoquinodimethane (TCNQ) and the enzyme acetylcholinesterase (AChE) or butyrylcholinesterase (BChE) immobilised on aminated silica particles. The results obtained indicated that the covalent immobilisation of the enzyme to aminated silica standardised the construction of biosensors independently of the enzyme origin or type. This provides a convenient method of construction especially for enzymes that leak easily from the surface of the biosensor.

Shen and Liu (2007:417) constructed a biosensor to detect cholesterol in solution through the enzymatic generation of hydrogen peroxide. They have chosen gold as the working electrode in the fabrication of a thick-film screen-printed cholesterol biosensor. The biosensor consisted of a thiol of *3*-mercaptopropionic acid (MPA), which was self-assembled onto the gold-working electrode forming a thin organic layer that served as the anchor for the enzyme immobilisation. Next a *1*-ethyl-*3*(*3*-dimethylamino propyl)carbodiimide methiodide (EDC) was used to immobilise the enzyme choline oxidase (ChOx) covalently on the gold working electrode through the carbodiimide coupling between the carboxyl (–COOH) groups of the self-assembled MPA layer and the amino (–NH$_2$) groups of the enzyme.

In the work done by Erlenkötter *et al.* (2000:82) screen-printed three-electrode sensors were constructed that consisted of a platinum working electrode, a carbon counter electrode and a pseudo Ag/AgCl reference electrode developed from

polymer thick-film inks. The amperometric transducers that were constructed allowed multi-analyte biosensors analysis for use in both batch and flow through systems. The results obtained indicated that the biosensors proved to be reproducible and well suited for the determination of hydrogen peroxide on using the oxidases as biocomponent. Furthermore, the biosensor construction employed a combination of two pre-treatment steps, an additional heat curing and an electrochemical pre-conditioning step that proved to be most helpful to reduce background current and settling time of the biosensors.

Ricci *et al.* (2003:165) reports the construction of a thick-film screen-printed sensor containing Prussian Blue (PB) as catalyst for the improved amperometric determination of H_2O_2. The sensor was constructed by the immobilisation of a single enzyme (glucose oxidase (GOD) or choline oxidase (ChOX)) or of two enzymes, acetylcholinesterase (AChE) co-immobilised with ChOX, on the surface of PB-modified screen-printed electrodes (SPEs) using glutaraldehyde and Nafion as binders. The choline biosensors showed reasonable detection limits, a high selectivity and a competitive long term stability, while similar results were obtained with the acetylcholinesterase biosensors.

The work done by Cagnini *et al.* (1995:85) describes the development of choline biosensor based on ruthenized-carbon screen-printed electrodes and its use for the monitoring of organophosphorus and carbamate pesticides. A 0.5% ruthenium mixed with activated carbon was used in the graphite-based ink for the working electrode surface, which increased the sensor's sensitivity towards hydrogen peroxide. The former electrode construction was used to construct the choline

biosensor with the choline oxidase immobilised by adsorption. This biosensor was then used to detect the inhibitory effect of organophosphorous and carbamate pesticides on acetylcholinesterase, and the procedure was optimised for the parameters of pH, buffer composition, incubation time and substrate concentration.

In the study by Hart *et al.* (1997:645) they have constructed screen-printed electrodes containing a layer of cobalt phthalocyanine, mixed with graphite ink and a layer of acetyl- or butyryl cholinesterase. The constructed sensors showed enzyme inhibition by standard solutions of organophosphates and the cholinesterase activity was inhibited by paraoxon and dichlorvos concentrations. Malathion only caused an inhibition of current generated by the electrodes that contained acetylcholinesterase as enzyme. The use of malathion also required a period of pre-incubation in the pesticide solution before addition of enzyme substrate was done. The results further showed that the addition of diluted commercial formulations of some organophosphate pesticides caused a rapid inhibition of the electrode function.

The work done by Wang *et al.* (1996:1903) describes the construction of a disposable amperometric inhibition biosensor that has been microfabricated with a screen-printing tyrosinase-containing carbon ink. The substrate used was catechol and the inhibition caused by the addition of various pesticides and herbicides were evaluated. In the construction of the tyrosinase thick-film devices, the enzyme was incorporated within the carbon ink, which is not the case in the construction of esterase-based disposable strips. These tyrosinase thick-film devices do also not require prolonged incubation in the presence of the inhibitor. The sensors were also

applied to untreated river water samples and the results showed good promise for on-site field analysis.

In another study by Hart and Collier (1998:111) screen-printed electrodes containing cholinesterase were constructed. The screen-printed electrodes contained one of three polymers consisting of hydroxyethyl cellulose, a co-polymer of vinyl pyrrolidone and dimethylaminoethyl methacrylate, and polyethyleneimine that served as a matrix for cholinesterase on the electrodes. When constructed the electrodes were exposed to drops of water or pesticide solution that were dried and their activity was assessed after 24 hours. When the enzyme matrix was constructed with hydroxyethyl cellulose, electrode activity was inhibited by water as well as by pesticides. With the use of the co-polymer of vinyl pyrrolidone and dimethylaminoethyl methacrylate, the electrodes showed only significant responses to pesticide. The results further showed that with the use of the co-polymer, the long-term storage stability of electrodes was the highest.

The work of Timur *et al.* (2004:132) reports the construction of thick-film biosensors that contain *Trametes versicolor* (TvL) and *Aspergillus niger* (AnL) laccases and *Agaricus bisporus* tissues (AbT), which were developed for the determination of phenolic compounds. Electrodeposited polyaniline (PANI) was used as the matrix for the immobilisation of the biocomponents in the preparation of the thick-film sensors. Different phenolic substances were evaluated with the sensors and optimum pH, temperature and thermal stabilities of the proposed systems were also detected.

2.2.6 Types of electrodes

2.2.6.1 Potentiometric electrodes

The simplest potentiometric technique is based on the concentration dependence of the potential, E, at reversible redox electrodes according to the Nernst equation:

$$E = E_0 + \frac{RT}{nF} \ln a_s$$

Eqn. 2.33

where, E_0 = standard redox potential

R = gas constant

T = absolute temperature

F = Faraday constant

n = number of exchanged electrons of the substance S

a_s = activity of the substance S.

In *ion selective electrodes* (ISE) the dissociation of groups contained in a sensitive membrane alters the charge density and causes changes of the membrane potential. The activity and the potential are logarithmically related. I order to account

for the influence of disturbing ions, e.g. of a substance P, a selectivity coefficient, $k_{S,P}$ is introduced to give the following equation:

$$E = const + \frac{RT}{Zs} \ln\left(as + k_{S,P}(a_P)^{ZsZp}\right)$$

Eqn. 2.34

where, Z represents the charge of the ion (Scheller and Schubert 1992:19).

The most important and common ion selective electrode making use of a "solid membrane" is the glass electrode for pH measurement. Although these electrodes have an outstanding selectivity for H^+ ions, glass electrodes are seldom used in enzyme electrodes because their sensitivity is affected by the buffer capacity of the measuring solution (Scheller and Schubert 1992: 19).

Other pH-sensing transducers used in biosensors are metal oxide electrodes. Not only the common antimony oxide electrode, but also the palladium oxide and iridium oxide probes have been coupled with immobilised enzymes. These sensors can be miniaturised by using chemical vapour deposition technology. These sensors are also mechanically more stable than glass electrodes. A disadvantage is the fact that the measuring signal of metal oxide electrodes is affected by redox active substances (Scheller and Schubert 1992:20).

2.2.6.2 Amperometric electrodes

Amperometric sensors are based on heterogeneous electron transfer reactions that are both the oxidation and reduction of electro-active substances. Oxygen and hydrogen peroxide (H_2O_2), being the co-substrate and the product of several enzyme reactions, as well as artificial mediators, e.g. ferricyanide, N-methylphenazinium ion (NMP^+), ferrocene and benzoquinone may be determined amperometrically (Scheller and Schubert 1992:24).

If there is an increase in the overvoltage, i.e. the deviation from the redox potential, the rate of the heterogeneous charge transfer process is enhanced so as to cause the rate of the whole process to become controlled by mass transfer. If these conditions exist, the diffusion current, I_d, is proportional to the concentration of the substance to be determined, S_0, giving the following equation:

$$I_d = nAFD_O \frac{S_0}{\delta}$$ Eqn. 2.35

where, δ = thickness of the diffusion layer (being constant at given convection),

Do = diffusion coefficient,

A = electrode surface area,

n = number of exchanged electrons

(Scheller and Schubert 1992:24).

The oxygen electrode is the most widely used amperometric electrode (Scheller and Schubert 1992:25).

2.2.6.3 Conductometric Measurement

Conductometric methods of measurement make use of non-Faradaic currents. It operates on an alternating current of low amplitude and a frequency in the range of 1 kHz. The measurement signal reflects the migration of all ions in the solution. This technique is therefore non-specific and may only be used for samples of identical conductivity. Disturbances encountered by deviating sample conductivity may largely be eliminated by combination of an enzyme-covered electrode pair with a pair of "reference" electrodes covered by the carrier containing no enzyme. Such arrangements may be fabricated by small-scale electronic production technology. An example has been the imprinting of Pt electrodes on ceramic substrates by the screen-printing technique.

In conductometric membrane sensors the two electrodes are separated from the measuring solution by a gas-permeable membrane. The diffusion processes of the measured gases are the same as in gas sensitive ISEs (Scheller and Schubert 1992:34).

2.3 Electrochemical Methods and Techniques

It is assumed for all the techniques discussed in this section that the analyte solution is quiet (i.e. still or unstirred) during the experimental performance, in order to ensure that mass transport by convection is absent. It is also assumed that an excess of ionic electrolyte has been added to the solution in order to ensure that mass transport by migration is also absent. The only form of mass transport remaining that will be considered is diffusion (Monk 2001:132).

2.3.1 Voltammetric Techniques

2.3.1.1.   Cyclic Voltammetry

In voltammetry the word root "voltam-" refers to both potential ("volt-") and current ("am-"). During any voltammetry experiment the potential of an electrode is varied while we simultaneously monitor the induced current (Monk 2001: 132). When cyclic voltammetry is performed, a solid electrode called the working electrode (WE) is employed. During an experiment the potential of the WE is ramped at a scan rate (v), and the resultant trace of current against potential is plotted in what is called a *voltammogram* (Monk 2001:156).

In *cyclic voltammetry* the potential is ramped from an *initial potential* (E_i) and at the end of its linear sweep, the direction of the potential scan is reversed, usually stopping at the initial potential. The potential may commence with further additional cycles. The potential at which the change in direction occurs is also known as the *switch potential* (E_λ). The scan rate between E_i and E_λ is the same as that between E_λ and E_i and the values of the scan rate $v_{forward}$ and $v_{reverse}$ are always written with positive numbers. In Figure 2.11 a voltammogram for a simple solution-phase couple is shown and it is also known as a *cyclic voltammogram* (CV) (Monk 2001:156).
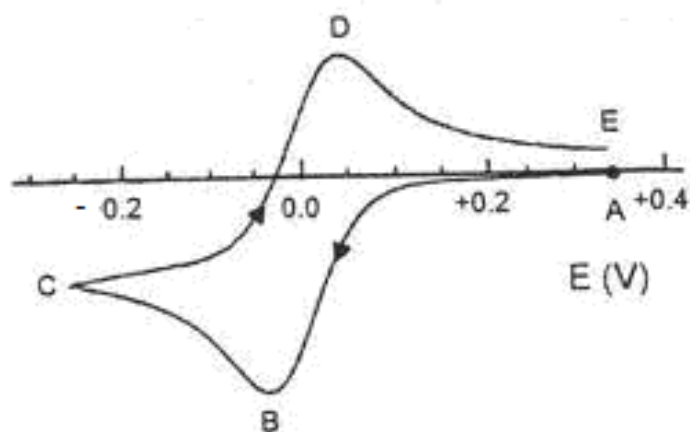
Figure 2.11   **A typical cyclic voltammogram exhibited by a species which undergoes a reversible reduction at $E^{o'} = 0.00$ V, where A represents the initial potential, B the cathodic peak, C the switch potential, D the anodic peak and E final potential (Zanello 2003:51).**

In the CV shown in Figure 2.12, a peak is formed in both the forward and reverse sides of the CV. The peaks look similar in shape and the reaction taking place in the reaction vessel is fully reversible, the magnitudes of the peaks will be identical. Oxidation usually takes place during the forward part of the CV, if scanned from a negative to a positive potential. The reverse part of the CV will then represent reduction taking place, with the potential running from a positive to a negative potential. If the potential is scanned from a negative to a positive value, then reduction would occur during the forward part of the CV scan and oxidation during the reverse CV scan. For a reversible reaction the CV usually has two peaks, one for each of oxidation and reduction taking place. The potential of the peak (E_p) can be identified and for the oxidation reaction taking place, the *anodic peak potential* is denoted as $E_{p,a}$. For the reduction reaction taking place, the *cathodic peak potential* is denoted as $E_{p,c}$. Similarly the current for the anodic reaction (I_p,a) and the cathodic reaction ($I_{p,c}$) can be identified. In voltammetry the magnitude of the current is proportional to concentration. Thus the equality in size between $I_{p(forward)}$ and $I_{p(reverse)}$ implies a quantitative retrieval of electromodified material, which follows from Faraday's laws (Monk 2001:157-159).

In cyclic voltammetry, the position of both the cathodic and anodic peaks gives us thermodynamic information of the redox couple used. The anodic and cathodic peak potentials also enable you to calculate the *formal electrode potential*, $E^{o\prime}$, as follows:

$$E^{\circ\prime} = \frac{E_{p,a} + E_{p,c}}{2}$$

Eqn. 2.36

The formal electrode potential (normally called the formal potential or the formal redox potential) is in concept similar to the standard electrode potential, E^{θ} (Monk 2001:159; Zanello 2003:57).

2.3.1.1.1 Diagnostic Criteria to Identify a Reversible Process

Certain diagnostic tests can be performed for the electrochemical reversibility of a redox couple, when cyclic voltammetry is performed. For a reversible system the following conditions should hold:

- $I_{pc} = I_{pa}$ or $\left| I_{pa} \div I_{pc} \right| = 1$

- The peak potentials ($E_{p,a}$ and $E_{p,c}$) are independent of the scan rate, v

- The formal potential is positioned midway between $E_{p,a}$ and $E_{p,c}$, so that ($E^{\circ\prime} = (E_{p,a} + E_{p,c})/2$

- I_p is proportional to $v^{\frac{1}{2}}$

- The separation between the peak potentials $E_{p,a}$ and $E_{p,c}$ is 59 mV/n for an n-electron couple at 25 °C (Monk 2001:158; Zanello 2003:56).

The value for the separation peak potential, ΔE_p, arises from the following relationship:

$$\Delta E_p = \frac{2.3 \cdot R \cdot T}{n \cdot F} \qquad \text{Eqn. 2.37}$$

which means that for reversible one-electron processes, the peak-to-peak separation assumes different values as a function of the temperature, as indicated in the following table (Zanello 2003:56):

T (°C)	50	25	20	10	0	-10	-20	-50
ΔE_p (mV)	64	59	58	56	54	52	50	44

The peak-to-peak separation, ΔE_p, is an important parameter since it relates to the *electrochemical reversibility* of an electrode reaction, i.e. the rate at which electrons are transferred. When the value of ΔE_p is measured, a departure of 10 – 20 mV from the theoretical value, especially at high scan rates, does not compromise the criterion of reversibility. This is due to the fact that the eventual presence of solution resistance, if not adequately compensated by the electrochemical instrumentation, tends to lay down the forward/reverse peaks system, thereby increasing the relative value of ΔE_p (Zanello 2003:56-57).

The chemical meaning of an electrochemical reversible process suggests that no important structural reorganisation accompanies the redox step. This will also be the case for an electrode process in which the rate of electron transfer is higher than the rate of mass transport (Zanello 2003:57).

When the peak current and potential is determined and the peak of the voltammogram is somewhat broad, it may be difficult to this determine this value. In such a case it is sometimes convenient to report the potential at $I_{p/2}$, called the *half-peak potential*, $E_{p/2}$, which can be determined with the equation (Bard and Faulkner 2001:231):

$$E_{p/2} = E_{\frac{1}{2}} + 1.09\frac{RT}{nF} = E_{\frac{1}{2}} + \frac{28.0}{n}mV \qquad \text{Eqn. 2.38}$$

Where Eqn. 2.38 holds at 25 °C. The value of $E_{\frac{1}{2}}$ is located halfway between E_p and $E_{p/2}$, and a convenient diagnostic for a Nernstian wave results in the following equation (Bard and Faulkner 2001:231):

$$\left|E_p - E_{p/2}\right| = 2.20\frac{RT}{nF} = \frac{56.5}{n}mV \qquad \text{Eqn. 2.39}$$

which also holds at 25 °C.

2.3.1.1.2 The Randles-Sevčik Equation

According to the above equation the magnitude of the peak current, I_p, in a cyclic voltammogram is a function of the temperature (T), bulk concentration

($c_{analyte}$), electrode area (A), the number of electrons transferred (n), the diffusion coefficient (D), and the speed at which the potential is scanned (v), according to the equation in 2.40 (Monk 2001:162):

$$I_p = 0.4463 \cdot n \cdot F \cdot A \cdot \left(\frac{nF}{RT}\right)^{\frac{1}{2}} \cdot D^{\frac{1}{2}} \cdot v^{\frac{1}{2}} \cdot c_{analyte} \qquad \text{Eqn. 2.40}$$

At 25 ℃ the above Eqn. 2.40 changes to (Bard and Faulkner 2001:231; Zanello 2003:54):

$$I_p = 2.69 \cdot 10^5 \cdot n^{3/2} \cdot A \cdot D^{\frac{1}{2}} \cdot c_{analyte} \cdot v^{\frac{1}{2}} \qquad \text{Eqn. 2.41}$$

The Randles-Sevčik equation is obeyed if a plot of peak current (I_p) against analyte concentration ($c_{analyte}$) yields a straight line. It also means that if the electrolyte composition is constant in terms of temperature, solvent, swamping electrolyte, then the Randles-Sevčik equation can be used to the determine the concentration of analyte by the construction of a suitable calibration curve. Furthermore, if Eqn. 2.41 is used in a plot of I_p (y-axis) against $v^{\frac{1}{2}}$ (x-axis), a straight line should also be obtained that passes through the origin with the slope equal to ($2.69 \times 10^5 \times n^{3/2} \times A \times D^{\frac{1}{2}} \times c_{analyte}$) as shown in Figure 2.12 (Monk 2001:164-165).
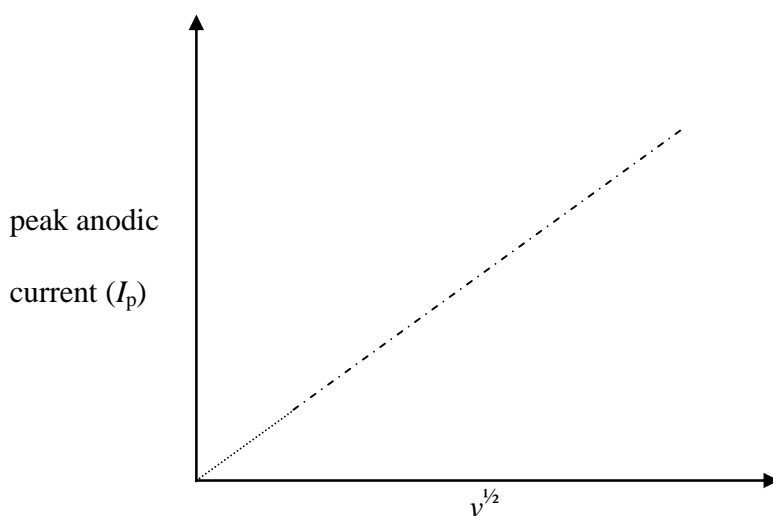
Figure 2.12   A Randles-Sevčik plot of I_p against $v^{1/2}$.

The Randles-Sevčik equation also enables the calculation of the other variables listed in Eqns. 2.40 and 2.41. That is, if the peak current (I_p) at a certain scan rate (v) is measured, knowing the area of the electrode (A), the diffusion coefficient (D) and the concentration (c) of the species under study, one is able to calculate the number of electrons (n) involved in the redox change. Similarly, if the number of electrons (n) is known, one can calculate the diffusion coefficient (D) of the species, and any of the other variables (Zanello 2003:54-55).

2.3.1.1.3 Diagnostic Criteria to Identify an Irreversible Process

The most marked feature of a cyclic voltammogram of a totally irreversible system is the total absence of a reverse peak. A typical cyclic voltammetric profile of an irreversible reduction process is shown in Figure 2.13. Whereas for the reversible case the value of $E_{p,c}$ is independent of the scan rate, for the irreversible case it is found that $E_{p,c}$ varies with the scan rate.
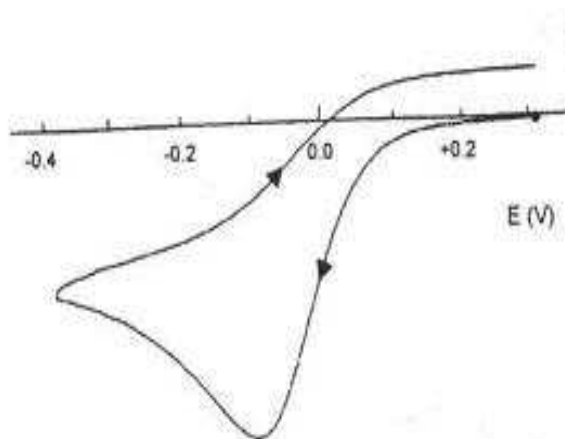
Figure 2.13   A typical cyclic voltammogram for an irreversible reduction process (Zanello 2003:60).

At $I_{p/2}$, the value of the *half-peak potential*, $E_{p/2}$, can be determined at 25 ℃ with the equation (Zanello 2003:61):

$$\left| E_p - E_{p/2} \right| = \frac{1.857 \cdot R \cdot T}{\alpha \cdot n_\alpha \cdot F} = \frac{47.7}{\alpha \cdot n_\alpha} (mV) \qquad \text{Eqn. 2.42}$$

where Eqn. 2.42 is commonly used to calculate the values of $\alpha \cdot n_\alpha$. It often happens that the value of $n = 1$ (or $n_\alpha = 1$), which then enables the calculation of the value of α (transfer coefficient). For an irreversible process the precise dependence of E_p with scan rate is expressed in the following equation (Zanello 2003:61):

$$E_p = E^{o\prime} - \frac{R \cdot T}{\alpha \cdot n_\alpha \cdot F} \cdot \left[0.780 + \ln\left(\frac{D^{\frac{1}{2}}}{k^o} \right) + \ln\left(\frac{\alpha \cdot n_\alpha \cdot F \cdot v}{R \cdot T} \right)^{\frac{1}{2}} \right]$$

$$\text{Eqn. 2.43}$$

which allows for the calculation of the heterogeneous rate constant, k^o, if the values of $E^{o\prime}$ and D is known.

The following tests should identify whether an electrochemical process is irreversible (Zanello 2003:61):

- There is no reverse peak

- The $I_{p,c}$ is proportional to $v^{\frac{1}{2}}$

- The value of $E_{p,c}$ shifts $- 30/\alpha.n_\alpha$ for each decade increase in v

- $\left| E_p - E_{p/2} \right| = \frac{48}{\alpha \cdot n_\alpha} mV$.

The property of the current for an irreversible process can be expressed by the following equation (Zanello 2003:61):

$$I_p = 0.227 \cdot n \cdot F \cdot A \cdot C \cdot k^o \cdot e^{-\frac{\alpha \cdot n_\alpha \cdot F}{R \cdot T}\left(E_p - E^{\circ'}\right)}$$

Eqn. 2.44

which can be used in a plot of $\ln I_p$ against $(E_p - E^{\circ'})$ that should give a straight line with a slope equal to $(\alpha \cdot n_\alpha \cdot F / R \cdot T)$ and the value of the y-intercept equal to $\ln(0.227 \cdot n \cdot F \cdot A \cdot C \cdot k^o)$. The chemical meaning of an irreversible electrochemical process implies that a large activation barrier to the electron transfer takes place causing breakage of the original molecular frame with the formation of new species (Zanello 2003:62).

2.3.1.1.4 Diagnostic Criteria to Identify a Quasi-reversible Process

A quasi-reversible process refers to one occurring in the transition *zone* between reversible and irreversible behaviour, as shown in Figure 2.14. A quasi-reversible process is characterised by determining either the thermodynamic parameter $E^{\circ'}$ (formal potential) or the kinetic parameters α (transfer coefficient) and k^o (rate constant) (Zanello 2003:62-64).
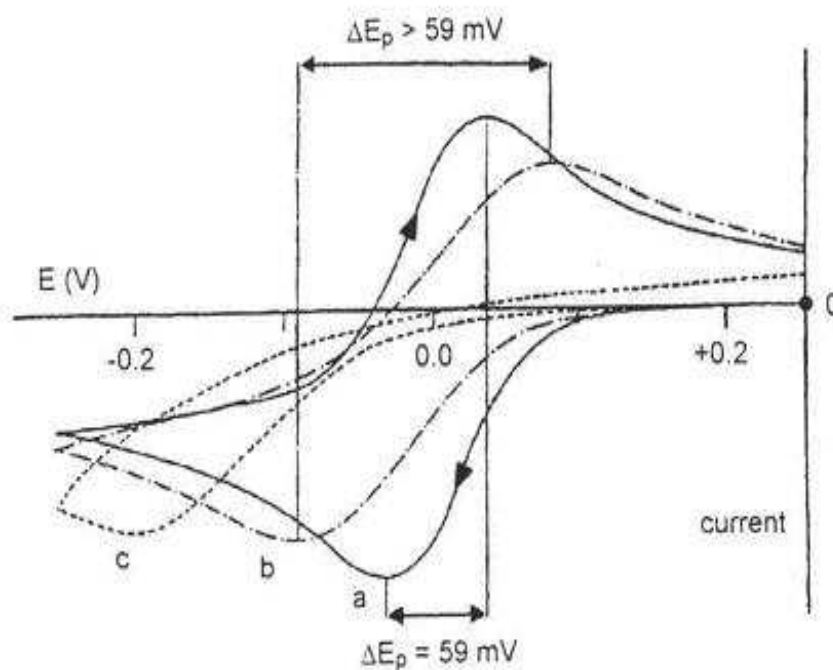
Figure 2.14   Qualitative behaviour of the cyclic voltammograms for a
                         reduction process having features of: a) reversibility; b)
                         quasireversibility; c) irreversibility. A = 0.5; E°′ = 0.00 V, T =
                         25 °C (Zanello 2003:64).

For a quasi-reversible electrochemical process the shape of the peaks and the peak-to-

peak separation (ΔE_p) depend, through a complex mathematical function Ψ, from α,

k^o and v as shown in the following equation (Zanello 2003:63):

$$\Psi = \frac{k^o \cdot \left[\dfrac{D_{ox}}{D_{red}}\right]^{\alpha/2}}{\left[D_{ox} \cdot \pi \cdot v \cdot \dfrac{n \cdot F}{R \cdot T}\right]^{1/2}}$$

Eqn. 2.45

and with the normal assumptions of $\alpha \approx 0.5$; $D_{ox} = D_{red} = D$, the above equation then becomes:

$$\Psi = \frac{k^o}{\left[\dfrac{\alpha \cdot n \cdot F \cdot v \cdot D}{R \cdot T}\right]^{1/2}}$$

Eqn. 2.46

With the use of Eqn. 2.46 the value of k^o can be calculated from a working curve containing Ψ, as shown in Figure 2.16.
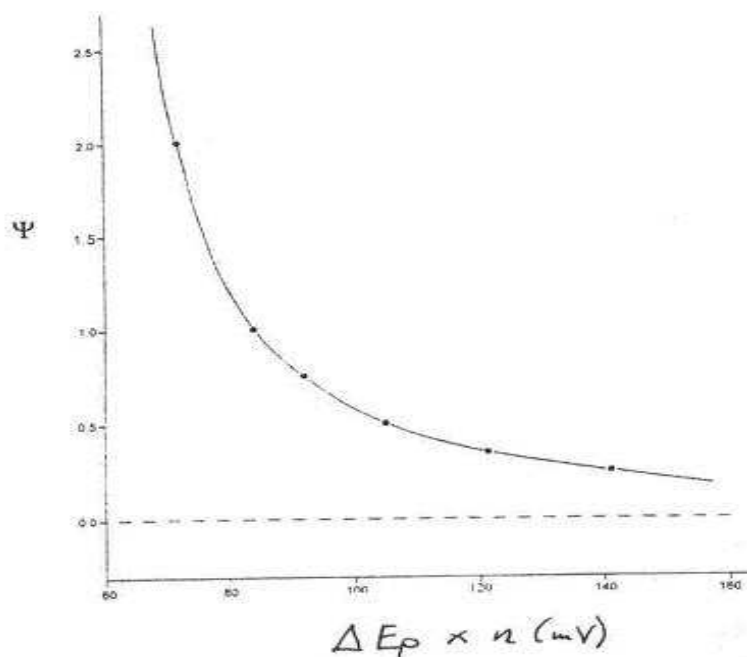
Figure 2.15   **Working curve used to calculate k^o from the peak-to-peak separation, ΔE_p (Zanello 2003:65).**

Figure 2.15 also shows that the peak-to-peak separation, ΔE_p, is plotted as a function of the parameter, Ψ. If the number of electrons (n) is known, as exchanged per molecule of Ox, measuring the value of ΔE_p at different scan rates, the corresponding value of Ψ can be obtained by using Eqn. 2.46 (Zanello 2003:63-64).

For a quasi-reversible system the following conditions should hold:

- /Ip/ increases with $v^{1/2}$ but is not proportional to it

- $\left| \dfrac{I_{p,a}}{I_{p,c}} \right| = 1$ provided $\alpha_c = \alpha_a = 0.5$

- ΔE_p is greater than $^{59}/_n$ mV and increases with increasing v

- $E_{p,c}$ shifts negatively with increasing v.

Furthermore, the chemical meaning of a quasi-reversible electrochemical process suggests that some important structural reorganisation accompanies the redox step, but it doesn't allow the molecular framework to undergo fragmentation (Zanello 2003:65-66).

2.3.2   Electrochemical Techniques Complementary to Cyclic Voltammetry

In the following paragraphs two techniques that are particularly useful in the analysis of partially overlapping processes are, i.e. differential pulse voltammetry and square wave voltammetry will be discussed. The last two techniques usually make use of the same equipment used for cyclic voltammetric measurements (Zanello 2003:110).

2.3.2.1   Square Wave Voltammetry

In Figure 2.16 it is shown that in Osteryoung Square Wave Voltammetry (OSWV), the perturbation of the potential with time consists of an in-phase combination of a staircase waveform of small and constant step height ($1 < \Delta E_{base} <$

40 mV) with periodic square wave pulses ($1 \leq \Delta E_{SW}$ (= ½ square wave amplitude) $\leq$ 250 mV). This last perturbation consists of pulses alternating in direction, i.e. succession of forward (reduction or oxidation) and reverse (oxidation and reduction) cycles ($1 \leq$ frequency SW ≤ 2000 Hz). The overall result obtained is a sequence of equally spaced steps: the forward step of height: $2 \Delta E_{SW} + \Delta E_{base}$; the reverse step of height: $-2\Delta E_{SW}$ (Zanello 2003:113).
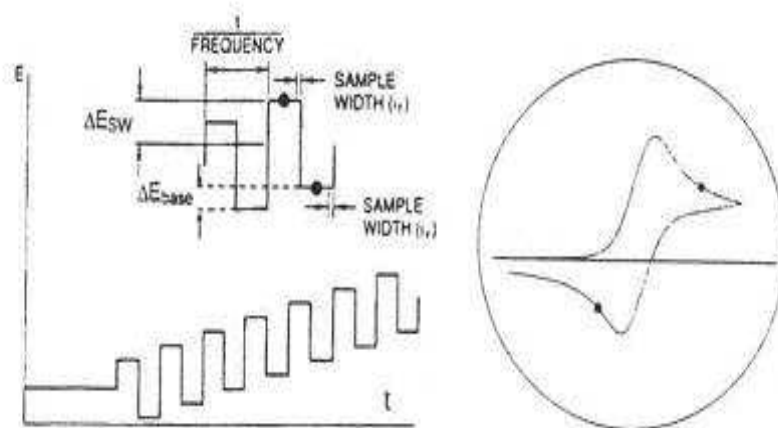
Figure 2.16   Potential-time perturbation on Osteryoung Square Wave
                   Voltammetry (Zanello 2003:114).

The resulting voltammograms that are obtained can be seen in Figure 2.17. The voltammograms is peak-shaped, but it consists of a differential curve between the

current recorded in the forward half-cycle and the current recorded in the reverse

half-cycle (Zanello 2003:114).
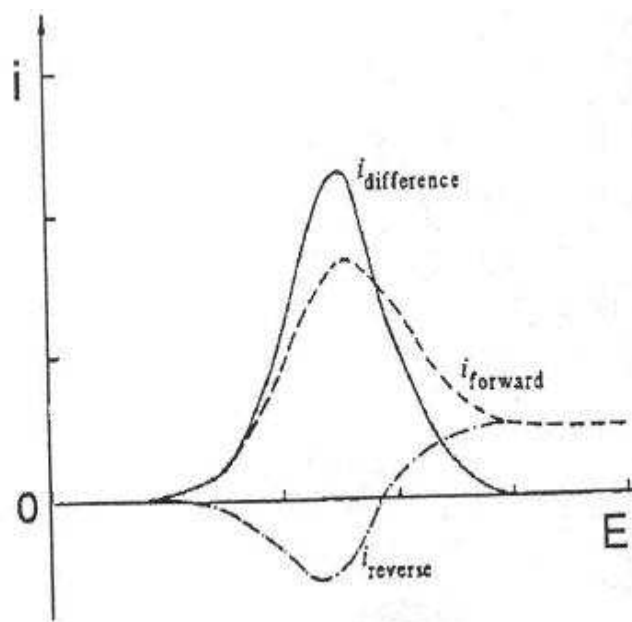
**Figure 2.17   Typical Osteryoung Square Wave voltammogram (Zanello
                     2003:114).**

In SWV, if ΔE_{SW} is small (about 50/n mV), it was found that the peak-potential for a

reversible electrochemical process virtually coincides with the formal electrode

potential. In addition to this, in the case of a reversible process the width of the peak

at half height, $\Delta E_{p/2}$ is given by the following two equations (Zanello 2003:115):

$$\Delta E_{p/2} = 4.90 \frac{R \cdot T}{n \cdot F}$$

Eqn. 2.47

or at a temperature of 25 ºC:

$$\Delta E_{p/2} = \frac{126}{n} mV$$

Eqn. 2.48

Therefore, OSWV can be very effectively used in solving almost overlapping processes. In OSWV higher scan rates than in Differential Pulse Voltammetry (DPV) is attained, from a few hundreds of mV/s to a few V/s. The value of the scan rate (obtained by the product *SW* frequency X ΔE_{base}) is around 0.2 V/s, a typical value for the scan rate of cyclic voltammetry. This also allows one to compete with the eventual presence of chemical complications coupled to the electron transfers (Zanello 2003:115).

2.3.2.2 Differential Pulse Voltammetry

The Differential Pulse voltammogram in Figure 2.18 shows that the perturbation of the potential with time consists in superimposing small constant-amplitude potential pulses ($10 < \Delta E_{pulse} < 100$ mV) upon a staircase waveform of steps of

constant height but they are smaller than the previous pulses ($1 < \Delta E_{base} < 5$ mV).

Some important parameters exist for Differential Pulse Voltammetry (DPV):

- the *pulse amplitude* (ΔE_{pulse}) is the height (in mV) of the applied potential,

- the *pulse width* is the length of the time (in ms) in which the pulse is maintained,

- the *sample width* is the time (in ms) at which the current is measured after the application of the potential pulse,

- the *pulse period* is the time (in ms) needed to make one cycle of variation of potential (Zanello 2003:111).
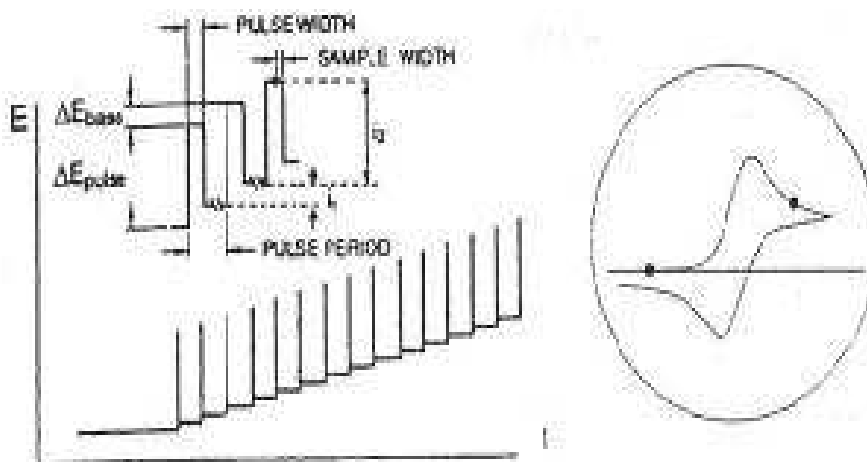
Figure 2.18   **Potential-time pulses in Differential Pulse Voltammetry (DPV) (Zanello 2003:111).**

In Figure 2.18 it is shown that during the pulse period the current is periodically sampled twice, i.e. before the pulse, i_1, and at the end of the pulse, i_2, respectively. It also shows that when the two currents are subtracted, i.e. $(i_2 - i_1)$, most of the capacitive currents are eliminated. This ensures that a differential-pulse voltammogram is a plot of the difference $(i_2 - i_1)$ against the potential increase. A typical differential pulse voltammogram is also shown in Figure 2.19 (Zanello 2003:111-112).
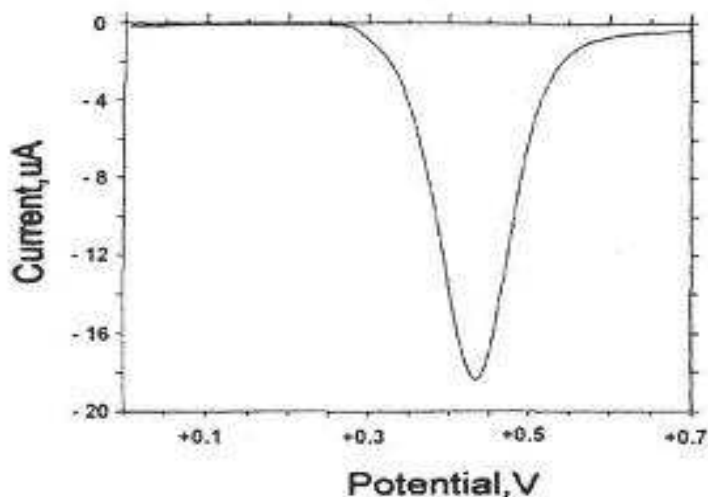
Figure 2.19   **A typical voltammogram in Differential Pulse Voltammetry (DPV) (Zanello 2003:112).**

In DPV it is noted that for reversible electron transfers, the peak potential is almost coincident with the formal potential, $E^{o'}$, value of the redox couple under study, according to the equation:

$$E_p = E^{o'} - \frac{\Delta E_{pulse}}{2}$$

Eqn. 2.49

but ΔE_{pulse} is usually low at approximately 50 mV.

The width of the peak at half height ($\Delta E_{p/2}$) for a reversible process can be calculated by the equation:

$$\Delta E_{p/2} = 3.52 \frac{R \cdot T}{n \cdot F}$$

Eqn. 2.50

or at a temperature of 25 ºC the equation becomes:

$$\Delta E_{p/2} = \frac{90.4}{n} (mV)$$

Eqn. 2.51

Differential pulse voltammetry (DPV) is particularly useful to determine accurately the formal electrode potentials of partially overlapping consecutive electron transfers. As shown in Figure 2.20 the cyclic voltammogram (CV) of a species undergoing two

closely spaced one-electron oxidations is compared to the relative differential-pulse

voltammogram (DPV). The DPV shows that the two processes are well separated

(Zanello 2003:111-113).
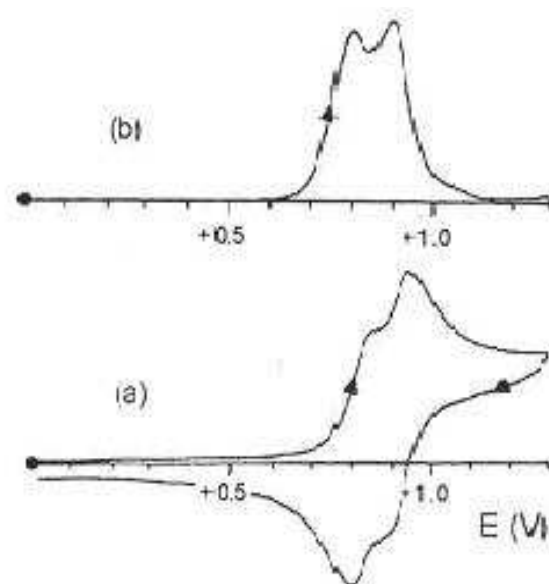
Figure 2.20   **Comparison between the results obtained for cyclic (0.2 V/s) and differential pulse (0.02 V/s) voltammetric responses of a redox species which undergoes two sequential one-electron oxidations (Zanello 2003:113).**

2.3.2.3   Chronoamperometry

The term *chronoamperometry* refers to the measurement of currents as a

function of time and is thought of as "controlled potential voltammetry" or

"controlled potential microelectrolysis" (occurring in an unstirred solution).

Chronoamperometry becomes a very useful technique in cases where cyclic voltammetry does not succeed in identifying the electrode mechanisms underlying certain redox changes. Furthermore, chronoamperometry measurements can be performed with the same equipment used for cyclic voltammetry.

Single potential step chronoamperometry is defined as the simplest chronoamperometric technique. This technique consists of applying an appropriate potential to an electrode, under the same stationary conditions similar to those of cyclic voltammetry. This then allows the electron transfer process under study, e.g. reduction, to run instantaneously to competion, while at the same time the decay of the generated current is monitored (Zanello 2003:123).

The *Cottrell equation* is defined as the fundamental law of chronoamperometry, which states that:

$$I = \frac{n \cdot F \cdot A \cdot D^{1/2} \cdot C^*}{n^{1/2}} \cdot \frac{1}{t^{1/2}} \qquad \text{Eqn. 2.52}$$

Equation 2.52 indicates that for a diffusion controlled process (not involving absorption processes) taking place at a planar electrode, the current decays following a function that is inversely proportional to the square root of time. From the equation it is also seen that the current is proportional to the electroactive species ($I \propto C^*$) present in the bulk of the solution (Zanello 2003:124).

In Figure 2.21 a typical chronoamperometric response is shown. It is clear from this diagram that for times $t < \tau$, the diagram represents the chronoamperometric

single step response. In this time interval (t < τ) the current-time curve follows the

Cottrel equation, therefore the cathodic current is expressed by the relationship:

$$I_c = n \cdot F \cdot A \cdot C * \cdot \left| \frac{D}{\pi \cdot t} \right|^{\frac{1}{2}}$$

Eqn. 2.53
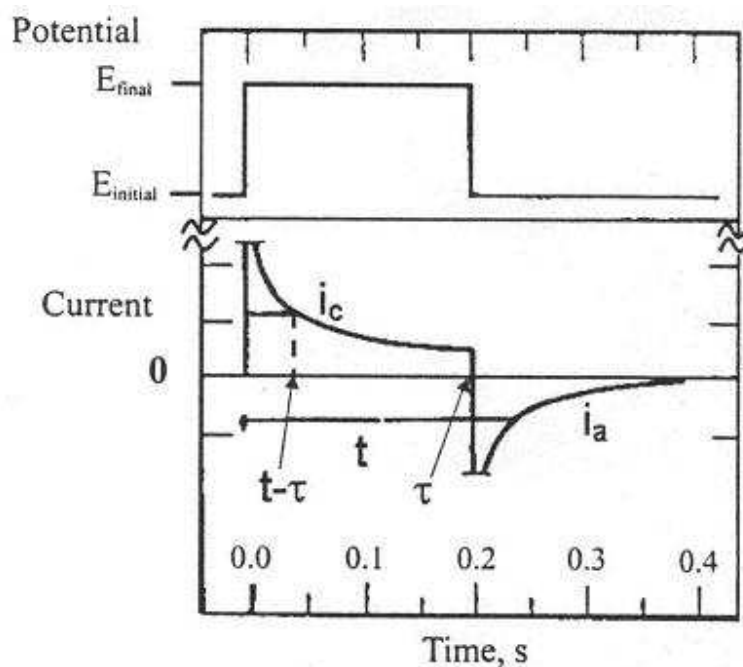
Figure 2.21   **Chronoamperometric double potential step experiment for the process: Ox + ne- ↔ Red; inversion time τ = 0.2 s. The top part of the diagram shows the perturbation of the potential applied to the working electrode with time (Zanello 2003:124).**

For times t > τ, where the reoxidation of the previously generated species Red takes place, Figure 2.21 represents the double potential step response. For these conditions the anodic current follows the equation:

$$I_a = \frac{n \cdot F \cdot A \cdot D^{\frac{1}{2}} \cdot C^*}{\pi^{\frac{1}{2}}} \left[\frac{1}{(t - \tau)^{\frac{1}{2}}} - \frac{1}{t^{\frac{1}{2}}} \right]$$

Eqn. 2.54

From Eqn. 2.54 it follows that the ratio between the return (at the time *t*) and forward (at the time *t-τ*) currents (expressed as the absolute value, since I_a and I_c have, conventionally, opposite signs) is equal to:

$$\left| \frac{I_a}{I_c} \right| = 1 - \left| \frac{\theta}{1 + \theta} \right|^{\frac{1}{2}}$$

Eqn. 2.55

where:

$$\theta = \frac{t - \tau}{\tau}$$

Eqn. 2.56

At this point, depending on whether or not the experimental data (i.e. the ratio between the anodic currents at the times t and the cathodic currents at the times *t-τ*) follow the trend shown in Figure 2.22, valid redox couples that undergo diffusion-

controlled processes, it is possible to gain information concerning the possible presence of coupled chemical reactions. It needs to be taken into account that the maximum time taken for a chronoamperometric experiment is of about 10seconds (Zanello 2003:125-126).
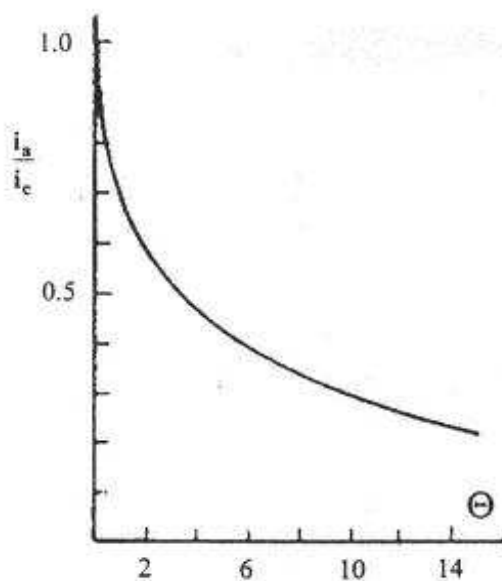
Figure 2.22 **The variation of the current ratio in a double potential step experiment for a simple reduction process (t > τ) (Zanello 2003:125).**

2.4 Self-Assembled Monolayers (SAMs)

2.4.1 Introduction

Extensive research has been done on self-assembled monolayers (SAMs) that are formed from long-chain amphiphiles. One of the reasons is that these films provide and interfacial region composed of a well-defined composition, structure, and thickness that can serve as an ideal model system in understanding various interfacial phenomena. These phenomena include wetting, adhesion, corrosion, catalysis, etc (Mazur and Krysinski 2001:3963; Berchmans *et al.* 1998:52; Sandhyarani *et al.* 1999:154).

The alkanethiols and its derivatives have been the subject of extensive study since these thiol monolayers can be used to influence the properties or topological structures of chemically or electrochemically synthesised conducting polymers. If a gold electrode (or transducer surface) is coated with a SAM, it allows pre-organisation in one plane followed by subsequent polymerisation. This is achieved by covalent or ionic immobilisation of the monomer molecules and their electrochemical oxidation that leads to the formation of molecular films of conducting polymers on the surface (Mazur and Krysinski 2001:3963; Mazur *et al.* 2002:145).

More importantly, thiol monolayers can also be patterned using a variety of techniques, in order for the monolayers to serve as molecular resists or templates for selective deposition of conducting polymers in preparation of different polymeric

domains on (transducer) surfaces (Mazur and Krysinski 2001:3964; Mazur *et al.* 1998:167-168).

Yourdshahyan *et al.* (2001:1) in their study also indicated that thiol monolayers hold special interest since the presence of a thiol group greatly strengthens the molecule-surface interactions, thereby inducing order in the layer. They also emphasised the fact that SAMs have important potential applications in industry that include the use in sensors, transducers, detectors, packaging, as insulating layers in integrated circuits, in functionalisation of surfaces, thin coatings for electrodes and in corrosion inhibition. In the case of the alkanethiols we get the methyl-terminated *1*-alkanethiols, μ-substituted *1*-alkanethiols of the formula $HS(CH_2)_nX$, where X is, for example, a halogen atom, or a hydroxyl, amino, carboxylic acid, ester, or nitrile group. Mixed monolayers of *1*-alkanethiols with different terminal substituents have also been employed. Besides the alkanethiols, these SAMs can also contain disulfide or thiolate groups in it (Kang *et al.* 2004:43; Zhang *et al.* 2002:150; Liu *et al.* 2002:295; Brito *et al.* 2003:53).

In a study by Zerulla *et al.* (1998:604) the aromatic thiol of *2*-mercaptobenzothiazole (MBT) was studied and compared to the alkanethiols. They have highlighted that MBT is known to form hydrophobic complexes with many metals and has been extensively used as a corrosion inhibitor or as a collector for mineral flotation. The structure of 2-mercaptobenzothiazole contains a nitrogen atom that acts as an additional ligator atom in a chelate type bonding at the surface and can be used as a tracer atom for the identification of adsorbed species. Self-assembled monolayers (SAMs) of *n*-alkanethiols can also be metallised for certain applications.

This represents a straightforward method to create ultrathin films on surfaces that contains tailormade chemical properties for certain applications (Zhang *et al.* 2001:68).

2.4.2   Reason for SAMs

Different strategies in the form of Langmuir-Blodget (LB) transfer and self-assembly techniques have been employed in the formation of monolayers on electrode surfaces. Self-assembled monolayer (SAM) formation has proved to give more rugged films since there is a strong chemisorption of suitable organo-sulphur compounds onto noble metal surfaces (Morrin *et al.* 2004:30). Very promising results have also been obtained for the formation of SAMs on gold electrodes in the construction of electrochemical biosensors. These advantages include:

(i)   improved electrocatalysis,

(ii)   freedom from surface fouling,

(iii)   and prevention of undesirable reactions competing kinetically with the desired electrode process (Morrin *et al.* 2004:30; Wang *et al.* 2000:88; Berchmans *et al.* 1998:52; Vergheese and Berchmans 2004:229).

In the application of alkanethiols, some has been functionalised with electron transfer mediators such as with tetrathiafulvalene and violegen that has been

successfully applied to biosensing (Morrin *et al.* 2004:30). Self-assembled monolayers of fullerene molecules have also been proposed due to their unique electronic, spectroscopic, and structural properties (Sahoo and Patnaik 2003:43).

An overview providing different approaches in using self-assembled monolayers (SAMs) and the rationale behind some of these approaches are listed below.

Felgenhauer *et al.* (2003:309) indicates that monolayers of thiol based organic molecules have been well recognized as convenient systems to control charge transfer at metal electrodes. Another advantage in the application of SAMs is provided by the possibility of controlling charge transfer systematically via the molecular structure of the SAM in molecule-based electronics and electrode modification.

The formation of SAMs of both organic and inorganic materials on solid substrates have also been the subject of intense study to investigate the possibility of applying various functionalities in view of possible applications in the fields of nanotechnology and nanoscience (Song *et al.* 2003:385).

Wang *et al*. (2000:457) also reports that for thiol self-assembled monolayers, the SAMs of alkanethiols have attracted a lot attention since they can be prepared on gold electrodes by a single one-step adsorption from a dilute solution. In contrast to this, studies performed on heteroaromatic thiols as SAMs are still rare (Wang *et al.* 2000:457).

In a study by Raj and Ohsaka (2003:69) it was indicated that the self-assembly technique can conveniently be applied to ensure that a stable and well-organised monolayer is obtained. Cooperative and homogenous behaviour of the

entire electrode surface is assured due to the high organisation of the monolayer on the electrode surface. SAMs also provides the flexibility in controlling the film thickness that is applied, since the electrochemical response at the SAM-modified electrode depends on the thickness. They have found that monolayers of long chain alkanethiols are too "thick" and would passivate the electrode surface, slowing down the electron transfer rate resulting in a small current response. To improve this situation, they have suggested the use of "thin" monolayers in order to shift from electron tunneling or spherical pinhole diffusion on the free site of the compact monolayer to semi-infinite diffusion. This will ensure that the electron transfer at the electrode no longer limits the electrochemical response, since fast electron transfer, good selectivity and high sensitivity can be achieved when "thin" monolayers are used. To achieve the latter, the use of SAMs of aromatic and heteroaromatic thiols was suggested. In the case of the aromatic thiols the molecules were found to be highly anisotropic and the intermolecular interactions are expected to be stronger than those between the alkanethiols, which may lead to different molecular packing structures. A total of 5 heteroaromatic thiols were suggested by their research, which is listed in Figure 2.23 below (Raj and Ohsaka 2003:70).

mercaptobenzimidazole
(MBI)

mercaptobenzothiazole
(MBT)

mercaptoimidazole
(MI)

mercaptopyrimidine
(MPM)
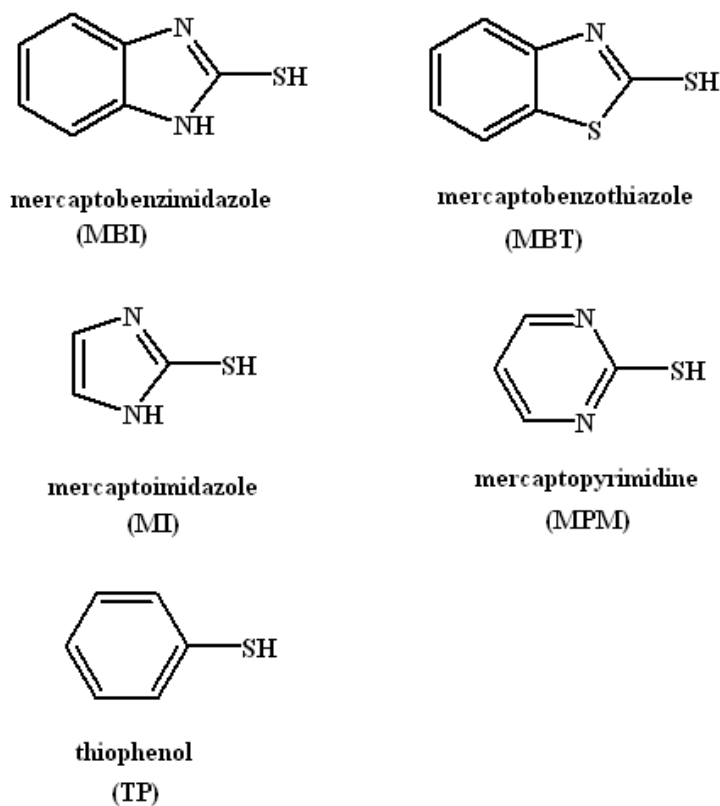
thiophenol
(TP)

Figure 2.23   Heteroaromatic thiols of mercaptobenzimidazole (MBI), mercaptoimidazole (MI), mercaptobenzothiazole (MBT), mercaptopyrimidine (MPM) and thiophenol (TP) (Raj and Ohsaka 2003:70).

In the work of Oyamatsu *et al*. (1999:59) it was reported that thiols having long alkylchains forms a highly packed SAM layer, which blocks the approach of electrochemically active species to the electrode substrate surfaces, resulting in a complete suppression of their reactions at the electrode. On the other hand, shorter alkylchains allow either electron tunnelling across the SAM or enable penetration of

electroactive species to the electrode substrate surface, which may result in a complete suppression of their reactions at the electrode.

Kerman *et al.* (2002:309) reported that SAMs provide molecular level control over the immobilisation of biomolecules such as enzymes, and ion-channels, as well as allowing the incorporation of a number of molecular functionalities within the biorecognition interface. Furthermore, they have found that in the case where an electrode was covered with an alkanethiol, it allowed surface coverage and orientation for DNA molecules to be immobilised on that surface when *2,6-anthroquinonedisulfonic acid* was used as the electrochemical label.

Brito *et al.* (2003:53) and Vergheese and Berchmans (2004:229) reported in their studies that SAMs hold several advantages specific for the field of electrochemistry. These advantages of using SAMs include the following:

i)   the SAMs can be employed as insulating barriers between an electrode and a redox couple, allowing the study of long range electron transfer,

ii)   it also allows the preparation of microarray electrodes that have potential applications in selective voltammetric detectors, or for measuring very fast electron transfer kinetics.

In the work done by Peng *et al.* (2004:291) it is reported that the spontaneous adsorption of thiols from solution or the vapour phase onto oxide-free metals (especially gold), provides a convenient method of functionalisation these surfaces. They further indicate that SAMs of ferrocene terminated thiols are the most widely used and best characterised in the category of mixed self-assembled systems.

SAMs have also been employed for the immobilisation of antibodies in immunosensing applications. A fast initial adsorption takes place since the thiols have a strong affinity towards gold, followed by a slower process whereby re-organisation of the S/S-H molecules on the gold surface takes place. It should be noted that the immobilisation of biological components can have a deleterious affect on activity. It is presumably attributed to the hindering of access to the active site when enzymes are used or the antigenic binding site when antibodies are used (Susmel *et al.* 2003:881; Park *et al.* 2004:667; Hleli *et al.* 2006:711).

The work of Mazur *et al.* (2002:145) reports the electrochemical deposition of conducting polymers on electrodes that are covered with thiol films. This technique leads to the preparation of ultrathin polymer-thiol layers that can be used as protective coatings for a variety of materials such as aluminium and steal. Alternatively it provides a platform for sensor construction in application in various fields (Mazur *et al.* 2002:145).

2.4.3   Mercaptobenzothiazole as SAM

Mercaptobenzothiazole (MBT) is a hetero-aromatic thiol containing a fused thiazole ring without a long alkyl chain and can form a compact and impervious monolayer on an electrode surface. MBT monolayers on gold gave higher thermal stability when compared to other alkane thiol monolayers and adsorbs with its

molecular plane perpendicular to the gold surface. The two differently bound sulphur-atoms in the structure of MBT is shown in Figure 2.24 to show the thione form (left) and the thiol form (right) of the compound (Zerulla *et al.* 1998:604; Vergheese and Berchmans 2004:229).
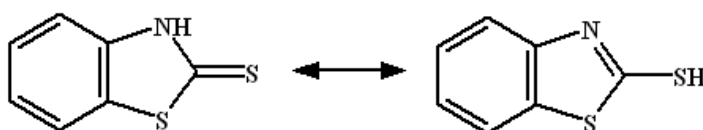
Figure 2.24   The chemical structure of mercaptobenzothiazole (MBT) showing the two differently bound sulphur-atoms (Zerulla *et al.* 1998:604).

Jun and Beng (2004:87-88) reports that electrochemical techniques are the most commonly used methods to characterise the SAM of MBT. They also confirmed the statement by Zerulla *et al.* (1998:604), which states that MBT forms a compact and impervious monolayer on an electrode surface and have suggested the binding to take place as shown in Figure 2.25 (Jun and Beng 2004:88).
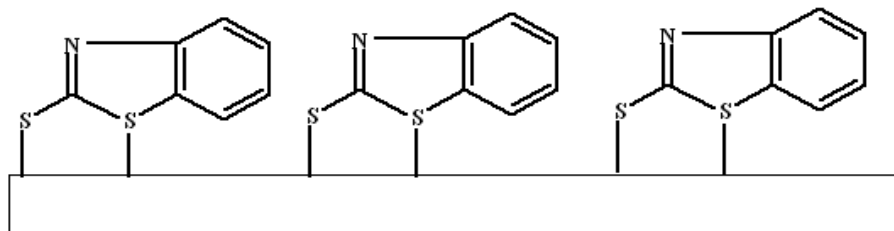
Figure 2.25   **The formation of a compact self-assembled monolayer of MBT on a gold surface (Jun and Beng 2004:88).**

A self-assembled monolayer (SAM) of mercaptobenzothiazole (MBT) has been used in the construction of different sensors and some of these applications will be listed and discussed below.

In a study by Wan and Yang (2002:131) they have used *2*-mercaptobenzothiazole (MBT) and formed an ordered chemically bound monolayer on a gold electrode surface through self-assembly. The gold-*2*-mercaptobenzothiazole (Au/MBT) SAM electrode was then used to investigate the electrochemical behaviour of folic acid, which in itself is electroactive and of considerable biological importance as part of the vitamin B complex.

Berchmans *et al.* (1998:52) indicated in their study that thiols containing a single aromatic ring such as thiophenol, with a single benzene ring, do not have good stability. Since the order and stability of a monolayer is reported to increase with an increase in chain length, they investigated MBT containg a fuzed thiazole ring but no

methylene chain and studied the influence of such a monolayer in electron transfer reactions.

Sandhyarani *et al.* (1999:154) studied the chemisorption and electrochemical roperties of *2*-mercaptobenzothiazole (MBT). They have found that the Au/MBT SAM allows the redox kinetics of ferro-ferricyanide to remain unhindered, while it blocks the under-potential deposition of copper and the redox behaviour of the ferrous-ferric system. This provided information for the possible use of a SAM to distinguish between inner- and outer-sphere electron transfer reactions. The results obtained through surface enhanced Raman spectroscopy (SERS) of MBT have conclusively established a near perpendicular geometry for a gold electrode and an almost parallel geometry for a silver electrode.

Vergheese and Berchmans (2004:229) indicated in their study that the compounds of imidazoles are important constituents of enzymes such as ascorbate oxidase and superoxide dismutase, whose metal complexes are responsible for important biological reactions. For this reason, mercaptobenzothiazole being a biomimetic is chosen as SAM and the structural integrity and compactness of the SAM formed with MBT and mixed monolayers of MBT are characterised by following the electron transfer kinetics with standard redox species (e.g. potassium ferrocyanide, hexa amine ruthenium (II) chloride).

In a study by Wang *et al.* (2000a:457) the properties of thioaromatic SAMs and heterocyclic thiol SAMs have been investigated. The SAM of *2*-mercaptobenzothiazole has been characterised by X-ray photoelectron spectroscopy (XPS) to investigate the properties of potential-dependent "opening and closing" of

the monolayer on a gold electrode. Impedance measurements have also been performed to investigate thin monolayer assemblies and electron transfer through them.

2.4.4   Influence of surfactants

In section 2.2.4.3 it was also reported that the conducting polymers can be doped with surfactants during the electroplymerisation of the polymer film onto the transducer surface. As an example PANI has been doped with polyvinylsulphonate to enhance the morphology and electrical conductivity of the polymer at non-acidic pH, thus rendering it ideal for the application in enzyme electrodes or immunosensors (Iwuoha *et al*. 1997:750-751; Killard *et al*. 1999:110-111).

Wang *et al.* (2000b:88) reports that surfactants can be used to improve the electron transfer of the electroactive species at the bare metal electrode. On the other hand, little attention has been paid to the electron transfer reaction taking place at a thiol modified gold electrode in the presence of surfactants. In their study thiols with different terminal groups (e.g. $-CH_3$, $-COOH$ and $-NH_2$) were prepared on gold electrodes using the self-assembling procedure. In the presence of the surfactants called hexadecyl trimethylammonium bromide (HTAB), hexadecyl pyridine bromide (HPB) and sodium dodecyl benzene sulfonate (SDBS), the electron-transfer reaction of potassium ferricyanide at the thiol modified gold electrode was investigated. The

results showed that the surfactants have some influence on the electron-transfer reaction at the thiol-modified gold electrode. In the case of cationic surfactants, some improvement in the reversibility of the redox reaction at the thiol-modified gold electrode was observed. For the anionic surfactants it was found that it causes some inhibition of electron transfer of the redox at both the methyl and carboxyl terminated thiol-modified gold electrodes.

In a study by Liu *et al.* (2003:2823) the influence of different surfactants on a gold-colloid modified electrode was investigated using cyclic voltammetry and electrochemical impedance techniques. It is reported that a thiol of *1,6*-hexanedithiol (HDT) was self-assembled on a gold electrode, while results obtained with a quartz crystal microbalance (QCM) indicated that some of the HDT molecules stood upright on the Au electrode and some molecules lay on their sides. The surfactants called cetyl trimethyl ammonium bromide (CTMAB) and sodium dodecyl benzene sulphonate (SDBS) were used to investigate their influence on the cathodic peak of Au-colloid modified electrode, and differences in their behaviors have been observed. Furthermore, the results have indicated that
anionic and cationic surfactants exhibit different behaviours on a SAM-modified gold electrode.

The work of Yang *et al.* (2005:679) investigated the barrier properties and electron transfer reactions of derivatised thiol SAMs on a gold electrode in the presence of surfactants. Derivatised thiols of *2*-mercaptoethanesulphonic acid (MES), *2*-mercaptoacetic acid (MAA) and *N*-acetyl-L-cysteine (NAC) were used. The ferricyanide negative redox probe was selected to indicate the electron-transfer

efficiency on the interface of the studied electrodes. The surfactants evaluated in this study included hexadecyl trimethylammonium bromide (HTAB), hexadecyl pyridine bromide (HPB) and sodium dodecyl benzene sulfonate (SDBS). The results have shown that by changing the surface structure of the SAMs, the different surfactants could regulate the barrier properties and electron-transfer efficiency in different ways. The cationic surfactant lowered the electrostatic repulsion between the negative redox probe and the negatively charged substituents of the thiol SAM, while enhancing the reversibility of electron transfer by virtue of increasing the redox probe concentration within the electric double-layer region. No significant effect or results were obtained for the neutral surfactant. The anionic surfactant hindered the acces and reaction of the redox probe with the electrode surface by electrostatic repulsion of same-sign charges.

2.5   Conducting Polymers

2.5.1   Introduction

The formation and characterisation of conducting polymers have received increasing attention, since it can be widely used in various applications of microelectronic devices, sensors and batteries (Palys *et al*. 2000:111; Tripathy *et. al*. 2002:65; Saxena and Malhotra 2003:293).

Recently, attention has also been given to the use of conducting polymers as active layers in chemical sensors, since there is evidence that adsorbed gas molecules and organic vapours can cause a change of electrical conductivity in the polymer matrix of organic metals. Conducting polymers can be electrochemically deposited that allows for the preparation of films at well-defined redox potential in the presence of a given counter ion. The counter ion further defines the level and characteristics of the doping reaction (Reemts *et al.* 2004:320).

Research has been done on a list of conducting polymers that include polyacetylene, polypyrrole, polyphthalocyanine, polythiophene, polyaniline and polyphenylene. Of these examples, polyaniline (PANI) has been the most promising representative and several reasons account for that. Aniline as monomer is relatively inexpensive, the polymerisation reaction proceeds with high yield and the polymerisation of the monomer to polyaniline is straightforward. Also note that the electrical properties of PANI are very sensitive to its chemical composition. For PANI itself potential applications include anti-corrosive coatings, in secondary batteries, electrochromic devices and electrochemical biosensors. Some of the advantages of utilising PANI-coated electrodes in biosensors include impressive signal amplification and the elimination of electrode fouling (Sakthivel *et al.* 1997:1747; Pruneanu *et al.* 1999:2733; Mathebe *et al.* 2004:115).

PANI as conducting polymer does not come without any disadvantages. In its conductive form, PANI is difficult to process since it is insoluble in common organic solvents and is unstable at melt processing temperatures. Recently, the introduction of

counter-ions induced the processability of PANI by doping it with functionalised protonic acids to increase its solubility (Kuo and Chen 1999:163).

2.5.2 Different conducting polymers

For conducting polymers to be used in applications, it needs to have excellent electronic and mechanical properties, solution or melt processability as well as high environmental stability. A list of conducting polymers widely used today is shown in Figure 2.26 and includes polyacetylene, polythiophene, poly(*3*-alkyl-thiophene), polypyrrole, polyisothiophene, polyethylene dioxythiophene, alkoxy-substituted polyparaphenylene, polyparaphenylene vinylene, poly(2,5-dialkoxy paraphenylene) vinylene, polyparaphenylene, ladder-type polyphenylenesulphide, polyheptadiyne, poly(3hexyl) thiophene and polyaniline (Saxena and Malhotra 2003:294).
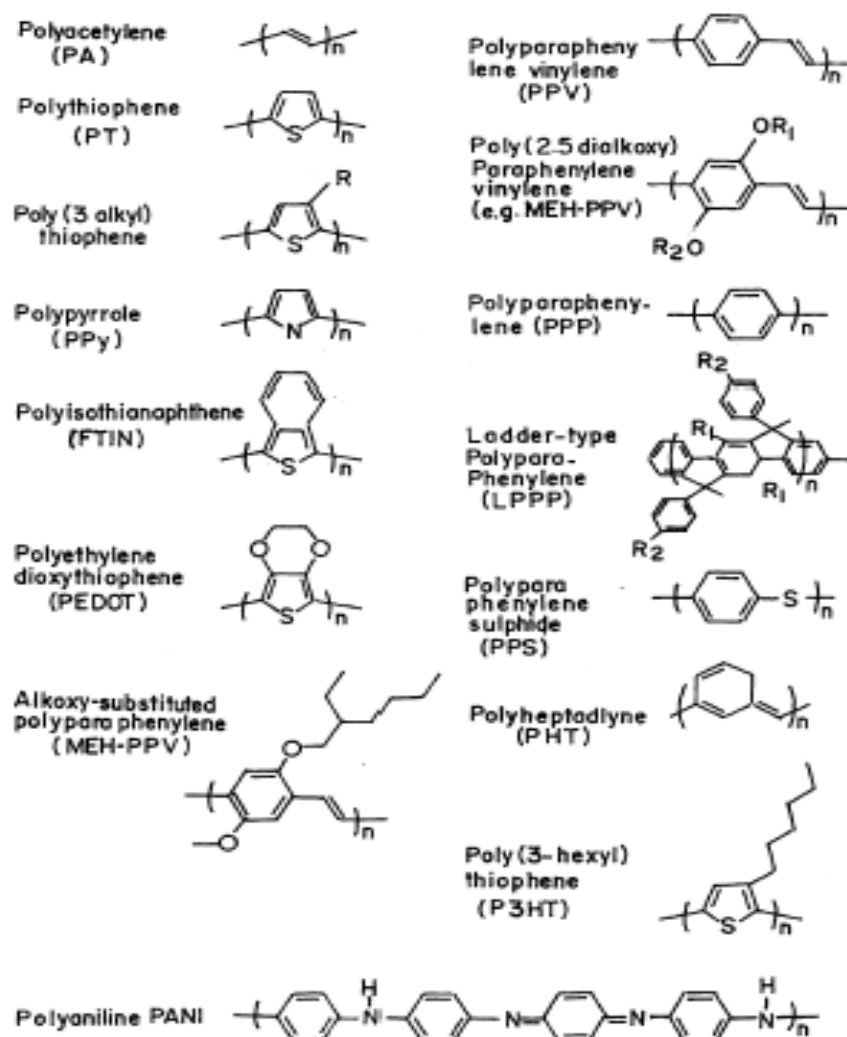
Figure 2.26   **Structures of a few conducting polymers (Saxena and Malhotra 2003:294).**

A change in emphasis in the areas of materials science and chemistry has opened new approaches to the areas of analytical sensing, which influences the design of sensors, particularly those that use electrochemical or spectroscopic transduction methods. In

this regard, the two groups of materials that have received widespread application in research include the conducting electroactive polymers (CEPs) and hydrogels. The application of conducting polymers has been widespread to include the areas of sensors, actuator components in microsurgical tools, controlled drug delivery systems, corrective implantable aids, life-like prosthetic limbs, actuators and artificial muscles. Since the early 1990s, CEPs have been extensively reported to function as thin films for batteries, sensors, ion-selective electrodes and solid-state devices (Brahim *et al.* 2003:123; Chaubey *et al.* 2000:97; Huang *et al.* 2003:88; Wen *et al.* 2001:451).

One conducting polymer that has received greater attention is polyaniline (PANI), due to its ease of preparation and well-behaved electrochemistry. PANI has been largely studied and characterised by electrochemical techniques that include cyclic voltammetry (CV), impedance spectroscopy, and also by thermal analysis. The use of PANI is not without difficulty due to its low solubility in common organic solvents that ultimate restricts its processability. One way to improve the solubility of PANI in organic solvents has been the use of functionalised acids as dopants. Dopants that have been commonly used include *p*-toluene-sulfonic acid (TSA), dodecyl benzene-sulphonic acid (DBSA) and camphor-sulphonic acid (CSA). The second option to improve the solubility of PANI is to use substituent groups in the polymer chain or use derivatives of aniline such as *2*-methoxy aniline (*o*-anisidine, OMA) and *2,5*- dimethoxy aniline (DMA). With the substitution route, problems arise when substitution is in the phenyl ring or *N*-position of polyaniline units, since it causes a decrease in the conductivity of the polymer. However, aniline substituted

with two methoxy groups such as *2,5-* dimethoxy aniline (DMA), has been reported to produce a soluble polymer of poly(*2,5*-dimethoxy aniline) (PDMA) with a conductivity similar to that of PANI (Chen *et al.* 2003:133; Alvial *et al.* 2004:3507).

2.5.2.1 Structure of polyaniline and its derivatives

2.5.2.1.1 Polyaniline, PANI

Polyaniline (PANI) represents one of the mostly widely used conducting polymers. The general structure of PANI is shown in Figure 2.27, where (1-y) is the average oxidation state.
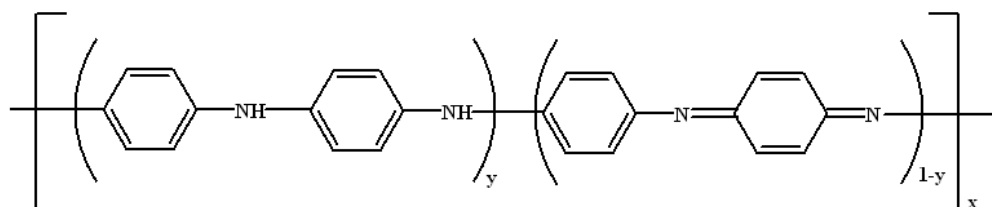
Figure 2.27   General structure of PANI (Wang and Jing 2005:154).

PANI exists in four different forms depending on its oxidation state. Form 1 is the leucoemeraldine base (LB, where 1-y = 0) where it's in the fully reduced state. Form 2 consists of the emeraldine base (EB, where 1-y = 0.5) that represents the half

oxidised state, where it is a semi-conductor composed of an alternation sequence of two benzenoid units (-B-) and one quinoid unit (=Q=). Form 3 is the pernigraniline base (PB, where 1-y = 1) that represents the fully oxidised state and PANI as a weak insulator exists. Form 4 is the conducting emeraldine salt (ES) state of PANI with the polymer having a green colour. The structures of the different oxidation states of leucoemeraldine base, emeraldine base and pernigraniline base is also shown in Figure 2.28 (Wang and Jing 2005:154; Hao 2003:3; Mathew *et al.* 2002:141; Albuquerque *et al.* 2000:19).
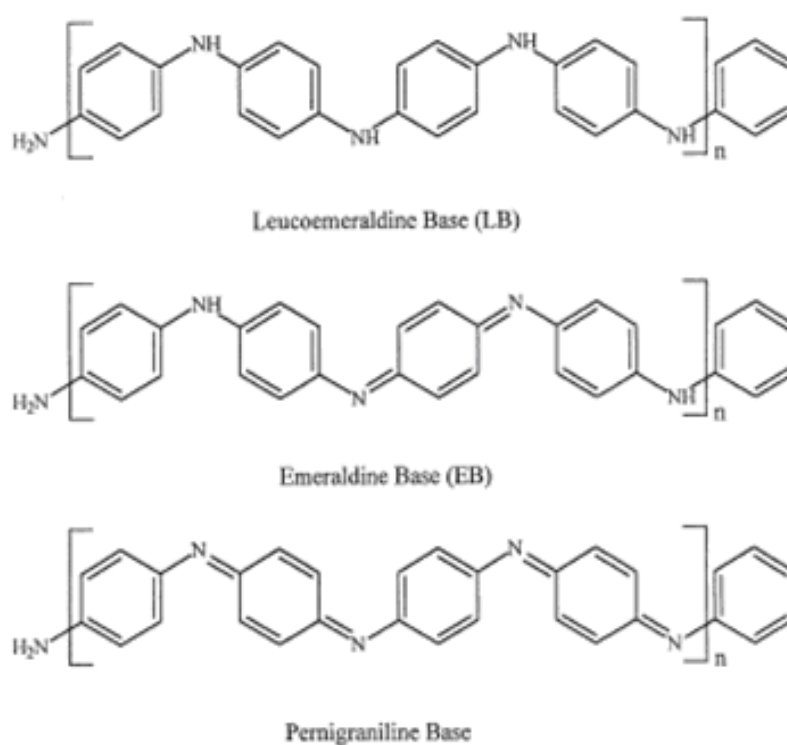
Figure 2.28   **The leucoemeraldine base, emeraldine base and pernigraniline base oxidation states of PANI (Mathew *et al.* 2002:141).**

The importance of PANI is further enhanced by its good stability in air, both in the isolating form (emeraldine base) and in the conducting form (emeraldine salt). PANI can be electrochemically prepared by polymerising the monomer aniline in acidic aqueous solutions under a constant voltage or using cyclic voltammetry. Quality PANI films are obtained when a great deal of the unreacted oxidised species is removed from solution, since these species can react with water that leads to polymer degradation through hydrolysis. Therefore, the deposition of PANI by cyclic voltammetry is preferred since the exposure time at anodic potential is short and reduction of the unreacted oxidised species will occur during the cathodic scan. Cyclic voltammetry further ensures that the incorporation of hydrolysis products of PANI decreases, resulting in a more conductive and thicker film that is produced (Pruneanu et al. 1999:2733).

The structures of intrinsically conductive polymers (ICPs) can be characterised by UV-Vis and X-ray photoelectron spectroscopy, with the former technique being favoured for its ease of operation. The UV-Vis spectrum of PANI in its base form is characterised by two absorption peaks at approximately 320 and 610 nm. The peak at 320 nm is often assigned to the π-π^* transition in the benzenoid structure, while the peak at 610 nm is attributed to the exciton formation in the quinoid rings. The last peak absorption is also ascribed to the blue colour of PANI base solutions in dimethyl formamide (DMF) or N-methyl pyrrolidnone (NMP) (Wang and Jing 2005:153).

In the case of PANI the redox states, proton content and steric hindrance are crucial factors in determining the polaronic states of polyanilines that are responsible for a high electrical conductivity of the polymer. During the electrochemical polymerisation of aniline by cyclic voltammetry, two types of doping exist in PANI. The PANI produced during polymerisation can exist in a base (EB), a bipolaron (ES) and two polarons (PB). The EB form of PANI contains benzenoid and quinonoid rings in a ratio of 3:1 in its structure. It is diamagnetic and insulating and its paramagnetic centres and conductivity would appear only if it is protonated (or doped). When protonation occurs, it leads to the appearance of positively charged paramagnetic polarons and diamagnetic bipolarons. In the next step the two polarons can recombine to form one bipolaron. It is this evident that conductivity can be a result of motions between polarons and bipolarons. The bipolarons is prevalent in the salt form of PANI (emeralsine base) (Grzeszczuk and Szostak 2003:257-258; Hao 2003:6).

2.5.2.1.2 Poly(o-methoxy aniline), POMA

In the polymerisation of conducting polymers, it is known that the morphological, electrical and structural properties of these polymers depend on the synthesis condictions such as monomer concentration, type of supporting electrolyte, solvent, pH, applied electrical potential and temperature. It is further well established that the rate of growth, morphology, optical, density and redox properties of

polyaniline (PANI) are affected by these properties. It has been shown that a derivative of PANI called poly(*o*-methoxyaniline) (POMA) has electrochemical properties similar to that of PANI. POMA can be synthesised chemically and electrochemically and is more soluble in common organic solvents than PANI. This enables POMA to be used for the manufacturing of free-standing films by Langmuir-Blodgett or self-assembling techniques (Widera *et al.* 1997:29; Patil *et al.* 1999a:298; Patil *et al.* 1999b:31; Kuramoto and Takahashi 1998:33).

As the interest in PANI as a conducting polymer was investigated, the interest has grown in the use of PANI derivatives. The poly(alkoxyanilines) and poly(alkylanilines) have been frequently studied as substituted PANI derivatives with more attention drawn to the poly(alkoxyanilines). The simplest poly(alkoxyaniline) of poly(*o*-methoxyaniline) have been prepared by both electropolymerisation and chemical oxidative polymerisation of *o*-, *m*- and *p*- methoxyaniline. However, only *o*-methoxyaniline has been found to form the PANI-type polymer during electrochemical synthesis, while the other isomers shows higher reactivity in the chemical polymerisation process. The general formula of POMA is presented in Figure 2.29 and when y = 0.5 POMA is found to be in the emeraldine oxidation state (Hasik *et al.* 2004:341).
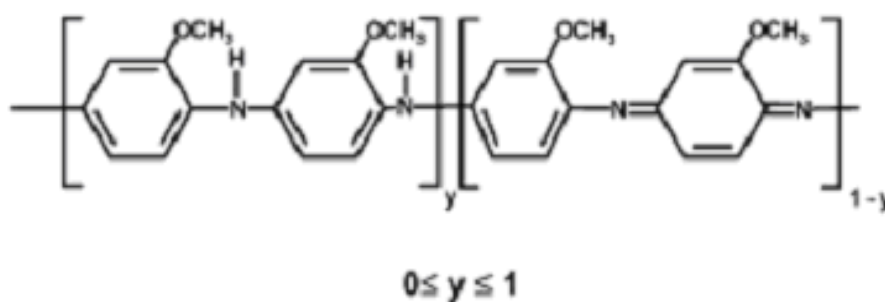
Figure 2.29 **The general formula of the POMA repeat unit with POMA being in the emeraldine oxidation state when y = 0.5 (Hasik *et al.* 2004:341).**

Interest has also been shown in PANI, POMA and other PANI-derivatives to synthesise these conducting polymers in the form of nanomaterials. The properties of PANI nanomaterials differ significantly from the properties of the corresponding macroscopic materials. A number of different methods can be used in the synthesis of conducting polymers in the micro- and nanscopic form. However, the most effective and simple techniques to form nanostructures is template synthesis. In template synthesis the desired material is obtained within a template that is subsequently dissolved to leave the material in the form of nanostructures that corresponds to the shape of the template. This technique has been investigated in the formation of PANI and POMA templates on polycarbonate membranes. This method can also be employed in the formation of conducting polymer nanotubes (Mazur *et al.* 2003:403; Tagowska *et al.* 2004:29; Delvaux *et al.* 2000:275).

More often nowadays attention is being drawn to nanoparticles to overcome the processability problems associated with polyaniline. Since the nanoparticles can be readily dispersed in aqueous media, the nanodimensional conducting polymers have also shown to exhibit unique properties such as greater conductivity and more rapid electrochemical switching speeds. Furthermore, the nanomaterials offer bulk handling solution characteristics with the material being controlled at nanoscale, and when combined with a biocomponent enables the fabrication of a sensor surface (Morrin *et al.* 2005:423; McCarthy *et al.* 2002:259).

2.5.2.1.3 Poly(2,5-dimethoxy aniline), PDMA

As described in earlier paragraphs, more work has been devoted to the study of substituted polyanilines in order to influence the optical properties of the polymer material and to enhance the solubility in organic solvents. Although substitution of PANI often results in decrease of conductivity, when aniline is substituted with two methoxy groups to form *2,5*-dimethoxyaniline (DMA), it is reported to produce a soluble polymer with conductivity similar to that of PANI. The structure of poly(*2,5*-dimethoxyaniline) (PDMA) is shown in Figure 2.30. As for PANI, the properties of its derivatives, e.g. PDMA, also depend on the synthesis conditions such as the type of supporting electrolyte, monomer concentration, applied potential, the type of solvent and pH (Palys *et al.* 2000:111; Alvial *et al.* 2004:3507; Huang *et al.* 2003:1765).
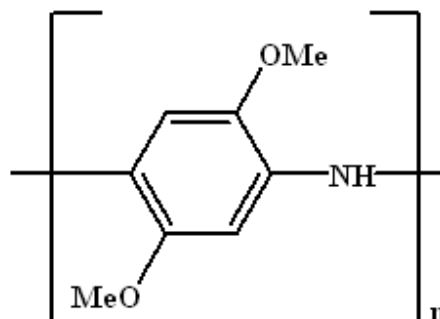
Figure 2.30   **The general formula of a single poly(2,5-dimethoxyaniline) (PDMA) unit.**

The chemistry of polyanilines is generally more complex with respect to other conducting polymers. This is due to the fact of their dependence on both the pH value and the oxidation states, described by three different forms of the polymer known as leucoemeraldine base (LB) (fully reduced form), emeraldine base (EB) (50% oxidised form), and pernigraniline base (PB) (fully oxidised form). The emeraldine base (EB) form is the most important one and its protonation by means of H^+ ions generated from protic acids gives the emeraldine salt form (ES), which is responsible for the strong increment of conducting properties. Since PDMA is more soluble and has conductivity similar to that of PANI, the anion present in the electrolyte medium influences the degradation of PDMA. In this regard PDMA has been reported to show redox transitions for leucoemeraldine to more oxidised PANI forms at lower potentials in comparison with PANI. The potential for converting PDMA to its fully oxidised state was found to be much less than in the case of PANI and has been

reported to be 0.27 V for PDMA, as compared to 0.70 V for PANI (Chen *et al.* 2003:133; Patil *et al.* 2004:57; Bavastrello *et al.* 2004:247).

Two classes of organic materials, e.g. conducting polymers and carbon nanotubes (CNTs), have gained enormous interest in recent years due to their attractive chemical and physical properties. An interesting application of both materials has seen the embedding of a little quantity of CNTs inside the PANI polymer matrix for the synthesis of nanocomposites. Recently a nanocomposite based on PDMA with embedded multiwalled carbon nanotubes (MWNTs) has been synthesised (Bavastrello *et al.* 2004:247).

2.5.3   Conducting mechanism of PANI

In section 2.5.2.1.1 it was shown that PANI exists in four different forms depending on its oxidation state (Wang and Jing 2005:154; Hao 2003:3; Mathew *et al.* 2002:141; Albuquerque *et al.* 2000:19).

The conducting mechanism of PANI is very specific since it is caused either by the oxidation of poly(leucoemeraldine base) (PLB) or by the protonation of the poly(emeraldine base) (PEB). It then undergoes a protonation/deprotonation process that is also referred to as an acid/base doping/dedoping process. This allows PANI to undergo inter-conversions among various oxidation states that are shown in Figure 2.31 (Hao 2003:5; Grzeszczuk and Szostak 2003:257-258; Laska 2004:13).
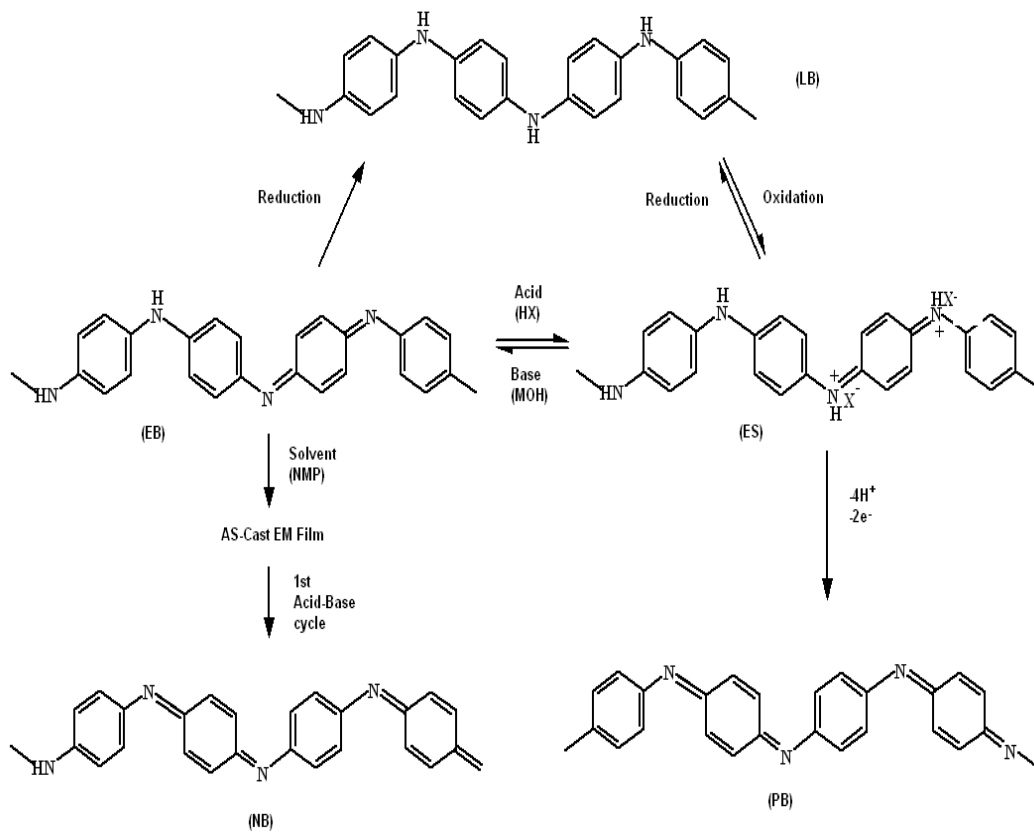
Figure 2.31   **Inter-conversions among various oxidation states and protonated/deprotonated states in PANI (Hao 2003:5).**

The increasing interest in the use of polyaniline (PANI) as a conjugated polymer stems from its uniqueness among other conjugated polymers, because its properties can be reversibly controlled by both redox doping and protonation (Tripathy *et. al.* 2002:65).

Redox activity of PANI enables variations in the relationship between the reduced amine and the oxidised imine groups in the polymer backbone, as shown in Figure 2.28. Figure 2.28 further shows that the reduced amine and oxidised imine groups of PANI results in the polymer being in three possible oxidation states, namely leucoemeraldine (LB), emeraldine (EB) and pernigraniline (PB). PANI systems are also of interest due to their ability to conduct electricity and related electrical properties. The use of protonic doping can result in a conductivity increase of the material by more than 10 orders of magnitude, from a non-conducting regime to good insulators to nearly metallic conductivity (Tripathy *et al*. 2002:66; Premvardhana *et al.* 2001:157).

If the EB form of PANI is subjected to protonic acid doping, it results in the formation of a polyelectrolyte, i.e. the polymer bearing a number of ionisable groups. The polyelectrolyte molecule can also be considered as an ideal molecular wire possessing metallic properties. Although the protonic acid doping is simple, it is not the only way of obtaining the EB based polyelectrolyte. Other few direct factors include redox-active agents, ionic salts, environmental conditions such as solvate medium, which lead to the formation of the emeraldine based polyelectrolyte chains with specific properties. Furthermore, the properties of the polyelectrolyte in a solid state are additionally affected by chain-chain interactions and therefore are sensitive to local ordering (packing) of the chains (Tripathy *et al*. 2002:66).

2.5.4   Synthesis of polyaniline, PANI

Two methods are generally used for the preparation of conducting polymers and it includes electrochemical and chemical polymerisation. Electrochemical polymerisation involves electrochemical oxidation of the corresponding monomer on the electrode surface, which is then followed by precipitation of the polymer. This method allows for the easy and well-controlled preparation of polymer films but it can only be used with conductive substrates. The second method involves chemical polymerisation using the monomer solution and a chemical oxidant (e.g. ammonium persulfate) to a more bulk-like material that is precipitated from the reaction mixture. With chemical oxidation *in situ* or electroless deposition techniques can be used to directly prepare polymeric films and it involves immersion of a solid substrate into the solution containing the corresponding monomer and oxidant. Since the monomer undergoes oxidation, the substrate will be coated with a thin film of the resulting polymer (Mazur 2005:1; Fenelon *et al.* 2005:264; Avlyanov *et al.* 1995:205; Saxena and Malhotra 2003:293; Iwuoha *et al.* 2005:929).

During the synthesis of PANI, oxidative doping can be performed by both the chemical and electrochemical method from the fully reduced state [poly(leucoemeraldine base) (PLB)] of PANI. However, the oxidative doping level in the chemical process is very difficult to control but electrochemical doping can be used to solve this problem. During electrochemical synthesis it is controlled very well by the potential applied between the working and the counter electrode. The PLB form is readily oxidised to the poly(emeraldine salt) (PES) form with the counter ions

of the electrolyte (acids) inserting in the polymer backbone, Figure 2.31 (Hao 2003:4).

A typical cyclic voltammogram (CV) of the electropolymerisation of PANI, as shown in Figure 2.32, includes two main redox couples.
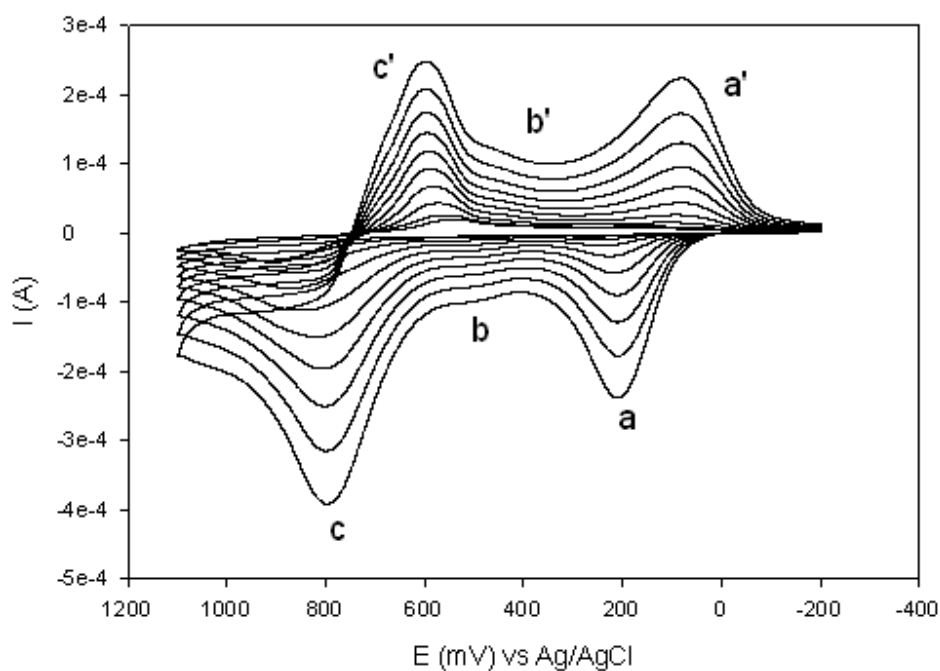
Figure 2.32   **The electropolymerisation of a PANI film in 1 M HCl on a gold (Au) electrode surface at scan rate of 40 mV/s is shown. Successive polymerisation cycles (10) are shown that corresponds to increases in thickness of the film during deposition.**

The CV in Figure 2.32 shows an anodic peak (a) at ± 0.2 V (vs Ag/AgCl) that is due to the transformation of leucoemeraldine base (LB) to emeraldine salt (ES). The second anodic peak (c) near 0.8 V (vs Ag/AgCl) corresponds to the oxidation of ES

followed by deprotonation of the polymer giving the fully oxidized pernigraniline salt (PS). On the reverse scan the reduction peak (c′) corresponds to the conversion of the pernigraniline salt (PS) to emeraldine salt (ES), while reduction peak (a′) is the emeraldine salt (ES) converted to leucoemeraldine base (LB). The middle peak (b/b′) around $\pm$ 0.5 V (vs Ag/AgCl) is essentially due to an adsorption of p-benzoquinone and hydroquinone during the growth of the polymer film (Hao 2003:6; Morrin *et al.* 2005:425-426; Mathebe *et al.* 2004:115-118).

When the conductive form of PANI is used in applications such as displays, semiconductor photo-electrode coatings and chemical sensors it is desirable to have a simple and straightforward deposition process that can produce smooth continuous conductive PANI films on a variety of different substrate materials with reproducible thickness. For such applications PANI can be deposited on smooth glass substrates from aqueous solutions of aniline and ammonium metavanadate. Ammonium metavanadate has also been used in the controlled polymerisation of aniline to deposit PANI on fabrics (Avlyanov *et al.* 1995:205).

Several oxidising agents can be used in the chemical preparation of polypyrrole, polythiophene and polyaniline from their monomers in aqueous solutions. These oxidising agents include $(NH_4)_2S_2O_8$, H_2O_2, $Ce(SO_4)_2$, $KMnO_4$, $K_2Cr_2O_7$, KIO_3, $FeCl_3$ and $Cu(ClO_4)_2 \cdot 6H_2O$. In the case of PANI deactivation or degradation of the polymer occurs when water is present in the polymerisation medium. To circumvent this problem, polymerisation in non-aqueous medium is required that will also ensure the electroactivity and stability of the polymers. The

electropreparation of polyaniline and polythiophene films in acetonitrile solutions containing anhydrous acid have been successfully demonstrated (Can *et al.* 1999:9).

Several methods (see section 2.5.2.1) and different synthesis conditions have been employed to improve the processability of PANI. The latest development reports the enzymatic synthesis of a water-soluble, electrically conducting PANI-sulphonated-polystyrene complex. With this process aniline is enzymatically polymerised in the presence of a polyelectrolyte that serves as a matrix within which the monomers align and preferentially react to form the water-soluble, electroactive PANI. This approach offers ease of synthesis, processability, electrical and chemical stability, and environmental compatibility (Wang *et al.* 1999:117).

The synthesis condictions is not only crucial in the polymerisation of PANI, but forms an essential part of the polymerisation of PANI-derivatives. In the case of *2,5*-dimethoxyaniline (DMA), it was found that it produces a soluble polymer with conductivity similar to that of PANI, while o-methoxyaniline (OMA) also produces a more soluble polymer. Notwithstanding, in the case of PANI-derivatives the synthesis conditions are also crucial and depend on the type of supporting electrolyte, monomer concentration, applied potential, the type of solvent and pH (Palys *et al.* 2000:111; Patil *et al.* 1999:298).

In recent developments attention has been drawn to the synthesis of nanoparticles that is incorporated in a polymer matrix. The synthesis of these materials combines the merits of conducting polymers and inorganic nanoparticles, since they have wide potential application in the diverse areas of chemistry, physics, electronic, optics, materials and biomedical science. It should however be noted that

conducting polymers are infusible in nature and generally insoluble in the usual solvents, and inorganic nanoparticles are easily aggregated because of their high surface energy. To synthesise these conducting polymer/inorganic nanocomposites is a big challenge since the nanoparticles are dispersed at the nanoscale in the composites. It is further made more difficult since a true nanocomposite cannot be obtained by simple blending or mixing in the melting state. One method reports the preparation of a PANI-nano-TiO_2 composite that is synthesised by encapsulating nano-TiO_2 particles through *in situ* emulsion polymerisation (Li *et al.* 2004:395).

When the dispersion of PANI is employed for the synthesis of a nanocomposite, the method of *in situ* polymerisation is superior to the post-polymerisation method. In this technique the aniline is polymerised within an aqueous acidic solution containing a suitable polymeric stabiliser in the *in situ* polymerisation method. Water soluble polymers such as poly(vinyl alcohol) (PVA), poly(vinyl pyrrolidone) (PVP), poly(acrylic acid) (PAA) and poly(styrene sulphonic acid) (PSSA) have been used as stabilisers for the *in situ* polymerisation method. After the polymerisation, stable PANI dispersions are generally obtained (Cho *et al.* 2004:15; Ge *et al.* 2005:1126).

Apart from a list of parameters, it has also been shown that the anions incorporated in the positively charged polymer during synthesis for charge compensation, have an influential effect on the growth rate, the morphology of the synthesised PANI, and the speed and extent of the electrochemical response. It therefore indicates that the growth rate of a PANI film is dependent on the type of anion. The anions can be grouped into two types, class A (BF_4^-; ClO_4^-; CF_3COO^-) and

class B (SO_4^{2-}; NO_3^-; Cl^-). The class A anions is known to promote a compact fibre-like structure, while the class B anions result in an open, granular structure Tang *et al.* 1996:1561).

2.5.5 Applications of conducting polymers

Electrosynthetic polymers have become increasingly important in the use of enzyme immobilisation matrices for biosensor preparation and applications (Iwuoha *et al.* 1997:750).

A tremendous interest in PANI (as mentioned in several previous paragraphs) exists for some time since it can be potentially applied:

➢ as antistatic agent for plastics,

➢ to produce conductive rubber and plastics composites,

➢ to produce electrochromic,

➢ in microelectronic devices,

➢ as component of electrochemical batteries,

➢ as chemical sensors in solution,

➢ in optical waveguides,

➢ as catalyst for chemical reactions,

➢ as antioxidant for rubbers and plastics,

➢ as key component in gas-sensing devices for "electronic nose"' set-ups (Cataldo and Maltese 2002:1791; Huang *et al.* 1997:1375).

PANI-based sensors and electrochromic displays proofs to the most promising among the practical applications proposed for PANI. This is due to the fact that both devices require application of electrical potential and direct contact with the active redox media that alter their properties with respect to time and their usage (Matseeva *et al.* 2001:343; Huang *et al.* 2002:155).

PANI has also received attention because of possible applications wherein PANI is used for the acceleration of redox processes taking place at the PANI electrode. To this extent PANI and its derivatives have been used as electrode materials in electrocatalytic processes. It has been showed that PANI films are effective as electro-catalysts in the anodic oxidation of both inorganic ions and hydroquinone. In the conducted studies it was found that these reactions are made possible by the fact that the redox potentials of almost all redox couples studied at PANI electrodes, are within the potential range of the conducting form of PANI, which is the emeraldine form. A more positive electrode potential exists for the emeraldine form of PANI, as compared to that of the leucoemeraldine: emeraldine transition. Furthermore, the higher electrical conductivity of the emeraldine form of PANI enables the electrode reactions to proceed at the polymer-solution interface (Malinauskas and Holze 1999:184).

The use of conducting polymers in sensor construction has been increasing and particularly polyaniline based biosensors have been reported for applications in potentiometric analysis, electrochemical studies, immunosensors and in pesticide

determination with immobilised cholinesterase (Langer *et al.* 2004:140; Mathebe *et al.* 2004:115; Iwuoha *et al.* 2005:929).

Conducting polymers for use in polymer actuators have also reveived increased attention due to their potential application in advanced robotics, artificial muscle, and new medical devices. When the actuators are based on conducting polymers such as polyaniline, polypyrrole and polythiophene, they have an added advantage of being lightweight, have a large strain and can be operated at low potentials (Li *et al.* 2004:4769).

2.5.6 Importance of conducting polymers to biosensors

Polyaniline (PANI) has been used for sensor application since it exhibits two redox couples in the convenient potential range to facilitate an enzyme-polymer charge transfer. PANI is also relatively stable and its solubility in various solvents makes it an attractive candidate for the technical development of a biosensor (Malhotra *et al.* 2005:92).

One of the limitations of PANI as a material for enzyme electrode construction is its instability at basic or neutral pH, since it loses electrochemical activiy and electronic conductivity because of the deprotonation of the nitrogen sites of the oxidised form of PANI. This can be circumvented by using PANI films that contains a polyanion as a counterion since these films are known to be electronically conductive even at a neutral and basic pH. The same argument holds for PANI-

derivatives containing anionic groups (Tatsuma *et al.* 2001:180; Yang *et al.* 2005:125).

Several types of biosensors have been developed in the last decades since conducting polymers acts as a three-dimensional matrix for the immobilisation of enzymes where reactants can be converted to products. When conducting polymers are immobilised on metal substrates they have an organised molecular structure that permits the three-dimensional structure for the immobilisation of the active catalysts and preserve their activity for long duration. This property of conducting polymers together with its functionality as a membrane has provided several opportunities for the development of sensors (Santhanam 1998:1259; Sadik 1999:839; Ngamna *et al.* 2005:85).

The electronic conducting properties and unique chemical and biochemical properties of conducting polymers have ensured that they have numerous (bio)analytical and technological applications. This further allow ease of synthesis and deposition onto a conductive surface of a given substrate from monomer solutions by electrochemical polymerisation a, with precise electrochemical control of their formation rate and thickness. Once electrodes are coated with conducting polymers under mild conditions, it opens up enormous possibilities for the immobilisation of biomolecules and bi-affinity or biorecognising reagents. The co-immobilisation of other molecules such as enzymatic co-factors or charge-transfer mediators through entrapment within the electropolymerised films or by covalent binding on these films permits the fabrication of reagentless biosensors (Vidal *et al.* 2003:93; Borole *et al.* 2006:1; Malhotra and Singhal 2003:331).

The mode of operation of a chemically modified sensor under amperometric conditions is simple in concenpt. The redox active substrate of interest reacts with the catalytically active sites immobilised in the polymer matrix rather than at the underlying support electrode. The electrocatalysis follows a three-dimensional process that is fairly effective. This enables electron transfer between the substrate and the catalytic site and the kinetics of the substrate/product transformation is normally governed by the properties of the mediating electractive polymer film. Important factors that may influence reactivity inlcude the degree of conductivity of the polymer film, the catalytic properties of the mediating sites, the nature of the interaction between the active site and substrate, and the morphology of the polymer film (Lyons *et al.* 1998:1947).

2.5.7   Immobilisation of enzymes on conducting polymers

In section 2.2.3.2.3 it was reported that the most commonly used enzyme immobilisation techniques for designing and development of specific sensors include physical adsorption, entrapment, intermolecular cross-linking and covalent binding of the biomaterial.

Although these several techniques exist for the immobilisation of enzymes, some of them suffer from drawbacks. The method of physical adsorption is known to be prone to leaching and shows instability, whereas the covalent linking technique

results in reduced activity of the biomaterial. The Langmuir-Blodgett technique is known to be an important method for the immobilisation of a desired biomolecule. With the Langmuir-Blodgett technique highly ordered and desired orientation of the enzyme molecules can be obtained (Malhotra *et al.* 2005:92).

Another technique that has been used for the immobilisation of biomolecules is the entrapment of the enzyme in the backbone of the conducting polymer in order to have the transfer of electrons between the redox centre and the polymer chain. However, this technique is not without its own problems especially in the case of PANI where the highly acidic conditions required for polymer growth are incompatible with the conditions required for entrapment of the enzyme in the growing polymer network (Georganopoulou *et al.* 2000:291; Tatsuma *et al.* 2001:180). To circumvent the problem of acidic conditions influencing the enzyme entrapment, the incorporation of a dopant such as polyvinyl sulphonate (PVS) can be used since it leads to enhanced morphology and conductivity at neutral pH (Killard *et al.* 1999:109).

2.5.8   Influence of surfactants

In section 2.5.2.1 it was described that one way to improve the solubility of PANI in organic solvents has been the use of functionalised acids as dopants. Dopants that have been commonly used include *p*-toluene-sulfonic acid (TSA),

dodecyl benzene-sulphonic acid (DBSA) and camphor-sulphonic acid (CSA). Some of the research activities that has involved the use of dopants/surfactants in the synthesis of PANI are outlined below.

Bernard *et al.* (1997:785) reported in their study that polyaniline (PANI) is a very interesting electro-chromic material that has been used in display devices and smart windows. When PANI is doped with mineral acid solutions, PANI can be protonated by a functionalised acid such as camphorsulphonic acid (CSA) and the compound then displays a remarkable stability during the electrochromic cyclings.

Cai *et al.* (1997:209) indicated that PANI is known to be easily degradable due to the over-oxidation hydrolysis in acidic electrolyte that reduces the quality and stability of the polymer film. Introducing a surfactant can provide the polymer a hydrophobic micro-effect with a controlled electrochemical catalysis, effecting the orientation and solubilisation due to the formation of micelles, thereby greatly improving the quality of the polymer films. They have further found that the use of camphor sulphonic acid (CSA) increased the conductivity of the PANI film, while the use of dodecyl benzenesulphonic acid (DBSA) produced PANI with higher quality and reduced disorder.

Cataldo and Maltese (2002:1791) also found in their study that the solubility and processability of PANI can be improved by the use of dopants such as camphor sulphonic acid (CSA), dodecyl benzensulphonic acid (DBSA) or alkylene phosphates. This resulted in the PANI being more conductive and it was possible to cast films of doped PANI or to grow films on opportune substrates by spinning.

Rannou *et al.* (1999:827) have found in their study that processible PANI with metallic type conductivity can be prepared by solution using a three component system comprising of PANI, camphor sulphonic acid (CSA) and *m*-cresol (MC). The results have shown that both the solutions of PANI-CSA in *m*-cresol and the films cast from solution, exhibit spectral properties characteristic of strongly delocalised charge carriers, indicative of metallic type behaviour.

In a study by Huang *et al.* (2002:155) they have also employed functional acids as dopants to improve the stability of PANI. They have used *p*-toluene-sulphonic acid (TSA), camphor sulphonic acid (CSA) and dodecyl benzensulphonic acid (DBSA) with a substituted aniline of *2*-methoxyaniline (*o*-anisidine) to improve solubility. The results have further shown that the substituent groups present in the units of the polymer chain caused a decrease in the stiffness of the polymer chain and resulted in better solvation. However, with the substituted aniline they have observed a decrease in conductivity noticed for polymers of substituted anilines with substitution in the phenyl ring or *N*-position. When aniline have two substituted methoxy groups as with *2,5*-dimethoxyaniline (DMA), a more soluble polymer of poly(*2,5*-dimethoxyaniline) (PDMA) is obtained, with a conductivity similar to PANI. Huang *et al.* (2003:1765) have indicated in another study that the improvement in the solubility with the use of the dopants can also be attributed to the polar nature of the substituents, which promote compatibility between the polymer and the solvent.

2.6   Acetylcholinesterase (AChE) as enzyme

2.6.1   Introduction

The enzyme called acetylcholinesterase (AChE) is an essential enzyme for nerve tissue. The principal biological role of AChE is to terminate the synaptic signal by catalysing the hydrolysis reaction of the neurotransmitter acetylcholine (ACh), after it has been released at cholinergic synapses. AChE is further considered as one of the fastest known enzymes with a high turnover number. In terms of its molecular structure, the enzyme monomer is an α/β protein and consists of a large central mixed β-sheet surrounded by 15 α-helices. The enzyme can be found in two major forms, e.g. asymmetric and globular form. The asymmetric form is further characterised by the presence of a collagen-like tail, while the globular form is heterogeneous. The globular form can be amphiphilic and non-amphiphilic depending on the basis of their capacity to associate with micelles (Dziri *et al.* 1998:56; Johnson *et al.* 2003:38948; Aslanian *et al.* 1995:37).

It is further said that acetylcholine (ACh) and its metabolite choline (Ch) are neurotransmitters and play important roles in brain chemistry. These two neurotransmitters participate in various functions that include learning and memory formation, development and maintenance of addiction. This makes the determination of ACh and Ch very important from a clinical perspective and their determination are based on the following enzyme reactions:

$$\text{ACh } + \text{ H}_2\text{O} \xrightarrow{\text{AChE}} \quad \text{Acetate } + \text{ Ch} \qquad\qquad \text{Eqn. 2.57}$$

$$\text{Ch } + \text{ O}_2 \xrightarrow{\text{ChOD}} \quad \text{betaine aldehyde } + \text{ 2 H}_2\text{O}_2 \qquad\qquad \text{Eqn. 2.58}$$

These two reactions in equations 2.57 and 2.58 indicate that the current generated by the oxidation of hydrogen peroxide is linearly related to Ch, while ACh is converted to Ch enzymatically using the enzyme AChE and the oxidation current is turn proportional to ACh (Yang *et al.* 2005:205; Martorell *et al.* 1997:305; Brochier *et al.* 2001:18296).

Acetylcholinesterase (AChE; EC. 3.1.1.7) and its sister compound butyrylcholinesterase (BuChE; EC. 3.1.1.8) are serine esterases that belongs to the same protein family. Both these enzymes are inhibited by organophosphate and carbamate pesticide compounds that can cause severe poisoning. AChE is also thought to exert non-cholinergic functions, particularly in neural development, while no clear physiological function bas been assigned to BuChE. BuChE seems to play a non-cholinergic role in neurogenesis and neural disorders. AChE and BuChE can be distinguished functionally, primarily on the basis of substrate specificity. It is known that AChE hydrolyses ACh much faster than other choline esters (e.g. propionylcholine) and is vitually inactive on butyrylcholine (BuCh), while on the other hand BuChE not only hydrolyses BuCh well, but also ACh at an appreciable rate (Masson *et al.* 1998:41; Masson *et al.* 2002:313; Sfiez-Valero and Vidal 1996:210 ; Forget *et al.* 2002:85; Nieto-Cerón *et al.* 2004:129).

The original substrate for AChE and BuChE (e.g. acetylcholine and butyrylcholine) can be substituted with the electroactive substrates of acetylthiocholine (ATCh) and butyrylthiocholine (BTCh), which are hydrolysed in the same proportion as Ch to produce thiocholine and the corresponding carboxylic acid. These reactions will take place on the surface of the biosensor that features AChE or BuChE and since thiocholine is electroactive, it is commonly incorporated into amperometric biosensors. The reactions between thiocholine and the enzyme cholinesterase (ChE) are as follows (Martorell *et al.* 1997:305; Komersov *et al.* 2005:353).

thiocholine ester + H$_2$O $\xrightarrow{\text{ChE}}$ thiocholine + carboxylic acid   Eqn. 2.59
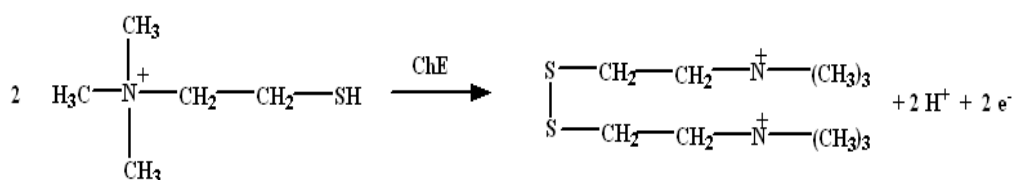
Eqn. 2.60

As indicated in the above paragraphs, AChE plays a key role in cholinergic transmission in mammals and the enzyme effectively terminates the chemical impulse at rates that are similar to a diffusion-controlled process allowing a rapid and repetitive response. AChE is inhibited by organophosphate and carbamate pesticide compounds, which interfere with the aforementioned process and this may lead to a

severe impairment of nerve functions or even death. It is also for this reason that insect AChE is the biological target of predominant insecticides used in agriculture. Although the AChE inhibitors are useful, they pose severe environmental and health risks at the same time. Therefore a growing interest in faster and more sensitive detection systems for these compounds (Schulze *et al.* 2003:201; Singh *et al.* 1999:703; Forget *et al.* 2002:85; Silva Filho *et al.* 2004:247).

AChE is also the topic of study in the fields of Pharmacology and Medicine. The reason for this is the interest in Alzheimer's disease (AD), where the loss of cholinergic neurotransmission in the brain contributes to the salient cognitive and behavioural disturbances. In the treatment of AD, several AChE inhibitors have successfully reached the market, which include tacrine, donepezil and rivastigmine (Darvesh *et al.* 2005:211; Tezer 2005:133; Toda *et al.* 2003:1935; Giacobini 2004:433; Bolognesi *et al.* 2003:917).

2.6.2   Structure of AChE

The structure of AChE has been studied to understand the structural basis of the high catalytic efficieny of AChE. With the technique of X-ray crystallography it was revealed that AChE has a narrow active site gorge some 20 Å deep with two separate ligand binding sites.

The acylation site (A-site) at the bottom of the gorge contains residues involved in a catalytic triad (His-447, Glu-334, and Ser-203) as well as Trp-86, which orientates the trimethylammonium group of acetylcholine prior to hydrolysis. The peripheral site (P-site) consists of a binding pocket near the surface of the enzyme at the mouth of the gorge and specifically binds certain ligands like the neurotoxin fasciculin and the fluorescent probes propidium and thioflavin T (Johnson *et al.* 2003:38948; Masson *et al.* 2002:313; Jung *et al.* 2003:65).

A three-dimensional view of the active center gorge of mammalian acetylcholinesterase is shown in Figure 2.33 (Carlacci *et al.* 2004:143):
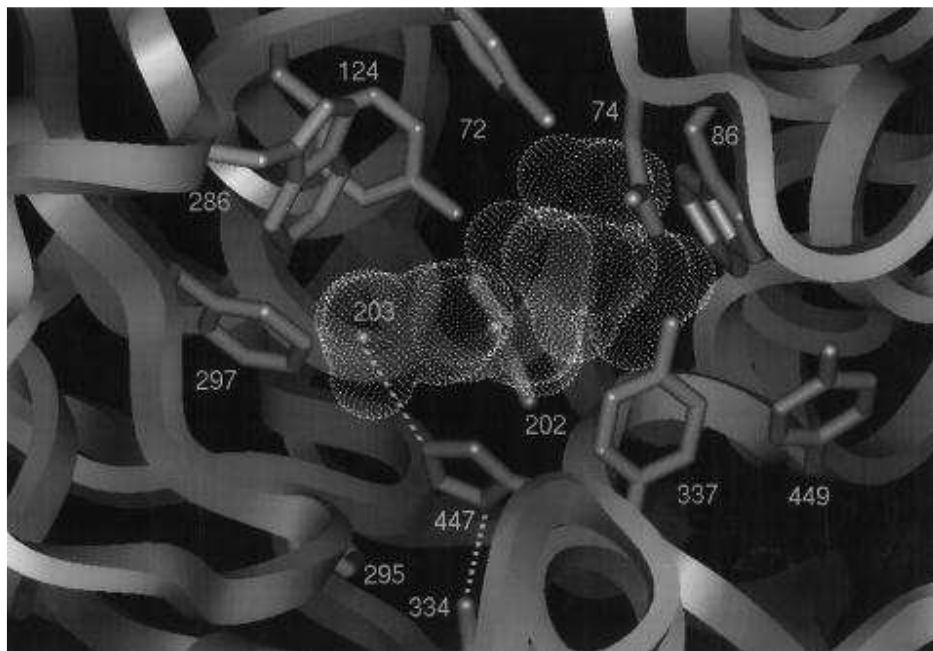
Figure 2.33   **View of the active center gorge of mammalian acetylcholinesterase (Carlacci *et al.* 2004:143).**

When the active centre gorge of mammalian AChE in Figure 2.33 is viewed, the following characteristics will be applicable:

➢ The gorge is 18 to 20 Å in depth in a molecule of 40 Å diameter and is heavily lined with aromatic amino acid side chains.

➢ Side chains from several sets of critical residues are shown emanating from the α carbon of the α carbon-amide backbone.

➢ A catalytic triad between Glu 334, His 447 and Ser 203 is shown by dotted lines to denote the hydrogen-bonding pattern.

➢ This renders Ser 203 more nucleophilic to attack the carbon of acetylcholine (shown in white with the van der Waals surface).

➢ This leads to formation of an acetyl enzyme, which is deacetylated rapidly.

➢ The acyl pocket outline by Phe 295 and 297 is of restricted size in acetylcholinesterase. In butyrylcholinesterase, these side chains are aliphatic, increasing the size and flexibility in the acyl pocket.

➢ The choline subsite lined by the aromatic residues Trp 86, Tyr 337 and Tyr 449 and the anionic residue Glu 202.

➢ A peripheral site which resides at the rim of the gorge encompasses Trp 286, Tyr 72, Tyr 124 and Asp 74. This site modulates catalysis by binding inhibitors or, at high concentrations, a second substrate molecule (Carlacci *et al.* 2004:143; Lin *et al.* 1999:2683; Toda *et al.* 2003:1940; Khalid *et al.* 2004:1995; Stojana *et al.* 2004:53; Krasinski *et al.* 2005:6686).

Another view of the center of the AChE enzyme is provided in Figure 2.34.
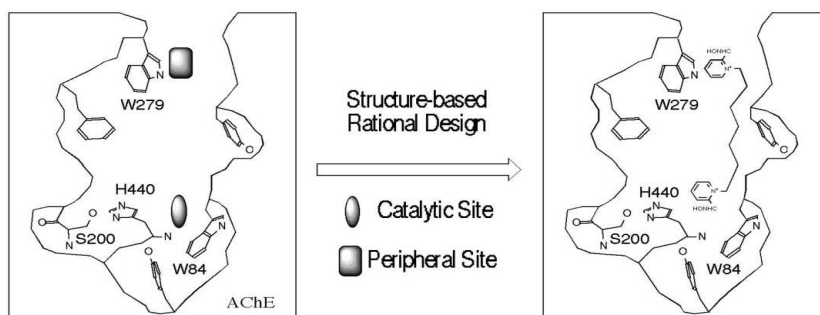
Figure 2.34 **Diagrammatic representation of catalytic and peripheral sites in human AChE (hAChE), (Pang *et. al.* 2003:499).**

In Figure 2.34 it can be seen that a catalytic site and a peripheral site in the enzyme gorge can be identified (Pang et al. 2003:499).

When the above structures of AChE are viewed, it provides evidence for the fact that at the synapse and neuromuscular junction the entire course of signal transmission, which is the release of acetylcholine (ACh), its diffusion across the synaptic cleft, its reversible interaction with the nicotinic ACh receptor and finally the hydrolysis by acetylcholine (AChE), occurs within a few milliseconds (Silman and Sussman 2005:293; Johnson and Moore 2004:448).

2.6.3   Acetylcholine (ACh) as substrate

Acetylcholine (ACh) is said to be one of the first neurotransmitters to be discovered. The chemical structure of the compound and the reaction with the enzyme AChE (see also section 2.6.1) is shown in Figure 2.35 (Yang *et al.* 2005:205; Martorell *et al.* 1997:305):
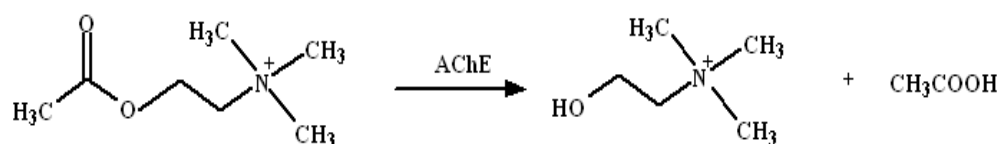
Figure 2.35   Chemical structure of acetylcholine and the hydrolysis reaction with acetylcholinesterase Yang *et al.* 2005:205; Martorell *et al.* 1997:305):

Importantly, acetylcholine is metabolised into choline and acetic acid in the presence of acetylcholinesterase, as shown in Figure 2.35 (Yang *et al.* 2005:205; Martorell *et al.* 1997:305).

Acetylcholine can be produced synthetically by using the enzyme choline acetyltransferase, which uses acetyl co-enzyme A and choline as substrates for the formation reaction. Another route consists of using dietary choline and phosphatidylcholine as the sources of free choline for acetylcholine synthesis (Messer 2000:1).
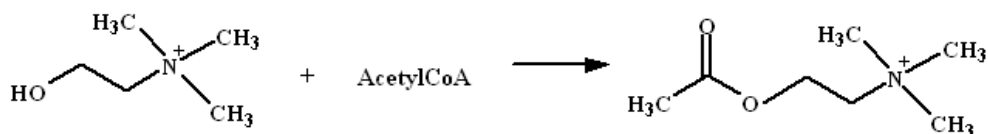
Figure 2.36   **Chemical reaction representation of acetylcholine synthesis (Messer 2000:1).**

2.6.4   Interaction between AChE enzyme and ACh as substrate

AChE as an enzyme is also a biological catalyst. It therefore increases the rate of the chemical reaction in which it is involved, without being consumed during the chemical reaction. AChE as an enzyme is also highly specific with respect to the reaction being catalysed. The reaction catalysed by AChE is shown in Figure 2.37. In Figure 2.37 below the binding of ACh to the active site of AChE and the catalysis at the active site in the enzyme gorge is shown.
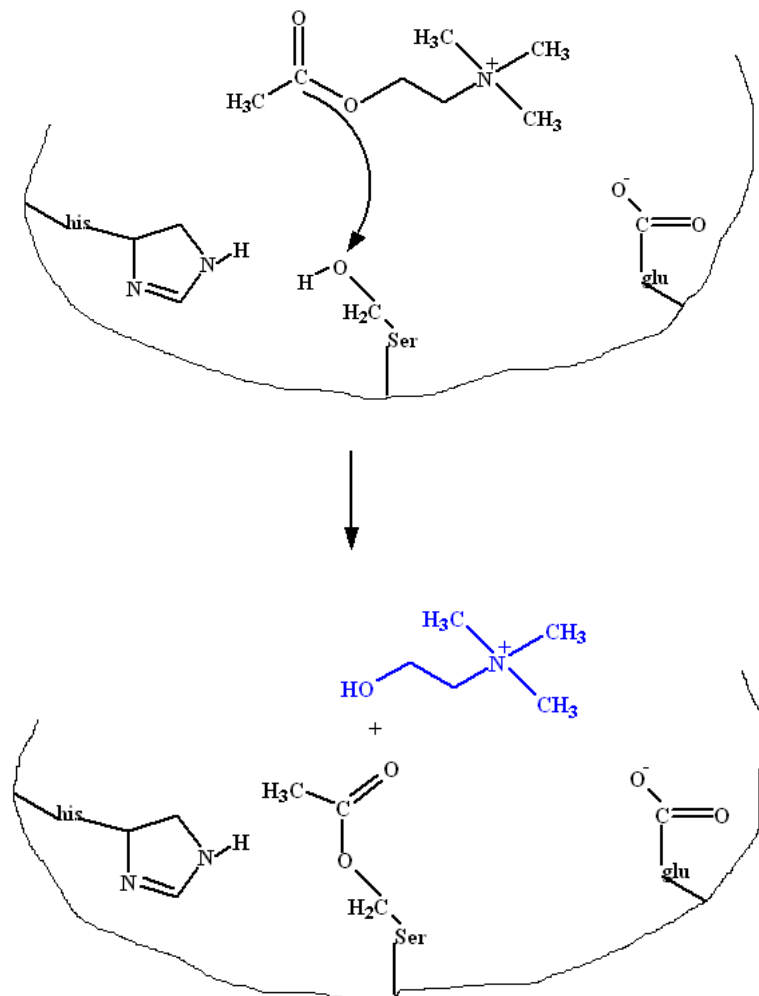
Figure 2.37   **Binding of ACh to the active site of AChE and the catalysis at the active site in the enzyme gorge (Wasilewski 2005:1).**

In Figure 2.37 it can be seen that the amino side chains of AChE play an important role in forming the enzyme-substrate complex and more directly in the catalytic process. The first step involved in any enzyme catalysed reaction is the binding of the substrate to the active site of the enzyme. This is facilitated by the interactions

between the substrate and the amoni-acyl side chains of the enzyme. This often involves non-covalent interactions and includes electrostatic attractions, hydrogen bonding and van der Waal's attractions (Wasilewski 2005:1). The negatively charged residues can interact favourably with the positively charged amino group. In AChE the histidine residue is near the serine residue and may stabilise the conformation of the active site via hydrogen bonding. In fact the activity of the enzyme is pH dependent with maximum activity at a pH value consistent with the pKa value of the histidine residue. In addition to amino acid residues involved in the formation of the enzyme-substrate complex, there are also those involved more directly in the catalysis. When the serine residue located at the active site is viewed, it can be seen that it contains a nucleophilic hydroxyl group that reacts with the acyl carbon on acetylcholine. This leads to the serine being acylated and the choline leaving the group (Wasilewski 2005:1).

In Figure 2.38 a more detailed mechanism of the bond formation and cleavage in the reaction between ACh and AChE is shown.
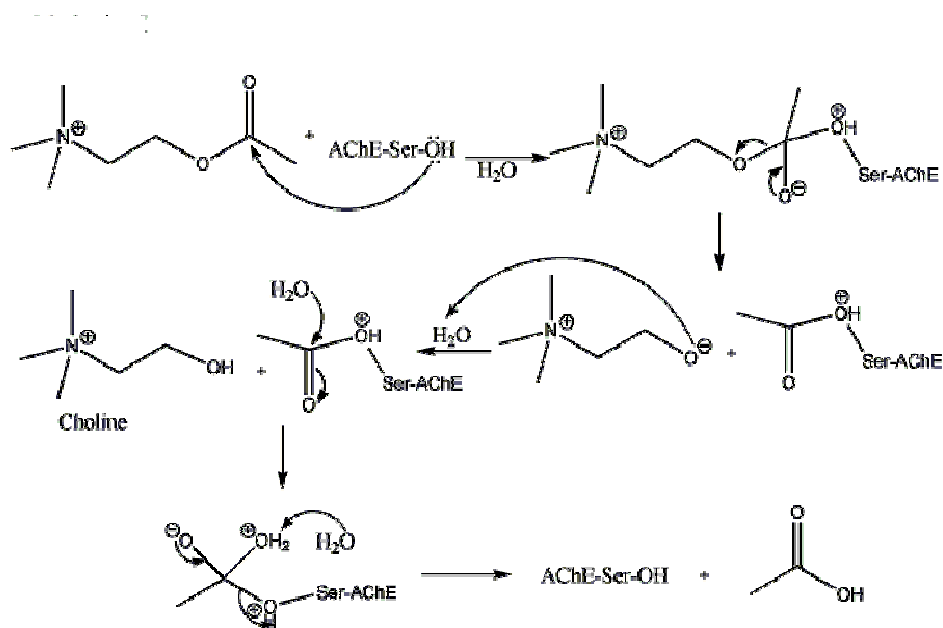
Figure 2. 38   **The detailed reaction mechanism showing the bond formation and cleavage between AChE and ACh (Glaser et al. 2005:7346).**

The mechanism in Figure 2.38 indicates that the electron pair of the hydroxyl group in AChE reacts with the carbonyl group of acetylcholine. This leads to the formation of choline with an acetate molecule attached to AChE molecule. The O-atom of the water molecule then reacts with the carbonyl group of the acetate molecule attached to AChE, which then leads to the formation of acetic acid while the AChE enzyme molecule is reformed (Glaser *et al*. 2005:7346; Ekholm 2004:28).

In any enzyme catalysed reaction, the enzyme is not consumed during the course of the reaction, therefore it must be regenerated before the reaction is complete. In Figure 2.39 the acetylated serine residue must be hydrolysed before the reaction is complete and then the enzyme is capable of catalysing a new reaction.
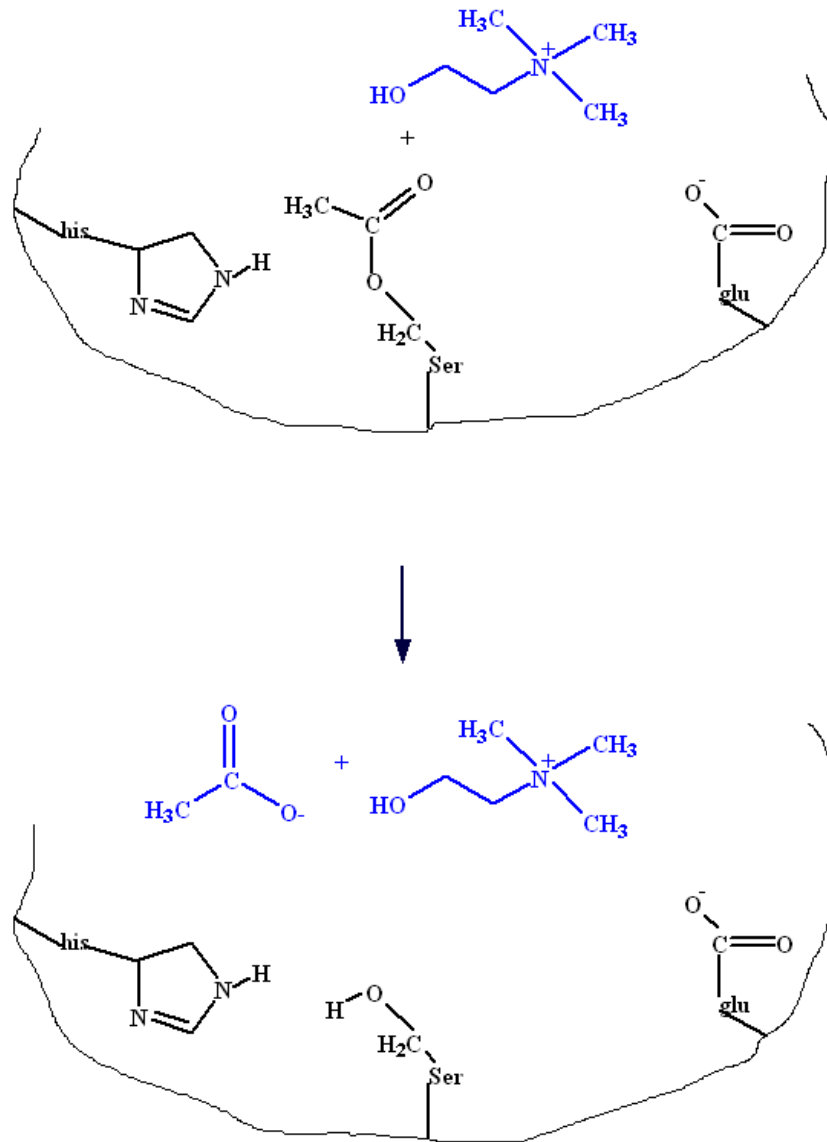
Figure 2.39   **Hydrolysis of acetylated serine residue and AChE enzyme regeneration (Wasilewski 2005:1).**

Figure 2.39 also shows that as a result of the hydrolysis of the acetylated serine residue, acetate is formed. Once the choline and acetate have diffused from the active site, the AChE enzyme is capable of binding more substrate and repeating the catalysis reaction (Wasilewski 2005:1; Chouteau *et al.* 2005:273; Schuvailo *et al.* 2005:87).

2.6.5   Interaction between AChE and organophosphates and carbamates

When AChE is attacked by inhibitors they target two target sites on the enzyme, which is the active site and the peripheral site on the enzyme. When inhibitors attack the active site of AChE, they prevent the binding of a substrate molecule, or its hydrolysis by reacting irreversibly with the catalytic serine as in the case of organophosphates and carbamates pesticide compounds (Simon *et al.* 1999:27740; Pond and Coyne 1996:363).

The most important chemical reactions between the AChE enzyme and the organophosphate pesticide compound, take place directly at the phosphorous atom. The P-X bond is easily broken by a nucleophilic reagent, such as water or hydroxyl group. The organophosphorous compound acts by binding to the acetylcholine binding site. It then transfers a phosphate group to the hydroxyl group of the AChE enzyme. The phosphorylated AChE enzyme is no longer capable of hydrolyzing

acetylcholine and due to the strength of the P-O bond, since the phosphate ester is very stable (Glaser *et al.* 2005:7348; Simon *et al.* 1999:27740).

In Figure 2.40 the reaction mechanism showing the bond formation and cleavage between the AChE enzyme and an organophosphate pesticide is illustrated (Glaser *et al.* 2005:7348).
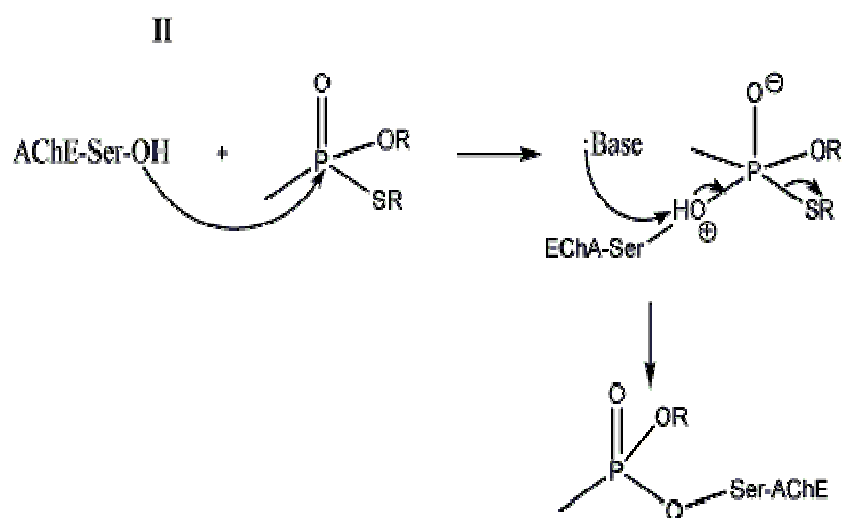
Figure 2.40 **Reaction mechanism for the reaction between the AChE enzyme and an organophosphate pesticide (Glaser et al. 2005:7348).**

Inhibitors are classified as substances that interact with an enzyme and result in a decrease in the enzyme activity. Furthermore, inhibitors can be classified as reversible or irreversible, depending on the lifetime of the enzyme-inhibitor complex. Organophosphates are classified as irreversible inhibitors, which react with the serine residue at the active site of AChE and remain attached. A similar reaction occurs with

the carbamates, but the reaction is not as long-lived as for organophosphates (George *et al.* 2003:45512).

In the top section of Figure 2.41 it can be seen that in the case of the organophosphates, the nucleophilic hydroxyl group of the serine residue located at the active site of AChE, reacts with the P-atom of the organophosphate. This results in a covalently bound organophosphate (Wasilewski 2005:1).

The bottom section of Figure 2.41 shows the same nucleophilic hydroxyl group reacting with the carbonyl carbon of the carbamates, resulting in a covalently bound carbamate, similar to the reaction obtained when acetylcholine is used. This results in inactivation of the enzyme since the hydroxyl group is no longer available to attack the acetylcholine substrate (Wasilewski 2005:1).
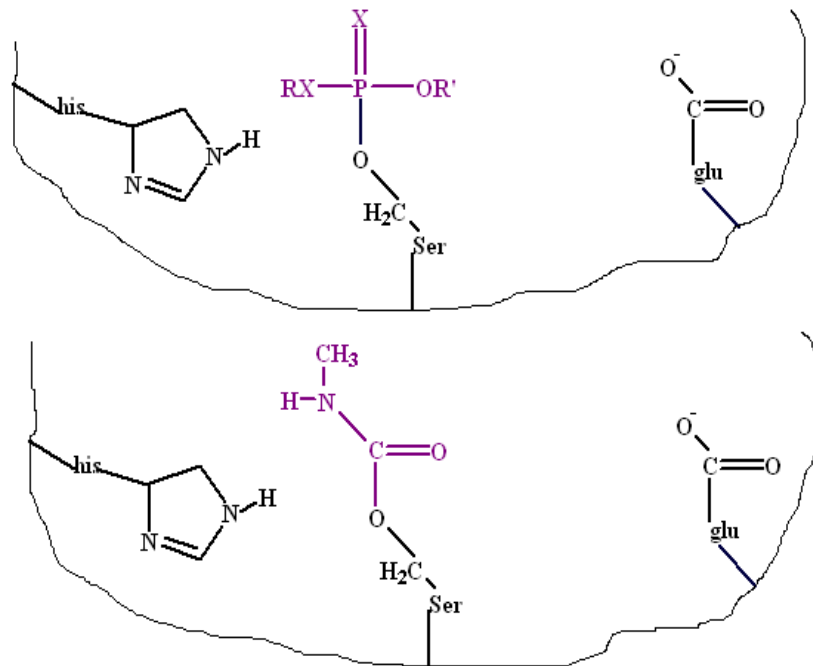
Figure2.41   **In the diagram the top section shows the covalently linked organophosphate and in the bottom part the carbamate compound, as it is linked to the serine residue of AChE (Wasilewski 2005:1).**

It should be noted that organophosphates and carbamates can also inhibit the AChE in non-target organisms, including mammals. Their acute toxicity to mammals is due to their effect on the nervous system of animals (Wasilewski 2005:1; Worek *et al.* 1999:73; Schuh *et al.* 2002:176).

2.6.6   AChE in Biosensors

Biosensors that are aimed at the detection and measurement of organophosphorus and carbamate pesticides will contain acetylcholinesterase (AChE) or butyrylcholinesterase (BuChE) as the biological component. The use of organophosphorus and carbamate pesticides are widespread in agriculture because they are less persistent in the environment than organochlorides such as DDT, aldrin, lindane, etc. (Martorell *et al.* 1997:305).

Some of the different approaches and techniques that have been reported in the development of AChE biosensors are discussed and listed below.

In the work done by Pandey *et al.* (2000:109) graphite paste electrodes were constructed that contained a mediator and immobilised choline oxidase (ChO) and acetylcholinesterase (AChE). Acetylthiocholine (ATCh) was used as substrate that was recognised by AChE to detect organophosphorous compounds based on the percent inhibition principle in the presence of these pesticides.

Varfolomeyev *et al.* (2002:2311) reports the construction of amperometric biosensors to detect neurotoxins (including organophosphorous and carbamate pesticides) by use of multi-enzymatic systems that contain cholinesterase (ChE) and choline oxidase (ChO). Butyrylcholinesterase (BChE) was used and the inhibition of this enzyme was proportional to the quantity of neurotoxins in the sample. In the sensor BChE activity was detected in accordance with the rate of appearance of hydrogen peroxide as a result of multi-enzymatic transformation of the substrate called butyrylcholine (BuCh).

The work done by Choi *et al.* (2001:937) reports the development of an improved fibre-optic biosensor for the simple and direct detection of organophosphorous compounds. No measurment of pH change was required but the sensor still consisted of an AChE immobilised Langmuir-Blodgett film. The sensor further used the substrate *o*-nitrophenyl acetate that is converted into a yellow product *o*-nitrophenol, by the enzyme activity of AChE. The hydrolysis of the substrate by AChE is complete, but in th epresence of an inhibitor, the amount of yellow product is reduced. This is measured in terms of change in absorbance and with different amounts of yellow product formed, it can be related to the amount of organophosphorous compound detected.

Sotiropoulou and Chaniotakis (2005:199) constructed an amperometric biosensor for the detection of organophosphorous pesticides based on nanoporous carbon nanostructures used as the enzyme immobilisation matrix. The adsorption of organic compounds such as pesticides onto activated carbon surfaces is a well-known phenomenon and in this sensor construction the carbon matrix was also used as the sensor transducer, since its resistance is very low, while it maintains a high surface area. Furthermore, since the sensor design protocol does not require the use of any organic matrices that would passivate the electrode surface, the nanostructure of the carbon aided the stabilisation of the enzymes.

In another study by Sotiropoulou *et al.* (2005:2347) genetically engineered AChE was used to improve the analytical characteristics of the corresponding constructed biosensor. The genetically engineered enzyme showed impressive

improvements in the development of inhibitor biosensors and delivered a biosensor

that has a very low detection limit for the pesticide called dichlorvos.

Andreescu *et al.* (2002:171) reports the construction of new immobilisation

processes for the development of AChE screen-printed sensors. Three different

immobilisation methods have been used and in the first approach AChE was

immobilised in a PVA-SbQ photopolymer for pesticide detection. In the second

approach the AChE was encapsulated in a sol-gel matrix, while in the third approach

the AChE was immobilised by metal-chelate affinity. For each approach the

parameters of operational and storage stability, linear range, sensitivity and response

time have been investigated.

Bucur *et al.* (2005:195) reports the construction of disposable screen-printed

electrodes (SPEs) that were modified with cobalt phtalocyanine to mediate the

oxidation of thiocholine, which is the product of the enzymatic hydrolysis of the

substrate acetylthiocholine. In this sensor the oxidation current of the thiocoline is

proportional to the activity of the immobilised AChE and this sensor was then used to

detect omethoate as a model organophosphorous analyte.

The work of Ivanov *et al.* (2002:75) reports the construction of polyaniline-

modified electrodes that were used in the construction of cholinesterase (ChE)

sensors for the detection of enzyme inhibitors such as organophosphorous and

carbamate pesticides. The electrodes were constructed by using the drop-coating

method with a 0.5 % polyaniline (PANI) solution in chloroform that contained the

dopant camphorsulphnic acid (CSA) as well as phenol and was left to dry at room

temperature. Acetylcholine iodide (AChI) was used as substrate to facilitate the hydrolysis reaction with ChE.

Gulla *et al.* (2002:133) constructed an amperometric biosensor for organophosphorus pesticide detection by using reactivation of the immobilised acetylcholinesterase in the biosensor. This was done since there exists a serious problem with the reuse of these pesticide biosensors due to the strong inhibition of the AChE enzyme by the organophosphorus pesticides. To overcome the problem of irreversible enzyme inhibition in the application of AChE-based biosensors, reactivation of the enzyme by oximes was proposed and investigated. Since the inhibition of AChE by organophosphorus pesticide occurs by binding of the phosphoryl group of the pesticide molecule to the serine group present in the active site of the enzyme, this problem can be overcome by using oximes that are nucleophilic compounds, able to remove the phosphorous group bound to serine in the active center of AChE.

Nunes *et al.* (2004:107) have constructed disposable screen-printed electrodes with *7,7,8,8*-tetracyanoquinodimethane (TCNQ) as mediator in graphite paste that facilitates the electrochemical oxidation of thiocholine at 100mV (vs. Ag/AgCl). Different techniques for AChE immobilisation in the TCNQ mediator were investigated and the AChE behaviour in these different set-ups were evaluated and compared.

2.6   Pesticides

Pesticides (herbicides, fungicides, insecticides) are considered to be one of the principal classes of environmental pollutants throughout the world and millions of tonnes are used annually in agriculture, medicine and industry. Pesticides can also be carcinogenic, citogenic and are able to produce bone marrow diseases, infertility, as well as immunological and respiratory diseases (Pogačnik & Franko 1999:569; Nunes *et al.* 1999:37; Albareda-Sirvent *et al.* 2001:35).

Organophosphorous and carbamate pesticide compounds have been widely used in the agricultural industry as pesticides and insecticides. These two pesticides have low environmental pesistence and high effectiveness but they exhibit high acute toxicity in humans. These pesticides further act by inhibiting the enzyme acetylcholinesterase (AChE) that results in accumulation of acetylcholine (ACh) at cholinergic receptor sites, causing excessive stimulation of cholinergic receptors. It is therefore important to find sensitive, rapid and reliable techniques for the determination of these pesticide compounds, in order to protect the environment and human health (Karousos *et al.* 2002:189; Del Carlo *et al.* 2004:651; Vakurov *et al.* 2004:1118; Fedosseeva *et al.* 2000:55).

2.6.1   Organophosphates

2.6.1.1 Introduction

Organophosphate pesticides account for about half of the insecticides used in most developed countries. A large number of organophosphate pesticides metabolise to dialkyl phosphate metabolites and other specific metabolites. There are six dialkyl phosphate metabolites; each of these can be produced from the metabolism of more than one organophosphate pesticide (Glaser 2000:1-3; Sogor and Vilanov 2002:215).

The   general   formula   for   the   dialkylphosphate   metabolites   of organophosphorous pesticides can be represented as follows:
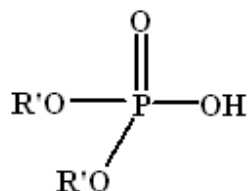
Figure 2.42   **General formula for the dialkylphosphate metabolites of organophosphorous pesticides, where R' can be methyl or ethyl substitutes (Glaser 2000:1-3).**

A breakdown of the different metabolites of organophosphorous pesticides and their common names are shown in Table 2.1.

Table 2.1 **Examples of the six different metabolites of organophosphorous pesticides, its chemical structure and common names are shown (Glaser 2000:1-3).**

Alkyl phosphate group	Chemical structure	Common or other names
Dimethylphosphates (DMP)	$(MeO)_2$-P(O)-OH	Azinphos-ethyl Azinphos-methyl Chlorpyrifos methyl Chlorpyrifos DDVP (Dichlorvos) Dimethoate Fenitrothion Malathion Methyl Parathion Trichlorfon Bromophos-ethyl
Dimethylthiophosphates (DMTP)	$(MeO)_2$-P(S)-OH	Azinphos-methyl Chlorpyrifos methyl Fenthion Malathion Methyl parathion
Diethylphosphates (DEP)	$(EtO)_2$-P(O)-OH	Chlorpyrifos Diazinon Ethion Parathion Terbufos
Diethylthiophosphates (DETP)	$(EtO)_2$-P(S)-OH	Chlorethoxyphos Chlorpyrifos Disulfon Ethion Parathion
Dimethyldithiophosphates (DMDTP)	$(MeO)_2$-P(S)-SH	Azinphos methyl Dimethoate Malathion Methidathion Phosmet
Diethyldithiophosphates (DEDTP)	$(EtO)_2$-P(S)-SH	Disulfon Ethion Phorate Terbufos

The general formula for the dialkylthiophosphate metabolites of organophosphorous pesticides can be can be represented as follows:

$$
\begin{array}{c}
\text{S} \\
\parallel \\
\text{R'O}\!-\!\text{P}\!-\!\text{OH} \\
\diagup \\
\text{R'O}
\end{array}
$$
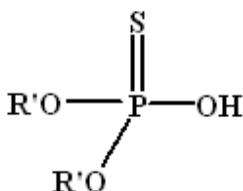
Figure 2.43   **General formula for the dialkylthiophosphate metabolites of organophosphorous pesticides, where R' can be methyl or ethyl substitutes (Glaser 2000:1-3).**

The general formula for the dialkyldithiophosphate metabolites of organophosphorous pesticides can be represented as follows:

$$
\begin{array}{c}
\text{S} \\
\parallel \\
\text{R'O}\!-\!\text{P}\!-\!\text{SH} \\
\diagup \\
\text{R'O}
\end{array}
$$
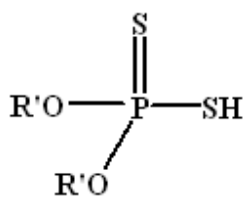
Figure 2.44   **General formula for the dialkyldithiophosphate metabolites of organophosphorous pesticides, where R' can be methyl or ethyl substitutes (Glaser 2000:1-3).**

Organophosphate pesticides act by interfering with the transmission of signals in the nervous systems of both insects and humans, if humans are exposed in high enough amounts of the pesticides. Organophosphate pesticides injure and even kill large numbers of people around the world every year, and have been associated with chronic nervous system damage in people who survive poisoning (Glaser 2000:1-3; Worek *et al.* 2004:2237).

2.6.1.2 Nature and effects of organophosphates

Most organophosphates are insecticides although a few are listed as organophosphate pesticides. Organophosphates were developed during the early 19th century, but their effects on insects, which are similar to their effects on humans, were discovered in 1932. Some are very poisonous (used in World War II as nerve agents) but they are usually not persistent in the environment (Glaser 2000:1-3; Varfolomeyev *et al.* 2002:2311; WHO 1986a:39).

Organophosphates affect the nervous system by reducing the ability of an enzyme called cholinesterase (ChE), to function properly in regulating a neurotransmitter called acetylcholine (ACh). Acetylcholine helps transfer nerve impulses from a nerve cell to a muscle cell or another nerve cell. If acetylcholine is not properly controlled by cholinesterase, the nerve impulses or neurons remain active longer than they should. Over stimulating the nerves and muscles and causing

symptoms such as weakness or paralysis of the muscles (Glaser 2000:1-3; Kato *et al.* 2004:64; Ali *et al.* 2005:58; WHO 1986b:58).

2.6.2 Carbamates

2.6.2.1 Introduction

The carbamates referred to in this study are that mainly used in agriculture, as insecticides, fungicides, herbicides, nematocides, or sprout inhibitors. Furthermore, they are used as biocides for industrial or other applications and in household products. These chemicals are part of the large group of synthetic pesticides that have been developed, produced, and used on a large scale in the last 40 years (WHO 1986c:1).

The general formula for the carbamates (where R^1 and R^2 are alkyl or aryl groups) as pesticides is as follows:

$$R^1HN - \overset{\overset{\displaystyle O}{\|}}{C} - OR^2$$
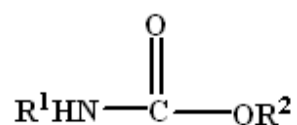
Figure 2.45   **General .formula for the carbamates as pesticides (WHO 1986:1).**

More than 50 carbamates are known to date. It consists of three classes of carbamate pesticides that can be divided into (WHO 1986c:2):

I)   The carbamate ester derivatives, used as insecticides (and nematocides), which are generally stable and have a low vapour pressure and low water solubility.

II)   The carbamate herbicides (and sprout inhibitors) which have the general structure $R^1NHC(O)OR^2$, in which R^1 and R^2 are aromatic and/or aliphatic moieties.

III)   On the other hand, the carbamate fungicides contain a benzimidazole group.

2.6.2.2 Physical and Chemical Properties

Generally simple esters or *N* -substituted derivatives of carbamic acid are unstable compounds, especially under alkaline conditions. Decomposition takes place, and the parent alcohol, phenol, ammonia, amine, and carbon dioxide are formed. The salts and esters of substituted carbamic acid are more stable than carbamic acid. This enhanced stability is the basis for the synthesis of many derivatives that are biologically active pesticides (WHO 1986d:1).

Carbamate ester derivatives are crystalline solids of low vapour pressure with variable, but usually low, water solubility. They are moderately soluble in solvents such as benzene, toluene, xylene, chloroform, dichloromethane, and 1,2-

dichloroethane. In general, they are poorly soluble in non-polar organic solvents such as petroleum hydrocarbons but highly soluble in polar organic solvents such as methanol, ethanol, acetone, dimethylformamide, etc. (WHO 1986d:2).

The carbamate derivatives with herbicidal action (such as pyrolan and dimetilan) are substantially more stable to alkaline hydrolysis than the methyl carbamate derivatives (carbaryl and propoxur), which have an insecticidal action. For example, the half-life of carbaryl is 15 min at pH 10 compared with 10 days at pH 7. However, pyrolan and dimetilan do not hydrolyse in the pH range of 4 - 10. The instability of these compounds with alkali solution is of use for decontamination and clean-up processes (WHO 1986d:2).

In acid fresh water, which is characteristic of the lakes and streams in heavily forested Canada, aminocarb would be rather stable and would persist long enough to be bioaccumulated by various trophic levels of food chains. Furthermore, the carbamate fungicides of carbendazim, benomyl, and thiophanates are related. Carbendazim and benomyl are derivatives of benzimidazole. Carbendazim is slowly hydrolysed by alkali solution to 2-aminobenzimidazole, but it is stable as acid-forming water-soluble salts. Benomyl breaks down to methyl 2-benzimidazole carbamate (MBC) in water. Benomyl is rather unstable in common solvents (WHO 1986c:2-3; Sogor and Vilanov 2002:215).

The names, chemical structure, and pesticidal activity of the principal carbamates are presented in Table 2.2 (WHO 1986c:2-3).

Table 2.2 **Relationship between the chemical structure and pesticidal activity of different carbamates and their common names are shown (WHO 1986c:2-3).**

Pesticidal activity	Chemical structure	Common or other names
Insecticide	CH_3-NH-C(O)-O-aryl	aldoxycarb, allyxycarb, aminocarb, BPMC, bendiocarb, bufencarb, benfuracarb, butacarb, carbanolate, carbaryl, carbofuran, cloethocarb, dimetilan, dioxacarb, ethiofencarb, formetanate, hoppcide, isoprocarb, trimethacarb, MPMC, methiocarb, metolcarb, mexacarbate, pirimicarb, promacyl, promecarb, propoxur, MTMC, XMC, xylylcarb
	CH_3-NH-C(O)-O-N-alkyl	aldicarb, methomyl, oxamyl, thiofanox, thiodicarb
Herbicide	aryl-NH-C(O)-O-alkyl	asulam, barban, carbetamide, chlorbufam, desmedipham, phenmedipham, swep
	aryl-NH-C(O)-O-aryl	dichlormate, karbutilate, terbucarb
Herbicide	aryl-NH-C(O)-O-alkyl	propham, chlorpropham and sprout-inhibitors
Fungicide	aryl-NH-C(O)-O-alkyl	benomyl, carbendazim, thiophanate-methyl, thiophanate-ethyl

2.6.2.3 Metabolism and mode of action

Most carbamates are active inhibitors of acetylcholinesterase (AChE) and they do not require metabolic activation. However, some carbamates, such as the benzimidazole carbamates, do not have anticholinesterase activity. Carbamates undergo metabolism, and the metabolites are generally less toxic than the parent compound, although some exceptions exist. The metabolism of carbamates is basically the same in mammals, insects, and plants, and the toxic effects of carbamates are similar in mammals and insects. Carbamates do not accumulate in the mammalian body, but are rapidly excreted, mainly through the urine (WHO 1986d:3; Sogor and Vilanov 2002:215).

Carbamates are effective insecticides by virtue of their ability to inhibit acetylcholinesterase (AChE) in the nervous system. AChE catalyses the hydrolysis of the neurotransmitter acetylcholine (ACh) to choline and acetic acid. Acetylcholine (ACh) is the synaptic mediator of nerve impulses in the nervous system of mammals and insects (WHO 1986d:3-4):

(a)   as a neurotransmitter in the brain of mammals, and in the central nervous system of insects,

(b)   as a pre-ganglionic neurotransmitter in the autonomic nervous system of mammals,

(c)   in post-ganglionic nerve endings of the autonomic nervous system,

(d)   at the neuromuscular junction of skeletal muscle.

Carbamates, like organophosphates, can inhibit esterases that have serine in their catalytic centre. These are called serine-esterases or beta-esterases. Although the inhibition of serine-esterases other than AChE is not significant for the toxicity of the compounds, it may have significance for the potentiation of toxicity of other compounds after long-term low-level exposure (WHO 1986d:3-4; Sogor and Vilanov 2002:215).

2.6.3   Chemical structures of specific pesticides used in this study

2.6.3.1 Specific organophosphate pesticides used in this study

In the following paragraphs the chemical structure of each of the organophosphorous pesticides used in this study and its IUPAC name is shown.

In Figure 2.46 the chemical structure of diazinon is shown:
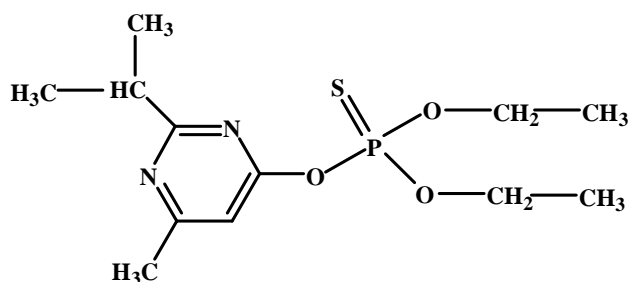
Figure 2.46   **Chemical structure of the organophosphate called diazinon; IUPAC name:** *O,O*-**diethyl** *O*-**2-isopropyl-6-methylpyrimidin-4-yl phosphorothioate (Wood 2005:1).**

In Figure 2.47 the chemical structure of chlorpyrifos is shown:
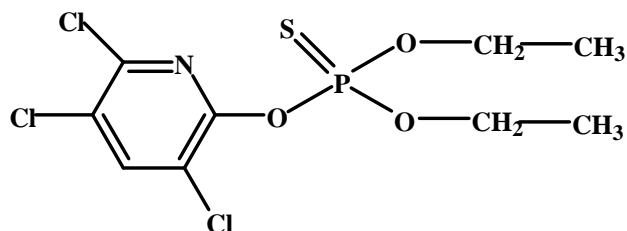
Figure 2.47   Chemical   structure   of   the   organophosphate   called
chlorpyrifos; IUPAC name: *O,O*-diethyl *O*-3,5,6-trichloro-2-
pyridyl phosphorothioate (Wood 2005:1).

In Figure 2.48 the chemical structure of fenthion is shown:
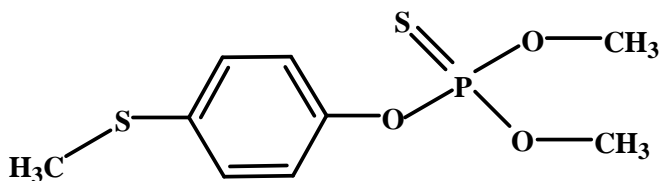
Figure 2.48   Chemical structure of the organophosphate called fenthion;
IUPAC   name: *O,O*-dimethyl   *O*-4-methylthio-*m*-tolyl
phosphorothioate (Wood 2005:1).

In Figure 2.49 the chemical structure of parathion-methyl is shown:
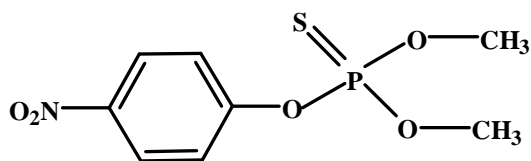
Figure 2.49   **Chemicl structure of the organophosphate called parathion-methyl; IUPAC name: O,O-dimethyl O-4-nitrophenylphosphorothioate (Wood 2005:1).**

In Figure 2.50 the chemical structure of malathion is shown:
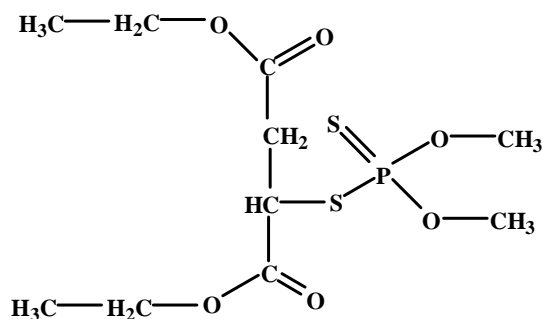
Figure 2.50   **Chemical structure of the organophosphate called malathion; IUPAC name: diethyl (dimethoxythiophosphorylthio) succinate OR *S*-1,2-bis(ethoxycarbonyl)ethyl *O,O*-dimethyl phosphorodithioate (Wood 2005:1).**

2.6.3.2 Specific carbamate pesticides used in this study

In the following paragraphs the chemical structure of each of the carbamate pesticides used in this study and its IUPAC name is shown.

In Figure 2.51 the chemical structure of carbofuran is shown:
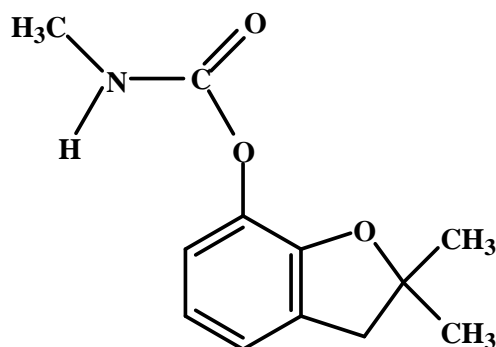
Figure 2.51 **Chemical structure of the carbamate called carbofuran; IUPAC name: 2,3-dihydro-2,2-dimethylbenzofuran-7-yl methylcarbamate (Wood 2005:2).**

In Figure 2.52 the chemical structure of carbaryl is shown:
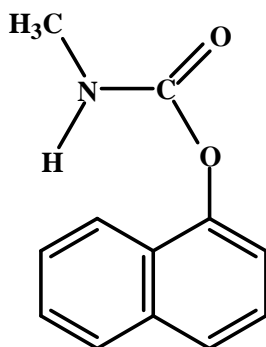
Figure 2.52 **Chemical structure of the carbamate called carbaryl; IUPAC name: 1-naphthyl methylcarbamate (Wood 2005:2).**

In Figure 2.53 the chemical structure of dioxacarb is shown:
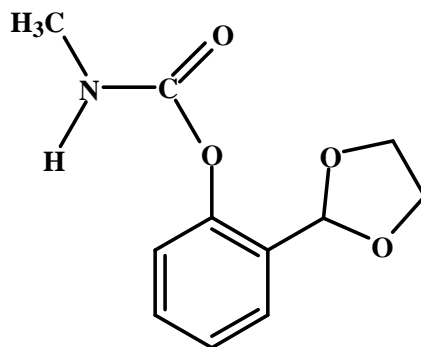
Figure 2.53   **Chemical structure of the carbamate called dioxacarb; IUPAC name: 2-(1,3-dioxolan-2-yl)phenyl methylcarbamate (Wood 2005:2).**

In Figure 2.54 the chemical structure of aldicarb is shown:
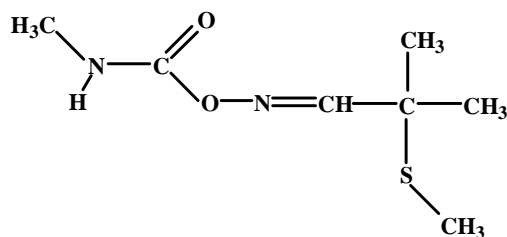
Figure 2.54   **Chemical structure of the carbamate called aldicarb; IUPAC name: (*EZ*)-2-methyl-2-(methylthio) propionaldehyde *O*-methylcarbamoyloxime (Wood 2005:2).**

In Figure 2.55 the chemical structure of methomyl is shown:
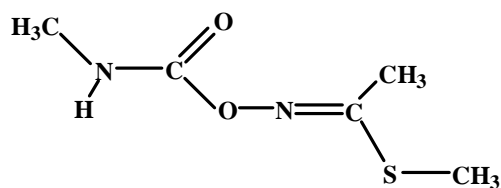
Figure 2.55   **Chemical structure of the carbamate called methomyl; IUPAC name: *S*-methyl (*EZ*)-*N*-(methylcarbamoyloxy) thioacetimidate (Wood 2005:2).**

2.6.4   Pesticides detection

Pesticides can generally be detected in aqueous solutions. However, pesticides are generally characterised by a low solubility in water and a high solubility in organic solvents. Extraction and concentration of pesticides from solid matrices such as fruits and vegetables are thus commonly carried out in organic solvents. The ability of enzymes to work in non-aqueous solvents has been proved for many years. Depending on the nature and the amount of the solvent, the enzyme activity can be strongly affected when experiments are carried out in these media. Some enzymes like glucose oxidase or tyrosinase work in various organic solvents as well as in water, but in all cases a minimal amount of water is required to retain catalytic activity (Andreescu *et al.* 2002:170; Zhang *et al.* 2005:5110).

Since organophosphorus and carbamate pesticides are widely used in agriculture, their presence in water, food and animal feed presents a potential hazard due to the high mammalian toxicity of these pesticides. Usually the enzymatic

determination of these insecticides using free or immobilised cholinesterases enzymes are performed, but these methods are suitable only for polar compounds soluble in water. This poses potential problems since organophosphorous and carbamate insecticides are comparatively insoluble in water and highly soluble in organic solvents. In order to detect very low concentrations of these insecticides in water or food samples, they require prior concentration or extraction using organic solvents (Campanella *et al.* 2001:244; Palchetti *et al.* l997:31).

The detection of organophosphorous and carbamate pesticides have been a contentious issue since these pesticides have a low solubility in water but a high solubility in organic solvents. For standard analytical procedures an organic solvent extraction is necessary when real samples such as fruit, vegetables, water and soil are analysed. The application of enzymatic biosensors for pesticide detection has become essential in the analysis of these samples and although several successes have been reported, it also comes with its own limitations. Enzyme activity is strongly influenced by the presence of organic solvents since it interacts with the aqueous layer around the enzyme molecule and usually a decrease in activity is reported. In the case of non-polar solvents, it is reported to interact slightly with the aqueous layer, while water-soluble polar solvents have a more dramatic influence. The detection of pesticides using the enzyme inhibition principle is an established procedure. It may involve the immobilisation of acetylcholinesterase (AChE) in a polymer matrix on a metal electrode and the determining of the initial response value of the constructed biosensor. This is then

by immersing the electrode in an organic solvent for 10 – 30 min and the repeated

determination of the reduced response of the biosensor after exposure to the inhibitor

(Palchett *et al.* l997:31; Evtugyn *et al.* 1998:468; Padilla *et al.* 2000:49; Padilla *et al.*

2004:1477).

CHAPTER 3

Experimental Methods of Investigation

3.1   Introduction

In this chapter the preparation procedures for the self-assembled monolayer, monomer electropolymerisation, enzyme electrode and biosensor construction are presented. This is followed by the electrochemical and analytical techniques for the AChE-biosensor investigation of organophosphorous and carbamate pesticides in 0.1 M phosphate, saline buffer (pH 7.2) and aqueous organic solvent solutions.

3.2   Reagents and Materials

The reagents aniline (99%), *o*-methoxyaniline (99+%) (OMA), poly(*4*-styrene sulphonic acid) (18 wt% solution in water) (PSSA), potassium dihydrogen phosphate (99+%), disodium hydrogen phosphate (98+%) and diethyl ether (99.9%) were obtained from Aldrich, Germany. The acetylthiocholine chloride (99%) was obtained from Sigma, Germany. The *2,5*-dimethoxyaniline (>97%) (DMA), mercaptobenzothiazole (MBT), acetylcholinesterase (AChE, from Electrophorus

electricus, EC 3.1.1.7; ~ 850 U/mg), acetylcholine chloride (99%), acetone (>99.8%, pestanal) and *n*-hexane (>95%, pestanal) were obtained from Fluka, Germany. The hydrogen peroxide (30%) and the organic solvents ethanol (99.9%, absolute grade), acetonitrile (99.9%, pestanal grade) were purchased from Riedel-de Haën, Germany. The potassium chloride, sulphuric acid (95%), hydrochloric acid (32%) and ethanol (absolute, 99,9%) were obtained from Merck, South Africa. Organophosphate pesticides used in this study include fenthion, diazinon, chlorpyrifos, malathion and parathion-methyl. These pesticide standards were purchased from Riedel-de Haën, Germany. Carbamate pesticides used in this study include carbofuran, carbaryl, dioxacarb, aldicarb and methomyl. These pesticide standards were purchased from Riedel-de Haën, Germany.

Platinum (Pt) wires as counter electrodes were obtained from Sigma-Aldrich, South Africa. Alumina micropolish and polishing pads that were used for the polishing of the working electrode were obtained from Buehler, IL, USA.

3.3   Instrumentation

3.3.1 Potentiostat Set-up

All electrochemical protocols were performed and recorded with a computer interfaced to a BAS-50/W electrochemical analyser with BAS-50/W software

(Bioanalytical Systems, Lafayette, IN, USA), using either cyclic voltammetry (CV), Oysteryoung square wave voltammetry (OSWV), differential pulse voltammetry (DPV) or time-based amperometric modes. A conventional three electrode system was employed. The working electrode was a gold disc electrode (diameter: 1.6 mm; area: 2.01×10^{-2} cm²; Bioanalytical Systems, Lafayette, IN, USA). Silver/silver chloride (Ag/AgCl – 3 M NaCl type) was used as the reference electrode and a platinum wire was used as auxiliary electrode (Morrin *et al.* 2004:30).

3.4   Electrode Surface Preparation

Prior to use, gold electrodes were first polished on aqueous slurries of 1 μm, 0.3 μm and 0.05 μm alumina powder. After thorough rinsing in deionised water followed by acetone, the electrodes were etched for about 5 minutes in a hot 'Piranha' solution {1:3 (v/v) 30 % H_2O_2 and concentrated H_2SO_4} and rinsed again with copious amounts of deionised water. The polished electrodes were then cleaned electrochemically by cycling the potential scan between - 200 and + 1500 mV in 0.05 M H_2SO_4 at the scan rate of 40 mV.s^{-1} for 10 min or until the CV characteristics for a clean Au electrode were obtained.

The platinum (Pt) counter electrode was regularly cleaned before and after synthesis and in between synthesis and analysis. This involved flaming the Pt

electrode in a Bunsen burner until it was white hot, followed by rinsing with copious

quantities of deionised water (Morrin *et al.* 2004:64; Raj and Ohsaka 2003:69).

3.4.1 Preparation of mercaptobenzothiazole self-assembled monolayer on gold electrode

Self-assembled monolayer (SAM) of mercaptobenzothiazole (MBT) was

formed by immersing the cleaned Au electrode into an ethanol solution of 10 mM of

MBT for 2 hours. Initially the SAM of MBT was coated on the Au electrode for

different times of 0.5, 1.0, 1.5 and 2 hours respectively, to investigate the variable of

time on the MBT deposition on the Au electrode. After deposition the SAM electrode

was rinsed extensively with ethanol and water and kept in 0.1 M phosphate buffer

(pH 7.2) for later use (Mazur *et al.* 1998:167; Mazur and Krysiński, 2001:3963;

Mazur *et al.* 2003:403; Mazur *et al.* 2002:145).

3.4.2 Characterisation of Au/MBT SAM-modified electrode

A three electrode arrangement was set up in a sealed 10 ml electrochemical

cell containing either 0.1 M hydrochloric acid (HCl) solution or 0.1 M phosphate

buffer (pH 7.2) solution. After deposition of the MBT SAM on the Au electrode for

different times of 0.5, 1.0, 1.5 and 2.0 hours respectively, the Au/MBT electrode was

potentially scanned from – 200 mV to +1100 mV at a scan rate of 40 mV.s^{-1} in a 0.1 M phosphate buffer (pH 7.2) solution.

The Au/MBT SAM-modified electrode was then potentially scanned in the 0.1 M HCl solution from – 450 mV to + 950 mV (vs. Ag/AgCl) at different scan rates of 5, 10, 20, 40, 60, 80, 100, 200, 300, 400, 500 and 700 mV.s^{-1}. The cyclic voltammetry was performed for only cycle at the above scan rates and the different potential window was adopted to accommodate the shift in peak potentials at the high scan rates. Similarly, the Au/MBT SAM-modified electrode was potentially scanned in the 0.1 M phosphate buffer (pH 7.2) solution from – 750 mV to + 400 mV (vs. vs. Ag/AgCl) at different scan rates of 5, 10, 20, 40, 60, 80, 100, 200, 300, 400, 500 and 700 mV.s^{-1} (Raj and Ohsaka 2003:69; Morrin *et al.* 2004:64).

3.5   Synthesis of polyaniline films onto gold disk (Au), MBT SAM modified electrode

3.5.1 Polymerisation of *o*-methoxyaniline (OMA)

A three electrode arrangement was set up in a sealed 10 ml electrochemical cell. Poly(*o*-methoxyaniline) (POMA) films were prepared by electropolymerisation from a 0.1 M *o*-methoxyaniline solution dissolved in 1 M hydrochloric acid (HCl), also containing 2 cm^3 of poly(*4*-styrene sulphonic acid) (PSSA), onto the previously prepared Au/MBT-modified electrode. Initial optimisation of the potential window

for electropolymerisation was performed. During electropolymerisation the potential was scanned from an initial potential (E_i) of – 500 mV to a switch potential (E_λ) of +1100 mV, at a scan rate of 20 mV/s vs. Ag/AgCl as a reference. The polymerisation process was stopped after 10 voltammetric cycles, to ensure a smooth and relatively thin polymer film surface was obtained.

The Au/MBT-poly(*o*-methoxyaniline) modified electrode was then rinsed with deionised water and used as the working electrode in subsequent studies. The electrode will be referred to as Au/MBT/POMA-PSSA for the gold-MBT-POMA-PSSA modified electrode (Mazur *et al.* 1998:167; Mazur and Krysiński, 2001:3963; Mazur *et al.* 2003:403; Mazur *et al.* 2002:145).

3.5.2 Polymerisation of *2,5*-dimethoxyaniline (DMA)

A three electrode arrangement was set up in a sealed 10 ml electrochemical cell. Poly(*2,5*-dimethoxyaniline) (PDMA) films were prepared by electropolymerisation from a 0.1 M *2,5*-dimethoxyaniline solution dissolved in 1 M hydrochloric acid (HCl), also containing 2 cm^3 of poly(*4*-styrene sulphonic acid) (PSSA), onto the previously prepared Au/MBT-modified electrode.

Initial optimisation of the potential window for electropolymerisation was performed. During electropolymerisation the potential was scanned from an initial potential (E_i) of – 200 mV to a switch potential (E_λ) of +1100 mV, at a scan rate of 40

mV/s vs. Ag/AgCl as a reference. The polymerisation process was stopped after 10 voltammetric cycles, to ensure a smooth and relatively thin polymer film surface was obtained.

The Au/MBT-poly(*2,5*-dimethoxyaniline) modified electrode was then rinsed with deionised water and used as the working electrode in subsequent studies. The electrode will be referred to as Au/MBT/PDMA-PSSA for the gold-MBT-PDMA-PSSA modified electrode (Mazur *et al.* 1998:167; Mazur and Krysiński, 2001:3963; Mazur *et al.* 2003:403; Mazur *et al.* 2002:145).

3.5.3 Polymerisation of aniline

A three electrode arrangement was set up in a sealed 10 ml electrochemical cell. Polyaniline (PANI) films were prepared by electropolymerisation from a 0.2 M aniline solution dissolved in 1 M hydrochloric acid (HCl) onto the previously prepared Au/MBT-modified electrode. The aniline/HCl solution was first degassed by passing argon (Ar) through the solution for approximately ten minutes and keeping the Ar blanket during electropolymerisation. Initial optimisation of the potential window for electropolymerisation was performed. During electropolymerisation the potential was scanned from an initial potential (E_i) of $-$ 200 mV to a switch potential (E_λ) of +1200 mV, at a scan rate of 40 mV/s vs. Ag/AgCl as a reference. The polymerisation process was stopped after 10 voltammetric cycles, to

ensure a smooth and relatively thin polymer film surface was obtained. No dopant

was added to aniline since the solubility of PANI is sufficient (see sections 2.5.4 and

2.5.8).

The Au/MBT-polyaniline modified electrode was then rinsed with deionised

water and used as the working electrode in subsequent studies. The electrode will be

referred to as Au/MBT/PANI for the gold-MBT-PANI modified electrode (Mathebe

et al. 2004:115; Mazur and Krysiński, 2001:3963; Iwuoha *et al.* 1997b:749).

3.5.4 Characterisation of Au/MBT/PANIs modified electrodes using cyclic voltammetry

A three electrode arrangement was set up in a sealed 10 ml electrochemical

cell. Each of the three different polymer modified electrodes of Au/MBT/POMA-

PSSA, Au/MBT/PDMA-PSSA and Au/MBT/PANI were then individually

potentially scanned in the 0.1 M HCl solution from $-$ 400 mV to $+$ 1100 mV (vs.

Ag/AgCl) at different scan rates of 5, 10, 20, 40, 60, 80, 100, 200, 300, 400, 500 and

700 mV.s^{-1}.

Similarly, the Au/MBT/POMA-PSSA, Au/MBT/PDMA-PSSA and

Au/MBT/PANI electrodes were potentially scanned in the 0.1 M phosphate buffer

(pH 7.2) solution from $-$ 400 mV to $+$ 1100 mV (vs. vs. Ag/AgCl) at different scan

rates of 5, 10, 20, 40, 60, 80, 100, 200, 300, 400, 500 and 700 mV.s^{-1} (Mathebe *et al.*

2004:115; Iwuoha *et al.* 1997b:749; Morrin *et al.* 2004:30).

3.6   Preparation of Au/MBT/PANI modified enzyme electrode

Following the electropolymerisation of a fresh PANI polymer film on an Au/MBT electrode, the Au/MBT/PANI electrode was transferred to a batch cell, containing 1 ml argon degassed 0.1 M phosphate buffer (pH 7.2) solution. The PANI polymer film was then reduced at a potential of – 500 mV (vs. Ag/AgCl) until a steady current was achieved, which took approximately thirty minutes.

Electrochemical incorporation of the enzyme acetylcholinesterase (AChE) onto the POMA-PSSA film was carried out next. This involved the addition of 60 μL of AChE to the 0.1 M phosphate buffer (pH 7.2) solution. After the enzyme solution was argon degassed, enzyme immobilisation was achieved by oxidation of the POMA-PSSA film in the presence of AChE at a potential of + 400 mV (vs. Ag/AgCl) until a steady current was achieved, which took approximately fourty minutes.

During the oxidation step, the enzyme AChE was electrostatically attached to the polymer film via an ion-exchange process. The biosensor was then rinsed with deionised water to remove any unbound enzyme and stored in the working 0.1 M phosphate buffer (pH 7.2) solution at 4 ℃. The resulting biosensor will be referred to as Au/MBT/POMA-PSSA/AChE biosensor.

The same procedure was followed for the preparation of the respective Au/MBT/PDMA-PSSA/AChE and Au/MBT/PANI/AChE biosensors. In the case of the Au/MBT/PANI/AChE bioelectrode, after enzyme incorporation the bioelectrode

was arranged vertically and then coated with a 2 μL drop of poly(vinyl acetate) (PVAc) solution (0.3 M) prepared in acetone and left to dry for 1 min. The resulting biosensor will be referred to as Au/MBT/PANI/AChE/PVAc biosensor (Mathebe *et al.* 2004:115; Iwuoha *et al.* 1997b:749; Morrin *et al.* 2004:30).

3.6.1   Voltammetric characterisation of Au/MBT/PANIs/AChE bioelectrode

A three electrode arrangement was set up in a sealed 10 ml electrochemical cell. A 2 ml test solution containing 0.1 M phosphate buffer, 0.1 M KCl (pH 7.2) was degassed with argon before the following voltammetric characterisations of each of the three bioelectrodes were performed.

A cyclic voltammogram (CV) of Au/MBT/POMA-PSSA/AChE in the absence of a substrate was then performed by applying a sequential linear potential scan between – 500 and + 1100 mV (vs. Ag/AgCl) at a scan rate of 5 mV.s^{-1}, in a 0.1 M phosphate buffer, 0.1 M KCl (pH 7.2) solution. Similarly, cyclic voltammograms were collected for each of the Au/MBT/PDMA-PSSA/AChE and Au/MBT/PANI/AChE/PVAc bioelectrodes in a 0.1 M phosphate buffer, 0.1 M KCl (pH 7.2) solution.

Osteryoung-type square wave voltammetry (SWV) in the absence of a substrate was then performed on Au/MBT/POMA-PSSA/AChE by applying a linear oxidative potential scan (anodic mode – one direction only) between – 500 and + 1100 mV (vs. Ag/AgCl) at a step potential of 4 mV, a frequency of 5 Hz, and a

square amplitude of 50 mV. Similar anodic square wave voltanmmograms were collected for each of the Au/MBT/PDMA-PSSA/AChE and Au/MBT/PANI/AChE/PVAc bioelectrodes in a 0.1 M phosphate buffer, 0.1 M KCl (pH 7.2) solution.

Differential pulse voltammetry (DPV) for the oxidation wave, in the absence of a substrate, was also performed on Au/MBT/POMA-PSSA/AChE by applying a linear potential scan (anodic mode) between – 500 and + 1100 mV (vs. Ag/AgCl) at a scan rate of 10 mV.s^{-1} and a pulse amplitude of 50 mV. The sample width, pulse width and pulse period were 17 ms, 50 ms and 200 ms, respectively. Similar anodic scan differential pulse voltammograms were collected for each of the Au/MBT/PDMA-PSSA/AChE and Au/MBT/PANI/AChE/PVAc bioelectrodes in a 0.1 M phosphate buffer, 0.1 M KCl (pH 7.2) solution (Mathebe *et al.* 2004:115; Iwuoha *et al.* 1997b:749; Morrin *et al.* 2004:30; Iwuoha and Smyth 2003:237).

3.7   Electrochemical measurements using AChE-based biosensors in the presence of acetylcholine as substrate

The electrochemical cell used for the electrocatalytic oxidation of acetylcholine (ACh) consisted of Au/MBT/POMA-PSSA/AChE, platinum wire and Ag/AgCl as the working, counter and reference electrode, respectively. A similar set-up was used for Au/MBT/PDMA-PSSA/AChE as the working electrode.

A 1 ml test solution containing 0.1 M phosphate buffer (0.1 M KCl, pH 7.2) solution was degassed with argon before any substrate was added and after each addition of small aliquots of 0.01 M acetylcholine (ACh). Cyclic, square wave and differential pulse voltammetry were used to measure the responses of the AChE-based biosensor towards Ach (Fedosseeva *et al.* 2000:55; Joshi *et al.* 2005: 54; Sotiropoulou *et al.* 2005b:2347).

3.7.1 Cyclic Voltammetric Analysis of Au/MBT/POMA-PSSA/AChE biosensor

Cyclic voltammetry (CV) was performed at a slow scan rate of 5 mV.s^{-1} to study the catalytic oxidation of ACh by applying a linear potential scan between + 100 mV and + 800 mV (vs. Ag/AgCl). The cyclic voltammogram was first obtained in the absence of the substrate ACh, followed by analysis in the presence of ACh as substrate.

Sequential 20 ml aliquots of 0.01M acetylcholine (ACh) were then added to the 1 ml of 0.1 M phosphate buffer (0.1 M KCl, pH 7.2) solution, degassed with argon and a blanket of gas was kept for the duration of the experiment. The phosphate buffer solution was stirred after each addition of ACh. This was done to ensure homogeneity of the solution before measurements were taken. The same procedure was repeated for the Au/MBT/PDMA-PSSA/AChE biosensor (Morrin *et al.* 2004:30; Mathebe *et al.* 2004:115; Iwuoha *et al.* 1997b:749).

3.7.2   Square Wave Voltammetric Analysis of Au/MBT/POMA-PSSA/AChE biosensor

Osteryoung-type square wave voltammetry (OSWV) was performed immediately after cyclic voltammetric analysis with the AChE-based biosensor in 1 ml of 0.1 M phosphate buffer (0.1 M KCl, pH 7.2) solution, containing different concentrations of ACh as the substrate under anaerobic conditions (system kept under an argon blanket). The anodic difference square wave voltammogram (SWV) was collected in an oxidation direction only by applying a linear potential scan between + 100 mV and + 800 mV (vs. Ag/AgCl), at a step potential of 4 mV, a frequency of 5 Hz, and a square wave amplitude of 50 mV. The SWV was first obtained in the absence of the substrate ACh, followed by analysis in the presence of ACh as substrate. The same procedure was repeated for the Au/MBT/PDMA-PSSA/AChE biosensor (Morrin *et al.* 2004:30; Iwuoha and Smyth 2003:237).

3.7.3   Differential Pulse Voltammetric Analysis of Au/MBT/POMA-PSSA/AChE biosensor

Differential pulse voltammetry (DPV) immediately followed SWV analysis with the AChE-based biosensor in 1 ml of 0.1 M phosphate buffer (0.1 M KCl, pH 7.2) solution, containing different concentrations of ACh as the substrate under anaerobic conditions (system kept under an argon blanket).

The anodic difference differential pulse voltammogram (DPV) was collected in an oxidation direction only by applying a linear potential scan between + 100 mV and + 800 mV (vs. Ag/AgCl), at a scan rate of 10 mV.s^{-1} and a pulse amplitude of 50 mV. The sample width, pulse width and pulse period were 17 ms, 50 ms and 200 ms, respectively. The DPV was first obtained in the absence of the substrate ACh, followed by analysis in the presence of ACh as substrate. The same procedure was repeated for the Au/MBT/PDMA-PSSA/AChE biosensor (Morrin *et al.* 2004:30; Iwuoha and Smyth 2003:237).

3.8   Electrochemical measurements using AChE-based biosensors in the presence of acetylthiocholine as substrate

The electrochemical cell used for the electrocatalytic oxidation of acetylthiocholine (ATCh) consisted of Au/MBT/PANI/AChE/PVAc, platinum wire and Ag/AgCl as the working, counter and reference electrode, respectively.

A 1 ml test solution containing 0.1 M phosphate (0.1M KCl, pH 7.2) solution was degassed with argon before any substrate was added and after each addition of small aliquots of 0.01 M acetylthiocholine (ATCh). Cyclic, square wave and differential pulse voltammetry were used to measure the responses of the AChE-based biosensor towards ATCh as substrate (Joshi *et al.* 2005: 54; Sotiropoulou *et al.* 2005b:2347; Pritchard *et al.* 2004:765).

3.8.1 Cyclic Voltammetric Analysis of Au/MBT/PANI/AChE/PVAc biosensor

Cyclic voltammetry (CV) was performed at a slow scan rate of 10 mV.s^{-1} to study the catalytic oxidation of ATCh by applying a linear potential scan between – 400 mV and + 1800 mV (vs. Ag/AgCl). The cyclic voltammogram was first obtained in the absence of the substrate ATCh, followed by analysis in the presence of ATCh as substrate.

Sequential 20 ml aliquots of 0.01 M acetylthiocholine (ATCh) were then added to the 1 ml of 0.1 M phosphate buffer (0.1 M KCl, pH 7.2) solution, degassed with argon and a blanket of gas was kept for the duration of the experiment. The phosphate buffer solution was stirred after each addition of ATCh. This was done to ensure homogeneity of the solution before measurements were taken (Morrin *et al.* 2004:30; Mathebe *et al.* 2004:115; Iwuoha *et al.* 1997b:749).

3.8.2   Square Wave Voltammetric Analysis of Au/MBT/ PANI/AChE/PVAc biosensor

Osteryoung-type square wave voltammetry (OSWV) was performed immediately after cyclic voltammetric analysis with the AChE-based biosensor in 1 ml of 0.1 M phosphate buffer (0.1 M KCl, pH 7.2) solution, containing different concentrations of ATCh as the substrate under anaerobic conditions (system kept under an argon blanket). The anodic difference square wave voltammogram (SWV) was collected in an oxidation direction only by applying a linear potential scan between – 400 mV and + 1800 mV (vs. Ag/AgCl), at a step potential of 4 mV, a frequency of 5 Hz, and a square wave amplitude of 50 mV. The SWV was first obtained in the absence of the substrate ATCh, followed by analysis in the presence of ATCh as substrate (Morrin *et al.* 2004:30; Iwuoha and Smyth 2003:237).

3.8.3   Differential Pulse Voltammetric Analysis of Au/MBT/ PANI/AChE/PVAc biosensor

Differential pulse voltammetry (DPV) immediately followed SWV analysis with the AChE-based biosensor in 1 ml of 0.1 M phosphate buffer (0.1 M KCl, pH 7.2) solution, containing different concentrations of ATCh as the substrate under anaerobic conditions (system kept under an argon blanket). The anodic difference

differential pulse voltammogram (DPV) was collected in an oxidation direction only by applying a linear potential scan between – 400 mV and + 1800 mV (vs. Ag/AgCl), at a scan rate of 10 mV.s^{-1} and a pulse amplitude of 50 mV. The sample width, pulse width and pulse period were 17 ms, 50 ms and 200 ms, respectively. The DPV was first obtained in the absence of the substrate ATCh, followed by analysis in the presence of ATCh as substrate (Morrin *et al.* 2004:30; Iwuoha and Smyth 2003:237).

3.9   Inhibitory studies of AChE-based biosensors in the presence of pesticide inhibitors

3.9.1 Inhibitory studies of Au/MBT/POMA-PSSA/AChE biosensor

A new biosensor as described in Section 3.6 was prepared each time a new organophosphorous or carbamate pesticide was studied. The electrochemical cell consisted of Au/MBT/POMA-PSSA/AChE, platinum wire and Ag/AgCl as the working, counter and reference electrode, respectively. A 1 ml test solution containing 0.1 M phosphate (0.1 M KCl, pH 7.2) solution was degassed with argon before any substrate was added and after each addition of small aliquots of 0.01M acetylcholine (ACh).

Cyclic, square wave and differential pulse voltammetric measurements were performed after each addition of ACh up to a maximum concentration of 1.1 mM. This was followed by the addition of a 0.16 ppb aqueous organic solvent solution of

either organophosphate or carbamate pesticide to the cell solution with voltammetric measurements performed after each addition. Cyclic voltammetry (CV) was performed at a scan rate of 5 mV.s^{-1} by applying a linear potential scan between + 100 mV and + 800 mV (vs. Ag/AgCl).

The anodic difference square wave voltammogram (SWV) was collected in an oxidation direction only by applying a linear potential scan between + 100 mV and + 800 mV (vs. Ag/AgCl), at a step potential of 4 mV, a frequency of 5 Hz, and a square wave amplitude of 50 mV.

The anodic difference differential pulse voltammogram (DPV) was collected in an oxidation direction only by applying a linear potential scan between + 100 mV and + 800 mV (vs. Ag/AgCl), at a scan rate of 10 mV.s^{-1} and a pulse amplitude of 50 mV. The sample width, pulse width and pulse period were 17 ms, 50 ms and 200 ms, respectively. The same sets of experiments were performed on the Au/MBT/PDMA-PSSA/AChE biosensor to test the effect of the organophosphorous and carbamate pesticides (Morrin *et al.* 2004:30; Iwuoha and Smyth 2003:237; Del Carlo *et al.* 2004: 651; Joshi *et al.* 2005: 54).

3.9.2 Inhibitory studies of Au/MBT/ PANI/AChE/PVAc biosensor

A new biosensor as described in Section 3.6 was prepared each time a new organophosphorous or carbamate pesticide was studied. A new biosensor was also

prepared for each of the six concentrations of the organophosphorous or carbamate pesticides studied. The electrochemical cell consisted of Au/MBT/PANI/AChE/PVAc, platinum wire and Ag/AgCl as the working, counter and reference electrode, respectively. A 1 ml test solution containing 0.1 M phosphate (0.1 M KCl, pH 7.2) solution was degassed with argon before any substrate was added and after each addition of small aliquots of 0.01M acetylthiocholine (ATCh).

Inhibition plots for each of the organophosphorous and carbamate pesticides detected were obtained using the percentage inhibition method. The following procedure was used. The biosensor was first placed in a stirred 1ml of 0.1 M phosphate (0.1 M KCl, pH 7.2) solution (anaerobic conditions) and multiple additions of a standard acetylthiocholine (ATCh) substrate solution was added until a stable current and a maximum concentration of 2.4 mM were obtained. This steady state current is related to the activity of the enzyme in the biosensor when no inhibitor was present. This was followed by incubating the biosensor in anaerobic conditions for 20 min with a standard pesticide phosphate buffer-organic solvent mixture. This was followed by multiple additions of a standard ATCh substrate solution (anaerobic conditions), to a fresh 1ml of 0.1 M phosphate (0.1 M KCl, pH 7.2) solution (anaerobic conditions) and multiple additions of a standard acetylthiocholine (ATCh) substrate solution was again added, until a stable current was obtained. The maximum concentration of acetylthiocholine (ATCh) was again 2.4 mM. The percentage inhibition was then calculated using the formula (Albareda-Sirvent *et al.* 2000:137; Sotiropoulou and Chaniotakis 2005a:199; Wilkins *et al.* 2000:786):

$$I\% = \frac{(I_1 - I_2)}{I_1} \; X \; 100 \qquad\qquad \text{Eqn. 3.1}$$

where I% is the degree of inhibition, I_1 is the steady-state current obtained in buffer solution, I_2 is the steady-state current obtained after the biosensor was incubated for 20 min in phosphate buffer-organic solvent mixture.

Cyclic, square wave and differential pulse voltammetric measurements were performed after each addition of ATCh up to a maximum concentration of 2.4 mM. Cyclic voltammetry (CV) was performed at a scan rate of 10 mV.s^{-1} by applying a linear potential scan between – 400 mV and + 1800 mV (vs. Ag/AgCl). For some experimental runs the anodic difference square wave voltammogram (SWV) was collected in an oxidation direction only by applying a linear potential scan between – 400 mV and + 1800 mV (vs. Ag/AgCl), at a step potential of 4 mV, a frequency of 5 Hz, and a square amplitude of 50 mV.

The anodic difference differential pulse voltammogram (DPV) was collected in an oxidation direction only by applying a linear potential scan between – 400 mV and + 1800 mV (vs. Ag/AgCl), at a scan rate of 10 mV.s^{-1} and a pulse amplitude of 50 mV. The sample width, pulse width and pulse period were 17 ms, 50 ms and 200 ms, respectively (Morrin *et al.* 2004:30; Iwuoha and Smyth 2003:237).

3.10. Optimisation of acetylcholinesterase (AChE) enzyme loading

The operation of the Au/MBT/PANI/AChE/PVAc biosensor was evaluated at different amounts of AChE enzyme incorporated into the biosensor. To achieve this, 0.1 M phosphate buffer, 0.1 M KCl (pH 7.2) solutions were prepared from AnalaR grades of anhydrous disodium hydrogenorthophosphate and sodium dihydrogenorthophosphate dihydrate, purchased from Aldrich, Germany. The potassium chloride was obtained from Merck, South Africa.

Following the electropolymerisation of a fresh PANI polymer film on an Au/MBT electrode, the Au/MBT/PANI electrode was transferred to a batch cell, containing 1 ml argon degassed 0.1 M phosphate buffer (pH 7.2) solution. The PANI polymer film was then reduced at a potential of – 500 mV (vs. Ag/AgCl) until a steady current was achieved, which took approximately thirty minutes.

Electrochemical incorporation of the enzyme acetylcholinesterase (AChE) onto the PANI film was carried out next. This involved the addition of 40 μL of AChE to the 0.1 M phosphate buffer (pH 7.2) solution. After the enzyme solution was argon degassed, enzyme immobilisation was achieved by oxidation of the PANI film in the presence of AChE at a potential of + 400 mV (vs. Ag/AgCl) until a steady current was achieved, which took approximately fourty minutes. The Au/MBT/PANI bioelectrode was arranged vertically and then coated with a 2 μL drop of poly(vinyl acetate) (PVAc) solution (0.3 M) prepared in acetone and left to dry for 1 min.. The

same procedure was followed to incorporate 60 and 80 µL of AChE enzyme into the PANI polymer surface.

Voltammetric characterisation was performed at a slow scan rate of 10 mV.s^{-1} to study the catalytic oxidation of ATCh by applying a linear potential scan between – 400 mV and + 1800 mV (vs. Ag/AgCl). The voltammograms were first obtained in the absence of the substrate ATCh, followed by analysis in the presence of ATCh as substrate. Sequential 20 ml aliquots of 0.01 M acetylthiocholine (ATCh) were then added to the 1 ml of 0.1 M phosphate buffer (0.1 M KCl, pH 7.2) solution, degassed with argon and a blanket of gas was kept for the duration of the experiment. The phosphate buffer solution was stirred after each addition of ATCh. This was done to ensure homogeneity of the solution before measurements were taken (Anitha *et al.* 2004:848; Nunes *et al.* 1999:37).

3.11 pH Optimisation for acetylcholinesterase (AChE) immobilised in Au/MBT/PANI/AChE biosensor

The operation of the Au/MBT/PANI/AChE/PVAc biosensor was evaluated at different pH values. To achieve this, 0.1 M phosphate buffer, 0.1 M KCl solutions were prepared from AnalaR grades of anhydrous disodium hydrogenorthophosphate and sodium dihydrogenorthophosphate dihydrate, purchased from Aldrich, Germany. The potassium chloride was obtained from Merck, South Africa.

The 0.1 M phosphate buffer, 0.1 M KCl solutions were prepared at different pH values of 6.0; 6.5; 7.2; 7.5 and 8.0. A 1 ml test solution containing 0.1 M phosphate buffer, 0.1 M KCl solution was degassed with argon before any substrate was added. The Au/MBT/PANI/AChE/PVAc biosensor was then evaluated in the 1 ml test solution with small aliquots of the substrate consisting of 0.01 M acetylthiocholine (ATCh) being added to the test solution, followed by degassing. The maximum current response of the biosensor was then obtained at the different pH values after 2 mM of the ATCh substrate was added to the Au/MBT/PANI/AChE/PVAc biosensor (Anitha *et al.*, 2004:848; Albareda-Sirvent *et al.*, 2001:35; Pritchard *et al.*, 2004:765; Bucur *et al.*, 2005a:1).

3.12   Long-term stability investigation of Au/MBT/PANI/AChE biosensor

The operation of the Au/MBT/PANI/AChE/PVAc biosensor was evaluated at different time intervals of 7 days for a total of 30 days, using one specific biosensor.

A 2 ml test solution containing 0.1 M phosphate buffer, 0.1 M KCl solution was degassed with argon before any substrate was added. The Au/MBT/PANI/AChE/PVAc biosensor was then evaluated in the 2 ml test solution with small aliquots of the substrate consisting of 0.01 M acetylthiocholine (ATCh) being added to the test solution, followed by degassing. The maximum current response of the biosensor was then obtained after 2 mM of the ATCh substrate was

added to the Au/MBT/PANI/AChE/PVAc biosensor. This procedure was performed

on 0, 7, 14, 21 and 28 days using one specific Au/MBT/PANI/AChE/PVAc biosensor

(Albareda-Sirvent *et al.*, 2001:35).

3.13   Temperature stability investigation of Au/MBT/PANI/AChE biosensor

The temperature stability of the Au/MBT/PANI/AChE/PVAc biosensor was

evaluated at different temperature values. To achieve this, the optimum temperature

for AChE activity in the constructed biosensor was determined by assaying the

biosensor at various temperatures of 10, 15, 20, 25, 30, and 35 ℃.

A 2 ml test solution containing 0.1 M phosphate buffer, 0.1 M KCl solution

was degassed with argon before any substrate was added, and incubated in a small

water bath for approximately 10 minutes at a specific temperature. The

Au/MBT/PANI/AChE/PVAc biosensor was then evaluated in the 2 ml test solution

with small aliquots of the substrate consisting of 0.01 M acetylthiocholine (ATCh)

being added to the test solution, followed by degassing. The maximum current

response of the biosensor was then obtained after 2 mM of the ATCh substrate was

added to the Au/MBT/PANI/AChE/PVAc biosensor. This procedure was performed

at 10, 15, 20, 25, 30, and 35 ℃ using different Au/MBT/PANI/AChE/PVAc

biosensors (Ricci *et al.*, 2003:165; Kuralay *et al.*, 2005:197).

3.14   Determination of the Limit of Detection (LOD)

A 1 ml test solution containing 0.1 M phosphate buffer, 0.1 M KCl solution was degassed with argon before any substrate was added. The AChE-biosensor was then evaluated in the 1 ml test solution by performing 10 replicate measurements on the 0.1 M phosphate buffer, 0.1 M KCl solution, or on any one of the analyte (standard pesticide) solutions at the lowest working concentration. A calibration graph of current (A) versus saline phosphate buffer or analyte concentration was then constructed for which the slope and the linear range was then determined. The limit of detection (LOD) was then calculated with the following equation:

$$LOD = \frac{3 \cdot \sigma_{n-1}}{m} = \frac{3 \cdot s}{m} \qquad \text{Eqn. 3.2}$$

where s is the standard deviation of the 10 replicate measurements on the 0.1 M phosphate buffer, 0.1 M KCl solution, or on any one of the analyte (standard pesticide) solutions at the lowest working concentration. The variable m represents the slope of the calibration graph in the linear range that is also equal to the sensitivity of the measurements performed.

CHAPTER 4

Assembly and Optimisation of Polyaniline-Based Enzyme Biosensors prepared on gold thiol-modified electrodes

4.1   Introduction

In this chapter the results for the assembling and optimisation of the substituted and unsubstituted polyaniline-based enzyme biosensors prepared on gold thiol-modified electrodes are presented and discussed. This will involve the discussion of the results for the assembling and characterisation of the:

(i)   self-assembled monolayer of mercaptobenzothiazole assembled on a gold electrode,

(ii)   electropolymerisation of (un)substituted polyanilines on the gold-modified electrode,

(iii)   substituted polyaniline-acetylcholinesterase bioelectrode(s) and corresponding biosensor(s),

(iv)   unsubstituted polyaniline-acetylcholinesterase bioelectrode and corresponding biosensor,

(v)   electrochemical measurements made using the AChE-biosensors in the presence of acetylcholine and acetylthiocholine as substrates.

The results obtained from the above optimisation and characterisation experiments were used in the actual assembly and testing of the organic phase (nano)biosensors for the determination of organophosphate and carbamate pesticide compounds.

4.2 Characterisation of mercaptobenzothiazole (MBT) monolayer on gold electrode

Electrode surfaces have been modified by the use of different strategies, of which one includes the formation of monolayers on the electrode surface. There are several motivations behind the modifications of the electrode surface which include: (i) improved electrocatalysis, (ii) freedom from surface fouling, and (iii) prevention of undesirable reactions competing kinetically with the desired electrode process (Raj *et al.* 2000:181).

The formation of self-assembled monolayers (SAMs) of organosulphur compounds on a gold electrode are of current research interest since the organosulphur compounds offer well organised, stable and compact self-assembled monolayers. SAM modified electrodes are used in the construction of electrochemical biosensors for the following reasons: (i) they can enhance the selectivity and sensitivity, (ii) improve the response time, (iii) decrease the overpotential, (iv) ease of preparation, (v) stability, and (vi) the possibility to introduce different chemical

functionalities (Raj *et al*. 2000:181; Mazur and Krysiński 2001:3963; Brito *et al*. 2003:53; Campuzano *et al*. 2002:92).

Thiol monolayers form a group of chemical compounds that can be used to influence the properties or topological structure of chemically or electrochemically synthesized conducting polymers. Thiols can be applied to pre-organise monomers in one plane to allow subsequent polymerization. This can be achieved by covalent or ionic immobilisation of monomer molecules and their electrochemical oxidation, leading to the formation of monomolecular films of conducting polymers on the surface (Mazur and Krysiński 2001:3963). The formation of a monolayer of mercaptobenzothiazole (MBT) was chosen, since it contains an aromatic ring with a fused thiazole ring, instead of a long alkyl chain.

For the thick-film electrode, a novel route was used for the preparation of the gold electrode before polymer layers was deposited. The gold electrode surface was first modified with a thiol self-assembling monolayer (SAM) of mercaptobenzothiazole (MBT). The thiol monolayer was applied to affect the deposition process and the selectivity of the polymer formation on the electrode surface (Brito *et al*. 2003:53). Figure 4.1 shows the cyclic voltammogram (CV) of a clean Au electrode (I) in 0.1 M phosphate buffer (pH 7.2) solution at a scan rate of 10 mV.s^{-1}, compared to the same electrode coated with the MBT monolayer (II) and scanned at 10 mV/s in a 0.1 M phosphate buffer (pH 7.2) solution over the same potential range. The results show that there is a change in the selectivity and sensitivity of the Au electrode surface. Figure 4.1 also shows that there is very little

redox response once the SAM of MBT is coated, indicating that MBT forms a closely

packed monolayer (Patil *et al.* 1999:298).
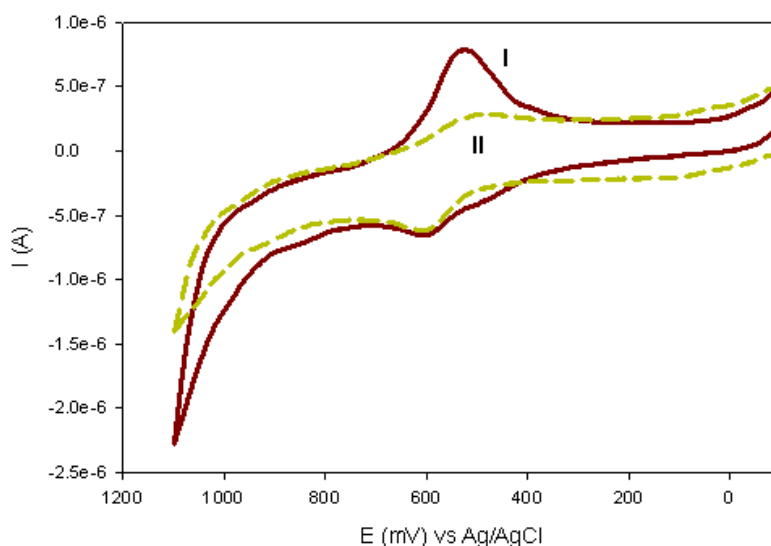
Figure 4.1 **Cyclic voltammogram recorded for a clean Au electrode in (I) and for the Au electrode plus MBT self-assembled monolayer (II) in 0.1 M phosphate buffer (pH 7.2), over a potential range of – 100 to + 1100 mV.**

Through experimentation it was decided on how long the MBT SAM will be coated

on the Au electrode. In Figure 4.2 the results for coating the MBT on the Au

electrode for 0.5, 1.0, 1.5 and 2.0 hours are shown. From the CV results it can be seen

that the redox couple obtained for the different times of MBT coating is different.

The formal potential ($E^{o\prime}$) for each of the hours of coating the MBT to the Au

electrode was calculated from the CV results. For 0.5 hours the formal potential was

calculated to be + 520.6 mV (vs. Ag/AgCl), for 1.0 hours it was found to be + 534.3

mV (vs. Ag/AgCl), for 1.5 hours it was + 537.7 mV (vs. Ag/AgCl) and for 2.0 hours

the value was + 536.9 mV (vs. Ag/AgCl). The formal potential (E$^{o\prime}$) was found to

increase from + 520.6 mV to + 537.7 mV (vs. Ag/AgCl) for 0.5 to 1.5 hours of

coating the MBT to the Au electrode, with a slight decrease in the formal potential to

+ 536.9 mV (vs. Ag/AgCl) for 2.0 hours of coating of the MBT SAM to the Au

electrode. The results obtained for the formal potential of the SAM coated at different

times thus provided the input to coat the MBT SAM on the Au electrode for 2 hours.
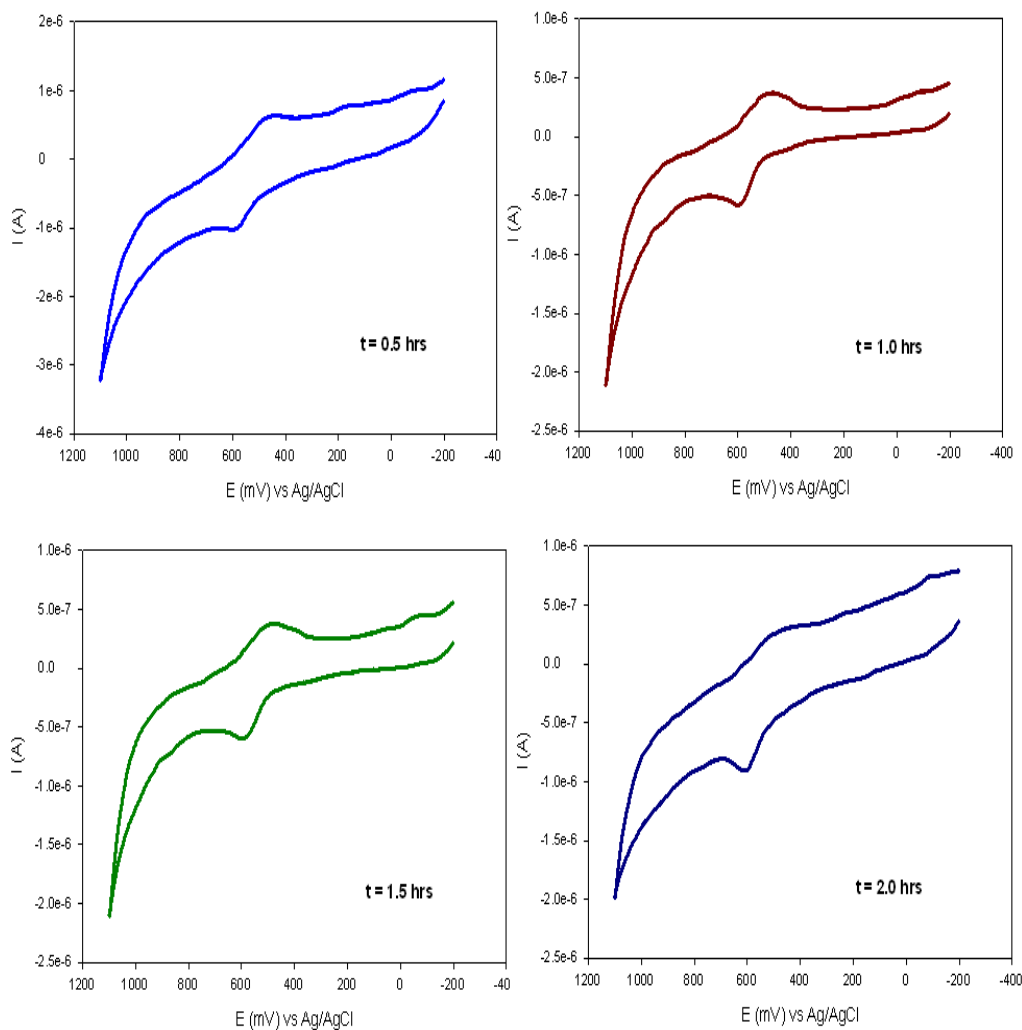
Figure 4.2   Cyclic voltammograms for MBT SAM coated on an Au electrode for 0.5, 1.0, 1.5 and 2.0 hours.

For the cyclic voltammograms (CVs) shown in Figure 4.2, the surface concentration (Γ_{MBT}) of the MBT SAM was calculated and compared to the different coating times. The surface concentration of the MBT film on the gold electrode was estimated from a plot of peak current (I_p) against scan rate (v) in accordance with Brown–Anson

analysis (Bard and Faulkner 2001:283) using Eqn. 4.3 (shown in section 4.2.1), where n represents the number of electrons transferred, F is the Faraday constant (96,584 C.mol^{-1}), Γ_{MBT} is the surface concentration of the MBT film (mol.cm^{-2}), A is the surface area of the electrode (0.0177 cm^2), v is the scan rate (V.s^{-1}), R is the gas constant (8.314 J.mol.K^{-1}), and T is the temperature of the system (298 K).

In Table 4.1 it can be seen that that as the contact time was increased for the coating of the MBT on the Au electrode, different values were obtained for the surface concentration of the MBT SAM on the Au electrode. The results also show that for a time of 2.0 hours the surface concentration was the highest.

Table 4.1   **The values of the calculated surface concentration (Γ) for the different contact times of the Au electrode in a 10 mM MBT solution.**

Time (t)	Surface concentration (Γ_{MBT}) mol.cm^{-2}
0.5	1.325×10^{-9}
1.0	5.092×10^{-10}
1.5	4.929×10^{-10}
2.0	1.228×10^{-8}

The values of Γ_{MBT} for the surface concentration of the MBT film in Table 4.1 also indicates that for the different electrode contact times with the MBT solution, only differences of approximately one order of magnitude were observed. Furthermore, the Γ_{MBT} value obtained after 2 hours of coating compares very well with a value of 2.8×10^{-10} mol.cm^{-2} calculated by Wan and Yang (2002:133) for the coating of MBT on a gold electrode surface.

Wang *et al.* (2000a:457) also reported in their research that 2 hours is the typical time required for the formation of a monolayer. The MBT thus provides a molecular resist or template upon which the polymer synthesis can be performed. The formation of the MBT SAM on the gold electrode surface is shown in Figure 4.3. In an acidic solution the protonisation of MBT occurs due to the free electron pair at the N atom. Wang *et al.* (2000a:457) has further shown that the MBT SAM shows an "opening" in an acidic solution and a "closing" in a neutral solution. The protonisation showed in Figure 4.3 shows that the monolayer carries a positive charge after protonisation. This may be followed by a structure reorientation of MBT on gold in an acidic solution, due to an electrostatic interaction between two positively charged MBT molecules. The resulting repulsion between the surface charges cause the SAM structure to open on the gold surface. Furthermore, since the MBT SAM carries a positive charge in an acidic solution, the charge plays an important role in electron transfer at a modified electrode. Since there is an interaction between charged MBT molecules, it is easy for a redox couple to penetrate the monolayer. When the MBT is positively charged, it can attract a negatively charged group such as $Fe(CN)_6^{3-/4-}$. It can thus be concluded that the N atoms at the MBT molecules play an important role in the electron transfer process, and as the MBT SAM is charged in an acidic solution, electron transfer can be promoted or inhibited according to the charge of the redox couple used (Wang *et al.* 2000a:457; Jun and Beng 2004:87).
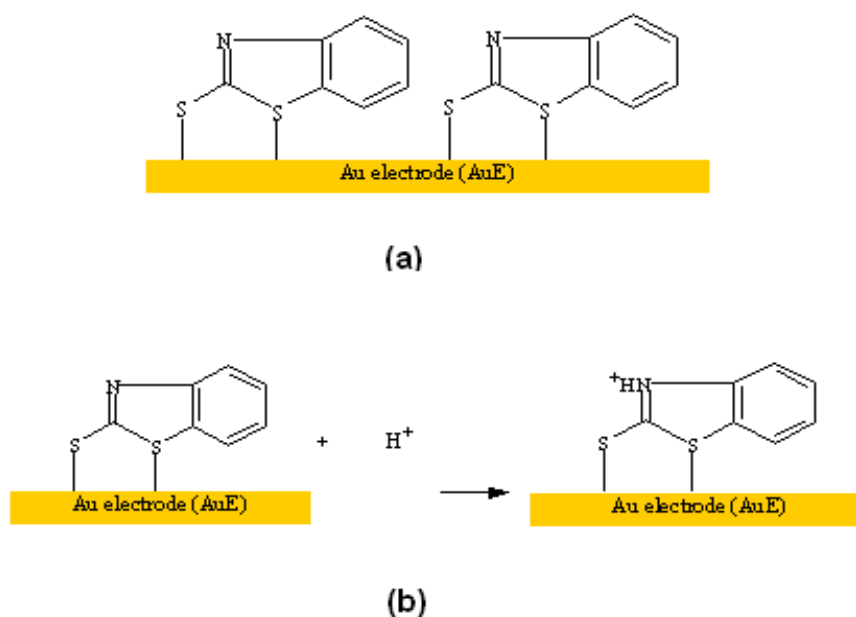
Figure 4.3   **In (a) the formation of the self-assembled monolayer (SAM) of mercaptobenzothiazole (MBT) on a gold electrode is shown, while in (b) the formation of a charged MBT monolayer in an acidic solution on a gold electrode is shown.**

4.2.1 Electropolymerisation of o-methoxyaniline (OMA)

Research has shown that the physical and chemical properties of polyanilines (PANIs) depend on the method of synthesis, whether it is chemical or electrochemical. Thus when PANIs are required for electrochemical applications, a conducting form will be required since the protonated PANIs exhibit higher conductivity and is best synthesised in acidic media (Pauliukaite *et al.* 2004:159).

The general formula of POMA is presented in Figure 4.4 (from Section 2.5.2.1.2,
Chapter 2) and when y = 0.5 POMA is found to be in the emeraldine oxidation state
(Hasik *et al.* 2004:341).
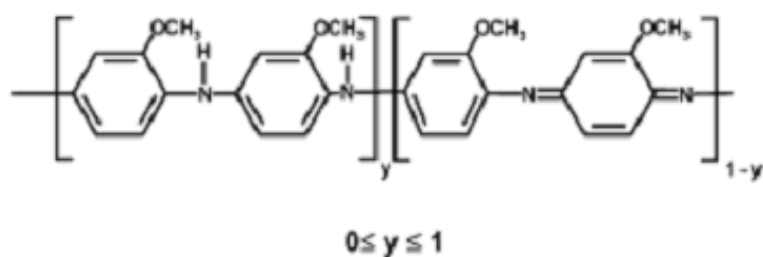
Figure 4.4   **The general formula of the POMA repeat unit with POMA being in the emeraldine oxidation state when y = 0.5 (Hasik *et al.* 2004:341).**

The electropolymerisation of OMA was first done at different scan rates of 10, 20, 40
and 100 $mV.s^{-1}$ respectively by repetitive cycling between – 500 and + 1100 mV (s.
Ag/AgCl), in a 1 M HCl solution to which the surfactant (dopant) poly(*4*-styrene
sulphonic acid) (PSSA) was also added. The reason for using the PSSA as surfactant
was to stabilise the polymer film that was synthesized on the gold electrode surface.
The cyclic voltammetric (CV) results for the electropolymerisation of OMA at the
different scan rates are shown in Figure 4.5.
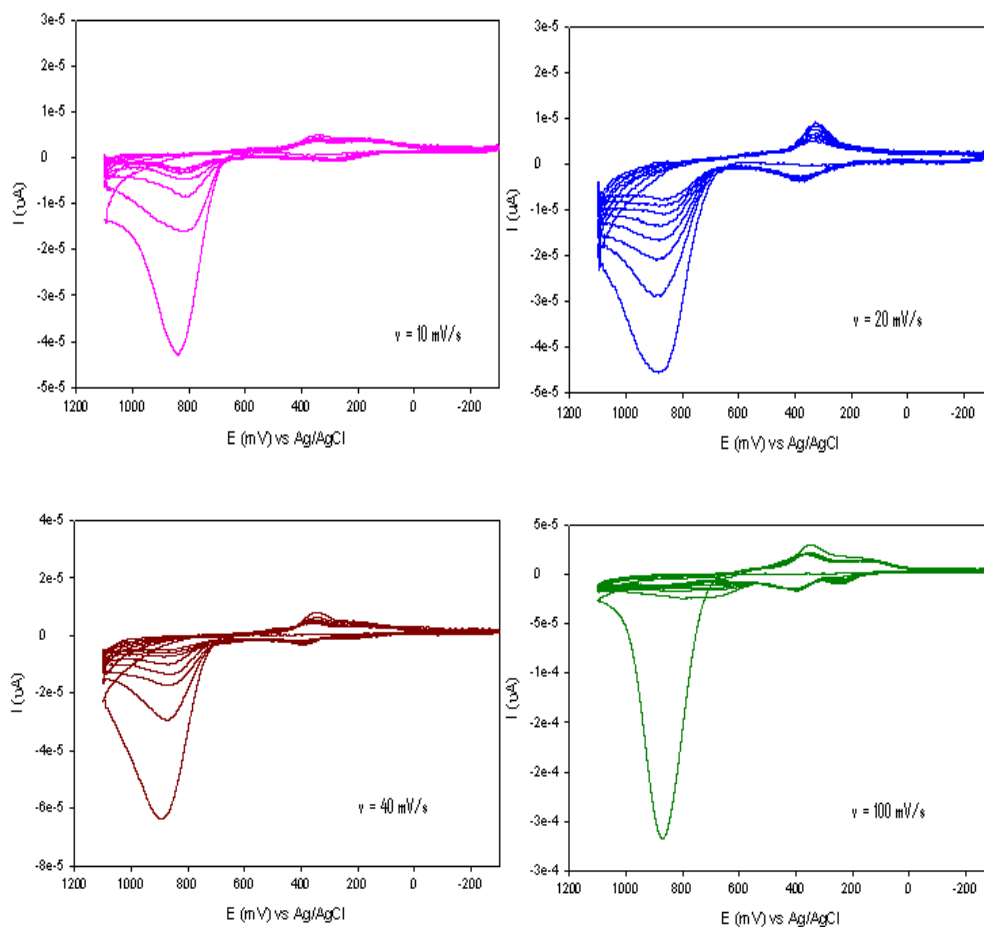
Figure 4.5   **Cyclic voltammograms for the electropolymerisation of POMA on an Au/MBT electrode at different scan rates of 10, 20, 40, 100 mV.s⁻¹.**

From the results in Figure 4.5 it can be seen that different cyclic voltammograms (CVs) were obtained for using different scan rates. For the entire scan rates employed, different shaped CVs showing the growth of a conducting polymer film on the Au electrode were obtained. The observation made is that the scan rate is either to slow or too fast. The best result was obtained with the scan rate of 20 mV.s⁻¹. A summary of the results for the electropolymerisation of POMA at different scan rates

is shown in Table 4.2. In Table 4.2 the results for the different kinetic parameters for the POMA-PSSA polymer film are also shown.

Table 4.2   **Comparison of the results for different kinetic parameters for the POMA-PSSA polymer electropolymerisation at different scan rates.**

Scan rate, v (mV/s)	Surface concentration (Γ^{*}_{POMA}), (mol.cm^{-2})	Electron diffusion coefficient (D_e), (cm^2.s^{-1})	Standard heterogeneous rate constant (k^o) (cm.s^{-1})	Peak potential separation, ΔE_p, (mV)
10	4.194×10^{-3}	1.151×10^{-13}	3.029×10^{-7}	59.1
20	5.559×10^{-3}	1.181×10^{-14}	1.372×10^{-8}	57.6
40	4.260×10^{-3}	1.113×10^{-13}	5.958×10^{-7}	41.4
100	8.537×10^{-3}	2.770×10^{-14}	4.699×10^{-7}	46.2

From the results in Table 4.2 it can be seen that the surface concentration (Γ^{*}_{POMA}) of the POMA-PSSA polymer film is of the same order of magnitude for the different scan rates at which the electropolymerisation was investigated. Different values for the electron diffusion coefficient (D_e) were obtained that are also of different orders of magnitude, indicating that electron transport along the polymer backbone occurs at different rates for the different scan rates used. On the other hand, no big differences in the surface concentration at the different scan rates were obtained. The values of the standard heterogeneous rate constant, k^o, for the analysis at different scan rates, are also of similar order of magnitude, except for the one at a scan rate of 20 mV.s^{-1} that are one order less. This further indicates that the transport of charge along the polymer chain was relatively slower at this scan rate, which resulted in the POMA

being fully oxidised and reduced as observed in the CV in Figure 4.5. The first redox couple for all CVs that is clearly visible in the CV at a scan rate of 20 mV.s-1, shows reversibility since the results in Table 4.2 gives a peak potential separation (ΔE_p) value that is approximately equal to 59 mV for a one electron process. Using the above results, it was then decided to perform electropolymerisation at a scan rate of 20 mV.s^{-1} as shown in Figure 4.6.

The cyclic voltammogram (CV) for the POMA polymer film was obtained by applying sequential linear potential between - 500 to + 1100 mV (vs. Ag/AgCl) at a scan rate of 20 mV.s^{-1}, as shown in Figure 4.6. The CV shows two prominent anodic peaks (+ 377.0 (a) and + 887.5 mV (c) vs. Ag/AgCl) with one prominent cathodic peak (+ 324.2 mV vs. Ag/AgCl) in (b). Previous studies (Iwuoha *et al.* 1997:749; Patil *et al.* 1999:298) attribute the two redox peaks for PANI and POMA to the transition of leucoemeraldine base (LB) to the emeraldine salt (ES) in (a) and ES to pernigraniline salt (PS) in (c). On the reverse scan the cathodic peak in (b) is attributed to the transformation from ES to LB. Repeated scanning of the potential resulted in an increase in the amplitude of the redox peaks, indicating that the polymer is polymerising at the Au/MBT surface and that the polymer is conducting. It also provides further evidence that the Au/MBT surface is conductive.
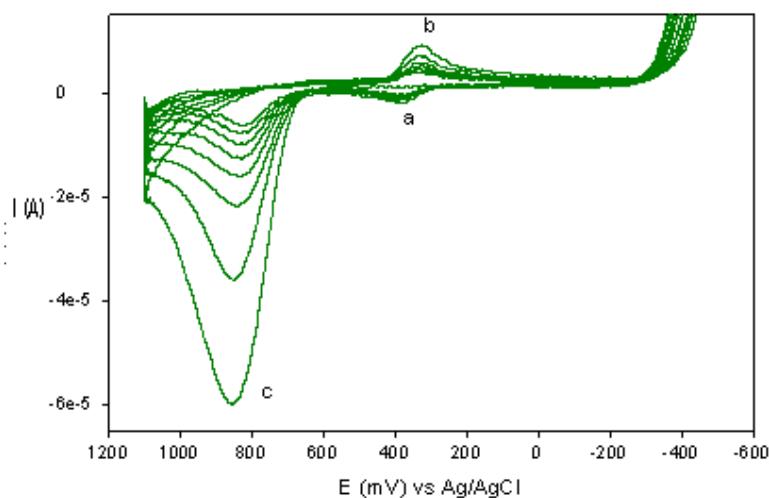
Figure 4.6   **Cyclic voltammogram obtained for the synthesis of POMA during repetitive cycling between – 500 and + 1100 mV in a 1 M HCl plus PSSA solution.**

The kinetic parameters of the electron transfer process for the POMA-PSSA polymer film characterised in HCl solution were calculated. The CV of the POMA-PSSA polymer film was used to calculate the rate parameter, ψ, for equation 4.1 (Zanello 2003:63-64). Equation 4.2 (Bard and Faulkner 2001:231) was used to calculate the number of electrons (n) transferred during electropolymerisation and found to be $n =$ 1. Equation 4.1 was further used to calculate k^o, the standard heterogeneous rate constant for the electron transfer reaction. The surface concentration of the POMA-PSSA polymer film, Γ^*_{POMA}, was calculated with equation 4.3 (Zanello 2003:107) and found to be $5.559 \ x \ 10^{-3}$ mol.cm^{-2}. The electron transport diffusion coefficient, D_e, was obtained from a Randle-Sevčik plot of Ip vs $v^{\frac{1}{2}}$ and found to be $1.181 \ x \ 10^{-14}$ cm².s^{-1}. Thus at 25 ºC, with $\alpha = 0.5$, the value of k^o was calculated as $1.372 \ x \ 10^{-8}$

cm.s^{-1}. The POMA polymer film thickness, L (cm), was estimated from the voltammetric charge passed during electropolymerisation using equation 4.4 (Iwuoha *et al.* 1997:749) and found to be 4.367 *x* 10^{-13} cm.

$$\Psi = \frac{k°}{\left[\dfrac{\alpha \cdot n \cdot F \cdot v \cdot D}{R \cdot T}\right]^{\frac{1}{2}}} \qquad \text{Eqn. 4.1}$$

$$\left|E_p - E_{p/2}\right| = 2.20 \frac{R \cdot T}{n \cdot F} \qquad \text{Eqn. 4.2}$$

$$I_p = \frac{n^2 \cdot F^2 \cdot A \cdot \Gamma^* \cdot v}{4 \cdot R \cdot T} \qquad \text{Eqn. 4.3}$$

$$\frac{I_{p,c}}{v^{\frac{1}{2}}} = \frac{0.446 \cdot (nF)^{3/2} \cdot D_e \cdot \Gamma^*}{L \cdot (RT)^{\frac{1}{2}}} = slope \qquad \text{Eqn. 4.4}$$

The variation of peak current and peak potential with scan rate was also analysed for the POMA-PSSA polymer films and the results are shown in Table 4.3.

Table 4.3   **Results for the effect of scan rate on anodic and cathodic peak current and peak potentials in CVs for electropolymerisation of POMA-PSSA on Au/MBT surface.**

Scan rate, v (mV.s^{-1})	Square root of scan rate, $v^{1/2}$ (mV.s^{-1})$^{1/2}$	Anodic peak current, $I_{p,a}$ (A) (x 10^{-6})	Cathodic peak current, $I_{p,c}$ (A) (x 10^{-6})	Anodic peak potential, $E_{p,a}$ (mV)	Cathodic peak potential, $E_{p,c}$ (mV)	Peak potential separation, ΔE_p, (mV)	$I_{p,a}/I_{p,c}$
10	3.16	-1.019	4.521	266.3	207.2	59.1	0.23
20	4.47	-9.418	17.59	386.4	328.8	57.6	0.54
40	6.32	-3.241	8.116	385.8	344.4	41.4	0.40
100	10.00	-15.29	30.14	394.6	348.4	46.2	0.51

For the kinetic parameters calculated in Table 4.3, is was found that the anodic peak potential increases as the scan rate increases form 10 to 20 mV.s^{-1} and remains relatively constant as the scan rate further increase to 100 mV.s^{-1}. A similar trend was observed for the cathodic peak potentials, while the peak potential separation (ΔE_p) are approximately equal to 59 mV for a one electron process as reported earlier. No clear conclusion of the $I_{p,a}/I_{p,c}$ ratio for the increase in scan rate could be made at this stage of the analysis as no clear trend was observed.

4.2.2 Electropolymerisation of 2,5-dimethoxyaniline (DMA)

The general formula of PDMA is presented in Figure 4.7 (from Section 2.5.2.1.3, Chapter 2) showing part of the structure of poly(2,5-dimethoxyaniline) (PDMA).
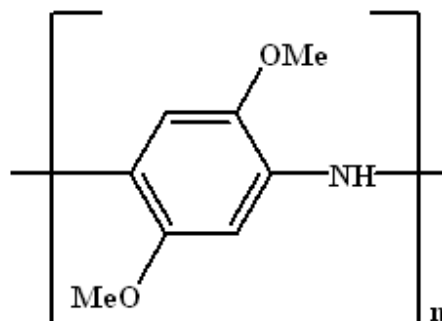
Figure 4.7   **The general formula of a single poly(2,5-dimethoxyaniline) (PDMA) unit.**

Similarly as for POMA, the electropolymerisation of *2,5*-dimethoxyaniline (DMA) was first done at different scan rates of 10, 20, 40 and 100 mV.s^{-1} respectively by repetitive cycling between – 200 and + 1100 mV vs. Ag/AgCl, in a 1 M HCl solution to which the surfactant (dopant) poly(*4*-styrene sulphonic acid) (PSSA) was also added. The CV results for the electropolymerisation of DMA at the different scan rates are shown in Figure 4.8.
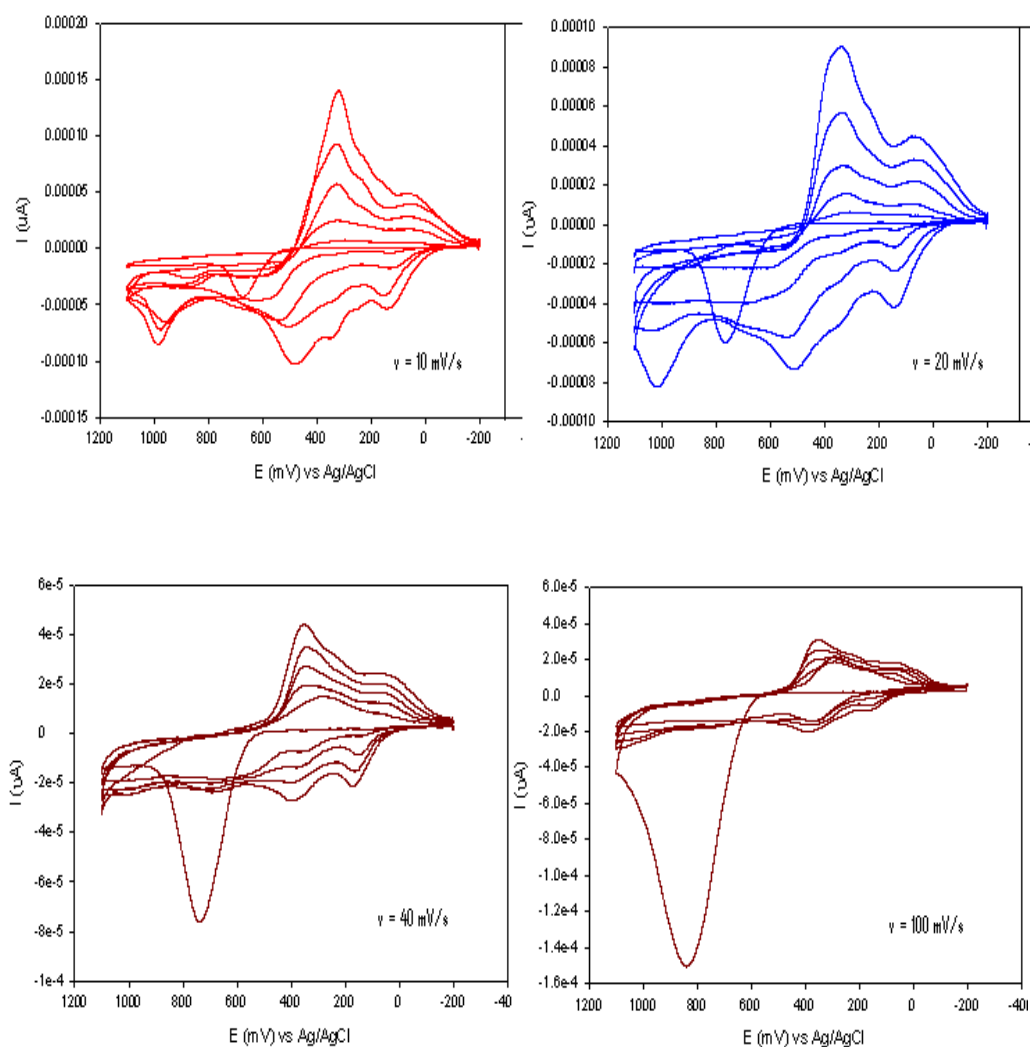
Figure 4.8   **Cyclic voltammograms for the electropolymerisation of PDMA on a Au/MBT electrode at different scan rates of 10, 20, 40, 100 mV.s^{-1}.**

In Table 4.4 a summary of the results for the different kinetic parameters for the PDMA-PSSA polymer electropolymerisation are shown.

Table 4.4   **Comparison of the results for different kinetic parameters for the PDMA-PSSA polymer electropolymerisation at different scan rates.**

Scan rate (mV/s)	Surface concentration (Γ^*_{PDMA}), (mol.cm^{-2})	Electron diffusion coefficient (D_e), (cm^2.s^{-1})	Standard heterogeneous rate constant (k^o) (cm.s^{-1})	Peak potential separation, ΔE_p, (mV)
10	1.520×10^{-1}	8.743×10^{-17}	8.348×10^{-9}	173.6
20	1.939×10^{-1}	5.373×10^{-17}	9.255×10^{-9}	173.4
40	2.200×10^{-2}	4.174×10^{-15}	1.154×10^{-7}	5.6
100	1.062×10^{-2}	1.791×10^{-14}	3.779×10^{-7}	38.4

From the results in Table 4.4 it can be seen that the surface concentration (Γ^*_{PDMA}) of the PDMA-PSSA polymer film is one order of magnitude higher at the slow scan rates of 10 and 20 mV.s^{-1}, as compared to the faster scan rates of 40 and 100 mV.s^{-1}. Again different values for the electron diffusion coefficient (D_e) were obtained that are also of different orders of magnitude, indicating that electron transport along the polymer backbone occurs at different rates. The values of the standard heterogeneous rate constant, k^o, are of the same order of magnitude for the slow scan rates and similarly for the faster scan rates. In the case of the scan rate of 40 mV.s^{-1}, the results for the kinetic parameters resulted in the scan rate being favoured for electropolymerisation, since the peak potential separation (ΔE_p) of 5.6 mV was also the lowest for the one electron transfer process.

The cyclic voltammogram (CV) for the PDMA polymer film was obtained by applying sequential linear potential between - 200 to +1100 mV at a scan rate of 40 mV/s, as shown in Figure 4.9. The CV shows prominent anodic peaks at + 111.5 (a),

+ 378.5 (c) and + 1008.3 mV (e) (vs. Ag/AgCl) respectively. One prominent cathodic

peak was observed at + 409.3 mV (d) (vs. Ag/AgCl) and a very smaller second

cathodic peak at + 29.5 mV (b) (vs. Ag/AgCl). Previous studies (Huang *et al.*

2002:155; Palys *et al.* 2000:111) attribute the two main redox peaks of PDMA to the

transition of leucoemeraldine base (LB) to the emeraldine salt (ES) in (a) and ES to

pernigraniline salt (PS) in (c). On the reverse scan the cathodic peak in (d) is

attributed to the transformation from PS to ES, while the peak in (b) accounts for the

transformation of ES to LB. Repeated scanning of the potential resulted in an increase

in the amplitude of the redox peaks, indicating that the polymer is polymerising at the

Au/MBT surface and that the polymer is conducting.
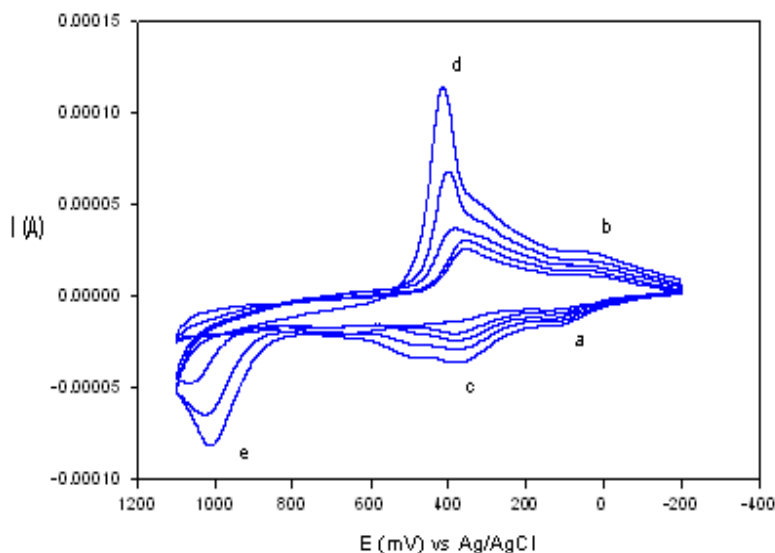
Figure 4.9   **Cyclic voltammogram obtained for the synthesis of PDMA during repetitive cycling between – 200 and + 1100 mV in a 1 M HCl plus PSSA solution.**

The kinetic parameters of the electron transfer process for the PDMA-PSSA polymer film characterised in HCl solution were calculated with $n = 1$, using Equation 4.1 (Zanello 2003:63-64). The surface concentration of the PDMA-PSSA film, Γ^*_{PDMA}, was calculated with equation 4.3 (Zanello 2003:107) and found to be $2.200 \; x \; 10^{-2}$ mol.cm^{-2}. From a Randel-Sevčik plot of i_p vs $v^{\frac{1}{2}}$, $D_e = 4.174 \; x \; 10^{-15}$ cm².s^{-1} was obtained. At 25 ºC and $\alpha = 0.5$, the value of k^o was calculated with equation 4.1 (Zanello 2003:283) and found to be $1.154 \; x \; 10^{-7}$ cm.s^{-1}. The PDMA film thickness, L (cm), was estimated with equation 4.4 (Iwuoha *et al.* 1997:749) and found to be $2.833 \; x \; 10^{-12}$ cm.

The variation of peak current and peak potential with scan rate was also analysed for the PDMA-PSSA polymer films and the results are shown in Table 4.5.

Table 4.5   **Results for the effect of scan rate on anodic and cathodic peak current and peak potentials in CVs for electropolymerisation of PDMA-PSSA on Au/MBT surface.**

Scan rate, v (mV.s^{-1})	Square root of scan rate, $v^{\frac{1}{2}}$ (mV.s^{-1})$^{\frac{1}{2}}$	Anodic peak current, $I_{p,a}$ (A) ($x \; 10^{-5}$)	Cathodic peak current, $I_{p,c}$ (A) ($x \; 10^{-5}$)	Anodic peak potential, $E_{p,a}$ (mV)	Cathodic peak potential, $E_{p,c}$ (mV)	Peak potential Separation, ΔE_p, (mV)	$I_{p,a}/I_{p,c}$
10	3.16	-11.32	7.999	515.5	341.9	173.6	1.42
20	4.47	-7.341	9.003	513.3	339.9	173.4	0.82
40	6.32	-3.594	6.253	404.8	410.4	5.6	0.57
100	10.00	-2.039	3.058	390.9	352.5	38.4	0.67

For the kinetic parameters calculated in Table 4.5, is was found that the anodic peak potential decreased as the scan rate increased, while no clear trend could be observed for the cathodic peak potentials. For the peak potential separation (ΔE_p) different values were obtained that were very big for the slow scan rates, while it was much smaller for the faster scan rates. Only at the fast scan rates the peak potential separation (ΔE_p) values were indicative of a one electron process taking place. No clear conclusion of the $I_{p,a}/I_{p,c}$ ratio for the increase in scan rate could be made at this stage of the analysis as no clear trend was observed.

4.3   Characterisation of the polymer films

4.3.1 Characterisation of Au/MBT/POMA-PSSA polymer film

The cyclic voltammograms (CVs) in Figures 4.10 shows the CV of a clean Au electrode (I) in 0.5 M H_2SO_4 at a scan rate of 40 mV.s^{-1}, compared to the same electrode coated with the MBT SAM (II) and scanned at 40 mV/s in a 0.1 M phosphate buffer (pH 7.2) solution over the same potential range.

On top of the MBT SAM the polymer film of POMA in (III) is shown in Figure 4.10. It can be seen in Figure 4.10 that the MBT SAM forms a closely packed monolayer on the Au surface, since the Au/MBT modified electrode in (II) showed no clear redox response. However, with the electropolymerisation of the POMA film,

it can be seen that the peak current increases. For the Au/MBT/POMA-PSSA polymer film the anodic peak potential ($E_{p,a}$) and cathodic peak potential ($E_{p,c}$) were found to be + 377.0 and + 324.2 mV (vs. Ag/AgCl) respectively. The formal potential ($E^{o\prime}$) was calculated to be + 350.6 mV (vs. Ag/AgCl).
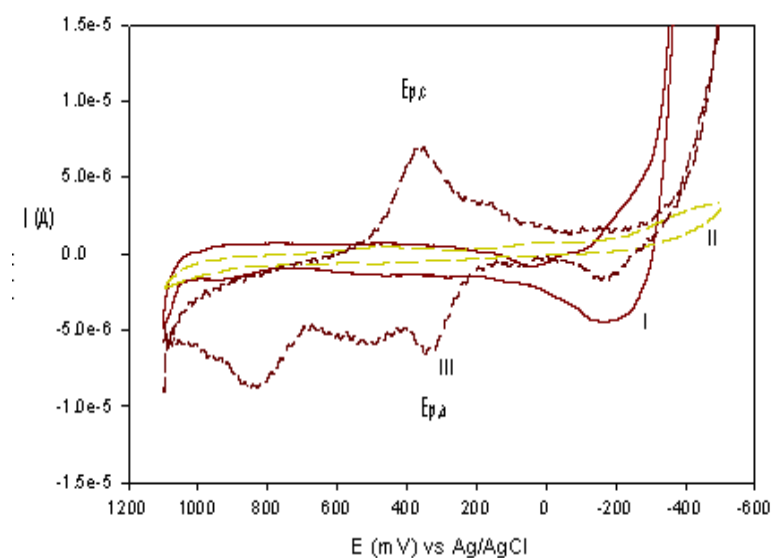
Figure 4.10 **Cyclic voltammogram of AuE + MBT + POMA-PSSA polymer film in 0.1 M phosphate buffer (pH 7.2) over a potential range of –500 to +1100 mV (vs. Ag/AgCl).**

In Figure 4.11 the CV results for the Au/MBT/POMA-PSSA polymer film at different scan rates in 0.1 M phosphate buffer, KCl (pH 7.2) solution is shown, with the arrows indicating the direction of increasing scan rate.
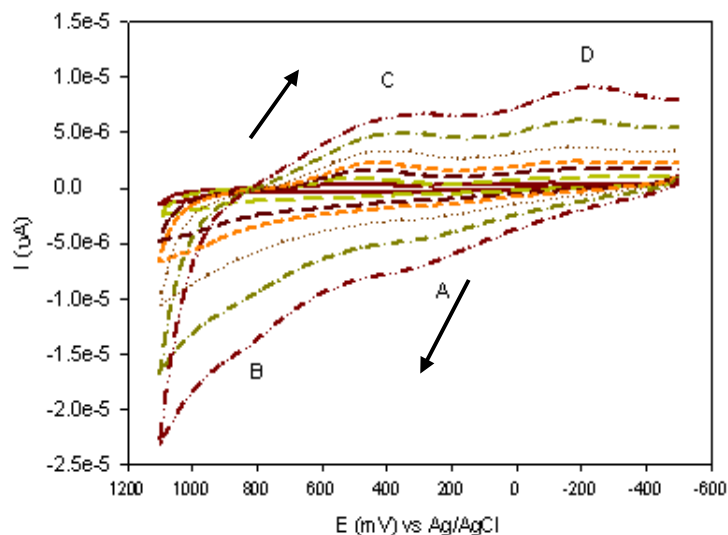
Figure 4.11   **Cyclic voltammograms for the Au/MBT/POMA-PSSA polymer film in 0.1 M phosphate buffer (pH 7.2) at different scan rates of 5, 20, 60, 100, 200, 400, 700 mV.s^{-1}.**

In Figure 4.11 the peaks in A and B are anodic, while peaks C and D are for the cathodic processes occurring. Figure 4.11 also indicates that the peak potentials of all four peaks are shifting to higher values as the scan rate is increased. The Randel-Sevčik equation was thus used to determine the rate of electron transport (D_e) within the polymer layer. The value for the surface concentration (Γ^*_{POMA}) of the POMA polymer film was also calculated. The surface concentration of the POMA-PSSA polymer film, Γ^*_{POMA}, was estimated in 0.1 M phosphate buffer (pH 7.2) and found to be 2.902 x 10^{-3} mol.cm^{-2}. The electron transport diffusion coefficient, D_e, was obtained from a Randle-Sevčik plot of I_p vs. $v^{1/2}$ and found to be 1.523 x 10^{-16} cm².s^{-1}.

Better redox activity was observed for the Au/MBT/POMA-PSSA polymer film at different scan rates in 0.1 M HCl than in 0.1 M phosphate buffer, KCl (pH 7.2) solution as shown in Figure 4.12, with the arrows indicating the direction of increasing scan rate.
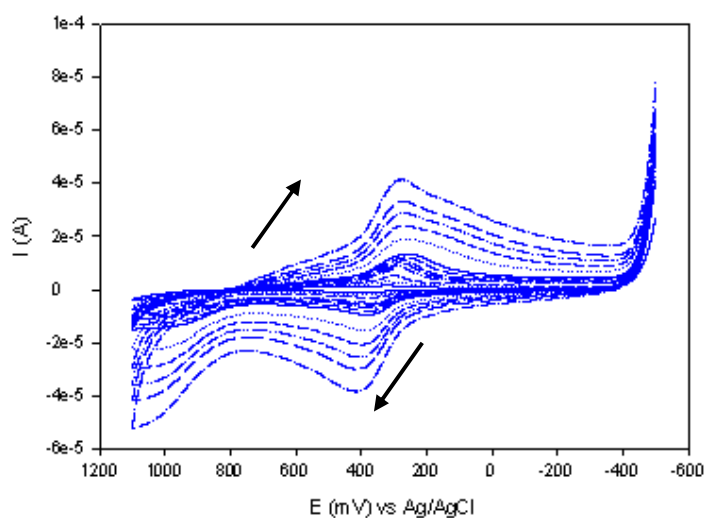
Figure 4.12   **Cyclic voltammograms for the Au/MBT/POMA-PSSA polymer film in 0.1 M HCl at different scan rates of 5, 10, 20, 40, 60, 80, 100, 200, 300, 400, 500, 700 mV.s^{-1}.**

Similarly, the CV results in Figure 4.12 indicate that for the POMA-PSSA polymer film, a distinct redox couple was observed. It also shows that the peak potentials shifted to higher values as the scan rate was increased. This is again observed in Figure 4.13 where the CVs of only certain scan rates are shown and the arrows indicate the direction. This was an indication that the Randel-Sevčik equation may be used to determine the rate of electron transport (D_e) within the polymer layer. The

value for the surface concentration (Γ^*_{POMA}) of the POMA polymer film was also calculated. In the 0.1 M HCl solution Γ^*_{POMA}, was found to be 5.559 x 10^{-3} mol.cm^{-2}, while the electron transport diffusion coefficient, D_e, was found to be 1.181 x 10^{-14} cm².s^{-1}.
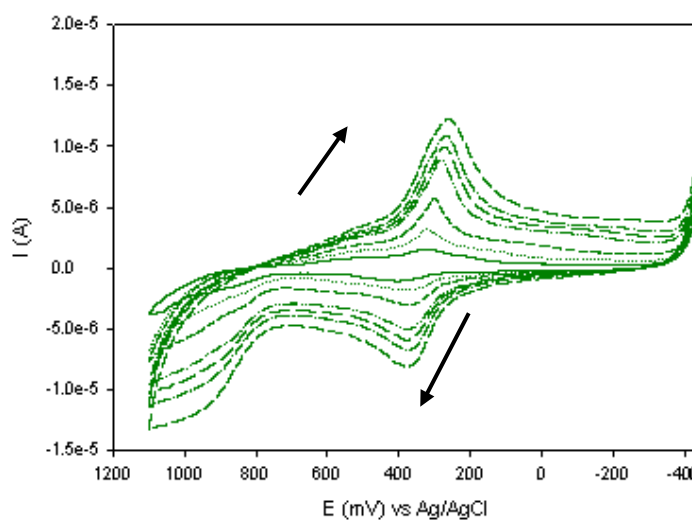
Figure 4.13 **Cyclic voltammograms for the Au/MBT/POMA-PSSA polymer film in 0.1 M HCl at different scan rates of 5, 20, 40, 60, 80, 100 mV.s^{-1}.**

The data of the CVs shown in Figures 4.12 and 4.13 were further evaluated and the results are shown in Table 4.6.

Table 4.6   **Results for the effect of scan rate on anodic and cathodic peak current and peak potentials in CVs for different scan rates in 0.1 M HCl solution.**

Scan rate, v (mV/s)	Square root of scan rate, $v^{1/2}$ (mV/s)$^{1/2}$	Anodic peak potential, $E_{p,a}$ (mV)	Anodic peak current $I_{p,a}$ (A) (x 10^{-6})	Cathodic peak potential, $E_{p,c}$ (mV)	Cathodic peak current, $I_{p,c}$ (A) (x 10^{-6})	Peak potential separation, ΔE_p (mV)	$I_{p,a}/I_{p,c}$
5	2.236	405.4	-1.032	324.3	1.488	81.1	0.69
10	3.162	382.3	-1.810	323.3	3.257	59.0	0.56
20	4.472	374.4	-2.936	299.8	5.670	74.6	0.52
40	6.325	374.4	-4.987	281.6	8.954	92.8	0.56
50	7.071	377.4	-5.705	271.3	10.17	106.1	0.56
60	7.746	373.0	-6.777	266.8	11.02	106.2	0.61
80	8.944	377.4	-8.064	258.0	12.10	119.4	0.67
100	10.000	381.8	-9.351	253.6	13.60	128.2	0.69
200	14.142	390.7	-15.52	262.4	19.06	128.3	0.81
300	17.321	399.5	-20.59	266.8	24.45	132.7	0.84
400	20.000	408.4	-25.01	271.3	29.28	137.1	0.85
500	22.361	412.8	-30.24	275.7	33.70	137.1	0.90
700	26.458	417.2	-38.34	280.1	42.09	137.1	0.91

The results in Table 4.6 were used to plot a graph of ΔE_p vs. scan rate (v) as shown in Figure 4.14. From the shape of the graph in Figure 4.14 it can be seen that it does not follow the Randles-Sevcik equation, since a straight line was not obtained that may be attributed to slow electron transfer kinetics in the polymer film.
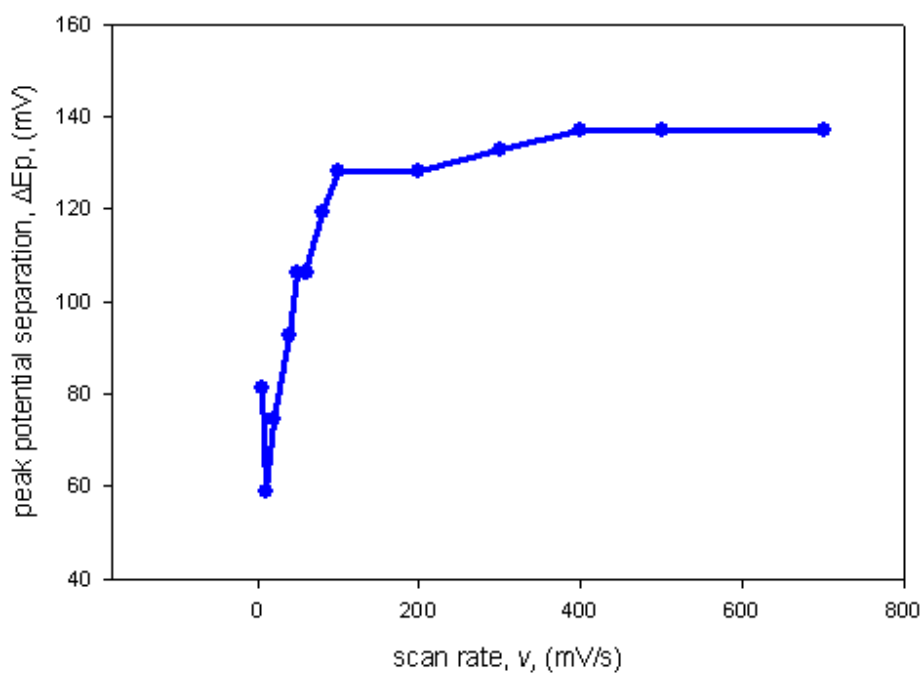
Figure 4.14   **Graph of peak potential separation (ΔE_p) vs. scan rate (v) for the Au/MBT/POMA-PSSA polymer film in 0.1 M HCl solution at different scan rates.**

On the other hand, the graph of anodic and cathodic peak current (Ip) vs. the square root of scan rate ($v^{1/2}$) in Figure 4.15, shows linearity which demonstrates that the process are absorption controlled.
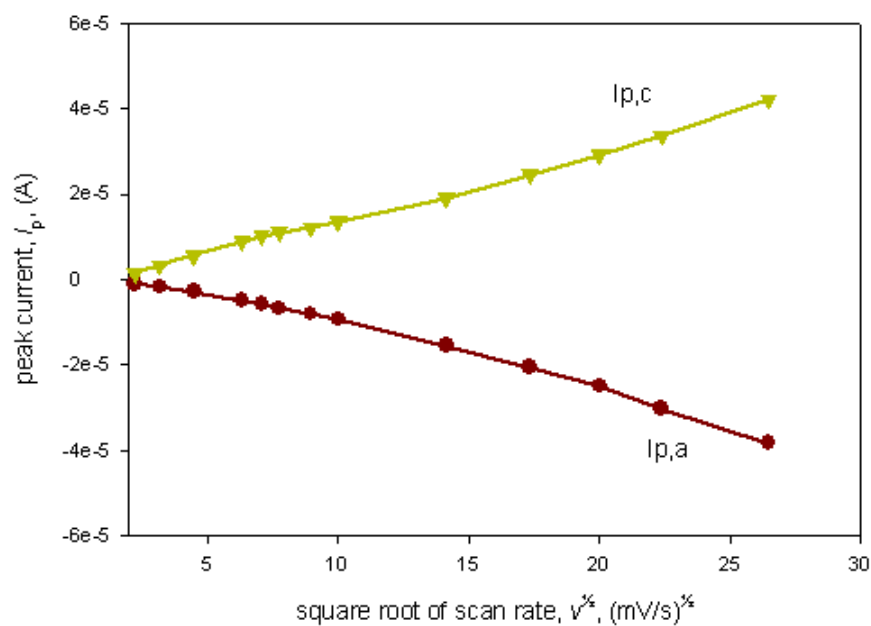
Figure 4.15   **Graph of anodic and cathodic peak current (I_p) vs. square root of scan rate ($v^{1/2}$) for the Au/MBT/POMA-PSSA polymer film in 0.1 M HCl solution at different scan rates.**

The results in Table 4.6 further indicate that the peak potential separation increases relatively with the scan rate, indicating some limitation due to charge transfer kinetics, with the results for the slow scan rates of 5 to 40 mV.s^{-1} indicating a reversible system, while the anodic and cathodic peak ratio ($I_{p,a}/I_{p,c}$) is less than unity. When the values for Γ^*_{POMA}, and D_e, are compared for the two solution used (i.e phosphate buffer and HCl), the following results are obtained, as shown in Table 4.7.

Table 4.7   **Surface concentration and electron transport coefficient for the POMA-PSSA polymer film.**

Solution	Surface concentration (Γ^*), $mol.cm^{-2}$	Electron transport coefficient, (D_e), $cm^2.s^{-1}$
0.1 M phosphate buffer (pH 7.2)	$2.902 \, x \, 10^{-3}$	$1.523 \, x \, 10^{-16}$
0.1 M HCl	$5.559 \, x \, 10^{-3}$	$1.181 \, x \, 10^{-14}$

From the results in Table 4.7 it can be deduced that the conductivity of the POMA-PSSA polymer film is representative of a conductive film and it is observed that the D_e value is approximately two orders of magnitude higher in the 0.1 M HCl solution as compared to the 0.1 M phosphate buffer, pH (7.2) solution.

4.3.2 Characterisation of Au/MBT/PDMA-PSSA polymer film

The cyclic voltammograms (CVs) in Figure 4.16 shows the CV of a clean Au electrode (I) in 0.5 M H_2SO_4 at a scan rate of 40 $mV.s^{-1}$, compared to the same electrode coated with the MBT SAM (II) and scanned at 40 $mV.s^{-1}$ in a 0.1 M phosphate buffer (pH 7.2) solution over the same potential range.
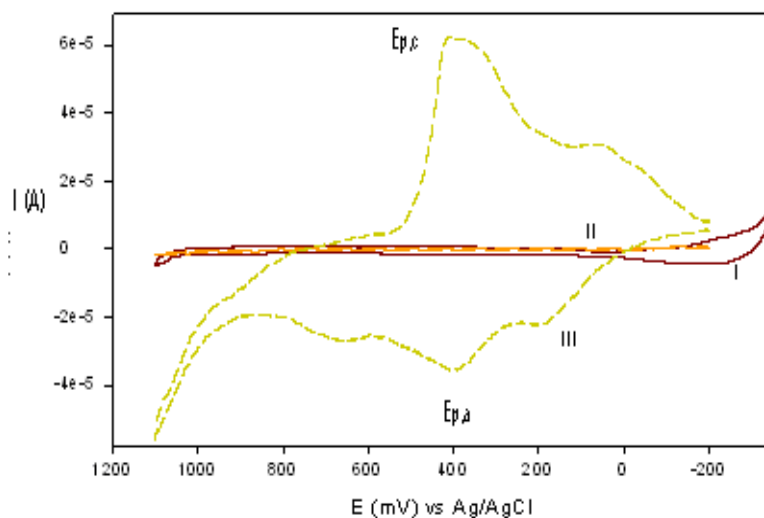
Figure 4.16   **Cyclic voltammogram of AuE + MBT + PDMA-PSSA polymer film in 0.1 M phosphate buffer (pH 7.2), over a potential range of –200 to +1100 mV.**

As previously, on top of the MBT SAM the polymer film of PDMA are shown in (III) in Figure 4.16. It can be seen in Figure 4.16 that the MBT SAM forms a closely packed monolayer on the Au surface, since the Au/MBT modified electrode in (II) showed no clear redox response. Again, with the electropolymerization of the PDMA film, it can be seen that the peak current increases. In the case of the Au/MBT/PDMA-PSSA polymer film the anodic peak potential ($E_{p,a}$) and cathodic peak potential ($E_{p,c}$) were found to be + 399.0 and + 405.9 mV (vs. Ag/AgCl) respectively. The formal potential ($E^{o\prime}$) was calculated to be + 402.5 mV (vs. Ag/AgCl).

In Figure 4.17 the CV results for the Au/MBT/PDMA-PSSA polymer film at

different scan rates in 0.1 M phosphate buffer (pH 7.2) solution is shown, with the

arrows indicating the direction of increasing scan rate.
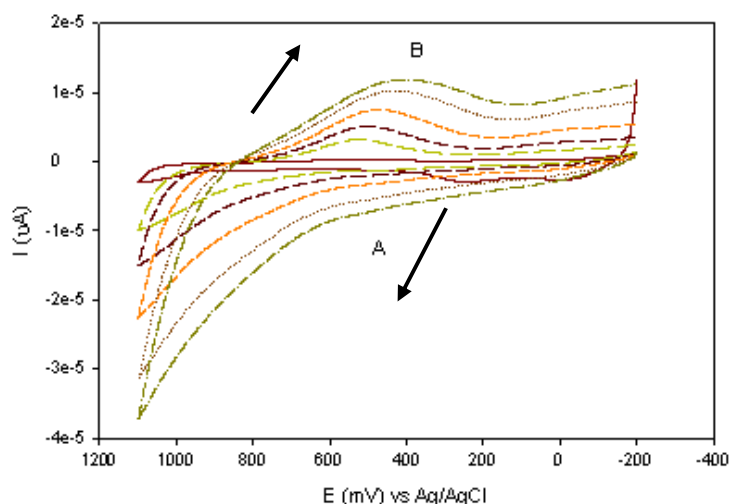
Figure 4.17   Cyclic voltammograms for the Au/MBT/PDMA-PSSA polymer film in
0.1 M phosphate buffer (pH 7.2) at different scan rates of 5, 50, 100,
200, 400, 600 mV.s^{-1}.

In Figure 4.17 the peak in A is anodic, while peak B is for the cathodic processes

occurring. Figure 4.17 also indicates that the peak potentials of the two peaks are

shifting to higher values as the scan rate is increased. The Randel-Sevčik equation

was thus used to determine the rate of electron transport (D_e) within the polymer

layer. The value for the surface concentration (Γ^*_{PDMA}) of the PDMA polymer film

was also calculated. The surface concentration of the PDMA-PSSA film, Γ^*_{PDMA},

was estimated in 0.1 M phosphate buffer (pH 7.2) solution and found to be 1.177 x

10^{-2} mol.cm^{-2}. From a Randel-Sevčik plot of I_p vs. $v^{\frac{1}{2}}$, the value for $D_e = 1.396 \, x \, 10^{-15}$ cm^2.s^{-1} was obtained.

In Figure 4.18 the CV results for the Au/MBT/PDMA-PSSA polymer film at different scan rates in 0.1 M HCl solution is shown, with the arrows indicating the direction of increasing scan rate.
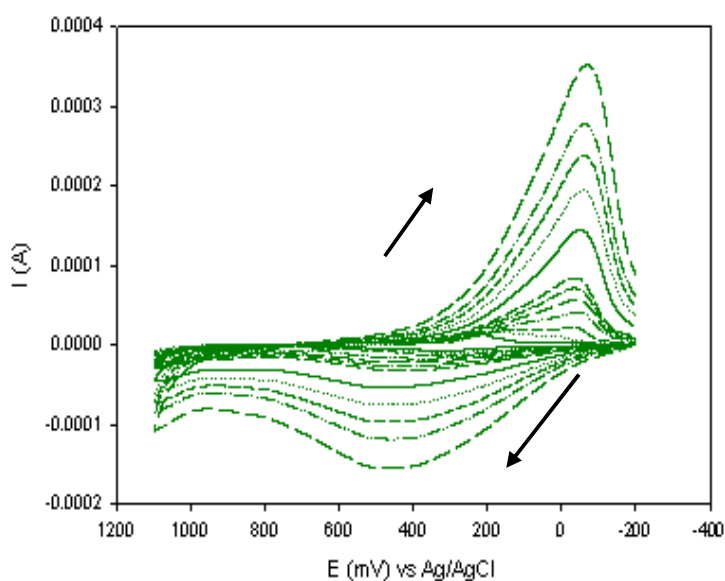
Figure 4.18   **Cyclic voltammograms for the Au/MBT/PDMA-PSSA polymer film in 0.1 M HCl at different scan rates of 5, 10, 20, 40, 60, 80, 100, 200, 300, 400, 500, 700 mV.s^{-1}.**

Similarly, the CV results in Figure 4.18 indicate that for the PDMA-PSSA polymer film, a distinct redox couple was observed. It also shows that the peak potentials shifted to higher values as the scan rate was increased, with the arrows indicating the direction of increasing scan rate. This is again observed in Figure 4.19 where the CVs

of only certain scan rates are shown. This was indication that the Randel-Sevčik equation may be used to determine the rate of electron transport (D_e) within the polymer layer. The value for the surface concentration (Γ^*_{PDMA}) of the PDMA polymer film was also calculated. In the 0.1 M HCl solution Γ^*_{PDMA}, was found to be 2.200 x 10^{-2} mol.cm^{-2}, while the electron transport diffusion coefficient, D_e, was found to be 4.174 x 10^{-15} cm².s^{-1}.
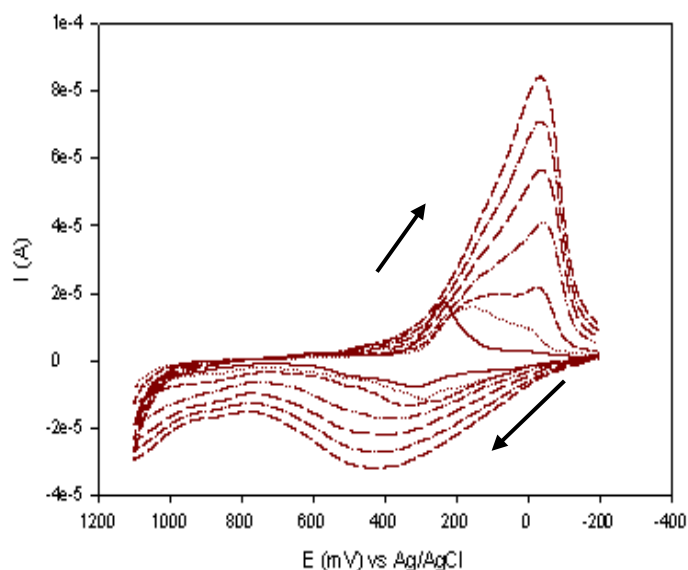
Figure 4.19   **Cyclic voltammograms for the Au/MBT/PDMA-PSSA polymer film in 0.1 M HCl at different scan rates of 5, 10, 20, 40, 60, 80, 100 mV.s^{-1}.**

The data of the CVs shown in Figures 4.18 and 4.19 were further evaluated and the results are shown in Table 4.8.

Table 4.8   **Results for the effect of scan rate on anodic and cathodic peak current and peak potentials in CVs for different scan rates in 0.1 M HCl solution.**

Scan rate, v (mV/s)	Square root of scan rate, $v^{1/2}$ (mV/s)$^{1/2}$	Anodic peak potential, $E_{p,a}$ (mV)	Anodic peak current $I_{p,a}$ (A) ($x\ 10^{-5}$)	Cathodic peak potential, $E_{p,c}$ (mV)	Cathodic peak current, $I_{p,c}$ (A) ($x\ 10^{-5}$)	Peak potential separation, ΔE_p (mV)	$I_{p,a}/I_{p,c}$
5	2.236	313.4	-0.7692	234.7	1.762	78.7	0.44
10	3.162	289.5	-1.147	159.4	1.566	130.1	0.73
20	4.472	334.0	-1.334	77.3	1.980	256.7	0.67
40	6.325	375.1	-1.717	-42.6	4.113	417.7	0.42
60	7.746	408.8	-2.210	-38.3	5.694	447.1	0.39
80	8.944	422.6	-2.593	-31.4	7.098	454.0	0.37
100	10.000	426.0	-3.160	-34.9	8.438	460.9	0.37
200	14.142	439.8	-5.266	-48.6	14.49	488.4	0.36
300	17.321	470.8	-7.454	-55.5	19.45	526.3	0.38
400	20.000	463.9	-9.663	-59.0	23.74	522.9	0.41
500	22.361	460.4	-11.73	-62.4	27.86	522.8	0.42
700	26.458	463.9	-15.55	-69.3	35.18	533.2	0.44

The results for the PDMA-PSSA polymer film in Table 4.8 were used to plot a graph of ΔE_p vs. scan rate (v) as shown in Figure 4.20. From shape of the graph in Figure 4.20 it can be seen that it does not follow the Randles-Sevcik equation, since a straight line was not obtained that may be attributed to slow electron transfer kinetics in the polymer film. This observation is similar as for the POMA-PSSA polymer film.
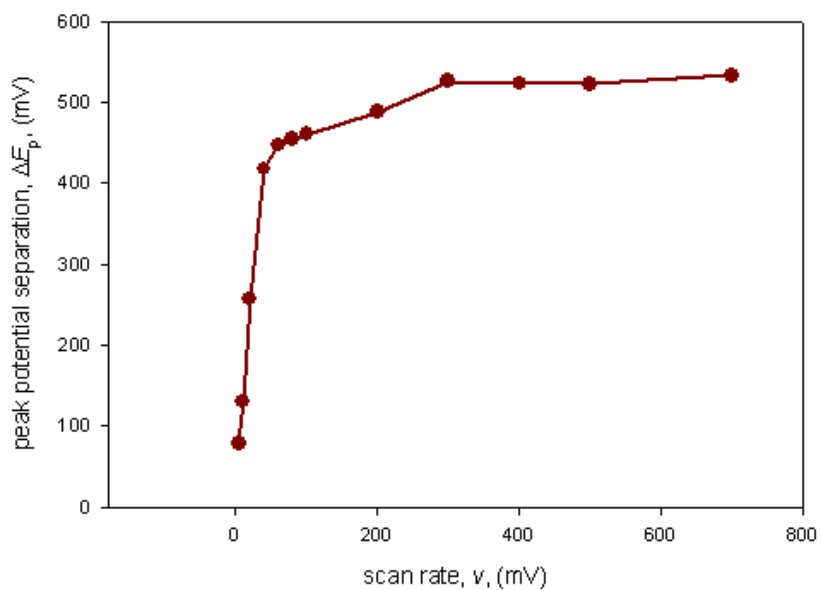
Figure 4.20   **Graph of peak potential separation (ΔE_p) vs. scan rate (v) for the Au/MBT/PDMA-PSSA polymer film in 0.1 M HCl solution at different scan rates.**

On the other hand, the graph of anodic and cathodic peak current (I_p) vs. the square root of scan rate ($v^{1/2}$) in Figure 4.21, shows linearity for the higher scan rates which demonstrates that the process are adsorption controlled. The graph further shows better linearity for the cathodic peak current results.
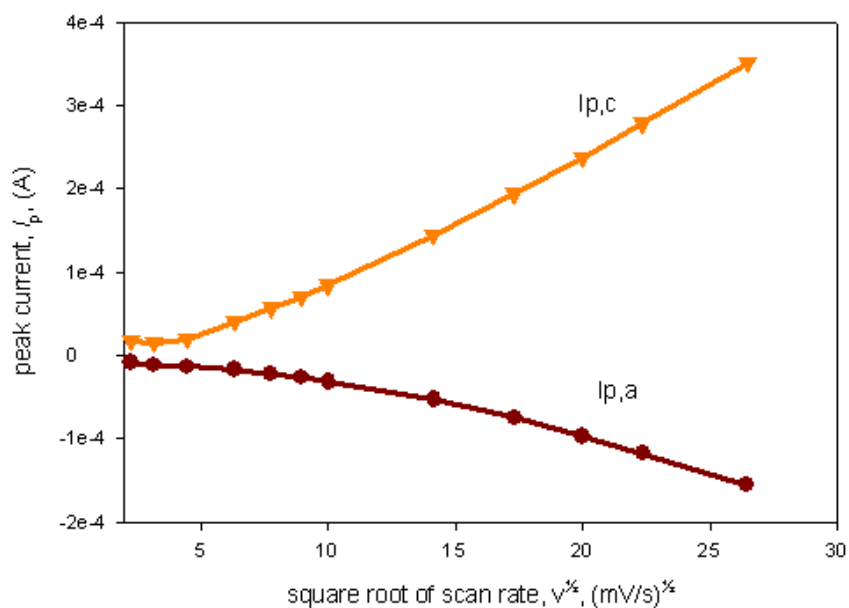
Figure 4.21   **Graph of anodic and cathodic peak current (I_p) vs. square root of scan rate ($v^{1/2}$) for the Au/MBT/PDMA-PSSA polymer film in 0.1 M HCl solution at different scan rates.**

Further analysis of the results in Table 4.8 shows that the peak-to-peak separation, ΔE_p, is significant as the scan rate increases. Again it was found that the anodic and cathodic peak ratio ($I_{p,a}/I_{p,c}$) is less than unity for the PDMA-PSSA polymer film, similar to the results obtained for the POMA-PSSA polymer film. Table 4.9 shows the values for Γ^*_{PDMA}, and D_e, as compared for the two solution used (i.e phosphate buffer and HCl).

Table 4.9   **Surface concentration and electron transport coefficient for the PDMA-PSSA polymer film.**

Solution	Surface concentration, (Γ^*), $mol.cm^{-2}$	Electron transport coefficient, (D_e), $cm^2.s^{-1}$
0.1 M phosphate buffer (pH 7.2)	1.177×10^{-2}	1.396×10^{-15}
0.1 M HCl	2.200×10^{-2}	4.174×10^{-15}

As reported for the POMA-PSSA polymer film, from the results in Table 4.2 it can be deduced that the conductivity of the PDMA-PSSA polymer film is very good and it is observed that the D_e value is of the same order of magnitude in both the 0.1 M HCl and 0.1 M phosphate buffer, pH (7.2) solutions.

Furthermore, when the D_e values for the POMA-PSSA polymer film (Table 4.7) is compared to that of the PDMA-PSSA polymer film, it is observed that it is approximately the same in the 0.1 M HCl solution, while there is one order of magnitude difference for the results in the 0.1 M phosphate buffer, pH (7.2) solution.

In summary, it was observed that the thickness of the polymer films were relatively higher for the substituted polyanilines (PANIs) as compared to the unsubstituted PANI (see section 4.6.1), which may also be attributed to the incorporation of the PSSA dopant in the electropolymerisation step, thereby creating a more bulky polymer, but with increased solubility.

4.4   Characterisation of the AChE-Bioelectrodes

4.4.1 Characterisation of Au/MBT/POMA-PSSA/AChE enzyme electrode

4.4.1.1 Voltammetric characterisation

In Figure 4.22 the CV results of the Au/MBT/POMA-PSSA/AChE enzyme electrode in 0.1 M phosphate buffer, KCl (pH 7.2) at a scan rate of 5 mV.s^{-1} is shown. For the same enzyme electrode the anodic difference SWV results are shown in Figure 4.23, with the DPV results shown in Figure 4.24. Square wave and differential pulse voltammetric results were collected for the enzyme electrode in order to compare the appearance of the redox peaks observed in the CV results.
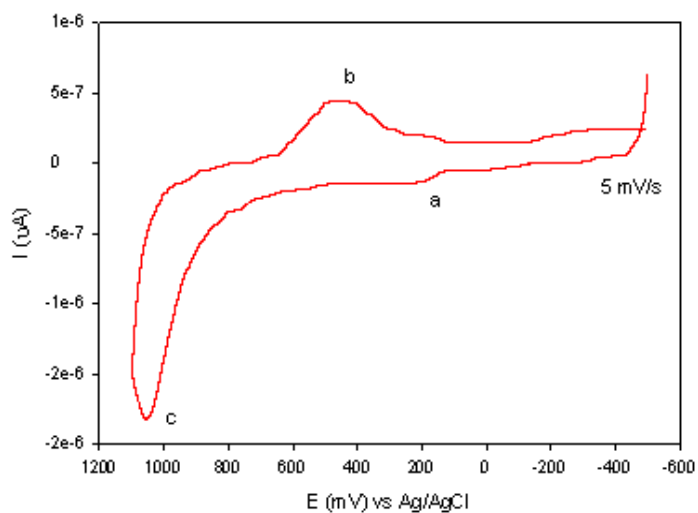
Figure 4.22   **CV results of Au/MBT/POMA-PSSA/AChE enzyme electrode in 0.1 M phosphate buffer, KCl (pH 7.2) at a scan rate of 5 mV.s^{-1}.**

During cyclic voltammetric (CV) characterisation it was observed that three peaks (two anodic and one cathodic) are obtained with their peak potentials at + 192.2 mV in (a), + 456.2 mV in (b) and + 1054.8 mV in (c) (vs. Ag/AgCl) in the potential window from – 500 to + 1200 mV.

The CV results were confirmed with the collection of the anodic difference SWV response, which was collected when the electrode was scanned oxidatively (anodic wave) from – 500 to + 1200 mV at a frequency of 25 Hz. Three peaks were obtained as shown in Figure 4.23 for the anodic difference SWV results with peaks potentials of + 236.2 mV in (a), + 539.9 mV in (b) and + 997.6 mV in (c) (vs. Ag/AgCl). These results compare relatively well with the results obtained using cyclic voltammetry.
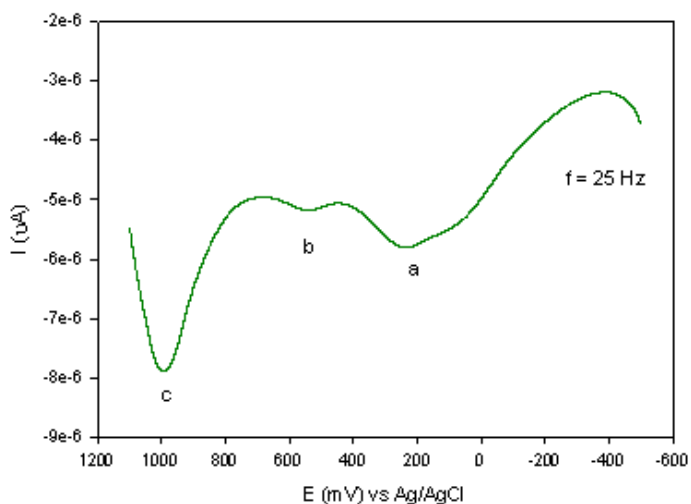
Figure 4.23   **Anodic difference SWV results of Au/MBT/POMA-PSSA/AChE enzyme electrode in 0.1 M phosphate buffer, KCl (pH 7.2) at a frequency of 25 Hz.**

The next step involved the correlation of the previous results with differential pulse voltammetry (DPV), performed in the same potential window at a scan rate of 10 mV.s^{-1}. The results obtained for the anodic difference DP voltammogram is shown in Figure 4.24, which confirmed the presence of the three peaks with peak potentials at + 196.6 mV in (a), + 504.6 mV in (b) and + 856.7 mV in (c) (vs. Ag/AgCl).
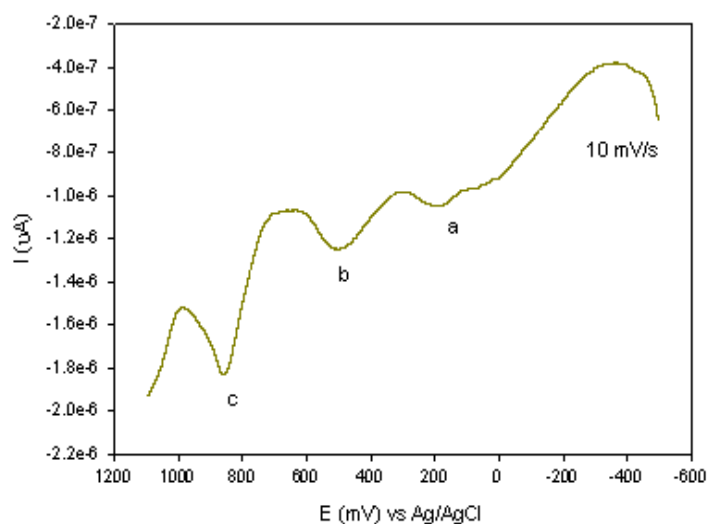
Figure 4.24   **DPV results of Au/MBT/POMA-PSSA/AChE enzyme electrode in 0.1 M phosphate buffer, KCl (pH 7.2) at a scan rate of 10 mV.s^{-1}.**

The voltammetric results showed in Figures 4.22 to 4.24 indicated that the enzyme electrode possesses electrochemical activity and based on these positive results the constructed sensor was evaluated by doing scan rate studies that are reported in the next section.

4.4.1.2 Cyclic voltammetric characterisation at different scan rates

In Figure 4.25 the CV results of the Au/MBT/POMA-PSSA/AChE enzyme electrode in 0.1 M phosphate buffer, KCl (pH 7.2) at different scan rates is shown, with the arrows indicating the direction of increasing scan rate.
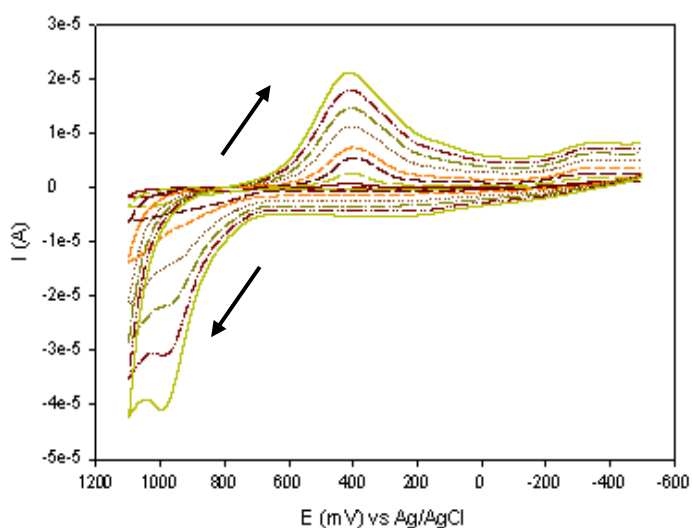
Figure 4.25   Cyclic voltammograms for the Au/MBT/POMA-PSSA/AChE enzyme electrode in 0.1 M phosphate buffer, KCl (pH 7.2) solution at different scan rates of 5, 20, 50, 100, 200, 300, 400, 500 mV.s^{-1}.

For the Au/MBT/POMA-PSSA/AChE enzyme electrode, the electron transport coefficient (D_e) and the value for the surface concentration ($\Gamma^*_{POMA/AChE}$) of the POMA-PSSA/AChE film was calculated. The value of $\Gamma^*_{POMA/AChE}$ was found to be

7.772 x 10^{-5} mol.cm^{-2} and that of D_e to be 1.2882 x 10^{-12} cm².s^{-1}. Using the above

results the heterogeneous rate constant, k^o, was calculated and found to be 3.167 x 10^{-9} cm.s^{-1}. Since the value of k^o is less than 10^{-5} cm.s^{-1}, an irreversible system exists and

electron transfer at the electrode is extremely slow. The important conclusion made

from the CV shown in Figure 4.25, is that the peak potentials are shifting to higher

values as the scan rate was increased, thus indicating that there is electron transport

along the polymer film to the enzyme immobilised in the polymer film.

4.4.2 Characterisation of Au/MBT/PDMA-PSSA/AChE enzyme electrode

4.4.2.1 Voltammetric characterisation

Figure 4.26 shows the CV results of the Au/MBT/PDMA-PSSA/AChE

enzyme electrode in 0.1 M phosphate buffer, KCl (pH 7.2) solution at a scan rate of 5

mV.s^{-1}, while the anodic difference SWV results are shown in Figure 4.27, with the

DPV results shown in Figure 4.28.

Similarly as for the first enzyme electrode, square wave and differential pulse

voltammetric results were used for this enzyme electrode in order to compare the

appearance of the redox peaks observed in the CV results. The CV results in Figure

4.26 shows two peaks (one anodic and one cathodic) which were observed at

potentials of + 1004.7 mV in (a) and at + 520.9 mV in (b) (vs. Ag/AgCl), respectively.
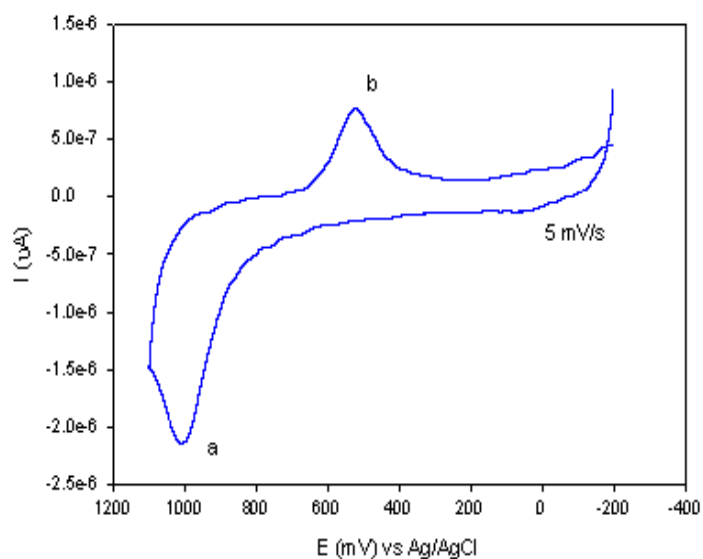
Figure 4.26   **CV response of Au/MBT/PDMA-PSSA/AChE enzyme electrode in 0.1 M phosphate buffer, KCl (pH 7.2) solution at a scan rate of 5 mV.s^{-1}.**

The two peaks observed in the CV results were confirmed with the SWV results in Figure 4.27, which was collected when the electrode was scanned oxidatively (anodic wave) from – 500 to + 1200 mV at a frequency of 35 Hz. The results compare very well with the CV results and 2 peaks were observed at potentials of + 378.5 mV in (b) and + 885.1 mV in (a) (vs. Ag/AgCl), respectively.
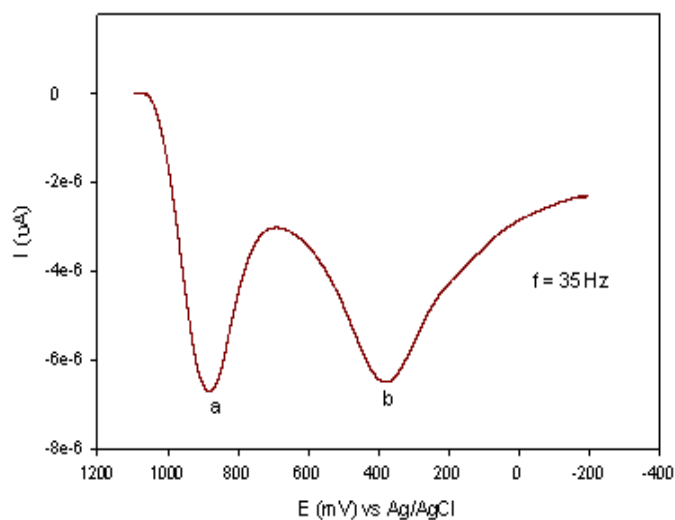
Figure 4.27   **Anodic difference SWV response of Au/MBT/PDMA-PSSA/AChE enzyme electrode in 0.1 M phosphate buffer, KCl (pH 7.2) solution at a frequency of 35 Hz.**

The two peaks observed in the CV results were next confirmed with the DPV results, collected in the same potential window at a scan rate of 10 mV.s^{-1}. The results obtained are showed in Figure 4.28 and shows 2 peaks at potentials of + 418.4 mV in (b) and + 858.5 mV in (a) (vs. Ag/AgCl) respectively. A third peak was observed at a potential of + 68.1 mV (vs. Ag/AgCl), which are attributed to the use of MBT.
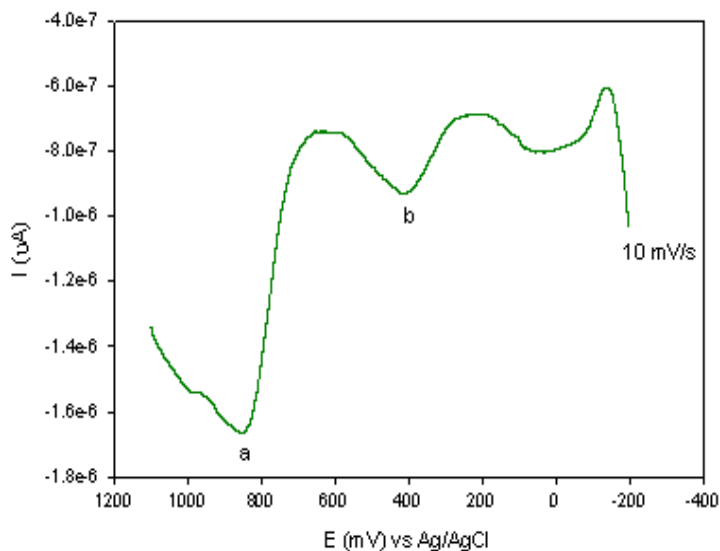
Figure 4.28   DPV of Au/MBT/PDMA-PSSA/AChE enzyme electrode in 0.1 M
phosphate buffer, KCl (pH 7.2) solution at a scan rate of 5 mV.s^{-1}.

The voltammetric results showed in Figures 4.26 to 4.28 indicate that the enzyme
electrode possesses electrochemical activity and based on these positive results the
constructed sensor was evaluated by doing scan rate studies that are reported in the
next section.

4.4.2.2 Cyclic voltammetric characterisation at different scan rates

In Figure 4.29 the CV results of the Au/MBT/PDMA-PSSA/AChE enzyme
electrode in 0.1 M phosphate buffer, KCl (pH 7.2) at different scan rates is shown,
with the arrows indicating the direction of increasing scan rate.
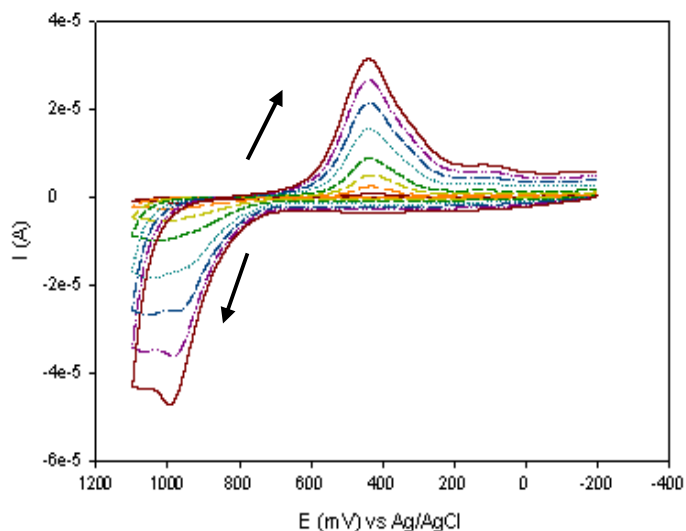
Figure 4.29   **Cyclic voltammograms for the Au/MBT/PDMA-PSSA/AChE enzyme electrode in 0.1 M phosphate buffer, KCl (pH 7.2) solution at different scan rates of 5, 20, 50, 100, 200, 300, 400, 500 mV.s^{-1}.**

Similarly, for the Au/MBT/PDMA-PSSA/AChE enzyme electrode, the electron transport coefficient (D_e) and the value for the surface concentration ($\Gamma^*_{PDMA/AChE}$) of the PDMA-PSSA/AChE film was calculated. The value of $\Gamma^*_{PDMA/AChE}$ was found to be 4.1024 x 10^{-3} mol.cm^{-2} and that of D_e to be 2.601 x 10^{-15} cm².s^{-1}. Using the above results the heterogeneous rate constant, k^o, was calculated and found to be 1.423 x 10^{-10} cm.s^{-1}. Since the value of k^o is less than 10^{-5} cm.s^{-1}, an irreversible system exists and electron transfer at the electrode is extremely slow. In Table 4.10 the values for the calculated heterogeneous rate constants for the respective Au/MBT/POMA-

PSSA/AChE and Au/MBT/PDMA-PSSA/AChE enzyme electrodes are listed and compared.

Table 4.10   **Comparison of the calculated heterogeneous rate constants for the POMA-PSSA/AChE and PDMA-PSSA/AChE enzyme electrodes.**

Enzyme electrode constructed	Heterogeneous rate constant, (k^o), $cm.s^{-1}$
Au/MBT/POMA-PSSA/AChE	3.167×10^{-9}
Au/MBT/PDMA-PSSA/AChE	1.423×10^{-10}

The results in Table 4.10 shows that electron transport at the two constructed enzyme electrodes occur at a difference of one order, with the POMA-PSSA/AChE bioelectrode having a faster rate of transfer. As for the results obtained in Figure 4.25, the important conclusion made from the CV in Figure 4.29, is that the peak potentials are shifting to higher values as the scan rate was increased, thus indicating that there is electron transport along the polymer film to the enzyme immobilised in the polymer film.

4.5   Electrochemical measurements using AChE-based biosensors in the presence of acetylcholine as substrate

4.5.1   Voltammetric characterisation of successive acetylcholine (ACh) substrate addition to Au/MBT and Au/MBT/POMA-PSSA electrodes

In this section the interaction between the Au/MBT SAM modified electrode and the substrate acetylcholine, ACh, will be discussed. This will be followed by the discussion of the results obtained for the interaction between the polymer film and ACh. Finally, the results obtained for the interaction between enzyme electrodes and ACh will be discussed. The results for each of the individual sections of the constructed thick film electrode were collected to ensure that the correct response for the substrate, ACh, with the enzyme acetylcholinesterase, AChE, was obtained and recorded.

4.5.1   Voltammetric characterisation of successive ACh addition to Au/MBT electrode

The reaction between the Au/MBT electrode and ACh was performed to investigate the cyclic voltammetric response at the electrode to the substrate addition. This information was collected to evaluate the biosensor's unique response once the ACh interacts with the enzyme acetylcholinesterase, AChE.

In Figure 4.30 the cyclic voltammetric results for the successive ACh substrate addition to Au/MBT electrode in 0.1 M phosphate buffer, KCl (pH 7.2) at a scan rate of 10 $mV.s^{-1}$ is shown. The potential was scanned between – 500 and + 1100 mV.
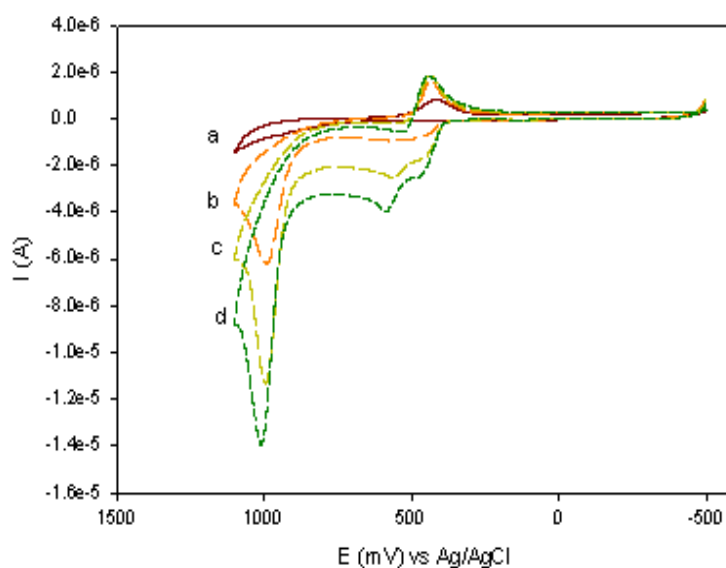
Figure 4.30   **CV of successive ACh substrate addition to Au/MBT electrode in 0.1 M phosphate buffer, KCl (pH 7.2) solution at a scan rate of 10 $mV.s^{-1}$.**

From the results obtained in Figure 4.30, it was evident that an anodic response was obtained as sequential additions of 0.1 M ACh was added to the Au/MBT electrode in saline phosphate buffer solution. The oxidative current has increased as the ACh concentration increased. In the CV response the ACh concentration is 0.0 mM in (a), 0.2 mM in (b), 0.6 mM in (c) and 1.0 mM in (d). It was also observed that an increase

in the anodic peak potential ($E_{p,a}$) at $\pm$ 1000 mV (vs. Ag/AgCl) was obtained when increasing amounts of ACh was added. Another increase in the anodic current was observed at a peak potential of $\pm$ 500 mV (vs. Ag/AgCl), which is smaller as compared to the second peak.

4.5.2 Voltammetric characterisation of successive ACh addition to Au/MBT/POMA-PSSA polymer film

Further investigation involved the reaction between the POMA-PSSA polymer film and ACh to determine the cyclic voltammetric response at the electrode to the substrate addition. This information was collected to determine how the POMA-PSSA polymer film responds to the ACh addition.

The results in Figure 4.31 shows the cyclic voltammetric response for the successive ACh substrate addition to the POMA-PSSA polymer film in 0.1 M phosphate buffer, KCl (pH 7.2) solution at a scan rate of 5 mV.s^{-1}. The potential was again scanned between $-$ 500 and $+$ 1100 mV.
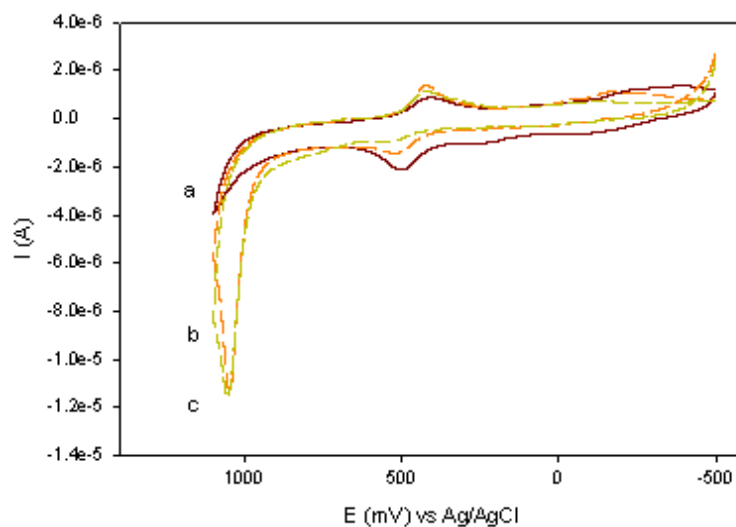
Figure 4.31   **CV response of successive ACh substrate addition to Au/MBT/POMA-PSSA polymer film in 0.1 M phosphate buffer, KCl (pH 7.2) solution at a scan rate of 5 mV.s^{-1}.**

The CV results in Figure 4.31 show that a redox response was obtained as the concentration of the ACh was increased. The results further show that the oxidative current of the redox peak increased as the ACh concentration was increased. The CV in (a) represents the addition of 0.0 mM of ACh to the polymer film and the formal potential ($E^{o\prime}$) calculated for the redox peak, amounts to + 455.7 mV (vs. Ag/AgCl). When 0.4 mM of ACh was added in (b), the value of $E^{o\prime}$ was + 472.9 mV (vs. Ag/AgCl) and for 1.0 mM of ACh added in (c), the $E^{o\prime}$ was calculated as + 484.95 mV (vs. Ag/AgCl). The main conclusion drawn from these results was that an increase in oxidative current was observed when successive additions of the ACh substrate were made to the polymer film.

4.5.3   Voltammetric characterisation of successive ACh addition to Au/MBT/PDMA-PSSA polymer film

As for the POMA-PSSA polymer film, another investigation involved that of the reaction between the PDMA-PSSA polymer film and ACh to determine the cyclic voltammetric response at the electrode to the substrate addition. Figure 4.32 shows the cyclic voltammetric results for the successive ACh substrate addition to the PDMA-PSSA polymer film in 0.1 M phosphate buffer, KCl (pH 7.2) solution at a scan rate of 5 mV.s^{-1}. The potential was also scanned between – 500 and + 1100 mV.
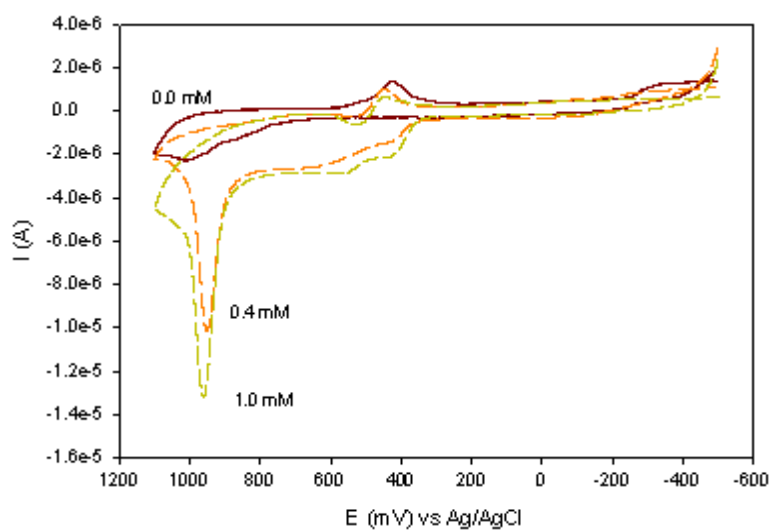
Figure 4.32   **CV response of successive ACh substrate addition to Au/MBT/PDMA-PSSA polymer film in 0.1 M phosphate buffer, KCl (pH 7.2) solution at a scan rate of 5 mV.s^{-1}.**

The CV results in Figure 4.32 shows that a different redox peak was obtained for the PDMA-PSSA polymer film, as compared to the POMA-PSSA polymer film in Figure 4.31. Again the formal potentials ($E^{o\prime}$) of the individual CVs was calculated and found to be + 719.2 mV (vs. Ag/AgCl) for 0.0 mM of ACh added, + 441.2 mV (vs. Ag/AgCl) for 0.4 mM of ACh added and + 438.9 mV (vs. Ag/AgCl) for 1.0 mM of ACh added. Another observation that was made is that not a clear redox peak was obtained when the ACh substrate was added to the polymer film, but that the anodic peaks are shifting and a second more definite oxidation peak is formed at a potential of approximately ± 953 mV (vs. Ag/AgCl). The anodic peak potentials for the second peaks were observed at + 968.3 mV (vs. Ag/AgCl) for 0.0 mM of ACh added, + 956.4 mV (vs. Ag/AgCl) for 0.4 mM of ACh added and + 962.5 mV (vs. Ag/AgCl) for 1.0 mM of ACh added. The next step in the biosensor construction involved the immobilisation of the enzyme called acetylcholinesterase (AChE) to test the effect of substrate addition once the enzyme is incorporated in the polymer film.

In summary, the experiments performed in sections 4.5.1, 4.5.2 and 4.5.3 were conducted to show that specific experimental results were obtained when the substrate acetylcholine (ACh) reacts with the Au/MBT, Au/MBT/POMA-PSSA and Au/MBT/PDMA-PSSA films. The results obtained in these experiments have also shown that ACh is not involved in non-specific interactions in the thick-film biosensor constructed.

4.5.4   Voltammetric characterisation of successive acetylcholine (ACh) substrate addition to Au/MBT/POMA-PSSA/AChE biosensor

In this section the interaction between the enzyme, AChE, and the substrate acetylcholine, ACh, will be discussed. The enzyme AChE was incorporated into the POMA-PSSA polymer film and the Au/MBT/POMA-PSSA/AChE biosensor was constructed. In Figure 4.33 the CV responses of the Au/MBT/POMA-PSSA/AChE biosensor to successive ACh substrate additions under anaerobic conditions are shown. The first results were collected by applying sequential linear potential scan between − 800 to + 500 mV (vs. Ag/AgCl), at a scan rate of $5mV.s^{-1}$. The CVs were performed at the slow scan rate of $5 \ mV.s^{-1}$, to ensure that the fast enzyme kinetics could be monitored.
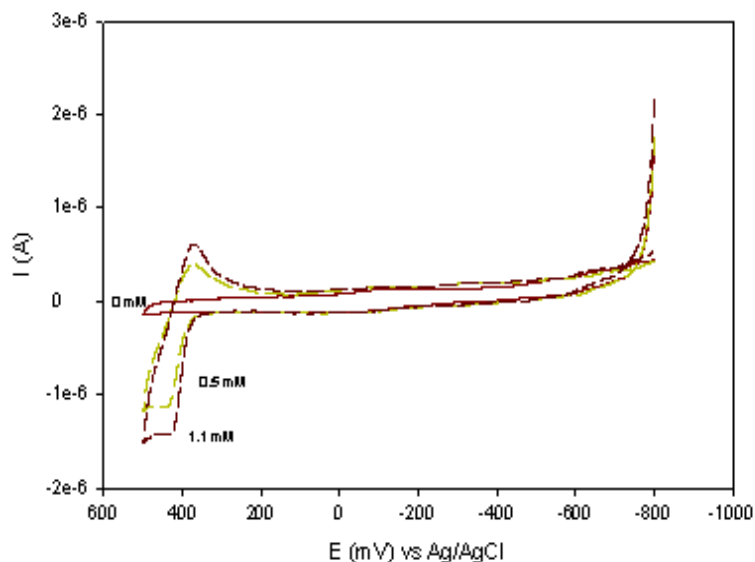
Figure 4.33   **CV response of successive ACh substrate addition to Au/MBT/POMA-PSSA/AChE sensor in 0.1 M phosphate buffer, KCl (pH 7.2) solution at a scan rate of 5 mV.s^{-1}.**

From the CV results in Figure 4.33 it was seen that a clear biosensor response was obtained when ACh interacted with the AChE enzyme electrode. Since the increase in anodic current was established to be between a potential window of +100 to +800 mV (vs. Ag/AgCl), it was decided to repeat the above reaction within the indicated potential window. Therefore, in Figure 4.33 the CV response of the Au/MBT/POMA-PSSA/AChE enzyme electrode to successive ACh substrate addition is shown, this time applying sequential linear potential scan between + 100 to + 800 mV (vs. Ag/AgCl), at a scan rate of 5 mV.s^{-1}.
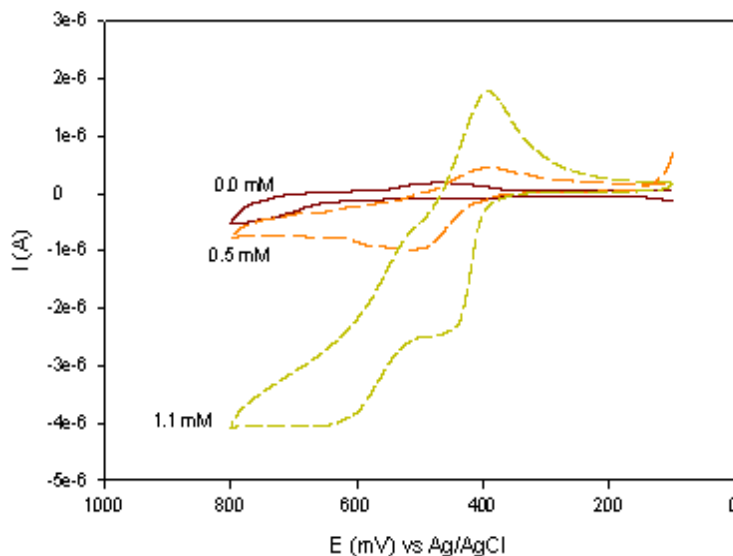
Figure 4.34   **CV response of successive ACh substrate addition to Au/MBT/POMA-PSSA/AChE sensor in 0.1 M phosphate buffer, KCl (pH 7.2) solution at a scan rate of 5 mV.s^{-1}.**

For the CV results in Figure 4.34 it can be seen that a clear redox response was obtained when the substrate ACh was added to the Au/MBT/POMA-PSSA/AChE biosensor. A clear increase in oxidative current is observed as the ACh concentration was increased from 0.0 mM to 0.5 mM and further to 1.1 mM. Thus in phosphate buffer, KCl (pH 7.2) solution the oxidative peak current shifted and increased with increasing acetylcholine (ACh) concentration. Furthermore, it also shows that the thiol, MBT, coated with POMA-PSSA can effectively mediate the transfer of electrons between the enzyme acetylcholinesterase and the gold electrode. In Figure 4.35 a calibration curve for the successive addition of ACh substrate to the Au/MBT/POMA-PSSA/AChE biosensor is showed. The calibration curve was

constructed in order to apply Michealis-Menten kinetics and calculate the apparent

Michaelis-Menten constant for the biosensor response.
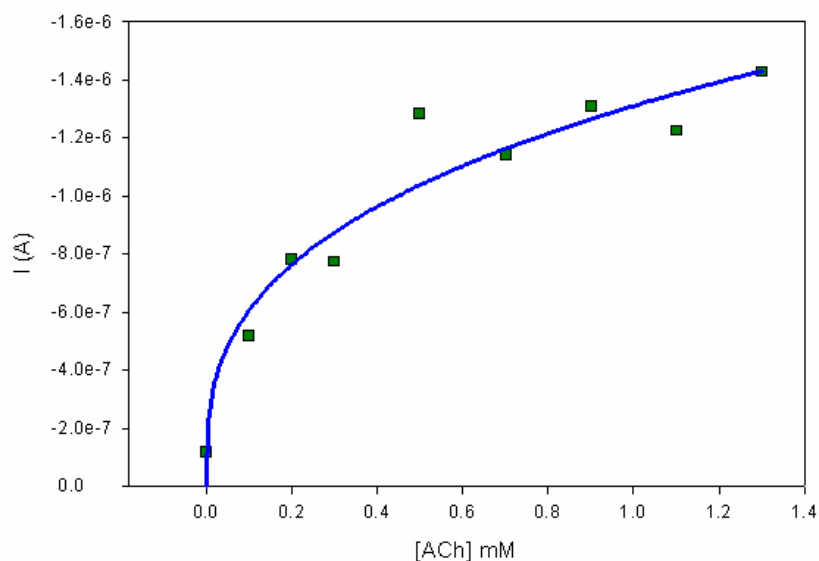
Figure 4.35   **Calibration curve of current vs. substrate concentration for the**
successive addition of ACh as substrate to the Au/MBT/POMA-
PSSA/AChE biosensor in 0.1 M phosphate buffer KCl (pH 7.2)
solution.

From the shape of the curve in Figure 4.35, it can be seen that the biosensor exhibit

Michaelis-Menten kinetics for most of the data plotted. Next the sensitivity of the

biosensor was estimated to be 7.194 x 10^{-7} M, while the limit of detection was

calculated and found to be 0.113 M. The apparent Michaelis-Menten constant, K_m^{app},

was calculated to be 2.085 mM and the maximum current, I_{max}, was 1.500 x 10^{-6} A.

The anodic difference SWV results obtained for the above biosensor response are displayed in Figure 4.36 indicating that similar voltammetric responses for the electrocatalytic oxidation of acetylcholine at the Au/MBT/POMA-PSSA/AChE biosensor under anaerobic conditions were observed.
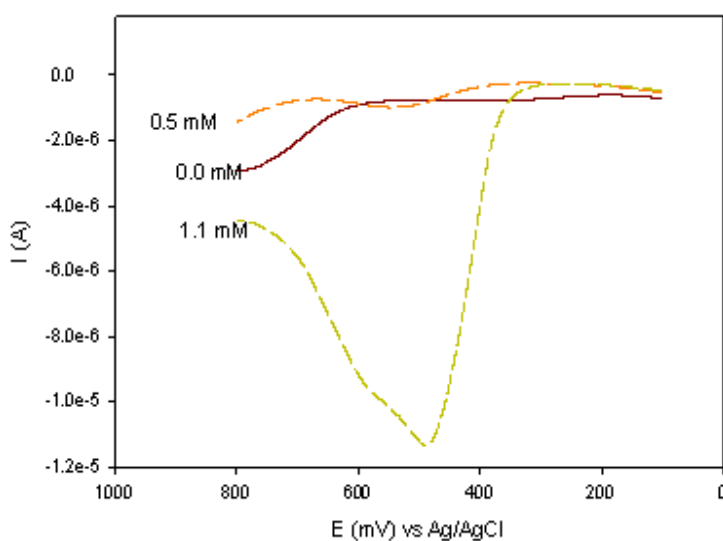
Figure 4.36   **Anodic difference SWV response of successive ACh substrate addition to Au/MBT/POMA-PSSA/AChE biosensor in 0.1 M phosphate buffer, KCl (pH 7.2) solution at a frequency of 5 Hz, and in a potential window from + 100 to + 800 mV.**

In Figure 4.36 it is seen that the increase in peak heights upon addition of ACh is just as pronounced when compared with the results observed in CV in Figure 4.34. The results in Figure 4.36 further indicate that a peak potential, $E_{peak,}$ at + 489.4 mV (vs. Ag/AgCl) for 1.1 mM of ACh added to the biosensor was obtained.

A similar electrocatalytic response as the one observed for the SWV results reported above was obtained for the DPV results shown in Figure 4.37.
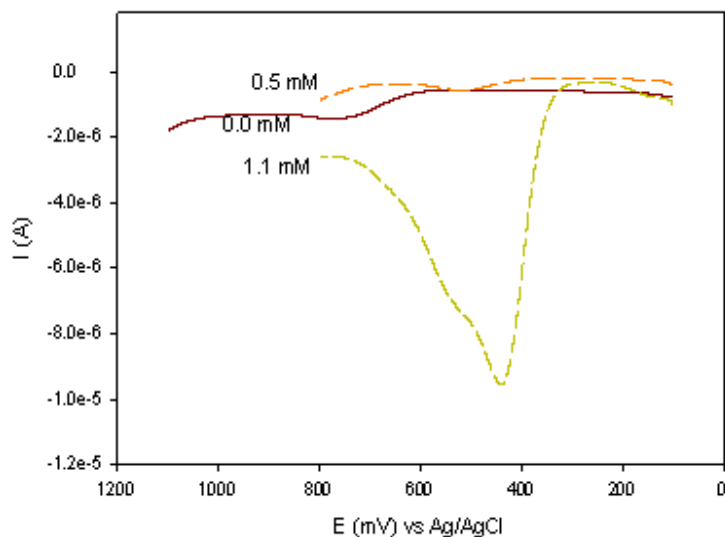
Figure 4.37   **DPV response of successive ACh substrate addition to Au/MBT/POMA-PSSA/AChE sensor in 0.1 M phosphate buffer, KCl (pH 7.2) solution at a scan rate of 10 mV.s^{-1}, and in a potential window of + 100 to + 800 mV.**

The DPV results in Figure 4.37 shows the voltammetric responses for the electrocatalytic oxidation of acetylcholine at the Au/MBT/POMA-PSSA/AChE biosensor, indicating that a peak potential, E_{peak}, of + 440.3 mV (vs. Ag/AgCl) for 1.1 mM of ACh added to the biosensor, is obtained. The peak potentials obtained in the SWV and DPV responses are relatively close at approximately the same range of potential.

4.5.5 Voltammetric characterisation of successive acetylcholine (ACh) substrate addition to Au/MBT/PDMA-PSSA/AChE biosensor

The next step was to test the functioning of the constructed Au/MBT/PDMA-PSSA/AChE enzyme electrode as a biosensor. The cyclic voltammograms (CVs) for the successive addition of ACh substrate to the Au/MBT/PDMA-PSSA/AChE biosensor under anaerobic conditions are shown in Figure 4.38. The results were collected by applying a sequential linear potential scan between $-$ 800 to $+$ 500 mV (vs. Ag/AgCl), at a scan rate of 5 mV.s^{-1}. The CVs were performed at this slow scan rate to ensure that the fast enzyme kinetics could be monitored.
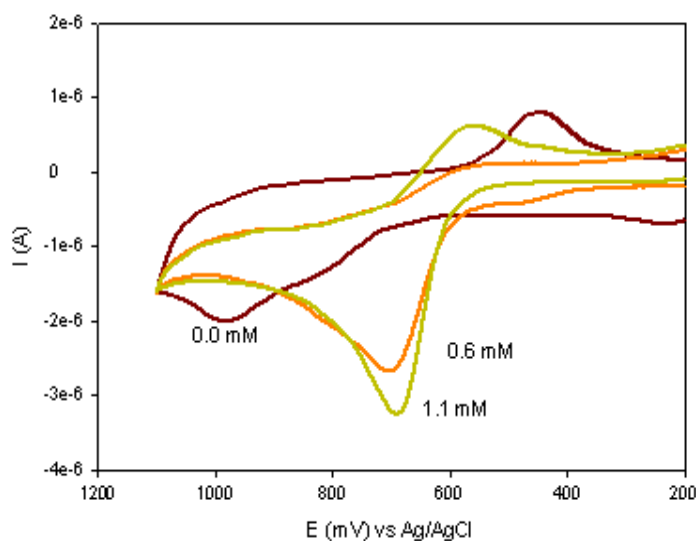
Figure 4.38   **CV response of successive ACh substrate additions to Au/MBT/PDMA-PSSA/AChE biosensor in 0.1 M phosphate buffer, KCl (pH 7.2) solution, with the potential scanned between +200 to +1100 mV at a scan rate of 5 mV.s^{-1}.**

In Figure 4.38 a clear increase in oxidative current is observed as the ACh concentration was increased from 0.0 mM to 0.6 mM and further to 1.1 mM, while a shift in potential is also evident. The formal potentials (E$^{o\prime}$) of the individual CVs shown in Figure 4.38 were calculated and found to be + 716.9 mV (vs. Ag/AgCl) for 0.0 mM of ACh added, compared to + 637.1 mV (vs. Ag/AgCl) for 0.6 mM of ACh added and lastly + 627.8 mV (vs. Ag/AgCl) for 1.1 mM of ACh added.

In Figure 4.39 a calibration curve for the successive addition of ACh substrate to the Au/MBT/PDMA-PSSA/AChE biosensor is displayed. The calibration curve was constructed in order to apply Michealis-Menten kinetics and calculate the

apparent Michaelis-Menten constant for the biosensor response. These results will

also be used to compare the catalytic capability of the two different substituted

polyanilines (PANIs) of POMA and PDMA.
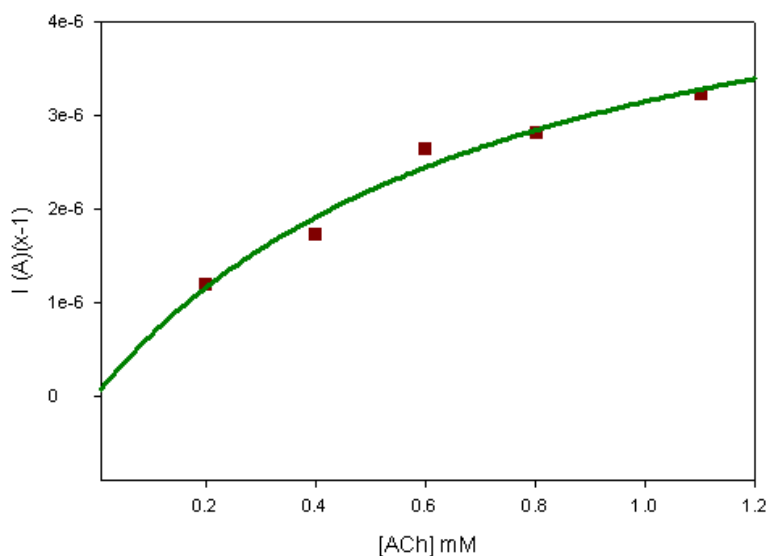
Figure 4.39   **Calibration curve of current vs. substrate concentration for the successive addition of ACh as substrate to the Au/MBT/PDMA-PSSA/AChE biosensor in 0.1 M phosphate buffer KCl (pH 7.2) solution.**

The shape of the curve in Figure 4.39 suggests that the biosensor exhibit Michaelis-

Menten kinetics for most of the data plotted. The sensitivity of the biosensor was

estimated to be 2.713 x 10^{-6} M, while the limit of detection was calculated and found

to be 0.019 M. The apparent Michaelis-Menten constant, K_m^{app}, was calculated to be

1.290 mM, and the maximum current, I_{max}, was 3.500 x 10^{-6} A.

When the results for the biosensor parameters of sensitivity, apparent
Michaelis-Menten constants and detection limits are compared, the values showed in
Table 4.11 are obtained.

Table 4.11   **Comparison of calculated values obtained for the kinetic parameters of
Au/MBT/POMA-PSSA/AchE and Au/MBT/PDMA-PSSA/AChE
biosensors, respectively.**

Biosensor	Sensitivity (M)	Apparent Michaelis-Menten constant, (K_m^{app}) (mM)	Detection limit (M)
Au/MBT/POMA-PSSA/AChE	$7.194 \, x \, 10^{-7}$	2.085	0.113
Au/MBT/PDMA-PSSA/AChE	$2.713 \, x \, 10^{-6}$	1.290	0.019

From the results in Table 4.11, it can be seen that the sensitivity of the
Au/MBT/PDMA-PSSA/AChE biosensor is one order higher than that of the
Au/MBT/POMA-PSSA/AChE biosensor, while the apparent Michaelis-Menten
constant (K_m^{app}) is also smaller for the Au/MBT/PDMA-PSSA/AChE biosensor and
its detection limit is smaller than that of the Au/MBT/POMA-PSSA/AChE biosensor.
Since the apparent Michaelis-Menten constant (K_m^{app}) can be used to predict the ease
with which a substrate partitions into the film of a biosensor, the results above show
that the Au/MBT/PDMA-PSSA/AChE biosensor would be more effective when
applied for analysis.

To verify the CV responses obtained for the successive addition of acetylcholine to the Au/MBT/PDMA-PSSA/AChE biosensor, square wave – and differential pulse voltammetric results under anaerobic conditions, were also obtained for each addition of the substrate.

The results for the square wave voltammograms (SWVs) for successive ACh addition to the biosensor measured at 5 Hz are shown in Figure 4.40. These SWVs were recorded under anaerobic conditions and the net (difference between forward and reverse currents) SWV responses were obtained.
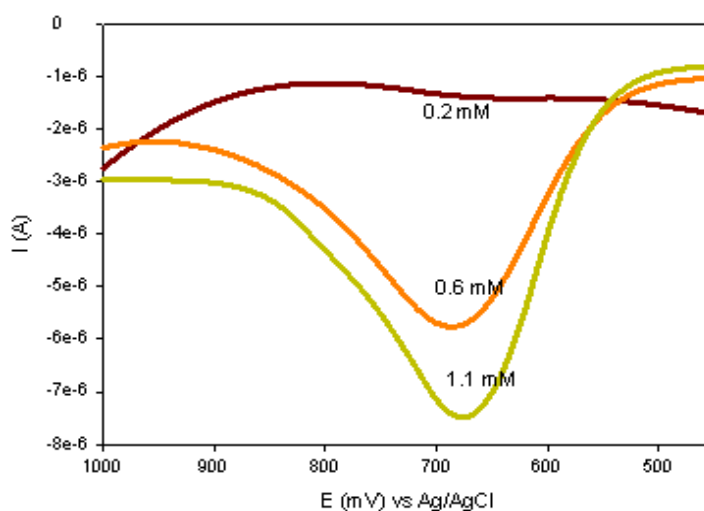
Figure 4.40   **SWV response of successive ACh substrate additions to the Au/MBT/PDMA-PSSA/AChE biosensor in 0.1 M phosphate buffer, KCl (pH 7.2) solution, with the potential scanned between +400 to +1000 mV at a frequency of 5 Hz.**

The SWV responses in Figure 4.40 shows an increase in peak current heights upon the successive additions of ACh as substrate, with the results more pronounced around a specific potential of approximately + 785 mV (vs. Ag/AgCl) as compared with those observed in the CVs in Figure 4.38. The results further shows that the enhancement of the peak current observed is consistent with an electrocatalytic effect.

For the SWV responses it was observed that when 0.2 mM of ACh was added in (a), the peak potential was found to be + 690.9 mV (vs Ag/AgCl). At higher ACh concentrations of 0.6 mM in (b) and 1.1 mM in (c) the corresponding peak potentials were found to be + 686.3 mV and + 678.3 mV (vs. Ag/AgCl), respectively.

The same electrocatalytic effect observed with the SWV responses were obtained for the DPV responses for each successive addition of ACh to the Au/MBT/PDMA-PSSA/AChE biosensor, as shown in Figure 4.41.
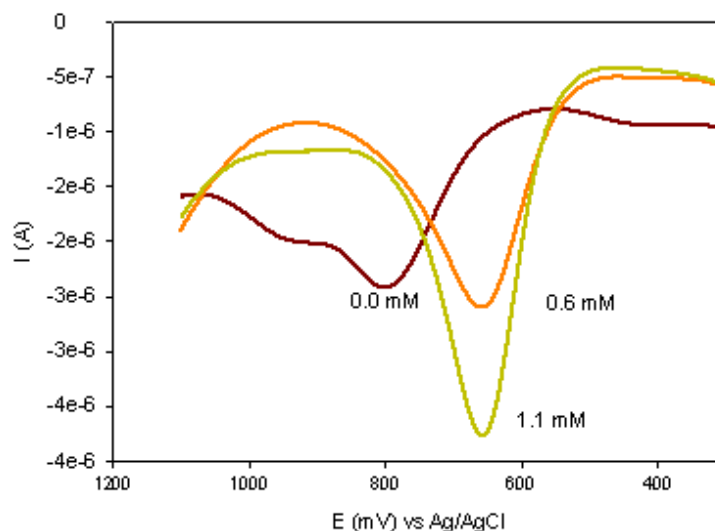
Figure 4.41   DPVs of successive ACh substrate additions to the
Au/MBT/PDMA/PSSA/AChE biosensor in 0.1 M phosphate buffer,
KCl (pH 7.2) solution, with the potential scanned between +400 to
+1000 mV at a scan rate of 10 mV.s^{-1}.

The shift in peak potentials observed in the DPV response shows similar peak

potential (E_{peak}) values as that obtained for the CV response for successive ACh

substrate addition to the biosensor. In Figure 4.41 the values of E_{peak} were obtained at

+ 800.8 mV (vs. Ag/AgCl) for 0.2 mM of ACh, + 659.7 mV (vs. Ag/AgCl) for 0.6

mM of ACh, and + 657.0 mV (vs. Ag/AgCl) for 1.1 mM of ACh added.

The results in all of section 4.5 have thus shown that the electrocatalytic

oxidation of acetylcholinesterase, ACh, was observed at both Au/MBT/POMA-

PSSA/AChE and Au/MBT/PDMA-PSSA/AChE biosensors, in which a novel MBT

self-assembled monolayer was used in the construction of the thick-film biosensor. It was further observed that the reaction is very specific when acetylcholine (ACh) as substrate reacts with the enzyme acetylcholinesterase (AChE) in the thick-film biosensors constructed. This conclusion is drawn from the specific results obtained for sections 4.5.1, 4.5.2 and 4.5.3 as compared to the results reported in sections 4.5.4 and 4.5.5.

4.6 Electrochemical measurements using AChE-based biosensors in the presence of acetylthiocholine as substrate

For the next set of experiments, it was decided to use the unsubstituted polyaniline (PANI) that is less soluble. With that it was also decided to use acetylthiocholine (ATCh) as substrate for the enzyme acetylcholinesterase (AChE), since ATCh is electroactive and can undergo both oxidation and reduction reactions at the sensor electrode. It is known that when AChE is immobilised on the working electrode surface, its interaction with the substrate produces an electroactive compound. To achieve this, acetylthiocholine (ATCh) can be used to substitute the original substrate of AChE, called acetylcholine (ACh). ATCh is thus also hydrolysed in the same manner as ACh, producing thiocholine (TCh) and acetic acid. The electrons that are generated during the electrochemical reaction are collected and the final current is a quantitative measure of the enzyme's activity. The above reactions

that occur on the biosensor surface are shown in equations 4.5 and 4.6 (Nunes *et al.* 2004:110):

$$\text{ATCh} \quad + \quad \text{H}_2\text{O} \quad \xrightarrow{\text{AChE}} \quad \text{TCh} \quad + \quad \text{HA} \qquad \text{Eqn. 4.5}$$
Acetylthiocholine **thiocholine** **acetic acid**

$$2\,\text{TCh}_{(\text{red})} \quad \longrightarrow \quad \text{TCh} \quad + \quad 2\,\text{H}^+ \quad + \quad 2\,\text{e}^- \qquad \text{Eqn. 4.6}$$
(dimeric)
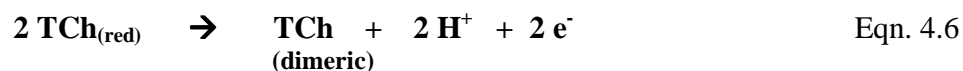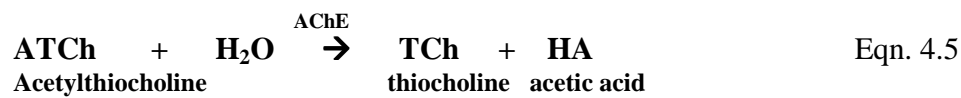
4.6.1 Characterisation of Au/MBT/PANI polymer film

The electropolymerisation of aniline was next done on an Au/MBT SAM-modified electrode at a scan rate of 40 mV.s^{-1} by repetitive cycling between – 200 and + 1100 mV (vs. Ag/AgCl), in a 1 M HCl solution. The result for the polyaniline (PANI) polymer film is shown in Figure 4.42.
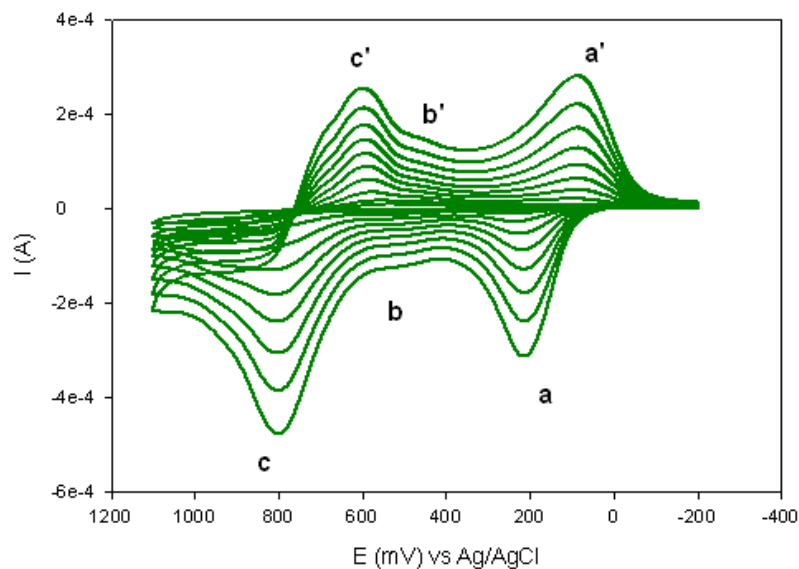
Figure 4.42 **Cyclic voltammogram (CV) obtained for the Au/MBT/PANI electroplymerisation during repetitive cycling between – 200 and + 1100 mV (vs. Ag/AgCl) in a 1M HCl solution at a scan rate of 40 mV.s^{-1}.**

The electrodeposition of polyaniline (PANI) was carried out using cyclic voltammetry in a solution containing 0.2 M aniline in a 1 M HCl aqueous solution, with the result shown in Figure 4.42. The potentialwas swept between – 200 and + 1100 mV (vs. Ag/AgCl), since PANI shows very good redox activity within this region at acidic pH. The CV obtained in Figure 4.42 shows two main peaks (a) and (c), which corresponds to the transformation of leucoemeraldine base (LB) to emeraldine salt (ES) and the emeraldine salt (ES) to pernigraniline salt (PS) respectively. The reverse scan shows the main peaks (c') and (a') that corresponds to the conversion of pernigraniline salt (PS) to emeraldine salt (ES) and emeraldine salt

(ES) to leucoemeraldine base (LB). The small redox couple (b/b') can be attributed to impurities such as benzoquinone and hydroquinone. Multiscan voltammetry resulted in an increase in the redox peaks which indicates the formation of conducting polymer at the Au/MBT surface. It also provides further evidence that the Au/MBT surface is conductive. Polyaniline was used as a mediator in this biosensor construction to harvest its dual role as immobilization matrix for AChE and use its electrocatalytic activity towards thiocholine for amperometric sensing.

The kinetic parameters of the electron transfer process for the PANI polymer film were calculated. The CV of the PANI polymer film was used to calculate the rate parameter, ψ, for equation 4.1 (Zanello 2003:283). Equation 4.2 (Bard and Faulkner 2001:168) was used to calculate the number of electrons (n) transferred during electropolymerisation and found to be $n = 1$. Equation 4.1 was further used to calculate k^o, the standard heterogeneous rate constant for the electron transfer reaction. The surface concentration of the POMA-PSSA polymer film, Γ^*_{PANI}, was calculated with equation 4.3 (Zanello 2003:283) and found to be 2.582×10^{-1} mol.cm^{-2}. The electron transport diffusion coefficient, D_e, was obtained from a Randle-Sevčik plot of I_p vs $v^{\frac{1}{2}}$ and found to be 2.844×10^{-9} cm².s^{-1}. Thus at 25 °C, with $\alpha = 0.5$, the value of k^o was calculated as 1.176×10^{-8} cm.s^{-1}. The PANI polymer film thickness, L (cm), was estimated from the voltammetric charge passed during electropolymerisation using equation 4.4 (Iwuoha *et al.* 1997:749) and found to be 6.777×10^{-8} cm.

The parameters obtained (in HCl solution) for the PANI polymer film were then compared to that of the POMA-PSSA and PDMA-PSSA polymer films, calculated in previous sections and are shown in Table 4.12.

Table 4.12   **Comparison of the results for different kinetic parameters for the PANI, POMA-PSSA, and PDMA-PSSA polymer electropolymerisation on the Au/MBT modified electrode.**

Polymer film	Scan rate, v (mV/s)	Surface concentration (Γ^*), (mol.cm^{-2})	Electron diffusion coefficient (D_e), (cm^2.s^{-1})	Standard heterogeneous rate constant (k^o), (cm.s^{-1})	Polymer film Thickness L, (m)
POMA-PSSA	20	5.559×10^{-3}	1.181×10^{-14}	1.372×10^{-8}	4.367×10^{-13}
PDMA-PSSA	40	2.200×10^{-2}	4.174×10^{-15}	1.154×10^{-7}	2.833×10^{-12}
PANI	40	2.582×10^{-1}	2.844×10^{-9}	1.176×10^{-8}	6.777×10^{-8}

From the results in Table 4.12, it can be concluded that the surface concentration of the electrosynthesized polymer is the highest for PANI, although the same number of cycles were applied during electropolymerisation. The results further shows that the transport of electrons along the polymer chain is the fastest in the unsubstituted PANI polymer film, while it is the slowest in the dimethoxy substituted PDMA polymer film. The results obtained for k^o is the highest for PDMA, indicating that the rate of electron transfer is the fastest for the PDMA polymer film. The thickness of the polymer films were the highest for the substituted polyanilines (PANIs), which may

also be attributed to the incorporation of the PSSA dopant in the electropolymerisation step, thereby creating a more bulky polymer.

4.6.1.1 Cyclic voltammetric (CV) characterisation at different scan rates

In Figure 4.43 the CV results for the Au/MBT/PANI polymer film at different scan rates in 0.1 M phosphate buffer, KCl (pH 7.2) solution is shown, with the arrows indicating the direction of increasing scan rate.
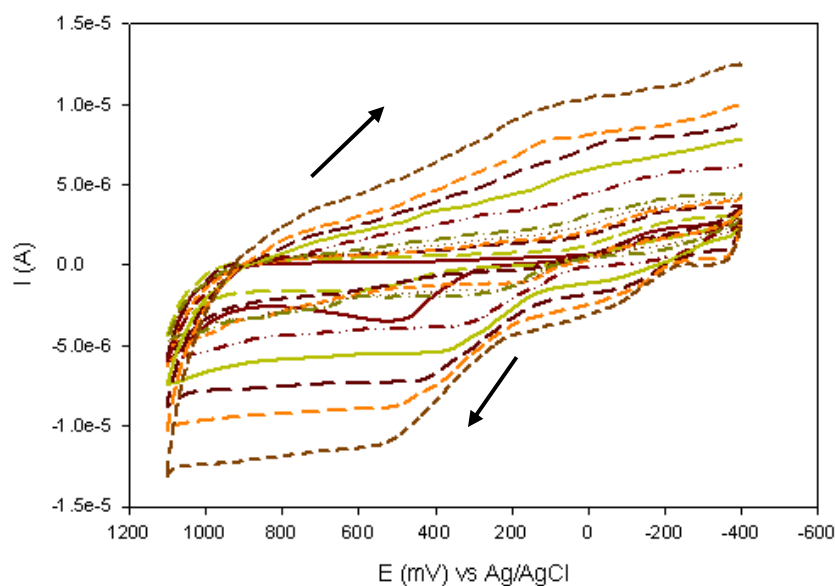
Figure 4.43   **Cyclic voltammograms for the Au/MBT/PANI polymer film in 0.1 M phosphate buffer, KCl (pH 7.2) solution at different scan rates of 5, 10, 20, 40, 60, 80, 100, 200, 400, 500, 700 mV.s^{-1}.**

In Figure 4.43 it was observed that the redox activity of the Au/MBT/PANI polymer film in 0.1 M phosphate buffer, KCl (pH 7.2) solution was not as good as expected, although an anodic peak was observed at + 520.3 mV (vs. Ag/AgCl) and a cathodic peak at +192.8 mV (vs. Ag/AgCl). It was also observed that the peak potentials of the single redox couple were shifting to higher values as the scan rate was increased. The Randel-Sevčik equation was thus used to determine the rate of electron transport (D_e) within the polymer film. From a Randel-Sevčik plot of I_p vs. $v^{1/2}$, the value for $D_e = 1.440 \ x \ 10^{-10}$ cm².s^{-1} was obtained. The heterogeneous rate constant, k^o, was calculated and found to be $1.059 \ x \ 10^{-10}$ cm.s^{-1}. Since the value of k^o is less than 10^{-5} cm.s^{-1}, an irreversible system exists and electron transfer at the electrode is extremely slow.

In Figure 4.44 the CV results for the Au/MBT/PANI polymer film at different scan rates in 0.1 M HCl solution is shown, with the arrows indicating the direction of increasing scan rate.
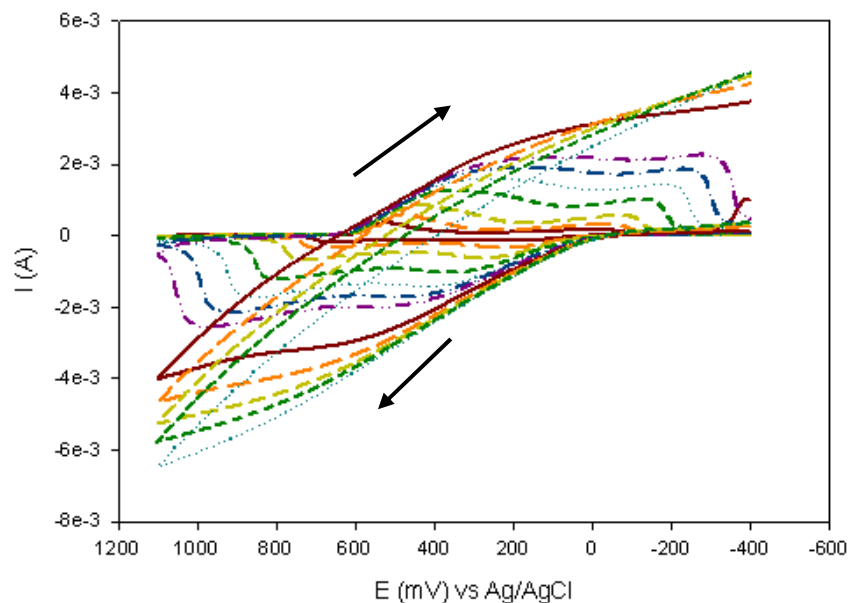
Figure 4.44   **Cyclic voltammograms for the Au/MBT/PANI polymer film in 0.1 M HCl solution at different scan rates of 5, 10, 20, 40, 60, 80, 100, 200, 400, 500, 700 mV.s^{-1}.**

Viewing the results of the scan rates studies done in 0.1 M HCl solution, Figure 4.44, it was observed that at slower scan rates of less than 200 mV.s^{-1}, two distinct redox couples were observed that were reduced to just one redox couple at high scan rates. The redox couples were however found to be irreversible since the peak separation potentials for the two peaks were too high. However, since it was observed that the peak potentials of the two redox couples were shifting to higher values as the scan rate was increased, the Randel-Sevčik equation was applied to determine the rate of electron transport (D_e) within the polymer film. From a Randel-Sevčik plot of I_p vs $v^{\frac{1}{2}}$, the value for $D_e = 2.844 \ x \ 10^{-9}$ cm².s^{-1} was obtained. The heterogeneous rate

constant, k^o, was calculated and found to be 1.176 x 10^{-8} cm.s^{-1}. Since the value of k^o

is less than 10^{-5} cm.s^{-1}, an irreversible system exists and electron transfer at the

electrode is extremely slow. A summary of the results for the different kinetic

parameters of the Au/MBT/PANI polymer film is shown in Table 4.13.

Table 4.13   **Comparison of the results for different kinetic parameters for the PANI polymer film on the Au/MBT SAM electrode is shown.**

Solution	Scan rate (mV/s)	Electron diffusion coefficient (D_e), $(cm^2.s^{-1})$	Standard heterogeneous rate constant (k^o) m.s^{-1}
0.1 M phosphate buffer (pH 7.2)	40	1.440 x 10^{-10}	1.059 x 10^{-10}
0.1 M HCl	40	2.844 x 10^{-9}	1.176 x 10^{-8}

From the results in Table 4.13 it can be concluded that the rate of electron transport

along the polymer chain is faster in the HCl solution (as compared to the saline

phosphate buffer solution). The rate of electron transfer to the electrode is also faster

in the HCl solution, as compared to the result of the saline phosphate buffer solution.

The data of the CVs shown in Figures 4.44 were further evaluated and the

results are shown in Table 4.14.

Table 4.14   **Results for the effect of scan rate on anodic and cathodic peak current and peak potentials in CVs for different scan rates in 0.1 M HCl solution.**

Scan rate v, (mV/s)	Square root of scan rate, $v^{1/2}$, $(mV/s)^{1/2}$	Anodic peak current, $I_{p,a}$, (A) $(x\,10^{-4})$	Anodic peak potential, $E_{p,a}$, (mV)	Cathodic peak current, $I_{p,c}$, (A) $(x\,10^{-4})$	Cathodic peak potential, $E_{p,c}$, (mV)	Peak potential separation, DE_p, (mV)	$I_{p,a}/I_{p,c}$
5	2.236	-2.04	661.9	3.52	524.9	137.0	0.58
10	3.162	-3.75	694.2	5.81	476.5	217.7	0.65
20	4.472	-6.79	733.6	8.39	439.2	294.4	0.81
40	6.325	-12.2	801.8	12.4	345.9	455.9	0.98
60	7.746	-17.1	866.4	16.0	263.9	602.5	1.07
80	8.944	-21.7	923.8	19.1	189.3	734.5	1.14
100	10.000	-25.7	970.4	21.8	129.6	840.8	1.18
200	14.142	-29.5	586.5	31.0	28.9	557.6	0.95
300	17.321	-34.8	636.8	31.2	2.8	634.0	1.11
400	20.000	-37.6	633.2	30.4	-23.3	656.5	1.24
500	22.361	-39.3	643.9	28.8	-23.3	667.2	1.37
700	26.458	-40.1	622.4	25.9	-8.4	630.8	1.55

The results for the PANI polymer film coated on an Au/MBT modified electrode, shown in Table 4.14 were used to plot a graph of ΔE_p vs. scan rate (v) as shown in Figure 4.45. From the shape of the graph in Figure 4.45 it can be seen that it does not follow the Randles-Sevčik equation, especially for the scan rates higher than 100 mV.s^{-1}, since a straight line was only obtained for the scan rates less than and equal to 100 mV.s^{-1}. These results thus indicate that at high scan rates slow electron transfer kinetics are observed in the polymer film.
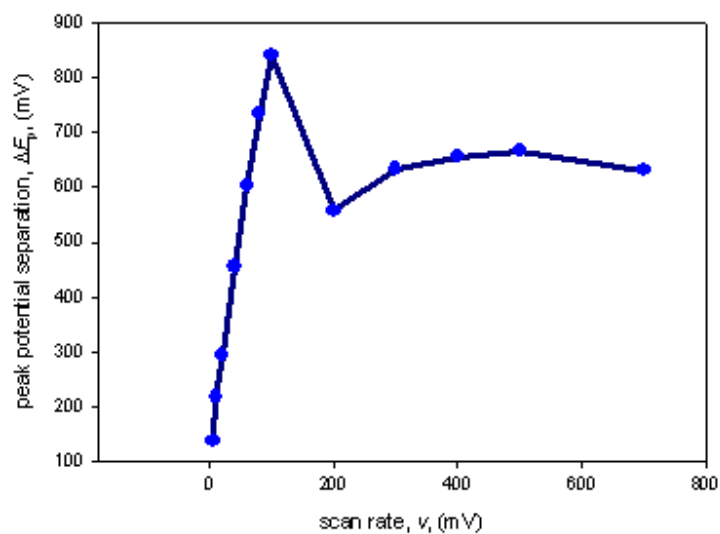
Figure 4.45   **Graph of peak potential separation (ΔE_p) vs. scan rate (v) for the Au/MBT/PANI polymer film in 0.1 M HCl solution at different scan rates.**

Secondly, the graph of anodic and cathodic peak current (I_p) vs. the square root of scan rate ($v^{1/2}$) in Figure 4.46, shows linearity only for the scan rates less than and equal to 100 mV.s^{-1}, which demonstrates that the process are absorption controlled only at slow scan rates, correlating with the results obtained in Figure 4.45.
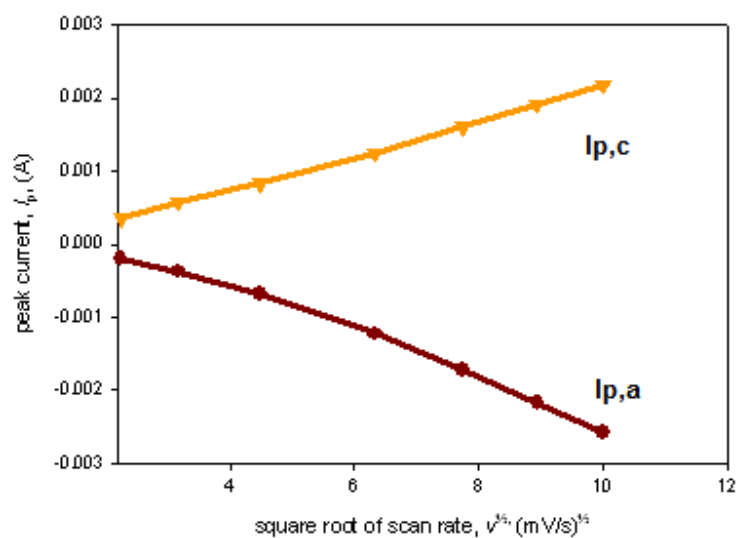
Figure 4.46   **Graph of anodic and cathodic peak current (I_p) vs. square root of slow scan rate ($v^{\frac{1}{2}}$) for the Au/MBT/PANI polymer film in 0.1 M HCl solution at different scan rates.**

The results in Table 4.14 further indicate that the peak potential separation increases relatively with the scan rate for the slow scan rates, indicating some limitation due to charge transfer kinetics, with the results for the slow scan rates of 5 to 100 mV.s^{-1} indicating a reversible system. The anodic and cathodic peak ratio ($I_{p,a}/I_{p,c}$) is equal to unity for the scan rates of 40 to 300 mV.s^{-1}.

4.6.2 Characterisation of Au/MBT/PANI/PVAc polymer film

This stage represents the final stage of constructing a thick-film biosensor as several layers are added to the transducer to form the biosensor for the organic phase pesticide studies.

Usually, a thick-film biosensor comprises of layers of special inks (or pastes) that are deposited sequentially onto an insulating support or substrate (Albared-Sirvent *et al.* 2000:153). The Au/MBT/PANI biosensor was constructed by coating a SAM of MBT on an Au electrode, followed by PANI electropolymerisation, which was followed by the immobilisation of the enzyme AChE, and next a layer of poly(vinyl acetate) (PVAc) was coated on top of all the layers to get the final biosensor.

Poly(vinyl acetate) is a polymer that is often used as a primary ingredient for the formation of glue that is odourless, non-flammable and suitable for use at low temperatures (Arshak *et al.* 2006:200).

In this section the electrochemical properties of the Au/MBT/PANI/PVAc sensor was investigated to establish the performance and redox activity of the electrode in 0.1 M phosphate buffer, KCl (pH 7.2) and 0.1 M HCl solutions, respectively. The results obtained are displayed and discussed in the following paragraphs.

4.6.2.1 Cyclic voltammetric characterisation at different scan rates

In Figure 4.47 the CV results for the Au/MBT/PANI/PVAc polymer film at different scan rates in 0.1 M phosphate buffer, KCl (pH 7.2) solution is shown, with the arrows indicating the direction of increasing scan rate.
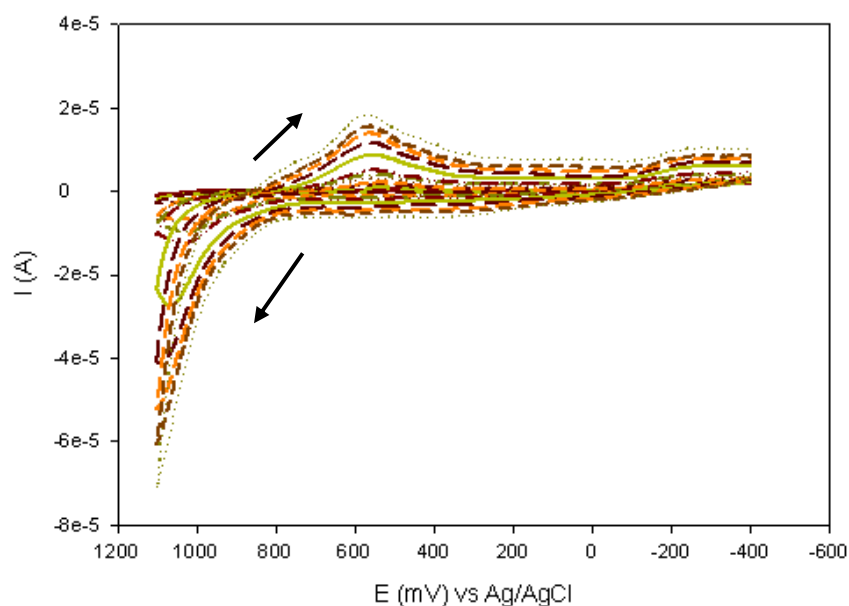
Figure 4.47   Cyclic voltammograms for the Au/MBT/PANI/PVAc polymer film in 0.1 M phosphate buffer, KCl (pH 7.2) solution at different scan rates of 5, 10, 20, 40, 60, 80, 100, 200, 400, 500, 700 mV.s^{-1}.

The CVs in Figure 4.47 for the scan rate studies done in 0.1 M saline phosphate buffer (pH 7.2) solution, shows that one redox couple is evident at slow scan rates, while the anodic peaks diminish at high scan rates. Since it was observed that the

peak potentials of the redox couple were shifting to higher values as the scan rate was

increased, the Randel-Sevčik equation was applied to determine the rate of electron

transport (D_e) within the polymer film. From a Randel-Sevčik plot of I_p vs $v^{1/2}$, the

value for $D_e = 5.985 \ x \ 10^{-15}$ cm².s^{-1} was obtained. The heterogeneous rate constant, k^o,

was calculated and found to be $2.159 \ x \ 10^{-10}$ cm.s^{-1}. Since the value of k^o is less than

10^{-5} cm.s^{-1}, an irreversible system exists and electron transfer at the electrode is

extremely slow.

In Figure 4.48 the CV results for the Au/MBT/PANI/PVAc polymer film at

different scan rates in 0.1 M HCl solution is shown.
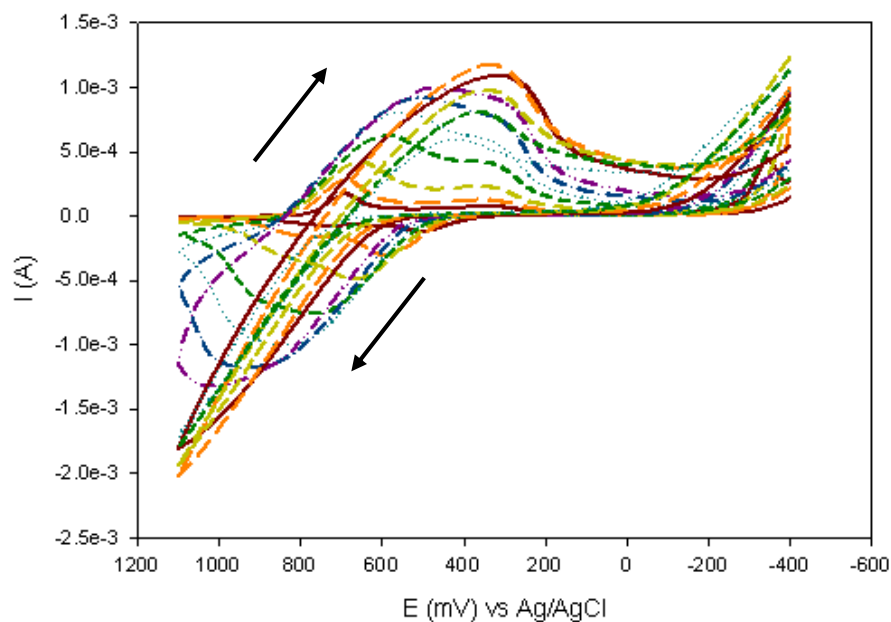
Figure 4.48   **Cyclic voltammograms for the Au/MBT/PANI/PVAc polymer film in
0.1 M HCl solution at different scan rates of 5, 10, 20, 40, 60, 80, 100,
200, 400, 500, 700 mV.s^{-1}.**

Similarly as for the CVs in Figure 4.47 for the scan rate studies done in 0.1 M saline

phosphate buffer (pH 7.2) solution, it was found in Figure 4.48 that one redox couple

is evident at slow scan rates, while the anodic peaks diminish at high scan rates, for

the scan rate results collected in 0.1 M HCl solution. For the results collected at

slower scan rates, it was observed that the peak potentials of the redox couple were

shifting to higher values as the scan rate was increased, the Randel-Sevčik equation

was applied to determine the rate of electron transport (D_e) within the polymer film.

The surface concentration of the PANI-PVAc polymer film was estimated to be 1.002

x 10^{-8} mol.cm^{-2}. From a Randel-Sevčik plot of I_p vs $v^{\frac{1}{2}}$, the value for $D_e = 5.519$ x 10^{-16} cm².s^{-1} was obtained. The heterogeneous rate constant, k^o, was calculated and

found to be 6.555 x 10^{-11} cm.s^{-1}. Since the value of k^o is less than 10^{-5} cm.s^{-1}, an

irreversible system exists and electron transfer at the electrode is extremely slow.

A summary of the results for the different kinetic parameters of the

Au/MBT/PANI/PVAc polymer film is shown in Table 4.15.

Table 4.15   **Comparison of the results for different kinetic parameters for the PANI/PVAc polymer film on the Au/MBT SAM electrode is shown.**

Solution	Scan rate (mV/s)	Electron diffusion coefficient (D_e), (cm²·s^{-1})	Standard heterogeneous rate constant (k^o) m.s^{-1}
0.1 M phosphate buffer (pH 7.2)	40	5.985 x 10^{-15}	2.159 x 10^{-10}
0.1 M HCl	40	5.519 x 10^{-16}	6.555 x 10^{-11}

An analysis of the results in Table 4.15 indicate that the rate of electron transport along the polymer chain is faster in the saline phosphate buffer solution, while the rate of electron transfer to the electrode is one order of magnitude slower in the HCl solution, as compared to the saline phosphate buffer solution.

The data of the CVs shown in Figure 4.48 were further evaluated and the results are shown in Table 4.16.

Table 4.16   **Results for the effect of scan rate on anodic and cathodic peak current and peak potentials in CVs for different scan rates in 0.1 M HCl solution.**

Scan rate v, (mV/s)	Square root of scan rate, $v^{1/2}$, (mV/s)$^{1/2}$	Anodic peak current, $I_{p,a}$, (A) ($x\ 10^{-4}$)	Anodic peak potential, $E_{p,a}$, (mV)	Cathodic peak current, $I_{p,c}$, (A) ($x\ 10^{-4}$)	Cathodic peak potential, $E_{p,c}$, (mV)	Peak potential separation, DE_p, (mV)	$I_{p,a}/I_{p,c}$
5	2.236	-1.225	506.7	1.654	692.8	-186.1	0.74
10	3.162	-3.091	594.3	2.686	692.8	-98.5	1.15
20	4.472	-4.920	666.7	4.134	655.5	11.2	1.19
40	6.325	-7.562	773.3	6.193	592.1	181.2	1.22
60	7.746	-10.08	834.3	8.009	554.8	279.5	1.26
80	8.944	-11.81	925.7	9.149	502.6	423.1	1.29
100	10.000	-13.25	1009.5	9.933	476.5	533.0	1.33
200	14.142	-15.91	1009.5	1.096	319.8	689.7	1.45
300	17.321	-19.24	1066.7	1.182	338.5	728.2	1.63
400	20.000	-16.58	1028.6	9.673	353.4	675.2	1.71
500	22.361	-5.717	822.7	8.064	375.8	446.9	0.71
700	26.458	-13.26	994.3	5.968	420.5	573.8	2.22

The results for the PANI/PVAc polymer film coated on an Au/MBT modified electrode, shown in Table 4.16 were used to plot a graph of ΔE_p vs. scan rate (v) as

shown in Figure 4.49. From the shape of the graph in Figure 4.49 it can be seen that it does not follow the Randles-Sevcik equation, especially for the scan rates higher than 100 mV.s^{-1}, since a straight line was only obtained for the scan rates less than and equal to 100 mV.s^{-1}. These results thus indicate that at high scan rates slow electron transfer kinetics are observed in the polymer film. The same trend was observed for the Au/MBT/PANI polymer film in Figure 4.45.
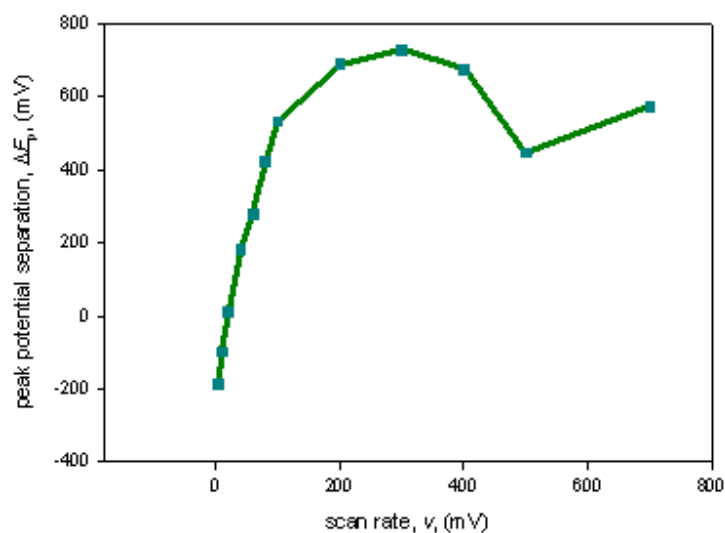
Figure 4.49   **Graph of peak potential separation (ΔE_p) vs. scan rate (v) for the Au/MBT/PANI/PVAc polymer film in 0.1 M HCl solution at different scan rates.**

Next the graph of anodic and cathodic peak current (I_p) vs. the square root of scan rate ($v^{\frac{1}{2}}$) as shown in Figure 4.50 was plotted, which again only showed linearity for the scan rates less than and equal to 100 mV.s^{-1}, which demonstrates that the process

are adsorption controlled only at slow scan rates, correlating with the results obtained

in Figure 4.48.
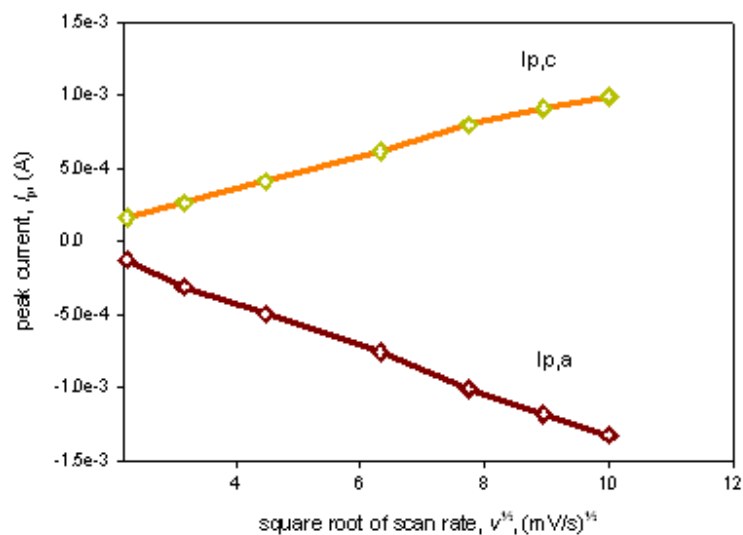
Figure 4.50   **Graph of anodic and cathodic peak current (I_p) vs. square root of slow scan rate ($v^{1/2}$) for the Au/MBT/PANI/PVAc polymer film in 0.1 M HCl solution at different scan rates.**

Further analysis of the results in Table 4.16 indicate that the peak potential separation

increases relatively with the scan rate for the slow scan rates, indicating some

limitation due to charge transfer kinetics, with the results for the slow scan rates of 5

to 100 mV.s^{-1} indicating a reversible system, while the anodic and cathodic peak ratio

($I_{p,a}/I_{p,c}$) is equal to unity for the scan rates of 10 to 200 mV.s^{-1}.

Next the different kinetic parameters calculated for the different

configurations of polymers constructed in this chapter were listed in order to compare

the different polymer films. The kinetic parameters of the polymers were evaluated in

0.1 M HCl solution. A summary of the kinetic parameters are given in Table 4.17.

Table 4.17   **Comparison of the results for different kinetic parameters calculated for the different configurations of polymer films constructed in this study.**

Polymer film	Surface concentration, (Γ^*), (mol.cm^{-2})	Electron diffusion coefficient (D_e), (cm^2.s^{-1})	Standard heterogeneous rate constant (k^o) m.s^{-1}
POMA-PSSA	5.559×10^{-3}	1.181×10^{-14}	4.367×10^{-13}
PDMA-PSSA	2.200×10^{-2}	4.174×10^{-15}	2.833×10^{-12}
[£]PANI-PVS	1.890×10^{-7}	6.460×10^{-8}	1.982×10^{-6}
PANI	2.582×10^{-1}	2.844×10^{-9}	6.777×10^{-8}
PANI-PVAc	1.002×10^{0}	5.519×10^{-16}	6.555×10^{-11}

From the results in Table 4.17 it can be seen that the surface concentration of the

polymer film was found to be highest when PANI was electropolymerised on the

Au/MBT modified electrode followed by drop-coating of the PVAC layer, while the

lowest surface concentration was recorded for the POMA-PSSA polymer film. When

these values are compared with that for a PANI film doped with polyvinyl sulphonate

(PVS), it is found that the surface concentration is much higher for the polymer

configurations used in this study. However, electron transport along the polymer

backbone is the fastest in the PANI-PVS polymer film when the D_e values are

compared, indicating that the conductivity is better in this film, compared to that of

---

[£] Iwuoha *et al.* (1997). Biosensors & Bioelectronics, 12(8): 749-761.

the POMA-PSSA, PDMA-PSSA and PANI-PVAc polymer films. The values obtained for the heterogeneous rate constant, k^o, compare relatively well for the POMA-PSSA, PDMA-PSSA and PANI-PVAc polymer films, although they differ from each other in one order of magnitude, also indicating that electron transfer is relatively slow. These results clearly show the influence of the different surfactants when incorporated into the different polyanilines (compared to the use of only PANI), as the results for the surface concentration, electron diffusion coefficient, and standard heterogeneous rate constant for the different polymer films were compared.

4.6.3 Characterisation of Au/MBT/PANI/AChE/PVAc thick-film electrode

4.6.3.1 Voltammetric characterisation

In Figure 4.51 the CV results of the Au/MBT/PANI/AChE/PVAc enzyme electrode in 0.1 M phosphate buffer, KCl (pH 7.2) at a scan rate of 10 mV.s^{-1} is shown. For the same enzyme electrode the anodic difference SWV results are shown in Figure 4.52, with the DPV results shown in Figure 4.53.

The CV response in Figure 4.51 was collected just after immobilisation of the enzyme AChE in the PANI polymer matrix, followed by drop coating of the PVAc polymer. The potential was swept between - 400 and + 1800 mV.
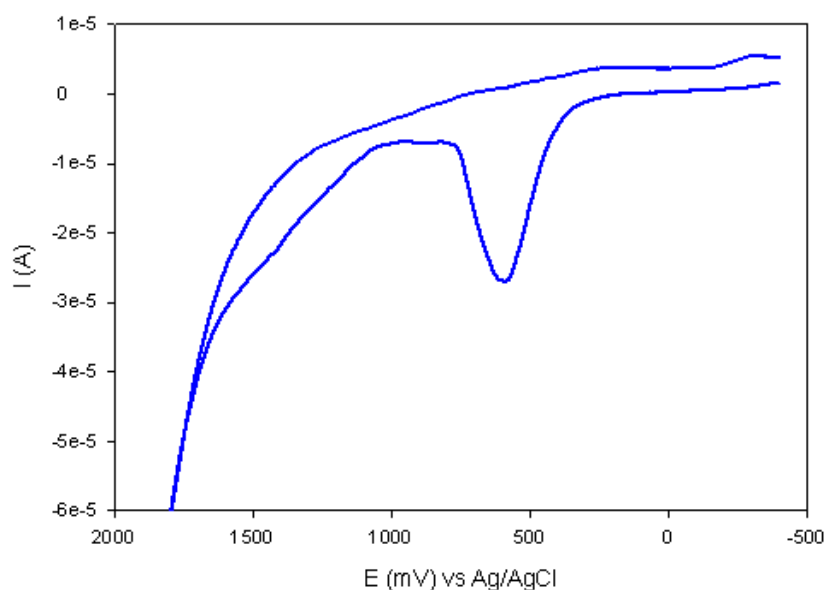
Figure 4.51   **CV response of Au/MBT/PANI/AChE/PVAc enzyme electrode in 0.1 M phosphate buffer, KCl (pH 7.2) solution at a scan rate of 10 mV.s^{-1}.**

The cyclic voltammetric results in Figure 4.51 show an anodic peak that was observed at a potential of + 568.5 mV (vs. Ag/AgCl).

The results of the square wave voltammograms (SWVs) for the Au/MBT/PANI/AChE/PVAc enzyme electrode measured at 20 Hz are shown in Figure 4.52. This SWV response was recorded under anaerobic conditions and the net (difference between forward and reverse currents) SWV responses were obtained. The anodic peak observed in the CV results was confirmed with the SWV results, which showed a strong anodic peak at a potential of + 1178.5 mV (vs. Ag/AgCl). The second anodic peak observed below 0 V (vs. Ag/AgCl) can be attributed to the MBT SAM layer on the Au surface.
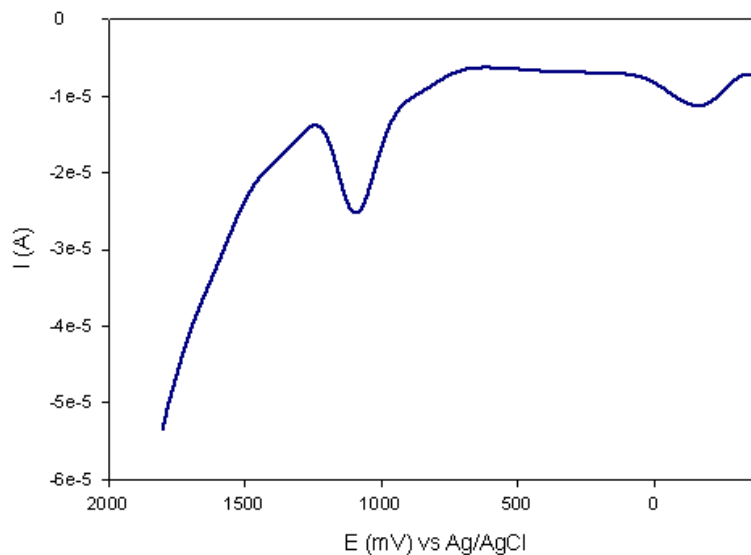
Figure 4.52   **SWV response of Au/MBT/PANI/AChE/PVAc enzyme electrode in 0.1 M phosphate buffer, KCl (pH 7.2) solution at a frequency of 20 Hz.**

The same enzyme electrode response observed with the SWV response was obtained for the DPV response of the Au/MBT/PANI/AChE/PVAc enzyme electrode, when the potential was scanned between – 400 and + 1800 mV as shown in Figure 4.53.
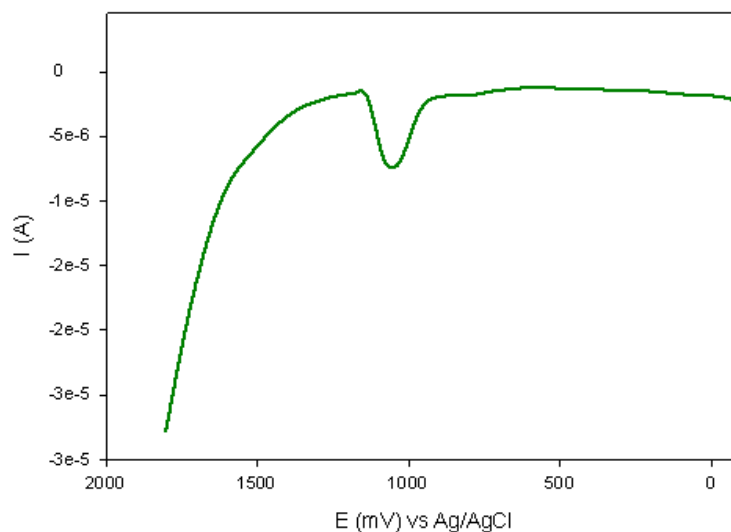
Figure 4.53   **DPV response of Au/MBT/PANI/AChE/PVAc enzyme electrode in 0.1 M phosphate buffer, KCl (pH 7.2) solution at a scan rate of 10 mV.s⁻¹.**

Next, the anodic peak observed in the CV results was also confirmed with the DPV results in Figure 4.53, which showed a single peak at a potential of + 1079.3 mV (vs. Ag/AgCl). This peak potential was in relatively the same vicinity as the SWV response observed.

4.6.3.2 Voltammetric characterisation of successive acetylthiocholine (ATCh) substrate addition to Au/MBT/PANI/AChE/PVAc biosensor

In Figure 4.54 the CV responses of the Au/MBT/PANI/AChE/PVAc biosensor to successive ATCh substrate additions under anaerobic conditions are

shown. The first results were collected by applying sequential linear potential scan between $-$ 400 to $+$ 1800 mV (vs. Ag/AgCl), at a scan rate of 10 mV.s^{-1}. The CVs were performed at the scan rate of 10 mV.s^{-1}, to ensure that the fast enzyme kinetics could be monitored.

The three CVs for successive 0.01 M ATCh substrate additions to Au/MBT/PANI/AChE/PVAc biosensor in 2 ml of 0.1 M phosphate buffer, KCl (pH 7.2) solution are shown in Figure 4.54. When 0.0 mM of ATCh was added, the peak current (I_p) was observed at $-$ 5.532 x 10^{-5} A, at 0.6 mM of ATCh added it was observed at $-$ 7.459 x 10^{-5} A, while at 0.9 mM of ATCh added it was observed at $-$ 7.981 x 10^{-5} A. A clear shift in peak current (I_p) was observed as the concentration of the substrate, ATCh, as increased indicating the electrocatalytic functioning of the biosensor. Figure 4.54 further illustrates that in increase in the reductive current is also observed, but the magnitude is smaller when compared to the increases in oxidative current. This clearly illustrates that the oxidative response of the biosensor to ATCh addition is preferred.
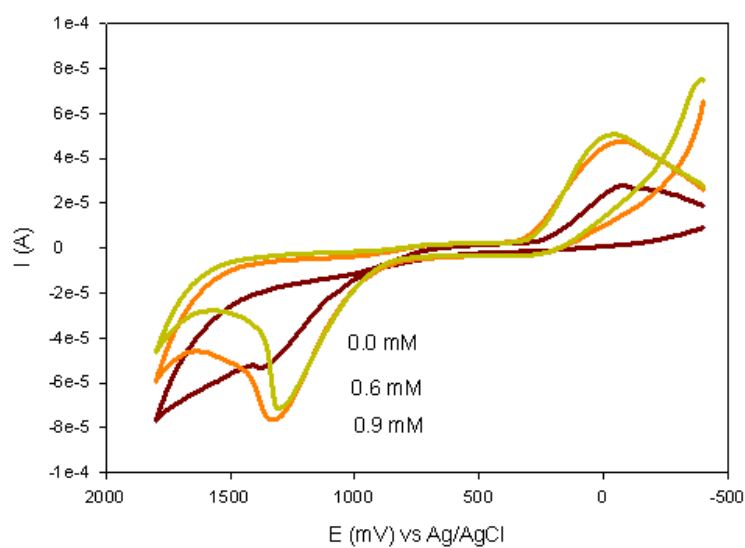
Figure 4.54   **CV response of successive ATCh substrate addition to Au/MBT/PANI/AChE/PVAc biosensor in 0.1 M phosphate buffer, KCl (pH 7.2) solution at a scan rate of 10 mV.s^{-1}.**

In Figure 4.55 a calibration curve for the successive addition of ATCh substrate to the Au/MBT/PANI/AChE/PVAc biosensor is shown. The calibration curve was constructed in order to apply Michealis-Menten kinetics and calculate the apparent Michaelis-Menten constant for the biosensor response.
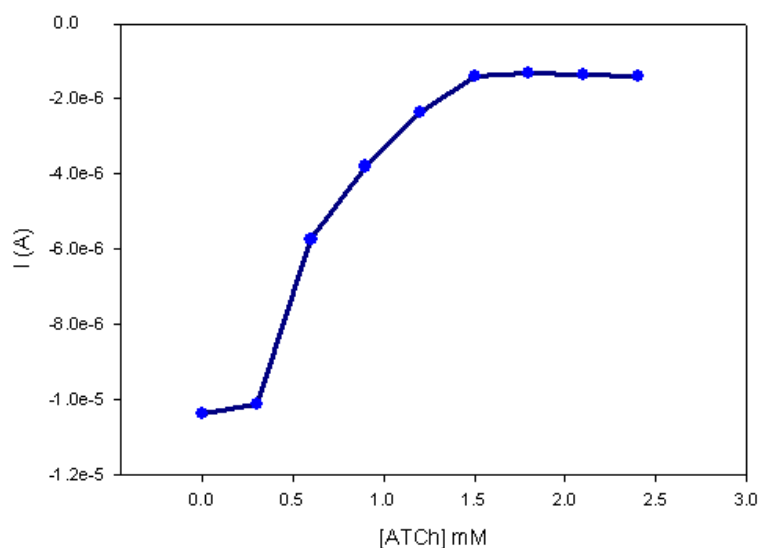
Figure 4.55   **Calibration curve of current vs. substrate concentration for the successive addition of ATCh as substrate to the Au/MBT/PANI/AChE/PVAc biosensor in 0.1 M phosphate buffer KCl (pH 7.2) solution.**

From the shape of the curve in Figure 4.55 it was deduced that the biosensor exhibit Michaelis-Menten kinetics for most of the data plotted. The sensitivity of the biosensor was estimated to be 4.793 x 10^{-6} M, while the limit of detection was calculated and found to be 0.478 M. The apparent Michaelis-Menten constant, K_m^{app}, was calculated to be 0.292 M, and the maximum current, I_{max}, was 1.400 x 10^{-6} A.

The results obtained in Figure 4.56 was repeated by scanning the potential in a different potential window, to again establish if an increase in anodic current can be obtained for successive ATCh substrate additions to the Au/MBT/PANI/AChE/PVAc biosensor. The anodic currents observed were relatively small, but the same increase in anodic current was obtained and the results shown in Figure 4.56 was narrowed

down by showing the potential sweep between + 600 and + 1300 mV at a scan rate of
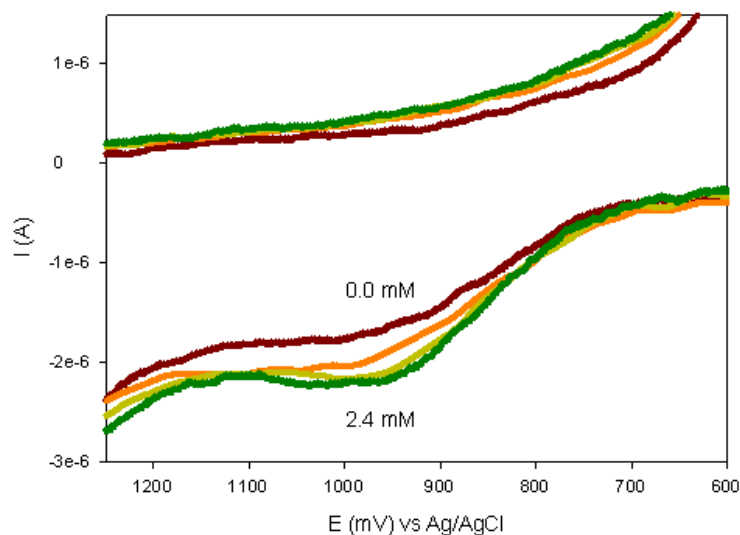
10 mV.s^{-1}.

Figure 4.56   **CV response of successive ATCh substrate addition to Au/MBT/PANI/AChE/PVAc biosensor in 0.1 M phosphate buffer, KCl (pH 7.2) solution at a scan rate of 10 mV.s^{-1}.**

For the CV results shown in Figure 4.56 it can be seen that a clear redox response

was obtained when the substrate ATCh was added to the

Au/MBT/PANI/AChE/PVAc biosensor. A clear increase in oxidative current is

observed as the ATCh concentration was increased from 0.0 mM to 2.4. Thus in

phosphate buffer, KCl (pH 7.2) solution the oxidative peak current shifted and

increased with increasing acetylthiocholine (ATCh) concentration. Furthermore, it

also shows that the thiol, MBT, coated with the PANI/AChE/PVAc film can

effectively mediate the transfer of electrons between the enzyme acetylcholinesterase (AChE) and the gold electrode.

In the next step the DPV response of the Au/MBT/PANI/AChE/PVAc biosensor was monitored for the successive addition of ATCh substrate and a similar electrocatalytic response as the one observed for the CV results reported above, was obtained for the DPV results as shown in Figure 4.57.
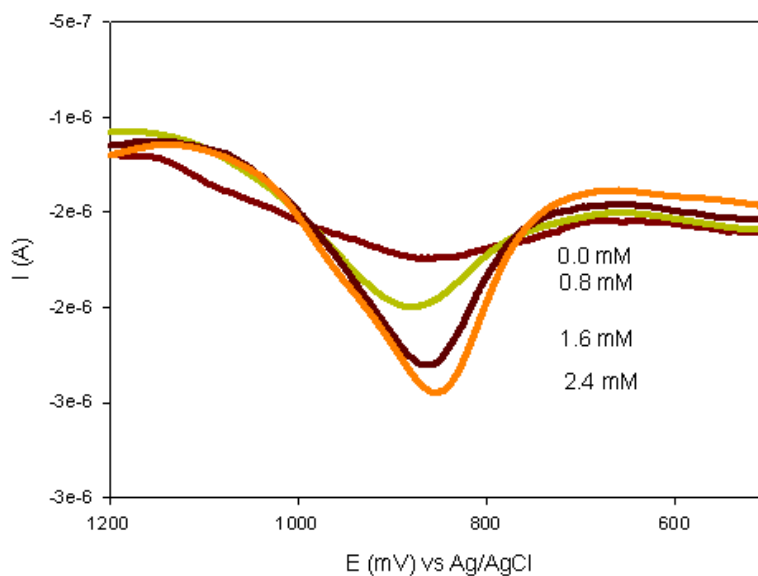
Figure 4.57   **DPV response of successive ATCh substrate addition to Au/MBT/PANI/AChE/PVAc biosensor in 0.1 M phosphate buffer, KCl (pH 7.2) solution at a scan rate of 10 mV.s^{-1}, and in a potential window of + 500 to + 1200 mV.**

The DPV results in Figure 4.57 shows the voltammetric responses for the electrocatalytic oxidation of acetylthiocholine at the Au/MBT/PANI/AChE/PVAc

biosensor. The DPV responses shows an increase in peak current heights upon the successive additions of ATCh as substrate, with the results more pronounced around a specific potentials as compared with those observed in the CV responses in Figure 4.56.

The peak current, $I_{peak,}$ for specific concentrations of the ATCh substrate added in Figure 4.57 was - 1.737 x 10^{-6} A for 0.0 mM of ATCh added, followed by - 1.992 x 10^{-6} A for 0.8 mM of ATCh, then - 2.314 x 10^{-6} A was obtained for 1.6 mM of ATCh added, while it was - 2.448 x 10^{-6} A for the highest concentration of 2.4 mM of ATCh added. These results clearly indicated that a biosensor was established and that AChE as enzyme was hydrolysing the substrate ATCh, with the increase in oxidative current as the preferred route of reaction.

CHAPTER 5

Application of AChE-Poly(*o*-methoxyaniline) and AChE-Poly(*2,5*-dimethoxyaniline) Biosensors for the Determination of Selected Organophosphate and Carbamate Pesticide Compounds in 0.1 M Phosphate buffer (pH = 7.2) Saline Solution

5.1   Introduction

In this chapter the results for the application of the AChE-Poly(*o*-methoxyaniline) and AChE-Poly(*2,5*-dimethoxyaniline) biosensors that were constructed, are discussed to determine and investigate its performance for the determination of selected organophosphate and carbamate pesticide compounds in 0.1 M phosphate buffer (pH = 7.2) saline solution.

Voltammetric results were collected for the Au/MBT/POMA-PSSA/AChE and Au/MBT/PDMA-PSSA/AChE biosensors, before and after 20 minutes of incubation in selected pesticide solutions, to investigate its response to successive acetylcholine (ACh) substrate addition under anaerobic conditions in 0.1 M phosphate buffer, KCl (pH 7.2) solution.

5.2   Design of Au/MBT/POMA-PSSA/AChE or Au/MBT/POMA-PSSA/AChE biosensor for pesticide detection

Acetylcholinesterase as an enzyme belongs to the family of hydrolase and the main player in its catalytic mechanism is the catalytic triad shown in Figure 5.1. This triad is a coordinated structure consisting of three essential amino acids of histidine, serine and aspartic acid (Krasinski *et al.* 2005:6686; Manetsch *et al.* 2004:12809).
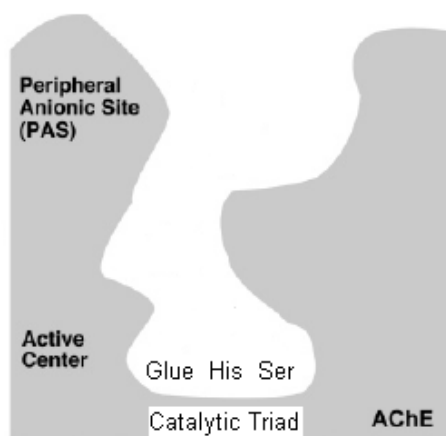
Figure 5.1   **Schematic representation of the active gorge of the AChE enzyme with its catalytic triad situated at the base of the gorge (Krasinski et al. 2004:6688).**

Acetylcholinesterase is also referred to as a serine esterase and has an anionic binding site that attracts the positively charged quaternary ammonium group of acetylcholine. The serine hydroxyl group attacks and cleaves the ester, an example of base catalysis, after it has been deprotonated by a neighbouring histidine group in the triad. After

ester hydrolysis has taken place, the enzyme is regenerated (Woster 2001:128). However, when inhibitors such as the organophosphate and carbamate pesticides interact with the AChE serine hydroxyl group, the nucleophilic hydroxyl group of the serine residue located at the active site of AChE reacts with the P-atom of the organophosphate. This results in a covalently bound organophosphate. Similarly, the serine hydroxyl group can react with the carbonyl carbon of the carbamates, resulting in a covalently bound carbamate, similar to the reaction obtained when acetylcholine is used. This results in inactivation of the enzyme since the hydroxyl group is no longer available to attack the acetylcholine substrate (Schulze *et al.* 2005:5823-5824).

With the working of the enzyme and substrate catalysis explained in the above paragraphs, the following amperometric biosensor design and mechanism was proposed to explain the biosensor reaction taking place as shown in Figure 5.2.
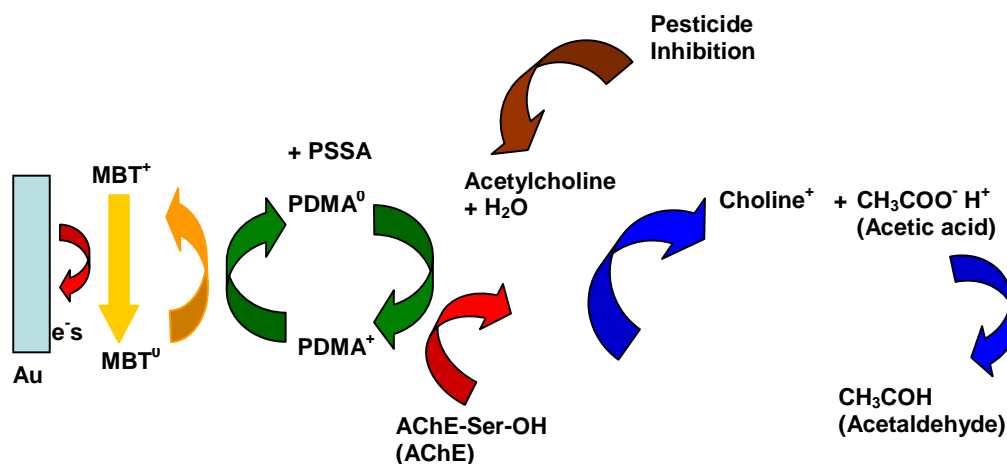
Figure 5.2   **A schematic representation of the Au/MBT/PDMA-PSSA/AChE biosensor reaction occurring at the gold electrode, with the pesticide inhibitor effect also included.**

In Figure 5.2 a proposed schematic representation for the Au/MBT/PDMA-PSSA/AChE biosensor is shown, but the polymer PDMA can be replaced by the second polymer used, *i.e.* POMA, to represent the Au/MBT/POMA-PSSA/AChE biosensor. It further shows that as acetylcholine is hydrolysed by acetylcholinesterase, it forms choline and acetic acid. The acetic acid is in turn reduced by poly(*2,5*-dimethoxyaniline) (PDMA) to form acetaldehyde as the PDMA loses an electron. In return the conducting PDMA polymer accepts an electron from mercaptobenzothiazole as it is oxidised through interaction with the gold electrode.

5.2.1 Acetic acid evaluation at both biosensor interfaces

Evidence to prove that acetic acid was indeed reduced to form acetaldehyde was collected by interacting the respective Au/MBT/PDMA-PSSA and Au/MBT/POMA-PSSA polymer films with successive additions of 0.01 M acetic acid, which was added to a 0.1 M phosphate buffer, KCl (pH 7.2) solution containing the electrode coated with the respective polymers.

In Figure 5.3 (a) it can be seen how the reduction current in the CV increases as the concentration of acetic acid is increased in the 0.1 M phosphate buffer, KCl solution (pH 7.2) solution containing the Au/MBT/POMA-PSSA polymer electrode. This

increase in the reduction current was confirmed with the DPV results shown in Figure

5.3 (b).
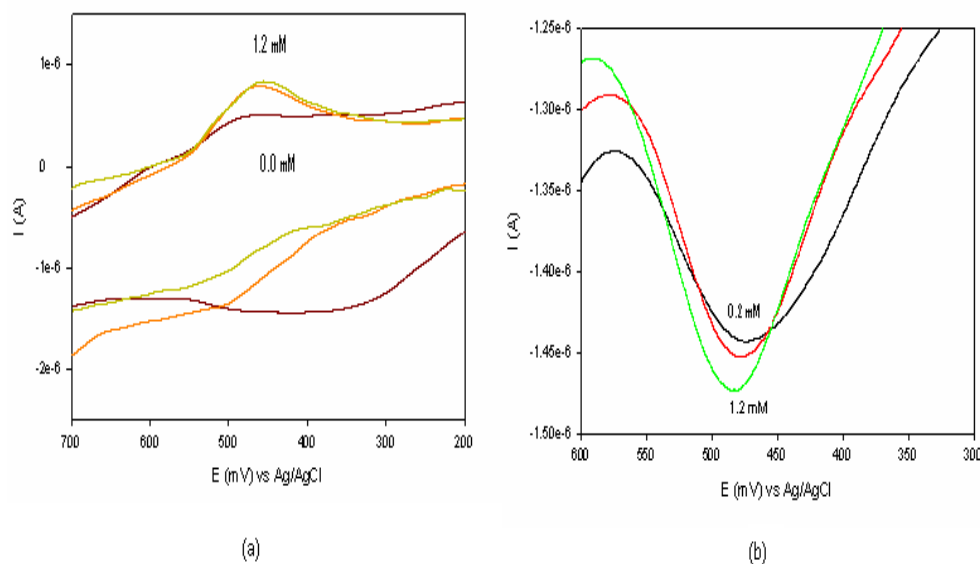
Figure 5.3   **Cyclic voltammetric (CV) results in (a) collected at scan rate of 10 mV.s^{-1} and differential pulse voltammetric (DPV) results in (b) collected at a scan rate of 10 mV.s^{-1} are shown for the increasing addition of acetic acid to the Au/MBT/POMA-PSSA polymer film.**

Similarly in Figure 5.4 (a) an increase in the reduction current of the CV was

observed when the acetic acid interacted with the Au/MBT/PDMA-PSSA polymer

electrode in the 0.1 M phosphate buffer, KCl solution (pH 7.2) solution. The DPV

results in Figure 5.4 (b) confirm the increase in reduction current as observed in the
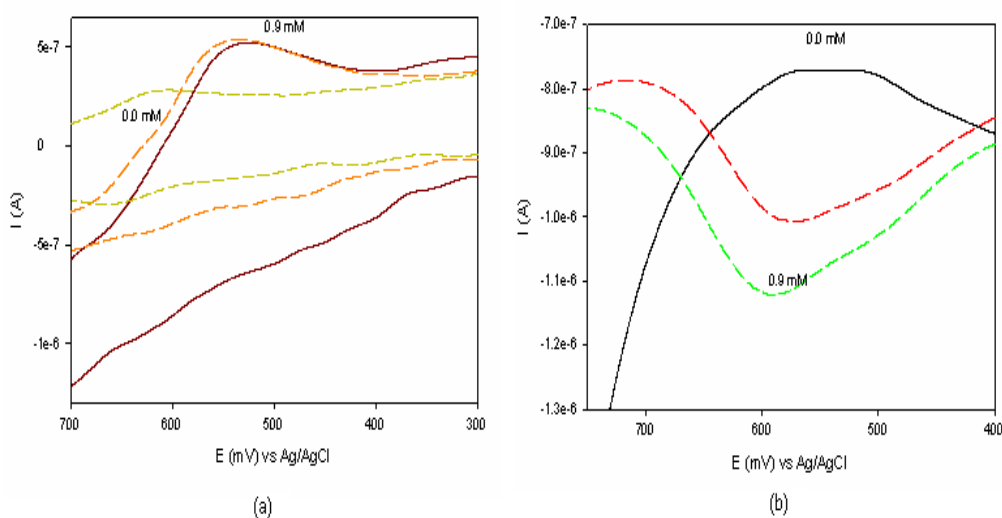
CV results.

Figure 5.4   **Cyclic voltammetric (CV) results in (a) collected at a scan rate of 10 mV.s^{-1} and differential pulse voltammetric (DPV) results in (b) collected at a scan rate of 10 mV.s^{-1} are shown for the increasing addition of acetic acid to the Au/MBT/PDMA-PSSA polymer film.**

The voltammetric results (CV and DPV) observed in Figures 5.3 and 5.4 have thus validated the amperometric biosensor design proposed in Figure 5.2, showing that as acetylcholine is hydrolysed by AChE into choline and acetic acid, the acetic acid is in turn reduced by the polymer to acetaldehyde.

5.3   Application of AChE-Poly(o-methoxyaniline) Biosensor in 0.1 M Phosphate buffer (pH = 7.2) Saline Solution

5.3.1   Successive acetylcholine (ACh) substrate addition to Au/MBT/POMA-PSSA/AChE biosensor

The cyclic voltammograms (CVs) for the successive addition of ACh substrate to the biosensor under anaerobic conditions are shown in Figure 5.5. It is seen in Figure 5.5 that the oxidative current of the cyclic voltammograms are increasing as the ACh concentration is increased from 0.0 mM to 1.1 mM in phosphate buffer, KCl (0.1 M, pH 7.2). In the CV where no ACh was added, the anodic peak potential ($E_{p,a}$) and the cathodic peak potential ($E_{p,c}$) were found to be + 438.5 and + 461.5 mV (vs. Ag/AgCl) respectively, with a formal potential ($E^{o\prime}$) of + 456.0 mV (vs. Ag/AgCl). When the ACh concentration was increased to 0.5 mM, it gave $E_{p,a}$ = + 515.9 mV and $E_{p,c}$ = + 389.2 mV (vs Ag/AgCl) with a formal potential of + 452.5 mV (vs. Ag/AgCl). At the ACh concentration equal to 1.1 mM, it was found that $E_{p,a}$ = + 470.9 mV and $E_{p,c}$ = + 392.1 mV (vs Ag/AgCl) with a formal potential of + 431.5 mV (vs. Ag/AgCl).
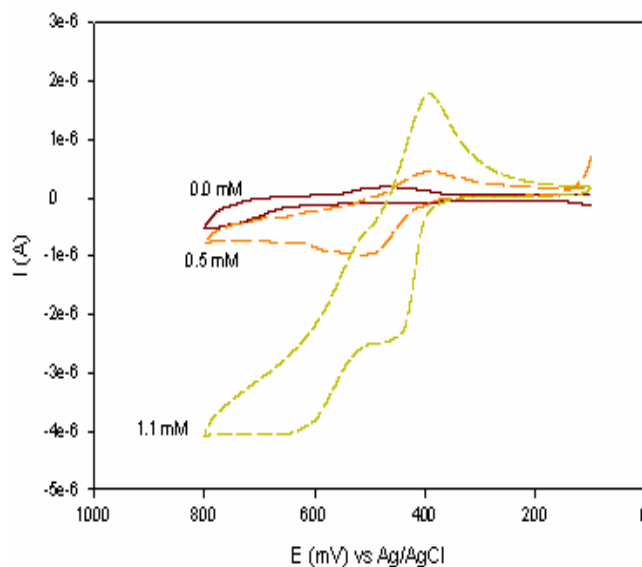
Figure 5.5   **Cyclic voltammograms for successive acetylcholine (ACh) substrate additions to the Au/MBT/POMA-PSSA/AChE biosensor in 0.1 M phosphate buffer, KCl (pH 7.2) solution, with the potential scanned between + 100 to + 800 mV at a scan rate of 5 mV.s^{-1}.**

The CV results in Figure 5.5 therefore indicate that the ACh is hydrolysed by AChE as observed by the CV response obtained, with the anodic current increasing from -7.827 x 10^{-7} A (for 0.0 mM of ACh added), to -9.800 x 10^{-7} A (for 0.5 mM of ACh added) and further to -1.126 x 10^{-5} A (for 1.1 mM of ACh added). These results thus indicate that a functioning biosensor has been developed.

In the next step of the biosensor development and analysis, the CV results obtained were verified by collecting the DPV responses for the same concentrations of ACh substrate added to the Au/MBT/POMA-PSSA/AChE biosensor. The DPV results obtained are displayed in Figure 5.6.
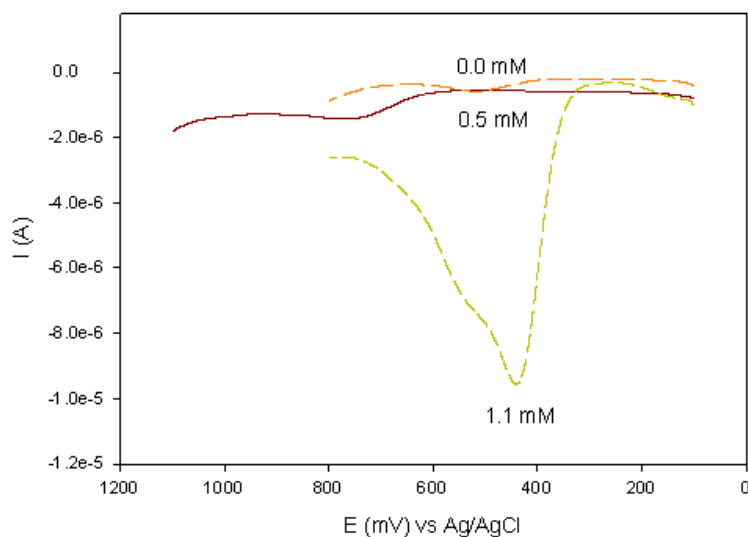
Figure 5.6 **Differential pulse voltammograms for successive acetylcholine (ACh) substrate additions to the Au/MBT/POMA-PSSA/AChE biosensor in 0.1 M phosphate buffer, KCl (pH 7.2) solution, with the potential scanned between + 100 to + 800 mV at a scan rate of 10 mV.s^{-1}.**

The results shown in Figure 5.6 indicate that a similar increase in anodic current was observed in the DPV responses as observed for the CV responses, with the anodic current increasing from -5.546 x 10^{-7} A (for 0.0 mM of ACh added), to -5.885 x 10^{-7} A (for 0.5 mM of ACh added) and further to -9.571 x 10^{-6} A (for 1.1 mM of ACh added). With this analysis the trend in the biosensor analysis observed in the CV responses was confirmed.

5.3.2 Detection of an organophosphorus and carbamate pesticides

When inhibitors such as the organophosphorous pesticides are present in a solution matrix, they inhibit the serine hydroxyl active centre of the AChE enzyme, producing an electroactive product that diminishes and signal decreases are shown. The decrease observed is related to the concentration of the pesticide. It should also be noted that one of the major limitations in the detection of organophosphorous and carbamate pesticides, is the irreversible inhibition of the enzyme in the biosensor, disabling the reuse of the devices. This limitation can be circumvented with single-use biosensors (Lin *et al.* 2005:1124).

In Figure 5.7 the molecular structures of the organophosphorous pesticide called diazinon and the carbamate pesticide called carbofuran are shown.
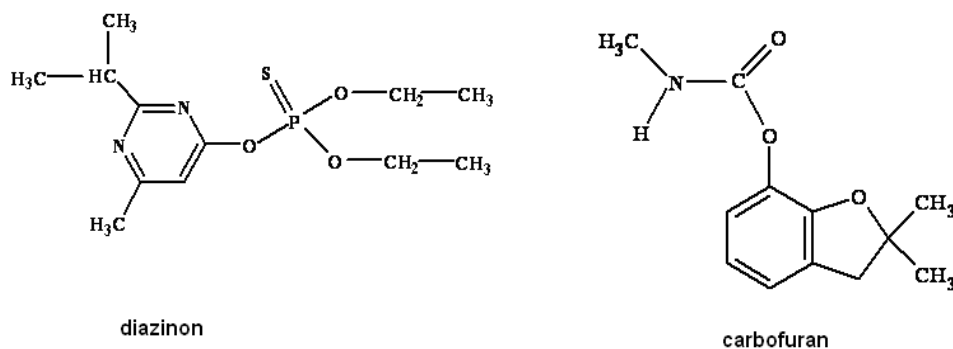
Figure 5.7   **Shows the molecular structure of the organophosphorous pesticide called diazinon and the carbamate pesticide called carbofuran.**

When the serine hydroxyl group of AChE has reacted with the phosphorous atom of an organophosphorous inhibitor, or with the carbonyl group of a carbamate inhibitor, the serine hydroxyl group of the enzyme is left inactive since the hydroxyl group is no longer available to attack the acetylcholine substrate. This results in a diminished or reduced signal which is detected by the amperometric biosensor device (Simon *et al.* 1999:27740; Pond and Coyne 1996:363).

5.3.3 Diazinon detection with the Au/MBT/POMA-PSSA/AChE/ACh biosensor

With the functioning of the Au/MBT/POMA-PSSA/AChE biosensor now established, the next step in the biosensor analysis focussed on the voltammetric characterisation of successive diazinon pesticide additions to the Au/MBT/POMA-PSSA/AChE biosensor.

In Figure 5.8 the CV results for the successive diazinon pesticide addition to Au/MBT/POMA-PSSA/AChE biosensor in 0.1 M phosphate buffer, KCl (pH 7.2) solution at a scan rate of 5 mV.s^{-1}, is shown.

<table>
</table>
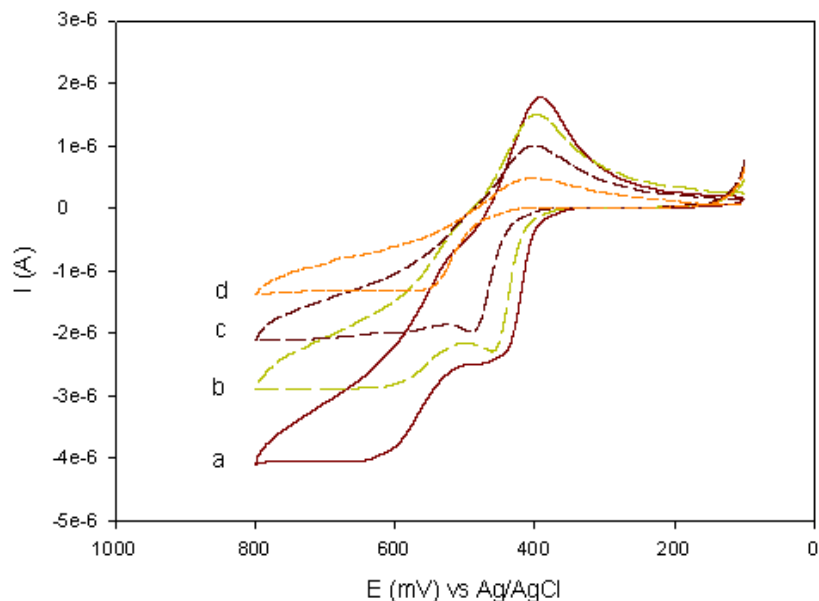
Figure 5.8 **CV response of successive diazinon pesticide addition to Au/MBT/POMA-PSSA/AChE biosensor in 0.1 M phosphate buffer, KCl (pH 7.2) solution at a scan rate of 5 mV.s^{-1}.**

The CV results in Figure 5.8 show the addition of 1.1 mM of ACh substrate to the biosensor in (a), while a shift in anodic current was observed when the additions of diazinon pesticide concentrations of 0.18 ppb in (b), 0.51 ppb in (c) and 1.19 ppb in (d) were made to the biosensor.

When 1.1 mM of ACh was added to the biosensor, the anodic current has increased to - 2.462 x 10^{-6} A for the first anodic peak observed. With 0.18 ppb of diazinon added, the anodic current decreased to - 2.290 x 10^{-6} A, next it further decreased to - 1.982 x 10^{-6} A with the diazinon concentration at 0.51 ppb, while for the highest concentration of 1.19 ppb of diazinon, the anodic current decreased to - 1.299 x 10^{-6} A. This shift towards a decrease in anodic current shown in the CV

results can be attributed to the inhibition of the AChE enzyme by the diazinon pesticide, since the AChE is now unable to fully perform its hydrolysis action of the substrate. Another observation made was the presence of a second less prominent anodic peak that diminished as the pesticide concentration increased.

In Figure 5.9 the anodic difference square wave voltammetric (SWV) results for the successive diazinon pesticide addition to the Au/MBT/POMA-PSSA/AChE biosensor in 0.1 M phosphate buffer, KCl (pH 7.2) solution is shown.
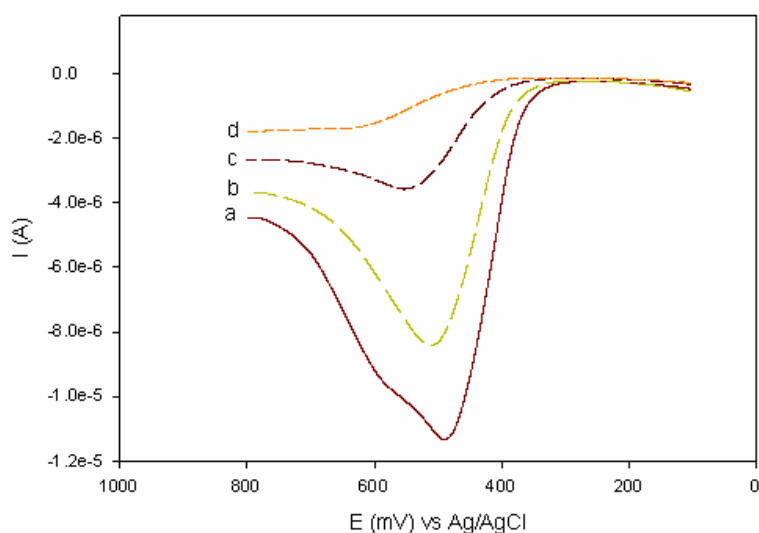
Figure 5.9   **Anodic difference SWV response for successive diazinon pesticide additions to the Au/MBT/POMA-PSSA/AChE biosensor in 0.1 M phosphate buffer, KCl (pH 7.2) solution, with the potential scanned between + 100 and + 800 mV at a frequency of 5 Hz.**

The results displayed in Figure 5.9 were collected to verify the CV responses for the successive diazinon pesticide additions shown in Figure 5.8. The SWV responses

indicate that for the addition of 1.1 mM of ACh substrate in (a), an anodic peak current of - 9.542 x 10^{-6} A were obtained, which decreased to - 8.421 x 10^{-6} A for 0.18 ppb of diazinon added in (b), then decreasing to - 3.581 x 10^{-6} A for 0.51 ppb of diazinon added in (c), finally decreasing to - 1.673 x 10^{-6} A for the highest concentration of 1.19 ppb of diazinon added in (d). These responses were in accordance with the CV results obtained.

In Figure 5.10 the differential pulse voltammetric (DPV) results for the successive diazinon pesticide addition to the Au/MBT/POMA-PSSA/AChE biosensor in 0.1 M phosphate buffer, KCl (pH 7.2) solution is shown.
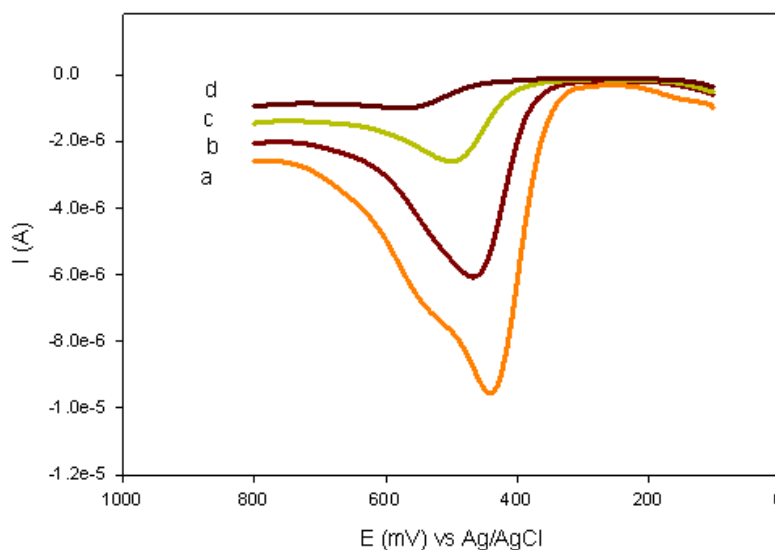
Figure5. 10   **DPV response for successive diazinon pesticide additions to the Au/MBT/POMA-PSSA/AChE biosensor in 0.1 M phosphate buffer, KCl (pH 7.2) solution, with the potential scanned between + 100 and + 800 mV at a scan rate of 10 mV.s^{-1}.**

The DPV results shown in Figure 5.10 shows the same trend observed in the SWV results, with the anodic current decreasing as the diazinon pesticide concentration was increased. For the addition of 1.1 mM of ACh substrate in (a), an anodic peak current of - 9.544 x 10^{-6} A were obtained, which decreased to - 6.069 x 10^{-6} A for 0.18 ppb of diazinon added in (b), then decreasing to - 2.603 x 10^{-6} A for 0.51 ppb of diazinon added in (c), finally decreasing to - 1.006 x 10^{-6} A for the highest concentration of 1.19 ppb of diazinon added in (d). The DPV results showed anodic currents that correlate well with that obtained for the SWV results.

In Figure 5.11 a calibration curve of current versus diazinon concentration is shown that was used for studying the Michaelis-Menten behaviour of the biosensor in the presence of the organophosphate inhibitor.
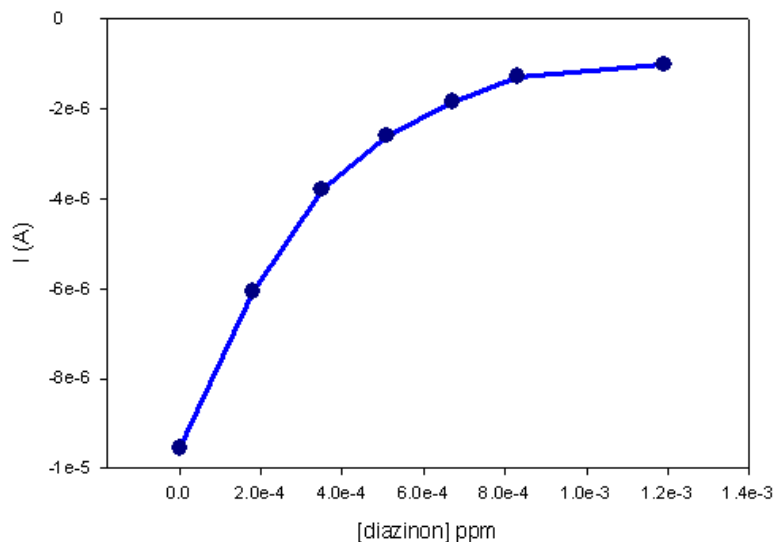
Figure 5.11   **Calibration curve of current vs. pesticide concentration for the successive addition of diazinon as pesticide to the Au/MBT/POMA-PSSA/AChE biosensor in 0.1 M phosphate buffer, KCl (pH 7.2) solution.**

From the shape of the curve in Figure 5.11 it can be seen that as the diazinon concentrations were increased, gradual decrease in peak current response was observed, with the current starting to limit off as the diazinon concentration neared saturation. This is a clear indication that the kinetics of the immobilised enzyme for the enzyme-inhibitor reaction display Michaelis-Menten plot characteristics. The Michaelis-Menten constant for the inhibitor (K_m^{Inhib}) was calculated and found to be 0.105 ppb, and the maximum current, I_{max}, was 1.101 x 10^{-6} A.

In the next step either the SWV or DPV results were used to calculate the percentage inhibition using the formula (Albareda-Sirvent *et al.* 2000:137; Sotiropoulou and Chaniotakis 2005:199; Wilkins *et al.* 2000:786):

$$I\% = \frac{(I_1 - I_2)}{I_1} X\ 100,$$ Eqn. 5.1

where $I\%$ is the degree of inhibition, I_1 is the current obtained after the addition of ACh substrate, and I_2 is the current obtained after pesticide addition to the biosensor.
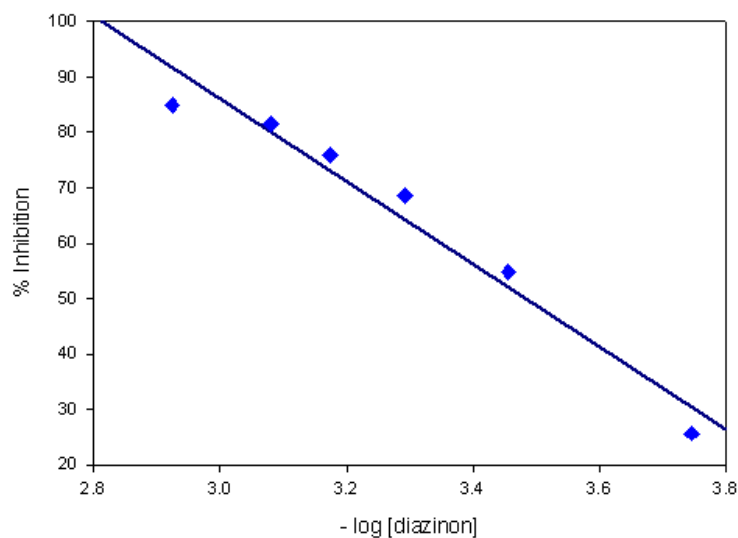
Figure 5.12   **Inhibition plot of Au/MBT/POMA-PSSA/AChE biosensor by diazinon inhibitor in 0.1 M phosphate buffer, KCl (pH 7.2) solution, after the addition of 1.1 mM of ACh as substrate.**

By plotting the percentage inhibition of the enzyme activity against the natural logarithm of pesticide concentration as shown in Figure 5.12, the results allowed us to determine the theoretical detection limit for the specific pesticide involved. The detection limit for diazinon was calculated to be 0.069 ppb. Figure 5.12 also shows that as the concentration of diazinon was increased, substantial inhibition of the biosensor was observed of between 82 to 85%.

5.3.4   Carbofuran detection with the Au/MBT/POMA-PSSA/AChE/ACh biosensor

The Au/MBT/POMA-PSSA/AChE biosensor was next applied in the detection of the carbamate pesticide called carbofuran. In Figure 5.13 the differential pulse voltammetric (DPV) results for the successive carbofuran pesticide addition to the Au/MBT/POMA-PSSA/AChE biosensor in 0.1 M phosphate buffer, KCl (pH 7.2) solution is shown. The carbofuran pesticide concentrations used are 0.18 ppb in (b), 0.51 ppb in (c) and 1.19 ppb in (d), whereas in (a) the highest concentration of 1.1 mM of the substrate ACh was added. The potential was scanned between + 100 and + 1000 mV, although the results are shown in a smaller potential window in order to show the trend observed more clearly.
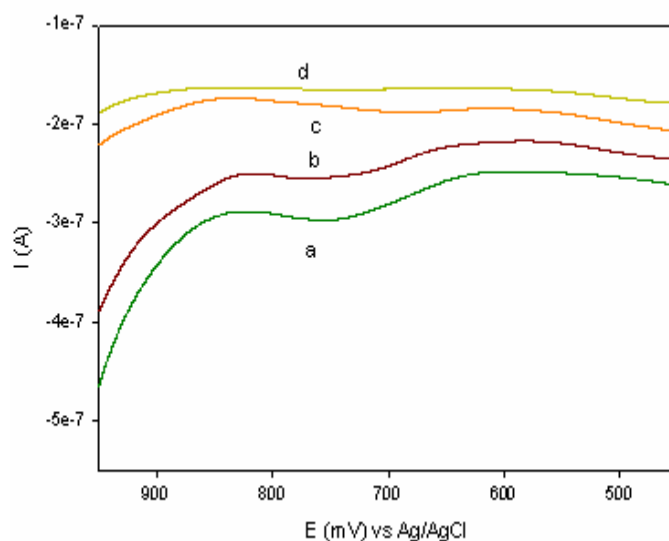
Figure5. 13   **DPV response for successive carbofuran pesticide additions to the Au/MBT/POMA-PSSA/AChE biosensor in 0.1 M phosphate buffer, KCl (pH 7.2) solution, with the potential scanned between + 100 and + 800 mV at a scan rate of 10 mV.s^{-1}.**

The DPV results shown in Figure 5.13 shows that the anodic current is decreasing as the carbofuran pesticide concentration was increased. For the addition of 1.1 mM of ACh substrate in (a), an anodic peak current of - 2.979 x 10^{-7} A were obtained, which decreased to - 2.547 x 10^{-7} A for 0.18 ppb of carbofuran added in (b), then decreasing to - 1.880 x 10^{-7} A for 0.51 ppb of carbofuran added in (c), finally decreasing to - 1.655 x 10^{-7} A for the highest concentration of 1.19 ppb of carbofuran added in (d).

In Figure 5.14 a calibration curve of current versus carbofuran concentration is shown that was used for studying the Michaelis-Menten behaviour of the biosensor in the presence of the carbamate inhibitor.
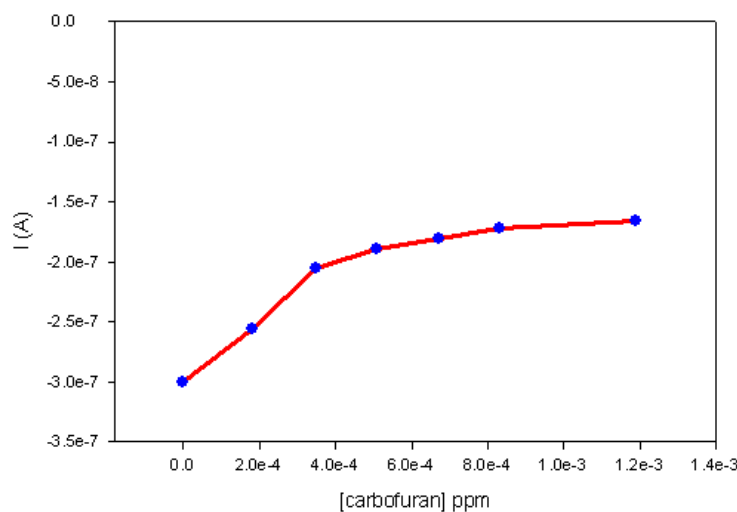
Figure 5.14   **Calibration curve of current vs. pesticide concentration for the successive addition of carbofuran as pesticide to the Au/MBT/POMA-PSSA/AChE biosensor in 0.1 M phosphate buffer, KCl (pH 7.2) solution.**

Similar enzyme-inhibitor reaction kinetics was observed in Figure 5.14 as was seen for diazinon as pesticide. From the shape of the curve in Figure 5.14 it can be seen that as the carbofuran concentrations was increased, gradual increase in peak current response was observed, with the current starting to limit off as the carbofuran concentration neared saturation. Again, it was a clear indication that the kinetics of the immobilised enzyme for the enzyme-inhibitor reaction display Michaelis-Menten plot characteristics. The Michaelis-Menten constant for the inhibitor (K_m^{Inhib}) was calculated and found to be 0.557 ppb, and the maximum current, I_{max}, was 1.501 x 10^{-7} A.

Similarly, a plot of the percentage inhibition of the enzyme activity against the natural logarithm of pesticide concentration as shown in Figure 5.15 was plotted for carbofuran as pesticide.
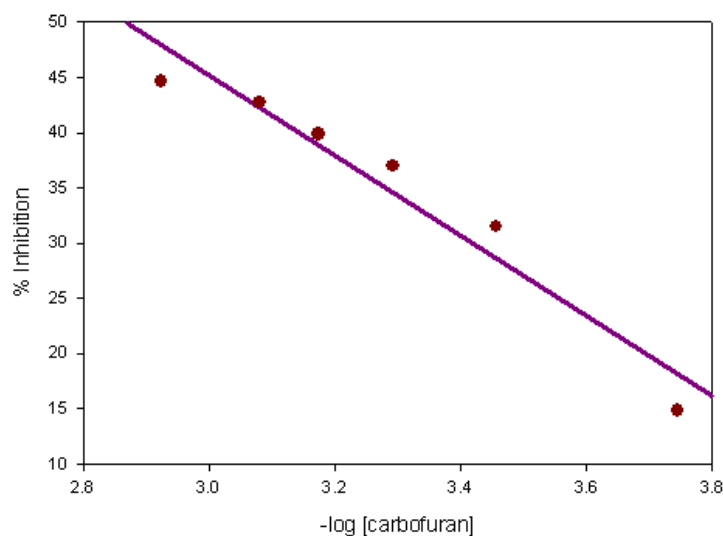
Figure 5.15   **Inhibition plot of Au/MBT/POMA-PSSA/AChE biosensor by diazinon inhibitor in 0.1 M phosphate buffer, KCl (pH 7.2) solution, after the addition of 1.1 mM of ACh as substrate.**

The results in Figure 5.15 allowed us to determine the theoretical detection limit for the specific pesticide involved. The detection limit for carbofuran was calculated to be 0.057 ppb. Figure 5.15 also shows that as the concentration of carbofuran was increased, lower inhibition of the biosensor as compared to that of diazinon was observed and found to be approximately 45%. From the percentage inhibition plot results in Figures 5.12 and 5.15 it was observed that for the same pesticide

concentrations, the enzyme is slightly more inhibited by diazinon than by carbofuran for the whole concentration range, also showing that the biosensor is less sensitive to carbofuran. The results of Albareda-Sirvent *et al.* (2005:41) for carbofuran obtained with a graphite-paste thick-film amperometric biosensor were compared to that of carbofuran detected in this study. It was found that Albareda-Sirvent et al. (2005:41) obtained a lower detection limit of 0.047 ppb, as compared to the detection limit of 0.057 ppb obtained in this study.

5.4   Application of AChE-Poly(2,5-dimethoxyaniline) 0.1 M Phosphate buffer (pH = 7.2) Saline Solution

5.4.1   Successive acetylcholine (ACh) substrate addition to Au/MBT/PDMA-PSSA/AChE sensor

The cyclic voltammograms (CVs) for the successive addition of ACh substrate to the biosensor under anaerobic conditions are shown in Figure 5.16. In the cyclic voltammetric study it was observed that the oxidative current of the cyclic voltammograms are increasing as the ACh concentration was increased from 0.0 mM to 1.1 mM in phosphate buffer, KCl (0.1 M, pH 7.2) solution.
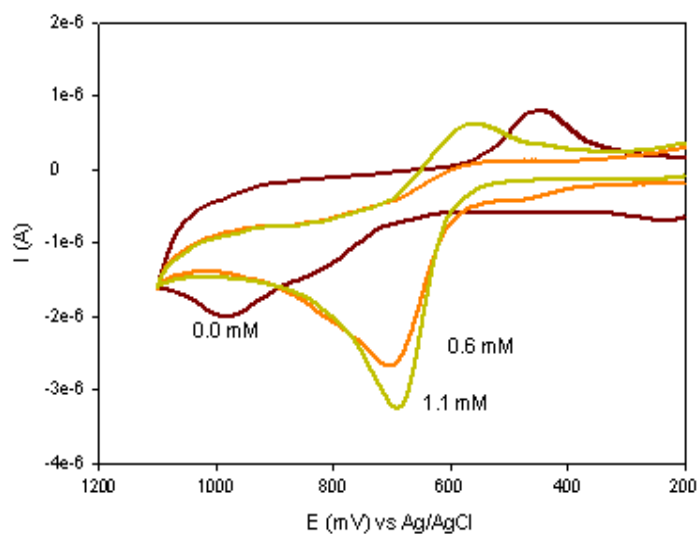
Figure 5.16 **CV response of successive ACh substrate additions to Au/MBT/PDMA-PSSA/AChE biosensor in 0.1 M phosphate buffer, KCl (pH 7.2) solution, with the potential scanned between - 200 to + 1100 mV at a scan rate of 5 mV.s^{-1}.**

A clear increase in oxidative current is observed in Figure 5.16 as the ACh concentration was increased from 0.0 mM to 0.6 mM and further to 1.1 mM, while a shift in potential is also evident. For the CV responses the anodic current increased from - 1.999 x 10^{-6} A (for 0.0 mM of ACh added), to - 2.668 x 10^{-6} A (for 0.6 mM of ACh added) and further to - 3.249 x 10^{-6} A (for 1.1 mM of ACh added). The results therefore indicate that the ACh is hydrolysed by AChE, thus indicating that a functioning biosensor has been developed.

To verify the CV responses obtained for the successive addition of acetylcholine to the Au/MBT/PDMA-PSSA/AChE biosensor, square wave voltammetric results were also obtained for each addition. The results for the square

wave voltammograms (SWVs) for successive ACh addition to the biosensor measured at 5 Hz are shown in Figure 5.17. These SWVs were recorded under anaerobic conditions and the net (difference between forward and reverse currents) SWV responses were obtained.
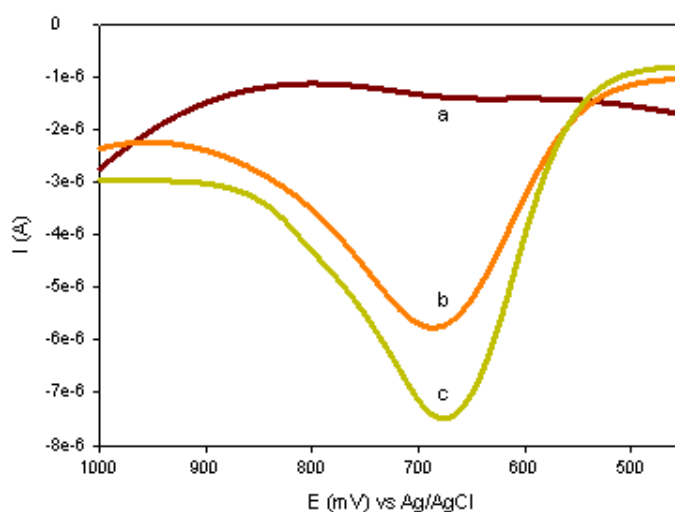
Figure 5.17   Square wave voltammograms (SWVs) for successive acetylcholine (ACh) substrate additions to the Au/MBT/PDMA-PSSA/AChE sensor in 0.1 M phosphate buffer, KCl (pH 7.2), with the potential scanned between - 200 to + 1100 mV at a frequency of 5 Hz.

The SWV responses are also increasing when it was scanned oxidatively (anodic wave), showing a similar trend as the one observed for the CV responses with increasing ACh addition. At 0.0 mM ACh in (a) the anodic current was - 1.422 x 10^{-6} A, which increased to - 5.759 x 10^{-6} A at 0.6 mM ACh in (b), while the anodic current finally increased to - 7.479 x 10^{-6} A at 1.1 mM ACh in (c). Since the

Au/MBT/PDMA-PSSA/AChE biosensor was now functioning properly, it was ready to be used for the pesticide detection.

5.4.2 Detection of an organophosphorus and carbamate pesticides

As indicated earlier, when the serine hydroxyl group of AChE has reacted with the phosphor atom of an organophosphorous inhibitor, or with the carbonyl group of a carbamate inhibitor, the serine hydroxyl group of the enzyme is left inactive since the hydroxyl group is no longer available to attack the acetylcholine substrate. This results in a diminished or reduced signal which is detected by the amperometric biosensor device (Simon *et al.* 1999:27740; Pond and Coyne 1996:363).

The next step in the biosensor evaluation was to determine whether the same inhibiting effect that was observed with the Au/MBT/POMA-PSSA/AChE biosensor, can be observed when PDMA was used as the conducting polymer in the Au/MBT/PDMA-PSSA/AChE biosensor. The results obtained in the evaluation of the latter biosensor are discussed in the following paragraphs.

5.4.3 Diazinon detection with the Au/MBT/PDMA-PSSA/AChE biosensor

The constructed Au/MBT/PDMA-PSSA/AChE biosensor with poly(*2,5-*dimethoxyaniline) as polymer was also tested and evaluated for the detection of diazinon and carbofuran as pesticides. In Figure 5.18 the anodic difference square wave voltammetric (SWV) results for the successive diazinon pesticide addition to the Au/MBT/PDMA-PSSA/AChE/ACh biosensor in 0.1 M phosphate buffer, KCl (pH 7.2) solution is shown.
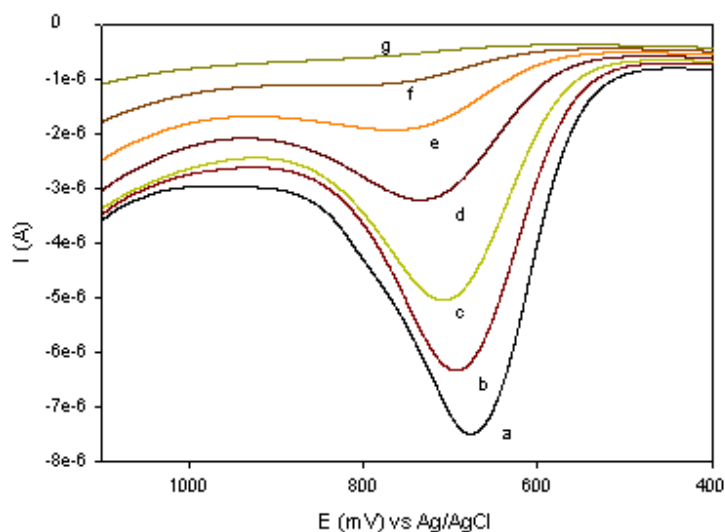
Figure 5.18   Square wave voltammetric (SWV) results for successive diazinon pesticide additions to the Au/MBT/PDMA-PSSA/AChE biosensor in 0.1 M phosphate buffer, KCl (pH 7.2) solution, with the potential scanned between + 400 to +1100 mV at a frequency of 5 Hz.

The results in Figure 5.18 show the addition of 1.1 mM of ACh substrate in (a), while a shift in anodic current is observed after the addition of diazinon pesticide concentrations of 0.18 ppb in (b), 0.35 ppb in (c), 0.51 ppb in (d), 0.67 ppb in (e), 0.83 ppb in (f) and 1.19 ppb in (g).

When 1.1 mM of ACh was added to the biosensor, the anodic current has increased to - 7.479 x 10^{-6} A for the first anodic peak observed in (a). The anodic current next decreased to - 6.324 x 10^{-6} A in (b), then to - 5.041 x 10^{-6} A in (c), then to - 3.215 x 10^{-6} A in (d), then to - 1.931 x 10^{-6} A in (e), then to - 1.113 x 10^{-6} A in (f), and finally to - 6.196 x 10^{-7} A in (g) for the highest concentration of diazinon added. The decreasing shift in anodic current shown in the SWV results can thus be attributed to the inhibition of the AChE enzyme by carbofuran as pesticide.

In Figure 5.19 a calibration curve of current versus diazinon concentration is shown that was used for studying the Michaelis-Menten behaviour of the biosensor in the presence of the organophosphate inhibitor.
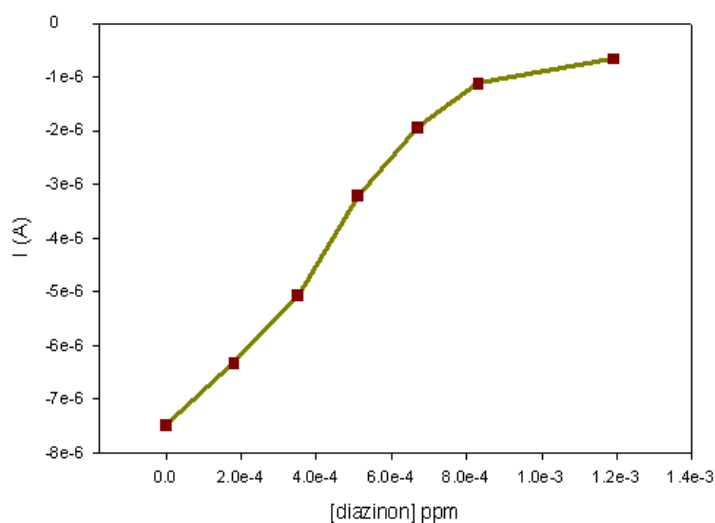
Figure 5.19   **Calibration curve of current vs. pesticide concentration for the successive addition of diazinon as pesticide to the Au/MBT/PDMA-PSSA/AChE biosensor in 0.1 M phosphate buffer, KCl (pH 7.2) solution.**

Since the enzyme AChE was immobilised in PDMA as polymer for this biosensor, a calibration curve of current vs. pesticide concentration was also used to study the kinetic behaviour of the enzyme in the presence of the inhibitor. From the shape of the curve in Figure 5.19 it can be seen that as the diazinon concentrations was increased, gradual increase in peak current response was observed, with the current starting to limit off as the diazinon concentration neared saturation. This is a clear indication that the kinetics of the immobilised enzyme for the enzyme-inhibitor reaction display Michaelis-Menten plot characteristics. The Michaelis-Menten constant for the inhibitor (K_m^{Inhib}) was calculated and found to be 0.067 ppb, and the maximum current, I_{max}, was 6.50×10^{-7} A.

Next the SWV results were used to calculate the percentage inhibition using the formula in equation 5.1 (Albareda-Sirvent *et al.* 2000:137; Sotiropoulou and Chaniotakis 2005:199; Wilkins *et al.* 2000:786):

$$I\% = \frac{(I_1 - I_2)}{I_1} X \ 100,$$
                                                                        Eqn. 5.1

where $I\%$ is the degree of inhibition, I_1 is the current obtained after the addition of ACh substrate, and I_2 is the current obtained after pesticide addition to the biosensor.

As the diazinon pesticide concentration was increased an increase in the percentage inhibition detected by the biosensor was observed. The obtained results have further indicated that when the enzyme membrane was exposed to diazinon concentrations of 1.19 ppb, substantial inhibition of 94% of the enzyme was observed.
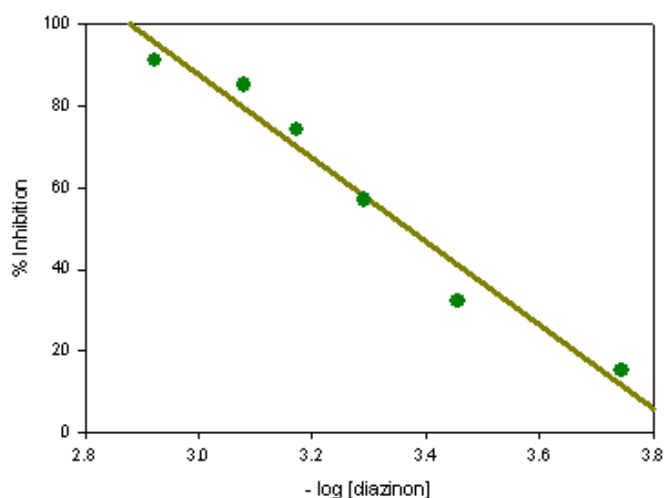
Figure 5.20   **Inhibition plot of Au/MBT/PDMA-PSSA/AChE biosensor by diazinon inhibitor in 0.1 M phosphate buffer, KCl (pH 7.2) solution, after the addition of 1.1 mM of ACh as substrate.**

By plotting the percentage inhibition of the enzyme activity against the natural logarithm of pesticide concentration as shown in Figure 5.20, the results allowed us to determine the theoretical detection limit for the specific pesticide involved. The detection limit for diazinon was calculated to be 0.138 ppb.

5.4.4 Carbofuran detection with the Au/MBT/PDMA-PSSA/AChE biosensor

The carbamate pesticide called carbofuran was next evaluated with the Au/MBT/PDMA-PSSA/AChE biosensor. In Figure 5.21 the differential pulse voltammetric (DPV) results for the successive carbofuran pesticide addition to the

Au/MBT/PDMA-PSSA/AChE biosensor in 0.1 M phosphate buffer, KCl (pH 7.2) solution is shown. The potential was scanned between - 200 and + 1100 mV, although the results are shown in a smaller potential window in order to show the trend observed more clearly.
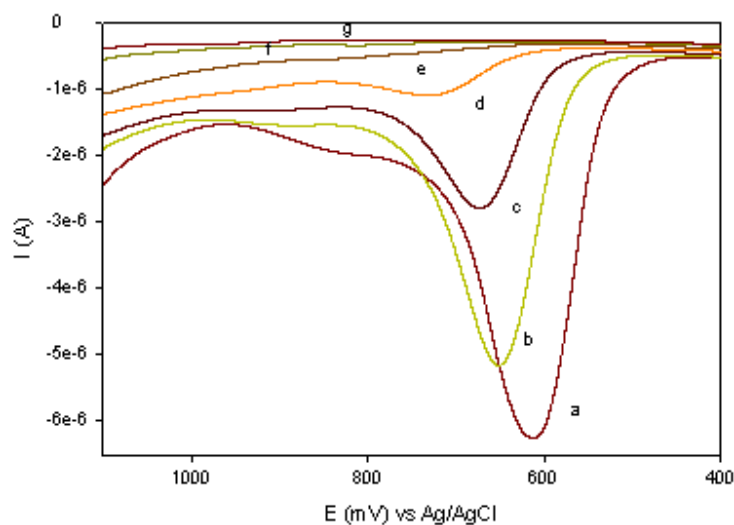
Figure 5.21   **Differential pulse voltammetric (DPV) results for successive carbofuran pesticide additions to the Au/MBT/PDMA-PSSA/AChE/ACh biosensor in 0.1 M phosphate buffer, KCl (pH 7.2) solution, with the potential scanned between - 200 to + 1100 mV at a scan rate of 10 mV.s^{-1}.**

The results in Figure 5.21 display the results for the addition of 1.1 mM of ACh substrate in (a), while a shift in anodic current is observed after the addition of carbofuran pesticide concentrations from 0.18 ppb in (b), 0.35 ppb in (c), 0.51 ppb in (d), 0.67 ppb in (e), 0.83 ppb in (f) to 1.19 ppb in (g).

When 1.1 mM of ACh was added to the biosensor, the anodic current has increased to - 6.254 x 10^{-6} A for the first anodic peak observed in (a). The anodic current next decreased to - 5.173 x 10^{-6} A in (b), then to - 2.798 x 10^{-6} A in (c), then to - 1.108 x 10^{-6} A in (d), then to - 5.690 x 10^{-7} A in (e), then to - 3.554 x 10^{-7} A in (f), and finally to - 3.442 x 10^{-7} A in (g) for the highest concentration of carbofuran added. This shift in anodic current shown in the DPV results can again be attributed to the inhibition of the AChE enzyme by the carbofuran pesticide.

In Figure 5.22 a calibration curve of current versus carbofuran concentration is shown that was used for studying the Michaelis-Menten behaviour of the biosensor in the presence of the organophosphate inhibitor.
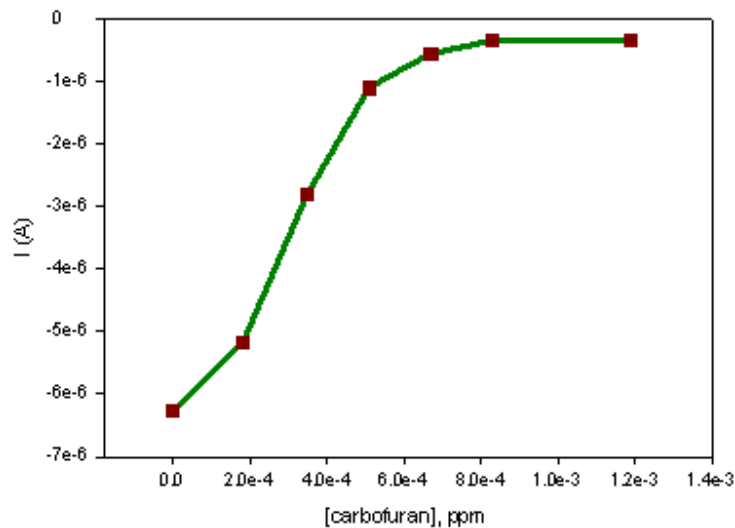
Figure 5.22   **Calibration curve of current vs. pesticide concentration for the successive addition of carbofuran as pesticide to the Au/MBT/PDMA-PSSA/AChE biosensor in 0.1 M phosphate buffer, KCl (pH 7.2) solution.**

From the shape of the curve in Figure 5.22 it can be seen that as the carbofuran concentrations was increased, gradual increase in peak current response was observed, with the current limiting off as the carbofuran concentration reached saturation. This was a clear indication that the kinetics of the immobilised enzyme for the enzyme-inhibitor reaction display Michaelis-Menten plot characteristics. The Michaelis-Menten constant for the inhibitor (K_m^{Inhib}) was calculated and found to be 0.027 ppb, and the maximum current, I_{max}, was $3.350 \ x \ 10^{-7}$ A.

As the Carbofuran pesticide concentration was increased an increase in the percentage inhibition detected by the biosensor was observed. The obtained results in Figure 5.23 have further indicated that when the enzyme membrane was exposed to carbofuran concentrations of 1.19 ppb, substantial inhibition of 95% of the enzyme was observed.
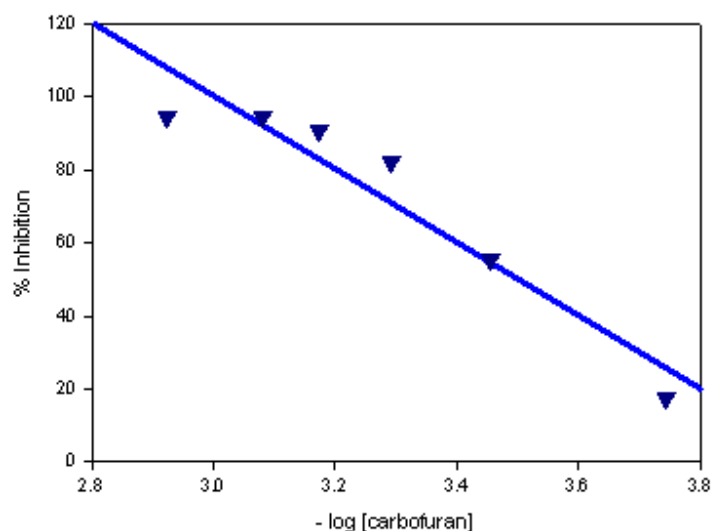
Figure 5.23   **Inhibition plot of Au/MBT/PDMA-PSSA/AChE biosensor by carbofuran inhibitor in 0.1 M phosphate buffer, KCl (pH 7.2) solution, after the addition of 1.1 mM of ACh as substrate.**

The results in Figure 5.23 allowed us to determine the theoretical detection limit for the specific pesticide involved. The detection limit for carbofuran was calculated to be 0.110 ppb. Figure 5.23 also shows that as the concentration of carbofuran was increased, a similar level of inhibition of the biosensor as compared to that of diazinon was observed and found to be approximately 95%. From the percentage inhibition plot results in Figures 5.20 and 5.23 it was observed that at high pesticide concentrations, the enzyme is inhibited to relatively the same degree by diazinon and carbofuran, when PDMA was used as polymer matrix for enzyme immobilisation.

The results for the different kinetic parameters of the Au/MBT/POMA-PSSA/AChE and Au/MBT/PDMA-PSSA/AChE biosensors interaction with diazinon

and carbofuran as pesticides was compared and shown in Table 5.1, while the results were also compared to that obtained for another biosensor applied to the similar classes of pesticides.

Table 5.1   **Summary and comparison of kinetic parameters calculated for the Au/MBT/POMA-PSSA/AChE and Au/MBT/PDMA-PSSA/AChE biosensors interaction with diazinon and carbofuran as pesticides.**

Technique	Pesticide	Michaelis-Menten constant for inhibitor (K_m^{Inhib}) (ppb)	% Inhibition	Detection limit (ppb)
POMA-PSSA polymer	diazinon	0.105	85	0.069
PDMA-PSSA polymer	diazinon	0.067	94	0.138
[¥]Graphite-epoxy composite	paraoxon	*n.d.*	67	0.165
POMA-PSSA polymer	carbofuran	0.557	50	0.057
PDMA-PSSA	carbofuran	0.027	95	0.110
[¥]Graphite-epoxy composite	carbofuran	*n.d.*	68	0.047
n.d. = not determined				

From the results in Table 5.1 it can be seen that the highest degree of inhibition was obtained for the PDMA-PSSA polymer film when diazinon as pesticide was

---

[¥] Albareda-Sirvent *et al*. (2001). Analytica Cimica Acta, 442: 35-44.

evaluated, while the lowest degree of inhibition was obtained for the graphite-epoxy composite with a similar class of pesticide. On the other hand the lowest detection limit was obtained with the POMA-PSSA polymer film.

When carbofuran as pesticide was evaluated, the highest degree of inhibition was obtained with the PDMA-PSSA polymer film, while the lowest degree of inhibition was obtained for the POMA-PSSA polymer film. When the detection limits are compared, the lowest value was obtained for the graphite-epoxy composite.

The Au/MBT/POMA-PSSA/AChE and Au/MBT/PDMA-PSSA/AChE biosensors were not evaluated to determine the long-term and temperature stability of the individual thick-film biosensors, since solubility problems were encountered as the polymer films fell off the transducer surface.

CHAPTER 6

Application of an Acetylcholinesterase-Polyaniline Biosensor for the Determination of a Series of Organophosphate and Carbamate Pesticide Compounds in Aqueous Organic Solvent Solutions

6.1   Introduction

This chapter focuses on the results obtained for the application of the Acetylcholinesterase-Polyaniline (AChE-PANI) biosensor that were constructed to determine and investigate the determination of certain organophosphate and carbamate pesticide compounds in selected aqueous organic solvent solutions.

Initially the AChE-Poly(*o*-methoxyaniline) and AChE-Poly(*2,5*-dimethoxyaniline) biosensors that were constructed, were used to determine selected organophosphate and carbamate pesticide compounds in aqueous organic solvent solutions. However, several difficulties were encountered with these biosensors since the polymer film containing the AChE enzyme fell of the transducer surface when the biosensors were applied in the aqueous organic solvent solutions. This was attributed to the increased solubility of the substituted polyanilines (e.g. POMA and PDMA) as compared to the unsubstituted PANI.

The Au/MBT/PANI/AChE/PVAc electrocatalytic biosensor device was constructed by encapsulating acetylcholinesterase (AChE) as enzyme in the PANI polymer composite, followed by the coating of poly(vinyl acetate) (PVAc) on top to secure the biosensor film from falling off. The voltammetric results (see section 6.3.1) have shown that the current shifts anodically as the Au/MBT/PANI/AChE/PVAc biosensor responded to successive acetylthiocholine (ATCh) substrate addition under anaerobic conditions in 0.1 M phosphate buffer, KCl (pH 7.2) solution.

One of the main aims of this research was the construction of a device that can be further developed into a sensor for pesticide monitoring on-site in the field. Wilkins *et al.* (2000:786) indicates that one of the most effective strategies in pollution control is to rapidly determine the source of the pollutant and the magnitude of its threat by using on-site measurement.

6.2   Design of an Au/MBT/PANI/AChE/PVAc biosensor for pesticide detection

In this work it is demonstrated that a gold disc electrode can be coated with a mercaptobenzothiazole (MBT) self-assembled monolayer (SAM) prior to polyaniline electropolymerisation, followed by AChE immobilisation and poly(vinyl acetate) coating in creating a thick film electrode for sensitive organophosphorous pesticide detection. The dual role of polyaniline, which shows electrocatalytic activity towards

thiocholine and serves as an immobilisation matrix for the AChE as an enzyme and that of poly(vinyl acetate) (PVAc) as a binder in this thick-film electrode is demonstrated.

Different technologies exist to develop thick-film biosensors for pesticide detection (Albareda-Sirvent *et al.* 2001:35; Joshi *et al.* 2005:54). Albareda-Sirvent *et al.* (2000:153) divide these different technologies into three categories of (i) multiple-layer deposition with biological deposition by hand or electrochemically, (ii) using screen-printing techniques of composite inks or pastes in two or more steps with biological deposition done by screen-printing, (iii) using a one-step deposition layer also called the biocomposite strategy. One of the main aims of this work was to develop an electrode which can be exposed to organic solutions containing potential inhibitors without having the polymer layer after separating from the electrode surface after use thereby using poly(vinyl acetate) as the binder to circumvent this problem. Cellulose acetate is known to be used as a synthetic resin in screen-printing inks to improve printing qualities or as a selective membrane over platinum anodes to reduce interferences (McGovern *et al.* 2005:657; Hart *et al.* 1999:7).

The detection of pesticides in non-aqueous environments has been reported but few publications refer to the use of immobilised AChE biosensors in non-aqueous media. Organophosphorous and carbamate pesticides are characterised by a low solubility in water and a higher solubility in organic solvents. It is for this fact that the extraction and concentration of pesticides from fruits, vegetables, etc. are carried out in organic solvents. It is known that some enzymes, e.g. glucose oxidase, work well in both water and organic solvents, while other enzymes require a minimum amount

of water to retain catalytic activity. To circumvent the problem of hydrophilic solvents stripping the enzymes of essential water of hydration necessary for enzymatic activity, it is recommended that 1 – 10% water be added to the organic solvent for sufficient hydration of the active site of the enzyme (Wilkins *et al.* 2000:786; Klibanov 2003:427; Andreescu *et al.* 2002:169; Palchetti *et al.* 1997:315; Iwuoha *et al.* 1995:661).

Polyaniline (PANI) was used as a mediator in this biosensor construction to harvest its dual role as immobilisation matrix for AChE and use its electrocatalytic activity towards thiocholine (TCh) for amperometric sensing. With that in mind, the following amperometric sensor design and mechanism is proposed and explained.
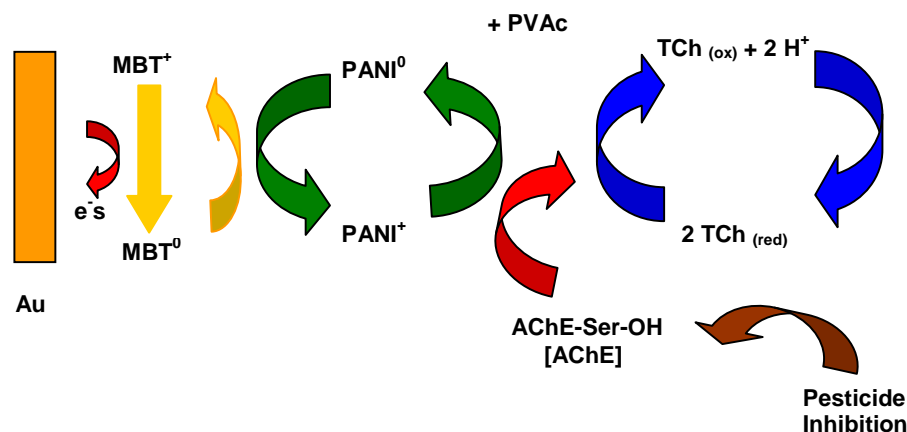
Figure 6.1   **The schematic representation of the Au/MBT/PANI/AChE/PVAc biosensor reaction occurring at the gold SAM modified electrode ([§]Somerset *et al.* 2007:300).**

[§] Biosensor reaction scheme published in Somerset *et al.* (2007). Journal of Environmental Science and Health Part B, 42:297-304.

In Figure 6.1 the schematic representation for the biosensor reaction taking place is presented. In Figure 6.1 it can be seen that as acetylthiocholine (ATCh) is catalysed by acetylcholinesterase (AChE), it forms thiocholine (TCh) and acetic acid. Thiocholine is electroactive and is oxidised in the reaction. In return the conducting PANI polymer reacts with thiocholine and also accepts an electron from mercaptobenzothiazole as it is oxidised through interaction with the gold electrode.

6.3   Evaluation of AChE-Polyaniline Biosensor in 0.1 M Phosphate buffer (pH 7.2) Saline Solution

6.3.1   Successive acetylthiocholine (ATCh) substrate addition to Au/MBT/PANI/AChE/PVAc biosensor

In Chapter 4, section 4.6.3.2, it was shown that a functioning biosensor was established with the addition of acetylthiocholine (ATCh) as substrate to the Au/MBT/PANI/AChE/PVAc biosensor. Some of those results are revisited here, since it is applicable to the biosensor mechanism explained here.

In Figure 6.2 the CV responses of the Au/MBT/PANI/AChE/PVAc biosensor to successive ATCh substrate additions under anaerobic conditions are shown. The first results were collected by applying sequential linear potential scan between - 400 to + 1800 mV (vs. Ag/AgCl), at a scan rate of 10 mV.s^{-1}. The CVs were performed at the scan rate of 10 mV.s^{-1}, to ensure that the fast enzyme kinetics could be

monitored. The three CVs for successive 0.01 M ATCh substrate additions to Au/MBT/PANI/AChE/PVAc biosensor in 2 ml of 0.1 M phosphate buffer, KCl (pH 7.2) solution are shown in Figure 6.2. When 0.0 mM of ATCh was added, the peak current (I_p) was observed at - 5.532 x 10^{-5} A, at 0.6 mM of ATCh added it was observed at - 7.459 x 10^{-5} A, while at 0.9 mM of ATCh added it was observed at - 7.981 x 10^{-5} A. A clear shift in peak current (I_p) was observed as the concentration of the substrate, ATCh, was increased indicating the electrocatalytic functioning of the biosensor. Figure 6.2 further illustrates that in increase in the reductive current is also observed, but the magnitude is smaller when compared to the increases in oxidative current. This clearly illustrates that the oxidative response of the biosensor to ATCh addition is preferred.
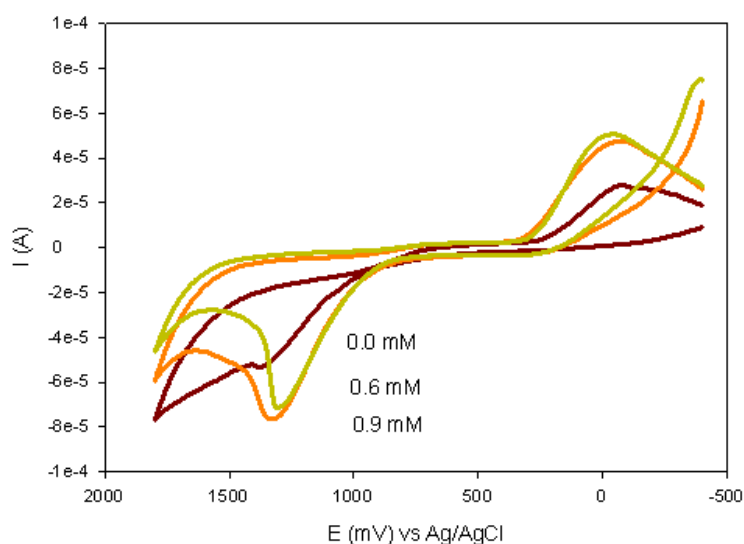
Figure 6.2   **CV response of successive ATCh substrate addition to Au/MBT/PANI/AChE/PVAc biosensor in 0.1 M phosphate buffer, KCl (pH 7.2) solution at a scan rate of 10 mV.s^{-1}.**

In the next step the DPV response of the Au/MBT/PANI/AChE/PVAc biosensor was monitored for the successive addition of ATCh substrate and a similar electrocatalytic response as the one observed for the CV results reported above, was obtained for the DPV results as shown in Figure 6.3.
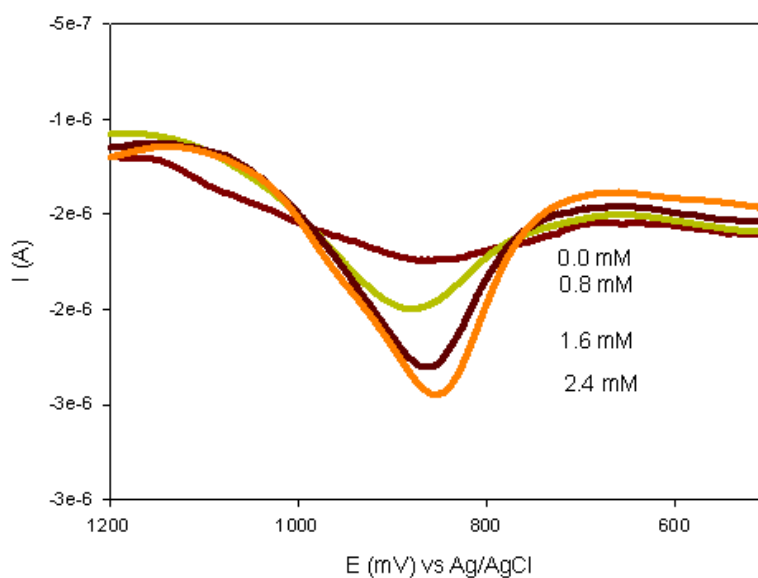
Figure 6.3   **DPV response of successive ATCh substrate addition to Au/MBT/PANI/AChE/PVAc biosensor in 0.1 M phosphate buffer, KCl (pH 7.2) solution at a scan rate of 10 mV.s^{-1}, and in a potential window of + 500 to + 1200 mV.**

The DPV results in Figure 6.3 are show in a shorter potential window to highlight the observed increase in anodic peak current. The results show the voltammetric responses for the electrocatalytic oxidation of acetylthiocholine at the

Au/MBT/PANI/AChE/PVAc biosensor. The DPV responses shows an increase in peak current heights upon the successive additions of ATCh as substrate, with the results more pronounced around a specific potentials as compared with those observed in the CV responses in Figure 6.2.

The peak current, $I_{\text{peak,}}$ for specific concentrations of the ATCh substrate added in Figure 6.3 was - 1.737 x 10^{-6} A for 0.0 mM of ATCh added, followed by - 1.992 x 10^{-6} A for 0.8 mM of ATCh, then - 2.314 x 10^{-6} A was obtained for 1.6 mM of ATCh added, while it was - 2.448 x 10^{-6} A for the highest concentration of 2.4 mM of ATCh added. These results clearly indicated that a biosensor was established and that AChE as enzyme was hydrolysing the substrate ATCh, with the increase in oxidative current as the preferred route of reaction.

6.4 Optimal Acetylcholinesterase (AChE) Enzyme Loading of Au/MBT/PANI/AChE/PVAc Biosensor

The amount of enzyme incorporated during the biosensor construction is an important element during construction and it affects the sensor's limit of detection. If the aim of the biosensor is to achieve the lowest possible detection, only a minimum amount of enzyme must be used (Sotiropoulou *et al.* 2005:201; Evtugyn *et al.* 1998:479; Bucur *et al.* 2004:217).

In Figure 6.4 the results for the amperometric response of the Au/MBT/PANI/AChE/PVAc biosensor to different amounts of the enzyme AChE incorporated into the biosensor is shown.
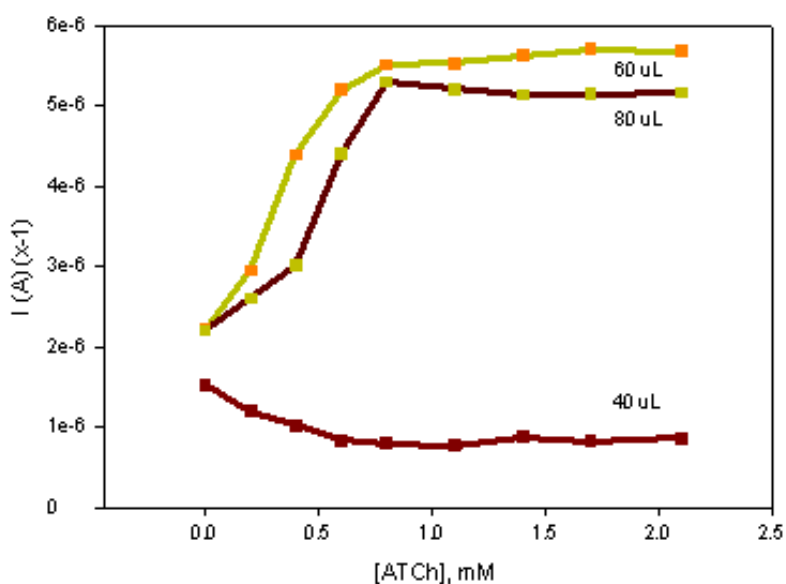
Figure 6.4   **The amperometric response of the AChE biosensor to different amounts of enzyme incorporated into the biosensor. These responses were measured in a 0.1 M phosphate buffer, KCl (pH 7.2) solution at 25 °C.**

Since the enzyme AChE was incorporated into the PANI polymer matrix by adsorption at fixed potential, different amounts of the enzyme was dissolved in a 1 ml of 0.1 M phosphate buffer (pH 7.2) solution. From the results in Figure 6.4 it can be seen that the biggest increase in current for the successive addition of ATCh substrate, was experienced when the biosensor had 60 µL of AChE dissolved in 1 ml

of 0.1 M phosphate buffer (pH 7.2) solution. The results obtained when 80 µL of AChE was used, does not show a very big difference in the current response when compared to the use of 60 µL of AChE. In both these cases it is observed that the biosensor response to ATCh substrate addition starts to level off after 1.0 mM of the substrate has been added. When the results for the use of 60 and 80 µL of AChE is compared to that of the 40 µL of AChE, a big difference in the amperometric response was observed, with the current increasing in several magnitudes. When a small amount of enzyme is incorporated into the biosensor, a very small response in anodic current was thus observed. Therefore, optimal enzyme loading is important and should be optimised as it has an effect on the detection limit of the constructed biosensor.

6.5   pH effect on the Immobilised AChE in Au/MBT/PANI/AChE/PVAc Biosensor

The pH value of the working solution is usually regarded as the most important factor in determining the performance of a biosensor and its sensitivity towards inhibitors. It is thus a rule that the pH maximum of the enzyme activity is evaluated as most appropriate for the substrate and inhibitor determination. And there is agreement that the pH-dependence of the observed inhibiting effect often corresponds to that of the response of a biosensor (Evtugyn *et al.* 1998:475-476; Yang *et al.* 2005:205).

It is for this reason that the operation of the biosensor was evaluated at different pH values. Other researchers (Palchetti *et al.* l997:315; Hart *et al.* 1997:645; Cagnini *et al.* 1995:85) have shown that the optimal working pH for the cholinesterases is near 7.5 but it depends on the polymer matrix used for enzyme immobilisation, although working pH values between 8 and 9 have also been reported (Albareda-Sirvent *et al.* 2001:38).

In Figure 6.5 the results for the investigation into the effect of different pH values on the working of the Au/MBT/PANI/AChE/PVAc biosensor is displayed.
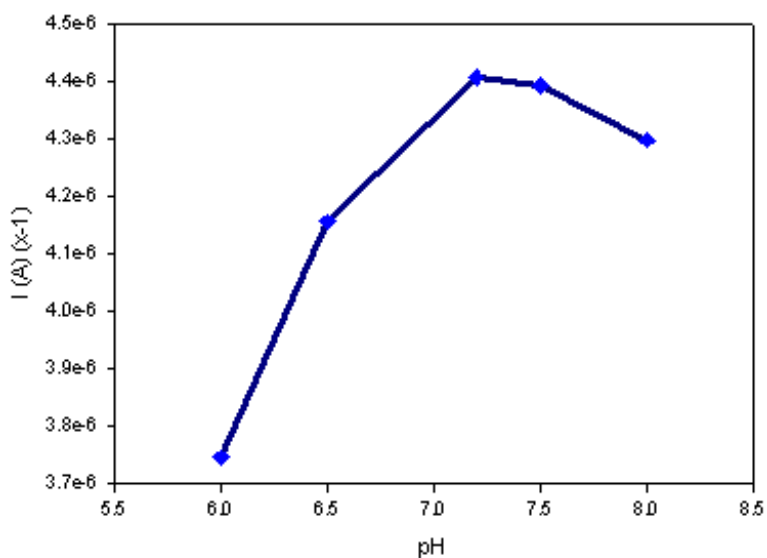
Figure 6.5   **Graph displaying the effect of pH on the Au/MBT/PANI/AChE/PVAc biosensor in 0.1 M phosphate buffer, KCl (pH 7.2) solution with 2 mM of ATCh added.**

The Au/MBT/PANI/AChE/PVAc biosensor was evaluated at pH values of 6.0; 6.5; 7.2; 7.5 and 8.0 in a 2 ml of 0.1 M phosphate buffer (pH 7.2) solution, to which a total of 2 mM of ATCh substrate was added. The results obtained are shown in Figure 6.5 indicating that the highest anodic current was obtained at pH = 7.2, while the result for pH = 7.5 is nor far off. The response profile thus indicate that an optimum pH can be obtained between 7.0 and 7.5, which falls within the range reported in literature (Sen *et al.* 2004:1265; Arkhypova *et al.* 2003:1047) for the optimum pH of the free enzyme activity in solution. The results further illustrates that enzyme incorporated in the Au/MBT/PANI/AChE/PVAc biosensor, was easily accessed by the buffer solution and the acetylthiocholine used as substrate in the buffer solution.

6.6   Long-term Stability Determination of Au/MBT/PANI/AChE/PVAc Biosensor

The Au/MBT/PANI/AChE/PVAc biosensor that was prepared under optimum conditions was tested at 25 ℃ to determine the long-term stability of the biosensor. The biosensor was stored at 4 ℃ for a length of approximately 30 days and the biosensor was tested every 7 days by adding the substrate ATCh to a 2 ml of 0.1 M phosphate buffer, KCl (pH 7.2) solution, containing the biosensor, and measuring the current at every addition. The results obtained for the successive addition of the substrate to the biosensor on 0, 7, 14, 21 and 28 days are displayed in Figure 6.6.
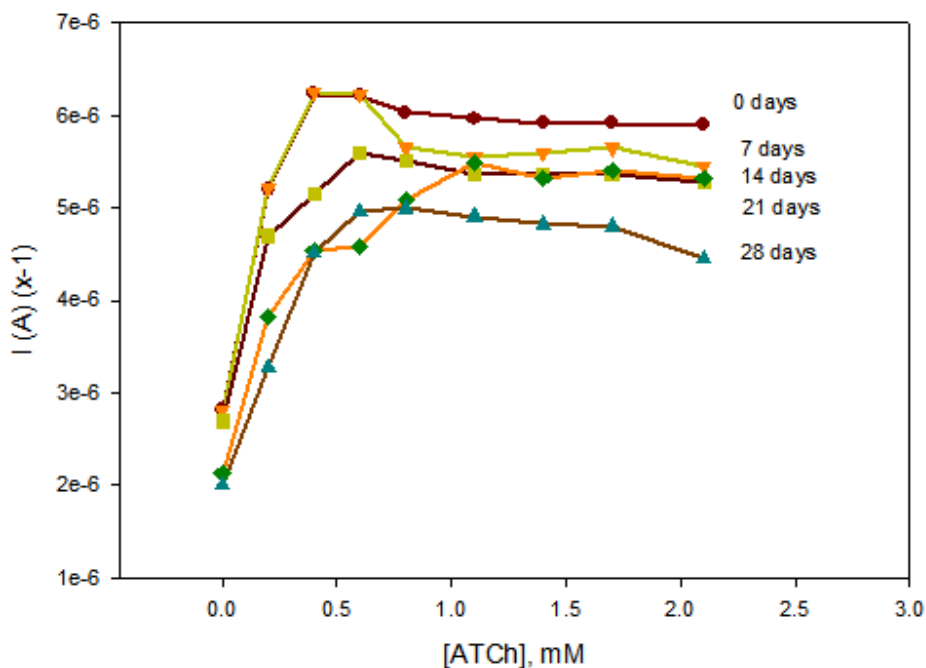
Figure 6.6   **Graph displaying the results for the long-term stability of the Au/MBT/PANI/AChE/PVAc biosensor in 0.1 M phosphate buffer, KCl (pH 7.2) solution at 25 ºC, for successive additions of the ATCh substrate.**

From the results in Figure 6.6 it can be seen that the biosensor responses reach a maximum current within the first 0.4 to 1.1 mM of substrate added to the biosensor. After 1.1 mM of substrate added it reaches a plateau and minimum changes in the current is observed. The results further indicate a gradual decrease in the first 21 days, with a bigger difference in current observed on the 28th day of biosensor response measured. On the first day of analysis, the maximum current (I_{max}) for the biosensor was measured at - 6.234 x 10^{-6} A, while on the 28th day after construction

the biosensor response at I_{max} was - 4.957 x 10^{-6} A. The difference in current response on the 28th day was 20% of the initial value. In the work done by Sen *et al.* (2004:1261) a polyvinylferrocenium modified Pt electrode was constructed and the amperometric response of the biosensor to choline and acetylcholinesterase was measured, indicating that the enzyme electrode responses gradually decreased in the first 25 days.

During the long-term stability studies of the Au/MBT/PANI/AChE/PVAc biosensor, a total of four measurements were made with the biosensor on a specific day to determine any variation in the readings obtained. This was further done to determine the operational stability of the biosensor during the long-term stability testing. The results obtained for the maximum current (I_{max}) of the four readings taken on a specific day, are displayed in Figure 6.7.
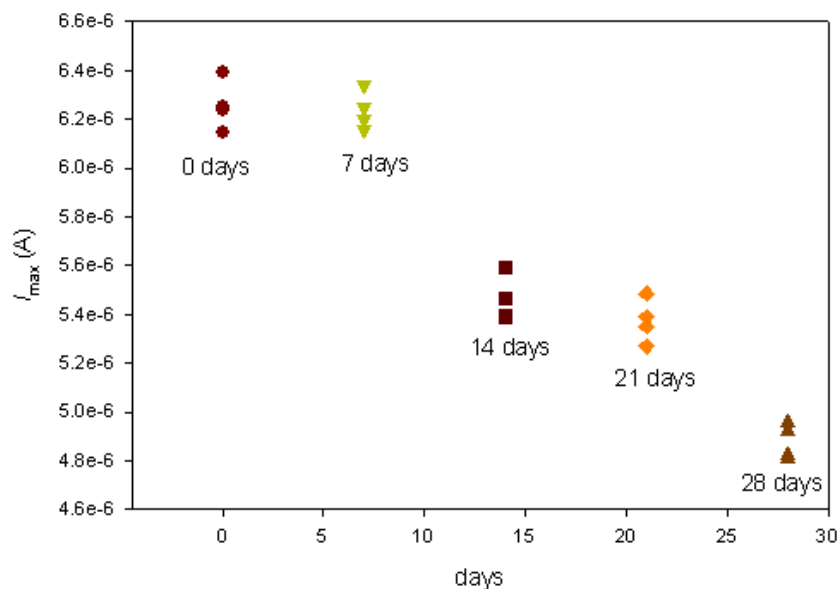
Figure 6.7 **Graph of variation in maximum current (I_{max}) vs. days in long-term stability determination ($n = 4$) of the Au/MBT/PANI/AChE/PVAc biosensor in 0.1 M phosphate buffer, KCl (pH 7.2) solution at 25 ºC, for 2.0 mM of ATCh added.**

The results shown in Figure 6.7 indicate firstly that there were some variation in the readings obtained on a specific day, but the deviation is relatively small indicating that the biosensor was stable during the period of investigation. The results in the graph also shows that during the first 7 days of construction, the values of I_{max} obtained are relatively close at the same maximum current, while there is a drop in the current at day 14, which on the other hand was relatively close to the maximum current obtained after 21 days of construction. After 28 days there was a drop in the

maximum current of the biosensor during analyses, which agree with the results

shown in Figure 6.6.

6.7   Temperature Stability Investigation of Au/MBT/PANI/AChE/PVAc Biosensor

Another critical factor in the determination of the activity and stability of a

biosensor, is the temperature at which measurements are performed (Sen *et al.*

2004:1261; Yang *et al.* 2005:205; Timur *et al.* 2004:132). The response of the

Au/MBT/PANI/AChE/PVAc biosensor to successive additions of the substrate ATCh

in a 2 ml of 0.1 M phosphate buffer, KCl (pH 7.2) solution, was determined at

different temperatures varying from 10 to 35 ºC. In Figure 6.8 the results obtained for

the response of the enzyme AChE at different temperatures are shown.
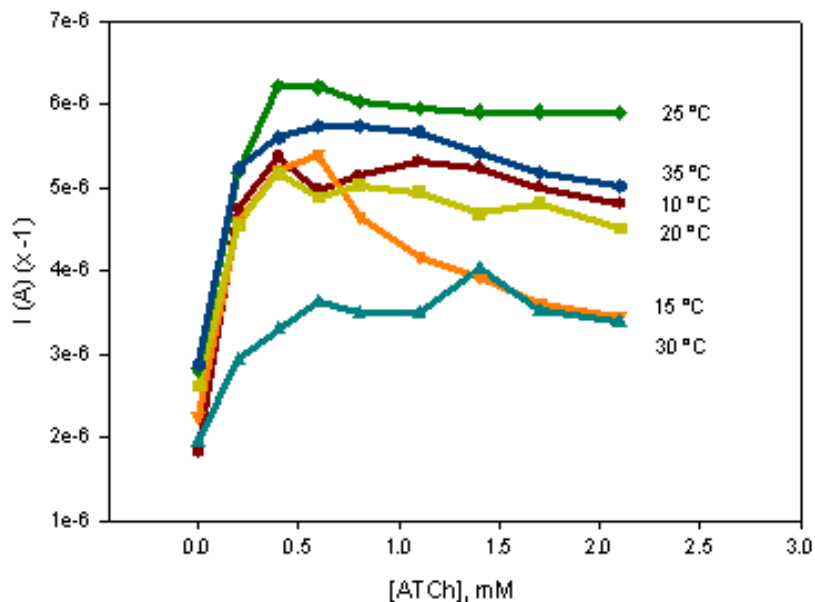
Figure 6.8   **Graph displaying the effects of temperature on the activity of the enzyme in the Au/MBT/PANI/AChE/PVAc biosensor in 0.1 M phosphate buffer, KCl (pH 7.2) solution.**

The results in Figure 6.8 shows that for the six temperatures investigated, maximum current (I_{max}) was reached within 0.6 to 1.0 mM of ATCh substrate added, indicating that the enzyme AChE responded favourably to most temperatures evaluated. The activity of the immobilised enzyme reached a maximum at 25 ºC, with the highest current obtained at this temperature. At the low temperatures of 10, 15 and 20 ºC, it was observed that the activity of the enzyme was relatively similar during the first 0.5 mM of ATCh substrate added. On the other hand, the higher temperatures of 30 and 35 ºC gave mixed results with the activity of the enzyme high at 35 ºC, while the

lowest activity was obtained for 30 ºC. At 15 ºC, it was observed that after maximum

current was reached at 0.6 mM of substrate added, there was a big decrease in the

activity of the enzyme, which can be attributed to denaturation of the enzyme. At

none of the other temperatures investigated, the same effect was observed.

In the next step the maximum current (I_{max}) obtained for each temperature was

estimated and the results are plotted in Figure 6.9.
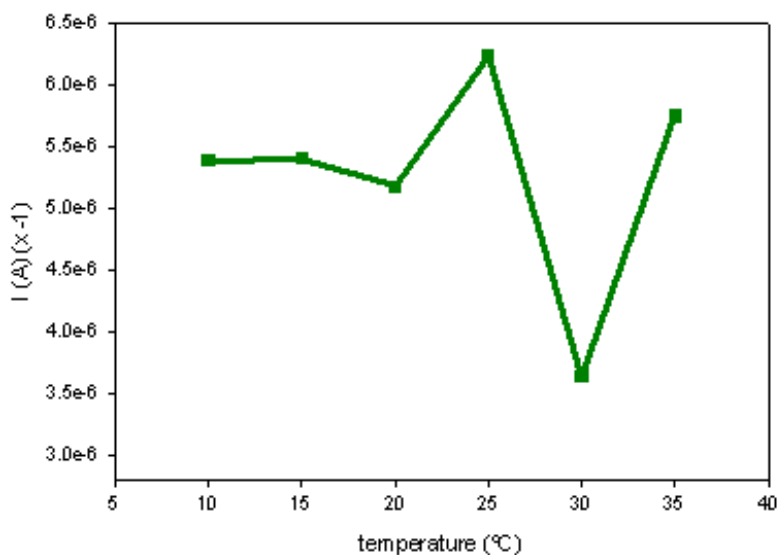
Figure 6.9   **Graph displaying the maximum current (I_{max}) obtained at different temperatures for the Au/MBT/PANI/AChE/PVAc biosensor in 0.1 M phosphate buffer, KCl (pH 7.2) solution, evaluated at 10, 15, 20, 25, 30 and 35 ºC.**

When the values obtained for the maximum current at the different temperatures

(Figure 6.9) are compared, it is observed that the activity of the enzyme AChE

remained relatively constant at the low temperatures and that optimum activity was

detected at a temperature of 25 ℃. The activity of the biosensor dropped at 30 ℃, while an increase in activity was observed when the biosensor was evaluated at 35 ℃. Although a good response was obtained at 35 ℃, the effect of high temperatures on the long-term stability of the enzyme was uncertain at this stage, therefore operation of the biosensor at 25 ℃ was chosen for this study.

6.8 The Effect of Polar Organic Solvents on the Amperometric Behaviour of the Au/MBT/PANI/AChE/PVAc Biosensor

It is known that organic solvents can induce extensive changes in the activity and specificity of an enzyme. This is because the enzyme's structure and reactivity depends on several non-covalent interactions in the biocatalyst, which includes hydrogen bonding, ionic, hydrophobic, and van der Waals interactions. Enzymes have further evolved to maintain their structural stability in aqueous medium, but organic solvents are known to disrupt the abovementioned forces of interaction in the enzyme, causing changes in the kinetic and thermodynamic behaviour of the enzyme (Iwuoha *et al.* 1997a:53). Any changes that occur in solvent hydrophobicity, dielectric constant and water content of the reaction medium, affect the ability of enzymes to use their free energy of binding with a substrate, leading to changes in substrate specificity and reactivity (Iwuoha *et al.* 1997a:56; Dordick 1992:259). The solvents media that can be used for biosensing can be classified into two groups, i.e. anhydrous organic media and water-containing media. In the case of anhydrous

organic media, it refers to pure solvents or a mixture of pure organic solvents that may be polar or non-polar in nature. On the other hand, water-containing organic media consist of micro-aqueous systems, water-organic solvent mixtures, water and immiscible organic solvent biphasic systems and reverse micellar solutions (Iwuoha *et al.* 1997a:56; Chatterjee and Russell 1992:1069). The term micro-aqueous reaction media are associated with the non-polar organic solvents that are immiscible with water. Since it is known that enzymes generally require essential water of hydration for activity, it is essential that non-polar solvents be saturated with water before they are used as reaction media for biosensing. These systems will contain a water content that is very insignificant when compared to the water content of organic solvents, and it depends on the ability of the solvent to absorb water. Since the so-called anhydrous aqueous systems require a minimum amount of water for enzyme activity, it is more suitable to refer to such a system as a micro-aqueous solution (Iwuoha *et al.* 1997a:56; Borzeix *et al.* 1992:791). In the case of polar organic solvents, they can be used as systems that contain some amount of water. The hydration of polar solvents ensures that the flexibility, structure and local dielectric constant of the enzyme redox site environment, stay as much as possible, unaltered. If the effect of increased solvent polarity occurs, it will weaken the electrostatic forces in the enzyme, which will lead to water partitioning out of the enzyme into the bulk solvent. Therefore, biosensors exhibit much greater reactivity in the presence of polar organic solvents that contain some amount of water (Iwuoha *et al.* 1997a:56).

6.8.1 The effect of polar organic solvents on AChE activity

The effect of organic solvents on the activity of AChE in the constructed Au/MBT/PANI/AChE/PVAc biosensor has been studied in the presence of polar organic solvents containing a 0 – 10% aqueous solution of water. The polar organic solvents used in this study includes acetonitrile, acetone and ethanol. The response of the Au/MBT/PANI/AChE/PVAc biosensor was first measured in a 0.1 M phosphate buffer, KCl (pH 7.2) solution, in the presence of a fixed concentration of ATCh. The biosensor was thereafter incubated for 20 minutes in an aqueous-solvent mixture or the pure organic solvent. The response of the Au/MBT/PANI/AChE/PVAc biosensor was then again measured in a 0.1 M phosphate buffer, KCl (pH 7.2) solution, in the presence of a fixed concentration of ATCh. The results of the two respective measurements were then used to calculate the percentage inhibition using the formula (Albareda-Sirvent *et al.* 2000:137; Sotiropoulou and Chaniotakis 2005:199; Wilkins *et al.* 2000:786):

$$I\% = \frac{(I_1 - I_2)}{I_1} X\ 100, \qquad\qquad \text{Eqn. 6.1}$$

where $I\%$ is the degree of inhibition, I_1 is the steady-state current obtained in buffer solution after the addition of ATCh substrate, and I_2 is the steady-state current obtained after the AChE biosensor was incubated for 20 minutes in the organic solvent. In Figure 6.10 the results obtained for the inhibition of AChE in the

Au/MBT/PANI/AChE/PVAc biosensor after 20 minutes of incubation in (a) 10% water-organic solvent mixture, (b) 5% water-organic solvent mixture, and pure organic solvent is shown.
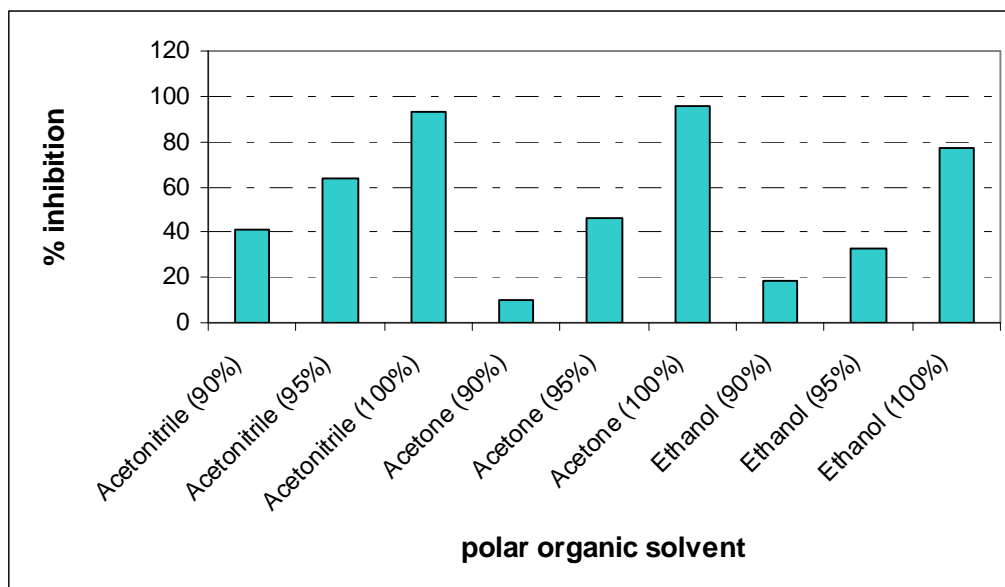
Figure 6.10   **Results obtained for the inhibition of AChE in the Au/MBT/PANI/AChE/PVAc biosensor after 20 minutes of incubation in (a) 10% water-organic solvent mixture, (b) 5% water-organic solvent mixture, and pure organic solvent. The ATCh concentration was 2.0 mM.**

From the results in Figure 6.10 it can be seen that for the three different 10% water-organic solvent mixtures investigated, the lowest decrease in catalytic activity of AChE was observed in acetone, compared to acetonitrile and ethanol. For the 5% water-organic solvent mixtures, ethanol had the lowest decrease on the catalytic

activity of AChE, while in the pure polar organic solvent it was observed that ethanol had again the lowest decrease on the catalytic activity of AChE.

In Figure 6.11 the individual results obtained for the inhibition of AChE in the Au/MBT/PANI/AChE/PVAc biosensor after 20 minutes of incubation in a 10% water-organic solvent mixture is shown.
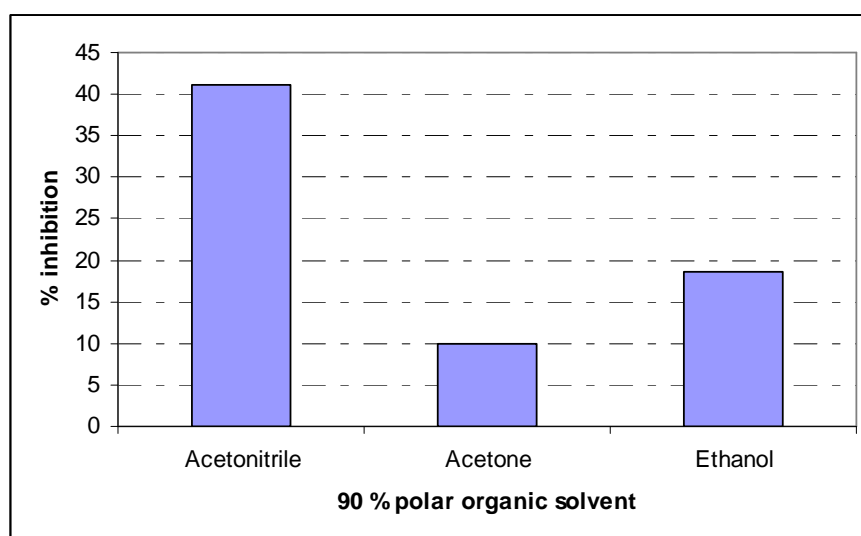
Figure 6.11 **Results obtained for the inhibition of AChE in the Au/MBT/PANI/AChE/PVAc biosensor after 20 minutes of incubation in a 10% water-organic solvent mixture. The ATCh concentration was 2.0 mM.**

The results in Figure 6.11 indicate that the highest decrease in the catalytic activity of AChE was observed when the biosensor was exposed to acetonitrile, while the lowest decrease was observed in acetone. If one looks at the use of organic solvents in biocatalysis, research have shown that enzymes have a high activity in hydrophobic

solvents that have a log P value greater than 4. On the other hand, enzyme activity will be low in hydrophilic solvents with a log P value less than 2, where P is the octanol/water partition coefficient of a specific organic solvent (Iwuoha *et al.* 1997b:756). The log P values of the polar solvents used in this study are - 0.33, - 0.23 and - 0.24 for acetonitrile, acetone and ethanol respectively (Konash and Magner 2006:116). Since the log P values of the three solvents shown in Figure 6.11 are less than 2, it was expected that the AChE activity will not be high since the solvents are hydrophilic. The effect of adding 10% water to keep the active centre of the AChE enzyme hydrated during the biosensor studies, have helped showing that only 10% inhibition of the AChE catalytic activity was observed in acetone.

In Figure 6.12 the cyclic voltammetric (CV) results obtained for investigating the effect of an acetone-aqueous mixture on the enzyme AChE in the Au/MBT/PANI/AChE/PVAc biosensor is shown.
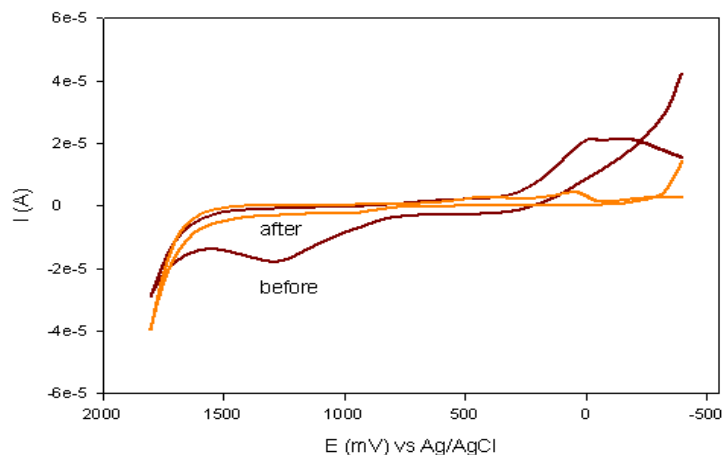
Figure 6.12   **Results for the cyclic voltammetric (CV) response of the
Au/MBT/PANI/AChE/PVAc biosensor in a 0.1 M phosphate buffer,
KCl (pH 7.2) solution in the presence of 2 mM ATCh, before and after
exposure to a 90% acetone-aqueous organic solvent mixture.**

In the CV results it was found that when the Au/MBT/PANI/AChE/PVAc biosensor was incubated in acetone for 20 minutes, a good decrease in the anodic current at a potential of approximately 1250 mV (vs. Ag/AgCl) was observed after analysis, as shown in Figure 6.12. This decrease in current corresponds with the results shown in Figure 6.11, showing the effect of acetone on the catalytic activity of the enzyme AChE.

Next the differential pulse voltammetry (DPV) responses of the Au/MBT/PANI/AChE/PVAc biosensor (Figure 6.13) were collected to check on whether the same trends observed with the CV responses are obtained.
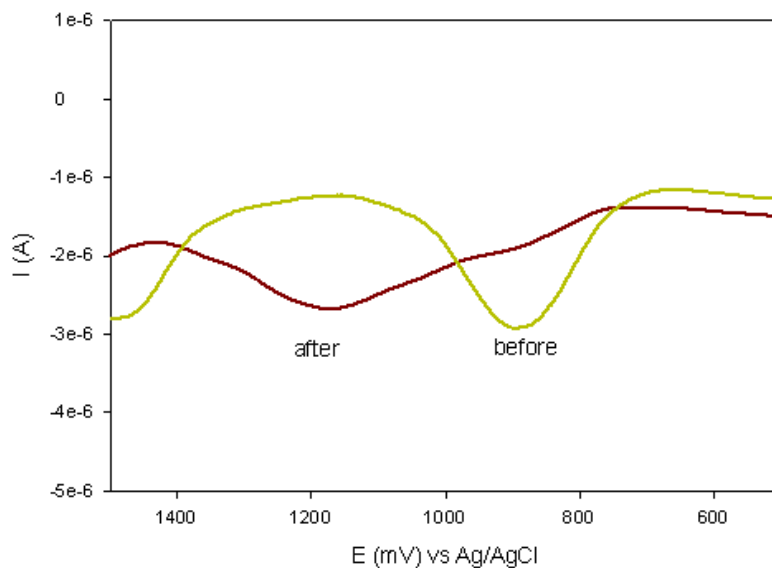
Figure 6.13   **Results for the differential pulse voltammetric (DPV) response of the Au/MBT/PANI/AChE/PVAc biosensor in a 0.1 M phosphate buffer, KCl (pH 7.2) solution in the presence of 2 mM ATCh, before and after exposure to a 90% acetone-aqueous organic solvent mixture.**

In Figure 6.13 the DPV results for the inhibiting effect of a 90% acetone-aqueous organic solvent mixture on AChE, shows two changes that occurred in the DPV results. First a shift in potential was observed as the peak potential (E_p) before inhibition was observed at + 901.2 mV (vs. Ag/AgCl), while after inhibition it was at + 1195.3 mV (vs. Ag/AgCl). Secondly, there was a decrease in anodic current to account for the decrease in catalytic activity of AChE due to the exposure to acetone.

Figure 6.14 shows the individual results obtained for the inhibition of AChE in the Au/MBT/PANI/AChE/PVAc biosensor after 20 minutes of incubation in a 5% water-organic solvent mixture.
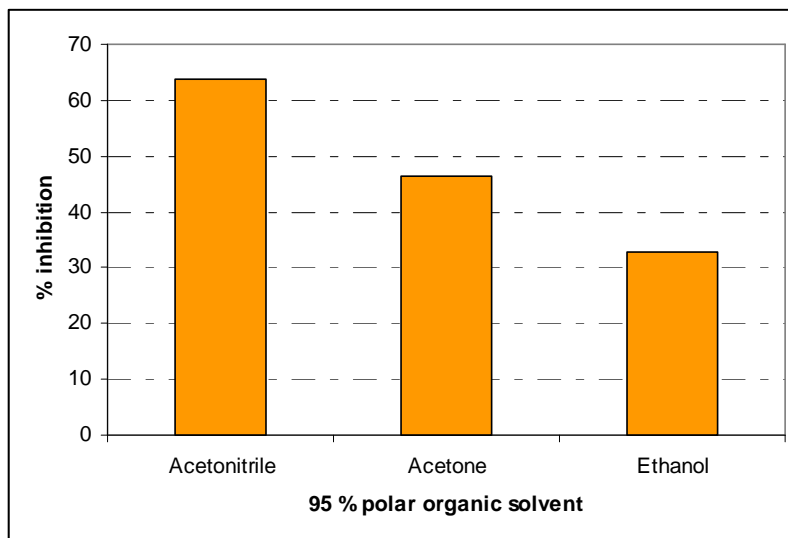
Figure 6.14   **Results obtained for the inhibition of AChE in the Au/MBT/PANI/AChE/PVAc biosensor after 20 minutes of incubation in a 5% water-organic solvent mixture. The ATCh concentration was 2.0 mM.**

The results in Figure 6.14 shows that the highest inhibition experienced by AChE as enzyme in the Au/MBT/PANI/AChE/PVAc biosensor was in acetonitrile as solvent, while the lowest inhibition was experienced in ethanol. Since the enzyme was incubated in 5% water-organic solvent mixtures, a higher degree of inhibition was seen from the results when it is compared to that in Figure 6.11, in which 10% water-organic solvent mixtures were evaluated. This can be attributed to the fact that less

water was used in the water-organic solvent mixtures under discussion, as compared to the first results reported. When 5% water-organic solvent mixtures were used, the lowest inhibition observed was 10% for acetone, while for the 10% water-organic solvent mixtures, the lowest inhibition observed were 33% for ethanol.

When the cyclic voltammetric (CV) results in Figure 6.15 are viewed, the inhibiting effect of ethanol on the enzyme AChE in the Au/MBT/PANI/AChE/PVAc biosensor can be seen. Although the potential window used in the collection of the CV results was - 400 to + 1800 mV at a scan rate of 10 mV.s^{-1}, a shorter potential window is shown below, to highlight the anodic and cathodic peaks in the CV obtained.
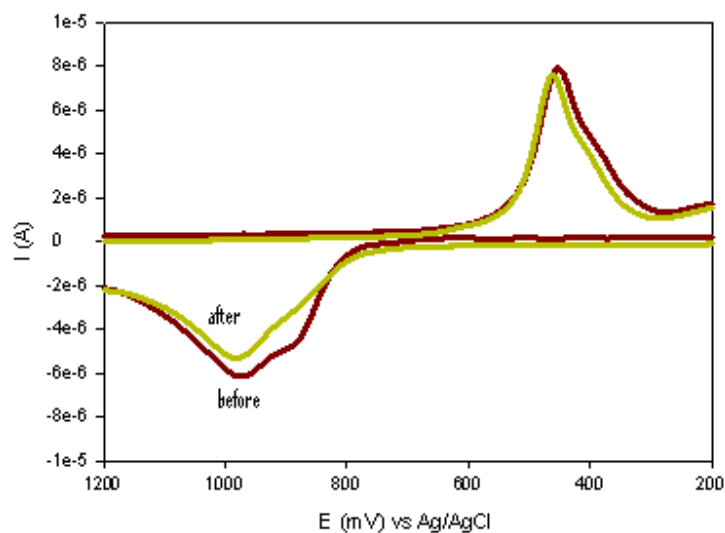
Figure 6.15   **Results for the cyclic voltammetric (CV) response of the Au/MBT/PANI/AChE/PVAc biosensor in a 0.1 M phosphate buffer, KCl (pH 7.2) solution in the presence of 2 mM ATCh, before and after exposure to a 95% ethanol-aqueous organic solvent mixture.**

The CV results in Figure 6.15 indicate that good redox behaviour was observed for the AChE enzyme in the Au/MBT/PANI/AChE/PVAc biosensor, before and after exposure to a 95% ethanol-aqueous organic solvent mixture. In the above CV it was also observed that the reduction peaks observed at approximately + 568.3 mV (vs. Ag/AgCl), had higher cathodic currents as compared to the results for the anodic currents. This result can be attributed to two factors. First, the substrate called acetylthiocholine (ATCh) is electroactive and undergoes both oxidation and reduction when it is hydrolysed by the enzyme AChE. Secondly, due to the influence of the 95% ethanol-aqueous organic solvent mixture on the enzyme, it was observed that the inhibition caused by the solvent had a stronger influence on the oxidation process occurring and the reduction of ATCh was favoured.

In Figure 6.16 the DPV responses for the inhibiting effect of an ethanol-aqueous mixture on the enzyme AChE in the Au/MBT/PANI/AChE/PVAc biosensor is shown. A shorter potential window between + 600 and + 1100 mV is shown in order to highlight the effect of the inhibition observed.
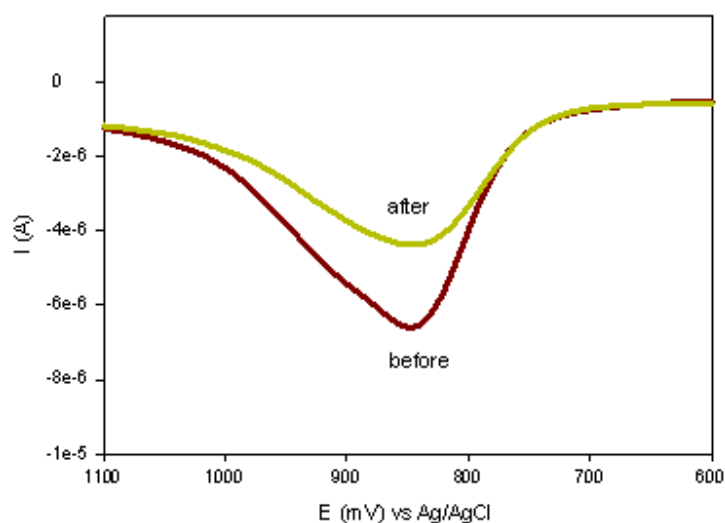
Figure 6.16   **Results for the differential pulse voltammetric (DPV) response of the Au/MBT/PANI/AChE/PVAc biosensor in a 0.1 M phosphate buffer, KCl (pH 7.2) solution in the presence of 2 mM ATCh, before and after exposure to a 95% ethanol-aqueous organic solvent mixture.**

The results in Figure 6.16 clearly show the inhibiting effect of the 95% ethanol-aqueous organic solvent mixture on the catalytic activity of the enzyme AChE. The decrease in anodic current was observed at a potential of approximately + 847.6 mV (vs. Ag/AgCl). Although not shown here, the higher cathodic currents observed in the CV results in Figure 6.15, was not observed in the DPV results.

Figure 6.17 shows the individual results obtained for the inhibition of AChE in the Au/MBT/PANI/AChE/PVAc biosensor after 20 minutes of incubation in a pure organic solvent.
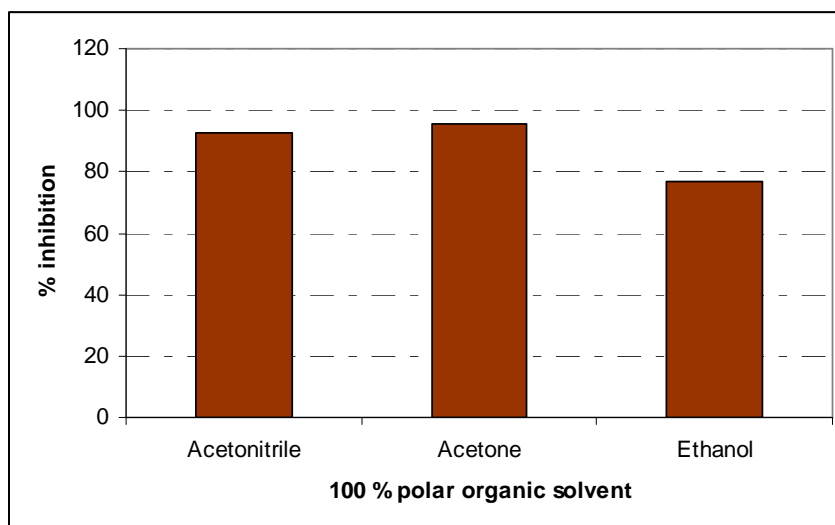
Figure 6.17   **Results obtained for the inhibition of AChE in the Au/MBT/PANI/AChE/PVAc biosensor after 20 minutes of incubation in a pure organic. The ATCh concentration was 2.0 mM.**

The results obtained for the exposure of the enzyme to pure organic solvents are shown in Figure 6.17. When the results in Figure 6.17 are compared to that in Figures 6.10, 6.11 and 6.14, it is observed that the highest inhibiting effect on the enzyme AChE, was experienced when the enzyme was exposed to the pure organic solvents. The individual inhibition results obtained are 93% in acetonitrile, 96% in acetone and 77% in ethanol. The lowest percentage inhibition of the enzyme AChE was experienced in ethanol, therefore suggesting that the assay of the pesticides in pure ethanol solvent will deliver good results. It further suggests that ethanol will be a good extraction organic solvent, with the added effect of good solubility of ATCh and pesticides in the solvent, eliminating the need to avoid the inactivation effect of the solvent on biosensor response (Wilkins *et al.* 2000:789).

For the CV results shown in Figure 6.18, it was observed that a strong oxidation peak was observed at approximately + 1251.6 mV (vs. Ag/AgCl) before the Au/MBT/PANI/AChE/PVAc biosensor was exposed to the ethanol solvent.
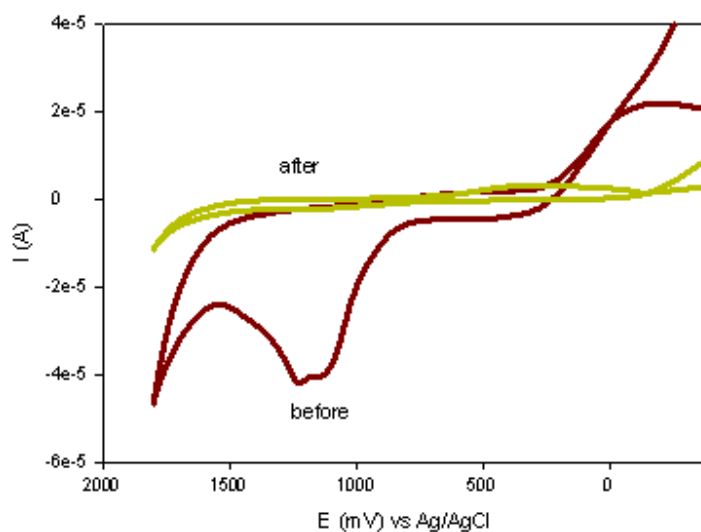
Figure 6.18   **Results for the cyclic voltammetric (CV) response of the Au/MBT/PANI/AChE/PVAc biosensor in a 0.1 M phosphate buffer, KCl (pH 7.2) solution in the presence of 2 mM ATCh, before and after exposure to a 100% ethanol organic solvent.**

After 20 minutes of incubation in the ethanol solvent, a relatively high decrease in the anodic peak current was observed while a good cathodic peak was also obtained as shown in Figure 6.18. The CV results clearly show the inhibiting effect of the pure ethanol solvent on the catalytic activity of the enzyme AChE.

When the DPV responses are viewed in Figure 6.19, anodic peak currents
were observed at a potential of approximately + 885.2 mV (vs. Ag/AgCl) for the
Au/MBT/PANI/AChE/PVAc biosensor in the pure ethanol solvent.
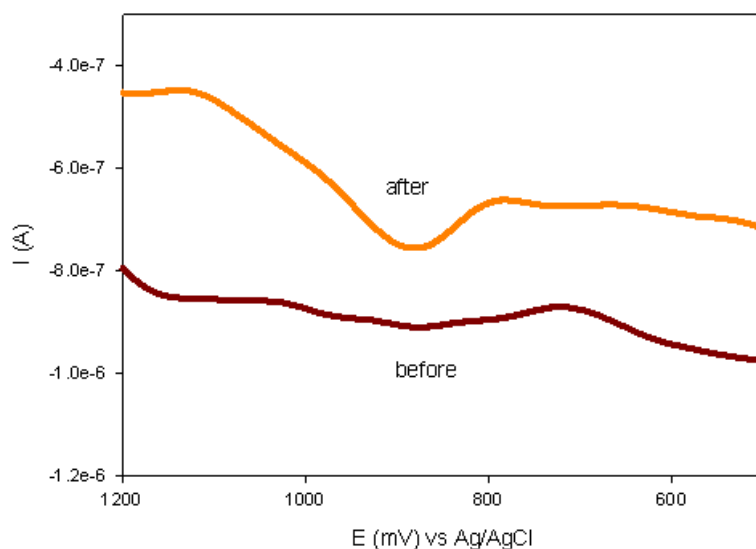
Figure 6.19   **Results for the differential pulse voltammetric (DPV) response of the
                         Au/MBT/PANI/AChE/PVAc biosensor in a 0.1 M phosphate buffer,
                         KCl (pH 7.2) solution in the presence of 2 mM ATCh, before and after
                         exposure to a 100% ethanol organic solvent.**

In order to highlight the peak data of the results, the DPV responses are again shown
in a shorter potential window between + 400 and + 1200 mV, collected at a scan rate
of 10 mV.s^{-1}. Closer analysis of the DPV responses in Figure 6.19 shows that a broad
anodic peak was obtained at approximately + 885 mV (vs. Ag/AgCl) before the
Au/MBT/PANI/AChE/PVAc biosensor was exposed to pure ethanol solvent. The

anodic peak obtained after incubation is more pronounced and a clear shift in anodic

current is seen to correspond with the inhibition results shown in Figure 6.17.

In summary the results obtained for the percentage inhibition of the enzyme

AChE in the different polar aqueous-solvent mixtures that were investigated, are

shown in Table 6.1.

Table 6.1   **Summary of the results obtained for the percentage inhibition of the enzyme AChE in the different polar aqueous-solvent mixtures investigated.**

Polar organic solvent	Log P	% Inhibition of enzyme, AChE, in different solvent mixtures		
		90% aqueous-solvent mixture	95% aqueous-solvent mixture	100% pure solvent
acetonitrile	-0.33	41	63	93
acetone	-0.23	**10**	47	96
ethanol	-0.24	18	**33**	**77**

The results in Table 6.1 indicate that a 90% aqueous-solvent mixture of acetone and

water gave the best results and the smallest degree of inhibition of the electrocatalytic

effect of AChE in the Au/MBT/PANI/AChE/PVAc biosensor investigated. The

results obtained for the 95% aqueous-solvent mixtures and the pure polar organic

solvents clearly indicate the solvent hydrating effect of the three solvent investigated

increases as the amount of water is decreased. These results are in line with the

investigations reported by Evtugyn *et al.* (1998:465) on the presence of water and in

the enzyme's active centre.

6.8.2 Nature of polar organic solvents

In this paragraph the nature of the polar organic solvents were investigated and the relationships between the hydrophobicity, hydrophilicity, dielectric constant or viscosity of the solvents used in the biosensor study are discussed.

The response of the Au/MBT/PANI/AChE/PVAc biosensor was first measured in a 0.1 M phosphate buffer, KCl (pH 7.2) solution, in the presence of a fixed concentration of ATCh. The biosensor was thereafter incubated for 20 minutes in an aqueous-solvent mixture or the pure organic solvent. The response of the Au/MBT/PANI/AChE/PVAc biosensor was then again measured in a 0.1 M phosphate buffer, KCl (pH 7.2) solution, in the presence of a fixed concentration of ATCh. In Figure 6.20 the results for the calibration curves obtained after successive addition of the substrate ATCh to 0.1 M phosphate buffer, KCl (pH 7.2) solutions before and after incubation of the AChE biosensor in 90% polar organic-aqueous solvent mixtures is shown.
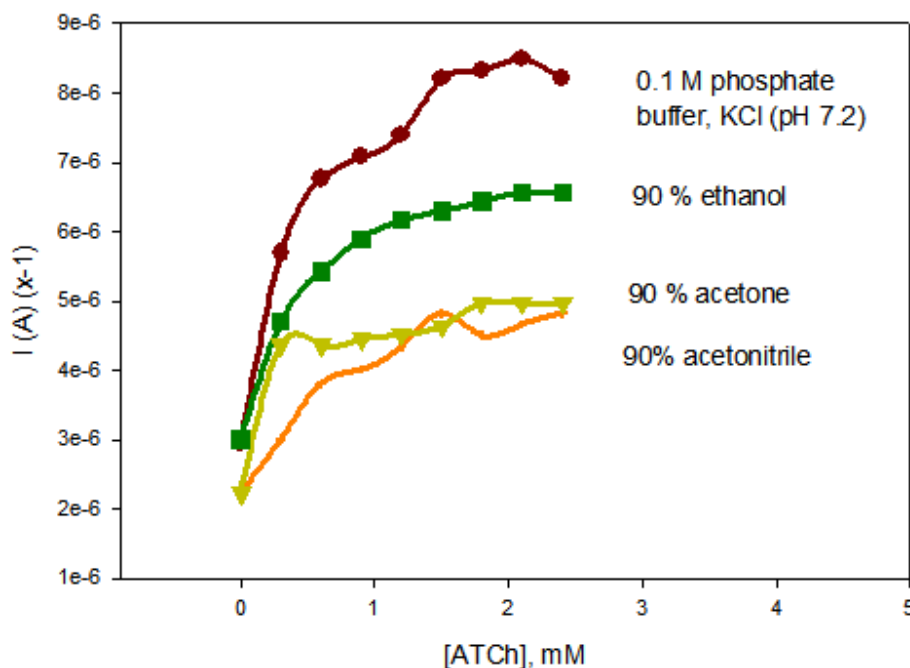
Figure 6.20   **Calibration curves for successive 0.01 M ATCh additions to 0.1 M phosphate buffer, KCl (pH 7.2) solutions before and after incubation of the AChE biosensor in 90% polar organic-aqueous solvent mixtures. The ATCh concentration was 2.4 mM.**

The results shown in Figure 6.20 indicate that there was a decrease in current response for the AChE biosensor in all three 90% polar-aqueous solvent mixtures to which the enzyme AChE was exposed. If the maximum current obtained in the phosphate buffer saline solution is used as reference, it is clearly seen from the results that the maximum current is lower in the 90% ethanol-water, acetone-water and acetonitrile-water solvent mixtures. The current vs. potential results for the last three polar organic-aqueous solvent mixtures, also indicate that after the enzyme AChE was exposed to the 90% ethanol-water solvent mixture, it was still able to function

relatively well, while exposure to the other two polar organic-aqueous solvent mixtures reduced the response of the enzyme to the substrate. Furthermore, the log P values of the polar solvents used in this study are - 0.33, - 0.23 and - 0.24 for acetonitrile, acetone and ethanol respectively (Konash and Magner 2006:116). Since the log P values of the three solvents shown in Figure 6.20 are less than 2, it was expected that the AChE activity will be reduced since the solvents are hydrophilic.

In Figure 6.21 the results for the calibration curves obtained after successive addition of the substrate ATCh to 0.1 M phosphate buffer, KCl (pH 7.2) solutions before and after incubation of the AChE biosensor in 95% polar organic-aqueous solvent mixtures is shown.
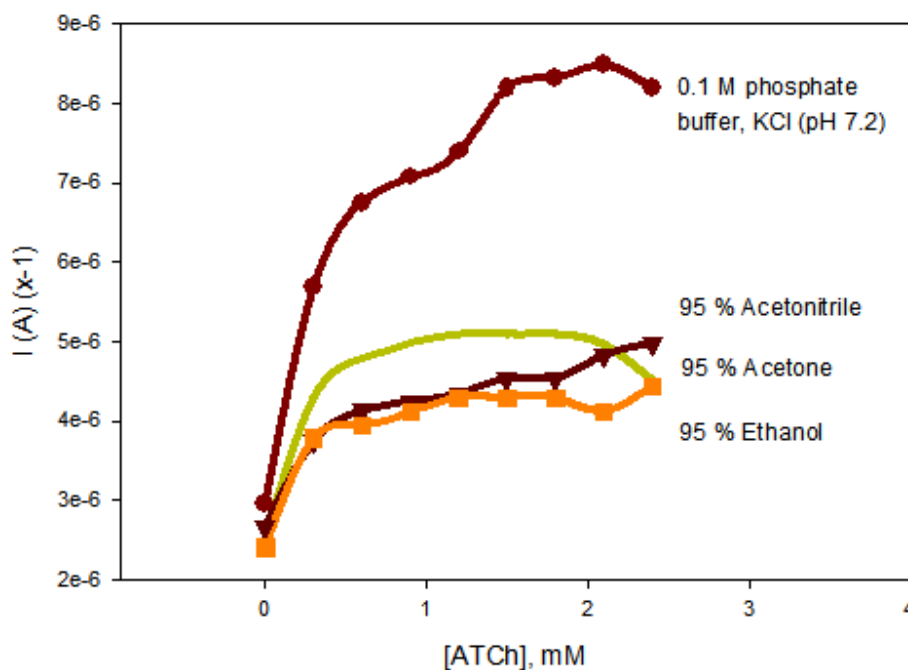
Figure 6.21   **Calibration curves for successive 0.01 M ATCh additions to 0.1 M phosphate buffer, KCl (pH 7.2) solutions before and after incubation of the AChE biosensor in 95% polar organic-aqueous solvent mixtures. The ATCh concentration was 2.4 mM.**

The above results in Figure 6.21 show the effect of a reduced amount of water used with the different polar organic solvents investigated. After incubation of the AChE biosensor in the 95% polar organic-aqueous solvent mixtures, it was observed that the current vs. potential results was more reduced as compared to the results for the phosphate buffer saline solution and that obtained in Figure 6.20. The results further shows that a reduction in the amount of water used in the polar organic-aqueous solvent mixtures for incubation reduced the response of the AChE biosensor to

substrate addition afterwards. This further indicates that hydration of the enzyme active centre by water plays an important role in the functioning of the biosensor.

The results for the incubation of the AChE biosensor in 100% pure polar organic solvents are shown in Figure 6.22.
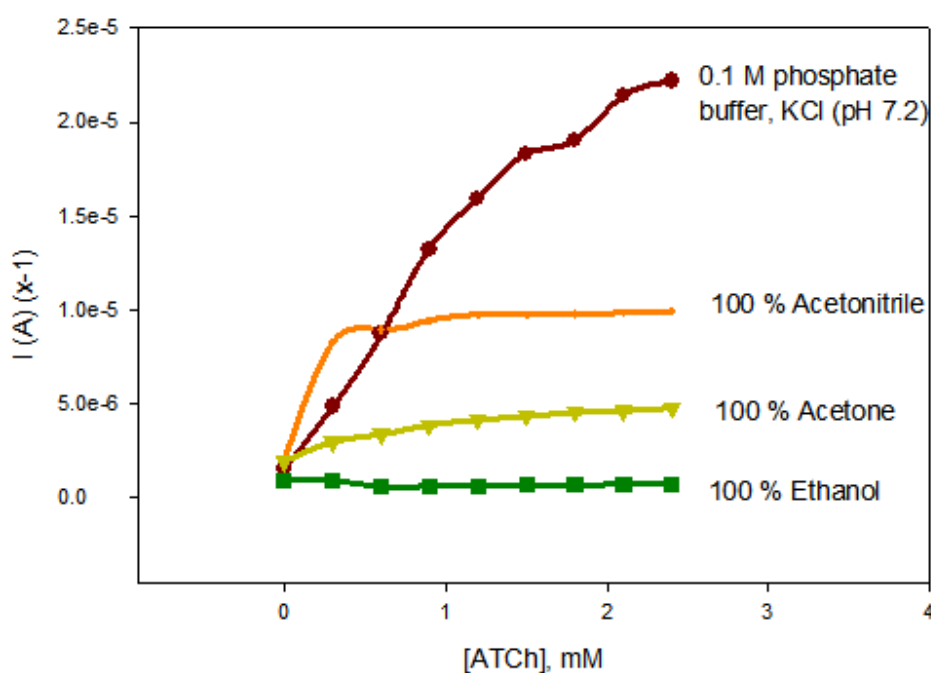
Figure 6.22   Calibration curves for successive 0.01 M ATCh additions to 0.1 M phosphate buffer, KCl (pH 7.2) solutions before and after incubation of the AChE biosensor in 100% organic solvent solutions. The ATCh concentration was 2.4 mM.

For the results shown in Figure 6.22 it was observed that the response of the AChE biosensor after incubation in the 100% pure polar organic solvents, showed diminishing currents as compared to the current response obtained in phosphate

buffer saline solution. For the three pure polar organic solvents used during incubation, it was seen that the current vs. potential results after exposure to acetonitrile, shows the least diminishing effect. Evtugyn *et al.* (1998:480-481) have indicated that a 30 minute incubation in pure acetonitrile does not significantly alter the activity of AChE, whereas in an alcohol a definite diminishing of the enzyme activity occurs. This influence is seen in the lowest current response obtained after the AChE biosensor was exposed to a 100% ethanol solution.

In order to further understand the polar organic solvents used in this study, their log *P*, viscosity and dielectric constants were compared to investigate its affect on the biosensor's performance. Iwuoha *et al.* (1997a:67) indicated that the viscosity of a solvent affects the diffusibility of the substrate as well as its partitioning into the enzyme membrane. The parameter called the dielectric constant is a measure of the relative permittivity and it governs the ability of solvents to weaken the electrostatic forces around the enzyme's charged and polar active site (Fatibello-Filho and Vieira 2000:340-341).

In Table 6.2 the values of log *P*, the viscosity and dielectric constants of the polar organic solvents of acetonitrile, acetone and ethanol is shown.

Table 6.2   **Physical and chemical properties of selected polar solvents used in this study and the biosensor responses obtained in the specific solvents (Konash and Magner 2006:121; Iwuoha et al. 1997a:68).**

Parameters	Acetonitrile	Acetone	Ethanol
log P	-0.33	-0.23	-0.24
Dynamic viscosity, v (x 10^{-3} $cm^2.s^{-1}$)	4.7	4.1	15.3
Dielectric constant, ε	37.5	20.7	25.0

For the results in Table 6.2 it can be seen that ethanol has the highest dynamic viscosity, while acetonitrile has the highest value for the dielectric constant. The solvent properties of acetone tend to be in the middle for the three solvents compared above. The effect of the dynamic viscosity on the enzyme behaviour will therefore be more influenced by ethanol with the highest dynamic viscosity. On the other hand, with acetonitrile having the highest dielectric constant, its influence on the catalytic activity of the enzyme will be the highest.

In Table 6.3 the results for the apparent kinetic characteristics of the Au/MBT/PANI/AChE/PVAc biosensor after incubation in 90% polar organic-aqueous solvent mixtures is shown.

Table 6.3   **Results for the apparent kinetic characteristics of the Au/MBT/PANI/AChE/PVAc biosensor after incubation in 90% polar organic-aqueous solvent mixtures.**

Parameters	Acetonitrile (90%)	Acetone (90%)	Ethanol (90%)
Sensitivity ($A.M^{-1}$)	8.85×10^{-6}	2.98×10^{-7}	9.68×10^{-7}
K_m^{app} (mM)	5.54	16.8	6.82
I_{max} (A)	4.9×10^{-6}	5.0×10^{-6}	6.6×10^{-6}

The results in Table 6.3 indicate that the sensitivity of the AChE biosensor after incubation in the 90% polar organic-aqueous solvent mixtures is the lowest for acetone and the highest for acetonitrile. Different values were also obtained for the apparent Michaelis-Menten constant (K_m^{app}), indicating that these values depend on the solvent medium. The value of K_m^{app} was the lowest after incubation in acetonitrile that has the highest sensitivity. Furthermore, the value of the maximum current (I_{max}) that indicate the response of the biosensor at saturation concentration of the substrate, was of the same order of magnitude for the three different 90% polar organic-aqueous solvent mixtures.

In Table 6.4 the results for the apparent kinetic characteristics of the Au/MBT/PANI/AChE/PVAc biosensor after incubation in 95% polar organic-aqueous solvent mixtures is shown.

Table 6.4   **Results for the apparent kinetic characteristics of the Au/MBT/PANI/AChE/PVAc biosensor after incubation in 95% polar organic-aqueous solvent mixtures.**

Parameters	Acetonitrile (95%)	Acetone (95%)	Ethanol (95%)
Sensitivity $(A.M^{-1})$	1.33×10^{-6}	3.39×10^{-7}	5.72×10^{-6}
K_m^{app} (mM)	3.83	15.0	7.86
I_{max} (A)	5.1×10^{-6}	5.1×10^{-6}	4.5×10^{-6}

In the case of the 95% polar organic-aqueous solvent mixtures, the results in Table 6.4 shows that the sensitivity of the AChE biosensor after incubation in acetonitrile and ethanol were the highest but of the same order. The values of the apparent Michaelis-Menten constant (K_m^{app}), again showed a dependency of these values on the solvent medium with the value obtained after incubation in acetonitrile being the lowest. The value of the maximum current (I_{max}) was again of the same order of magnitude for the three different 95% polar organic-aqueous solvent mixtures that the biosensor was incubated in.

In Table 6.5 the results for the apparent kinetic characteristics of the Au/MBT/PANI/AChE/PVAc biosensor after incubation in 100% pure polar organic solvent is shown.

Table 6.5　　　**Results for the apparent kinetic characteristics of the Au/MBT/PANI/AChE/PVAc biosensor after incubation in 100% pure polar organic solvents.**

Parameters	Acetonitrile (100%)	Acetone (100%)	Ethanol (100%)
Sensitivity (A.M^{-1})	1.97×10^{-6}	8.58×10^{-7}	7.71×10^{-7}
K_m^{app} (mM)	5.59	5.6	0.934
I_{max} (A)	1.1×10^{-5}	4.8×10^{-6}	7.2×10^{-7}

The results obtained in Table 6.5 indicate that after incubation of the AChE biosensor in the 100% pure polar organic solvent, the sensitivity due to acetone and ethanol was found to be of the same order and lower than when it was exposed to acetonitrile. The value of the apparent Michaelis-Menten constant (K_m^{app}) was the lowest after incubation of the sensor in ethanol, while in Figure 6.17 it was shown that the enzyme AChE inhibition was the lowest in 100% pure ethanol solvent. The value of the maximum current (I_{max}) was different for the three different 100% pure polar organic solvents investigated, with the highest value obtained after incubation in acetonitrile and the lowest for ethanol.

In summary, the results tabulated in Tables 6.1, 6.2 and 6.3 have shown for the 90% aqueous-solvent mixtures that acetone has the lowest sensitivity, which is in line with the results of the solvent's dynamic viscosity and dielectric constant. Therefore, acetone was chosen as the solvent for the pesticide studies since a much lower inactivation effect on the biosensor response due to the solvent can be expected.

6.9   The Effect of Non-Polar Organic Solvents on the Amperometric Behaviour of the Au/MBT/PANI/AChE/PVAc Biosensor

6.9.1 The effect of non-polar organic solvents on AChE activity

The effect of organic solvents on the activity of AChE in the constructed Au/MBT/PANI/AChE/PVAc biosensor has been studied in the presence of non-polar organic solvents containing a 0 – 10% aqueous solution of water. The non-polar organic solvents used in this study are n-hexane and diethyl ether. The same working principle discussed in section 6.8.1 was used to study the inhibiting effect of the polar organic solvents and to calculate the percentage inhibition for these solvents. The log *P* values of the non-polar solvents used in this study are 3.5 and 0.85 for n-hexane and diethyl ether respectively (Campanella *et al.* 1998:595; Ruiz *et al.* 2000:229).

Figure 6.22 shows the results obtained for the inhibition of AChE in the Au/MBT/PANI/AChE/PVAc biosensor after 20 minutes of incubation in (a) 10% water-organic solvent mixture, (b) 5% water-organic solvent mixture, and pure organic solvent, for n-hexane and diethyl ether used as non-polar organic solvents. These two non-polar organic solvents were subjected to rigorous shaking, after the addition of water has been done, in order to assure that it was saturated with water before the incubation experiments were done.
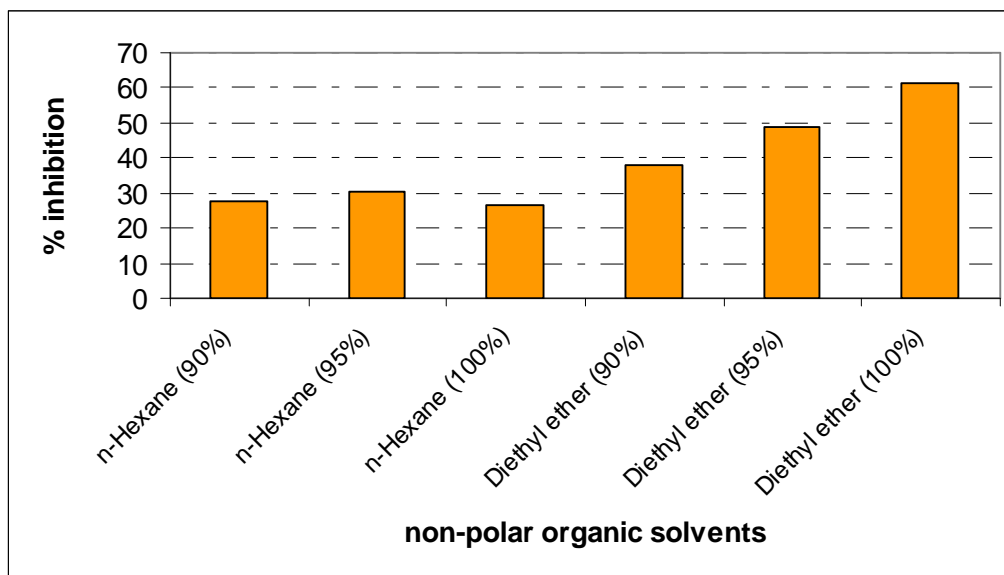
Figure 6.23   **Results obtained for the inhibition of AChE in the Au/MBT/PANI/AChE/PVAc biosensor after 20 minutes of incubation in (a) 10% water-organic solvent mixture, (b) 5% water-organic solvent mixture, and pure organic solvent. The ATCh concentration was 2.0 mM.**

Once again the attention is drawn to the log *P* values of the organic solvents used in this study. Previously it was indicated that research has shown that the use of organic solvents in biocatalysis, is directed by these values since enzymes with a high activity in hydrophobic solvents, have a log *P* value greater than 4. On the other hand, enzyme activity will be low in hydrophilic solvents with a log *P* value less than 2, where *P* is the octanol/water partition coefficient of a specific organic solvent (Iwuoha *et al.* 1997b:756).

The results in Figure 6.23 indicate that n-hexane showed the lowest inhibiting effect on the enzyme for the 10% water-organic solvent mixtures, as well as for the

5% water-organic solvent mixtures and the pure non-polar organic solvents. In essence, the lowest decrease in catalytic activity of AChE was observed in n-hexane as compared to diethyl ether. Since n-hexane has a log P value of 3.5, which is much higher than the 0.85 for diethyl ether, it is expected that n-hexane will deliver better results and a less inhibiting effect on the enzyme AChE.

Figure 6.24 shows the individual results obtained for the inhibition of AChE in the Au/MBT/PANI/AChE/PVAc biosensor after 20 minutes of incubation in a 10% water-organic solvent mixture.
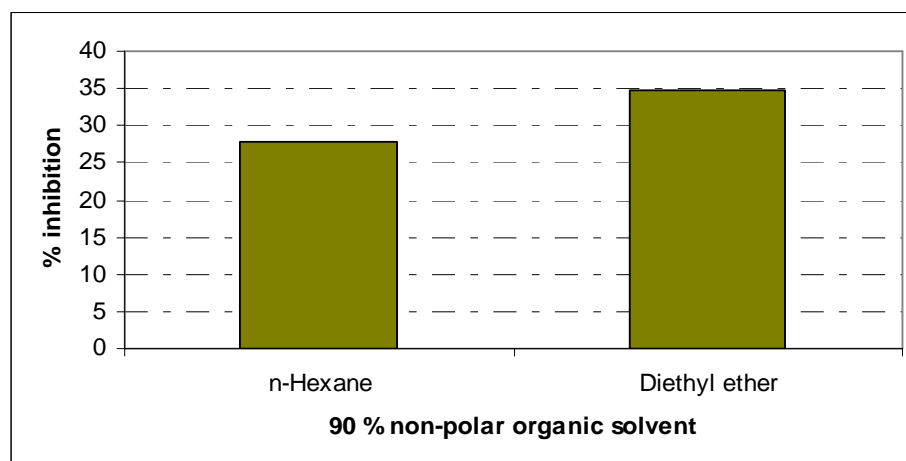
Figure 6.24   **Results obtained for the inhibition of AChE in the Au/MBT/PANI/AChE/PVAc biosensor after 20 minutes of incubation in a 10% water-organic solvent mixture. The ATCh concentration was 2.0 mM.**

Since there was a relatively high amount of water added to the non-polar organic solvents, the results in Figure 6.24 shows that the inhibiting effect of the solvents on

the enzyme AChE was not more than 35% for diethyl ether. *n*-Hexane showed the lowest decrease in the catalytic activity of AChE. When the results for the 10% water-organic solvent mixtures with the least inhibition results are compared, it was found that the 90% acetone-aqueous organic solvent mixture had an inhibition effect of 10%, while the 90% n-hexane-aqueous organic solvent mixture had an inhibition effect of 28%.

In Figure 6.25 the CV responses for the inhibiting effect of a 90% n-hexane-aqueous mixture on the enzyme AChE in the Au/MBT/PANI/AChE/PVAc biosensor is shown. A shorter potential window between 0 and + 1100 mV is shown in order to highlight the effect of the inhibition observed.
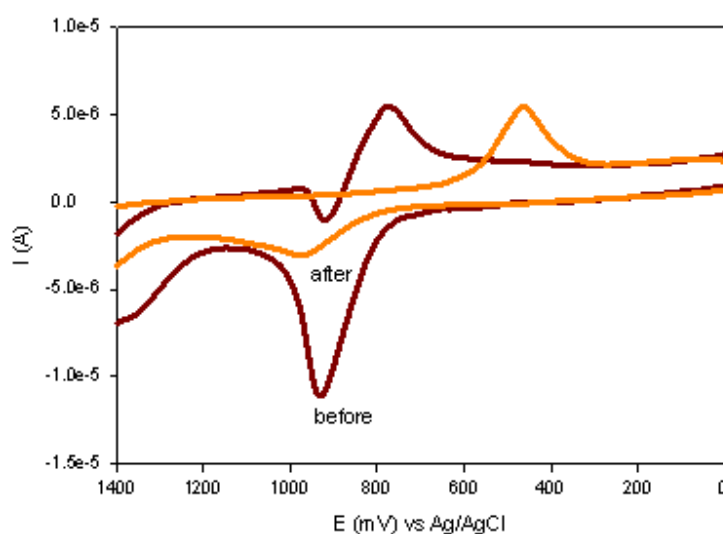
Figure 6.25   **Results for the cyclic voltammetric (CV) response of the Au/MBT/PANI/AChE/PVAc biosensor in a 0.1 M phosphate buffer, KCl (pH 7.2) solution in the presence of 2 mM ATCh, before and after exposure to a 90% n-hexane aqueous-organic solvent mixture.**

For the CV results in Figure 6.25 it was observed that the anodic current obtained at approximately + 938.3 mV (vs. Ag/AgCl) before incubation, has decreased considerably to show a lower anodic current at approximately + 976.2 mV (vs. Ag/AgCl) after incubation. The CV response obtained before the incubation also has a funny dip in the reduction results at + 925.6 mV (vs. Ag/AgCl) that can not be accounted for. Furthermore, the CV results obtained after incubation has shown a reduction peak (at + 446.8 mV (vs. Ag/AgCl)) with a cathodic current that is higher than that of the anodic current, which can be attributed to the effect of the 90 % n-hexane-aqueous organic solvent mixture on the enzyme AChE.

For the differential pulse voltammetric (DPV) responses of the Au/MBT/PANI/AChE/PVAc biosensor shown in Figure 6.26, good redox activity was observed.
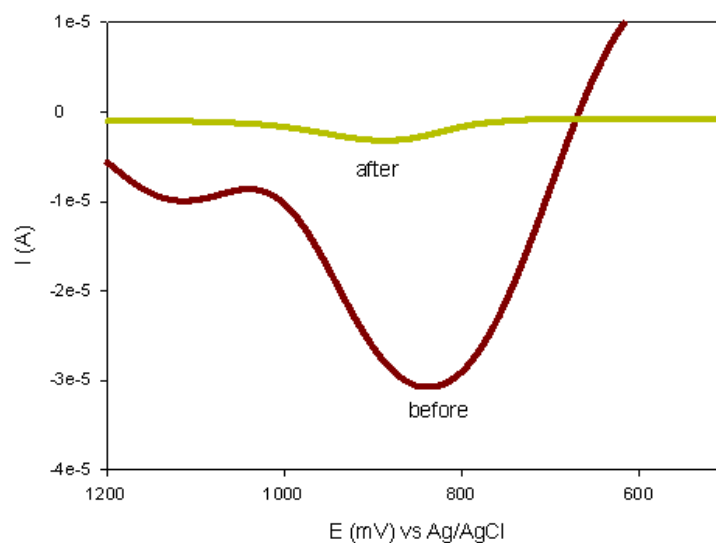
Figure 6.26   **Results for the differential pulse voltammetric (DPV) response of the Au/MBT/PANI/AChE/PVAc biosensor in a 0.1 M phosphate buffer, KCl (pH 7.2) solution in the presence of 2 mM ATCh, before and after exposure to a 90% n-hexane aqueous-organic solvent mixture.**

The DPV responses obtained in the 90% n-hexane-aqueous organic solvent mixture in Figure 6.26 has shown a good anodic peak (E_p = + 836.4 mV (vs. Ag/AgCl)) for the DPV results collected before incubation. A relatively big decrease in anodic current was observed after incubation, which corresponds with the CV results obtained in Figure 6.25. The anodic peak potential was observed after inhibition at approximately + 889.7 mV (vs. Ag/AgCl).

In Figure 6.27 the individual results obtained for the inhibition of AChE in the Au/MBT/PANI/AChE/PVAc biosensor after 20 minutes of incubation in a 5% water-organic solvent mixture is shown.
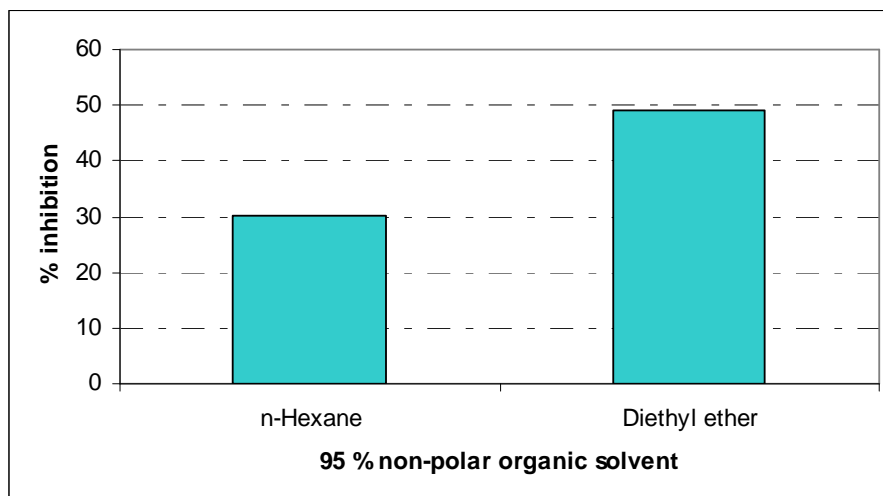
Figure 6.27   **Results obtained for the inhibition of AChE in the Au/MBT/PANI/AChE/PVAc biosensor after 20 minutes of incubation in a 5% water-organic solvent mixture. The ATCh concentration was 2.0 mM.**

The amount of water added to the non-polar solvents was decreased at this stage of the investigation and an increase in inhibition was observed in the 95% water-organic solvent mixtures for n-hexane and diethyl ether. In the case of the 90% water-organic solvent mixtures, the percentage inhibition obtained in n-hexane and diethyl ether was 28% and 35% respectively. The above results in Figure 6.27 indicate a percentage inhibition of 30% and 49% for n-hexane and diethyl ether respectively.

When the CV results for the above analysis are viewed in Figure 6.28, it is observed that good redox behaviour for the biosensor was obtained before incubation, with a relatively huge decrease in redox activity after incubation has occurred. A shorter potential window between + 100 and + 1300 mV is shown in order to highlight the effect of the inhibition observed.
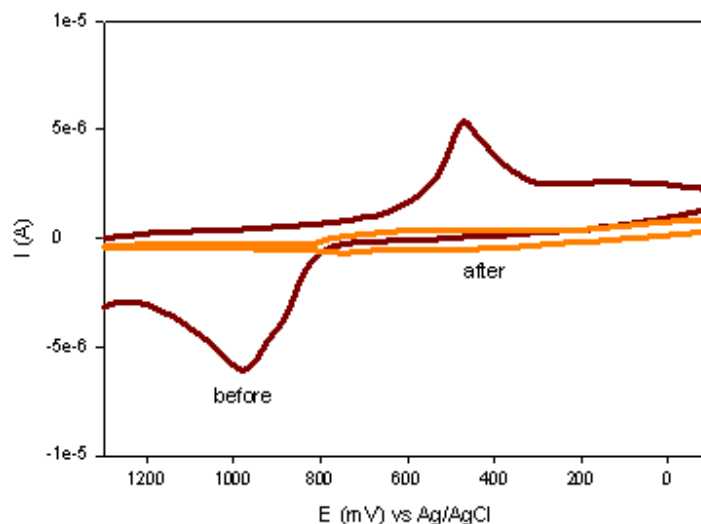
Figure 6.28   **Results for the cyclic voltammetric (CV) response of the Au/MBT/PANI/AChE/PVAc biosensor in a 0.1 M phosphate buffer, KCl (pH 7.2) solution in the presence of 2 mM ATCh, before and after exposure to a 95% n-hexane aqueous-organic solvent mixture.**

The CV results in Figure 6.28 show that prominent redox peaks were observed in the CV obtained for the biosensor before incubation was done. Although a strong reduction peak is seen in the CV results before incubation, the magnitude of the cathodic current (E_p = + 475.6 mV (vs. Ag/AgCl)) is less than that of the anodic current (E_p = + 995.7 mV (vs. Ag/AgCl)) for ATCh used as substrate. The magnitude of the redox peaks observed after incubation in the 95% *n*-hexane aqueous-organic solvent mixture, are considerably smaller when compared to the before incubation results, highlighting the 30% inhibition of the catalytic activity of the enzyme AChE in the biosensor.

When the DPV responses in Figure 6.29 are viewed, it again shows the good redox activity obtained before inhibition, as compared to the decrease in redox activity observed after incubation as was observed in the CV results.
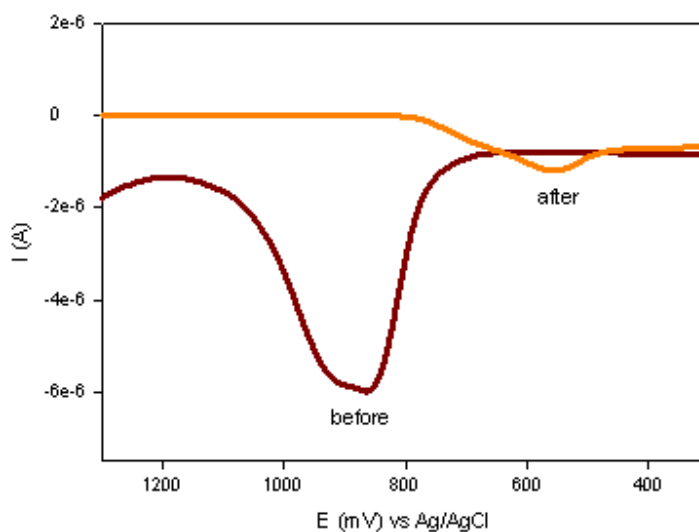
Figure 6.29   **Results for the differential pulse voltammetric (DPV) response of the Au/MBT/PANI/AChE/PVAc biosensor in a 0.1 M phosphate buffer, KCl (pH 7.2) solution in the presence of 2 mM ATCh, before and after exposure to a 95% n-hexane aqueous-organic solvent mixture.**

In Figure 6.29, the anodic current of - 5.997 x 10^{-6} A obtained before incubation at + 852.3 mV (vs. Ag/AgCl), shows the good redox activity obtained that correlates with the CV results in Figure 6.28. After incubation a relatively high decrease in anodic current was observed and an anodic current of - 1.189 x 10^{-6} A at a peak potential of + 569.1 mV (vs. Ag/AgCl) was obtained. The DPV results are consistent with the CV results shown in Figure 6.28.

In Figure 6.30 the individual results obtained for the inhibition of AChE in the Au/MBT/PANI/AChE/PVAc biosensor after 20 minutes of incubation in a pure organic solvent mixture is shown.
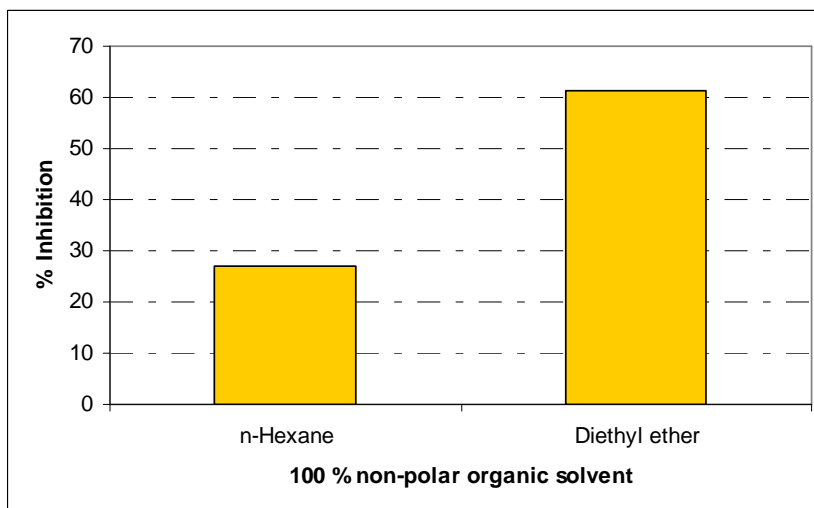
Figure 6.30   **Results obtained for the inhibition of AChE in the Au/MBT/PANI/AChE/PVAc biosensor after 20 minutes of incubation in a pure organic solvent. The ATCh concentration was 2.0 mM.**

The results obtained for the inhibition of the enzyme AChE in pure organic solvent (Figure 6.30) indicates that the lowest percentage inhibition of the enzyme was obtained in pure organic solvent. The percentage inhibition experienced by the enzyme AChE in n-hexane has decreased from 28% in the 90% *n*-hexane-aqueous organic solvent mixture, to 30% in the 95% *n*-hexane-aqueous organic solvent mixture, and finally to 27% in the 100% pure organic solvent. Although the decrease

was relatively small, it is significant indicating that the n-hexane can also be used for pesticide extraction and analysis purposes.

In Figure 6.31 the cyclic voltammetric (CV) results obtained for investigating the effect of a *n*-hexane-aqueous mixture on the enzyme AChE in the Au/MBT/PANI/AChE/PVAc biosensor is shown.
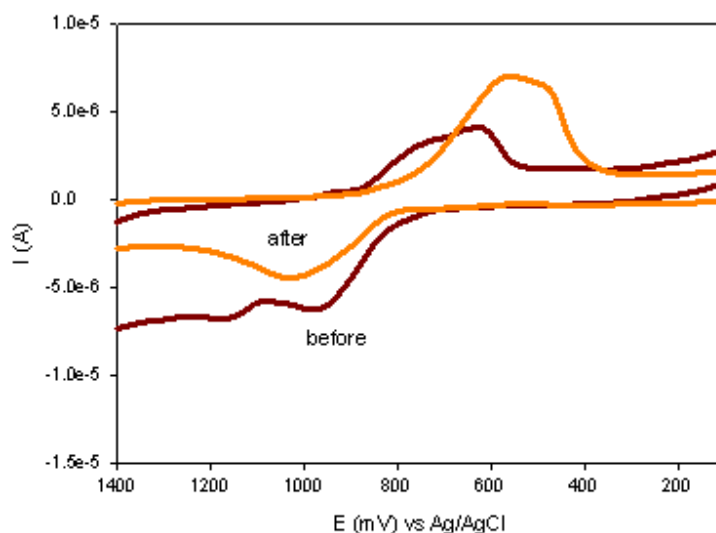
Figure 6.31   **Results for the cyclic voltammetric (CV) response of the Au/MBT/PANI/AChE/PVAc biosensor in a 0.1 M phosphate buffer, KCl (pH 7.2) solution in the presence of 2 mM ATCh, before and after exposure to 100% n-hexane organic solvent.**

The CV results in Figure 6.31 shows that good redox activity was obtained for the Au/MBT/PANI/AChE/PVAc biosensor after it was incubated in the n-hexane pure organic solvent. The CV results obtained before incubation shows a strong anodic peak at approximately + 962.5 mV (vs. Ag/AgCl), while the magnitude of the

cathodic current is smaller than that of the anodic current. A decrease in the anodic current was obtained after incubation in the pure organic solvent, with the cathodic peak bigger than the anodic one for the CV results after incubation. This is again attributed to the effect of the pure organic solvent on the enzyme AChE.

The results collected for the DPV responses are shown in Figure 6.32, indicating that a decrease in anodic current was also obtained for the solvent effect on the enzyme AChE.
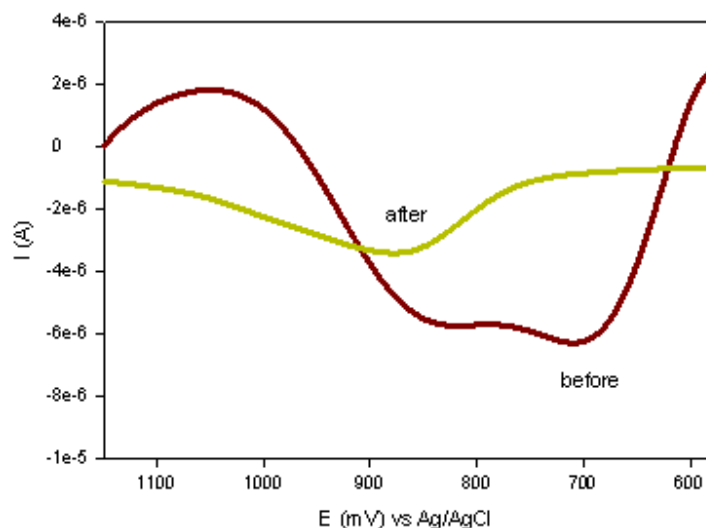
Figure 6.32   **Results for the differential pulse voltammetric (DPV) response of the Au/MBT/PANI/AChE/PVAc biosensor in a 0.1 M phosphate buffer, KCl (pH 7.2) solution in the presence of 2 mM ATCh, before and after exposure to 100% n-hexane organic solvent.**

The DPV results (Figure 6.32) further indicate that a strong anodic peak was obtained at a potential of approximately + 710.5 mV (vs. Ag/AgCl) and that the anodic current

then decreased after incubation to deliver an anodic peak at approximately + 873.8 mV (vs. Ag/AgCl). This decrease in anodic current is consistent with the results observed in the CV responses shown in Figure 6.31.

In summary the results obtained for the percentage inhibition of the enzyme AChE in the different non-polar aqueous-solvent mixtures that were investigated, are shown in Table 6.6.

Table 6.6   **Summary of the results obtained for the percentage inhibition of the enzyme AChE in the different non-polar aqueous-solvent mixtures investigated.**

Non-polar organic solvent	Log P	% Inhibition of enzyme, AChE, in different solvent mixtures		
		90% aqueous-solvent mixture	95% aqueous-solvent mixture	100% pure solvent
n-hexane	3.5	28	30	27
diethyl ether	0.85	35	49	62

The results in Table 6.6 indicate that the *n*-hexane non-polar solvent showed the least inhibitory effect on the electrocatalytic activity of the Au/MBT/PANI/AChE/PVAc biosensor, despite water being present or absent. The percentage inhibition values obtained also shows small differences between the values further indicating the relatively small effect on the activity of AChE by *n*-hexane as solvent. These findings indicate that n-hexane can also be used as solvent for pesticide extraction and analysis purposes.

6.9.2 Nature of non-polar organic solvents

In this paragraph the nature of the non-polar organic solvents were investigated and the relationships between the hydrophobicity, hydrophilicity, dielectric constant or viscosity of the solvents used in the biosensor study are discussed.

The response of the Au/MBT/PANI/AChE/PVAc biosensor was first measured in a 0.1 M phosphate buffer, KCl (pH 7.2) solution, in the presence of a fixed concentration of ATCh. The biosensor was thereafter incubated for 20 minutes in an aqueous-solvent mixture or the pure organic solvent. The response of the Au/MBT/PANI/AChE/PVAc biosensor was then again measured in a 0.1 M phosphate buffer, KCl (pH 7.2) solution, in the presence of a fixed concentration of ATCh.

In Figure 6.33 the results for the calibration curves obtained after successive addition of the substrate ATCh to 0.1 M phosphate buffer, KCl (pH 7.2) solutions before and after incubation of the AChE biosensor in 90% non-polar organic-aqueous solvent mixtures is shown.
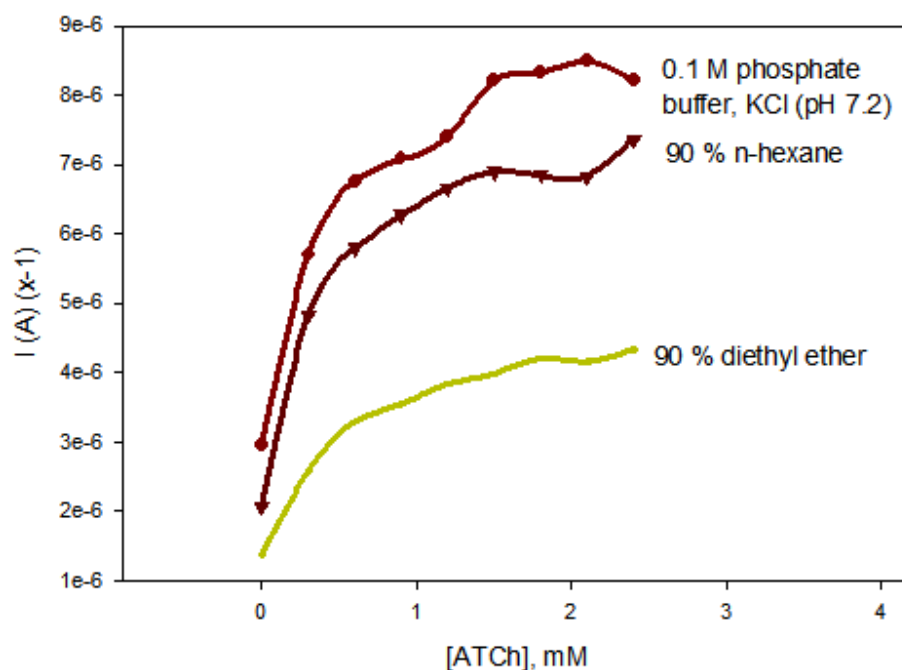
Figure 6.33   **Calibration curves for successive 0.01 M ATCh additions to 0.1 M phosphate buffer, KCl (pH 7.2) solutions before and after incubation of the AChE biosensor in 90% non-polar organic-aqueous solvent mixtures. The ATCh concentration was 2.0 mM.**

Since the log *P* values of the two non-polar organic solvents shown in Figure 6.33 are 3.5 for *n*-hexane and 0.85 for diethyl ether, it is expected that the enzyme activity of the biosensor will be less reactive in diethyl ether which is a hydrophilic solvent. In the case of n-hexane with a log *P* value between 2 and 4, the solvent medium will provide a reaction medium of intermediate enzyme activity (Campanella *et al.* 1998:595; Ruiz *et al.* 2000:229; Iwuoha *et al.* 1997a:57).

The results shown in Figure 6.33 indicate that there was a decrease in the catalytic response of the AChE biosensor after it was incubated in 90% non-polar

organic-aqueous solvent mixtures. The reduction in catalytic activity was of a higher degree when the AChE biosensor was incubated in diethyl ether as compared to *n-*hexane.

In Figure 6.34 the results for the calibration curves obtained after successive addition of the substrate ATCh to 0.1 M phosphate buffer, KCl (pH 7.2) solutions before and after incubation of the AChE biosensor in 95% non-polar organic-aqueous solvent mixtures is shown.
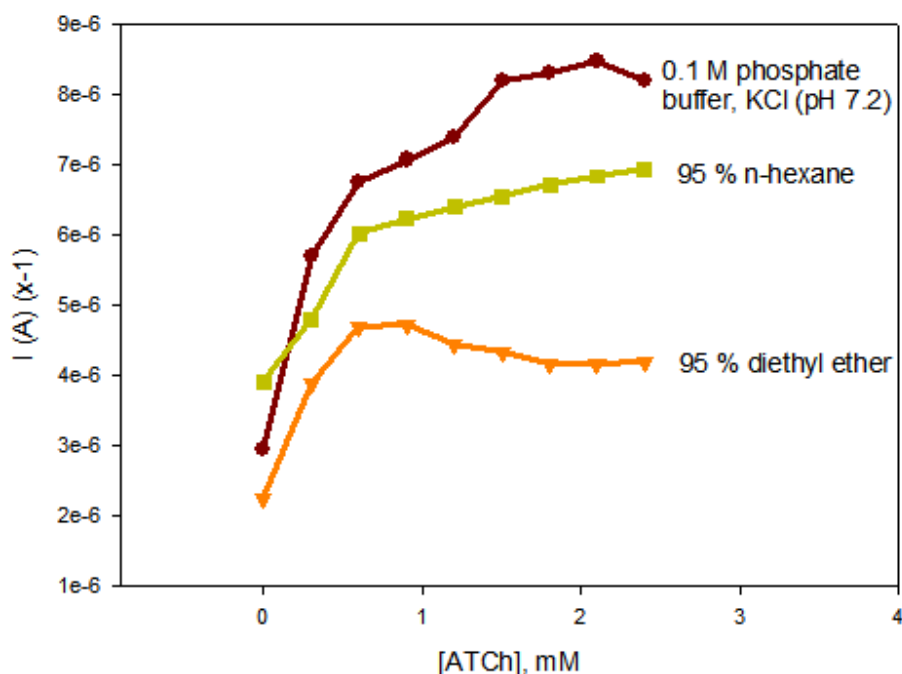
Figure 6.34   **Calibration curves for successive 0.01 M ATCh additions to 0.1 M phosphate buffer, KCl (pH 7.2) solutions before and after incubation of the AChE biosensor in 95% non-polar organic-aqueous solvent mixtures. The ATCh concentration was 2.0 mM.**

The results obtained for the incubation of the AChE biosensor in 95% non-polar organic-aqueous solvent mixtures is shown in Figure 6.34. These results indicate that after incubation a reduction in the catalytic activity of the enzyme AChE was observed, which was higher in diethyl ether as compared to *n*-hexane. Since diethyl ether has a log *P* value of 0.85 that is less than 2, the hydrophilic character of the solvent played a crucial part in the reduction of the enzyme's activity. On the other hand, incubation in *n*-hexane (log *P* = 3.5) had an intermediate effect on the

enzyme's activity and a smaller reduction in the enzyme's catalytic activity as showcased by the above results.

The results for the incubation of the AChE biosensor in 100% pure non-polar organic solvents are shown in Figure 6.35.
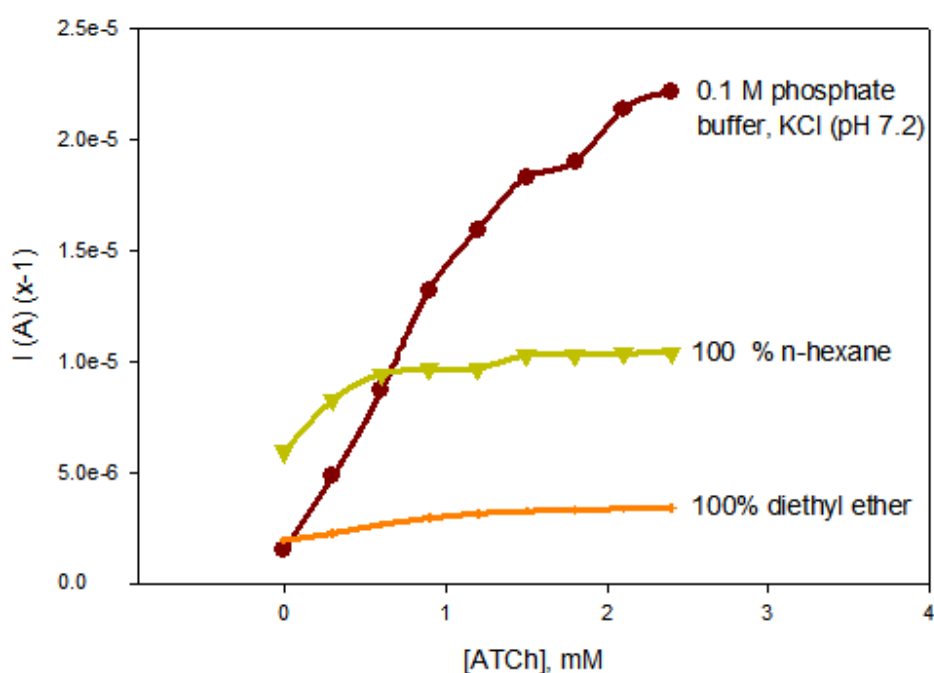
Figure 6.35   **Calibration curves for successive 0.01 M ATCh additions to 0.1 M phosphate buffer, KCl (pH 7.2) solutions before and after incubation of the AChE biosensor in 100% pure non-polar solvent solutions. The ATCh concentration was 2.0 mM.**

The results obtained after the exposure of the AChE biosensor to pure non-polar organic solvents are shown in Figure 6.35. Again the log P values of the two non-polar solvents were a good indicator as to how they would affect the enzyme's

activity after incubation of the AChE biosensor. The reduction in the catalytic activity of the enzyme AChE, was thus higher when it was incubated in diethyl ether, as compared to *n*-hexane and even more drastic when compared to the current response seen in phosphate buffer saline solution.

For the non-polar organic solvents, their log *P*, viscosity and dielectric constants were also compared to investigate its affect on the biosensor's performance. In Table 6.7 the values of log *P*, the viscosity and dielectric constants of the non-polar organic solvents of *n*-hexane and diethyl ether is shown.

Table 6.7   **Physical and chemical properties of selected polar solvents used in this study and the biosensor responses obtained in the specific solvents (Campanella *et al.* 1998:595; Ruiz *et al.* 2000:229)**

Parameters	*n*-Hexane	Diethyl ether
log *P*	3.5	0.85
Dynamic viscosity, v (x 10^{-3} cm^2.s^{-1})	4.66	3.11
Dielectric constant, ε	2.0	4.3

For the dynamic viscosity, it is observed in Table 6.7 that n-hexane has the highest value of the two non-polar solvents, therefore the diffusion of the substrate to the enzyme will be the highest in this solvent. The solvent diethyl ether has the highest dielectric constant and its influence on the catalytic activity of the enzyme will also be the highest. More accurately, diethyl ether will have a higher ability to weaken the electrostatic forces around the enzyme's charged and polar active site.

In Table 6.8 the results for the apparent kinetic characteristics of the Au/MBT/PANI/AChE/PVAc biosensor after incubation in 90% non-polar organic-aqueous solvent mixtures is shown.

Table 6.8   **Results for the apparent kinetic characteristics of the Au/MBT/PANI/AChE/PVAc biosensor after incubation in 90% non-polar organic-aqueous solvent mixtures.**

Parameters	n-Hexane (90%)	Diethyl ether (90%)
Sensitivity (A.M^{-1})	7.74 x 10^{-7}	1.45 x 10^{-6}
K_m^{app} (mM)	5.81	5.09
I_{max} (A)	4.5 x 10^{-6}	7.4 x 10^{-6}

The values obtained for the sensitivity of the biosensor after incubation in the two 90% non-polar organic-aqueous solvent mixtures are shown in Table 6.8. The results indicate that the sensitivity of the biosensor after incubation in diethyl ether is one order of magnitude bigger than after incubation in *n*-hexane. The values obtained for the apparent Michaelis-Menten constant (K_m^{app}) of the biosensor after incubation in the two solvent mixtures are relatively the same. The value of the maximum current (I_{max}) gives an indication of the response of the biosensor at saturation concentration of the substrate, and the above results shows that the values obtained in each of the solvents after incubation, are of the same order of magnitude.

In Table 6.9 the results for the apparent kinetic characteristics of the Au/MBT/PANI/AChE/PVAc biosensor after incubation in 95% non-polar organic-aqueous solvent mixtures is shown.

Table 6.9   **Results for the apparent kinetic characteristics of the Au/MBT/PANI/AChE/PVAc biosensor after incubation in 95% non-polar organic-aqueous solvent mixtures.**

Parameters	n-Hexane (95%)	Diethyl ether (95%)
Sensitivity (A.M^{-1})	2.68×10^{-6}	7.54×10^{-7}
K_m^{app} (mM)	1.79	9.61
I_{max} (A)	4.8×10^{-6}	7.25×10^{-6}

For the results in Table 6.9 it was observed that the sensitivity of the biosensor after incubation in *n*-hexane was one order of magnitude higher than that of diethyl ether. A big difference in the values for the apparent Michaelis-Menten constant (K_m^{app}) was obtained after incubation of the biosensor in the two solvent mixtures with the value of n-hexane being the lowest. The value of the maximum current (I_{max}) obtained for the biosensor response after incubation in each of the above solvents are of the same order of magnitude.

In Table 6.10 the results for the apparent kinetic characteristics of the Au/MBT/PANI/AChE/PVAc biosensor after incubation in 100% pure non-polar organic-aqueous solvent mixtures is shown.

Table 6.10   **Results for the apparent kinetic characteristics of the Au/MBT/PANI/AChE/PVAc biosensor after incubation in 100% non-polar organic solvents.**

Parameters	n-Hexane (100%)	Diethyl ether (100%)
Sensitivity $(A.M^{-1})$	8.25×10^{-7}	9.33×10^{-7}
K_m^{app} (mM)	4.24	11.8
I_{max} (A)	3.5×10^{-6}	1.1×10^{-5}

The results obtained for the response of the biosensor after incubation in the 100% pure non-polar organic solvents are shown in Table 6.10. These results indicate that the sensitivity of the biosensor was of the same order of magnitude after exposure to both solvents. A big difference in the values for the apparent Michaelis-Menten constant (K_m^{app}) was obtained after incubation of the biosensor in the two solvent mixtures with the value of n-hexane being the lowest. The value of the maximum current (I_{max}) obtained for the biosensor response after incubation in each of the above solvents was the highest in diethyl ether and the lowest in n-hexane.

6.10   Organophosphorous Pesticide Detection with Au/MBT/PANI/AChE/PVAc Biosensor

A new biosensor was prepared each time a new organophosphorous pesticide was studied since the pesticides inhibit the enzyme AChE irreversibly (Albareda-

Sirvent *et al.* 2001:35). A new biosensor was prepared for each of the five concentrations of the respective organophosphorous pesticides studied.

6.10.1 Voltammetric results of Au/MBT/PANI/AChE/PVAc biosensor analysis of organophosphates

The differential pulse voltammetric (DPV) responses of the Au/MBT/PANI/AChE/PVAc biosensor for the analysis of standard organophosphate pesticide samples, incubated in acetone-saline phosphate buffer solution, were recorded for each of the five different pesticides investigated.

In Figure 6.36 the DPV responses for the calibration of the Au/MBT/PANI/AChE/PVAc biosensor to 2.4 mM of the substrate ATCh before incubation and the respective responses obtained after incubation in different diazinon pesticide concentrations are shown.
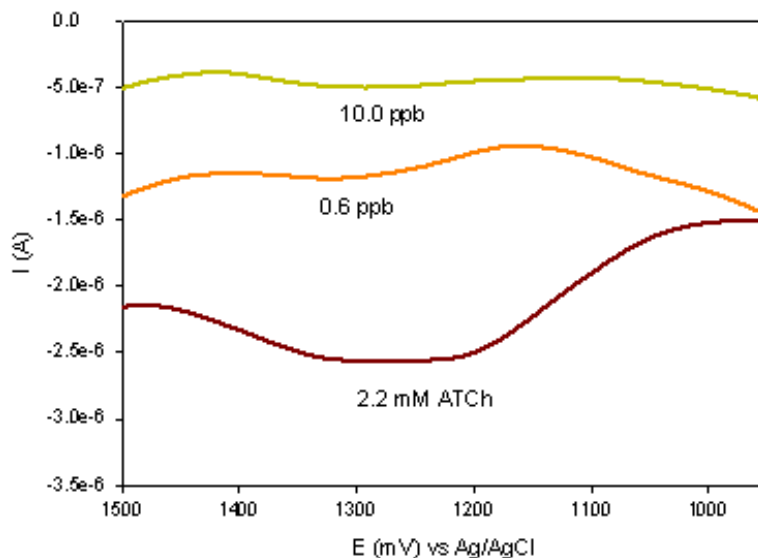
Figure 6.36   **Results for the DPV responses obtained after diazinon pesticide inhibition studies at different concentrations.**

The results in Figure 6.36 indicate that an anodic peak was obtained at approximately + 1275.4 mV (vs. Ag/AgCl) after 2.4 mM of the substrate ATCh was added to the AChE biosensor. After incubation of the biosensor in a 0.6 ppb diazinon standard solution, a decrease in the anodic current was observed when the AChE biosensor was subjected to successive additions of ATCh as substrate. A similar decrease was observed when the AChE biosensor was incubated in a 10.0 ppb diazinon standard solution. The maximum anodic current obtained decreased as the diazinon pesticide concentration was increased.

In Figure 6.37 the DPV responses for the calibration of the Au/MBT/PANI/AChE/PVAc biosensor to 2.4 mM of the substrate ATCh before incubation and the respective responses obtained after incubation in different fenthion pesticide concentrations are shown.

Figure 6.37   Results for the DPV responses obtained after fenthion pesticide inhibition studies at different concentrations.

The results obtained for the inhibition studies of the AChE biosensor performed in fenthion standard pesticide solutions are shown in Figure 6.37. The first result indicates that an anodic peak was obtained at approximately + 1047.8 mV (vs. Ag/AgCl) after 2.4 mM of the substrate ATCh was added to the AChE biosensor. After incubation of the biosensor in different concentrations of standard fenthion pesticide concentrations, it was observed that the anodic peak potentials were

obtained at different potentials after substrate addition to the biosensor. A smaller decrease in anodic current was also obtained for the lowest pesticide concentration, compared to the highest pesticide concentration added, which may be attributed to a higher degree of inhibition by fenthion as pesticide.

In Figure 6.38 the DPV responses for the calibration of the Au/MBT/PANI/AChE/PVAc biosensor to 2.4 mM of the substrate ATCh before incubation and the respective responses obtained after incubation in different parathion-methyl pesticide concentrations are shown.

Figure 6.38   **Results for the DPV responses obtained after parathion-methyl pesticide inhibition studies at different concentrations.**

Figure 6.38 shows the voltammetric results obtained after 2.4 mM of the substrate ATCh was added to the AChE biosensor, as well as for the highest and lowest standard pesticide concentrations used in the biosensor inhibition studies. The results

show that after ATCh addition, an anodic peak was obtained at approximately +

1018.9 mV (vs. Ag/AgCl). After incubation studies in different standard pesticide

concentrations, the anodic peak potentials had shifted to approximately + 910.3 mV

(vs. Ag/AgCl). Furthermore, it was observed that there was a relatively high decrease

in anodic current after incubation in a 0.6 ppb parathion-methyl standard pesticide

solution. This decrease was relatively smaller when the standard pesticide

concentration was increased to 10.0 ppb.

In Figure 6.39 the DPV responses for the calibration of the

Au/MBT/PANI/AChE/PVAc biosensor to 2.4 mM of the substrate ATCh before

incubation and the respective responses obtained after incubation in different

malathion pesticide concentrations are shown.

Figure 6.39   **Results for the DPV responses obtained after malathion pesticide inhibition studies at different concentrations.**

The results in Figure 6.39 indicate that an anodic peak was obtained at approximately + 1378.6 mV (vs. Ag/AgCl) after 2.4 mM of the substrate ATCh was added to the AChE biosensor. A shift in the peak potential values occurred after the biosensor was incubated in the different malathion standard pesticide concentrations and was subjected to ATCh substrate addition afterwards. For malathion as pesticide a relatively bigger decrease in anodic current was observed between the different pesticide concentrations evaluated.

In Figure 6.40 the DPV responses for the calibration of the Au/MBT/PANI/AChE/PVAc biosensor to 2.4 mM of the substrate ATCh before incubation and the respective responses obtained after incubation in different chlorpyrifos pesticide concentrations are shown.

Figure 6.40   **Results for the DPV responses obtained after chlorpyrifos pesticide inhibition studies at different concentrations.**

Figure 6.40 shows the voltammetric results obtained after 2.4 mM of the substrate ATCh was added to the AChE biosensor, as well as for the highest and lowest standard pesticide concentrations used in the biosensor inhibition studies. The voltammetric results further shows anodic peak data around an average peak potential of + 875.9 mV (vs. Ag/AgCl). After incubation studies in different standard pesticide concentrations, the anodic peak current decreased for 0.6 ppb of chlorpyrifos added, with a further decrease in anodic current when the chlorpyrifos concentration was 10.0 ppb.

The voltammetric results obtained for the analysis of the organophosphorous standard pesticide solutions with the Au/MBT/PANI/AChE/PVAc biosensor, indicate for all five different pesticides evaluated that the electrocatalytic activity of the AChE enzyme is reduced as the pesticide concentration is increased.

6.10.2 Inhibition plots for standard samples

Inhibition plots for each of the organophosphorous pesticides detected were obtained using the percentage inhibition method. This involved the biosensor being first placed under a stirred 1 ml of 0.1 M phosphate (0.1M KCl, pH 7.2) solution (anaerobic conditions) and multiple additions of a standard acetylthiocholine (ATCh) substrate solution was added until a stable current and a maximum concentration of 2.4 mM were obtained. This steady state current is related to the activity of the enzyme in the biosensor when no inhibitor was present. This was followed by incubating the biosensor in anaerobic conditions for 20 min with a standard pesticide saline acetone-phosphate buffer mixture. This was followed by multiple additions of a standard ATCh substrate solution (anaerobic conditions), to a fresh 1ml of 0.1 M phosphate (0.1M KCl, pH 7.2) solution (anaerobic conditions) and multiple additions of a standard acetylthiocholine (ATCh) substrate solution was again added, until a stable current was obtained. The maximum concentration of acetylthiocholine (ATCh) was again 2.4 mM. The percentage inhibition was then calculated (Albareda-

Sirvent *et al.* 2000:137; Sotiropoulou and Chaniotakis 2005a:199; Wilkins *et al.* 2000:786):

In Table 6.11 the results calculated for the percentage inhibition of the AChE enzyme after incubation in pesticide solutions are shown.

Table 6.11   **Table of results for the percentage inhibition values obtained at the six different organophosphorous pesticide concentrations investigated with the Au/MBT/PANI/AChE/PVAc biosensor.**

- log [pesticide]	% I$_{diazinon}$	% I$_{fenthion}$	% I$_{parathion-methyl}$	% I$_{malathion}$	% I$_{chlorpyrifos}$
0.222	36.15	18.07	14.40	31.96	43.42
0.000	41.80	25.30	22.18	41.55	51.71
-0.301	57.00	36.09	34.10	59.10	60.00
-0.699	60.84	48.16	55.93	67.43	67.49
-0.845	66.37	59.97	67.21	71.65	72.05
-1.000	78.59	67.70	81.64	75.59	78.61

From the results in Table 6.11 it can be seen that for the six different organophosphorous pesticides investigated with the Au/MBT/PANI/AChE/PVAc biosensor, an increase in the percentage inhibition was observed as the concentration of the standard pesticide solutions were increased. At a pesticide concentration of 0.6 ppb used, the lowest percentage inhibition was obtained with parathion-methyl as pesticide, while with the same concentration of pesticide used, the highest percentage inhibition was obtained with chlorpyrifos as pesticide. When 10.0 ppb of pesticide concentration was used, the lowest percentage inhibition was obtained with fenthion as pesticide, compared to the highest percentage inhibition obtained with parathion-methyl as pesticide. The above results shown in Table 6.11 were then used to

construct graphs of percentage inhibition vs. – log [pesticide] that is shown in Figure 6.41.
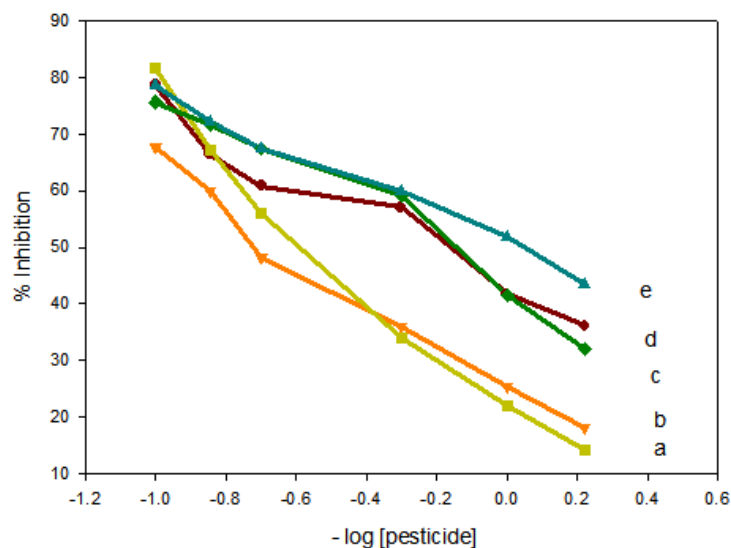
Figure 6.41   **Graph of percentage inhibition vs. – log [pesticide] for all the different organophosphorous pesticides investigated with the Au/MBT/PANI/AChE/PVAc biosensor.**

The results in Figure 6.41 show the combined plot for the percentage inhibition vs. – log [pesticide] results for the six different organophosphorous standard pesticide solutions investigated. The graph in (a) represents the results for parathion-methyl, in (b) fenthion, in (c) malathion, in (d) diazinon and in (e) chlorpyrifos.

The results further indicate that the effect of the pesticides called parathion-methyl and fenthion on the AChE biosensor response are relatively similar, since the results for the inhibition plots of these two pesticides are close. Next it is observed in Figure

6.41 that the results for the inhibition plots of malathion, diazinon and chlorpyrifos

can be grouped together, since their inhibition plots falls close to each other. Further

analyses of the inhibition plots were done and the results are shown in Table 6.12.

Table 6.12   Results for the different parameters calculated from the inhibition plots of the Au/MBT/PANI/AChE/PVAc biosensor detection of standard organophosphorous pesticide solutions ($n = 2$).

Organophosphorous pesticides					
Pesticide	Sensitivity (%I/decade)	Detection limit (ppb)	Detection limit (ppt)	Detection limit (nM)	Regression coefficient
Diazinon	-31.25	0.0147	41.7	0.137	0.9461
Fenthion	-39.55	0.230	230.0	0.826	0.9810
parathion-methyl	-53.66	0.388	388.0	1.332	0.9766
Malathion	-35.24	0.0623	62.3	0.189	0.9679
Chlorpyrifos	-26.68	0.0127	12.7	0.018	0.9875

The results in Table 6.12 shows the parameters calculated from the inhibition plots of

the Au/MBT/PANI/AChE/PVAc biosensor for the detection of standard

organophosphorous pesticide solutions. These parameters include the sensitivity and

the detection limit estimated from the inhibition plots. The lowest sensitivity was

obtained for chlorpyrifos as pesticide, while the highest sensitivity was obtained for

parathion-methyl as pesticide. Furthermore, the sensitivity of three of the pesticides,

i.e. diazinon, fenthion and malathion fall within the same range. Chlorpyrifos

represents a more powerful organophosphate than the rest of the four pesticides

studied (due to the three chlorine atoms substituted in its pyridine ring structure) and

with the constructed Au/MBT/PANI/AChE/PVAc biosensor, a very good sensitivity

was obtained. For parathion-methyl as pesticide the highest sensitivity was obtained for this study, which is also higher than the 48% sensitivity reported by Lin *et al.* (2004:149) obtained with a disposable carbon nanotube modified screen-printed biosensor.

6.10.2.1 Determination of standard organophosphorous pesticide concentrations at nanomolar levels

The direct detection of pesticides has been the driving force of intense scientific and industrial research, since the organophosphates and carbamates are used extensively in agricultural processes such as crop an animal protection, storage of products, and in stables and homes for pest control. It is for this reason that enzyme-based biosensors have emerged as one of the most promising technologies for the direct monitoring of organophosphates and carbamates (Sotiropoulou and Chanitakis 2005a:199). Several researchers (Mulchandani *et al.* 2001:225; Sacks *et al.* 2000:2055; Rekha *et al.* 2000:499; Neufeld *et al.* 2000:323) have reported that systems that seem to offer the highest sensitivity are the biosensors that are based on the inhibition of cholinesterases. These biosensors also have their shortcomings, which include the lack of a sensitive detection limit since the lowest detection limit reported in literature until now is 10^{-9} M for the detection of organophosphates (Sotiropoulou and Chanitakis 2005a:199; Bachman and Schmid 1999:95; Jeanty *et al.* 2001:119).

The results in Table 6.12 show very good detection limits for the standard samples of the five organophosphates investigated with the Au/MBT/PANI/AChE/PVAc biosensor. When the results for the detection limits shown in nanomolar concentrations are viewed, several interesting findings were obtained. These include the lowest nanomolar detection limit for chlorpyrifos of 0.018 nM and the higher of 1.332 nM for parathion-methyl. Lin *et al.* (2004:149) reported a detection limit of 0.05 μM parathion-methyl with a disposable carbon nanotube modified screen-printed biosensor, which is higher than the detection limit obtained in this study. The results in Table 6.12 also reports detection limits of 0.137 and 0.826 nM for diazinon and fenthion respectively. Wilkins *et al.* (2000:790) reported detection limits for diazinon and fenthion of 0.8 and 1.0 μM respectively, collected with an amperometric AChE biosensor based on the thiocholine-hexacyanoferrate reaction.

6.11   Carbamate Pesticide Detection with Au/MBT/PANI/AChE/PVAc Biosensor

A new biosensor was prepared each time a new carbamate pesticide was studied since the pesticides inhibit the enzyme AChE irreversibly (Albareda-Sirvent *et al.* 2001:35). A new biosensor was also prepared for each of the five concentrations of the respective carbamate pesticides studied.

6.11.1 Voltammetric results of Au/MBT/PANI/AChE/PVAc biosensor analysis of carbamates

Similarly, the DPV responses of the Au/MBT/PANI/AChE/PVAc biosensor for the analysis of standard carbamate pesticide samples, incubated in acetone-saline phosphate buffer solution, were also recorded for each of the five different pesticides investigated.

The DPV responses for the calibration of the Au/MBT/PANI/AChE/PVAc biosensor to 2.4 mM of the substrate ATCh before incubation and the respective responses obtained after incubation in different dioxacarb pesticide concentrations are shown in Figure 6.42.
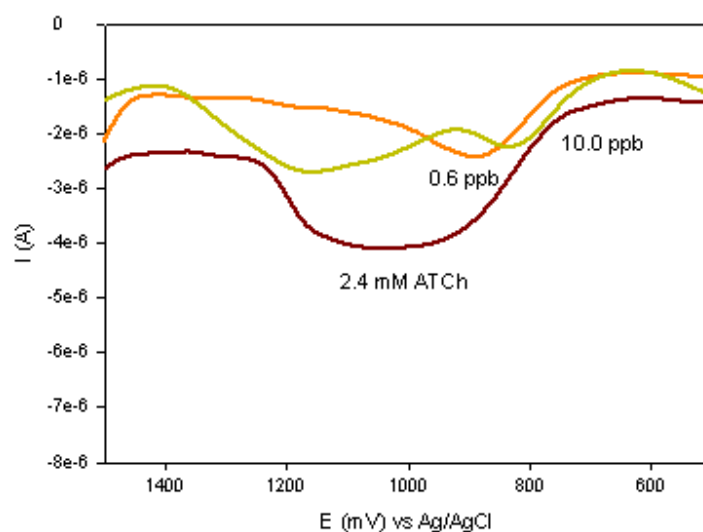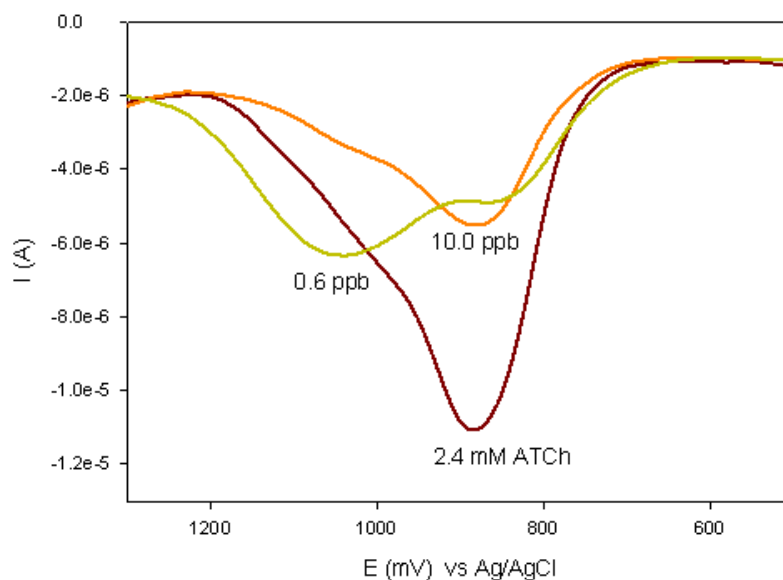
Figure 6.42   **Results for the DPV responses obtained after dioxacarb pesticide inhibition studies at different concentrations.**

The results obtained for the inhibition studies of the AChE biosensor performed in dioxacarb standard pesticide solutions are shown in Figure 6.42. The first result indicates that an anodic peak was obtained at approximately + 892.7 mV (vs. Ag/AgCl) after 2.4 mM of the substrate ATCh was added to the AChE biosensor. After incubation studies in the lowest standard pesticide concentration, the anodic peak potential had shifted to approximately + 1051.9 mV (vs. Ag/AgCl). Furthermore, it was observed that there was a relatively high decrease in anodic current after incubation in a 0.6 ppb dioxacarb standard pesticide solution. A similar

decrease in anodic current was observed when the standard pesticide concentration was increased to 10.0 ppb.

The DPV responses for the calibration of the Au/MBT/PANI/AChE/PVAc biosensor to 2.4 mM of the substrate ATCh before incubation and the respective responses obtained after incubation in different aldicarb pesticide concentrations are shown in Figure 6.43.
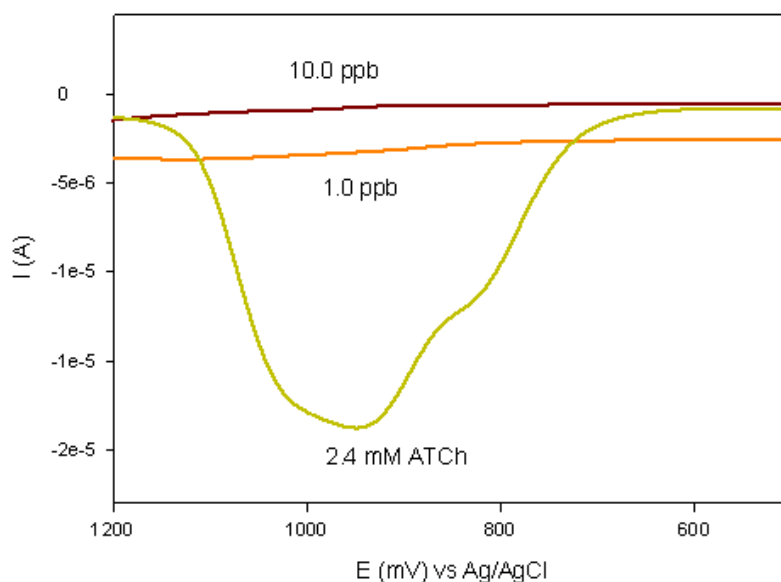
Figure 6.43   **Results for the DPV responses obtained after aldicarb pesticide inhibition studies at different concentrations.**
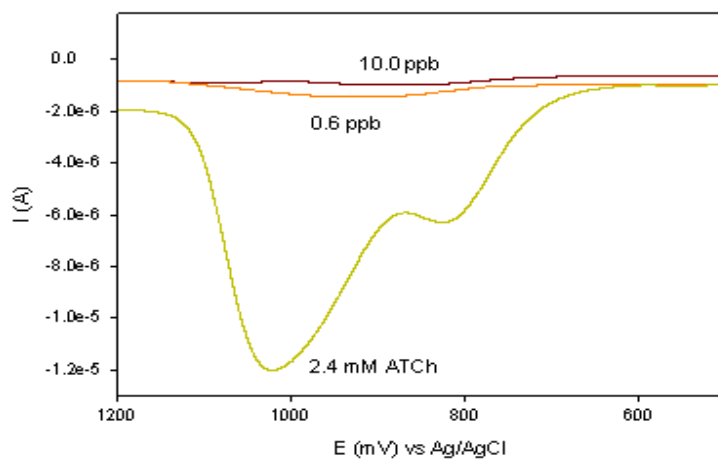
Figure 6.43 shows the voltammetric results obtained after 2.4 mM of the substrate ATCh was added to the AChE biosensor, as well as for the highest and lowest aldicarb standard pesticide concentrations used in the biosensor inhibition studies. A

strong anodic peak was obtained at a potential of approximately + 955.2 mV (vs. Ag/AgCl) when 2.4 mM of the susbtrate was added before incubation in a pesticide standard solution. After incubation of the AChE biosensor in 1.0 ppb aldicarb standard solution, a relatively high decrease in anodic current was observed. At a higher aldicarb standard pesticide concentration of 10.0 ppb, a further decrease in the anodic current was observed after incubation, when compared to the results obtained in phosphate buffer saline solution with 2.4 mM of ATCh added.

The DPV responses for the calibration of the Au/MBT/PANI/AChE/PVAc biosensor to 2.4 mM of the substrate ATCh before incubation and the respective responses obtained after incubation in different carbaryl pesticide concentrations are shown in Figure 6.44.
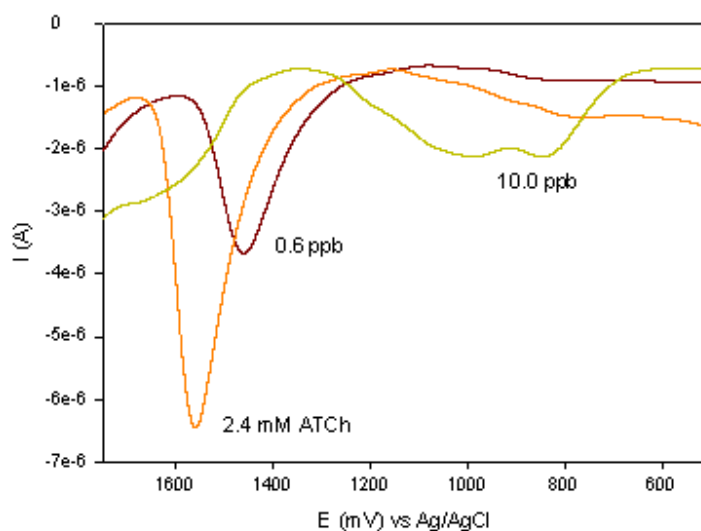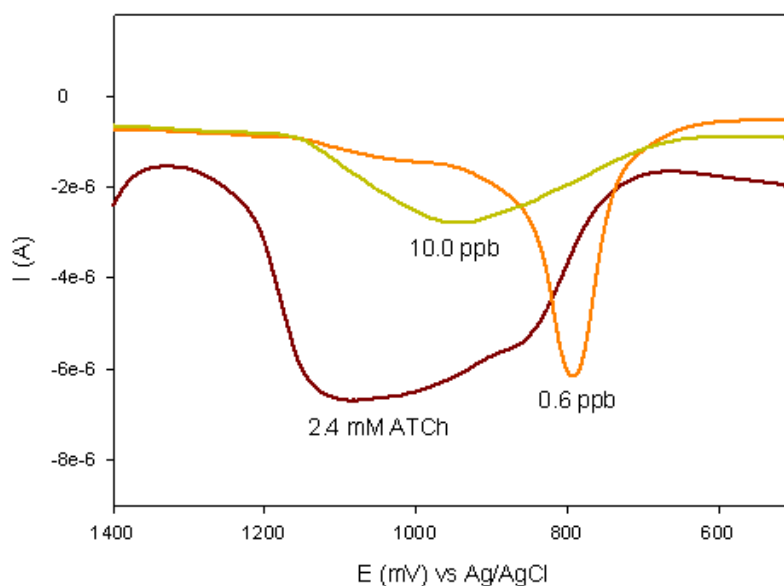
Figure 6.44   **Results for the DPV responses obtained after carbaryl pesticide inhibition studies at different concentrations.**

The results obtained for the inhibition studies of the AChE biosensor performed in carbaryl standard pesticide solutions are shown in Figure 6.44. The first result indicates that an anodic peak was obtained at approximately + 1097.6 mV (vs. Ag/AgCl) after 2.4 mM of the substrate ATCh was added to the AChE biosensor. After incubation of the biosensor in different concentrations of standard carbaryl pesticide concentrations, it was observed that the anodic peak potentials were obtained at different potentials after substrate addition to the biosensor. A relatively small decrease in anodic current was obtained after incubation of the biosensor in 0.6 ppb standard pesticide solution. A relatively bigger decrease in anodic current was obtained after the biosensor was incubated in 10.0 ppb standard pesticide solution.

The DPV responses for the calibration of the Au/MBT/PANI/AChE/PVAc biosensor to 2.4 mM of the substrate ATCh before incubation and the respective responses obtained after incubation in different carbofuran pesticide concentrations are shown in Figure 6.45.
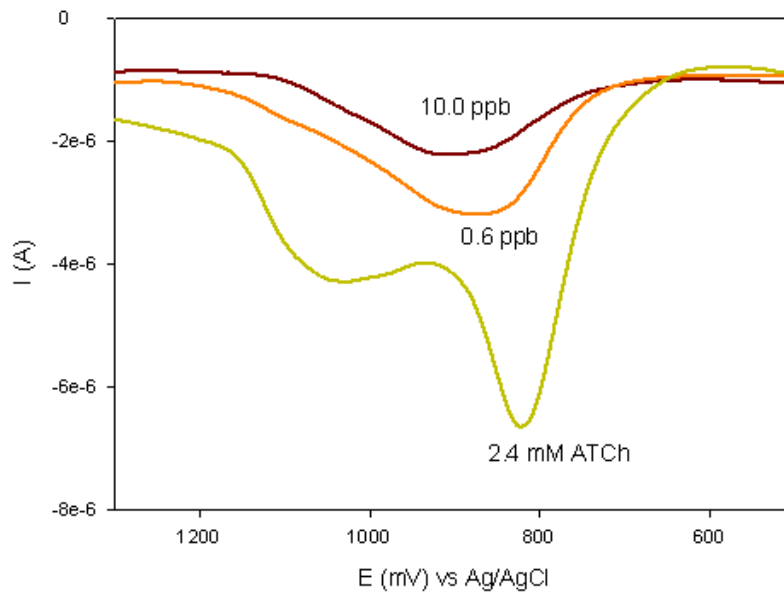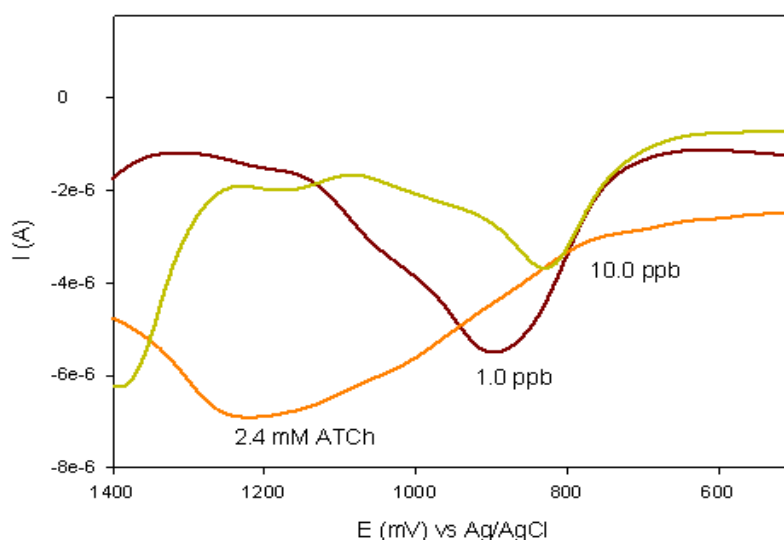

Figure 6.45   Results for the DPV responses obtained after carbofuran pesticide inhibition studies at different concentrations.

The results in Figure 6.45 indicate that an anodic peak was obtained at approximately + 1238.6 mV (vs. Ag/AgCl) after 2.4 mM of the substrate ATCh was added to the AChE biosensor. After incubation of the biosensor in different concentrations of standard carbofuran pesticide concentrations, it was observed that the anodic peak potentials were obtained at different potentials after substrate addition to the

biosensor. A good decrease in anodic current was observed after the biosensor was incubated in 1.0 ppb of standard pesticide solution, while a further decrease was observed for the highest concentration of standard pesticide solution used.

The DPV responses for the calibration of the Au/MBT/PANI/AChE/PVAc biosensor to 2.4 mM of the substrate ATCh before incubation and the respective responses obtained after incubation in different methomyl pesticide concentrations are shown in Figure 6.46.
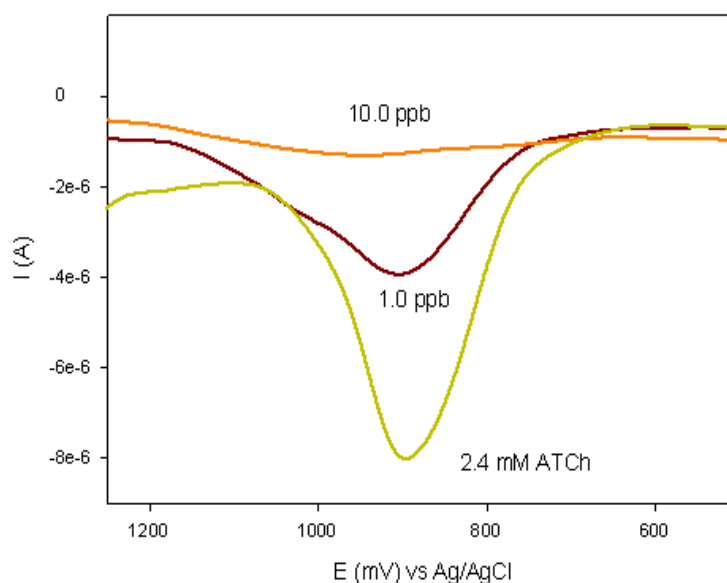
Figure 6.46   **Results for the DPV responses obtained after methomyl pesticide
                        inhibition studies at different concentrations.**

Figure 6.46 shows the voltammetric results obtained after 2.4 mM of the substrate ATCh was added to the AChE biosensor, as well as for the highest and lowest

standard pesticide concentrations used in the biosensor inhibition studies. The voltammetric results showed anodic peak potentials around a specific value of approximately + 902.8 mV (vs. Ag/AgCl) and a good decrease in the anodic current were obtained after incubation of the biosensor in standard pesticide solutions. The decrease in anodic peak current represents a good set of data showing the inhibitory effect of the methomyl standard pesticide solutions on the catalytic effect of AChE, when substrate solutions of ATCh was added after incubation.

The voltammetric results obtained for the analysis of the carbamate standard pesticide solutions with the Au/MBT/PANI/AChE/PVAc biosensor, indicate for all five different pesticides evaluated that the electrocatalytic activity of the AChE enzyme is reduced as the pesticide concentration is increased.

6.11.2 Inhibition plots for standard samples

Inhibition plots for each of the carbamate pesticides detected were obtained using the percentage inhibition method. This involved the biosensor being first placed in a stirred 1 ml of 0.1 M phosphate (0.1M KCl, pH 7.2) solution (anaerobic conditions) and multiple additions of a standard acetylthiocholine (ATCh) substrate solution was added until a stable current and a maximum concentration of 2.4 mM were obtained. This steady state current is related to the activity of the enzyme in the biosensor when no inhibitor was present. This was followed by incubating the

biosensor in anaerobic conditions for 20 min with a standard pesticide saline acetone-phosphate buffer mixture. This was followed by multiple additions of a standard ATCh substrate solution (anaerobic conditions), to a fresh 1ml of 0.1 M phosphate (0.1M KCl, pH 7.2) solution (anaerobic conditions) and multiple additions of a standard acetylthiocholine (ATCh) substrate solution was again added, until a stable current was obtained. The maximum concentration of acetylthiocholine (ATCh) was again 2.4 mM. The percentage inhibition was then calculated (Albareda-Sirvent *et al.* 2000:137; Sotiropoulou and Chaniotakis 2005a:199; Wilkins *et al.* 2000:786):

In Table 6.13 the results calculated for the percentage inhibition of the AChE enzyme after incubation in pesticide solutions are shown.

Table 6.13   **Table of results for the percentage inhibition values obtained at the six different carbamate pesticide concentrations investigated with the Au/MBT/PANI/AChE/PVAc biosensor.**

- log [pesticide]	% $I_{dioxacarb}$	% $I_{aldicarb}$	% $I_{carbaryl}$	% $I_{carbofuran}$	% $I_{methomyl}$
0.222	10.09	22.09	13.67	37.85	31.08
0.000	14.50	30.63	16.08	42.13	37.38
-0.301	23.52	40.71	21.27	45.44	46.02
-0.699	36.58	52.67	28.69	65.53	48.24
-0.845	46.70	67.18	35.51	71.04	52.84
-1.000	49.82	76.26	41.14	76.62	60.53

Table 6.13 shows the results for the six different carbamate pesticides investigated with the Au/MBT/PANI/AChE/PVAc biosensor. From these results it can be observed that an increase in the percentage inhibition was observed as the concentration of the standard pesticide solutions were increased. At a concentration

of 0.6 ppb used, the results showed the lowest percentage inhibition for dioxacarb as

pesticide. On the other hand, for the highest concentration of 10.0 ppb of pesticide

used, the highest percentage inhibition was obtained for aldicarb and carbofuran as

pesticides. The results in Table 6.13 were the used to plot graphs of percentage

inhibition vs. – log [pesticide] that is shown in Figure 6.47.
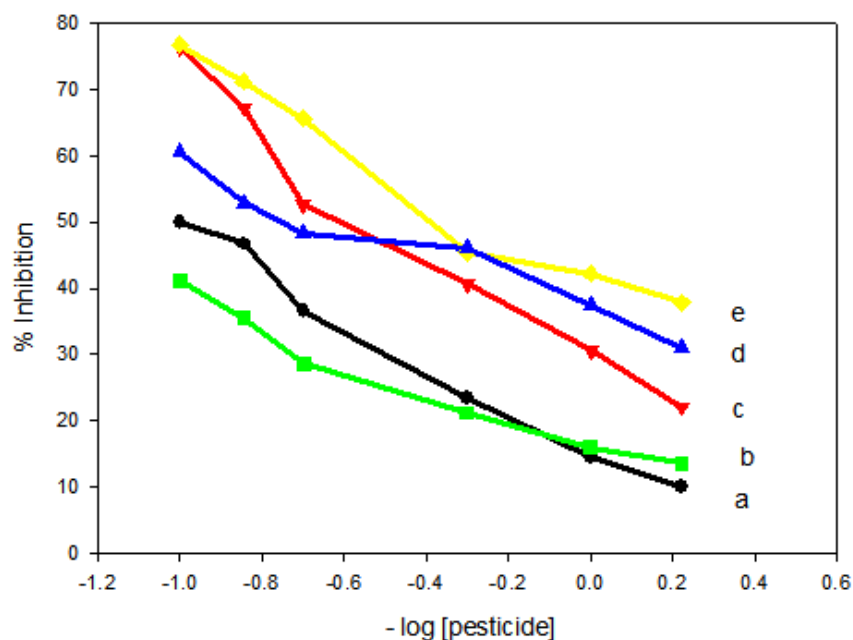
Figure 6.47   **Graph of percentage inhibition vs. – log [pesticide] for all the different
carbamate pesticides investigated with the
Au/MBT/PANI/AChE/PVAc biosensor.**

The results in Figure 6.47 show the combined plot for the percentage inhibition vs. –

log [pesticide] for the six different carbamate standard pesticide solutions

investigated. The different results showcased in the graph are that of dioxacarb in (a),

carbaryl in (b), aldicarb in (c), methomyl in (d) and carbofuran in (e). From the results it is also evident that the effects of the pesticides called dioxacarb and carbaryl on the AChE biosensor response are relatively similar, since the results for the inhibition plots are very close at low pesticide concentrations. In the case of the other three pesticides called aldicarb, methomyl and carbofuran, the results in Figure 6.47 shows that the effects of these three pesticides on the AChE biosensor response are relatively similar.

In Table 6.14 the results calculated for the percentage inhibition of the AChE enzyme after incubation in pesticide solutions are shown.

Table 6.14   **Results for the different parameters calculated from the inhibition plots of the Au/MBT/PANI/AChE/PVAc biosensor detection of standard carbamate pesticide solutions ($n = 2$).**

Carbamate pesticides					
Pesticide	**Sensitivity (%l/decade)**	**Detection limit (ppb)**	**Detection limit (ppt)**	**Detection limit (nM)**	**Regression coefficient**
dioxacarb	-33.84	0.351	351.0	1.572	0.9830
aldicarb	-42.33	0.230	230.0	1.209	0.9676
carbaryl	-21.92	0.177	177.0	0.880	0.9581
carbofuran	-33.20	0.055	55.0	0.249	0.9590
methomyl	-21.04	0.018	18.0	0.111	0.94552

Table 6.14 shows the results for the different parameters calculated from the inhibition plots of the Au/MBT/PANI/AChE/PVAc biosensor for the detection of standard carbamate pesticide solutions. These include the data for the sensitivity and the detection limits estimated from the inhibition plots. Analysis of the data for the

five different pesticides shows that methomyl and carbaryl have the lowest sensitivity, while aldicarb has the highest sensitivity. When the results of the organophosphates in Table 6.12 are compared to that of the carbamates in Table 6.14, it was observed that with the Au/MBT/PANI/AChE/PVAc biosensor, the lowest sensitivity was obtained for carbamates. This value is 21.04% for methomyl as pesticide. When the sensitivity of carbofuran is reviewed a value of 33.30 % was obtained that is much higher than the value of 7.73% obtained by Albareda-Sirvent *et al.* (2001:41), which have used a graphite-epoxy screen-printed thick film biosensor for the detection of pesticides.

6.11.2.1   Determination of standard organophosphorous pesticide concentrations at nanomolar levels

When the detection limits obtained for the carbamates with the Au/MBT/PANI/AChE/PVAc biosensor in Table 6.14 are viewed, it is observed that an increasing trend in the nanomolar concentration was obtained. The lowest detection limit of 0.111 mM was obtained for methomyl, while the highest detection limit of 1.572 mM was obtained for dioxacarb. In the case of carbofuran, a detection limit of 0.249 nM was obtained with the AChE biosensor, while Albareda-Sirvent *et al.* (2001:41) have reported a detection limit of 0.212 nM for carbofuran. These two values are within the same range. In a study done by Nunes *et al.* (1999:37) a highly sensitive amperometric biosensor consisting of carbon paste modified with cobalt(II) phthalocyanine and acetylcellulose was constructed for the determination of trace

carbamates in fruit, vegetables and water samples. In this study Nunes *et al.* (1999:44-45) have reported detection limits[ξ] of 52.558 nM for aldicarb, 2.485 nM for carbaryl, 0.452 nM for carbofuran and 0.308 nM for methomyl. In this study lower detection limits for these four carbamates have been obtained, which are 1.209 nM for aldicarb, 0.880 nM for carbaryl, 0.249 for carbofuran and 0.111 nM for methomyl. These results show that the thick film Au/MBT/PANI/AChE/PVAc biosensor is more sensitive than the biosensor constructed by Nunes *et al.* (2000:37).

Analysis of the results in sections 6.10.2.1 and 6.11.2.1, shows that an amperometric AChE-biosensor with improved detection limits for organophosphorous and carbamate pesticides has been obtained. The novel use of mercaptobenzothiazole (MBT) as a self-assembled monolayer (SAM) in the construction of the Au/MBT/PANI/AChE/PVAc biosensor, has proved to be useful in delivering a biosensor with high sensitivity and good reproducibility.

[ξ] Nunes *et al.* (1999). Analytica Chimica Acta, 399:45. Reported results converted from $\mu g.L^{-1}$ to nM values.

CHAPTER 7

Summary and Conclusions

7.1 Introduction

In this chapter the results from the work presented in this dissertation is summarised. The main objective proposed at the beginning of this dissertation, *i.e. to expand the current existing knowledge base for both the physical and chemical properties of organic phase amperometric biosensors for the detection of organophosphorous and carbamate pesticides in organic solvents, is re-examined.* A summary of each individual chapter is given to recap the main and important findings and conclusions for that chapter. Recommendations are made for the path of future work, and the overall significance of the study is discussed.

7.2   Summary of Individual Chapters

7.2.1 Chapter 1

In this chapter the theme of this dissertation, which focused on the development and characterisation of a suitable organic phase amperometric biosensor for the detection of organophosphorous and carbamate pesticides in organic solvents, have been introduced. It further provided a brief description of the different elements of this dissertation and a discussion of the motivation, aims and objectives, and the layout of the dissertation.

7.2.2 Chapter 2

In chapter 2 a description was first given of what a biosensor or chemical sensor is followed by a description of the different components of a biosensor. This was followed by a description of the evolvement of different generations of biosensors and a review of the literature surrounding the sciences and differentiation of biosensors. Next the rationale behind the use and construction of organic phase enzyme electrodes and the different elements of biosensors for inhibitor determination was discussed. This was followed by a discussion of the concept of thick-film biosensors and the voltammetric techniques used in the characterisation of biosensors (or sensors in general).

The rest of the literature review focussed on the different areas of interest in this study, which involved:

(i)   the use and function of self-assembled monolayers,

(ii)   the structure, synthesis and application of conducting polymers,

(iii)   the structure, catalytic activity and use of the enzyme acetylcholinesterase (AChE) in biosensors for pesticide detection,

(iv)   the physical and chemical properties of the organophosphorous and carbamate pesticides.

7.2.3 Chapter 3

Chapter 3 gave a concise description of the sample and experimental procedures used for the preparation and cleaning of the gold electrode, and the formation of a self-assembled monolayer (SAM) of mercaptobenzathiole (MBT) on the gold electrode. This was followed by a description of the *in situ* electropolymerisation procedures for the coating of unsubstituted and substituted polyanilines (PANIs) on the Au/MBT electrode. The next step involved the immobilisation of the enzyme acetylcholinesterase (AChE) into the polymer matrix and the coating of poly(vinyl acetate) in order to have a thick-film AChE biosensor, which was ready to use for the detection of standard solutions of organophosphorous and carbamate pesticides. A description of the electrochemical characterisation of the

biosensor was provided, which included techniques such as cyclic voltammetry, Osteryoung square wave voltammetry and differential pulse voltammetric techniques.

7.2.4 Chapter 4

In chapter 4 the results for the assembling and optimisation of the substituted (and unsubstituted) polyaniline-based acetylcholinesterase biosensors prepared on gold thiol-modified electrodes were presented and discussed. This involved the discussion of the results obtained for the assembling and characterisation of the:

(vi)   self-assembled monolayer of mercaptobenzothiazole assembled on a gold electrode,

(vii)   electropolymerisation of (un)substituted polyanilines on the gold thiol-modified electrode,

(viii)   substituted polyaniline-acetylcholinesterase bioelectrodes and corresponding biosensors,

(ix)   unsubstituted polyaniline-acetylcholinesterase bioelectrode and corresponding biosensor,

(x)   electrochemical measurements made using the AChE-biosensors in the presence of acetylcholine and acetylthiocholine as substrates.

7.2.5 Chapter 5

In chapter 5 it was demonstrated that the technique of applying a self-assembled monolayer (SAM) of mercaptobenzothiazole (MBT), can be used for pre-organisation on a gold (Au) electrode to allow subsequent polymerisation of a poly(*o*-methoxyaniline) plus poly(*4*-styrene sulphonic acid) [POMA-PSSA] and poly(*2,5*-dimethoxyaniline) plus poly(*4*-styrene sulphonic acid) [PDMA-PSSA] polymer films respectively. It was further shown that the Au/MBT/POMA-PSSA/AChE and Au/MBT/PDMA-PSSA/AChE thick-film biosensor configurations was successfully constructed as the characterisation results of the voltammetric studies, showed results for increases in the anodic peak potentials when the substrate acetylcholine (ACh) was added to the biosensor. In this manner the novel technique of using a SAM of mercaptobenzothiazole (MBT) was applied in the construction of a thick-film amperometric biosensor for pesticide evaluation. In addition, biosensor reaction mechanisms for the Au/MBT/POMA-PSSA/AChE and Au/MBT/PDMA-PSSA/AChE biosensors were proposed and the biosensors then applied to successfully detect standard organophosphorous and carbamate pesticides in a 0.1 M phosphate buffer, 0.1 M KCl (pH 7.2) solution.

Application of the Au/MBT/POMA-PSSA/AChE biosensor in 0.1 M phosphate buffer saline solution has shown inhibition of between 82 to 85% for diazinon, with a detection limit of 0.069 ppb. For the detection of carbofuran, a lower percentage inhibition of approximately 45% was achieved with detection limit of 0.057 ppb.

Application of the Au/MBT/PDMA-PSSA/AChE biosensor in 0.1 M phosphate buffer saline solution has shown diazinon inhibition of 94% with a detection limit of 0.138 ppb. In the case of carbofuran substantial inhibition of 95% was achieved with a detection limit of 0.110 ppb.

The above results have shown that the use of poly(*2,5*-dimethoxyaniline) plus poly(*4*-styrene sulphonic acid) [PDMA-PSSA] as polymer in the biosensor construction, has enhanced the catalytic activity of AChE as enzyme. Therefore, higher percentages of inhibition for both diazinon and carbofuran were achieved with this biosensor, while higher detection limits for the respective pesticides were also obtained.

7.2.6 Chapter 6

The main aim of chapter 6 was the construction of the Au/MBT/PANI/AChE/PVAc thick-film biosensor to investigate the determination of certain organophosphate and carbamate pesticide solutions in selected aqueous organic solvent solutions.

Initially the Au/MBT/POMA-PSSA/AChE and Au/MBT/PDMA-PSSA/AChE thick-film biosensors that were constructed were used to determine selected organophosphate and carbamate pesticide solutions in aqueous organic solvent solutions. However, several difficulties were encountered with these

biosensors since the polymer film containing the AChE enzyme fell off the transducer surface when the biosensors were applied in the aqueous organic solvent solutions. This was attributed to the increased solubility of the substituted polyanilines (e.g. POMA and PDMA) as compared to the unsubstituted PANI.

The Au/MBT/PANI/AChE/PVAc thick-film biosensor device was constructed by encapsulating acetylcholinesterase (AChE) as enzyme in the PANI polymer composite, followed by the coating of poly(vinyl acetate) (PVAc) on top to secure the biosensor film from falling off. The electroactive substrate called acatylthiocholine (ATCh) was also chosen to replace acetylcholine (ACh) as substrate, since ATCh has better redox activity and can both be oxidised and reduced to provide better movement of electrons in the amperometric biosensor. The voltammetric results have shown that the current shifts more anodically as the Au/MBT/PANI/AChE/PVAc biosensor responded to successive acetylthiocholine (ATCh) substrate addition under anaerobic conditions in 0.1 M phosphate buffer, KCl (pH 7.2) solution.

For the Au/MBT/PANI/AChE/PVAc biosensor, different factors and stability aspects in the construction of the biosensor was evaluated, which included:

(i)   the optimal enzyme loading,

(ii)   pH effect on the enzyme,

(iii)   long-term stability of the biosensor,

(iv)   temperature stability of the biosensor,

(v)   the effect of polar organic solvents,

(vi)   and the effect of non-polar organic solvents on the amperometric behaviour of

the biosensor.

In the next step the Au/MBT/PANI/AChE/PVAc biosensor was then applied

to detect a series of 5 organophosphorous and carbamate standard pesticide solutions.

The series of organophosphorous pesticides included diazinon, fenthion, parathion-

methyl, malathion and chlorpyrifos. The series of carbamate pesticides included

dioxacarb, aldicarb, carbaryl, carbofuran, and methomyl. Very good detection limits

for the standard pesticide solutions were obtained that are within the nanomolar

range. The individual results include 0.137 nM for diazinon, 0.826 nM for fenthion,

1.332 nM for parathion-methyl, 0.189 nM for malathion and 0.018 nM for

chlorpyrifos. For the carbamate pesticides, the individual results include 1.572 nM for

dioxacarb, 1.209 nM for aldicarb, 0.880 nM for carbaryl, 0.249 nM for carbofuran

and 0.111 nM for methomyl.

For some of the above results it was shown that the thick-film

Au/MBT/PANI/AChE/PVAc biosensor is more sensitive for the detection of

organophosphorous and carbamate pesticides, compared to other biosensor results

found in literature.

7.3   Critical Overview of this Dissertation

In the following paragraphs, the specific aims of this study are revisited to report whether the aims of this dissertation were achieved, and to give an overview of the successes and shortcomings of the study.

The first specific aim of this study was to coat a gold electrode with an appropriate self-assembled monolayer (SAM) of mercaptobenzothiazole (MBT), followed by *in situ* electropolymerisation of substituted and unsubstituted polyanilines (PANIs) in the presence or absence of a surfactant. The results obtained towards the achievement of this aim has shown that MBT can be successfully coated on a gold electrode to provide a platform for the electropolymerisation of poly(*o*-methoxyaniline) and poly(*2,5*-dimethoxyaniline) in the presence of the surfactant poly(*4*-styrene sulphonic acid). This provided platforms for the immobilisation of the enzyme AChE, in the construction of the corresponding biosensors that showed catalytic activity for the substrate called acetylcholine (ACh). The Au/MBT/POMA-PSSA/AChE and Au/MBT/PDMA-PSSA/AChE biosensors were then successfully applied in 0.1 M phosphate buffer, KCl (pH 7.2) solution using the substrate acetylcholine (ACh) and was characterised with different voltammetric techniques.

Future reactions should optimise the ratio between the monomers *o*-methoxyaniline and *2,5*-dimethoxyaniline with the surfactant poly(*4*-styrene sulphonic acid), to investigate if even better electrochemistry is observed for the resulting conducting polymer.

A second aim of the study involved the application and characterisation of the Au/MBT/POMA-PSSA/AChE and Au/MBT/PDMA-PSSA/AChE biosensors to standard organophosphate (e.g. diazinon, chlorpyrifos) and carbamate (e.g. carbofuran, carbaryl) pesticides in 0.1 M phosphate buffer, KCl (pH 7.2) solutions. In these experiments, the substrate called acetylcholine (ACh) was used as substrate for the enzyme AChE and some difficulties were experienced with the mechanism of the biosensor reaction. Since the substrate ACh is not electroactive, some experiments were done as to show that the one product of the enzyme hydrolysis reaction called acetic acid, is reduced to acetaldehyde. This result was successfully demonstrated and the results published, but on review it was best to change to an electroactive substrate such as acetylthiocholine (ATCh). Furthermore, it was successfully shown that the Au/MBT/POMA-PSSA/AChE and Au/MBT/PDMA-PSSA/AChE biosensors can detect organophosphorous and carbamate pesticides in 0.1 M phosphate buffer, KCl (pH 7.2) solutions. When the Au/MBT/POMA-PSSA/AChE and Au/MBT/PDMA-PSSA/AChE biosensors were applied in organic solvent media some problems were experienced and the polymer films fell off the electrode, thereby impeding any biosensor investigations. These results were then used as input to change the biosensor construction for the detection of organophosphorous and carbamate pesticides in organic solvent media.

A third aim of the study was the construction, characterisation, and optimisation of the electropolymerisation of unsubstituted polyaniline (PANI) on top of the Au/MBT electrode. This was followed by immobilisation of the enzyme AChE and coating of poly(vinyl acetate) (PVAc) to form the thick-film biosensor of

Au/MBT/PANI/AChE/PVAc. This was done to ensure that the polymer film does not fall off the electrode during the incubation studies of the biosensor in organic solvent media. The Au/MBT/PANI/AChE/PVAc biosensor was then successfully applied in 0.1 M phosphate buffer, KCl (pH 7.2) solution using the substrate acetylthiocholine (ATCh) and was characterised with different voltammetric techniques. Voltammetric studies were also performed to investigate if the PVAc doesn't impede the catalytic activity of the enzyme AChE towards the substrate ATCh, but no results to that extend was obtained. The Au/MBT/PANI/AChE/PVAc biosensor was then successfully applied to the study of organophosphorous and carbamate pesticides in pure and aqueous organic solvent mixtures of acetone, acetonitrile, ethanol, n-hexane and diethyl ether. The Au/MBT/PANI/AChE/PVAc biosensor was incubated for 20 minutes in the six different pesticide concentrations evaluated, and the effect of the pesticide inhibition was determined afterwards in 0.1 M phosphate buffer, KCl (pH 7.2) solution. No optimisation experiments were done to investigate if a shorter or longer incubation time will yield better inhibition results. Since the organophosphorous and carbamate pesticides inhibit the enzyme irreversibly, a new biosensor had to be constructed for each pesticide concentration that was evaluated. This is a time-consuming activity if you are not using disposable electrode platforms. This was also a shortfall of this study and it is proposed that disposable gold electrode platforms be used for evaluation of this Au/MBT/PANI/AChE/PVAc biosensor.

The fourth specific aim of this study was the application and characterisation of the Au/MBT/PANI/AChE/PVAc biosensor to real samples containing organophosphorous and carbamate pesticides. This was not attempted due to time

constraints and it is suggested that this research work be done in post-doctoral studies with the use of gold disposable electrode platforms.

7.4   Recommendations for Further Study

The following aspects of organic phase biosensors for the determination of organophosphate and carbamate pesticide compounds, presented in this work warrant further investigation.

1.   More work needs to be done to optimise the ratio between the monomers *o*-methoxyaniline and *2,5*-dimethoxyaniline with the surfactant poly(*4*-styrene sulphonic acid), to investigate if better electrochemistry is observed for the resulting conducting polymer.

2.   Further optimisation experiments should done to investigate if a shorter or longer incubation time, compared to the 20 minutes used in this study, will yield better inhibition results.

3.   It is proposed that disposable gold electrode platforms be used for evaluation of this Au/MBT/PANI/AChE/PVAc biosensor, since this will enable the investigator to study two or more pesticide concentrations at a time.

4.   The application and characterisation of the Au/MBT/PANI/AChE/PVAc biosensor to real samples containing organophosphorous and carbamate pesticides, was not attempted due to time constraints. It is suggested that this

research work be done in post-doctoral studies with the use of gold disposable

electrode platforms.

5.   It is also suggested that higher concentrations of the standard

       organophosphorous and carbamate pesticide solutions be evaluated, to

       determine the extent of inhibition obtained, and to determine whether the

       detection limit can be further improved.

7.5   Overall Significance of the Study

The results delivered in this dissertation have shown that novel use of

mercaptobenzothiazole (MBT) as a self-assembled monolayer (SAM) in the

construction of the Au/MBT/POMA-PSSA/AChE, Au/MBT/PDMA-PSSA/AChE

and Au/MBT/PANI/AChE/PVAc biosensors, has proved to be useful in delivering

biosensors that can be applied for the determination of organophosphorous and

carbamate pesticides. More specific, the novel use of mercaptobenzothiazole (MBT)

as a self-assembled monolayer (SAM) in the construction of the

Au/MBT/PANI/AChE/PVAc biosensor, has delivered a biosensor with high

sensitivity and good reproducibility. It was further shown that the presence of 10% or

5% of water in the aqueous-organic solvent mixtures plays an important role in the

detection and the selectivity of the AChE-biosensor towards pesticides. The AChE-

biosensors also show good characteristics and it appears to be very suitable for the

detection of pesticides in real samples. The applicability of these sensors as early

alarm systems to provide an estimation of the toxicity in food and environmental samples looks very promising.

The results obtained from this study that involved organic phase biosensors for the determination of organophosphate and carbamate pesticide compounds, have shown that the first two Au/MBT/POMA-PSSA/AChE and Au/MBT/PDMA-PSSA/AChE biosensors can be successfully applied to determine standard organophosphate and carbamate pesticides in 0.1 M phosphate buffer, KCl (pH 7.2) solutions.

Furthermore, the third Au/MBT/PANI/AChE/PVAc biosensor was successfully applied to the study of organophosphorous and carbamate pesticides in pure and aqueous organic solvent mixtures of acetone, acetonitrile, ethanol, n-hexane and diethyl ether.

With the construction of the Au/MBT/POMA-PSSA/AChE, Au/MBT/PDMA-PSSA/AChE and Au/MBT/PANI/AChE/PVAc biosensors, it was shown that the novel technique of using a self-assembled monolayer (SAM) of mercaptobenzothiazole (MBT) in the construction of thick-film amperometric biosensors for pesticide evaluation could be successfully achieved.

For some of the detection limits obtained with the thick film Au/MBT/PANI/AChE/PVAc biosensor, it was shown that more sensitive results for the detection of organophosphorous and carbamate pesticides can be achieved, compared to other biosensor results found in literature.

With the results obtained in this research, one closer step was taken to the construction of a device that can be further developed into a sensor for pesticide

monitoring on-site in the field. This is a significant development since one of the

most preventative measures in pollution control is to determine the source of the

pollutant and the magnitude of its threat rapidly by using on-site measurement.

CHAPTER 8

References

Abdollahi, M., Mostafalou, S., Pournourmohammadi, S. & Shadnia, S. (2004). Oxidative stress and cholinesterase inhibition in saliva and plasma of rats following subchronic exposure to malathion. *Comparative Biochemistry and Physiology Part C*, 137: 29–34.

Adányi N. & Váradi, M. (2004). Catalase-based thin-layer enzyme cell used in organic-phase FIA system for determination of moisture in oily foods *European Food Research & Technology*, 219: 432–437.

Albareda-Sirvent, M., Merkoći, A. & Alegret, S. (2001). Pesticide determination in tap water and juice samples using disposable amperometric biosensors made using thick-film technology. *Analytica Chimica Acta*, 442: 35–44.

Albareda-Sirvent, M., Merkoći, A. & Alegret, S. (2000). Configurations used in the design of screen-printed enzymatic biosensors. A review. *Sensors and Actuators B*, 69: 153–163.

Albuquerque, J.E., Mattoso, L.H.C., Balogh, D.T., Faria, R.M., Masters, J.G. & MacDiarmid, A.G.(2000). A simple method to estimate the oxidation state of polyanilines. *Synthetic Metals*, 113: 19–22.

Ali, H.M., Sharaf Eldeen, H.A. & Hikal, M.S. (2005). Selectivity, acetylcholinesterase inhibition kinetics, and quantitative structure–activity relationships of a series of N-(2-oxido-1,3,2-benzodioxa-phosphol-2-yl) amino acid ethyl or diethyl esters. *Pesticide Biochemistry and Physiology*, 83: 58–65.

Alvial, G., Matencio, T., Neves, B.R.A. & Silva, G.C. (2004). Blends of poly(2,5-dimethoxy aniline) and fluoropolymers as protective coatings. *Electrochimica Acta*, 49: 3507–3516.

Andreescu, S., Noguer, T., Magearu, V. & Marty, J-L. (2002a). Screen-printed electrode based on AchE for the detecton of pesticides in presensce of organic solvents. *Talanta*, 57: 169-176.

Andreescu, S., Barthelmebs, L. & Marty, J-L. (2002b). Immobilization of acetylcholinesterase on screen-printed electrodes: comparative study between three immobilization methods and applications to the detection of organophosphorus insecticides. *Analytica Chimica Acta*, 464: 171–180.

Arkhypova, V.N., Dzyadevych, S.V., Soldatkin, A.P., Elśkaya, A.V., Martelet, C. & Jaffrezic-Renault, N. (2003). Development and optimisation of biosensors based on pH-sensitive field effect transistors and cholinesterases for sensitive detection of solanaceous glycoalkaloids. *Biosensors and Bioelectronics*, 18: 1047-1053.

Arshak, K., Morris, D., Arshak, A., Korostynska, O. & Moore, E. (2006). PVAB, PVAc and PS pressure sensors with interdigitated electrodes. *Sensors and Actuators A*, 132: 199 – 206.

Aslanian, D., Gröf, P-I., Renault, F. & Masson, P. (1995). Raman spectroscopic study of conjugates of butyrylcholinesterase with organophosphates. *Biochimica et Biophysica Acta*, 1249: 37-44.

Avlyanov, J.K., Josefowicz, J.Y. & MacDiarmid, A.G. (1995). Atomic force microscopy surface morphology studies of 'in situ' deposited polyaniline thin films. *Synthetic Metals*, 73: 205-208.

Bachmann, T.T. & Schmid, R.D. (1999). A disposable multielectrode biosensor for rapid simultaneous detection of the insecticides paraoxon and carbofuran at high resolution. *Analytica Chimica Acta*, 401: 95–103.

Ballarin, B., Berrettoni, M., Carpani, I., Scavetta, E. & Tonelli, D. (2005). Electrodes modified with an electrosynthesised Ni/Al hydrotalcite as amperometric sensors in flow systems. *Analytica Chimica Acta*, 538: 219–224.

Bard, A.J. & Faulkner, L.R. (2001). *Electrochemical Methods. Fundamentals and Applications.* 2nd edition. New York: John Wiley & Sons, Inc.

Barkauskas, J. (1997). Investigation of conductometric humidity sensors. *Talanta*, 44: 1107-1112.

Basu, I., Subramanian, R.V., Mathew, A., Kayasthac, A.M., Chadha, A. & Bhattacharya, E. (2005). Solid state potentiometric sensor for the estimation of tributyrin and urea. *Sensors and Actuators*, B (107): 418–423.

Bavastrello, V., Stura, E., Carrara, S., Erokhin, V. & Nicolini, C. (2004).

Poly(2,5-dimethylaniline)–MWNTs nanocomposite: a new material for conductometric acid vapours sensor. *Sensors and Actuators B*, 98: 247-253.

Berchmans, S., Yegnaraman, V. & Rao, G.P. (1998). Self-assembled monolayers on electrode surfaces: a probe for redox kinetics. Short Communication. *Journal of Solid State Electrochemistry*, 3: 52-54.

Bernard, M-C., Bich, V.T., de Toressi, S.C. & Goff, A.H-L. (1997). Spectroelectrochemical characterization (OMA and Raman) of sulfonic acids – doped polyaniline. *Synthetic Metals*, 84: 785-786.

Bolognesi, M.L., Cavalli, A., Andrisano, V., Bartolini, M., Banzi, R., Antonello, A., Rosini, M. & Melchiorre, C. (2003). Design, synthesis and biological evaluation of ambenonium derivatives as AChE inhibitors. *Il Farmaco*, 58: 917-928.

Borole, D.D., Kapadi, U.R., Mahulikar, P.P. & Hundiwale, D.G. (2006). Conducting polymers: an emerging field of biosensors. *Designed Monomers and Polymers*, 9 (1): 1–11.

Borzeix, F., Monot, F. & Vandecasteele, J-P. (1992). Strategies for enzymatic esterification in organic solvents: Comparison of microaqueous, biphasic, and micellar systems. *Enzyme and Microbial Technology,* 14 (10): 791-797.

Brahim, S., Wilson, A.M., Narinesingh, D., Iwuoha, E. & Guiseppi-Elie, A. (2003). Chemical and Biological Sensors Based on Electrochemical Detection Using Conducting Electroactive Polymers. *Microchimica Acta*, 143: 123–137.

Brito, R., Tremont, R., Feliciano, O. & Cabrera, C.R. (2003). Chemical derivatization of self-assembled *3*-mercaptopropionic and 16-mercaptohexadecanoic acids at platinum surfaces with *3*-aminopropyltrimethoxysilane: a spectroscopic and electrochemical study. *Journal of Electroanalytical Chemistry*, 540: 53-59.

Brochier, L., Pontié, Y., Willson, M., Estrada-Mondaca, S., Czaplicki, J., Klaébé, A. & Fournier, D. (2001). Involvement of Deacylation in Activation of Substrate Hydrolysis by *Drosophila* Acetylcholinesterase. *Journal of Biological Chemistry*, 276 (1): 18296-18302.

Bucur, B., Danet, A.F. & Marty, J-L. (2004). Versatile method of cholinesterase immobilisation via affinity bonds using concanavalin A applied to the construction of a screen-printed biosensor. *Biosensors and Bioelectronics*, 20: 217–225

Bucur, B., Danet, A.F. & Marty, J-L. (2005a). Cholinesterase immobilisation on

the surface of screen-printed electrodes based on concanavalin A affinity. *Analytica Chimica Acta*, 530: 1–6.

Bucur, B., Dondoi, M., Danet, A. & Marty, J-L. (2005b). Insecticide identification using a flow injection analysis system with biosensors based on various cholinesterases. *Analytica Chimica Acta*, 539: 195–201.

Cagnini, A., Palchetti, I., Lionti, I., Mascini, M. & Turner, A.P.F. (1995). Disposable ruthenized screen-printed biosensors for pesticides monitoring *Sensors and Actuators*, B (24-25): 85-89.

Cai, L-T., Yao, S-B., & Zhou, S-M. (1997). Surfactant effects on the polyaniline film. *Synthetic Metals*, 88: 209-212.

Campanella, L., Favero, G., Sammartino, M.P. & Tomassetti, M. (1998). Further development of catalyse, tyrosinase and glucose oxidase based organic phase enzyme electrode response as a function of organic solvent properties. *Talanta*, 46: 595-606.

Campanella, L. Favero, G., Sammartino, M.P. & Tomassetti, M. (1999). Analysis of several real matrices using new mono-, bi-enzymatic, or inhibition organic phase enzyme electrodes. *Analytica Chimica Acta*, 393: 109-120.

Campanella, L., Favero, G., Persi, L., Sammartino, M.P., Tomassetti, M. & Visco, G. (2001). Organic phase enzyme electrodes: applications and theoretical studies. *Analytica Chimica Acta*, 426: 235-247.

Campuzano, S., Gálvez, R., Pedrero, M., Manuel de Villena, F.J. & Pingarrón, J.M. (2002). Preparation, characterization and application of alkanethiol self-assembled monolayers modified with tetrathiafulvalene and glucose oxidase at a gold disk electrode. *Journal of Electroanalytical Chemi*stry, 526: 92 – 100.

Can, M., Pekmez, K., Pekmez, N. &Yildiz, A. (1999). Electropolymerization of acetonitrile solutions containing aniline and thiophene. *Synthetic Metals*, 104: 9–17.

Carlacci, L., Millard, C.B. & Olson, M.A. (2004). Conformational energy landscape of the acyl pocket loop in acetylcholinesterase: a Monte Carlo-generalized Born model study. *Biophysical Chemistry*, 111: 143– 157.

Casella, I.G. & Contursi, M. (2005). Electrochemical and spectroscopic characterization of a tungsten electrode as a sensitive amperometric sensor of small inorganic ions. *Electrochimica Acta*, 50: 4146–4154.

Casey, V., Cleary, J., D'Arcy, G. & McMonagle, J.B. (2003). Calorimetric combustible gas sensor based on a planar thermopile array: fabrication, characterisation, and gas response. *Sensors and Actuators* B, 96: 114-123.

Castilh, T.J., Sotomayor, M.D.T. & Kubota, L.T. (2005). Amperometric biosensor based on horseradish peroxidase for biogenic amine determinations in biological samples. *Journal of Pharmaceutical and Biomedical Analysis*, 37: 785–791.

Cataldo, F. (2002a). On the action of ozone on undoped and doped alkyl and N-alkyl-substituted polyanilines. *Polymer Degradation and Stability*, 75: 99–106.

Cataldo, F. & Maltese, P. (2002b). Synthesis of alkyl and N-alkyl-substituted polyanilines. A study on their spectral properties and thermal stability *European Polymer Journal*, 38: 1791–1803.

Chao, Y., Yao, S., Buttner, W.J.& Stetter, J.R. (2005). Amperometric sensor for selective and stable hydrogen measurement. *Sensors and Actuators B*, 106: 784–790.

Chaplin, M. (2004). Hyperlink http://www.lsbu.ac.uk/biology/enztech/inhibition.html , accessed on 20 January 2006.

Chatterjee, S. & H.S. Maiti,. H.S. (2001). A novel method of doping PTC thermistor sensor elements during sintering through diffusion by vapour phase. *Materials Chemistry and Physics*, 67: 294-297.

Chatterjee, S. & Russell, A.J. (1992). Determination of equilibrium and individual rate constants for subtilisin-catalyzed transesterification in anhydrous environments. *Biotechnology and Bioengineering,* 40 (9): 1069-1077.

Chaubey, A., Pande, K.K., Singh, V.S. & Malhotra, B.D. (2000). Co-immobilization of lactate oxidase and lactate dehydrogenase on conducting polyaniline films. *Analytica Chimica Acta*, 407: 97–103.

Chellappan, R.R. & Ohsaka, T. (2001). Electroanalysis of ascorbate and dopamine at a gold electrode modified with a positively charged self-assembled monolayer. *Journal of Electroanalytical Chemistry*, 496: 44-49.

Chen, S-S., Wen, T-C. & Gopalan, A. (2003). Electrosynthesis and characterization of a conducting copolymer having S–S links. *Synthetic Metals*, 132: 133–143.

Cho, M.S., Park, S.Y., Hwang, J.Y. & Choi, H.J. (2004). Synthesis and electrical properties of polymer composites with polyaniline nanoparticles. *Materials Science and Engineering C*, 24: 15–18.

Choi, J-W., Kim, Y-K., Lee, I-H., Min, J. & Lee, W.H. (2001). Optical organophosphorus biosensor consisting of acetylcholinesterase/viologen hetero Langmuir–Blodgett film. *Biosensors and Bioelectronics*, 16: 937–943.

Chough, S.H., Mulchandani, A., Mulchandani, P., Chen, W., Wang, J. & Rogers, K.R. (2002). Organophosphorus Hydrolase-Based Amperometric Sensor: Modulation of Sensitivity and Substrate Selectivity. *Electroanalysis*, 14 (4): 273-276.

Chouteau, C., Dzyadevych, S., Chovelon, J-M. & Durrieu, C. (2004). Development of novel conductometric biosensors based on immobilised whole cell *Chlorella vulgaris* microalgae. *Biosensors and Bioelectronics*, 19: 1089-1096.

Chouteau, C., Dzyadevych, S., Durrieu, C. & Chovelon, J-M. (2005). A bi-enzymatic whole cell conductometric biosensor for heavy metal ions and pesticides detection in water samples. *Biosensors and Bioelectronics*, 21: 273–281.

Chowdary, G.V. & Prapulla, S.G. (2003). Enzymatic synthesis of ethyl hexanoate by transesterification. *International Journal of Food Science and Technology*, 38: 127–133.

Cosnier, S., Lepellec, A., Guidetti, B. & Rico-Lattes, I. (1998). Enhancement of biosensor sensitivity in aqueous and organic solvents using a combination of poly(pyrrole-ammonium) and poly(pyrrole-lactobionamide) films as host matrices. *Journal of Electroanalytical Chemistry*, 449: 165–171.

Cui, L., Swann, M.J., Glidle, A., Barker, J.R. & Cooper, J.M. (2000). Odour mapping using microresistor and piezo-electric sensor pairs. *Sensors and Actuators B*, 66: 94-97.

Dable, B.K., Booksh, K.S., Cavicchi, R. & Semancik, S. (2004). Calibration of microhotplate conductometric gas sensors by non-linear multivariate regression methods. *Sensors and Actuators B*, 101: 284-294.

Dable, B.K., Booksh, K.S., Cavicchi, R. & Semancik, S. (2004). Calibration of microhotplate conductometric gas sensors by non-linear multivariate regression methods. *Sensors and Actuators B*, 101: 284-294.

Darain, F., Park, D.S., Park, J-S., Chang, S-C. & Shim, Y-B. (2005). A

separation-free amperometric immunosensor for vitellogenin based on screen-printed carbon arrays modified with a conductive polymer. *Biosensors and Bioelectronics*, 20: 1780–1787.

Darvesh, S., McDonald, R.S., Penwell, A., Conrad, S., Darvesh, K.V., Mataija, D., Gomez, G., Caines, A., Walsh, R. & Martin, E. (2005). Structure–activity relationships for inhibition of human cholinesterases by alkyl amide phenothiazine derivatives. *Bioorganic and Medicinal Chemistry*, 13: 211–222.

Del Carlo, M., Mascini, M., Pepe, A., Diletti, G. & Compagnone, D. (2004). Screening of food samples for carbamate and organophosphate pesticides using an electrochemical bioassay. *Food Chemistry*, 84:651.

Delvaux, M., Duchet, J., Stavaux, P-Y., Legras, R. & Demoustier-Champagne, S. (2000). Chemical and electrochemical synthesis of polyaniline microand nano-tubules. *Synthetic Metals*, 113: 275–280.

Deo, R.P., Wang, J. Block, I., Mulchandani, A., Joshi, K.A., Trojanowicz, M., Scholz, F., Chen, W. & Lin, Y. (2005). Determination of organophosphate pesticides at a carbon nanotube/organophosphorus hydrolase electrochemical biosensor. *Analytica Chimica Acta*, 530: 185–189.

Diamond, D. (Ed.). (1998). *Principles of Chemical and Biological Sensors*. New York: John Wiley & Sons, Inc.

Di Natale,, C., Salimbeni, D., Paolesse, R., Macagnano, A. & D'Amico, A. (2000). Porphyrins-based opto-electronic nose for volatile compounds detection. *Sensors and Actuators B*, 65: 220-226.

Dordick, J.S. (1992). Designing Enzymes for Use in Organic Solvents. *Biotechnology Progress*, 8: 259-267.

Dücsǒ, C., Ádám, M., Fürjes, P., Hirschfelder, M.,Kulinyi, S. & Bársony, I. (2003). Explosion-proof monitoring of hydrocarbons by mechanically stabilised, integrable calorimetric microsensors. *Sensors and Actuators B*, 95: 189-194.

Dziri, L., Boussaad, S., Tao, N. & Leblanc, R.M. (1998). Effect of pH on acetylcholinesterase Langmuir and Langmuir–Blodgett films studied by surface potential and atomic force microscopy. *Thin Solid Films*, 327–329: 56–59.

Ekholm, M. (2001). Molecular Modeling of Substrates and Inhibitors of

Acetylcholin- and Butyrylcholinesterases. Unpublished Ph.D Thesis. Department of Chemistry, Laboratory for Instruction in Swedish, Faculty of Science, University of Helsinki, Helsinki, Finland.

Environmental Protection Agency (EPA), USA. (2006). *http://www.epa.gov/pesticides/about/* accessed on 19 April 2006.

Erdem, A., Pabuccuoulu, A., Meruc, B., Kerman, K. & Mehmet, Z. (2000). Electrochemical Biosensor Based on Horseradish Peroxidase for the Determination of Oxidizable Drugs. *Turkish Journal of Medical Sciences*, 30: 349-354.

Erlenko tter, A., Kottbus, M. & Chemnitius, G-C. (2000). Flexible amperometric transducers for biosensors based on a screen printed three electrode system. *Journal of Electroanalytical Chemistry*, 481: 82–94.

Evtugyn, G.A., Budnikov, H.C. & Nikolskaya, E.B. (1998). Sensitivity and selectivity of electrochemical sensors for inhibitor determination. *Talanta*, 46: 465-484.

Fatibello-Filho, O. & Vieira, I.C. (2000). Construction and analytical application of a biosensor based on stearic acid-graphite powder modified with sweet potato tissue in organic solvents. *Fresenius Journal of Analytical Chemistry*, 368: 338 – 343.

Fedosseeva, O.V., Uchida, H., Katsube, T., Ishimaru, Y. & Iida, T. (2000). Novel type cholinesterase sensor based on SPV measurement technique. *Sensors and Actuators B*, 65: 55-57.

Felgenhauer, T., Rong, H-T. & Buck, M. (2003). Electrochemical and exchange studies of self-assembled monolayers of biphenyl based thiols on gold. *Journal of Electroanalytical Chemistry*, 550-551: 309–319.

Fenelon, A.M. & Breslin, C.B. (2005). Polyaniline-coated iron: studies on the dissolution and electrochemical activity as a function of pH. *Surface and Coatings Technology*, 190: 264–270.

Fennouh, S., Casimiri, V. & Burstein, C. (1997). Increased paraoxon detection with solvents using acetylcholinesterase inactivation measured with a choline oxidase biosensor. *Biosensors and Bioelectronics*, 12(2): 97-104.

Forget, J., Livet, S. & Leboulenger, F. (2002). Partial purification and characterization of acetylcholinesterase (AChE) from the estuarine copepod *Eurytemora affinis* (Poppe). *Comparative Biochemistry and Physiology Part C*, 132: 85–92.

Galan-Vidal, C.A., Munoz, J. Dominguez, C. & Alegret, S. (1998). Glucose biosensor strip in a three electrode configuration based on composite and biocomposite materials applied by planar thick film technology. *Sensors and Actuators B*, 52: 257–263.

Ge, C., Doherty III, W.J., Mendes, S.B., Armstrong, N.R. & Saavedra, S.C. (2005). Voltammetric and waveguide spectroelectrochemical characterization of ultrathin poly(aniline)/poly(acrylic acid) films self-assembled on indium-tin oxide. *Talanta*, 65: 1126-1131.

George, K.M., Schule, T., Sandoval, L.E., Jennings, L.L., Taylor, P.& Thompson, C.M. (2003). Differentiation between Acetylcholinesterase and the Organophosphate-inhibited Form Using Antibodies and the Correlation of Antibody Recognition with Reactivation Mechanism and Rate. *Journal of Biological Chemistry*, 278 (46): 45512-45518.

Georganopoulou, D.G., Carley, R., Jones, D.A. & Boutelle, M.G. (2000). Development and comparison of biosensors for *in-vivo* applications. *Faraday Discussions*, 116: 291-303.

Giacobini, E. (2004). Cholinesterase inhibitors: new roles and therapeutic Alternatives. *Pharmacological Research*, 50: 433–440.

Glaser, L.C. (2000). *Wildlife Mortality Attributed to Organophosphorus and Carbamate Pesticides*. Report published by the National Wildlife Health Centre. 3 pp. WI: Madison, USA.

Glaser, R., Wu, H. & Lewis, M. (2005). Cytosine Catalysis of Nitrosative Guanine Deamination and Interstrand Cross-Link Formation. *Journal of American Chemical Society*, 127: 7346-7358.

Gooding, J.J., Hall, E.A.H. & Hibbert, D.B. (1999).From Thick Films to Monolayer Recognition Layers in Amperometric Enzyme Electrodes. *Electroanalysis*, 10 (16): 1130 – 1136

Greenhalgh, R., Baron, R.L., Desmoras, J., Engst, R., Esser, H.O. & Klein, W. 1980). Definition of persistence in pesticide chemistry. *Journal of Pure and Applied Chemistry*, 52: 2563-2566.

Grzeszczuk, M. & Szostak, R. (2003). Electrochemical and Raman studies on the redox switching hysteresis of polyaniline. *Solid State Ionics*, 157: 257–262.

Guardigli, M., Pasini, P., Mirasoli, M., Leoni, A., Andreani, A. & Roda, A.

(2005). Chemiluminescent high-throughput microassay for evaluation of acetylcholinesterase inhibitors. *Analytica Chimica Acta*, 535: 139–144.

Gulla, K.C., Gouda, M.D., Thakur, M.S. & Karanth, N.G. (2002). Reactivation of immobilized acetyl cholinesterase in an amperometric biosensor for organophosphorus pesticide. *Biochimica et Biophysica Acta*, 1597: 133–139.

Guo, Y., & Guadalupe, A.R. (1998). Screen-printable surfactant-induced sol–gel graphite composites for electrochemical sensors. *Sensors and Actuators B*, 46: 213–219.

Gupta, V.K. & Agarwal, S. (2005). PVC based *5,10,15,20*-tetrakis (*4*-methoxyphenyl) porphyrinatocobalt(II) membrane potentiometric sensor for arsenate. *Talanta*, 65: 730–734.

Gupta, M.N. & Roy, I. (2004). Enzymes in organic media. Forms, functions and Applications. *European Journal of Biochemistry*, 271: 2575–2583.

Halamek, J., Makower, A., Knosche, K., Skladal, P. & Scheller, F.W. (2005). Piezoelectric affinity sensors for cocaine and cholinesterase inhibitors. *Talanta*, 65: 337–342.

Hao, Q., Kulikov, V. & Mirsky, V.M. (2003). Investigation of contact and bulk resistance of conducting polymers by simultaneous two- and four-point technique. *Sensors and Actuators B*, 94: 352–357.

Hao, G. (2003). Development of Conductometric Polymer Sensor for Gaseous Hydrogen Chloride. Unpublished PhD Thesis. University of Regensburg, Germany.

Hart, A.L., Matthews, C., Collier, W.A. (1999). Estimation of lactate in meat extracts by screen-printed sensors. *Analytica Chimica Acta*, 386:7-12.

Hart, A.L., Collier, W.A. & Janssen, D. (1997). The response of screen-printed enzyme electrodes containing cholinesterases to organo-phosphates in solution and from commercial formulations. *Biosensors and Bioelectronics*, 12 (7): 645-654.

Hart, A.L. & Collier, W.A. (1998). Stability and function of screen printed electrodes, based on cholinesterase, stabilised by a co-polymer: sugar alcohol mixture. *Sensors and Actuators B*, 53: 111–115.

Hasik, M., Wenda, E., Paluszkiewicz, C., Bernasik, A. & Camrac, J. (2004). Poly(*o*-methoxyaniline)–palladium systems: effect of preparation conditions on physico-chemical properties. *Synthetic Metals*, 143: 341–350.

Hleli, S., Martelet, C., Abdelghani, A., Burais, N. & Jaffrezic-Renault. N. (2006). Atrazine analysis using an impedimetric immunosensor based on mixed biotinylated self-assembled monolayer. *Sensors and Actuators B*, 113: 711–717.

Hou, Y. (2005). *Elaboration Et Characterisation De Biofilms Pour Micro Et Nanobiocapteurs Olfactifs*. Unpublished Ph.D thesis. Fance, Lyon: I'Ecole Centrale De Lyon.

Huang, J., Hao, Y., Lin, H., Zhang, D., Song, J, & Zhou, D. (2003). Preparation and characteristic of the thermistor materials in the thick-film integrated temperature_ humidity sensor. *Materials Science and Engineering*, B99: 523-526.

Huang, L-M., Wen, T-C. & Gopalan, A. (2002). In situ UV-visible spectroelectrochemical studies on electrochromic behavior of poly(*2,5*-dimethoxy aniline). *Synthetic Metals*, 130: 155-163.

Huang, L-M., Wen, T-C. & Gopalan, A. (2003). Synthesis and characterization of soluble conducting poly(aniline-co-2, 5-dimethoxyaniline). *Materials Letters*, 57: 1765–1774.

Huang, L-M., Wen, T-C., Gopalan, A. & Ren, F. (2003). Structural influence on the electronic properties of methoxy substituted polyaniline/aluminum Schottky barrier diodes. *Materials Science and Engineering B*, 104: 88–95.

Huang, Z., Wang, P-C. Feng, J. & MacDiarmid, G. (1997). Selective deposition of films of polypyrrole, polyaniline and nickel on hydrophobic/hydrophilic patterned surfaces and applications. *Synthetic Metals*, 85: 1375-1376.

Inci, M.N., Barton, J.S. & Jones, J.D.C. (1997). A fibre-optic thermometric sensor based on the thermo-optic effect of titanium dioxide coatings, *Optics and Laser Technology*, 29 (3): 121-124.

Ippolito, S.J., Kandasamy, S., Kalantar-Zadeh, K. & Wlodarskia, W. (2005). Hydrogen sensing characteristics of WO_3 thin film conductometric sensors activated by Pt and Au catalysts. *Sensors and Actuators B*, 108: 154-158.

Ivanov, A.N., Lukachova, L.V., Evtugyn, G.A., Karyakina, E.E., Kiseleva, S.G., Budnikov, H.C., Orlov, A.V., Karpacheva, G.P. & Karyakin, A.A. (2002). Polyaniline-modified cholinesterase sensor for pesticide determination. *Bioelectrochemistry*, 55: 75–77.

Iwuoha, E.I., Adeyoju, O., Dempsey, E., Smyth, M.R., Liu, J., Wang, J. (1995).

Investigation of the effects of polar organic solvents on the activity of tyrosinase entrapped in a poly(ester-sulphonic acid) polymer. *Biosensors and Bioelectronics*, 10: 661-667.

Iwuoha, E.I., Smyth, M.R. & Lyons, M.E.G. (1997a). Organic phase enzyme electrodes: kinetics and analytical applications. *Biosensors and Bioelectronics*, 12: 53-75.

Iwuoha, E.I., De Villaverde, D.S., Garcia, N.P., Smyth, M.R. & Pingarron, J.M. (1997b). Reactivities of organic phase biosensors. 2. The amperometric behaviour of horseradish peroxidase immobilised on a platinum electrode modified with an electrosynthetic polyaniline film. *Biosensors and Bioelectronics*, 12: 749-761.

Iwuoha, E.I. Wilson, A., Howel, M., Mathebe, N.G.R. Montane-Jaime, K. Narinesingh, D. & Guiseppi-Elie, A. (2005). Cytochrome P_{450} 2D6 (CYP2D6) Bioelectrode for Fluoxetine. *Analytical Letters*, 37 (5): 929-941.

Iwuoha, E.I. & Smyth, M.R. (2003). Reactivities of organic phase biosensors: 6. Square-wave and differential pulse studies of genetically engineered cytochrome P450cam (CYP101) bioelectrodes in selected solvents. *Biosensors and Bioelectronics*, 18: 237- 244.

Jeanty, G., Ghommidh, C. & Marty, J-L. (2001). Automated detection of chlorpyrifos and its metabolites by a continuous flow system-based enzyme sensor. *Analytica Chimica Acta*, 436: 119–128.

Jin, W. & Brennan, J.D. (2002). Properties and applications of proteins encapsulated within sol-gel derived materials. *Analytica Chimica Acta*, 461: 1-36.

Johnson, G. & Moore, S.W. (2004). Identi.cation of a structural site on acetylcholinesterase that promotes neurite outgrowth and binds laminin-1 and collagen IV. *Biochemical and Biophysical Research Communications*, 319: 448–455.

Johnson, J.L., Cusack, B., Hughes, T.F., McCullough, E.H., Fauq, A., Romanovskis, P., Spatola, A.F. & Rosenberry, T.L. (2003).Inhibitors Tethered Near the Acetylcholinesterase Active Site Serve as Molecular Rulers of the Peripheral and Acylation Sites. *Journal of Biological Chemistry*, 278 (40): 38948-38955.

Joshi, K.A., Tang, J., Haddon, R., Wang, J., Chen, W., Mulchandania, A. (2005).

A Disposable Biosensor for Organophosphorus Nerve Agents Based on Carbon Nanotubes Modified Thick Film Strip Electrode. *Electroanalysis,* 17: 54-58.

Jun, Y.Y. & Beng, K.S. (2004). Electrochemical study of monolayers of heterocyclic thiols self-assembled on polycrystalline gold electrode: the effect of solution pH on redox kinetics. *Electrochemistry Communications*, 6: 87–90.

Jung, D.I., Shin, Y.J., Lee, E.S., Moon, T., Yoon, C.N. & Lee, B.H. (2003). Acetylcholinesterase(AChE)-Catalyzed Hydrolysis of Long-Chain Thiocholine Esters: Shift to a New Chemical Mechanism. *Chemical Society*, 24 (1): 1 65-69.

Jun, Y. Y. & Beng, K. S. (2004). Electrochemical study of monolayers of heterocyclic thiols self-assembled on polycrystalline gold electrode: the effect of solution pH on redox kinetics. *Electrochemistry Communications,* 6: 87 – 90.

Kang, Y., Won, D-J., Kim, S.R., Seo, K., Choi, H-S., Lee, G., Noh, Z., Lee, T.S. & Lee, C. (2004). Self-assembled monolayer of the aromatic thioacetate on the gold surface. *Materials Science and Engineering C*, 24: 43–46.

Karousos, N.G., Aouabdi, S., Way, A.S. & Reddy, S.M. (2002). Quartz crystal microbalance determination of organophosphorus and carbamate pesticides. *Analytica Chimica Acta*, 469: 189–196.

Karube, I. & Nomura, Y. (2000). Enzyme sensors for environmental analysis. *Journal of Molecular Catalysis B: Enzymatic*, 10: 177-181.

Kato, Y., Tanaka, T. & Miyata, T. (2004). Comparison of kinetic properties of a hydrophilic form of acetylcholinesterase puri.ed from strains susceptible and resistant to carbamate and organophosphorus insecticides of green rice leafhopper (Nephotettix cincticeps Uhler). *Pesticide Biochemistry and Physiology*, 79: 64–73.

Keane, A., Phoenix, P., Ghoshal, S. & Lau, P.C.K. (2002). Exposing culprit organic pollutants: A Review. *Journal of Microbiological Methods*, 49: 103-119.

Kerman, K., Ozkan, D., Kara, P., Meric, B., Gooding, J.J. & Ozsoz, M. (2002). Voltammetric determination of DNA hybridisation using methylene blue and self-assembled alkanethiol monolayer on gold electrodes. *Analytica Chimica Acta*, 462:39–47.

Khalid, A., Haq, Z., Anjum, S., Khan, M.R., Rahman, A. & Choudhary, M.I. (2004). Kinetics and structure–activity relationship studies on pregnane-type steroidal alkaloids that inhibit cholinesterases. *Bioorganic and Medicinal Chemistry*, 12: 1995–2003.

Khmelnitsky, Y.L., Hilhorst, R., Visser. A.J. & Veeger, C. (1993). Enzyme inactivation and protection during entrapment in reversed micelles. *European Journal of Biochemistry*, 211: 73-77.

Killard, A.J., Zhang, S., Zhao, H., John, R., Iwuoha, E.I. & Smyth, M.R. (1999). Development of an electrochemical flow injection immunoassay (FIIA) for the real-time monitoring of biospecific interactions. *Analytica Chimica Acta,* 400: 109–119.

Kim, J-D. & Nam, S-R. (1997). Development of a micro-depth control system for an ultra-precision lathe using a piezo-electric actuator. *International Journal of Mechanical Tools Manufacturing,* 37 (4): 495-509.

Kimura, M. & Toshima, K. (2003). Thermistor-like pn junction temperature-sensor with variable sensitivity and its combination with a micro-air-bridge heater. *Sensors and Actuators A*, 108: 239-243.

Klibanov, A.M. (1989). Enzymatic catalysis in anhydrous organic solvents. *Trends in Biochemical Sciences*, 14 (4): 141-144.

Klibanov, A.M. (2003). Asymmetric enzymatic oxidoreductions in organic solvents. *Current Opinion in Biotechnology*, 14:427–431.

Kok, F.N. & Hasirci, V. (2004). Determination of binary pesticide mixtures by an acetylcholinesterase–choline oxidase biosensor. *Biosensors and Bioelectronics*, 19: 661–665.

Komersova, A., Komers, K. & Zdraizilova, P. (2005). Kinetics of hydrolysis of acetylthiocholine and acetylcholine by cholinesterases. *Extended Abstracts/ Chemico-Biological Interactions*, 157–158: 353–434.

Konash, A. & Magner, E. (2006). Characterization of an organic phase peroxide biosensor based on horseradish peroxidase immobilized in Eastman AQ. *Biosensors and Bioelectronics*, 22: 116–123.

Krasinski, A., Radic, Z., Manetsch, R., Raushel, J., Taylor, P., Sharpless, K.B. & Kolb, H.C. (2005). In Situ Selection of Lead Compounds by Click Chemistry: Target-Guided Optimization of Acetylcholinesterase Inhibitors. *Journal of American Chemical Society*, 127: 6686-6692.

Kröger, S., Setford, S.J. & Turner, A.P.F. (1998). Assessment of glucose oxidase behaviour in alcoholic solutions using disposable electrodes. *Analytica Chimica Acta*, 368: 219-231.

Kryger, G., Silman, I. & Sussman, J.L. (1999). Structure of acetylcholinesterase complexed with E2020 (AriceptÒ): implications for the design of new anti-Alzheimer drugs. *Structure*, 7: 297–307.

Kukla, A.L., Kanjuk, N.I., Starodub, N.F. & Shirshov, Y.M. (1999). Multienzyme electrochemical sensor array for determination of heavy metal ions. *Sensors and Actuators B*, 57: 213-218.

Kuo, C-T. & Chen, C-H. (1999). Characterization of polyaniline doped with diphenyl phosphate. *Synthetic Metals*, 99: 163–167.

Kuralay, F., Özyörük, H. & Yıldız, A. 2005. Potentiometric enzyme electrode for urea determination using immobilized urease in poly(vinylferrocenium) film. *Sensors and Actuators B*, 109: 194–199.

Kuramoto, N. & Takahashi, Y. (1998). Oxidative polymerisation of dodecylbenzenesulfonic acid *o*-anisidine salt in organic solvent with electron receptor. *Reactive and Functional Polymers*, 37: 33-38.

Lan, Y. Kocher, M.F. & Smith, J.A. (1999). Opto-electronic Sensor System for Laboratory Measurement of Planter Seed Spacing with Small Seeds. *Journal Agricultural &.Engineering Resources,* 72: 119-127.

Langer, J.J. Filipiak, M., Kecinska, J., Jasnowska, J., Włodarczak, J. & Buładowski, B. (2004). Polyaniline biosensor for choline determination. *Surface Science*, 573: 140–145.

Laska, J. (2004). Conformations of polyaniline in polymer blends. *Journal of Molecular Structure*, 701: 13–18.

Law, K.A. & Higson, S.P.J. (2005). Sonochemically fabricated acetylcholinesterase micro-electrode arrays within a flow injection analyser for the determination of organophosphate pesticides. *Biosensors and Bioelectronics*, 20: 1914–1924.

Lee, W-Y., Kim, S-R., Kim, T-H., Lee, K.S., Shin, M-C. & Park, J-K. (2000). Sol–gel-derived thick-film conductometric biosensor for urea determination in serum. *Analytica Chimica Acta*, 404: 195–203.

Li, H-P., Li, J-H., Li, G-C. & Jen, J-F. (2004). Simultaneous determination of

airborne carbamates in workplace by high performance liquid chromatography with fluorescence detection. *Talanta*, 63 (3): 547-553.

Li, J., Tan, S.N. & Oh, J.T. (1998). Silica sol-gel immobilized amperometric enzyme electrode for peroxide dtermination in the organic phase. *Journal of Electroanalytical Chemistry*, 448: 69-77.

Li, X., Wang, G., Li, X. & Lu, D. (2004). Surface properties of polyaniline/nano-TiO_2 composites. *Applied Surface Science*, 229 (1-4): 395-401.

Li, W., Johnson, C.L. & Wang, H-L. (2004). Preparation and characterization of monolithic polyaniline–graphite composite actuators. *Polymer*, 45: 4769–4775.

Lin, G., Lai, C-Y. & Liao, W-C. (1999). Molecular Recognition by Acetylcholinesterase at the Peripheral Anionic Site: Structure-Activity Relationships for Inhibitions by Aryl Carbamates. *Bioorganic and Medicinal Chemistry*, 7: 2683-2689.

Lin, Y., Lu, F., Wang, J. (2004). Disposable Carbon Nanotube Modified Screen-Printed Biosensor for Amperometric Detection of Organophosphorous Pesticides and Nerve Agents. *Electroanalysis*, 16 (1-2): 145 – 149.

Liu, S-J. & Tubino, M., (1998). A thermistor as a sensor in gas phase flow injection analysis. *Analytica Chimica Acta*, 366: 5-10.

Liu, G., Rodriguez, J.A., Dvorak, J., Hrobek, J. & Jirsak, T. (2002). Chemistry of sulfur-containing molecules on Au(111): thiophene, sulfur dioxide, and methanethiol adsorption. *Surface Science*, 505: 295–307.

Liu, Y., Zhang, Z., Nie, L. & Yao, S. (2003). Study on the influence of anionic and cationic surfactant on Au-colloid modified electrode function by cyclic voltammetry and electrochemical impedance techniques. *Electrochimica Acta*, 48: 2823-2830.

Lyons, M.E.G., Bannon, T., Hinds, G. & Rebouillat, S. (1998). Reaction/diffusion with Michaelis–Menten kinetics in electroactive polymer films Part 2. The transient amperometric response. *Analyst*, 123: 1947–1959.

McCarthy, P.A., Huang, J., Yang, S-C. & Wang, H-L. (2002). Synthesis and Characterization of Water-Soluble Chiral Conducting Polymer Nanocomposites. *Langmuir*, 18: 259-263.

Majumder, C., Mizuseki, H. & Kawazoe, Y. (2003). Thiophene thiol on the Au(III) surface: Size-dependent adsorption study. *Journal of Chemical*

Physics, 118 (21): 1-8.

Makower, A., Halamek, J., Skladal, P., Kernchen, F. & Scheller, F.W. (2003).
New principle of direct real-time monitoring of the interaction of
cholinesterase and its inhibitors by piezolectric biosensor. *Biosensors and
Bioelectronics*, 18: 1329-1337.

Malinauskas, A. & Holze, R. (1999). A UV-vis spectroelectrochemical study of
redox reactions of solution species at a polyaniline electrode in the conducting
and the reduced state. *Journal of Electroanalytical Chemistry*, 461: 184–193.

Malhotra, B.D. & Singhal, R. (2003). Conducting polymer based biomolecular
electronic devices. *Pramana - Journal of Physics*; 61 (2): pp. 331–343.

Malhotra, B.D., Singha, R., Chaubey, A., Sharma, S.K. & Kumar, A. (2005).
Recent trends in biosensors. *Current Applied Physics*, 5: 92–97.

Marty, J-L., Leca, B. & Noguer, T. (1998). Biosensors for the detection of
pesticides. *Analusis Magazine*, 26 (6): 144-148

Martorell, D., Cospedes, F., Martinez-Fobregas, E. & Alegret, S. (1997).
Determination of organophosphorus and carbamate pesticides using a
biosensor based on a polishable, *7,7,8*-tetracyanoquino-dimethane-modified,
graphite-epoxy biocomposite. *Analytica Chimica Acta*, 337: 305-313.

Mashhadizadeh, M.H., Shoaei, I.S. & Monadi, N. (2004). A novel ion selective
membrane potentiometric sensor for direct determination of Fe(III) in the
presence of Fe(II). *Talanta*, 64: 1048-1052.

Masson, P., Froment. M-T., Fortier, P-L., Visicchio, J-E., Bartels, C.F. &
Lockridge, O. (1998). Butyrylcholinesterase-catalysed hydrolysis of aspirin, a
negatively charged ester, and aspirin-related neutral esters. *Biochimica et
Biophysica Acta*, 1387: 41-52.

Masson, P., Schopfer, L.M., Bartels, C.F., Froment, M-T., Ribes, F., Nachon, F.
& Lockridge, O. (2002). Substrate activation in acetylcholinesterase induced
by low pH or mutation in the π-cation subsite. *Biochimica et Biophysica Acta,*
1594: 313-324.

Mashhadizadeh, M.H., Shoaei, I.S. & Monadi, N. (2004). A novel ion selective
membrane potentiometric sensor for direct determination of Fe(III) in the
presence of Fe(II). *Talanta*, 64: 1048-1052.

Mathebe, N.G.R., Morrin, A. & Iwuoha, E.I. (2004). Electrochemistry and

scanning electron microscopy of polyaniline/peroxidase-based biosensor. *Talanta*, 64: 115–120.

Mathew, R., Mattes, B.R. & Espe, M.P. (2002). A solid state NMR characterization of cross-linked polyaniline powder. *Synthetic Metals*, 131: 141–147

Matseeva, E.S., Patil, R.C. & Tejera, M.J.G. (2001). Optical evidence of electrochemical modification of polyaniline induced by tetra-fluoro-hydroquinone. *Synthetic Metals*, 123: 343 – 348.

Mathews, C.K. & Van Holde, K.E. (1990). *Biochemistry*. Redwood City, California: The Benjamin/Cummings Publishing Company.

Mazur, M., Krysinski, P. & Jackowska, K. (1998). Electrochemical deposition of poly(o-anisidine) and polypyrrole at octadecanethiol coated gold electrodes. *Thin Solid Films*, 330: 167-172.

Mazur, M. & Krysiński, P. (2001). Bulk- and surface-initiated chemical in situ polymerization of 2,5-dimethoxyaniline and *2*-methoxyaniline on thiol-coated gold electrodes. *Electrochimica Acta*, 46: 3963–3971.

Mazur, M., Krysinski, P. & Palys, B. (2002). Preparation of ultrathin films of polyaniline and its derivatives by electrochemical deposition on thiol modified gold. *Journal of Electroanalytical Chemistry*, 533: 145-152.

Mazur, M., Tagowska, M., Pałys, B. & Jackowska, K. (2003). Template synthesis of polyaniline and poly(2-methoxyaniline) nanotubes: comparison of the formation mechanisms. *Electrochemistry Communications*, 5: 403–407.

Mazur, M. (2005). Preparation of poly(3-methylthiophene) thin films by in situ polymerization. *Thin Solid Films*, 472: 1– 4.

McCarthy, P.A., Huang, J., Yang, Z-C. & Wang, H-L. (2002). Synthesis and Characterization of Water-Soluble Chiral Conducting Polymer Nanocomposites. *Langmuir*, 18: 259-263.

McGovern, S.T., Spinks, G.M., Wallace, G.G. (2005). Micro-humidity sensors based on a processable polyaniline blend. *Sensors and Actuators B*, 107:657–665.

Messer, Jr., W.S. (2000). Professor of Medicinal and Biological Chemistry at the University of Toledo. www.utoledo.edu, available online on 3 July 2005.

Moghimi, M., Bagherinia, M.A., Arvand, M. & Zanjanchi, M.A. (2004).

Polymeric membrane sensor for potentiometric determination of vanadyl ions. *Analytica Chimica Acta*, 527: 169–175.

Moghimi, M., Arvand, M., Javandel, R. & Zanjanchi, M.A. (2005). Picrate ion determination using a potentiometric sensor immobilized in a graphite matrix. *Sensors and Actuators B*, 107 (1): 296-302.

Monk, P. (2001). *Fundamentals of Electro-Analytical Chemistry.* Chichester: John Wiley & Sons Ltd.

Montesinos, T., Pérez-Munguia, S., Valdez, F. & Marty, J-L. (2001). Disposable cholinesterase biosensor for the detection of pesticides in water-miscible organic solvents. *Analytica Chimica Acta*, 431: 231-237.

Morales, J.A., O'Sullivan, S.J. & Cassidy, J.F. (2004). Studies on conducting polymer-based sensing membranes with tri-iodide organic salts for vapour detection. *Sensors and Actuators B*, 105 (2): 266-270.

Morrin, A. (2002). Characterisation and optimisation of an amperometric biosensor for use in electrochemical immunosensing. Report for Transfer to PhD Register. Dublin City University, Ireland.

Morrin, A., Moutloali, R.M., Killard, A.J., Smyth, M.R., Darkwa, J. & Iwuoha, E.I. (2004). Electrocatalytic sensor devices: (I) cyclopentadienylnickel(II) thiolato Schiff base monolayer self-assembled on gold. *Talanta*, 64: 30–38.

Morrin, A., Ngamna, O., Killard, A.J., Moulton, S.E., Smyth, M.R. & Wallace, G.G. (2005). An Amperometric Enzyme Biosensor Fabricated from Polyaniline Nanoparticles. *Electroanalysis*, 17: 423-430.

Mulchandani, A., Chen, W., Mulchandani, P., Wang, J. & Rogers, K.R. (2001). Biosensors for direct determination of organophosphate pesticides. Review. *Biosensors and Bioelectronics*, 16: 225–230.

Neufeld, T., Eshkenazi, I., Cohen, E. & Rishpon, J. (2000). A micro flow injection electrochemical biosensor for organophosphorus pesticides. *Biosensors and Bioelectronics*, 15: 323–329.

Newman, J.D., Tigwell, L.J., Warner, P.J. & Turner, P.F. (2001). Biosensors: Boldly going into the new millennium. *Sensor Review*, 21: 268-271.

Ngamna, O., Morrin, A., Moulton, S.E., Killard, A.J., Smyth, M.R. & Wallace, G.G. (2005). An HRP base d biosensor using sulphonated polyaniline. *Synthetic Metals*, 153: 185–188.

Nieto-Cerón, S., Moral-Naranjo, M.T., Muñoz-Delgado, E., Vidal, C.J. & Campoy, F.J. (2004). Molecular properties of acetylcholinesterase in mouse spleen. *Neurochemistry International*, 45: 129–139.

Niwa, O., Horiuchi, T., Morita, M., Huang, T. & Kissinger, P.T. (1996). Determination of acetylcholine and choline with platinum-black ultramicroarray electrodes using liquid chromatography with a post-column enzyme reactor. *Analytica Chimica Acta*, 318: 167-173.

Noguer, T., Leca, B., Jeanty, G. & Marty, J-L. (1999). Biosensors based on enzyme inhibition: Detection of organophosphorus and carbamate insecticides and dithiocarbamate fungicides. *Field Analytical Chemistry & Technology*, 3 (3): 171-178.

Nunes, G.S., Barceló, D., Grabaric, B.S.;Diaz-Cruz, J.M. & Ribeiro, M.L. (1999). Evaluation of a highly sensitive amperometric biosensor with low cholinesterase charge immobilized on a chemically modified carbon paste electrode for trace determination of carbamates in fruit, vegetable and water samples. *Analytica Chimica Acta*, 399: 37–49.

Nunes, G.S., Jeanty, G. & Marty, J-L. (2004). Enzyme immobilization procedures on screen-printed electrodes used for the detection of anticholinesterase pesticides. Comparative study. *Analytica Chimica Acta*, 523: 107–115.

Oyamatsu, D., Kuwabata, S. & Yoneyama, H. (1999). Underpotential deposition behavior of metals onto gold electrodes coated with self-assembled monolayers of alkanethiols. *Journal of Electroanalytical Chemistry*, 473: 59–67.

Padilla, S., Buzzard, J. & Moser, V.C. (2000). Comparison of the role of esterases in the differential age-related sensitivity to chlorpyrifos and methamidophos. *Neurotoxicology*, 21: 49-56.

Padilla, S., Sung, H.J. & Moser, V.C. (2004). Further assessment of an in vitro screen that may help identify organophosphorus pesticides that are more acutely toxic to the young. *Journal of Toxicology and Environmental Health, Part A: Current Issues*, 67: 1477-1489.

Palchetti, I., Cagninia, A., Del Carlo, M., Coppi, C., Mascini, M. & Anthony P.F. Tumer, A.P.F. (1997). Determination of anticholinesterase pesticides in real samples using a disposable biosensor. *Analytica Chimica Acta*, 337: 31-321.

Palys, B., Kudelski, A., Stankiewicz, A. & Jackowska, K. (2000). Influence of anions on formation and electroacitivity of poly-*2,5*-dimethoxyaniline. *Synthetic Metals*, 108: 111–119.

Pandey, P.C., Upadhyay, S., Pathak, H.C., Pandey, C.M.D. & Tiwari, I. (2000). Acetylthiocholineracetylcholine and thiocholinercholine electrochemical biosensorsrsensors based on an organically modified sol–gel glass enzyme reactor and graphite paste electrode. *Sensors and Actuators B*, 62: 109–116.

Pang, Y-P., Kollmeyer, T.M., Hong, F., Lee, J-C., Hammond, P.I., Haugabouk, S.P. & Brimijoin, S. (2003). Rational Design of Alkylene-Linked Bis-Pyridiniumaldoximes as Improved Acetylcholinesterase Reactivators. *Chemistry and Biology*, 10: 491–502.

Pang, Y-P., Quiram, P., Jelacic, T., Hong, F. & Brimijoin, S. (1996). Highly Potent, Selective, and Low Cost Bis-tetrahydroaminacrine Inhibitors of Acetylcholinesterase. Steps Toward Novel Drugs for Treating Alzheimer's Disease. *The Journal of Biological Chemistry*, 271 (39): 23646–23649.

Park, I-S., Kima, D-K, Adanyi, N., Varadi, M. & Kima, N. (2004). Development of a direct-binding chloramphenicol sensor based on thiol or sulfide mediated self-assembled antibody monolayers. *Biosensors and Bioelectronics*, 19: 667–674.

Pauliukaite, R., Brett, C.M.A. & Monkman, A.P. (2004). Polyaniline fibres as electrodes. Electrochemical characterisation in acid solutions. *Electrochimica Acta*, 50: 159–167.

Patil, S., Mahajan, J.R., More, M.A. & Patil, P.P. (1999). Influence of supporting electrolyte on the electrochemical synthesis of poly(*o*-methoxyaniline) thin films. *Materials Letters*, 39: 298–304.

Patil, S., Mahajan, J.R., More, M.A. & Patil, P.P. (1999). Electrochemical synthesis of poly(*o*-methoxyaniline) thin effect of post treatment. Materials Chemistry and Physics, 58: 31-36.

Patil, V., Sainkar, S.R. & Patil, P.P. (2004). Growth of poly(*2,5*-dimethoxyaniline) coatings on low carbon steel. *Synthetic Metals*, 140: 57–63.

Peng, Z., Qu, X. & Dong, S. (2004). Co-assembly of ferrocene-terminated and alkylthiophene thiols on gold and its redox chemistry modulated by surfactant adsorption. *Journal of Electroanalytical Chemistry*, 563: 291–298.

Peres, L.O., Varela, H., Garcia, J.R., Fernandes, M.R., Torresi, R.M., Nart, F.C. & Gruber, J. (2001). On the electrochemical polymerization of poly(*p*-phenylene vinylene) and poly(*o*-phenylene vinylene). *Synthetic Metals*, 118: 65-70.

Pijanowska, D.G., A.J. Sprenkels, A.J., Van der Linden, H., Olthuis, W.,

Bergveld, P. & Van den Berg, A. (2004). A flow-through potentiometric sensor for an integrated microdialysis system. *Sensors and Actuators B*, 103: 350-355.

Pogačnik, L. & Franko, M. (1999). Determination of organophospahate and carbamate pesticides in spiked samples of tap water and fruit juices by a biosensor with photothermal detection. *Biosensors and Bioelectronics*, 14: 569-578.

Pond, A.L., Coyne, C.P., Chamberst, H.W. & Chumbers, J.E. (1996). Identification and Isolation of Two Rat Serum Proteins with A-Esterase Activity toward Paraoxon and Chlorpyrifos-oxon. *Biochemical Pharmacology*, 52: 363-369.

Premvardhan, L., Peteanu, L.A., Wang, P-C. & MacDiarmid, A.G. (2001). Electronic properties of the conducting form of polyaniline from electroabsorption measurements. *Synthetic Metals*, 116: 157-161.

Pritchard, J., Law, K., Vakurov, A., Millner, P. & Higson, S.P.J. (2004). Sonochemically fabricated enzyme microelectrode arrays for the environmental monitoring of pesticides. *Biosensors and Bioelectronics*, 20: 765-772.

Pruneanu, S., Veress, E., Marian, I. & Oniciu, L. (1999). Characterization of polyaniline by cyclic voltammetry and UV-Vis absorption spectroscopy. *Journal of Materials Science*, 34**:** 2733–2739.

Quintino, M.D.M., Winnischofer, H., Nakamura, M., Araki, K., Toma, H.E. & Angnes, L. (2005). Amperometric sensor for glucose based on electrochemically polymerized tetraruthenated nickel-porphyrin. *Analytica Chimica Acta*, 539: 215–222.

Raj, C.R., Gobi, K.V. & Ohsaka, T. (2000). Electrocatalytic oxidation of NADH at the self-assembled monolayer of nickel(II) macrocycle on gold electrode. *Bioelectrochemistr*y, 51: 181-186.

Rao, V.K., Rai, G.P., Agarwal, G.S. & Suresh, S. (2005). Amperometric immunosensor for detection of antibodies of *Salmonella typhi* in patient serum. *Analytica Chimica Acta*, 531: 173–177.

Reay, R.J., Flannery, A.F., Stroment, C.W., Kounaves, S.P. & Kovacs, G.T.A. (1996). Microfabricated electrochemical analysis system for heavy metal detection. *Sensors and Actuators B*, 34: 450-455.

Raj, C.R. & Ohsaka, T. (2003). Voltammetric detection of uric acid in the

presence of ascorbic acid at a gold electrode modified with a self-assembled monolayer of heteroaromatic thiol. *Journal of Electroanalytical Chemistry*, 540: 69-77.

Rannou, P., Pron, A. & Nechschein, M. (1999). UV-vis-NIR Studies of new PANI/dopant/solvent associations with metallic-like behaviour. *Synthetic Metals*, 101: 827-828.

Reay, R.J., Flannery, A.F., Stroment, C.W., Kounaves, S.P. & Kovacs, G.T.A. (1996). Microfabricated electrochemical analysis system for heavy metal detection. *Sensors and Actuators B*, 34: 450-455.

Reemts, J., Parisi, J. & Schlettwein, D. (2004). Electrochemical growth of gas-sensitive polyaniline thin films across an insulating gap. *Thin Solid Films*, 466:320– 325.

Rekha, K., Gouda, M.D., Thakur, M.S. & Karanth, N.G. (2000). Ascorbate oxidase based amperometric biosensor for organophosphorous pesticide monitoring. *Biosensors and Bioelectronics*, 15: 499–502.

Reynolds, D.R. & Riley, J.R. (2002). Remote-sensing, telemetric and computer-basedtechnologies for investigating insect movement: a survey of existing and potential techniques. *Computers and Electronics in Agriculture*, 35: 271-307.

Ricci, F., Amine, A., Palleschi, G. & Moscone, D. (2003). Prussian Blue based screen printed biosensors with improved characteristics of long-term lifetime and pH stability. *Biosensors and Bioelectronics*, 18: 165-174.

Rosini, S. & Siebert, E. (2005). Electrochemical sensors for detection of hydrogen in air: model of the non-Nernstian potentiometric response of platinum gas diffusion electrodes. *Electrochimica Acta*, 50 (14): 2943-2953.

Ronzani , N. Effet de solvants sur l'acetylcholinestérase. (1993). *Tetrahedron Letters*, 34 (24): 3867-3870.

Ruiz, A.I., Malave, A.J., Felby, C. & Griebenow, K. (2000). Improved activity and stability of an immobilized recombinant laccase in organic solvents. *Biotechnology Letters*, 22: 229–233.

Sacks, V., Eshkenazi, I., Neufeld, T., Dosoretz, C. & Rishpon, J. (2000). Immobilized Parathion Hydrolase: An Amperometric Sensor for Parathion. *Analytical Chemistry*, 72: 2055-2058.

Sadik, O.A. (1999). Bioaffinity Sensors Based on Conducting Polymers: A Short Review. *Electroanalysis*, 11 (12): 839-844.

Sahoo, R.R. & Patnaik, A. (2003). Binding of fullerene C60 to gold surface functionalized by self-assembled monolayers of 8-amino-1-octane thiol: a structure elucidation. *Journal of Colloid and Interface Science*, 268: 43–49.

Sakthivel, S., Shekar, B.C., Mangalaraj, D., Narayandass, B.S.K., Venkatachalamb, S. & Prabhakaran, P.V. (1997). Structure, Dielectric, AC and DC Conduction Prpoerties of Acid Doped Polyaniline Films. *European Polymer Journal*, 33 (10-12): 1747-1752.

Sharma, S.K., Sehgal, N. & Kumar, A. (2003). Biomolecules for development of biosensors and their applications. *Current Applied Physics*, 3: 307–316.

Sandhyarani, N., Skanth, G., Berchmans, S., Yegnaraman, V. & Pradeep, T. (1999). A Combined Surface-Enhanced Raman–X-Ray Photoelectron Spectroscopic Study of 2-mercaptobenzothiazole Monolayers on Polycrystalline Au and Ag Films. *Journal of Colloid and Interface Science*, 209**:** 154–161.

Santhanam, K.S.V. (1998). Conducting polymers for biosensors: Rationale based on models. *Pure and Applied Chemistry,* 70 (6): 1259-1262.

Saxena, V. & Malhotra, B.D. (2003). Prospects of conducting polymers in molecular electronics. *Current Applied Physics*, 3: 293–305.

Scheller, F. & Schubert, F. (1992). *Techniques and Instrumentation in Analytical Chemistry – Volume 11: Biosensors*. Amsterdam: Elsevier Science Publishers B.V.

Schuh, R.A., Lein, P.J., Beckles, R.A. & Jett, D.A. (2002). Noncholinesterase Mechanisms of Chlorpyrifos Neurotoxicity: Altered Phosphorylation of Ca^{2+}/cAMP Response Element Binding Protein in Cultured Neurons. *Toxicology and Applied Pharmacology*, 182: 176–185.

Schulze, H., Vorlova, S., Villatte, F., Bachmann, T.T. & Schmid, R.D. (2003). Design of acetylcholinesterases for biosensor applications. *Biosensors and Bioelectronic*s, 18: 201-209.

Schuvailo, O.N., Dzyadevych, S.V., Elskaya, A.V., Gautier-Sauvign, S., Csoregic, E., Cespuglio, R. & Soldatkin, A.P. (2005). Carbon fibre-based microbiosensors for in vivo measurements of acetylcholine and choline. *Biosensors and Bioelectronics*, 21: 87–94.

Sen, S., Gülce, A. & Gülce, H. (2004). Polyvinylferrocenium modified Pt

electrode for the design of amperometric choline and acetylcholine enzyme electrodes. *Biosensors and Bioelectronics*, 19: 1261–1268.

Sfiez-Valero, J. & Vidal, C.J. (1996). Biochemical properties of acetyl- and butyrylcholinesterase in human meningioma. *Biochimica et Biophysica Acta*, 1317: 210-218.

Sergeyeva, T.A., S.A. Piletsky, T.A., Brovko, A.A., Slinchenko, E.A., Sergeeva, L.M. & Elskaya, A.V. (1999). Selective recognition of atrazine by molecularly imprinted polymer membranes. Development of conductometric sensor for herbicides detection. *Analytica Chimica Acta*, 392: 105-111.

Shvarev,A.E., Rantsan, D.A. & Mikhelson, K.N. (2001). Potassium-selective conductometric sensor. *Sensors and Actuators B*, 76: 500 – 505.

Sharma, R.K. & Goel, A. (2004). Development of a Cr(III)-specific potentiometric sensor using Aurin tricarboxylic acid modified silica. *Analytica Chimica Acta*, 534: 137-142.

Sharma, S.K., Sehgal, N., Kumar, A. (2003). Biomolecules for development of biosensors and their applications. *Current Applied Physics*, 3: 307-316.

Shen, J. & Liu, C-C. (2007). Development of a screen-printed cholesterol biosensor: Comparing the performance of gold and platinum as the working electrode material and fabrication using a self-assembly approach. *Sensors and Actuators B*, 120: 417–425.

Silman, I. & Sussman, J.L. (2005). Acetylcholinesterase: "classical" and "non-classical" functions and pharmacology. *Current Opinion in Pharmacology*, 5: 293–302.

Silva-Filho, M.V., Oliveira, M.M., Salles, J.B., Cunha Bastos, V.L.F., Cassano, V.P.F.& Cunha Bastos, J. (2004). Methyl-paraoxon comparative inhibition kinetics for acetylcholinesterases from brain of neotropical fishes. *Toxicology Letters*, 153: 247–254.

Simon, S., Le Goff, A., Frobert, Y., Grassi, J. & Massoulié, J. (1999). The Binding Sites of Inhibitory Monoclonal Antibodies on acetylcholinesterase. Identification of a novel regulatiry site at the putative "back door". *Journal of Biological Chemistry*, 274 (39): 27740-27746.

Singh, A.K., Flounders, A.W., Volponi, J.V., Ashley, C.S., Wally, K. & Schoeniger, J.S. (1999). Development of sensors for direct detection of

organophosphates. Part I: immobilization, characterization and stabilization of acetylcholinesterase and organophosphate hydrolase on silica supports. *Biosensors and Bioelectronics*, 14: 703–713.

Sirotkin, V.A., Zazybin, A.G., Osipova, O.L., Solomonov, B.N, Faizullin, D.A. & Fedotov, V.D. (2000). Solubility and secondary structure of bovine pancreatic chymotripsin in water-acetonitrile mixtures. *Khimiya*, 41 (6): 114-117.

Snejdarkova, M., Svobodova, L., Evtugyn, G., Budnikov, H., Karyakin, A., Nikolelis, D.P. & Hianik, T. (2004). Acetylcholinesterase sensors based on gold electrodes modified with dendrimer and polyaniline. A comparative research. *Analytica Chimica Acta*, 514: 79–88.

Sogor, M.A. & Vilanov, E. (2002). Enzymes involved in the detoxification of organophosphorus, carbamate and pyrethroid insecticides through hydrolysis. Review Article. *Toxicology Letters*, 128: 215–228.

Song, W., Okamura, M., Kondo, T. & Uosaki, K. (2003). Electron and ion transport through multilayers of Au nanoclusters covered by self-assembled monolayers. *Journal of Electroanalytical Chemistry*, 554-555: 385-393.

Sotiropoulou, S. & Chaniotakis, N.A. (2005a). Lowering the detection limit of the acetylcholinesterase biosensor using a nanoporous carbon matrix. *Analytica Chimica Acta*, 530: 199–204.

Sotiropoulou, S., Fournier, D. & Chaniotakisa, N.A. (2005b). Genetically engineered acetylcholinesterase-based biosensor for attomolar detection of dichlorvos. Short Communication. *Biosensors and Bioelectronics*, 20: 2347–2352.

Stojana, J.Golicinika, M. & Fournier, D. (2004). Rational polynomial equation as an unbiased approach for the kinetic studies of Drosophila melanogaster acetylcholinesterase reaction mechanism. *Biochimica et Biophysica Acta*, 1703: 53–61.

Strassberger, M. & Waller, H. (2000). Active noise reduction by structural control using piezo-electric actuators. *Mechatronics,* 10: 851-868.

Stryer, L. (1981). *Biochemistry*. 2nd edition. San Francisco: W.H. Freeman and Company.

Sun, B. & Huang, D. (2001). Vibration suppression of laminated composite beams with a piezo-electric damping layer. *Composite Structures*, 53: 434–447.

Susmel, S., Guilbault, G.G. &O'Sullivan, C.K. (2003). Demonstration of labeless

detection of food pathogens using electrochemical redox probe and screen printed gold electrodes. *Biosensors and Bioelectronics*, 18: 881-889.

Suye, S., Matsuura , T., Kimura, T., Zheng, H., Hori, T., Amano, Y., & Katayama, H. (2005). Amperometric DNA sensor using gold electrode modified with polymerized mediator by layer-by-layer adsorption. *Microelectronic Engineering*, 81 (2-4): 441-447.

Szigeti a, Z., Bitter, I., Toth, K., Latkoczy, C., Fliegel, D.J., Detlef Günther, D. & Pretsch, E. (2005). A novel polymeric membrane electrode for the potentiometric analysis of Cu2+ in drinking water. *Analytica Chimica Acta*, 532, 129-136.

Tagowska, M., Mazur, M. & Krysinski, P. (2004). Covalently and ionically immobilised monomers on the gold surface. *Synthetic Metals*, 140: 29–35.

Tang, H., Kitani, A. & Shiotang, M. (1996). Effects of anions on electrochemical formation and overoxidation of polyaniline. *Electrochimica Acta*, 41: 1561-1567.

Tao, W., Pan, D., Liu, Y., Nie, L. & Yao, S. (2005). An amperometric hydrogen peroxide sensor based on immobilization of hemoglobin in poly(*o*-aminophenol) film at iron–cobalt hexacyanoferrate-modified gold electrode. *Analytical Biochemistry*, 338: 332–340.

Tatsuma, T., Ogawa, T., Sato, R. & Oyama, N. (2001). Peroxidase-incorporated sulfonated polyaniline–polycation complexes for electrochemical sensing of H_2O_2. *Journal of Electroanalytical Chemistry*, 501: 180–185.

Teller, C., Halamek, J., Makower, A., Fournier, D., Schulze, H. & Scheller, F.W. (2006). A piezoelectric sensor with propidium as a recognition element for cholinesterases. *Sensors and Actuators B*, 113: 214-221.

Tezer, N. (2005). Ab initio molecular structure study of alkyl substitute analogues of Alzheimer drug phenserine: structure–activity relationships for acetyl- and butyrylcholinesterase inhibitory action. *Journal of Molecular Structure: THEOCHEM*, 714: 133–136.

Timur, S., Pazarlioglu, N., Pilloton, R. & Telefoncu, A. (2004). Thick film sensors based on laccases from different sources immobilized in polyaniline matrix. *Sensors and Actuators B*, 97: 132–136.

Toczylowska, R., Pokrop, R., Dybko, A. & Wroblewski, W. (2005). Planar potentiometric sensors based on Au and Ag microelectrodes and conducting polymers for flow-cell analysis. *Analytica Chimica Acta*, 540: 167-172.

Toda, N., Tago, K., Marumoto, S., Takami, K., Ori, M., Yamada, N., Koyama, N., Naruto, S., Abe, K., Yamazaki, R., Hara, T., Aoyagi, A., Abe, Y., Kaneko, T. & Kogen, H. (2003). Design, Synthesis and Structure–Activity Relationships of Dual Inhibitors of Acetylcholinesterase and Serotonin Transporter as Potential Agents for Alzheimer's Disease. *Bioorganic and Medicinal Chemistry*, 11: 1935–1955.

Tønning, E., Sapelnikova, S., Christensen, J., Carlsson, C., Winther-Nielsen, M. Dock, E., Solna, R., Skladal, P. Nørgaard, L., Ruzgas, T. & Emneus, J. (2005). Chemometric exploration of an amperometric biosensor array for fast determination of wastewater quality. *Biosensors and Bioelectronics*, 21: 608-617.

Trojanowicz, M. & Hitchman, M.L. (1996). Determination of pesticides using electrochemical biosensors. *Trends in Analytical Chemistry*, 15(1): 38-45.

Tripathy, S.K., Kumar, J. & Nalwa, H.S. (2002). *Handbook of Polyelectrolytes and Their Applications. Volume 2. Polyelectrolytes, Their Characterization and Polyelectrolyte Solutions.* California: American Scientific Publishers.

Tsai, H-C. & Doong, R-A. (2005). Simultaneous determination of pH, urea, acetylcholine and heavy metals using array-based enzymatic optical biosensor. *Biosensors and Bioelectronics*, 20: 1796–1804.

Tu, Y-F., Fu, Z-Q. & Chen, H-Y. (2001). The fabrication and optimization of the disposable amperometric biosensor. *Sensors and Actuators B*, 80: 101-105.

Tymecki, L., Zwierkowska, E. & Koncki, R. (2004). Screen-printed reference electrodes for potentiometric measurements. *Analytica Chimica Acta*, 526: 3–11.

Tzou, H.S., Smithmaitrie, P. & Ding, J.H. (2002). Micro-sensor electromechanics anddistributed signal analysis of piezo(electric)-elastic spherical shells. *Mechanical Systems and Signal Processing,* 16(2–3): 185-199.

Ulman, A., Kang, J.F., Shnidman, Y., Liao, S., Jordan, R., Choi, G-Y., Zaccaro, J., Myerson, A.S., Rafailovich, M., Sokolov, J. & Fleischer , J. (2000). Self-assembled monolayers of rigid thiols. *Reviews in Molecular Biotechnology*, 74: 175-188.

Vakurov, A., Simpson, C.E., Dalya, C.L., Gibson, T.D. & Millner, P.A. (2004). Acetylcholinesterase-based biosensor electrodes for organophosphate pesticide detection I. Modification of carbon surface for immobilization of acetylcholinesterase. *Biosensors and Bioelectronics*, 20: 1118–1125.

Vamvakaki, V., Fournier, D. & Chaniotakis, N.A. (2005). Fluorescence detection of enzymatic activity within a liposome based nano-biosensor. Short Communication. *Biosensors and Bioelectronics*, 21: 384–388.

Varamban, S.V., Ganesan, R. & Periaswami, G. (2005). Simultaneous measurement of emf and short circuit current for apotentiometric sensor using perturbation technique. *Sensors and Actuators B*, 104: 94-102.

Varfolomeyev, S., Kurochkin, I., Eremenko, A., & Efremenko, E. (2002). Chemical and biological safety. Biosensors and nanotechnological methods for the detection and monitoring of chemical and biological agents. *Pure and Applied Chemistry*, 74 (12): 2311–2316.

Vergheese, T.M. & Berchmans, S. (2004). Evaluation of monolayers and mixed monolayers formed from mercaptobenzothiazole and decanethiol as sensing platforms. *Materials Chemistry and Physics*, 83: 229–238.

Vidal, J-C., Garcia-Ruiz, E. & Castillo, J-R. (2003). Recent Advances in Electropolymerized Conducting Polymers in Amperometric Biosensors. *Microchimica Acta*, 143 (2-3): 93-111.

Wan, Q. & Yang, N. (2002). The direct electrochemistry of folic acid at a 2-mercaptobenzothiazole self-assembled gold electrode. *Journal of Electroanalytical Chemistry*, 527: 131-136.

Wang, B. & Dong, S. (2000). Organic-phase enzyme electrode for phenolic determination based on a functionalised sol-gel composite. *Journal of Electroanalytical Chemistry*, 487: 45-50.

Wang, Y. & Jing, X. (2004). Effect of solution concentration on the UV–vis spectroscopy measured oxidation state of polyaniline base. *Polymer Testing*, 24: 153–156.

Wang, J., Krause, R., Block, K., Musameh, M., Mulchandani, A. & Schoning, M.J. (2003). Flow injection amperometric detection of OP nerve agents based on an organophosphorus_/hydrolase biosensor detector. *Biosensors and Bioelectronics*, 18: 255-260.

Wang, J., Zeng, B., Fang, C. & Zhou, X. (2000a). Electrochemical Characteristics of *2*-Mercaptobenzothiazole Self-Assembled Monolayer on Gold. *Analytical Sciences*, 16*:* 457–461.

Wang, J., Zeng, B., Fang, C. & Zhou, X. (2000b). The influence of surfactants on

the electron-transfer reaction at self-assembled thiol monolayers modifying a gold electrode. *Journal of Electroanalytical Chemistry*, 484: 88–92.

Wang, J., Wu, L-H. & Angnes, L. (1991). Organic-Phase Enzymatic Assays with Ultramicroelectrodes. *Analytical Chemistry,* 63: 2993-2994.

Wang, X., Schreuder-Gibson, H., Downey, M., Tripathy, S. & Samuelson, L. (1999). Conductive fibers from enzymatically synthesized polyaniline *Synthetic Metals*, 107: 117–121.

Wang, J. Nascimento, V.B., Kane, S.A., Rogers, K., Smyth, M.R. & Angne, L. (1996). Screen-printed tyrosinase-containing electrodes for the biosensing of enzyme inhibitors. *Talanta*, 43: 1903-1907.

Wang, Y., Guo, C., Chen, Y., Hu, C. & Yu, W. (2003). Self-assembled multilayer films based on a Keggin-type polyoxometalate and polyaniline. *Journal of Colloid and Interface Science*, 264: 176–183.

Wang, Y. & Jing, X. (2005). Analysis Method. Effect of solution concentration on the UV–vis spectroscopy measured oxidation state of polyaniline base. *Polymer Testing*, 24: 153–156.

Wasilewski, J. (2005). Chemistry Department, University of Scranton, wasilewskij1@uofs.edu. http://academic.scranton.edu/faculty/CANNM1/biochemistry.html, available online, 7 July 2005.

Wen, T-C., Huang, L-M. & Gopalan, A. (2001). Spectroscopic and thermal properties of the copolymer of aniline with dithioaniline. *Synthetic Metals*, 123: 451-457.

White, B.J., Legako, J.A. & Harmon, H.J. (2003). Spectrophotometric detection of cholinesterase inhibitors with an integrated acetyl- or butyrylcholinesterase surface. *Sensors and Actuators B*, 89: 107–111.

Widera, J., Grochala, W., Jackowska, K. & Bukowska, J. (1997). Electrooxidation of *o*-methoxyaniline as studied by electrochemical and SERS methods. *Synthetic Metals*, 89: 29-37.

Williams, R.D., Boros, L.G., Kolanko, C.J. Jackman, S.M. & Eggers, T.R. (2004). Chromosomal aberrations in human lymphocytes exposed to the anticholinesterase pesticide isofenphos with mechanisms of leukemogenesis. *Leukemia Research*, 28: 947–958.

Wilkins, E., Carter, M., Voss, J., Ivnitski, D. (2000). A quantitative determination

of organophosphate pesticides in organic solvents. *Electrochemistry Communications*, 2:786–790.

Wolfbeis, O.S., Klimant, I., Werner, T., Huber, C., Kosch, U., Krause, C., Neurauter, G. & Durkop, A. (1998). Set of luminescence decay time based chemical sensors for clinical applications. *Sensors and Actuators B*, 51: 17–24.

Wood, A. (1995). Hyperlink http://www.hclrss.demon.co.uk/class_acaricides.html#carbamate_acaricides , accessed on 17 June 2005.

Worek, F., Mast, U., Kiderlen, D., Diepold, C. & Eyer, P. (1999). Improved determination of acetylcholinesterase activity in human whole blood. *Clinica Chimica Acta*, 288: 73–90.

Worek, F., Thiermann, H., Szinicz, L. & Eyer, P. (2004). Kinetic analysis of interactions between human acetylcholinesterase, structurally different organophosphorus compounds and oximes. *Biochemical Pharmacology*, 68: 2237–2248.

WHO, World Health Organization. (1986a). World Health Organization Metabolism and mode of action. Organophosphorus Insecticides: a General Introduction. WHO, Geneva, pp. 39–48.

WHO, World Health Organization. (1986b). Effects of organophosphorus insecticides on the nervous system. World Health Organization. Organophosphorus Insecticides: a General Introduction. WHO, Geneva, pp. 58–69.

World Health Organization. (1986c). *Environmental Health Criteria 64 – Carbamate Pesticides: A General Introduction*. 92 pp. Geneva: ISBN 92 4 154264 0

WHO, World Health Organization. (1986d). Carbamate pesticides. In: Environmental Health Criteria, 64. WHO, Geneva.

Wu, M-C. & Micheli, A.L. (2004). Calorimetric hydrocarbon sensor for automotive exhaust applications. *Sensors and Actuators B*, 100: 291-297.

Yang, M., Yang, Y., Yang, Y., Shen, G. & Yu, R. (2005). Microbiosensor for acetylcholine and choline based on electropolymerization/sol–gel derived composite membrane. *Analytica Chimica Acta*, 530: 205–211.

Yang, J., Kim, D.H., Hendricks, J.L. Leach, M., Northey, R. & Martin, D.C.

(2005). Ordered surfactant-templated poly(3,4-ethylenedioxythiophene) (PEDOT) conducting polymer on microfabricated neural probes. *Acta Biomaterialia*, 1: 125–136.

Yang, L., Wei, W., Xia, J., Tao, H. & Yang, P. (2005). Electrochemical Studies of Derivatized Thiol Self-Assembled Monolayers on Gold Electrode in the Presence of Surfactants. *Analytical Sciences*, 21: 679–684.

Yeh, W-M. & Ho, K-C. (2005). Amperometric morphine sensing using a molecularly imprinted polymer-modified electrode. *Analytica Chimica Acta*, 542: 76-82.

Yourdshahyan, Y., Zhang, H.K. & Rappe, A.M. (2000). *n*-alkyl thiol head-group interactions with the Au(III) surface. *Physical Review B*, 63: 1-4.

Zerulla, D., Szargan, U.R. & Chasse, T. (1998). Competing interaction of different thiol species on gold surfaces. *Surface Science*, 402–404: 604–608.

Zhang, W-W., Ren, X-M., Li, H-F., Lu, C-S., Hu, C-J., Zhu, H-Z. & Q-J. Meng. (2002). Study on Self-Assembled Monolayers of Functionalized Azobenzene Thiols on Gold: XPS, Electrochemical Properties, and Surface-Enhanced Raman Spectroscopy1. *Journal of Colloid and Interface Science*, 255: 150–157.

Zhang, X.G., Li, X.H. & Li, H.L. (2001). The Influence of Bromine Adsorption on Copper Electrodeposition on Polycrystalline Gold Electrodes Modified with Self-Assembled Monolayers. *Journal of Colloid and Interface Science*, 234: 68–71.

Zanello, P. (2003). *Inorganic Electrochemistry. Theory, Practice and Application*. Cambridge, UK: The Royal Society of Chemistry.

Zeaiter, J., Gomes, V.G., Romagnoli, J.A. & Barton, G.W. (2002). Inferential conversion monitoring and control in emulsionpolymerisation through calorimetric measurements. *Chemical Engineering Journal*, 89: 37-45.

Organophosphate Pesticides in Food. Hyperlink http://ww.epa.gov/oppsrrd1/op/primer.htm , accessed on 15 June 2005.

Hyperlink http://orion1.paisley.ac.uk/kinetics/Chapter_3/chapter3_1.html , accessed on 5 December 2005.

Hyperlink http://orion1.paisley.ac.uk/kinetics/Chapter_3/chapter3_1.html, accessed on 5 December 2005.

Hyperlink http://campus.northpark.edu/biology/cell/enzymes.html ,
        Accessed on 20 january 2006.

APPENDIX

Abstracts of Papers Published

1.   **Vernon S. Somerset, Michael J. Klink, Priscilla G. L. Baker and Emmanuel I. Iwuoha. (2007). Acetylcholinesterase-polyaniline biosensor investigation of organophosphate pesticides in selected organic solvents. Journal of Environmental Science and Health Part, B42: 297–304.**

The behavior of an amperometric organic-phase biosensor consisting of a gold electrode modified first with a mercaptobenzothiazole self-assembled monolayer, followed by electropolymerization of polyaniline in which acetylcholinesterase as enzyme was immobilized, has been developed and evaluated for organophosphorous pesticide detection. The voltammetric results have shown that the formal potential shifts anodically as the Au/MBT/PANI/AChE/PVAc thick-film biosensor responded to acetylthiocholine substrate addition under anaerobic conditions in selected organic solvent media containing 2% v/v 0.05 M phosphate buffer, 0.1 M KCl (pH 7.2) solution. Detection limits in the order of 0.147 ppb for diazinon and 0.172 ppb for fenthion in acetone-saline phosphate buffer solution, and 0.180 ppb for diazinon and 0.194 ppb for fenthion in ethanol-saline phosphate buffer solution has been achieved.

Keywords: Polyaniline;   mercaptobenzothiazole;   acetylcholinesterase; organophosphorous pesticides; diazinon and fenthion; organic phase biosensor.

2.   **Vernon S. Somerset, Michael J. Klink, Mantoa M. C. Sekota, Priscilla G. L. Baker, and Emmanuel I. Iwuoha. (2006). Polyaniline-Mercaptobenzothiazole Biosensor for Organophosphate and Carbamate Pesticides. *Analytical Letters*, 39: 1683–1698.**

Organophosphate and carbamate pesticides are powerful neurotoxins that impede the activity of cholinesterase enzyme leading to severe health effects. This study reports the development, characterization, and application of acetylcholinesterase (AChE) biosensors based on a gold electrode modified with mercaptobenzothiazole (MBT) self-assembled monolayer and either poly(o-methoxyaniline) (POMA) or poly(2,5-dimethoxyaniline) (PDMA) in the presence of polystyrene sulfonic acid (PSSA). The pesticide biosensors were applied in the aqueous phase detection of diazinon and

carbofuran pesticides using Osteryoung square wave voltammetry (SWV) and differential pulse voltammetry (DPV) at low frequencies. The results of the study showed that up to 94% inhibition of the MBT-polyaniline-based biosensors can be achieved in sample solutions containing 1.19 ppb of these neurotoxin pesticide compounds. Both Au/MBT/PDMA-PSSA/AChE and Au/MBT/POMAPSSA/AChE biosensors exhibited low detection limits, which were calculated using the percentage inhibition methodology. The Au/MBT/POMA-PSSA/AChE biosensor exhibited lower detection limits of 0.07 ppb for diazinon and 0.06 ppb for carbofuran than did the Au/MBT/PDMA-PSSA/AChE sensor system that had detection limits values of 0.14 ppb for diazinon and 0.11 ppb for carbofuran. The average sensitivity of the pesticide biosensor systems is 4.2 mA/ppb. A combination of the high sensor sensitivity and low detection limits means that it will be possible to deploy the polyaniline-based sensor systems as alarm devices for carbamate and organophosphate
pesticides.

Keywords: Polyaniline derivatives, mercaptobenzothiazole, acetylcholinesterase, organophosphate carbamate pesticides, diazinon, carbofuran

3.   **Emmanuel I. Iwuoha, Sipho E. Mavundla, Vernon S. Somerset, Leslie F. Petrik, Michael J. Klink, Mantoa Sekota, and Priscilla Bakers. (2006). Electrochemical and Spectroscopic Properties of Fly Ash–Polyaniline Matrix Nanorod Composites. Microchim Acta, 155: 453–458.**

Polyaniline (PANI) nanocomposites were prepared with fly ash (FA) either by aging the starting materials (aniline and FA) before oxidative polymerization or by including poly(styrene sulphonic acid) (PSSA) eliminating the aging step. The aging procedure formed polymer nanotubes that have cross-sectional diameters of 50–110 nm. The procedure involving PSSA produced nanorods and nanofibres composites that have diameters of 100–500 nm and length of up to 10 mm attributed to the presence of metal oxides and silica in FA. The electrochemical analysis of the PANI–PSSA–FA nanorod composites shows three redox couples with formal potentials, $E^{\circ\prime}(200mVs^{-1})$, values of 105mV, 455mV and 670mV, and conductance, C, value of 1.21_10_2 S. The UV-Vis spectroscopy of the polymeric nanorod shows absorption maxima at 340 and 370 nm (due to π-π^* transition of the benzoid rings), and 600–650 nm (due to charge transfer excitons of the quinoid structure), which are characteristic of emeraldine base.

Keywords: Cyclic voltammetry; fly ash; polyaniline nanorods; polyaniline nanotubes; poly(styrene sulphonic acid); polyaniline-fly ash composites; scanning electron microscopy.

4.   **V.S. Somerset, M.J. Klink, M. Sekota, P.G.L. Baker and E.I. Iwuoha. (2007). Acetylcholinesterasepoly(*2,5*dimethoxyaniline) pesticide (nano)biosensor for organophosphate pesticide detection. In E. Mvula, H.R. Lofty, I. Mapaure, S. Singh & B. Mapani (eds.). Proceedings of the East and Southern Africa Environmental Chemistry Workshop (ESAECW) and the Sixt Theoretical Chemistry Workshop in Africa (TCWA). University of Namibia, Windhoek, Namibia. 5-9 December 2005***: 89 – 102.*

A very sensitive amperometric sensor for the determination of organophosphate pesticides has been evaluated and electrochemically characterised. The biosensor was manufactured using a polyaniline (PANI) derivative called poly(*2,5*-dimethoxyaniline) (PDMA), which was prepared by *in situ* oxidative polymerisation of the monomer in acid solutions containing poly(styrene sulphonic acid) (PSSA) as stabiliser. The working electrode was first modified with a mercaptobenzothiazole (MBT) self-assembled monolayer (SAM), before being placed in the monomer solutions. The acetylcholinesterase enzyme was then immobilised within the polymer matrix. The inhibition of the biosensor amperometric response to acetylcholine (ACh) by Diazinon (an organophosphate pesticide) was used to construct a calibration curve for the pesticide. The cyclic voltammetric results have also shown that the formal potential shift anodically as the Au/MBT/PDMA-PSSA/AChE biosensor responded to acetylcholine (ACh) substrate addition under anaerobic conditions in 0.1 M phosphate buffer, KCl (pH 7.2). It was further established that the Au/MBT/PDMA-PSSA/AChE biosensor can be inhibited by up to 90% by Diazinon pesticide when applied in a 0.1 M phosphate buffer, KCl (pH 7.2) solution, to which the Diazinon pesticide was added.

Keywords: Poly(*2,5*-dimethoxyaniline);   Biosensor;   Mercaptobenzothiazole; Diazinon Pesticide; Acetylcholinesterase

5.   **Immaculate N. Michira, M. Klink, R. O. Akinyeye, V. Somerset, M. Sekota, A. Al-Ahmed, P. G. L Baker, Emmanuel I. Iwuoha. (2007). Anthracene Sulfonic Acid-Doped Polyanilines: Electrodynamics and Application as Amperometric Peroxide Biosensor.** *Book chapter: Recent Advances in Conducting Polymer (In Review)*

Polyaniline (PANi) is one of the most studied conducting polymers [1-4]. It has received great attention due to its good environmental stability, optical and electrochemical properties. Due to its light weight, flexibility and a reasonably facile processibility, PANi is finding use in the fabrication of electromagnetic interference shielding materials, and in broadband microwave adsorbing materials [5]. PANi has also merited applications in many other fields including; biosensor technology, electrochromic devices, energy storage systems and anticorrosion materials. The main drawback associated with this conducting polymer however, is its poor processibility both in melt and solution forms due to its stiff backbone and

insolubility in most organic and inorganic. Several strategies have been employed to make PANi more processable. One approach entails the introduction of substituents [6-8] on the aromatic ring or aromatic nitrogen, which distorts the rigid π-electron system and promotes organic/ aqueous solubility depending on the substituents type. Co-polymerization with aliphatic monomers, preparation of PANi blends/composites with other convectional polymers [9-11] have led to more soluble PANi. Also PANi colloidal dispersions have found use in many fields. PANi colloidal dispersions have been prepared through several methods. The polymerisation of aniline monomers in a micelle [2], emulsion [12], reversed micro- emulsion media [13] or in the presence of polymeric stabilizers have yielded colloidally stable PANi with submicrometer/nanometer-sized particles. Recently it has been discovered that the morphology of PANi can be as diverse as there are synthetic routes and reaction conditionality. PANi with needle-like or spherical shapes has been obtained through the dispersion polymerisation method in the presence of stabilizers [14]. Also microporous PANi has been fabricated by using colloidal assemblies as templates [14]. Elsewhere [aniline]:[β-NSA] micelles played a pseudo template role of facilitating the formation of PANi-β-NSA nano and microstructures [15]. Wei and Wan [16], synthesized amongst others, polyaniline hollow microspheres with diameter ranges of 450-1370 nm on aniline emulsion templates using β- NSA and ammonium persulfate as oxidant. PANi-dodecylbenzenesulfonic acid (DBSA) exhibited micromorphology [17] as camphor sulfonic acid-doped PANi showed fibrillar morphology. These sulfonic acids were found to play both surfactant and dopant roles.

6.   **V. Somerset, M. Klink, R. Akinyeye, M. Sekota, A. Al-Ahmed, P. Baker and E.I. Iwuoha. (2007). Spectroelectrochemical Reactivities of Novel Polyaniline Nanotube Pesticide Biosensors.** *Macromolecular Symposia, 2007 (In Press)*

The preparation and characterisation of electrosynthetic polyaniline nanomaterials doped with phenanthrene sulphonic acid (PSA) is being presented. The polymeric nanomaterials prepared include processable poly(*o*-methoxy aniline) (POMA) and poly(*2,5*-dimethoxy aniline) (PDMA). Spectroelectrochemical reactivities of the electroactive polymeric nanotube systems as well as the nanobiosensor systems were studied by SEM, FTIR, UV-Vis and Subtractively Normalised Fourier Transformed Infrared Spectroscopy (SNIFTIRS) techniques. Furthermore, cyclic and differential pulse voltammetric studies of the nanomaterials were also performed using platinum or thiol-modulated gold electrodes. The SEM studies confirmed the nanorod morphology of the polyanilines. The heterogeneous rate constant, k_o, for the nanopolymeric material and the diffusion coefficient of electrons, D_e, was calculated and found to be in agreement with values expected for electron hopping along conducting polymer chains. Organophosphate pesticide nanobiosensor devices were prepared by encapsulating acetylcholinesterase (AChE) in the nanopolymeric composite. The biosensor amperometric response to the organophosphate pesticide

called diazinon and the carbamate pesticide called carbofuran were studied. The sensor responses to pesticides followed typical electrochemical Michaelis-Menten kinetics.

Keywords: Spectroelectrochemistry; polyaniline; nanotube; pesticide; biosensor

7.   **Michira I. N, Klink M., Akinyeye R., Somerset V., Sekota M., Al-Ahmed A., Baker P. and Iwuoha E. (2007). Electrochemical Synthesis of Anthracene Sulfonic Doped Polyanilines: Spectroscopic Characterization and Application in Hydrogen Peroxide Sensing.** *Macromolecular Symposia, 2007 (In Press)*

Anthracene sulfonic acid doped polyaniline nanomaterials were prepared through the chemical oxidative polymerisation process. Ammonium peroxydisulfate (APS) was employed as oxidant. Scanning electron microscopy (SEM) results show the resultant polyaniline (PANi) materials exhibited nanofibrillar morphology with diameter sizes less than 300 nm. Using the nanofibrillar PANI, amperometric biosensors for H_2O_2 and erythromycin were constructed through the drop-coating technique. Anthracene sulfonic acid (ASA) doped PANi and the test enzymes horseradish peroxidase, (HRP), or cytochrome P_{450} 3A4, ($CYP_{450-3A4}$) were mixed in phosphate buffer solution before drop coating onto the electrode. The resultant biosensors displayed typical Michaelis-Menten behaviour. The apparent Michaelis-Menten constant obtained was 0.18 ± 0.01 mM and 0.80 ± 0.02 μM L^{-1} for the peroxide and erythromycin biosensor respectively. The sensitivity for the peroxide sensor was 3.3×10^{-3} A.cm^{-2}.mM^{-1}, and the detection limit was found to be 1.2×10^{-2} mM respectively. Similarly, the sensitivity for the erythromycin sensor was in the same order at 1.57×10^{-3} A.cm^{-2}.mM^{-1} and detection limit was found to be 7.58×10^{-2} μM.

Keywords: synthesis; doped polyaniline; enzymes; nanocomposites; electroactive